The Role of Pre-Receptor Steroid Metabolism in the Therapeutic Application of Glucocorticoids

By

Chloe Fenton

A thesis submitted to the University of Birmingham for the degree of

DOCTOR OF PHILOSOPHY

Institute of Metabolism and Systems Research

College of Medical and Dental Sciences

University of Birmingham

January 2020

Abstract

Glucocorticoids (GCs) are widely used in the treatment of chronic inflammatory diseases such as rheumatoid arthritis (RA). Unfortunately, their application is limited by side effects including GC-induced osteoporosis (GIO). The GC-activating enzyme 11β-hydroxysteroid dehydrogenase type 1 (11β-HSD1) has been shown to mediate side effects associated with therapeutic GCs, suggesting that 11β-HSD1 inhibition may be effective in managing their deleterious side effect profile. In this thesis, I have examined the contribution of 11β-HSD1 to therapeutic actions and off target bone side effects of therapeutic GCs in the TNF-transgenic (TNF-tg) murine model of chronic polyarthritis. TNF-tg animals receiving the GC corticosterone in drinking water (100 mg/L) demonstrated a significant reduction in markers of inflammation, disease activity, synovitis and inflammatory bone loss. In contrast, TNF-tg animals with transgenic deletion of 11β-HSD1 (TNF11βKO) showed a marked resistance to GC-induced changes showing more severe, persistent inflammation and inflammatory bone loss, despite being protected from GIO driven by suppression of anabolic bone formation. Local and systemic bone loss in TNF11βKO animals receiving GCs, was underpinned by increased inflammatory activation of osteoclasts. This study demonstrates a fundamental role for 11β-HSD1 in mediating the anti-inflammatory and bone protective actions of therapeutic GCs in murine models of chronic polyarthritis.

Acknowledgements

First and foremost, I would like to thank my supervisors, Dr Rowan Hardy, Prof Karim Raza and Prof Gareth Lavery, for their continued support throughout my PhD. Rowan; your enthusiasm, advice and friendship has been invaluable over the past three years, without which this thesis would not be possible. In particular, a special thanks for allowing me to conscientiously object to Coup without *too* much protest. Karim; your clinical knowledge and insights have broadened the perspective of this research and Gareth; who provided the 11β-HSD1 KO mouse on which the majority of this research is based. Additionally, I would like to thank Prof Mark Cooper who acted as an unofficial supervisor on this project and provided many interesting experimental ideas.

I would also like to acknowledge the Department of Musculoskeletal Pathology at the ROH, for processing and cutting sections for histology, and the BMSU, for supporting the animal work performed as part of this research. In addition, the diagrams in this thesis have been made with the help of Servier Medical Art (https://smart.servier.com/) unless otherwise stated.

I have been very fortunate to work amongst the other members of the Hardy lab, Justine and Claire, who have contributed to my scientific output both directly, by helping me in the lab, and indirectly, by supporting and encouraging me. I would like to say additional thank yous to the past students who have joined our group for shorter time periods but who have still made an impact. I also feel extremely lucky to have had the opportunity to work with such an inspiring and entertaining group of people at the IMSR, who have made my PhD experience so much fun. I would like to especially thank my Spice Girls; Michelle, Kat, Danni and Rachel and my Crime Club who have contributed substantially to my

enjoyment of the past few years. Also, to Amadeo, it's impossible to imagine what my PhD experience would have been like without you and I'm grateful for having your support and video game knowledge throughout.

I would also like to thank my friends from back home; Becca, Anna and Christabel, who have kept me going at the height of my stress with a continuous supply of memes and gossip.

Last, but certainly not least, I would like to thank my mum, dad and brother, for their endless love, support and encouragement. I am eternally grateful for all you have done for me and I would not be the person I am today without you.

Table of Contents

List of Figures

List of Tables

Abbreviations

•OH	Hydroxyl radical
11-DHC	11-dehydrocorticosterone
11β-HSD	11β-hydroxysteroid dehydrogenase
3'-UTR	3'-untranslated region
^{3}H	Tritium
Ab	Antibody
ACTH	Adrenocorticotropic hormone
AF	Activation function
AIA	Antigen induced arthritis
ANCA	Antineutrophil cytoplasmic antibodies
ANOVA	Analysis of variance
AP-1	Activator protein 1
ARE	AU-rich element
AU	Arbitrary units
BERSC	Birmingham Ethical Review Subcommittee
BMD	Bone mineral density
BMSU	Biomedical Service Unit
BMU	Basic multicellular unit
BSA	Bovine serum albumin
BSP	Bone sialoprotein
BV/TV	Bone volume/total volume C/EBP
	CCAAT/enhancer-binding
protein	
CAIA	Collagen antibody induced arthritis
CaR	Calcium sensor receptor
CBG	Corticosteroid-binding globulin
CBP	CREB-binding protein
cDNA	Complementary deoxyribonucleic acid

CHS	Contact hypersensitivity
CIA	Collagen induced arthritis
Col1	Type 1 collagen
COPD	Chronic obstructive pulmonary disease
Cort	Corticosterone
CREB	cAMP response element-binding protein
CRH	Corticotropin-releasing hormone
CRP	C-reactive protein
CT	Cycle threshold
CTSK	Cathepsin K
CTX-1	C-terminal telopeptide
DAS28	Disease activity score 28
DBD	DNA-binding domain
DC	Dendritic cell
Dkk1	Dickkopf1
DMARD	Disease modifying anti-rheumatic drug
DMEM	Dulbecco’s Modified Eagle Medium
dNTP	Deoxynucleotide triphosphates
EAE	Experimental autoimmune encephalomyelitis
ECM	Extracellular matrix
EIA	Enzyme immunoassay
ELISA	Enzyme-linked immunosorbent assay
ESR	Erythrocyte sedimentation rate
FCS	Fetal calf serum
FKBP	FK506-binding protein
FLS	Fibroblast-like synoviocytes
GC	Glucocorticoid
GFP	Green fluorescent protein

GILZ	GC-induced leucine zipper
GIO	Glucocorticoid-induced osteoporosis
GR	Glucocorticoid receptor
GRE	Glucocorticoid response element
GRIP-1	GR-interacting protein 1
H&E	Haematoxylin and Eosin
H6PD	Hexose-6-phosphate dehydrogenase
HA	Hyaluronic acid
HAT	Histone acetyltransferase
HCL	Hydrochloric acid
HDAC	Histone deacetylases
HPA	Hypothalamus-pituitary-adrenal
HRP	Horseradish peroxidase
HSC	Haematopoietic stem cell
Hsp	Heat shock protein
IBD	Inflammatory bowel disease
IFN-γ	Interferon-γ
IGF-1	Insulin-like growth factor 1
IL	Interleukin
IRDS	Infantile respiratory distress syndrome
JCA	Juvenile chronic arthritis
KO	Knockout
LBD	Ligand-binding domain
LC-MS	Liquid chromatography–mass spectrometry
LDL	Low density lipoprotein
LPS	Lipopolysaccharide
LRP	Low density lipoprotein receptors
MCP-1	Monocyte chemoattractant protein-1

M-CSF	Macrophage colony-stimulating factor
MHC	Major histocompatibility complex
Micro-CT	Micro- computed tomography
MIP2	Macrophage inflammatory protein 2
MKP-1	Mitogen-activated protein kinase phosphatase-1
MMP	Matrix metalloproteinase
MR	Mineralocorticoid receptor
mRNA	Messenger ribonucleic acid
MSC	Mesenchymal stem cell
mTOR	Mammalian target of rapamycin
MuRF1	Muscle RING-finger protein-1
NAD	Nicotinamide adenine dinucleotide
NADPH	Nicotinamide adenine dinucleotide phosphate
NFATc1	Nuclear factor of activated T-cells, cytoplasmic 1
NF-κB	Nuclear Factor kappa-light-chain-enhancer of activated B cells
NLS	Nuclear localisation sequence
NSAID	Non-steroidal anti-inflammatory drug
NTD	N-terminal domain
OA	Osteoarthritis
OD	Optical density
OPG	Osteoprotegrin
P1NP	Procollagen Type 1 N-Terminal Propeptide
PBMC	Peripheral blood mononuclear cells
PBS	Phosphate buffered saline
Pen/strep	Penicillin/Streptomycin
PGC-1	Peroxisome proliferator-activated receptor-γ coactivator
POMC	Pro-opiomelanocortin
PPi	Pyrophosphate

PTH	Parathyroid hormone
PVN	Paraventricular nucleus
qPCR	Quantitative polymerase chain reaction
RA	Rheumatoid arthritis
RANK	Receptor activator of nuclear factor kappa-B
RANKL	Receptor activator of nuclear factor kappa-B ligand
ROH	Royal Orthopaedic Hospital
ROI	Region of interest
ROS	Reactive oxygen species
Rpm	Revolutions per minute
RPMI	Roswell Park Memorial Institute
RT	Reverse transcription
SCID	Severe combined immunodeficient
SCN	Suprachiasmatic nuclei
SLPI	Secretory leukocyte protease inhibitor
Sost	Sclerostin
STIA	Serum transfer induced arthritis
SULT	Sulfotransferase
Tb.N	Trabecular number
Tb.Sp	Trabecular separation
Tb.Th	Trabecular thickness
TCR	T cell receptor
TF	Transcription factor
Tg	Transgenic
TGF-β	Transforming growth factor-β
TLC	Thin layer chromatography
TLR	Toll-like receptor
TMB	Tetramethylbenzidine

TNF	Tumour necrosis factor
TRAP	Tartrate-resistant acid phosphatase
TSLP	Thymic stromal lymphopoietin
TTP	Tristetrapolin
TUNEL	Terminal deoxynucleotidyl transferase dUTP nick end labelling
VDR	Vitamin D receptor
VDRE	Vitamin D response element
WT	Wildtype

Chapter 1: Introduction

Sections of this chapter have been previously published as part of a review article (2).

1.1 Glucocorticoids in the treatment of chronic polyarthritis

Rheumatoid arthritis (RA) is characterised by synovial hyperplasia, which leads to cartilage destruction and bone erosions; in addition to extra-articular complications, which include osteoporosis and muscle wasting (3-6). Glucocorticoids (GCs) are often used as a first line therapy in chronic inflammatory polyarthritides such as RA due to their potent anti-inflammatory and immunomodulatory properties (7-9). Unfortunately, administration of therapeutic GCs is limited due to a range of side effects, including osteoporosis and muscle wasting, associated with their long term use (10-15). In this thesis we have used murine models of chronic inflammatory polyarthritis to examine how therapeutic glucocorticoids and their pre-receptor metabolism influence disease pathophysiology and extra-articular manifestations of disease.

1.2 Glucocorticoids

In 1929, Philip Hench hypothesised that a secreted “anti-rheumatic substance X” may exist in humans. At the same time, Edward Kendall and Tadeusz Reichstein identified “Compound E” in the adrenal cortex. When injected into rheumatoid arthritis patients, compound E showed profound anti-inflammatory effects. In 1950, Hench, Reichstein and Kendall were awarded the Nobel Prize in Physiology or Medicine for their collective discovery and isolation of cortisone and since then numerous studies have centred on their therapeutic capacity (16).

Currently, synthetic GCs, such as dexamethasone, prednisolone and hydrocortisone, are some of the most effective treatments for inflammatory disorders such as asthma, inflammatory bowel disease (IBD), rheumatoid arthritis and other autoimmune diseases,

with approximately 1% of the adult population in the UK and US receiving GC treatment (17-19). Despite their efficacy, therapeutic GC use is limited due to the prevalence of detrimental side effects. Around 70% of patients receiving therapeutic GCs present with adverse effects such as GC-induced osteoporosis (GIO), muscle wasting, hypertension and central obesity (20-22). Therefore, there is currently an unmet need to better target GC therapies to promote the beneficial anti-inflammatory actions whilst bypassing their detrimental side effects.

1.2.1 Physiological roles of endogenous glucocorticoids

Glucocorticoids are steroid hormones produced by the adrenal glands in response to a number of physiological cues, and possess a wide variety of functions. The principal endogenous glucocorticoids in humans are cortisol and its inactive form cortisone, while in rodents the most common glucocorticoids are the active corticosterone and its inactive form 11-dehydrocorticosterone (11-DHC).

Glucocorticoids are named for their effects on glucose metabolism and homeostasis. In response to stress, GCs increase the serum level of glucose by promoting gluconeogenesis in the liver and suppressing uptake in skeletal muscle and adipose tissue. GCs can also promote hepatic storage of glycogen (23). Additionally, GCs impact on glucose metabolism via increasing secretion of glucagon, a hormone produced by α cells of the pancreas to increase serum glucose levels (24). The overall increase in serum glucose provides energy for the brain to promote maximal function under stressful conditions. GC effects on glucose metabolism counter the effects of insulin, which stimulate glucose uptake and glycolysis (25).

Glucocorticoids are required for the normal development and maintenance of many organs, with global glucocorticoid receptor (GR) knockout (KO) mice asphyxiating within a few hours of birth due to defective lung development (26). Antenatal GCs are often given to patients at risk of a pre-term delivery and have been shown to significantly decrease the prevalence of infantile respiratory distress syndrome (IRDS) (27). This seems to be due to GCs mediating the differentiation of type II alveolar cells, which secrete surfactant, a protein which prevents alveolar collapse (28). Similarly, endogenous GC signalling is required for the appropriate developmental of the heart. Mice lacking GR in cardiomyocytes and smooth muscle cells exhibited disorganisation of myofibrils and failure to upregulate genes involved in contraction and calcium signalling (29). GCs also regulate the development and maintenance of bone (see section 1.5.5).

One of the most prominent features of GCs is their potent anti-inflammatory and immunomodulatory actions. Studies have investigated the impact of endogenous GC signalling in specific cell types in various inflammatory conditions. In experimental autoimmune encephalomyelitis (EAE), widely used as a murine model of multiple sclerosis, cell specific GR KOs demonstrated that endogenous GCs act on T cells to induce apoptosis and subsequently reduce susceptibility and severity of EAE (30). Two arthritis models were used to investigate endogenous GC signalling in chondrocytes. K/BxN serum transfer-induced arthritis (STIA) and antigen-induced arthritis (AIA) in chondrocyte specific GR KO mice resulted in the exacerbation of joint swelling and inflammation, cartilage destruction and neutrophil activity (31). An additional study has utilised the immunosuppression associated with ageing to investigate the effects of endogenous GCs on macrophages. They found that the increase in GC levels in ageing mice results in a shift in polarisation of macrophages towards the pro-resolution M2

phenotype (32). The specific anti-inflammatory actions of GCs will be discussed further in section 1.4.1.

1.2.2 Synthesis and regulation

The synthesis of endogenous GCs is mediated by the hypothalamic-pituitary-adrenal (HPA) axis. Upon activation of the HPA axis, corticotropin-releasing hormone (CRH) is produced in the paraventricular nucleus (PVN) of the hypothalamus and released via the median eminence (33). CRH travels to the anterior pituitary of the pituitary gland to stimulate the expression of pro-opiomelanocortin (POMC) in corticotroph cells, which is cleaved to produce adrenocorticotropic hormone (ACTH). ACTH can then be secreted into the circulation where it migrates to the cortex of the adrenal gland to induce the synthesis of GCs (Fig 1.1) (34).

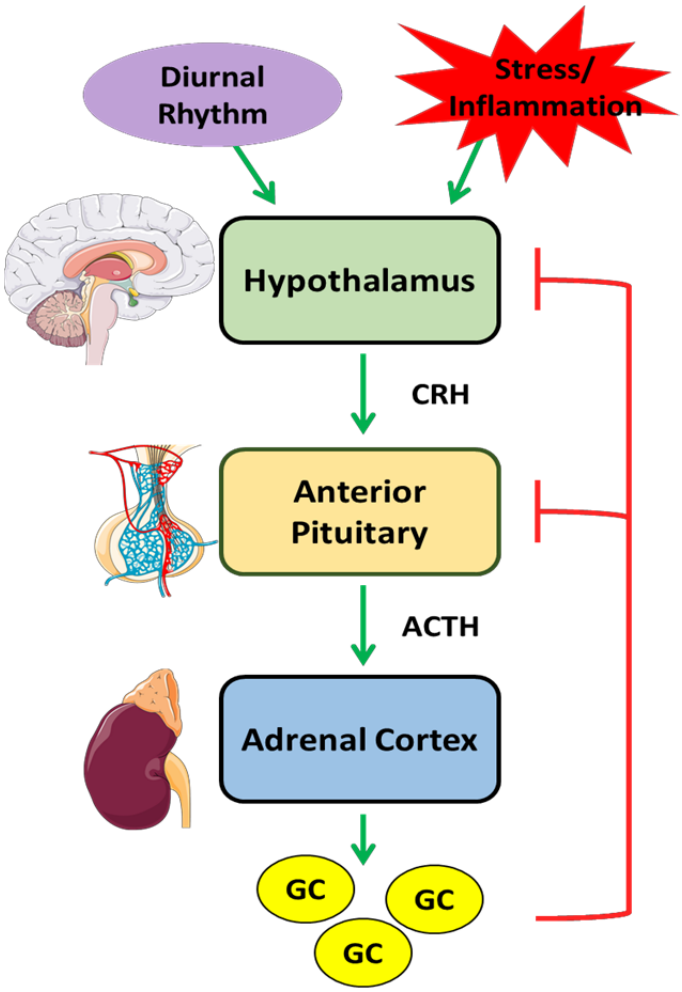

Figure 1. 1: The HPA axis

Activation of the HPA axis can be stimulated by factors such as the normal diurnal rhythm, stress and inflammation. CRH is produced and released from the PVN of the hypothalamus which triggers the production of ACTH in the pituitary gland. ACTH then migrates to the adrenal gland where it induces the synthesis of GCs. GCs can feedback on the pituitary and hypothalamus to inhibit their overproduction.

In the adrenal cortex, ACTH impacts on the GC precursor cholesterol by increasing cholesterol transport across the membrane of mitochondria and upregulating the expression of cholesterol esterase (35). The conversion of cholesterol to pregnenolone can lead to the production of mineralocorticoids, GCs and androgens via the catalysis by various key enzymes (summarised in Fig 1.2).

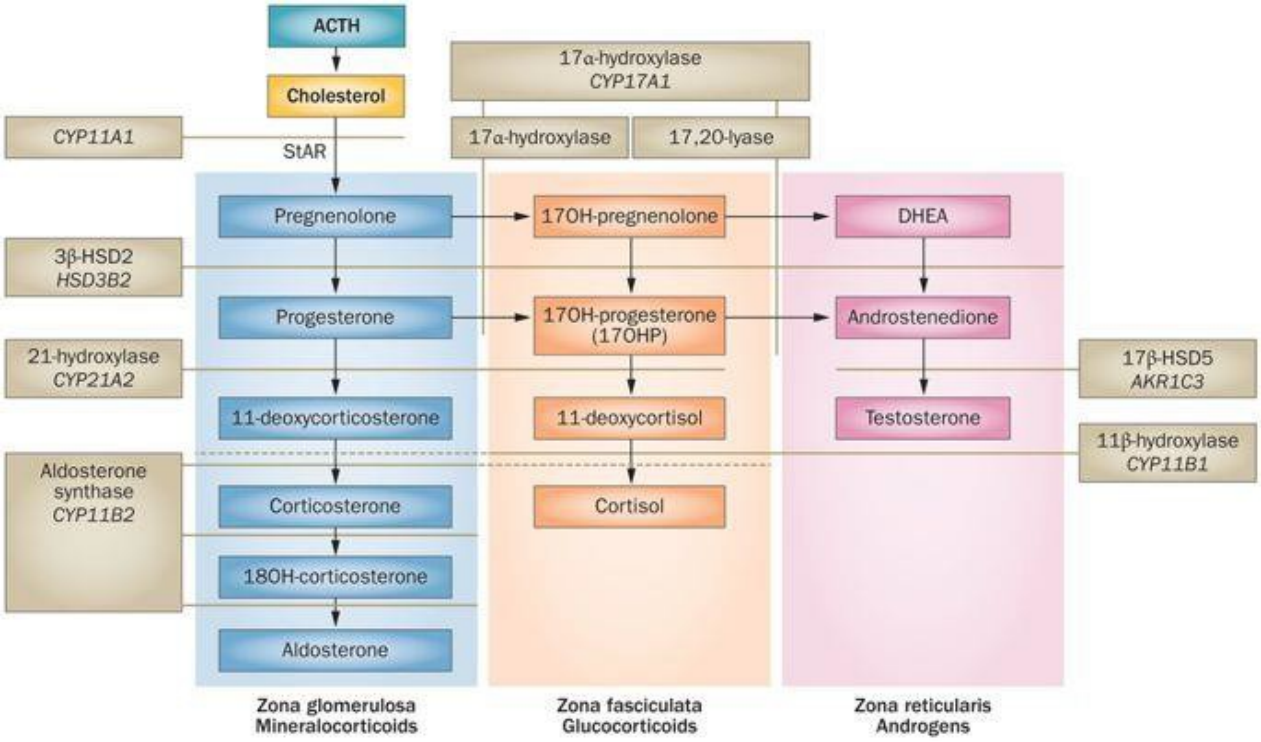

Figure 1. 2: Mineralocorticoid, glucocorticoid and androgen synthesis pathways from cholesterol.
Synthesis of mineralocorticoids, glucocorticoids and androgens from cholesterol in the adrenal cortex. Mineralocorticoid, GC and androgen pathways are highlighted in blue, orange and purple respectively. Enzymes catalysing each reaction are shown in grey boxes. Image taken from Han *et al.,* 2013 (1).

The HPA axis can be stimulated and inhibited by various factors. The circadian rhythm causes natural fluctuations in GC levels, with the peak increase occurring around wakening, in the early morning in diurnal animals, and in the evening in nocturnal animals. In contrast, HPA activation is at its lowest during the night in diurnal animals and during the day in nocturnal animals, corresponding to the rest-activity cycle of the animal (36). In response to light/dark signals from the retina via the retino-hypothalamic tract, a transcription factor known as Clock is activated and regulates downstream gene expression. The central clock is located in the hypothalamic suprachiasmatic nuclei (SCN) and can interact with the HPA axis via synapses which connect the SCN to the

PVN. Additionally, the clock system alters the sensitivity of the adrenal gland to ACTH which subsequently alters the production of GCs (37).

GCs play an important role in suppressing the immune response to prevent tissue damage, and support resolution of inflammation. Consequently, many pro-inflammatory cytokines can induce GC production via stimulation of the HPA axis, to negatively regulate inflammation in a feedback cycle. Cytokines can interact with each section of the HPA axis; hypothalamus, pituitary and adrenal gland. TNFα, IL-6 and IL-1 have been shown to activate CRH-producing neurons in the hypothalamus and subsequently stimulate the HPA axis via an upregulation of CRH levels (38-40). Utilisation of the murine pituitary tumour cell line AtT20 has revealed that IL-1, IL-2 and IL-6 increase the synthesis and release of ACTH from pituitary cells (41). For IL-1, and IL-2 this effect appeared to be due to increased expression of the ACTH precursor POMC (42). Additionally, administration of TNFα to rats by intravenous injections resulted in an increase in plasma levels of ACTH and corticosterone in a dose-dependent manner (39). Cytokines have also been shown to act directly on the adrenal gland to produce GCs. Both IL-1 and IL-6 treatment of cultured rat adrenal cells had the capacity to stimulate release of corticosterone independently and synergistically with ACTH (43-45).

Glucocorticoids also regulate their own production via negative feedback on the HPA axis in order to prevent overstimulation. This is achieved by both rapid non-genomic and delayed genomic mechanisms. Non-genomic HPA inhibition mechanisms have been suggested to decrease CRH release from the hypothalamus via the induction of endocannabinoid signalling which leads to suppression of the excitatory signals to the cells of the PVN (46). On the other hand, genomic inhibition by GCs appears to be

mediated by direct inhibition of CRH expression in the hypothalamic neurons and of POMC expression in pituitary corticotrophs (Fig 1.1) (47, 48).

1.2.3 Glucocorticoids in the circulation

An additional method by which GC actions are regulated is via their interaction with binding proteins. Around 80-90% of cortisol in the circulation is bound by corticosteroid-binding globulin (CBG) and 10-15% is bound by albumin, leaving only approximately 5% of the cortisol in the circulation unbound and able to bind to receptors (49). The steroid-binding site of CBG can be cleaved by neutrophil elastase which results in its irreversible destruction. This leads to the local increase in free GCs at sites of inflammation which suggests that CBG may play a role in targeted release of active GCs in areas where their actions are required (50). Although the plasma concentrations of albumin are around 1000 times more than that of CBG, its affinity for GCs is approximately 3 times lower. Albumin typically acts as a buffer to transient changes in plasma cortisol levels (51). In circumstances of CBG deficiency, albumin has been shown to be able to partially compensate for CBG actions by binding up to 75% of circulating cortisol, leaving only 25% biologically active GC in the blood (49).

1.2.4 Glucocorticoid receptor signalling

GCs readily diffuse across cell membranes due to their lipophilic nature and exert their effects through interactions with the intracellular glucocorticoid receptor. The GR is a ligand-inducible transcription factor and a member of the nuclear receptor superfamily encoded by the *NR3C1* gene. The protein is comprised of three functional domains; the

N-terminal domain (NTD), the DNA-binding domain (DBD), and the ligand-binding domain (LBD). The NTD includes a ligand-independent activation function 1 (AF1) region which interacts with chromatin modulators, co-regulators and transcriptional machinery to facilitate the initiation of transcription (52). Next to the NTD is the DBD which is required for GR binding to GC-response elements (GRE) situated in the promoter regions of GC-responsive genes. Additionally, the DBD contains the specific amino acid sequence necessary for the dimerization of the GR (53). The DBD is connected to the C-terminal LBD through a hinge region. The LBD contains a ligand-dependent AF2 region which undergoes a conformational change upon binding of ligand and allows interaction with co-activators such as SRC-1 (54, 55).

Two splice variants of the GR exist; GRα and GRβ. GRα and β have identical structure up to the C-terminal domain, in which GRβ has a truncated LBD. As a result of this, GRβ cannot bind GCs and GRα is the main mediator of classical GC effects. Conversely, GRβ has been shown to be an inhibitor of GRα gene regulation. This appears to be mediated via the heterodimerisation of GRα and GRβ to form an inactive receptor complex (56). Increased expression of GRβ has been demonstrated in peripheral blood mononuclear cells (PBMCs) from patients with GC-insensitive asthma, indicating a potential role for GRβ in therapeutic GC resistance (57).

The GR contains two nuclear localisation signals (NLS); NLS1 located in the DBD and NLS2 located in the LBD (58). In their unbound state, GRs form a multiprotein complex with chaperone proteins such as heat shock protein-70 (hsp70), hsp90 and FK506-binding protein 52 (FKBP52) which block the NLSs of the GR and prevent its translocation from the cytoplasm (59). Upon GC binding, the GR undergoes a conformational change which leads to the dissociation of chaperone proteins, exposure of the NLS and

subsequent translocation of the GC/GR complex to the nucleus where it can both transactivate and transrepress target genes (60).

The GR complex can regulate gene expression via both genomic and non-genomic mechanisms. The classical method of GR signalling includes GR homodimerization and binding to GREs in the promotor region of GC-responsive genes and recruiting coactivators such as CREB-binding protein (CBP), a histone acetyltransferase (HAT), which opens chromatin and allows transcription to take place (61). Negative GREs (nGRE) can also be present in genes and when the GR binds to these they can recruit histone deacetylases (HDAC) which close chromatin and prevent transcription, such as with the osteoblast specific gene osteocalcin and the pro-inflammatory cytokine thymic stromal lymphopoietin (TSLP) (62, 63).

Additionally, GCs can regulate genes that do not contain GREs. This is achieved by tethering of the GR to a transcription factor by protein-protein interactions without associating with the DNA directly, after which the GR can then recruit HDACs to inhibit the transcription of genes (64) (Fig 1.3).

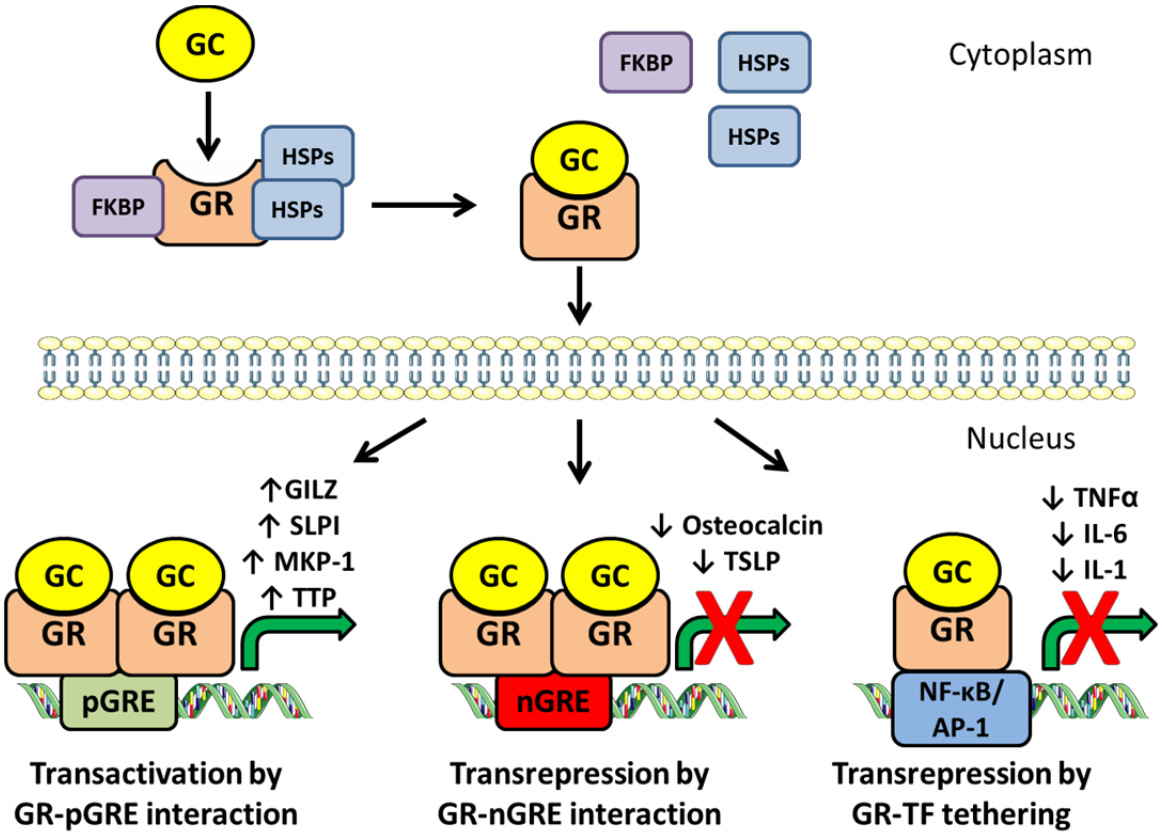

Figure 1. 3: Glucocorticoid receptor signalling pathways

GCs can readily diffuse across the membrane where they bind to the GR in the cytoplasm, causing a conformational change which results in the dissociation of molecular chaperones, such as HSPs and FKBP, subsequently exposing the NLS and causing nuclear localisation of the GC-GR complex. Here, the GR can dimerise and bind to either positive GREs (pGRE) to induce transcription of genes (e.g. GILZ, SLPI, MKP-1 and TTP) or negative GREs (nGRE) to inhibit the transcription of genes (e.g. osteocalcin, TSLP). Alternatively, the GR complex can signal as a monomer and tether to transcription factors (TFs) such as NF-κB or AP-1 to suppress the transcription of pro-inflammatory genes (e.g. TNFα, IL-6, IL-1).

1.2.5 Pre-receptor metabolism by 11β-HSDs

In addition to the HPA axis, active GC levels are also determined at the tissue level by the 11β-hydroxysteroid dehydrogenase (11β-HSD) enzymes. 11β-HSD1 is a bidirectional enzyme which *in vivo* predominantly reduces inactive GCs such as cortisone in humans and 11-DHC in rodents, to their active counterparts, cortisol or corticosterone (65). 11β-

HSD1 uses NADPH generated by the hexose-6-phosphate dehydrogenase (H6PD) enzyme to transfer a hydrogen to the inactive GC which upon reduction becomes active (Fig 1.4). H6PD null mice exhibit markedly higher dehydrogenase activity compared to WT indicating a switch in the direction of 11β-HSD1 activity dependent on the availability of cofactor (66). Several synthetic GCs such as prednisolone (active) and prednisone (inactive) are also converted via 11β-HSD metabolism, whilst others such as dexamethasone are resistant to reductase metabolism (67).

In contrast, 11β-HSD2 is a NAD+-dependent unidirectional dehydrogenase enzyme which converts active GCs to their inactive counterparts by removal of a hydrogen ion (68) (Fig 1.4). The main function of 11β-HSD2 is to protect the mineralocorticoid receptor (MR) from occupancy by GCs. The MR binds both mineralocorticoids and active GCs with high affinity, but cannot bind inactive GCs, thus 11β-HSD2 protects against inappropriate activation by cortisol (69).

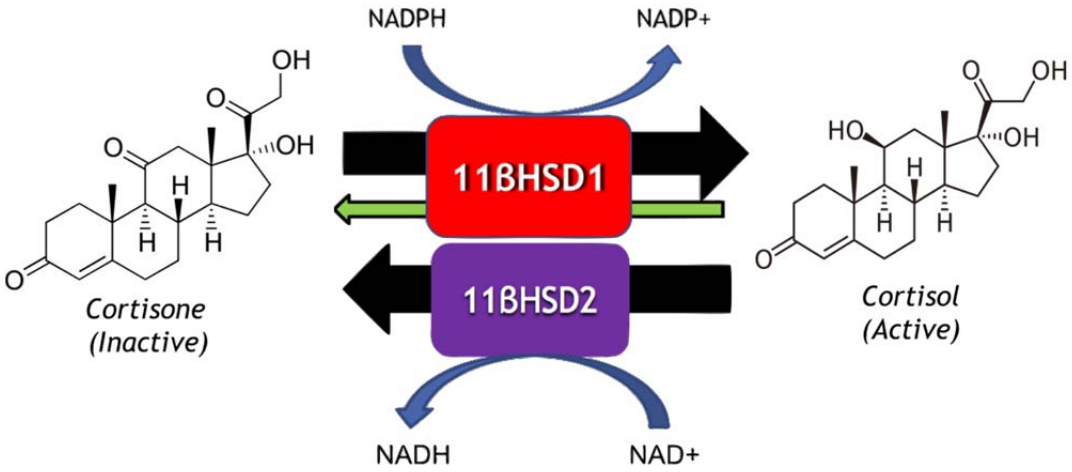

Figure 1. 4: 11β-HSD system of GC metabolism

11β-HSD1 is a bidirectional enzyme which *in vivo* predominantly converts inactive GCs (e.g. cortisone) to their active counterparts (e.g. cortisol) in a NADPH-dependent manner, whilst 11β-HSD2 is a NAD+-dependent enzyme which inactivates GCs.

1.2.6 Tissue specific expression of 11β-HSDs

11β-HSD1 is expressed in a wide array of tissues including the liver, muscle, adipose, skin, bone, and synovium (70-72). In contrast, 11β-HSD2 is largely expressed in mineralocorticoid-target tissues such as the kidney, colon, salivary and sweat glands (73-75). The expression of type 1 enzymes in the liver and type 2 enzymes in the kidney allow for the regulation of circulating metabolism, in which active GCs are inactivated by renal 11β-HSD2 and reactivated by hepatic 11β-HSD1 to determine systemic levels of GCs (76). As previously mentioned, approximately 95% of cortisol in the blood is bound to protein which reduces its biological activity. To increase the supply of active GCs to the local environment of a specific tissue, 11β-HSD1 is expressed. 11β-HSD2 generates cortisone which can travel freely via the circulation until it reaches target tissues which express type 1 enzymes. Here it can be locally reactivated to generate a high concentration of biologically active GC in a tissue-specific manner (70) (Fig 1.5).

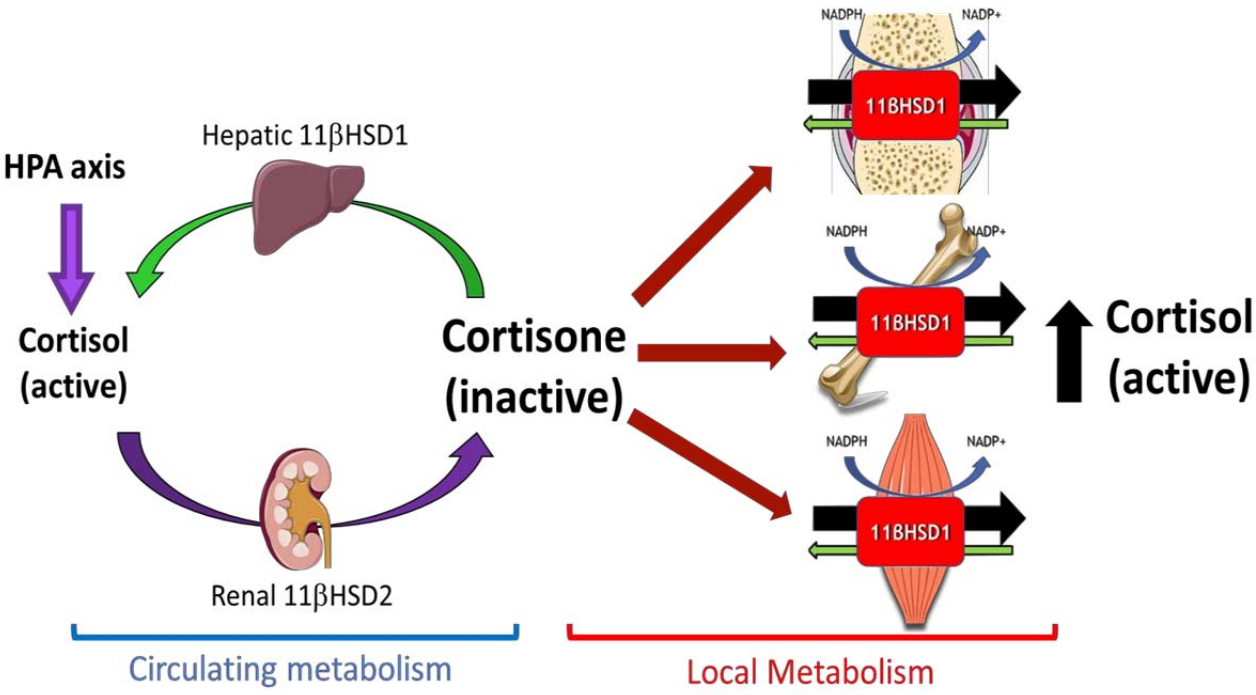

Figure 1. 5: Circulating and local metabolism of GCs by 11β-HSDs

Systemic levels of GCs are determined by circulating metabolism in which GCs are inactivated by renal 11β-HSD2 enzymes and reactivated by hepatic 11β-HSD1 enzymes. During local metabolism, inactive GC can travel unbound in the blood until it reaches tissues which express 11β-HSD1, such as the synovium, bone and muscle. Here, GCs are reactivated to produce elevated levels of biologically active GCs in the local environment.

1.2.7 Post receptor metabolism and clearance

For clearance of GCs from the body, membrane bound enzymes known as 5α- or 5β-reductases reduce the A-ring associated with the steroid structure to generate the relevant 5α/5β-dihydrosteroid. 3α or 3β-hydroxysteroid dehydrogenase enzymes facilitate the clearance process by further reduction to 3α/3β,5α/5β-tetrahydrosteroid (tetrahydrocortisol; THF, tetrahydrocortisone; THE) (77). Sulfotransferases (SULTs) can conjugate sulfate groups to tetrahydrosteroids which increases their water solubility and thus allows them to be excreted by the kidneys more efficiently (78, 79).

Tetrahydrosteroids can also be further metabolised to α or β-cortol or cortolone (from THF and THE, respectively) by the 20α or 20β-hydroxysteroid dehydrogenase enzymes. THF and THE, along with cortols, cortolones and free cortisol and cortisone, can be measured in the urine as markers of systemic 11β-HSD1 and 11β-HSD2 metabolism (80).

Cortisone and cortisol can also be metabolised by alternative pathways. It has recently been shown that the enzyme carbonyl reductase 1 can catalyse the reduction of cortisol to 20β-dihydrocortisol, a metabolite which is increased in the urine during obesity (354). In addition, 6β-hydroxylase enzymes can metabolise cortisol into 6β-hydroxycortisol (355). Cortisone can also be metabolised in a similar fashion to 20β-dihydrocortisone or 6β-hydroxycortisone.

1.3 Rheumatoid arthritis

Rheumatoid arthritis (RA) is a chronic inflammatory disease characterised by synovitis and progressive joint destruction that ultimately results in pain, physical disability and increased mortality; systemic inflammation is also a feature (81). In combination with other inflammatory arthropathies, such as psoriatic arthritis, these diseases are estimated to cost the US economy $304 billion per year (219). Around 2% of the adult population have an inflammatory arthritis, with the most frequent condition being RA. This is present in almost 1% of the population, with a two times greater prevalence in females than males, with smoking and obesity being additional risk factors (82, 83).

1.3.1 Normal joint physiology

A joint is characterised as the point where two separate bones meet, consisting of three main tissues; bone, cartilage and synovium (Fig 1.6).

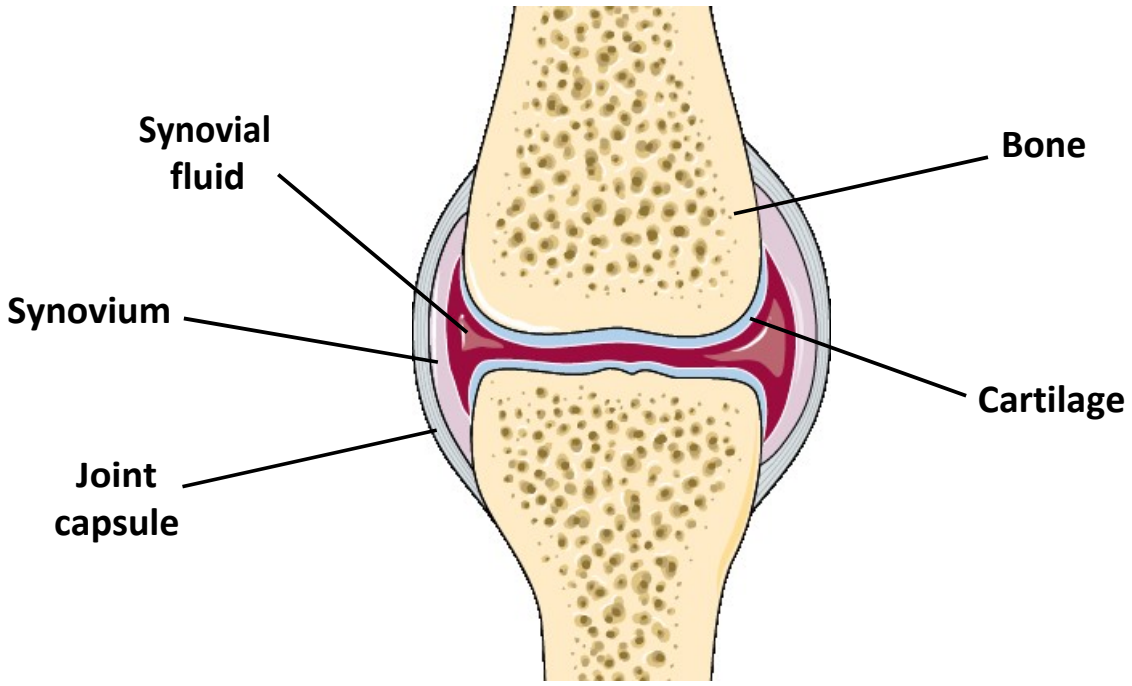

Figure 1. 6: Normal joint physiology

In normal joint physiology, the bone is surrounded by cartilage and the space in between the bones is filled with synovial fluid. The synovial fluid is contained by a synovial membrane, normally about one to two cells thick. The joint capsule encloses the joint.

The structure of bone will be discussed further in section 1.5.1. Surrounding the head of the bone is a layer of articular cartilage, which acts to provide a smooth surface in order to reduce friction during movement and to absorb shock (84). Cartilage is formed by an extracellular matrix (ECM) consisting mainly of water, proteoglycans and collagen. Within the ECM reside the chondrocytes, a specialised mesenchymal derived cell involved in the production and homeostasis of the cartilage via the synthesis of collagens and proteoglycans (85). The cartilage is formed of four zones with different properties and

functions; the superficial, middle, deep and calcified zones. Briefly, the superficial zone is a thin outer layer with a high number of flat chondrocytes which protects the deeper layers from the sheer stress of the synovial fluid. The middle zone is the largest zone, containing proteoglycans, collagen and relatively few chondrocytes which are typically of spherical morphology. The middle zone facilitates in the protection against compressive forces, however the greatest protection against compression is the deep zone. The deep zone harbours the highest proteoglycan content and the largest collagen fibrils. The chondrocytes sit alongside the collagen fibrils in a columnar orientation. Finally, the calcified zone attaches the collagen fibrils from the deep zone to the underlying subchondral bone, ensuring the secure anchoring of the cartilage to the bone. The calcified zone is sparsely populated with hypertrophic chondrocytes (86).

The joint is surrounded by synovial fluid, which acts as lubrication to further reduce friction, enclosed in a layer known as the synovial membrane. Under normal conditions, the intimal lining of the synovium which is in close contact with the synovial fluid is typically 1 to 2 cells thick, made up of approximately equal proportions of fibroblast-like synoviocytes (FLS) and macrophages. This layer acts as a physical barrier and FLS secrete lubricin and hyaluronic acid (HA) into the synovial fluid, which function to lubricate and increase the viscosity of the fluid (87, 88). The sublining layer of the synovium lines the inner region of the joint capsule and is relatively sparsely populated with FLS and macrophages, in addition to a blood vessel network (89).

1.3.2 Chronic joint inflammation

In patients with chronic inflammatory polyarthritis, the on-going inflammatory process within the synovium results in damage and destruction of the bone and cartilage. In RA the characteristic manifestation of synovitis occurs principally in the small joints, such as the proximal interphalangeal and metacarpophalangeal joints of the hand and affect joints in a symmetrical distribution (90). The structural damage associated with RA can begin prior to the onset of clinical symptoms and is driven by inflammation of the synovium which subsequently impacts on the adjacent bone and cartilage (91) (Fig 1.7).

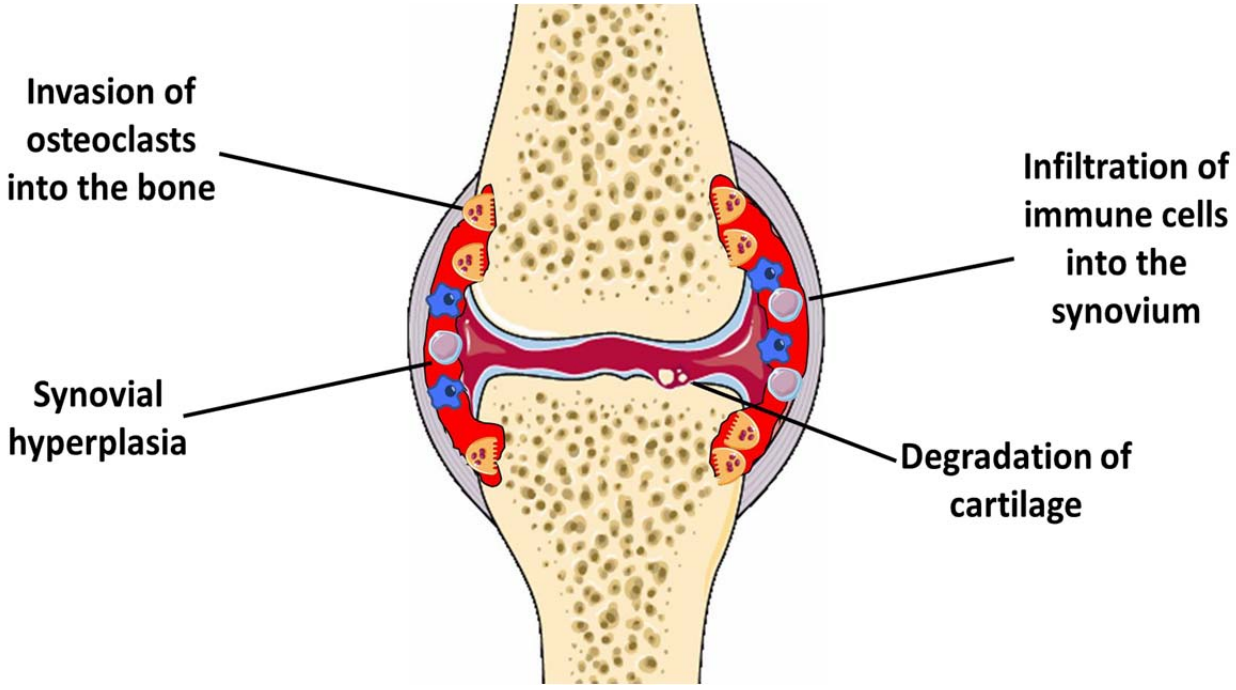

Figure 1. 7: Representation of an RA joint

In the joint of an RA patient, significant hyperplasia of the synovial membrane occurs mediated by immune cell infiltration and FLS expansion, which leads to the release of pro-inflammatory cytokines. These cytokines activate FLS and osteoclasts, which drive the destruction of cartilage and bone.

The precise mechanisms behind the initiation of inflammation in RA remain unknown, however it is well established that both genetic and environmental factors play a part. A

study using quantitative methods to analyse data from monozygotic and dizygotic twin studies determined that the heritability of RA was approximately 60%, indicating that the contribution of genetic factors is substantial to the pathogenesis of this disease (92).

One suggested mechanism for initiation of inflammation in RA is via stimulation of Toll-like receptors (TLR), expressed on cells such as dendritic cells (DCs) and monocytes which mediate the initial identification of pathogens and induce NF-κB signalling. Expression of both TLR2 and TLR4 is increased within FLS and synovial macrophages of RA patients relative to healthy controls (93). Furthermore, activation of TLR4 or 2 on RA FLS potently induces osteoclastogenesis via the upregulation of RANKL (94). The activation of the immune system leads to the infiltration of immune cells such as macrophages, T cells and B cells into the synovium, resulting in synovial hyperplasia and pannus formation. A prominent role has been suggested for activated FLS in immune cell recruitment with the fibroblast-derived T cell chemokine CXCL12 found to be overexpressed in the RA joint (95, 96). In addition, TGF-β, a cytokine expressed at high levels in the RA synovium, triggers the expression of the CXCL12 receptor, CXCR4, on T cells which provokes their retention in the synovium and prevents efflux from this site (97). Moreover, activated macrophages in the synovium secrete IL-1 which further contributes to leukocyte recruitment (98). In acute inflammation, resolution of inflammation requires the apoptosis of immune cells. However, in chronic inflammatory diseases such as RA, FLS and macrophages secrete type 1 interferons which prolongs the survival of T cells, contributing to the persistence of the immune response (96).

Activated immune cells secrete pro-inflammatory cytokines which contribute to increased osteoclastogenesis in the pannus and subsequent destruction of juxta-articular bone (as discussed in section 1.5.7). Osteoclasts can also resorb the calcified zone of cartilage

adjacent to the subchondral bone (99). Osteoclasts cannot, however, mediate the destruction of unmineralized cartilage, thus this is mediated by an alternative mechanism. It has been suggested that FLS are the main drivers of cartilage destruction within RA joints. RA FLS are able to invade into the unmineralized cartilage potentially by their expression of typically osteoclastogenic molecules such as cathepsin K (99-101). In addition, stimulation with pro-inflammatory cytokines such as TNFα, lymphotoxin and IL-1β leads to the expression of matrix degradation factors, including MMP-9 and -2, in synovial fibroblasts which facilitates the cartilage destruction as seen in the rheumatoid joint (102). A study used the severe combined immunodeficient (SCID) mouse to investigate the contribution of RA FLS to cartilage degradation in the absence of functioning lymphocytes and macrophages (103). Healthy human cartilage was transplanted into the mouse alongside human FLS from RA patients. RA FLS showed extensive invasion into the cartilage, as opposed to osteoarthritic (OA) FLS which showed minimal invasion and normal FLS which did not invade at all. RA FLS also expressed matrix-degrading enzymes such as cathepsins D, B and L which were not apparent in the FLS controls. Therefore, these results indicated that FLS in RA present with a distinct destructive phenotype that actively drives the degradation of cartilage, even when pro-inflammatory stimuli have been removed (104).

1.3.3 RA therapy

Presently, there is no cure for RA, however studies have shown that the initiation of anti-rheumatic therapy early in the course of the disease shows significant benefits in radiographic progression in the long-term. This would subsequently reduce the risk of functional disability, joint replacement surgeries and work disability (105). The current

commonly used treatments for RA can be categorised into four groups; non-steroidal anti-inflammatory drugs (NSAIDs), glucocorticoids, non-biologic disease modifying anti-rheumatic drugs (DMARDs) and biologic DMARDs. However, currently no one drug is able to treat every case of RA and drug resistance remains a problem within RA therapy (106). RA is often treated with a combination of drugs, and in severe cases with the pairing of a non-biologic DMARD such as methotrexate with a biologic DMARD such as anti-TNF therapy. Approximately 40% of patients will respond to monotherapy with methotrexate, compared to a response rate of between 56% to 67% with methotrexate in combination with a biologic therapy (107). Unfortunately, combination therapies have been associated with an increase in serious infections, particularly within the first six months of therapy initiation (108). NSAIDs are fast-acting drugs with anti-inflammatory and analgesic effects, thus they are generally used to bridge the gap between the effects of the slow-acting DMARDs since they cannot slow the radiographic progression of RA alone and are not disease modifying (109).

GCs are used in approximately 66% of RA patients globally with an estimated yearly cost of around $10 billion in the US (110). Unfortunately, despite the effective anti-inflammatory actions of GCs, their use is often associated with serious side effects as discussed in section 1.4.3. Thus, the development of targeted GC therapies, to harness their beneficial effects whilst bypassing their detrimental actions is required.

1.4 Therapeutic application of glucocorticoids in chronic inflammation

Due to the potent anti-inflammatory actions of glucocorticoids, synthetic derivatives, which mimic endogenous GC action on the immune system, have been produced for the

treatment of many chronic inflammatory diseases. A recent systematic review revealed that low dose GCs given alongside other DMARDs to treat early RA can substantially impede the progression rate of juxta-articular erosions compared to DMARD only controls (111). In addition, oral prednisolone therapy has been shown to significantly reduce infiltration of cells such as macrophages, T and B cells and FLS into the synovial lining (112). Consequently, GC treatment significantly reduces the number of tender and swollen joints in RA patients, as well as decreasing serum markers of inflammation (such as IL-6 and C-reactive protein (CRP)), and improving the disease activity score (DAS28) (113-115).

Commonly used synthetic GCs include hydrocortisone (synthetic cortisol), prednisolone and prednisone. Alterations to the structure of GCs can impact on their potency, activity and clearance. Prednisolone is the active form of prednisone synthesised by the introduction of a double bound between carbons 1 and 2 in the cortisol structure and is 4 times more potent than hydrocortisone, with a duration of action of 12-36 hours compared to hydrocortisone's 8-12 hours (116) (Fig 1.8). Prednisone differs from prednisolone in an identical fashion as cortisone to cortisol, requiring activation through the hydrogenation of the 11-keto-group. Addition of a methyl group to carbon 6 of prednisolone creates methylprednisolone, a more potent version of the GC, 5 times more potent than hydrocortisone, which has been suggested to exhibit fewer systemic side effects such as obesity and adrenal atrophy (117).

The addition of a fluoride molecule and a methyl group at positions 9α and 16, respectively, on prednisone results in the formation of dexamethasone (Fig 1.8). Dexamethasone is 30 times more potent than hydrocortisone and is much longer lasting,

with a duration of action of 36-72 hours. Due to the potency of dexamethasone, it is no longer used to treat RA in the UK (116).

Studies have shown that prednisolone/prednisone is more readily metabolised by 11β-HSD enzymes than cortisol/cortisone. Increased reduction of prednisone by 11β-HSD1 relative to cortisone may contribute to the higher levels of active GC in the circulation and increased potency of prednisone (118). In contrast, dexamethasone shows little oxoreductase or dehydrogenase metabolism by 11β-HSD1 or 2, respectively. However, whilst 11β-HSD2 is incapable of catalysing the conversion of inactive cortisone to active cortisol, it can in fact catalyse the conversion of inactive 11-dehydro-dexamethasone to active dexamethasone, exhibiting a marked difference between metabolism of different GC derivatives (118).

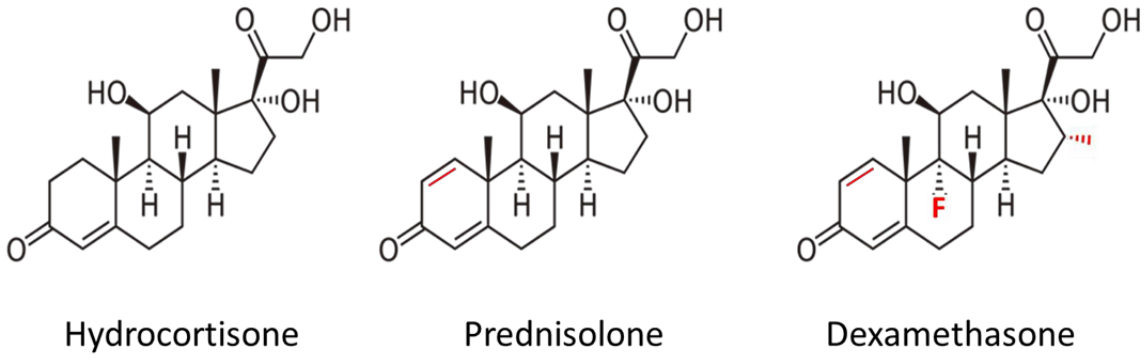

Figure 1. 8: Structural changes of synthetic GCs

Synthetically derived hydrocortisone is structurally identical to endogenously produced cortisol. Prednisolone differs from cortisol in the presence of a double bond between carbons 1 and 2. Dexamethasone also contains this double bond, in addition to the fluoride molecule and methyl group introduced into the structure. Changes to the structure of synthetic GCs are highlighted in red.

1.4.1 Anti-inflammatory actions of therapeutic glucocorticoids

Synthetic GCs used in the treatment of chronic inflammatory diseases can mediate their actions via transactivation of anti-inflammatory genes or transrepression of pro-inflammatory genes. Genes which exert anti-inflammatory effects such as secretory leukocyte protease inhibitor (SLPI), mitogen-activated protein kinase phosphatase-1 (MKP-1) and GC-induced leucine zipper (GILZ) are upregulated via the classical method of GC signalling through GRE binding (119-121). GCs also upregulate tristetraprolin (TTP), which has non-genomic downstream effects on pro-inflammatory cytokines, such as TNFα, via destabilisation of mRNA and thus reduced transcription and translation of the protein (122). As TNFα is at the apex of a pro-inflammatory cytokine cascade, this reduction in TNFα by GCs impacts on the production of downstream inflammatory mediators such as IL-1β and IL-6 (123).

GCs can also inhibit transcription factors which promote pro-inflammatory gene expression via tethering of GR to transcription factors and recruitment of HDACs (as previously discussed in 1.2.4). In particular, GCs inhibit NF-κB and AP-1 which regulate the transcription of various genes relating to inflammation such as TNF-α, IL-1 and IL-6 (124). Additionally, GCs can inhibit NF-κB signalling via an induction in its inhibitor IκBα, which sequesters the transcription factor in the cytoplasm, preventing it from influencing gene regulation (125).

GCs can impact on cells of the immune system both directly and indirectly. In dendritic cells (DCs), for example, GCs reduce maturation by significantly decreasing the expression of MHCII and co-stimulatory molecules such as CD80. Whenever T cells were stimulated with these GC treated DCs, the number of Th1 cells was reduced while Tregs producing anti-inflammatory IL-10 were increased (126). GCs typically induce apoptosis

in T cells, however Tregs are resistant to GC-induced apoptosis which may contribute to the shift towards increased Treg number during GC treatment (127). Additionally, GCs suppress the ability of neutrophils to adhere to the blood vessels by downregulating expression of the adhesion molecule E-selectin and ICAM-1 on endothelial cells, thus neutrophils cannot migrate to sites of inflammation (128).

As previously mentioned, GCs also influence macrophage polarisation promoting an anti-inflammatory/pro-resolution M2 phenotype and suppressing inflammatory M1 polarisation (32). A study using a mouse model of contact hypersensitivity, an inflammatory disease commonly treated with GCs, showed that the therapeutic actions of GCs were mediated by the GR on macrophages and neutrophils. Mice with a myeloid specific GR KO were unable to suppress pro-inflammatory cytokines such as IL-1, MCP-1 and MIP-2 in this model (129). Furthermore, GCs have been shown to increase the phagocytic capacity of macrophages which facilitates removal of pro-inflammatory mediators and apoptotic cells (130, 131).

1.4.2 Insights from GR^{dim} mouse

Until recently, it was believed that the anti-inflammatory actions of GCs were dependent on transrepression by monomeric GRs, whilst the adverse side effects of GC use relied on transactivation by homodimeric GR complexes (132). The development of the GR^{dim} mouse which possesses a mutation in the DBD region of the GR that prevents dimerization has allowed extensive investigation into this hypothesis (133). Studies have shown that GR^{dim} mice retain the ability to suppress AP-1 induced gene expression despite lacking the ability of GR dimerization (133, 134). In an acute inflammatory model

of phorbol ester induced oedema, GC treatment of GR^{dim} mice suppressed the infiltration of inflammatory cells at sites of inflammation and reduced swelling. Here, pro-inflammatory factors, such as TNFα, IL-6 and IL-1β in peritoneal macrophages and IL-2 and IFNγ in T cells were significantly suppressed to a similar extent upon treatment with dexamethasone. It was concluded that this was due to the continued ability of GR^{dim} mice to suppress NF-κB regulation of pro-inflammatory genes (135). In contrast, GR^{dim} mice were resistant to side effects of GC use such as changes in liver metabolism and glaucoma (136, 137). This work indicated the potential to use selective monomer ligands to specifically target the therapeutic anti-inflammatory effects of GCs, without triggering the adverse side effects.

However, recent evidence indicates that this is an oversimplified view of GC signalling. In an STIA model of inflammatory arthritis, GR^{dim} mice were resistant to the anti-inflammatory effects of dexamethasone, with persistent ankle swelling and immune cell infiltration. Thus, in this model GR dimerization was required for the anti-inflammatory effects of GCs (138). It is now known that GCs can increase the expression of anti-inflammatory genes, such as GILZ, via transactivation (121). Similarly, in the mouse model of TNF-induced acute lethal inflammation, GR^{dim} mice were resistant to the anti-inflammatory actions of GCs, failing to suppress the pro-inflammatory transcription factor STAT1. In this case, GR dimerization was contributing to transrepression, disputing the idea that only monomeric GR can induce this mechanism (139). Additionally, GR^{dim} mice are not resistant to GC-induced osteoporosis and muscle wasting, common side effects of GC use (140, 141).

The GR requires interaction with coactivators or corepressors in order to mediate its effects on gene expression. It is estimated that hundreds of coregulators exist which may

interact with the GR via its AF domains (142). In addition, it appears that expression of coregulators are specific to different cell types, with the expression of different GC-responsive genes requiring a particular coregulator or coregulator complex (143). Consequently, the possibility of targeting specific genes via this mechanism exists. One artificial GR ligand, known as AL-438, is able to induce a conformational change in the GR allowing the specific interaction of coactivator GR-interacting protein 1 (GRIP-1), whilst preventing interaction of peroxisomal proliferator-activated receptor γ coactivator-1 (PGC-1). GRIP-1 is involved in transcriptional repression of pro-inflammatory genes while PGC-1 is involved in upregulating glucose. In a carrageenan-induced paw oedema murine model, AL-438 treatment exhibited similar anti-inflammatory effects as prednisolone, but bone and glucose metabolism were protected from GC-induced negative effects (144). Therefore, although selective targeting of the GR appears to be more complicated than originally thought, a potential approach to achieving the anti-inflammatory effects of GCs whilst bypassing the negative side effects is still achievable via the modification of coregulators.

1.4.3 Glucocorticoid excess

Despite the potent therapeutic efficacy of GCs, their use is limited due to the prevalence of adverse side effects associated with GC excess. Cushing's syndrome is the name given to the collection of problems associated with prolonged exposure to either endogenous GCs, such as cortisol, or exogenous GC administration. Endogenous overproduction of GCs predominantly occurs as ACTH-dependent Cushing's syndrome, termed Cushing's disease, in the form of pituitary ACTH or CRH-producing tumours (145). Common symptoms of Cushing's syndrome include obesity, striae, muscle atrophy,

osteoporosis (see section 1.5.5), hypertension, hepatic steatosis and glucose intolerance (146). These symptoms are also common side effects of GC therapy in patients with chronic inflammatory diseases, with around 70% of patients developing adverse Cushingoid features during the initial 3 months of GC treatment (20).

1.4.4 The role of 11β-HSD1 in the metabolic effects of GC excess

In order to examine the contribution of 11β-HSD1 metabolism to the adverse side effect profile of GC excess, a global 11β-HSD1 KO mouse has been established. In a study by Morgan *et al*, 11β-HSD1 KO animals were exposed to supraphysiological levels of GCs, receiving 100 mg/L of corticosterone in the drinking water for five weeks. Whereas WT animals on this treatment developed many of the features of GC excess, such as hypertension, hepatic steatosis, glucose intolerance, muscle wasting and increased adiposity, 11β-HSD1 KO animals were protected from these adverse effects. Both GC treated WT and 11β-HSD1 KO animals showed a comparable reduction in adrenal weights and increases in serum corticosterone, confirming identical exposure to circulating GCs. Thus, it was concluded that 11β-HSD1 reactivation of GCs at target tissues mediates the detrimental metabolic side effects associated with GC use. These results indicated the potential of 11β-HSD1 inhibitors to prevent the negative effects of GC excess (70).

1.4.5 11β-HSD1 inhibitors in clinical trials

The use of 11β-HSD1 inhibitors to treat metabolic disorders is not a novel idea. Many studies have looked at the therapeutic potential of these agents in the treatment of

metabolic diseases such as type 2 diabetes and polycystic ovary syndrome. This began with the use of a non-selective 11β-HSD inhibitor known as carbenoxolone. Carbenoxolone resulted in reductions in glycogenolysis and glucagon-stimulated glucose production in patients with type 2 diabetes, whilst healthy individuals had reductions in total cholesterol levels. Although this approach showed promise for the treatment of metabolic complications of type 2 diabetes, carbenoxolone also inhibited renal 11β-HSD2, which resulted in a raise in blood pressure, highlighting the requirement for selective 11β-HSD1 inhibitors (147). This resulted in the development of the selective 11β-HSD1 inhibitor; INCB13739. INCB13739 was used to treat type 2 diabetes when metformin was inadequate to control the disease. This resulted in significant decreases in average blood glucose and fasting glucose levels. Here, significant dose-dependent decreases in body weight, total cholesterol, LDL cholesterol and triglyceride levels in patients with hyperlipidaemia were also reported (148). The selective 11β-HSD1 inhibitor, MK-0916, showed similar results in type 2 diabetic patients, with a further significant reduction in blood pressure (149). Consequently, these studies supported a role for 11β-HSD1 inhibitors in the treatment of metabolic diseases.

1.4.6 The regulation of 11β-HSD1 in inflammation

The GC activating enzyme 11β-HSD1 is potently up-regulated by pro-inflammatory cytokines and has been suggested to play an important role in the pathophysiology of chronic inflammatory diseases. A variety of cell types in the synovial tissue of RA patients have been shown to express 11β-HSD1, such as T cells, macrophages, endothelial cells and synovial fibroblasts (72). 11β-HSD1 activity in RA synovium has been shown to positively correlate with inflammatory markers in the serum, such as erythrocyte

sedimentation rate (ESR) (150). In addition, the activity of the enzyme is significantly increased in synovial fibroblasts, osteoblasts, adipocytes and myotubes in response to pro-inflammatory cytokines such as TNFα and IL-1 (72, 151-153). Glucocorticoids also increase the activity of 11β-HSD1 in both synovial fibroblasts and osteoblasts, with a synergistic upregulation identified when combined with pro-inflammatory cytokines (154). This led to an increased anti-inflammatory response to inactive GCs such as cortisone *in vitro*. This finding indicates that local cells of the joint can enhance the anti-inflammatory response by amplifying the levels of active GCs in the juxta-articular environment. Moreover, whilst human monocytes do not express 11β-HSD1, expression is induced following differentiation to macrophage (155). Macrophages polarised towards the pro-inflammatory M1 phenotype by LPS and IFNγ exposure have been shown to have a 9-fold increase in 11β-HSD1 mRNA levels compared to macrophages polarised to the pro-resolution M2 phenotype by IL-4 (156).

1.4.7 11β-HSD1 metabolised glucocorticoids in inflammation

Due to the regulation of 11β-HSD1 by pro-inflammatory cytokines, several studies have focused on the functional role of this enzyme during inflammation. We have previously used the global 11β-HSD1 KO mouse crossed with the TNF-tg inflammatory model of chronic polyarthritis (TNF11βKO) to determine the role of 11β-HSD1-mediated regulation of endogenous GCs during chronic inflammation. Lack of 11β-HSD1 lead to a much more severe form of arthritis, characterised by significantly exacerbated swelling and deformity of paws, significantly more synovitis and pannus formation, and significantly worse juxta-articular and systemic bone loss (157). An additional study showed that the increased inflammation in the TNF11βKO mouse also lead to increased inflammatory muscle

wasting, suggesting that 11β-HSD1 amplification of active GCs plays a fundamental role in suppressing inflammation (153). A mesenchymal specific 11β-HSD1 KO mouse was utilised to determine the role of FLS and osteoblast 11β-HSD1 in these phenotypes. These animals displayed comparable arthritis scores, synovitis, and systemic bone destruction to TNF-tg animals, indicating that mesenchymal-derived 11β-HSD1 does not mediate the anti-inflammatory actions of endogenous GCs in the TNF-tg mouse model (157).

The TNF11βKO mouse also exhibited increased infiltration of T cells, neutrophils and macrophages into the joint compared with TNF-tg animals, consistent with the reported increase in synovitis. Here, a shift in the M1/M2 ratio towards increased pro-inflammatory M1 macrophages was apparent in the TNF11βKO mouse compared to the TNF-tg animals, indicating a role for 11β-HSD1 in the polarisation of macrophages (157). In keeping with this, a separate study showed that 11β-HSD1 KO mice had a dramatic delay in the clearance of pro-apoptotic leukocytes by macrophages, which is a classic function of the M2 phenotype. *In vitro* experiments confirmed this finding, with 11β-HSD1 inhibitors preventing the ability of macrophages to increase phagocytosis in response to 11-DHC (158).

Overall, these results indicated that whilst 11β-HSD1 seems to mediate many of the negative side effects associated with GCs (see section 1.4.4), 11β-HSD1 inhibitors may be detrimental if administered during chronic inflammation by blocking their beneficial anti-inflammatory actions.

1.4.8 Side effects of glucocorticoid use in chronic polyarthritis

Glucocorticoids are widely utilised in the treatment of diseases such as RA, where they are utilised as a bridging therapy prior to traditional DMARDs and manage acute inflammatory flares. As previously mentioned (section 1.4.3), the side effects of therapeutic GC use are similar to that of endogenous GC excess, including osteoporosis, muscle atrophy and diabetes (146). Prednisolone is often initially administered at higher doses, at a maximum of 60 mg/day, which is then tapered down to between 7.5 – 30 mg/day to minimise the risk of side effects (159). The net effects of GCs on the bone during chronic inflammation will be discussed in detail in section 3.1. In addition to these side effects, GC treatment can result in the suppression of the HPA axis which persists even after the termination of therapy. This is commonly known as adrenal insufficiency. A systematic review found that between 13-63% of patients receiving exogenous GCs developed adrenal insufficiency which persisted 3 years after withdrawal in 15% of patients. This phenomenon was evident even in short-term low dose GC therapy and can result in problems such as nausea, fatigue and anorexia (160).

Both chronic inflammation and therapeutic GCs are recognised drivers of systemic muscle and bone loss, whilst their combined actions on bone metabolism are less well defined. To better delineate how these factors influence these processes requires an understanding of normal bone physiology and metabolism.

1.5 Bone

The skeleton is a highly metabolically dynamic organ which is constantly being remodelled, with approximately 10% of the entire skeleton being renewed each year

(161). The bone serves multiple functions within the body including; structural support and protection of internal organs, contributing to movement via interaction with muscles, providing an appropriate environment for haematopoiesis, and acting as a reserve for calcium and phosphate (162, 163). Dense cortical bone surrounds the bone marrow space and accounts for around 80% of the skeleton, whilst the more elastic trabecular bone forms a network of rod and plates within the bone marrow space and accounts for the remaining 20% (84). Bone consists of three main cell types; the mesenchymal-derived bone forming osteoblasts, the myeloid-derived bone resorbing osteoclasts, and the terminally differentiated osteoblasts known as osteocytes (164).

1.5.1 Structure of long bones

Five different types of bones exist; long, short, sesamoid, flat and irregular. Long bones consist of two main parts, the diaphysis and the epiphysis. The epiphysis is the region at either end of the bone containing the spongy trabecular bone, whilst the diaphysis is the shaft in the middle of the bone. Epiphyseal and diaphyseal regions are connected by a narrow area of metaphysis, which in growing bones harbours the epiphyseal growth plate. The diaphysis contains no trabecular bone, with the cortical bone surrounding a medullary cavity, containing the yellow bone marrow, a structure made up of mesenchymal cells and lipid droplets that gradually replaces the haematopoietic red bone marrow compartment with age (Fig 1.9) (165).

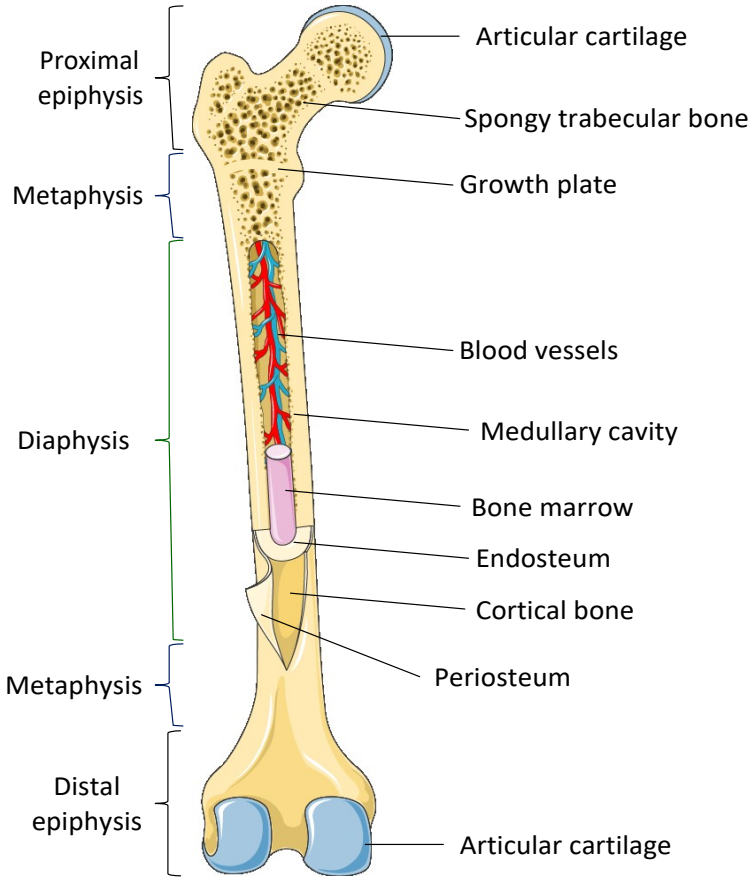

Figure 1. 9: Structure of a long bone.

Long bones are made up of epiphyseal, metaphyseal and diaphyseal regions. The epiphyseal region is made up of spongey trabecular bone and is surrounded by cartilage. The diaphyseal region consists of the medullary cavity which harbours the bone marrow. These regions are connected by the metaphyseal area that contains the epiphyseal growth plate.

Cortical bone is formed of functional units known as osteons. Osteons are cylindrical structures consisting of concentric layers of lamellar bone built around an inner cavity called a Haversian canal which houses the blood vessels (84). Additionally, the osteon contains lacunae in which osteocytes embedded in the bone reside (166) (Fig 1.10).

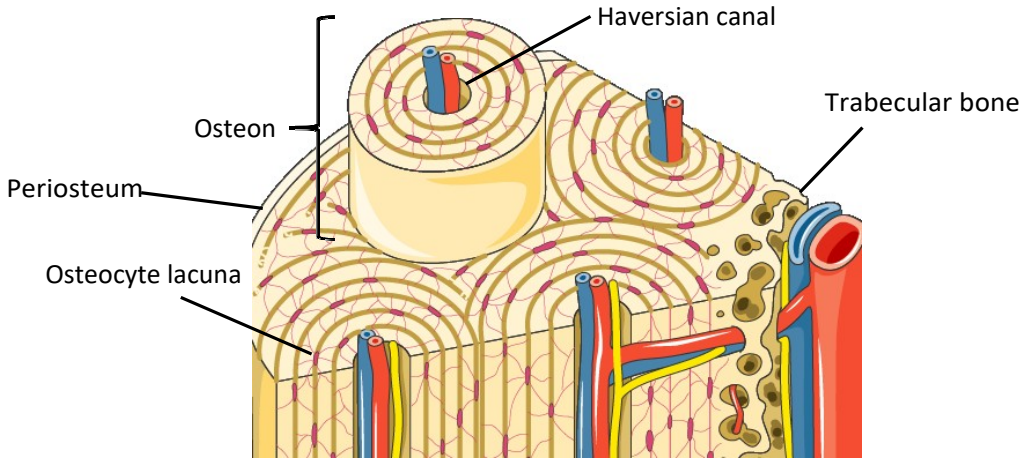

Figure 1. 10: Structure of cortical bone

Cortical bone is made up of functional units called osteons which consist of layers of lamellar bone arranged in concentric circles around a Harversian canal containing the blood vessels. Bone embedded osteocytes reside in lacuna in the osteon.

The inner side of the cortical bone is covered with a layer of connective tissue called the endosteum. Tethered to this are a range of cells including osteoblasts, mesenchymal stem cells (MSCs) and adipocytes. Recently, this endosteal niche has been shown to play a critical role in the maintenance of haematopoietic stem cells (HSCs) in the bone marrow and can induce vascular remodelling during development (167). The outer surface of the cortical bone is covered by a thin membrane composed of fibroblasts, elastin and collagen known as the periosteum, which contains the blood vessels and nerves that supply the bone. The periosteum plays a major role during bone regeneration, with a recent study showing that it contains a pool of MSCs which are the major source of chondrocytes during endochondral bone repair (168). Almost the entire surface of the bone is covered by periosteum, excluding the area where the epiphyses connect with

other bones at the joints. In this area, the bone is instead covered with a layer of articular cartilage to reduce friction (Fig 1.9) (84).

1.5.2 The bone remodelling cycle

In adults, bone undergoes a tightly regulated process of formation and resorption, allowing damage repair and facilitating mineral homeostasis of calcium and phosphorus. This process is known as the bone remodelling cycle and it is comprised of five consecutive steps; activation, resorption, reversal, formation and termination (164). The cycle occurs in what is known as a basic multicellular unit (BMU), which brings together the osteoblasts and osteoclasts in close proximity with access to a capillary blood supply and is enclosed by a canopy of bone lining cells (169). BMU structure varies depending on where they are situated. BMUs in the trabecular bone resemble a trench on the surface of the bone, whilst BMUs in the cortical bone are shaped like tunnels in the cortex formed by a “cutting cone” of osteoclasts. A “closing cone” of osteoblasts fills the tunnel and a new osteon is created (170).

During the initiation stage of bone remodelling, osteocytes sense signals such as structural damage, mechanical strain or hormones and can communicate to other cells via dendritic process. In the absence of initiating signals, osteocytes produce factors such as transforming growth factor-β (TGF-β) and the wnt inhibitors sclerostin (SOST) and Dickkopf1 (DKK1) which inhibit osteoclast and osteoblast differentiation (171). Signals such as bone matrix damage or immobilisation result in osteocyte apoptosis, which subsequently leads to a removal of the inhibitory signals and therefore facilitates osteoclastogenesis (172, 173). *In vitro* studies using conditioned media from apoptotic or

non-apoptotic osteocytes to treat osteoclasts have shown that treatment with apoptotic media increased osteoclast precursor migration and osteoclast formation by up to 64% and 450% respectively. Treatment with blocking antibodies revealed that these effects were at least partially mediated by receptor activator of nuclear factor kappa-β ligand (RANKL) (174) (Fig 1.11). Once osteocytes have recruited and triggered the differentiation of osteoclasts, the resorption stage can occur.

Differentiated, multinucleated osteoclasts must first adhere to the bone surface before resorption can occur. The cytoskeleton of osteoclasts is reorganised and four distinct membrane regions are formed; the sealing zone, the ruffled-border, the functional secretory domain and the basolateral domain. Upon stimulation with growth factors such as macrophage colony stimulating factor (M-CSF), osteoclasts form internal adhesion structures known as podosomes which consist of a membrane domain made up of integrins, encompassing an actin core (175). It has been hypothesised that the sealing zone is comprised of a dense network of podosomes (176, 177). Specifically, β3 integrin activation has been shown to control cytoskeletal reorganisation and appropriate formation of podosomes (178). Integrin activation allows the tight adherence of osteoclasts to the mineralised matrix, preventing the leakage of catalytic enzymes from the ruffled border into the surrounding environment. The cytoplasm of osteoclasts has been found to contain a high concentration of carbonic anhydrase, which serves to provide a constant supply of bicarbonate and protons (179). These protons can then be shuttled across the ruffled membrane via an H+-ATPase and chloride ions passively follow through chloride channels, which ultimately leads to the acidification of the resorption compartment and the degradation of the inorganic hydroxyapatite component of the bone (180, 181). At the basolateral domain, an anion exchanger releases

bicarbonate from the cell whilst taking up chloride ions. This allows the pH of the cytoplasm to remain neutral while also replenishing the chloride supply (182) (Fig 1.11).

In contrast, the predominantly type 1 collagen organic component of bone is broken down by lysosomal enzymes such as cathepsin K, which are secreted into the resorption space. These lysosomal enzymes operate under acidic conditions and require H+-ATPase proton pumps and chloride channels on the membrane of the lysosomes to facilitate their activity (183, 184). The proteolytic enzyme cathepsin K is one of the proteins housed within the lysosomes, and plays an important role in bone resorption due to its ability to degrade type 1 collagen fibres. A further function of cathepsin K is to cleave the repressive loop domain which inhibits the activity of tartrate-resistant acid phosphatase (TRAP) (185). TRAP is highly expressed on osteoclasts, specifically at the ruffled border and in intracellular vesicles (186). The exact mechanism of action of TRAP has yet to be determined. One theory by which TRAP catalyses bone matrix degradation is via the production of reactive oxygen species (ROS), such as hydroxyl radicals (•OH) (187). Resorbed bone matrix is transcytosed through the osteoclast and secreted via the functional secretory domain. TRAP has also been shown to be localised in these transcytotic vesicles, where it further degrades resorbed products, before being secreted into the extracellular matrix (Fig 1.11) (187).

Following the termination of the resorption phase, a shift towards an osteogenic environment promotes the reversal phase, aiding the coupling of resorption to formation. This remains a poorly understood stage of bone remodelling. One theory by which this coupling process occurs is via the release of growth factors from the bone matrix by resorption. Growth factors such as TGF-β and insulin-like growth factor-1 (IGF-1) are released during bone resorption and trigger the recruitment of mesenchymal stem cells

to the resorption lacunae, favouring osteoblast differentiation (188, 189). The Ephrin/Eph family members have also been implicated in this process. EphrinB2 is expressed on osteoclasts and it has been suggested that it can interact with its receptor EphB4 found on osteoblasts to simultaneously stimulate osteogenic differentiation whilst also suppressing the formation of preosteoclast cells via bi-directional signalling (Fig 1.11) (190).

Once mesenchymal progenitors have differentiated into mature osteoblasts, they begin to secrete molecules required for bone formation. Mature osteoblasts secrete an organic matrix rich in type 1 collagen, osteocalcin and bone sialoprotein (BSP) known as osteoid (191). Osteoid is then mineralised via the deposition of hydroxyapatite crystals. Hydroxyapatite is formed in matrix vesicles with transporters expressed on their surface, allowing the influx of calcium and phosphate ions. Eventually the hydroxyapatite crystals break through the membrane of the vesicle and are deposited as a mineralised nodule (192). The enzyme alkaline phosphatase is also present on the matrix vesicles, where it hydrolyses pyrophosphate (PPi) and promotes release of phosphate ions and with the sodium/phosphate co-transporter can provide the materials necessary for crystal formation and mineralisation of new bone (193). To prevent abnormal or overactive mineralisation, osteopontin is produced and secreted by osteoblasts and osteocytes in response to high levels of phosphate. Osteopontin binds to calcium in crystal surfaces and inhibits hydroxyapatite formation (Fig 1.11) (194).

Lastly, the final phase of termination occurs. When bone formation has finished, osteoblasts will either undergo apoptosis or become embedded in the bone and differentiate into osteocytes. One of the key factors in terminating the bone remodelling cycle is the production of the wnt inhibitor sclerostin by osteocytes. During the bone

remodelling cycle, expression of sclerostin is reduced to allow osteoblasts to differentiate via wnt signalling. During termination, newly differentiated osteocytes in the bone re-express sclerostin leading to the inhibition of osteoblast differentiation and subsequently the inhibition of bone formation (195) (Fig 1.11).

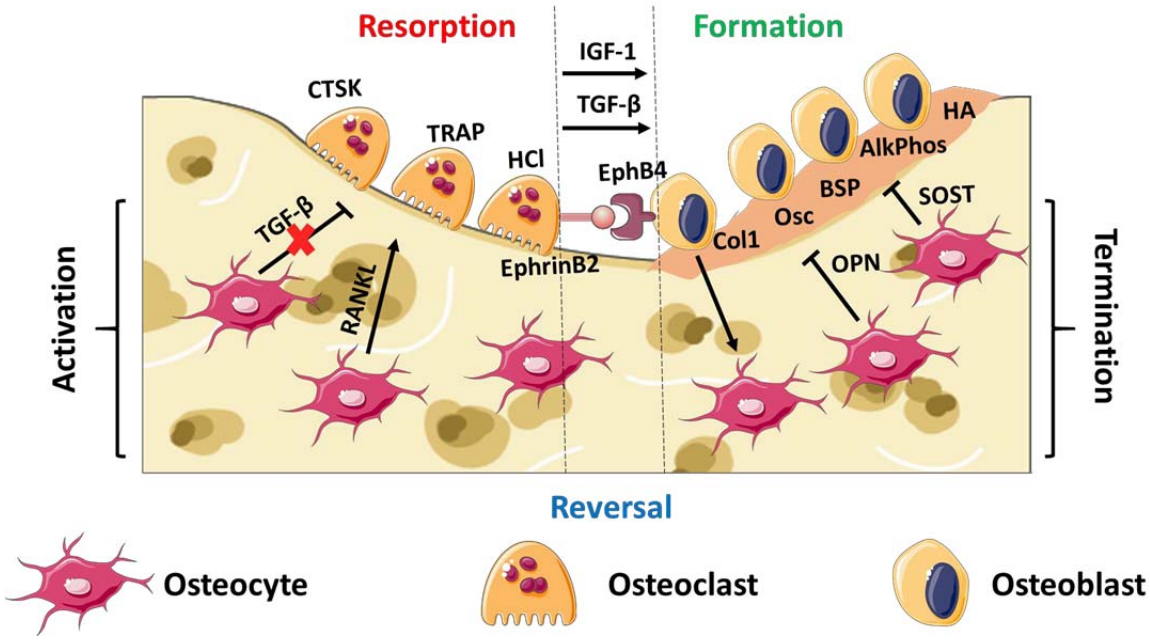

Figure 1. 11: The bone remodelling cycle

The bone remodelling cycle is activated by apoptosis of osteocytes, which inhibits the TGF-β inhibitory signal on osteoclasts, and by osteocyte signalling to osteoclasts via RANKL. Once activated, osteoclasts resorb the bone by producing hydrochloric acid (HCL) and enzymes such as cathepsin K (CTSK) and tartrate-resistant acid phosphatase (TRAP). Osteoblasts become activated by factors released from the resorbed bone such as IGF-1 and TGF-β, or by direct interactions with osteoclasts by EphrinB2/EphB4 signalling. Activated osteoblasts can then secrete type 1 collagen (Col1), osteocalcin (OSC), bone sialoprotein (BSP), alkaline phosphatase (AlkPhos) and hydroxyapatite (HA) to form new bone. After the formation stage is completed, termination occurs by inhibitory signals from osteocytes such, as osteopontin (OPN) and sclerostin (SOST), or by osteoblasts becoming embedded in the bone and differentiating into osteocytes.

1.5.3 Regulation of osteoblast differentiation

Bone remodelling must be tightly regulated to ensure that resorption and formation are balanced. Disruptions to the bone remodelling cycle can cause net bone loss or abnormal bone gain (196, 197). One key mechanism is mediated via factors that influence the differentiation of osteoblasts. Runx2 is the master regulator of osteoblast differentiation from mesenchymal progenitors by mediating the expression of osteoblast-specific genes such as osteocalcin, osteopontin and bone sialoprotein (198, 199). Runx2 requires phosphorylation to become activated, after which it can associate with enhancers, such as CCAAT/enhancer-binding proteins (C/EBP), on target genes and recruit factors that promote chromatin remodelling, such as the SWI/SNF complex that promotes transcriptional activation (200-202). Thus, factors which influence Runx2 signalling strongly influence osteoblast differentiation.

The wnt signalling pathway has been identified as a major regulator of Runx2. Canonical wnt signalling is required for the commitment of mesenchymal progenitor cells to the osteoblast lineage (203). Here, wnt pathway activation through their binding to the low density lipoprotein receptors (LRP) 5 and 6 results in β-catenin translocation to the nucleus, where it upregulates the expression of Runx2 (204, 205).

Consequently, factors which inhibit wnt signalling inhibit the differentiation of osteoblasts. Dickkopf1 (Dkk1) is a secreted protein which binds to the co-receptors LRP5/6 and antagonises the wnt signalling pathway (206). The wnt inhibitor sclerostin, produced by osteocytes, acts in a similar fashion by acting as an antagonist for LRP5/6 receptors (207).

Osteoblast differentiation can also be induced by hormonal mediators such as parathyroid hormone (PTH) which functions to maintain systemic calcium homeostasis under physiological conditions (208). PTH is synthesised in the parathyroid gland and secretion of PTH-containing vesicles is activated by low serum concentrations of calcium as determined by calcium sensor receptors (CaR) (209). Cells of the osteoblast lineage express the G-protein coupled receptor PTH1R, which binds PTH and can cause the activation of calcium mediated intracellular signalling pathways and protein kinase A dependent phosphorylation of transcription factors (210, 211). PTH can have both anabolic and catabolic roles on the skeleton depending on the duration of activation, i.e. continuous PTH stimulation results in suppression of osteoblastic bone formation whilst intermittent stimulation increases osteoblast activity (212, 213). PTH impacts on the proliferation of early osteoblasts by inducing the transcription of cyclin D during osteoblast development (214). Additionally, PTH increases the differentiation and activity of osteoblasts via an upregulation of alkaline phosphatase and an increase in anabolic IGF-1 signalling, which subsequently augments the production of type 1 collagen (215, 216). PTH signalling can also promote wnt signalling pathways by reducing Dkk1 expression and amplifying β-catenin expression and signalling (217).

Vitamin D can also regulate the concentration of calcium in the serum by improving absorption in the intestines. Vitamin D exerts its action via binding to the vitamin D receptor (VDR) which subsequently dimerises and binds to vitamin D response elements (VDRE) on genes to control transcription. In this way, vitamin D binds to and upregulates the gene-encoding the co-receptor LRP5 which leads to enhanced wnt signalling and osteoblast differentiation (218). Similarly, to PTH, vitamin D can also increase β-catenin

expression (219). Additionally, vitamin D can directly interact with Runx2 via VDREs which leads to the upregulation of osteocalcin (220).

1.5.4 Regulation of osteoclast differentiation

For osteoclasts, the main regulator of differentiation is the RANKL/RANK/ osteoprotegerin (OPG) system. M-CSF is essential for differentiation and survival of osteoclasts, however it cannot induce osteoclastogenesis alone and instead RANKL/RANK signalling is also required (221). Surface bound and secreted RANKL is expressed in osteoblasts, osteocytes, fibroblasts and activated B and T lymphocytes, whilst RANK is predominantly expressed on osteoclasts and their precursors (222-226). Upon binding with RANKL, RANK recruits TRAF6 to its cytoplasmic domain, activating a kinase signalling cascade that promotes osteoclast differentiation, activation and survival (227). Activation of NF-κB signalling pathway by RANKL/RANK signalling also activates NFATc1, the master regulator of osteoclast differentiation, which is associated with the expression of osteoclast-specific genes including those encoding TRAP and cathepsin K (228). RANKL also induces the expression of Atp6v0d2, a subunit of the proton pump, and DC-STAMP, which are required for the fusion of osteoclast precursors to form differentiated osteoclasts (229, 230). Of interest, transgenic mice that ubiquitously overexpress the soluble form of RANKL die *in utero*, and those overexpressing soluble RANKL in the liver exhibit a severe osteoporotic phenotype (231). Thus, tight control of RANKL/RANK signalling is critical in regulating bone metabolism. OPG is expressed by cells of the osteoblast lineage and acts as a decoy receptor for RANK, leading to inhibition of RANK/RANKL signalling pathways and suppression of osteoclastogenesis (232).

As previously mentioned, continuous PTH exposure results in increased bone resorption secondary to the increased production of RANKL and M-CSF. Additionally, PTH has been shown to have inhibitory effects on OPG expression in osteoblasts, which together with changes in RANK signalling, promotes bone resorption (233).

Other factors impacting on RANKL/RANK signalling include GCs and inflammation which are discussed in section 1.5.5 and 1.5.7 respectively.

1.5.5 Glucocorticoid-induced osteoporosis (GIO)

Another important hormonal factor in the regulation of bone homeostasis is glucocorticoid signalling. Under physiological conditions, GCs positively influence bone development and maintenance. Here, constitutively inactivating GC signalling through the overexpression of 11β-HSD2 in mature osteoblasts (resulting in their increased clearance) shifts the commitment of mesenchymal progenitor cells from osteoblasts to adipocytes (234). GCs have been shown to stimulate the expression of wnt7b and wnt10b in osteoblasts and promote osteoblast differentiation at low doses, whilst at higher doses GCs downregulate these wnt proteins and upregulate wnt inhibitors such as Dkk1 (235). Therefore, while low levels of GCs are beneficial for the bone, higher doses are detrimental. The best example of this is with GC-induced osteoporosis (GIO).

GIO is the most common form of secondary osteoporosis. Risk of fracture has been found to dramatically increase within 3 to 6 months of starting prednisolone therapy. The relative risk of any fracture was increased by 33% in patients receiving GCs, with particular increase in vertebral and hip fractures. The side effects of GC use on the bone were found to be markedly reversible after stopping treatment (21). While postmenopausal

osteoporosis is mediated by an increase in bone resorption by the osteoclasts, GIO is mediated primarily by a substantial inhibition of osteoblastic bone formation (236). Again, constitutively inactivating GC signalling through the overexpression of 11β-HSD2 in mature osteoblasts revealed that therapeutic GCs reduce bone strength and formation rate by suppressing their maturation and triggering their apoptosis (237).

The impact of GCs on osteoclasts is less clear. Several studies report that GC treatments result in a decrease in osteoclast number but an increase in osteoclast longevity, mediated via an increased M-CSF production (236, 238, 239). Further studies have reported conflicting results on the expression of osteoclastic genes in response to GCs. One study showed that dexamethasone treatment of murine calvarial bones resulted in increased mRNA levels of RANK, RANKL and OPG, leading to increased levels of TRAP and cathepsin K (240). Other studies found that OPG is either decreased, or that RANKL and OPG levels remain unchanged (238, 241, 242). These differential responses may be dependent on the differentiation stage or activation status of the osteoclasts (243). The variation in dose, method of administration and experimental model may also be responsible for the variation of results.

Since GCs are used clinically as immunosuppressive agents, the underlying inflammatory state of the patient must also be taken into account when investigating bone related effects.

1.5.6 Bone loss and muscle wasting in chronic inflammation

In addition to the localised juxta-articular complications associated with chronic inflammatory arthritis, systemic complications, such as bone loss and muscle wasting,

are also common. After one year of disease, patients with RA were found to have significantly lower bone mineral density (BMD) measurements at all sites examined when compared to healthy controls. This inversely correlated with clinical inflammatory markers such as serum C reactive protein (CRP) suggesting that systemic bone loss in RA is associated with severity of inflammation (244). The mechanisms behind inflammatory bone loss will be extensively covered in section 1.5.7. One study performed high-resolution CT scans of the radius bones of 90 RA patients and found that bone volume measurements (BV/TV) were significantly reduced in the RA group compared to healthy controls. The basis of this reduction in bone volume differed depending on the sex of the patient, with female RA patients having significantly lower trabecular number (Tb.N), whilst male RA patients had significantly reduced lower trabecular thickness (Tb.Th) compared to their respective controls (351).

Muscle wasting is also a systemic complication associated with inflammatory arthritis, with approximately two thirds of RA patients presenting with reductions in muscle mass (245). A study showed that RA patients had significant reductions in hip and knee muscle strength, endurance and aerobic capacity compared to healthy controls (246). In addition, one study reported that cross-sectional area of forearm muscles was significantly reduced in RA patients compared to controls, and this muscle atrophy, alongside increases in joint deformity and pain, lead to reductions in grip strength (247). Briefly, inflammatory muscle wasting is mediated by pro-inflammatory cytokine stimulated upregulation of MuRF1 and atrogin-1, genes associated with the proteasomal degradation pathway, and the disruption of the mTOR pathway, associated with protein synthesis, in the muscle (248, 249).

Bone loss, muscle wasting and physical inactivity in RA patients all contribute to an increase in fracture risk. Overall, RA patients have around a 30% increased risk of osteoporotic fractures at sites such as the hip, vertebrae, wrist and humerus (250). More specifically, a study showed that vertebral fractures in women with RA are over twice as common than in age-matched postmenopausal women (251). The contribution of inflammation to fracture risk can be difficult to ascertain due to the use of therapeutic GCs which also contribute to both reductions in bone mineral density and muscle strength, as previously described (1.5.5).

1.5.7 Mechanisms of Inflammatory bone loss

Glucocorticoids are commonly used to treat inflammation; however, inflammation in itself is a significant driver of systemic bone loss. A prominent mechanism associated with a shift toward net bone loss is the interaction of the activated immune system with bone cells. Chronic inflammation is associated with inflammatory bone loss, which can be triggered by both direct interactions with immune cells and by their production of pro-inflammatory cytokine mediators. In terms of resorption, cytokines can be split into two categories; pro-osteoclastogenic and anti-osteoclastogenic. Many of the pro-osteoclastogenic cytokines, including TNFα, IL-1β, IL-6, IL-8 and IL-17, mediate their actions via an upregulation of RANKL on fibroblasts and osteoblasts (252-255). Additionally, TNFα, IL-1β and IL-6 have been shown to act synergistically to increase RANKL (256). T and B cells also upregulate RANKL expression in response to stimulation with antigen. Activated T and B cells isolated from resorptive bone lesions of patients with periodontitis were able to induce osteoclastogenesis *in vitro* in a RANKL-dependent manner (224). However, the osteoclastogenic potential of a T cell depends on its specific

subset. Studies have shown that Th17 cells, which are commonly associated with autoimmune diseases, act as osteoclastogenic helper cells, whilst Th1 cells inhibit RANKL expression via IFNγ-induced degradation of TRAF6 and thus have anti-osteoclastogenic actions (257, 258). Th2 cells can also inhibit osteoclast differentiation via their production of the anti-osteoclastogenic IL-4 which downregulates NFATc1 expression and suppresses TNFα signalling (259).

TNFα also has important effects on the bone forming ability of osteoblasts in inflammation. TNFα treatment of osteoblasts precursors inhibits their differentiation by suppressing the DNA-binding ability of Runx2. This leads to inhibition of alkaline phosphatase expression and reduced matrix deposition (260). The pro-apoptotic properties of TNFα on osteoblasts have also been observed (261). Similarly, IL-6 treatment of osteoblasts leads to reductions in alkaline phosphatase activity and in the expression of Runx2 and osteocalcin. Mineralisation by osteoblasts is also dramatically reduced in a dose dependent manner, highlighting the inhibitory effects of this cytokine on osteoblast differentiation (262). Conflicting data has also been published highlighting the stimulatory effects of IL-6 on osteoblasts, suggesting that IL-6 mediates osteoblast differentiation via activation of the Stat3 transcription factor and inhibits TNFα-induced osteoblast apoptosis (261, 263). More research is needed to fully elucidate the role of specific cytokines in inflammatory bone loss, however it is widely accepted that this detrimental bone phenotype results from an imbalance in the bone remodelling cycle, shifting towards resorption and away from formation (264). A previous study attempted to reverse the bone loss observed in the human TNF-transgenic (TNF-tg) mouse by combined treatment with anti-TNF therapy in combination with anti-osteoclastic (OPG) and pro-osteoblastic agents (PTH). Anti-TNF and OPG treatments alone were sufficient

to inhibit osteoclast activity and prevent the development of further erosions. However, treatment with anti-TNF in combination with OPG and PTH, resulted in arrest of bone erosion development but also repair of existing bone erosions. These results indicate that repair of bone erosions requires a therapy which simultaneously controls inflammation while also shifting the osteoclast to osteoblast ratio in favour of the osteoblasts either by promoting osteoblastogenesis or suppressing osteoclastogenesis (265).

1.6 Mouse models of polyarthritis and inflammatory bone loss

Animal models of inflammatory arthritis have substantially enhanced the knowledge behind the pathogenesis of chronic inflammatory polyarthritis and informed therapeutic approaches. Commonly used models include the TNF-tg mouse, collagen-induced arthritis (CIA), collagen-antibody-induced arthritis (CAIA), K/BxN mouse and serum transfer induced arthritis (STIA) (266).

1.6.1 Strengths and weaknesses of commonly used models

Each model is associated with specific strengths and limitations. The CIA model uses an intradermal injection of homologous type 2 collagen alongside Freund's adjuvant to induce a chronic and progressive inflammatory polyarthritis. The disease progression is similar to that of human RA, with characteristic inflammatory infiltration into the synovium and erosion of the bone and cartilage of the joint. In addition, this model also mimics the breach of tolerance often seen in RA which leads to the production of auto-antibodies and type 2 collagen-specific T cells (267). The main limitation of the CIA model is that it is generally limited to the DBA/1 mouse strain, whilst the majority of transgenic models are generated in the C57BL/6 strain which is markedly more resistant to CIA induction (268).

Recent developments have been made towards inducing CIA in C57BL/6 mice, however the disease is milder and more variable than in DBA/1 mice and thus less reproducible (83, 269).

The CAIA overcomes this limitation through the transfer of CIA serum, containing collagen specific autoantibodies, into a C57BL/6 strain to generate acute inflammatory arthritis (270). The clinical progression of the disease closely resembles that of CIA, however the CAIA model does not include the involvement of the adaptive T and B cell immune responses (271). Thus, the CAIA model is not appropriate to study the contribution of the adaptive immune response to the pathogenesis of inflammatory arthritis.

Crossing mice with a transgenic T cell receptor (TCR) specific for a bovine RNase epitope (KRN mice) with mice expressing MHC class II molecule-Ag7 (such as the NOD mouse) generates the K/BxN model of chronic spontaneous inflammatory arthritis. The pathogenesis is driven by activation of the complement cascade and stimulation of pro-inflammatory cytokines such as TNFα and IL-1β. In addition, this model has high levels of autoantibodies and T cells specific to glucose-6-phosphate isomerase (272). Transferring the serum containing these antibodies to another mouse will also induce an acute resolving form of inflammatory arthritis with a well-established progression of disease, known as the serum transfer induced model. This can be performed in a wide variety of mouse strains (273). The drawback of these models is that glucose-6-phosphate isomerase antibodies do not appear to play a role in the development of human RA (274, 275).

1.6.2 The TNF-tg model of polyarthritis

The TNF-tg mouse model of chronic inflammatory polyarthritis is driven by the overexpression of human pro-inflammatory cytokine TNFα. The AU-rich element (ARE) typically present in the 3'-untranslated region (3'-UTR) of the human TNFα gene mediates the destruction of TNFα transcripts in resting cells to prevent gene expression. In the TNF-tg mouse, the human TNFα gene is modified to replace the 3'UTR containing the ARE with the 3'-UTR of the gene encoding β-globin. This leads to increased gene stability and thus constitutive translation of TNFα (276). Several lines of TNF-tg mice have been developed in which chronic inflammatory arthritis is consistently induced. The Tg197 line contains five transgene copies, producing a severe arthritic phenotype which, in homozygous mice, becomes fatal at 12-14 weeks. Consequently, due to the severity of disease, TNF-tg are bred with WT animals to produce heterozygous offspring (277).

Tg197 mice exhibit progressive inflammatory arthritis similar to human RA, with significant swelling of joints present from around four weeks of age, substantial hyperplasia and inflammatory infiltration, and juxta-articular bone and cartilage erosions. The effects triggered by the overexpression of TNFα helped highlight the important role of this cytokine in the pathogenesis of RA, and facilitated research examining anti-TNF therapies as a therapeutic, ultimately culminating in the anti-TNFα biological class of drugs (276). As with the CAIA model, the TNF-tg model is limited due to the lack of adaptive immunity in disease progression (278).

1.6.3 Bone and muscle phenotype of the TNF-tg mouse

TNFα has been widely implicated in the development of bone loss and muscle wasting in inflammation due to its activation of osteoclasts and induction of muscle specific ubiquitin ligases (279, 280). Thus, in addition to the similar local juxta-articular signs and clinical presentation of the TNF-tg mouse model to human RA, it also closely resembles the human disease in terms of systemic complications. Using micro-CT analysis of the tibias from the TNF-tg mouse, we have previously shown that there are significant reductions in bone volume, trabecular thickness and trabecular number in these animals compared to WT mice. Moreover, histological analysis has revealed that TRAP positive osteoclasts are highly abundant in the bones of TNF-tg animals. In addition to the osteoclast phenotype observed in the TNF-tg mouse, significant reductions in the mature osteoblast markers alkaline phosphatase and osteocalcin were also observed. Finally, the muscles of the TNF-tg animals have significant inflammatory muscle wasting with smaller muscle fibres, trends towards decreased quadriceps and tibialis anterior muscle size relative to WT counterparts, that result in decreased mobility (281).

1.7 Summary

Chronic inflammatory polyarthritis affects around 2% of the adult population and can leads to both juxta-articular manifestations, such as bone and cartilage destruction and joint deformity, and systemic problems, including inflammatory bone loss and muscle wasting. Together these contribute to physical disability, decreased quality of life and increased mortality. GCs have proven highly efficacious in the treatment of chronic inflammatory diseases via their potent anti-inflammatory and immunomodulatory actions, however their use is limited due to the prevalence of serious adverse effects such as GC-induced

osteoporosis. Understanding these processes remains paramount in the effective management of patients with chronic inflammatory disease, with further research necessary to tease apart the mechanisms behind the beneficial and detrimental actions of therapeutic GCs and facilitate the development of new, more targeted therapies.

1.8 Hypothesis

We predict that glucocorticoid activation by 11β-HSD1 will be central in mediating both the beneficial and detrimental effects of therapeutic GCs in the backdrop of chronic inflammatory disease.

1.9 Aims

The specific aims of this project were to:

- Examine the contribution of 11β-HSD1 metabolism of GCs to GIO using the 11β-HSD1 KO mouse (Chapter 3)
- Investigate the net effects of GCs on the bone in the TNF-tg mouse model of chronic inflammatory arthritis (Chapter 4)
- Establish the role of 11β-HSD1 in mediating the therapeutic anti-inflammatory effects of GCs in the TNF11βKO mouse (Chapter 5)
- Determine which cell types are mediating the anti-inflammatory effects of GCs in cell specific TNF11βKO mice (Chapter 5)
- Utilise the TNF11βKO mouse to investigate the role of 11β-HSD1 metabolism in GIO during chronic inflammation (Chapter 6)

Chapter 2: Materials and Methods

Unless otherwise stated all reagents were ordered from Sigma-Aldrich, Gillingham, UK.

All methods were carried out by me unless specifically stated.

2.1 Animal experiments

Procedures on animals were performed under guidelines by the Animal (Scientific Procedures) Act 1986 in accordance with the project licence (70/8582 or P51102987) and approved by the Birmingham Ethical Review Subcommittee (BERSC). All mice were from C57BL/6J strain. Mice were housed in the Biomedical Service Unit (BMSU) at 21-23°C and a humidity of approximately 55%. Mice were kept with *ad libitum* access to standard chow and water and a 12 hour light/dark cycle. An arthritic paw score (section 2.1.4) of greater than 10, a clinical score of over 16, or a loss of weight greater than 20% was characterised as the human endpoint for the mice. At seven weeks animals were culled using cervical dislocation. Male mice were exclusively utilised to avoid any fluctuations in responses based on differing estrous cycles of the mice since estrogen levels vary widely during the cycle and have been shown to have differing effects on the immune system (353).

2.1.1 TNF-Tg mice

TNF-transgenic (TNF-Tg) mice of the Tg197 line were obtained from Dr George Kollias of BSRC Alexander Fleming (Athens, Greece). Briefly, chronic inflammation is driven by the replacement of the inhibitory ARE in the 3'-UTR of the human TNFα gene with the 3'-UTR of the β-globulin gene, rendering it constitutively active (see section 1.6.2) (276). Tg197 mice have five copies of the transgene and develop severe arthritis, thus they are bred with wild-type (WT) mice in order to generate heterozygous offspring (277). Breeding animals were given Remicade (infliximab), a monoclonal antibody against human TNFα, which has been shown to decrease disease activity and improve breeding of animals

(282).

2.1.2 Generation of global KO mice

Global 11β-HSD1 knockout (11βKO) mice have been previously produced using the Cre-loxP system. Cre is a site-specific DNA recombinase protein encoded by the *cre* (cyclisation recombination) gene from bacteriophage P1, which recognises sites known as loxP sites on the genome and catalyses homologous recombination of DNA that is flanked by loxP sequences (283). This capacity of the cre-loxP system to efficiently manipulate DNA has been taken advantage of to produce animal models capable of deciphering the impact of specific proteins, for example the 11βKO mouse. Briefly, a targeting vector was designed, using the pBluescript SK(+) plasmid, which contained a lox-P flanked neomycin cassette at the 5' site of exon 5 of the *HSD11B1* gene and an extra loxP at the 3' site. DNA sequencing was used to verify the construct, after which it was linearised and electrophorated into the pluripotent embryonic stem cell line E14TG2a. Cells which were positive for the recombined trifloxed allele were selected for, expanded and injected into blastocysts from C57BL/6 mice. Male mice containing the recombinant allele were then crossed with WT females and the recombined allele was transmitted via the germline. Upon generation of mice heterozygous for the trifloxed allele, these animals were mated with zona pellucida 3 (Zp3)-Cre expressing mice, which leads to the deletion of the floxed allele. Germline transmission of the null allele occurs until homozygosity is achieved, resulting in the 11β-HSD1 global KO mouse (284). Global 11βKO mice were provided courtesy of Prof Gareth Lavery. Heterozygous TNF-tg mice were crossed with 11βKO mice to generate TNF11βKO mice.

2.1.3 Generation of cell specific KO mice

The Cre-loxP system was also used to generate the mesenchymal and myeloid specific KO mice. For mesenchymal specific KOs, *HSD11B1*$^{flx/flx}$ animals were crossed with Twist-2 cre mice. Twist2 is expressed in mesenchymal derived cell populations and twist-2 cre recombinase activity has been shown in populations such as synovial fibroblasts, chondrocytes and osteoblasts. *HSD11B1*$^{flx/flx/Twist2cre}$ (WT-Twist2) mice were mated with heterozygous TNF-Tg mice to produce TNF-Tg$^{flx/flx/Twist2cre}$ (TNF-Twist2) animals. Myeloid specific KO animals were bred in a similar way, using a LysM cre mouse, which has previously been shown to achieve a 70% recombination in macrophages, 90% in neutrophils, 16% in DCs and 26% in mast cells, with T and B cells almost completed unaffected (129).

2.1.4 Treatment and scoring

Four-week old male mice were scored twice weekly for clinical scores, and arthritic paw scores, as shown in table 2.1 and 2.2, for three weeks. Mice receiving GC treatment were supplied with *ad libitum* access to drinking water containing corticosterone (Cort) (Sigma, Gillingham, UK) at 50 µg/ml or 100 µg/ml for the duration of the scoring period. To prepare the corticosterone drinking water, 100 mg corticosterone was dissolved in 6 ml ethanol (or 50 mg in 3 ml) before being added to 1 L water (giving 0.6% ethanol overall). Corticosterone water was kept at 4°C in the dark when not in use and replaced twice weekly. During treatment, corticosterone water was administered in opaque drinking bottles to protect from light. Mice were culled at the end of the experiment by cervical

dislocation following exsanguination by cardiac puncture. Tibias were collected post mortem, one of which was fixed in 4% formalin before being transferred to 70% ethanol for storage, the other of which was homogenised for RNA isolation. Spines, front paws and livers were also formalin-fixed and stored in 70% ethanol prior to use. Adrenals were excised and weighed.

Table 2. 1: Scoring system for clinical parameters

	Score
Behaviour (assessed in home cage prior to handling)	
Normal interactions with cage mates	0
Reduced interest in roaming behaviour	2
Isolated from cagemates (provide additional house)	5
Mobility (assessed in a separate cage)	
Normal	0
Abnormal gait	1
Paddling (give analgesia)	2
Reluctance to stand up on hind legs (give analgesia)	3
Absence of load bearing (give analgesia)	5
Body weight (compared to an age-matched control)	
Normal (within 10% of age matched control)	0
>10 % weight loss (ensure food on cage floor)	2
>15% (give soft, palatable food)	5
Mouse Grimace Scale	
Not present	0
Mild	1
Moderate - give analgesia	2
Arthritic paw score (see table right)	
Normal	0
Total 1 - 3	1
Total 4 – 7	2
Total 8– 10	3
Total 11 - 12	4
Time since first signs of arthritis were detectable	
0-1 week	0
1-2 weeks	1
2-4 weeks	2
>4 weeks	4
Total score	
Sum all parameters	/25

Table 2. 2: Scoring system for arthritic paw scores

Arthritic paw score	
No swelling	0
Discolouration and/or mild deformity of <2 joints	1
Mild deformity affecting phalanges/metatarsals	2
Moderate deformity affecting multiple joints	3

2.2 Micro-CT imaging

Tibias, front limbs and spines were excised from mice post mortem and fixed in 4% formalin before being stored in 70% ethanol. A Skyscanner 1172 (Bruker Micro-CT, Belgium) was used to obtain X-ray images of the samples with source voltage and current settings set to 60 kV and 167 µA, respectively. Projections were taken after every 0.45° rotation at an exposure of 580 ms. Volumetric reconstruction by Feldkamp algorithm was performed for each sample using NRecon software (Bruker Micro-CT, Belgium) in order to generate a 3D model. For all reconstructions, a beam hardening correction of 20% was used and ring artefact correction was set to 4. A misalignment compensation within the range of ±5 was accepted, otherwise the sample was rescanned to minimise movement.

2.2.1 Quantitative µCT analysis

Reconstructed models of the tibias and spines could then be analysed using the CT-analyser software (CTan, Bruker Micro-CT, Belgium). CTan allows for the visualisation of the bone in cross-sectional slices. For spines, the 6th lumbar vertebra was chosen, and the region of interest (ROI) was drawn around the vertebral body (Fig 2.1 A-C). For tibias,

1 mm of bone (150 slices) directly under the growth plate in the metaphysis was chosen for analysis due to the high trabecular content. The region of interest (ROI) was drawn around the inner trabecular space for each slice (Fig 2.1 D-F). Upper and lower grey thresholds of 255 and 71 were chosen, respectively. The ROIs were then despeckled and 3D analysis was performed for bone volume/total volume (BV/TV), trabecular thickness (Tb.Th), trabecular number (Tb.N) and trabecular separation (Tb.Sp) with the analysis tools provided with the software. 3D meshes of the tibias were generated using MeshLab software.

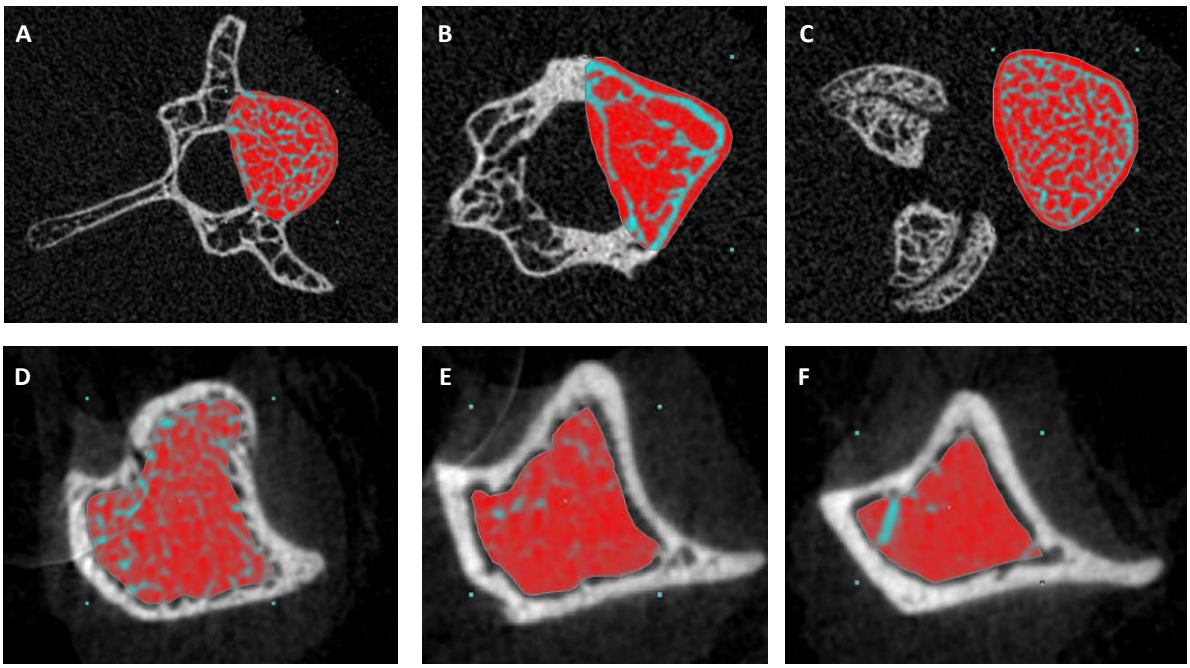

Figure 2. 1: Regions of interest selected for spines and tibias

A-C show cross-sectional images through the spine at the top (A), middle (B) and bottom (C) of the 6th lumbar vertebra. D-F show cross-sectional images through the tibia at the top (D), middle (E) and bottom (F) of the 1 mm section of bone chosen.

2.2.2 Qualitative µCT analysis

Reconstructed models of the front limbs were processed using CTan software (Bruker Micro-CT, Belgium). An upper grey threshold of 255 was used with a lower grey threshold of 100. Each scan was despeckled and processed in order to generate a .ply file which could be loaded onto MeshLab and modified using ambient occlusion. Each sample was scored blind by two independent people. Samples were scored for approximate area affected and erosion scores as shown in Table 2.3 for each region; the wrist, metacarpals and phalanges. Final scores were generated by multiplying area and erosions scores for each region and taking an overall total, an example of which is shown in Table 2.4

Table 2. 3: Criteria for area affected and erosion scores for qualitative scoring of front limbs

Approximate area affected	**0 = none**
	1 = a few, small localised areas
	2 = multiple small-medium areas
	3 = multiple medium-large areas or extensive
	4 = complete decalcification of joint (appears missing)
Erosion score	0 = normal, no signs of erosion
	1 = roughness
	2 = pitting
	3 = full thickness holes

Table 2. 4: Example of calculation of total erosion scores for qualitative scoring of front limbs

	Erosion score	Area affected	Total
Wrist region	3	1	3
Metacarpals	2	3	6
Phalanges	2	2	4
Total			**13**

2.2.3 ImageJ analysis of spines

ImageJ analysis of cross-sectional slices from spines was used as an extra analysis of bone loss. The slice used was determined by defining the top and bottom slices of the 6th lumbar vertebra and selecting the slice directly in the middle of these. The scale was set to 185.5398 pixels = 2 mm. The freehand selection tool was used to draw the first area of interest around the outside perimeter of the vertebra (as indicated by the red line Fig 2.2) and the second area of interest around the inner perimeter of the cortical bone (indicated with the yellow line Fig 2.2). The perimeter and area were recorded for each region of interest, and cortical area was calculated as total area minus inner area.

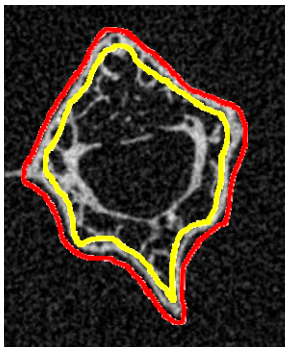

Figure 2. 2: Representative image showing areas of interest in the 6th lumbar vertebra.

The red line indicates the outside perimeter of the vertebra, whilst the yellow line indicates the inner perimeter of the cortical bone.

2.3 Osteoblast cell culture

Osteoblasts were isolated from mouse pup calvaria at 1-2 days old (prior to ossification of the skull) by a serial digestion method. All digestions were performed at 37°C in a shaking water bath and calvaria were washed in PBS after each incubation. Heads were removed after cervical dislocation, calvaria were isolated and ears were collected for genotyping. After washing in sterile PBS, each calvariae underwent an initial digestion with collagenase D (1 mg/ml, Sigma, Gillingham) in serum free Dulbecco's Modified Eagle Medium (DMEM, Sigma, Gillingham) for 10 minutes. The supernatant was removed using a 100 µm cell strainer and discarded. Samples then underwent a second collagenase digestion for 30 minutes. The resulting supernatant was removed and retained (Fraction 1). The calvaria were then digested with EDTA (4 mM) (Sigma, Gillingham, UK) in serum free DMEM for 10 minutes. The supernatant was removed and retained (Fraction 2). A final collagenase digestion was performed for 30 minutes, after which the supernatant was removed and retained (Fraction 3). Fractions 1, 2 and 3 were then combined and

centrifuged for 5 minutes at 1200 rpm. The pellet could then be resuspended in high-glucose DMEM (1% penicillin-streptomycin, 10% fetal calf serum [FCS]) and osteoblasts were plated at a density of 1 x 10^5 cells per well on a six well plate.

2.4 Co-culture

Cell culture methods were employed in order to investigate whether macrophages and fibroblasts communicate GC actions via paracrine signalling. Both direct co-culture techniques and indirect conditioned media assays were utilised for this.

2.4.1 Isolation of synovial fibroblasts

Fibroblasts were isolated from the synovial lining of tibias and paws of seven-week old mice. Front and hind limbs were dissected post mortem and sterilised in 70% ethanol after removal of skin. All steps after this were carried out in a tissue culture hood. Nails, fat, muscle and tendons were removed from the limbs. Tibias and both front and hind paws were isolated from each mouse. Individual bones of the paw were dissected apart to optimally expose the synovium on the metacarpals and carpal bones (metatarsal and tarsal bones for hind paws). Care was taken not to break any bones in order to avoid contamination by cells of the bone marrow compartment. The bones were then incubated at 37°C in enzymatic medium no.1 (DMEM containing 2% FCS, collagenase D [100 mg/ml, Sigma, Gillingham] and DNAse I [100mg/ml, Sigma, Gillingham]) for 45 minutes. The supernatant was discarded and the bones were then incubated at 37°C in enzymatic medium no.2 (DMEM containing 2% FCS, collagenase/dispase [100 mg/ml, Sigma, Gilligham] and DNAse I [100 mg/ml, Sigma, Gillingham]) for 30 minutes. EDTA (0.5M)

was added to the media and incubated for a further 5 minutes. The supernatant was filtered through a 70 µm cell strainer, centrifuged at 1200 rpm for 5 minutes and resuspended in high glucose DMEM (10%FCS, 5% pen/strep). Cells were plated onto a T25 cm^3 flask and allowed to become confluent. Cells were passaged 3 times before use to remove any macrophages.

2.4.2 Isolation of peritoneal macrophages

Tissue resident macrophages were extracted from mice via peritoneal lavage. After cervical dislocation, the skin of the mouse was gently removed to expose the lining of the peritoneal cavity. 10 ml of ice cold EDTA/PBS solution (2mM, sterile) was prepared for each mouse in a 20 ml syringe. 8 ml of the EDTA/PBS solution was injected into the peritoneum via the gonadal fat pad using a 0.5 mm x 25 mm 25 gauge hypodermic needle (B. Braun, Sheffield, UK). Care was taken throughout so as not to puncture any internal organs. The peritoneum was gently massaged to dislodge cells into the solution. A 1.1 mm x 50 mm 19 gauge hypodermic needle (Terumo, Birmingham, UK) needle was then used to inject the final 2 ml of EDTA/PBS solution into the peritoneal cavity. This was syringed in and out several times in order to further dislodge any cells still attached to the peritoneum. The fluid was then removed, avoiding any fat which may block the needle, and approximately 7-8 ml of the solution was recovered. The solution was centrifuged at 1200 rpm for 10 minutes and resuspended in Roswell Park Memorial Institute (RPMI, Sigma, Gillingham) 1640 medium (10% FCS, 1% pen/strep). Cells were plated at a density of 500,000 cells per ml.

2.4.3 Treatment of macrophage and FLS co-cultures

After being passaged 3 times, FLS from 11βKO mice were plated onto a 6 well plate. Peritoneal macrophages from WT animals were plated onto Nunc™ Polycarbonate Cell Culture Inserts (ThermoFisher, Paisley, UK) with a pore size of 3 μm and inserted into three of the wells. High glucose DMEM (10% FCS, 1% pen/strep) was supplemented with either 11-DHC (1000 nmol/L) or corticosterone (1000 nmol/L) in each well for 48 hours. Treatments were repeated in wells containing 11βKO FLS with no inserts as a control (Fig 2.3). After 48 hours, cells were lysed and RNA isolated.

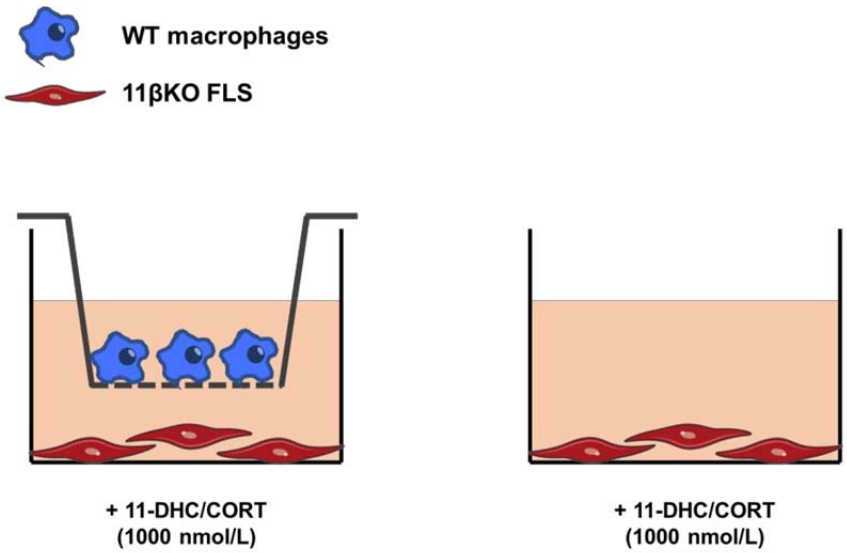

Figure 2. 3: The set-up of the co-culture experiments using Cell Culture Inserts

KO FLS are cultured in wells with the WT macrophages sitting on top in inserts and treated with either active corticosterone or inactive 11-DHC.

2.4.4 Conditioned media experiments

FLS and macrophages from both WT and 11βKO mice were isolated for conditioned media experiments. FLS from both genotypes were treated with either normal

unsupplemented media (con) or media supplemented with 1000 nmol/L 11-DHC for 48 hours, after which the conditioned media was removed and frozen at -80°C. Macrophages cultured from 11βKO animals were then treated with 200 µl (per ml) of FLS conditioned media for 24 hours (Fig 2.4). Media was collected and stored at -80°C for ELISA analysis. Cells were lysed, RNA isolated and GC responsive genes were analysed by qPCR to detect any changes. This experiment was also performed in reverse i.e. 11βKO FLS were treated with conditioned media from WT and 11βKO macrophages.

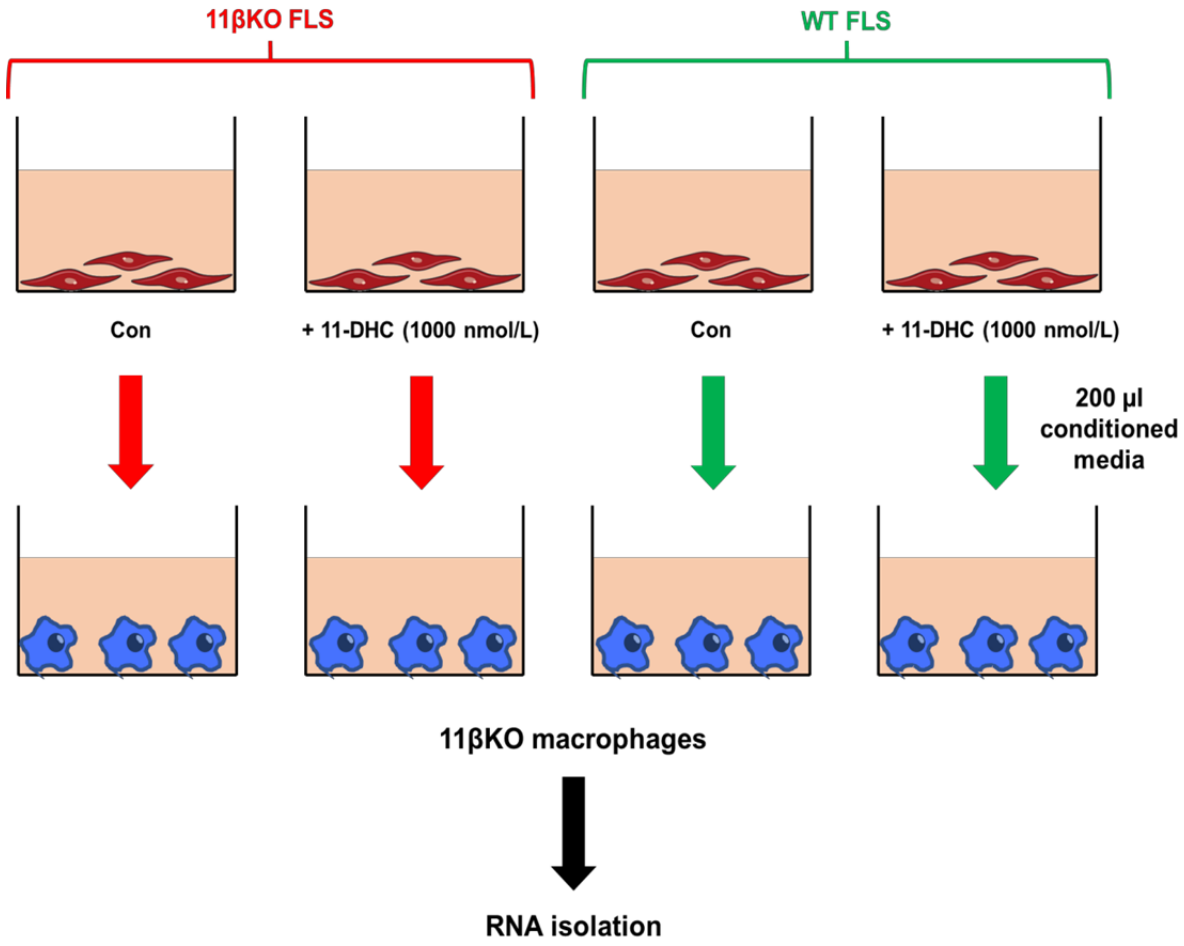

Figure 2. 4: Set up of conditioned media transfer experiments

WT and 11βKO fibroblasts were cultured in the absence or presence of 11-DHC. Media was collected and used to treat 11βKO macrophages. Experiments were also performed in reverse with macrophages providing the conditioned media and FLS being treated

2.5 RNA isolation and analysis

RNA was extracted from tissues and cells, quantified and reverse transcribed to complimentary DNA (cDNA). This cDNA could then be analysed by quantitative PCR (qPCR) to determine the levels of messenger RNA (mRNA) of genes of interest.

2.5.1 RNA isolation

RNA was extracted using the innuPREP RNA Mini Kit 2.0 (AnalytikJena, Jena, Germany). All centrifugation steps were performed at 4°C. To extract RNA from bone, tibias were dissected, removing all soft tissue, and homogenised in liquid nitrogen. Lysis buffer RL was added to the resulting powder and the mixture was centrifuged at 13,000 rpm for 5 minutes. For cells, lysis buffer RL was added directly to the plates followed by scraping of each well. The supernatant from the tissue or cells was transferred to a receiver tube with Spin Filter D. This was centrifuged at 12,000 rpm for 2 minutes to remove genomic DNA. Spin Filter D could then be discarded, and an equal volume of ethanol was added to the filtrate to allow precipitation of the RNA. The sample was transferred to a receiver tube with Spin Filter R and centrifuged at 12,000 rpm for 2 minutes. Spin Filter R binds the RNA and buffers can be flushed through the filter to wash the RNA. First, washing solution HS is added to the filter and centrifuged at 12,000 rpm for 1 minute. After discarding the filtrate, the same can be done with washing solution LS. The filter is then transferred to a fresh receiver tube and centrifuged at 12,000 rpm for 3 minutes in order to dry the RNA. Finally, 30 µl of RNAse free water is added to the filter and centrifuged at 8,000 rpm for 1 minute to elute the purified RNA into an elution tube. RNA concentration could then be quantified using a NanoDrop™ 1000 Spectrophotometer (ThermoFisher, Paisley, UK). All RNA was stored at -80°C prior to use.

2.5.2 Reverse transcription

Unstable RNA was reverse transcribed to the more stable cDNA for gene expression analysis using the High-Capacity cDNA Reverse Transcription Kit (ThermoFisher, Paisley, UK). 700 ng of RNA was added to 10 µl of a master mix of the kit's components (Table 2.5) and made up to 20 µl with RNAse free water. Samples were then run in a GeneAmp® PCR System 2700 (ThermoFisher, Paisley, UK) thermocycler at the pre-optimised conditions: 25°C for 10 minutes, 37°C for 120 minutes and 85°C for 5 minutes followed by 4°C until removal of samples. The resulting cDNA was stored at -20°C prior to use.

Table 2. 5: Volume of each component used per sample in reverse transcription master mix

Kit component	Quantity (µl) per sample
10x RT buffer	2.0
25x dNTP Mix	0.8
10x RT Random Primers	2.0
Multiscribe™ Reverse Transcriptase	1.0
RNAse free water	7.2

2.5.3 Quantitative real-time PCR (qPCR)

Real-time PCR utilises a fluorogenic probe in combination with specific primers to quantify the presence of a gene of interest. The TaqMan probe consists of a fluorescent molecule at the 5’ end and a quencher which inhibits the fluorescent signal at the 3’ end. Briefly, once the double-stranded DNA has been denatured to a single-stranded DNA template during the first reaction of the PCR process, the annealing step can occur allowing the probe and primers to bind to the gene of interest. During extension, the Taq DNA polymerase synthesises a new strand of DNA. Once it reaches the probe, the polymerase will utilise its 5’ exonuclease activity to cleave the fluorescent dye, releasing it from the inhibitory action of the quencher (Fig 2.5). Real-time PCR detects the level of fluorescence, which is directly proportional to the amount of the gene of interest. The amount of cycles required for the fluorescent signal to surpass the threshold is known as the cycle threshold (CT) value.

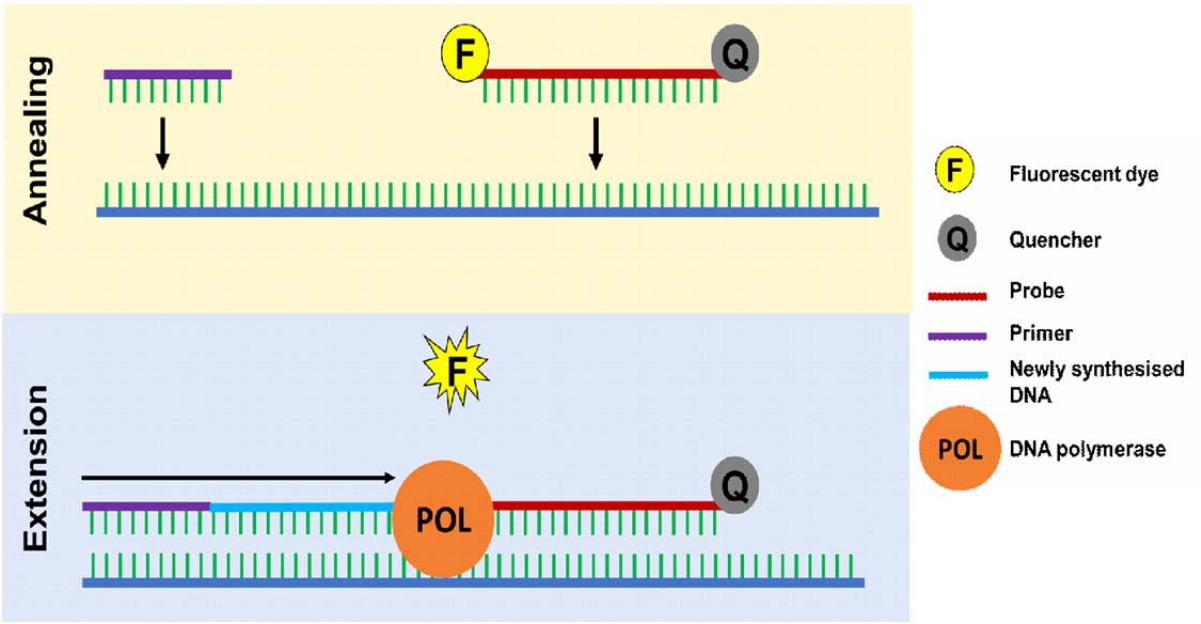

Figure 2. 5: How Taqman real-time PCR works

The Taqman probe consists of a quencher which inhibits the fluorescence of the dye. Upon binding to the gene of interest, DNA polymerase can cleave the dye from the quencher and a fluorescent signal is produced.

For each gene of interest, a master mix was prepared consisting of 5 µl SensiFAST™ Probe Lo-ROX (Bioline, Nottingham, UK), 0.5 µl of the specific TaqMan Gene Expression Assay probe (Applied Biosystems, Warrington, UK) and 3.5 µl RNAse free water per sample. 9 µl of the master mix was added to each well of a 96 well plate, followed by 1 µl of cDNA. All samples were added in duplicate. For each gene, a no sample control was added to the plate containing master mix only. For each sample, the housekeeping gene 18S was run as an internal control. The plate was sealed with a film, spun at 1200 rpm for 1 minute, and run on an ABI7500 qPCR machine (Applied Biosystems, Warrington, UK). The PCR program consisted of a pre-cycle step at 95°C for 10 minutes, followed by 95°C for 15 secs and 60°C for 1 minute for a total of 40 cycles. CT values were obtained for each gene, duplicate values were averaged and normalised to 18S (gene of interest

CT – 18S CT) which yielded a value referred to as a ΔCT value. ΔCT values were transformed using the equation $2^{-\Delta CT \times 1000}$ and expressed as arbitrary units (AU).

2.6 ELISA analysis

For analysis of proteins present in a sample, two types of assay were utilised; competitive enzyme immunoassays (EIA) and sandwich enzyme-linked immunosorbent assays (ELISA). To obtain serum from mice, blood was collected by cardiac puncture prior to cervical dislocation and allowed to clot for 30 minutes at room temperature. Blood samples were then centrifuged at 13,000 rpm for 30 minutes, after which serum could be aspirated and stored at -80°C prior to ELISA analysis. For samples obtained from cell culture experiments, media was collected from wells after the treatment period was over and stored at -80°C until required. All samples and standards were assayed in duplicate.

2.6.1 Principles of a sandwich ELISA

To detect the levels of a protein in a sample, a sandwich ELISA can be used. First, a capture antibody specific to the protein of interest is coated on to a microtiter plate. The sample is added, and any target protein present will bind to the capture antibody. After washing off unbound sample, a detection antibody specific to the target protein is added. The detection antibody is typically either bound to biotin or bound directly to the enzyme horseradish peroxidase (HRP). For biotin bound detection antibodies, the HRP is introduced in a separate step conjugated to streptavidin which will bind to the biotin. Finally, a colorimetric substrate for HRP (often tetramethylbenzidine [TMB] is used) can be added which will produce a coloured product proportional to the amount of target

protein present. The assay is stopped with the addition of an acid. The intensity of the colour produced can be compared to standards run alongside the samples, which contain a known concentration of target protein, and thus can be used to quantify sample protein concentrations (Fig 2.6).

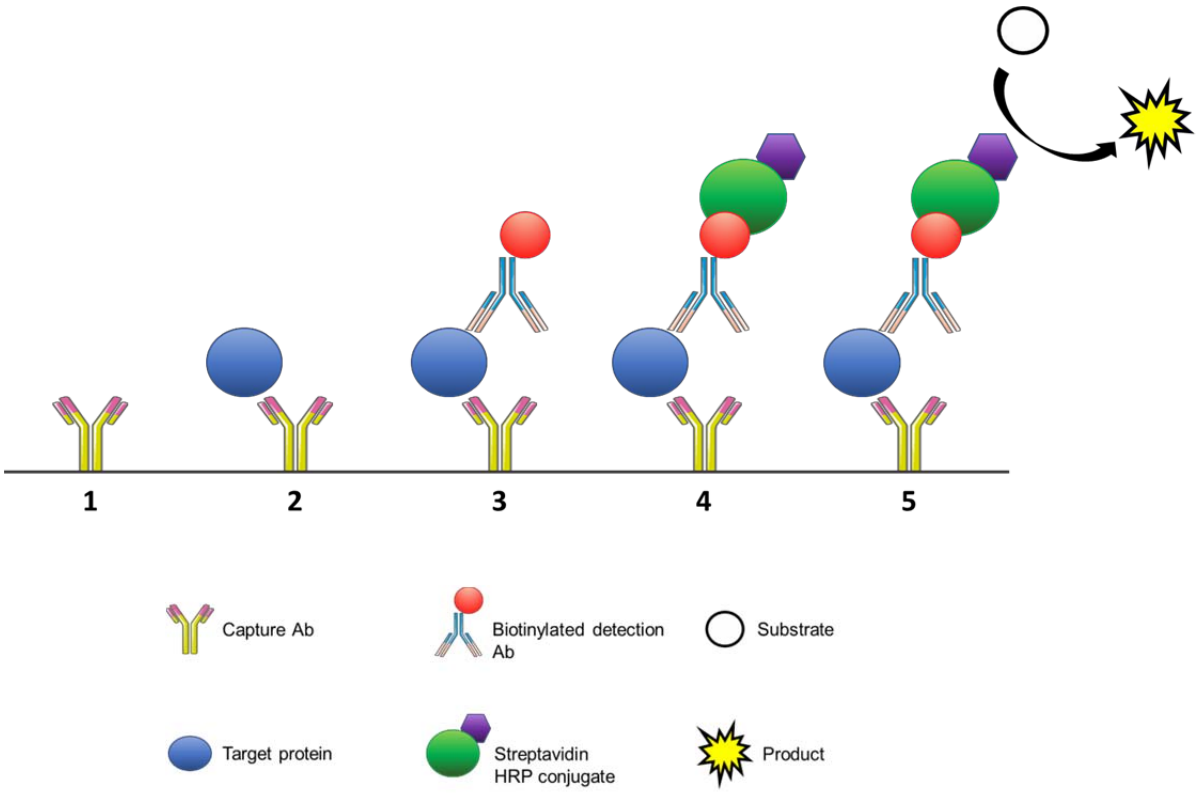

Figure 2. 6: Principles of a sandwich ELISA

A detection Ab coated to the plate recognises the protein of interest. A capture Ab conjugated to biotin also binds the protein, which the streptavidin-HRP conjugate can attach to. Upon addition of substrate, HRP mediates a colour change.

2.6.1.1 Mouse IL-6 ELISA

To measure the levels of the pro-inflammatory cytokine IL-6 in serum samples isolated from mouse blood or in the media collected from conditioned media experiments, a

commercially available mIL-6 ELISA kit (R&D Systems, Abingdon, UK) was used. Serum samples were diluted 1:2 prior to being added to the plate, while media samples were added neat. The microtiter plate provided with the kit is pre-coated with a monoclonal capture antibody specific to mouse IL-6. 50 µl Assay Diluent was added alongside 50 µl of sample or standard. Extra Assay Diluent was added to two wells in place of sample to act as a blank control. Samples were allowed to incubate with the capture antibody for 2 hours at room temperature. An adhesive strip was used to cover the plate during each incubation period. Wells were washed five times with the wash buffer provided and blotted against paper towels to dry. 100 µl of Mouse IL-6 Conjugate (polyclonal antibody specific for mIL-6 conjugated to HRP) was added to each well and incubated for 2 hours at room temperature. The wash step was repeated, following the addition of 100 µl of Substrate Solution (equal volumes of hydrogen peroxide and TMB). The TMB yields a blue colour when in contact with HRP. After a 30 minute incubation in the dark the reaction was stopped by the addition of Stop Solution (hydrochloric acid). The optical density (OD) was determined within 30 minutes using a VICTOR^3 1420 Multilabel counter (PerkinElmer, Llantrisant, UK) plate reader set to 450 nm. An average of the OD values for the duplicates was calculated and the value recorded for the blank control was subtracted from each average value. Standards were plotted against their known concentrations and the equation generated from the line of best fit was used to calculate the concentration of the samples. Samples were multiplied by any dilution factors used. Concentrations were plotted as pg/ml.

2.6.2 Principles of a competitive EIA

Another method often utilised to detect protein levels in a sample is the competitive EIA. A capture antibody specific to the protein of interest is coated onto a microtiter plate. Sample can then be added and the target protein will bind to the capture antibody. This is followed by the addition of the target protein conjugated to biotin. The biotin conjugated protein will compete with protein present in the sample to bind to the specific capture antibodies. Any unbound protein is washed away and streptavidin-conjugated HRP is introduced, which will bind to the biotinylated protein. Upon addition of a colorimetric substance (usually TMB), a colour change will occur in the presence of HRP. The reaction is stopped with the addition of an acid solution. A more intense colour change signifies more biotinylated protein bound to the capture antibody and thus less sample derived protein present. Colour intensity is therefore inversely proportional to the amount of target protein in the sample. This can be compared to standards of known concentration assayed alongside the sample, and target protein concentration can be calculated (Fig 2.7).

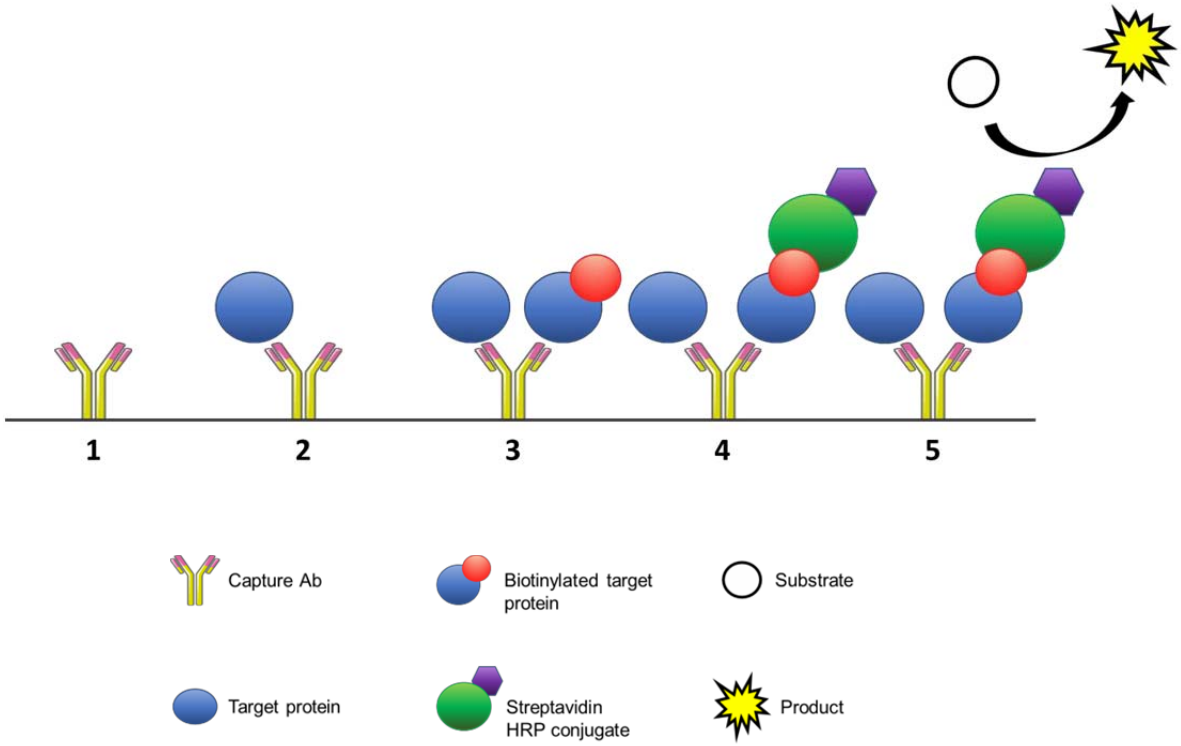

Figure 2. 7: Principles of a competitive EIA

The protein of interest binds to the capture Ab coated to the plate. Protein of interest with biotin attached is then added to compete for the Ab. Streptavdin-HRP conjugate binds the biotinylated protein and colour is produced when substrate comes in contact with HRP.

2.6.2.1 Mouse P1NP EIA

To detect systemic changes in bone formation in serum from mice, the Rat/Mouse P1NP EIA kit (ImmunoDiagnosticSystems, Tyne & Wear, UK) was used. The microtiter plate provided was pre-coated with a capture antibody specific to mouse P1NP. 50 µl of standard or control was added to the relevant wells of the plate. 5 µl of sample was added to each well alongside 45 µl of Sample Diluent, followed by 50 µl of P1NP Biotin. The plate was covered with an adhesive plate sealer and incubated at room temperature for 1 hour on a Titramax 100 microplate shaker (Heidolph, Schwabach, Germany) at approximately 500 rpm. The plate was washed twice with the wash buffer provided and

blotted against paper towels to dry. 150 µl of Enzyme Conjugate (HRP linked avidin) was added to each well and incubated at room temperature for 30 minutes. After repeating the wash step, 150 µl of TMB Substrate was added and this was incubated in the dark for a further 30 minutes at room temperature. 50 µl of Stop Solution (hydrochloric acid) was used to stop the reaction and the microtiter plate was read at 450 nm within 30 minutes of stopping. An average of the OD values for the duplicates was calculated and the value recorded for the blank control was subtracted from each average value. Values were multiplied by 10 to account for the sample dilution. Standards were plotted against their known concentrations and GraphPad Prism software was used to perform a non linear regression analysis to generate a standard curve and interpolate the unknown concentrations. Concentrations were expressed as ng/ml.

2.6.2.2 Mouse corticosterone EIA

Due to the fact that mice are nocturnal animals, their consumption of corticosterone water occurred predominantly at night during their active phase. Thus, to determine the levels of corticosterone in the serum, blood was collected between 11.00 p.m to 1.00 a.m. Serum was isolated as previously described in 2.6 and the Corticosterone Parameter Assay Kit (R&D Systems, Abingdon, UK) was utilised. Approximately 95% of corticosterone is bound by CBP which significantly reduces its bioavailability, thus this kit includes a Pretreatment E (trichloroacetic acid) which precipitates the bound corticosterone, allowing it to be removed from the assay. 50 µl of Pretreatment E was added to 50 µl of sample and incubated for 15 minutes at room temperature. After a centrifugation at 12,000 rpm for 4 minutes, the supernatant was decanted into a fresh tube whilst the precipitate was discarded. The supernatant was diluted 1:10 before use.

50 µl of Corticosterone Primary Antibody solution was coated onto the plate and incubated for 1 hour at room temperature, covered with an adhesive plate sealer. The plate was gently shaken on a microplate reader at approximately 500 rpm during the incubation period. The plate was washed four times using the wash buffer provided and dried by blotting on paper towels. 100 µl of Pretreatment F (buffer) and 50 µl sample, standard or Calibrator Diluent were added to the wells followed by 50 µl Corticosterone Conjugate. The plate was covered and incubated for 2 hours at room temperature with gentle shaking. The plate was washed as before and 200 µl of Substrate Solution was added. After a 30 minute incubation in the dark at room temperature, 100 µl Stop Solution was added and the plate was read on a plate reader set to 450 nm within 30 minutes. Protein concentration was calculated as described in 2.6.2.1 and expressed as ng/ml.

2.6.3 Mouse CTX-1 EIA

CTX-1 is the C-terminal telopeptide released into the blood upon degradation of type 1 collagen, thus it is often used as a serum marker of bone resorption. To measure CTX-1 in serum isolated from the mice, the RatLaps™ (CTX-1) EIA kit (ImmunoDiagnosticSystems, Tyne & Wear, UK) was used.

2.6.3.1 Principle

Although the CTX-1 EIA kit is a competitive assay and follows a similar concept as described with the previous competitive EIAs, the specifics of the assay are slightly different. As opposed to the capture antibody being coated onto the microtiter plate, in this case the plate is coated with streptavidin. A biotinylated target protein can then be

added, which will in turn bind the streptavidin. The sample is then added alongside the capture antibody specific for the target protein. Target protein in the sample and biotinylated target protein will compete for binding with the capture antibody. Sample derived target protein bound to antibody will not be attached to the plate and thus will be washed off. A detection antibody (anti-IgG) conjugated to HRP is added which binds to the capture antibody and any excess unbound antibody is washed off. When the TMB is added, a colour change will occur depending on the amount of HRP-conjugated antibodies still present in the well. This colour change is therefore inversely proportional to the amount of target protein in the sample (Fig 2.8).

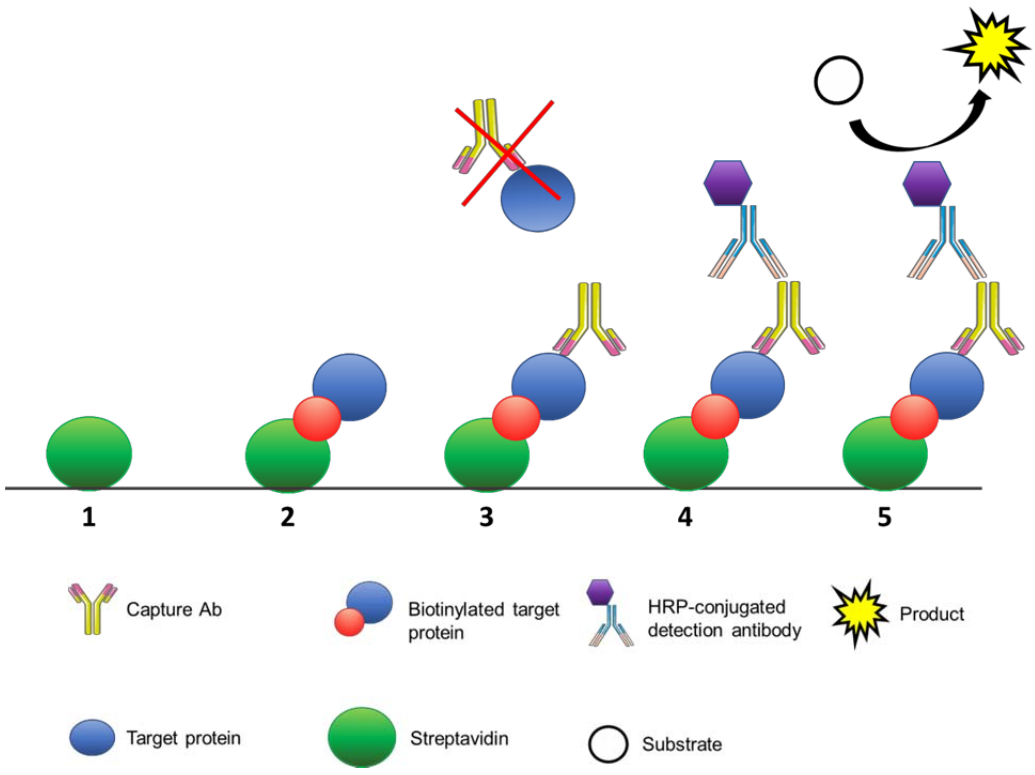

Figure 2. 8: Principle of the CTX-1 EIA

Streptavidin coated on the plate binds to biotinylated target protein. Detection Ab is added following the addition of sample, allowing sample protein and biotinylated protein to compete for Ab binding. Unbound Ab-protein complexes are washed away. A detection Ab conjugated to HRP recognises the capture Ab and produces a colour change on addition of substrate.

2.6.3.2 Method

100 µl of Biotinylated RatLaps antigen is added into a microtiter plate which had been pre-coated with streptavidin. The plate was covered with an adhesive strip and incubated for 30 minutes at room temperature. All wells were washed five times with the wash solution provided and blotted on absorbent paper to dry. 20 µl of each standard, sample or control was pipetted onto the plate, followed by 100 µl of Primary Antibody. This was covered and incubated overnight at 4°C. After repeating the wash step, 100 µl of Peroxidase conjugated anti-IgG was added to each well. Following a 1 hour incubation at room temperature, the plate was washed and 100 µl of Substrate Solution was applied to each well. The plate was incubated for a final 30 minutes at room temperature in the dark prior to the addition of 100 µl Stop Solution (sulfuric acid). Absorbance was measured on a plate reader at 450 nm within 30 minutes and protein concentration was calculated as previously described in 2.6.2.1. Concentrations were expressed as ng/ml.

2.7 11β-HSD1 enzyme activity assay

The enzymatic activity of 11β-HSD1 was determined by quantifying the amount of ^{3}H-11-DHC converted to ^{3}H-corticosterone using thin layer chromatography (TLC). TLC uses a mobile phase and a stationary phase to separate compounds based on their solubility. The stationary phase is the absorbent material that the TLC plate is composed of (typically silica) while the mobile phase is the solvent in the tank the plates are ran in (in this case, chloroform and ethanol). If a compound is more soluble in water, it will move slower up the plate as it favours the stationary phase, whereas less water-soluble compounds will move further up the plate with the mobile phase. The amount of ^{3}H-substrate can be

quantified using a BioScanner which detects the amount of radiation present in a sample, allowing the calculation of the percent of GC conversion during the assay.

2.7.1 Steroid treatment

For ex vivo tissue biopsies, tissues were excised and placed in glass tubes with 500 µl serum free DMEM and 2 µl ^{3}H-11-DHC alongside 0.5 µl of the relevant cold steroid. This was incubated at 37°C for 3 hours. After the incubation, samples were frozen at -20°C until required. For cell assays, cells were plated on a 12 well plate and allowed to become confluent. Once confluent, media was replaced with 1 ml serum free DMEM containing 4 µl ^{3}H-11-DHC and 1 µl cold steroid and incubated at 37°C for 3 hours. Media could then be moved to glass tubes and frozen at -20°C until required.

2.7.2 Thin layer chromatography

In order to quantify GC conversion rates samples were defrosted and TLC was performed. Tissue samples were weighed prior to assay. To extract the steroids from the media, 5 ml dichloromethane is added to each tube and the solution is vortexed before being centrifuged at 1500 rpm for 15 minutes. This separates the solution into an aqueous phase (the media) and an organic phase (the dichloromethane which contains the steroids). The aqueous phase is aspirated and the dichloromethane is evaporated on a Dri-Block® Heater DB100/3 (Techne, Staffordshire, UK) at 50°C with continuous air flow. The steroids can then be resuspended in 70 µl dichloromethane, vortexed and spotted onto a silica TLC plate (Sigma, Gillingham, UK) using a glass Pasteur pipette (VWR, Lutterworth, UK). ^{3}H-steroid controls were also spotted alongside the samples. The plate

is run in a tank containing 184 ml chloroform and 16 ml ethanol for 90 minutes, which allows the steroids to be separated based on their molecular makeup. The plate is then run on a AR-2000 bioscanner (Bioscan, Oxford, UK) to determine the radioactivity of each sample. Percentage steroid conversion was calculated using the counts from both inactive and active steroid peaks (Fig 2.9). From this the conversion rate could be calculated as follows:

Conversion rate = %conversion x (S/T) x (1/P)

In which S = steroid substrate concentration (pmol), T = time (hours), and P = protein concentration (for cells) or weight (for tissues) (mg). Activity was expressed as picomoles of steroid converted per mg of protein per hour (pmol/mg/hr).

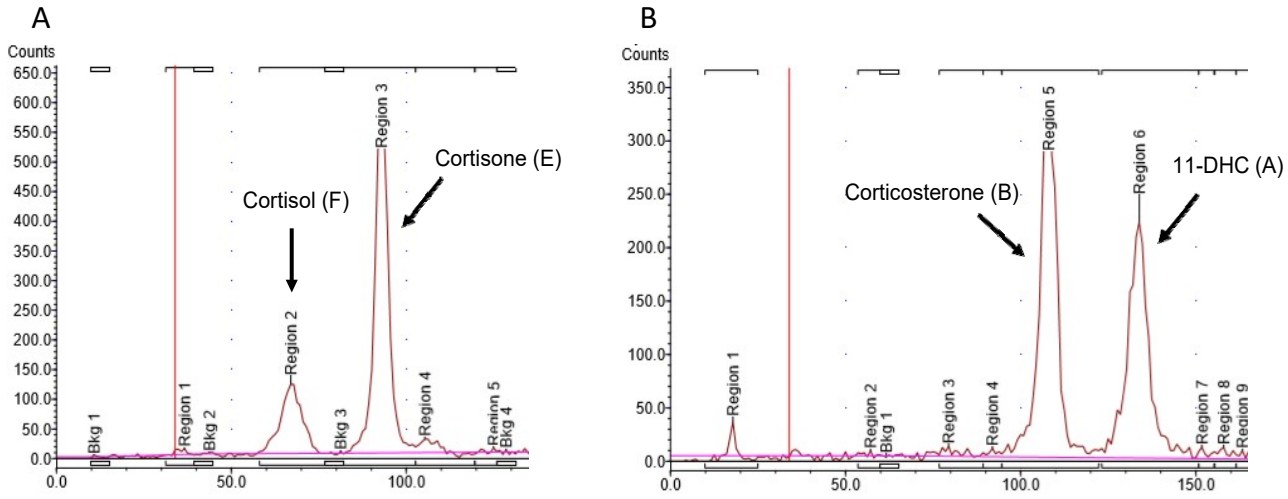

Figure 2. 9: Representative images of steroid peaks

A. Peaks representing human steroids, cortisol (F) and cortisone (E). B. Peaks representing murine steroids, corticosterone (B) and 11-DHC (A).

2.7.3 Protein concentration assay

A DC™ Protein Assay kit (BioRad, Watford, UK) was used to determine the protein concentration in cell cultures used for 11β-HSD1 conversion assays. Once media was removed for TLC analysis, RNase free water was pipetted into each well and plates were stored at -20°C until required. Protein standards were prepared by dissolving bovine serum albumin (BSA) (Sigma, Gillingham, UK) in water at varying concentrations (2 mg/ml, 1.5 mg/ml, 1 mg/ml, 0.5 mg/ml and pure water). Wells containing samples were scraped and 5 µl of each was removed and pipetted onto a 96 well plate alongside 5 µl of each standard. To prepare a working solution of Reagent A*, 20 µl of Reagent S was added per 1 ml of Reagent A. 25 µl Reagent A* and 200 µl Reagent B was then added to each sample or standard and incubated at room temperature for 15 minutes. This produces a colorimetric response which correlates to the concentration of protein present in the sample. Absorbance was read at 750 nm on a plate reader. Concentrations were calculated by plotting the absorbance values of the protein standards and obtaining an equation from the trendline. This equation was applied to the values measured from the samples and results were multiplied by the dilution factor from the volume of RNAse free water initially added to the sample.

2.7.4 Production of ^{3}H-11-DHC

In-house generation of ^{3}H-11-DHC by conversion of ^{3}H-corticosterone was performed using mouse placenta as a source of the GC-inactivating enzyme 11β-HSD2. Around 0.5 – 1 g of placenta was harvested from mice and homogenised in 2 ml potassium chloride solution (0.154 M). Tissue homogenate was centrifuged at 1500 rpm for 10 minutes at 4°C. The supernatant was aliquoted and stored at -80°C until required. 50 µl of

homogenised placenta was then added to 380 µl of potassium phosphate buffer (0.1 M, pH 7.6) with 20 µl of ^{3}H-corticosterone and 50 µl of NAD (10 mM) in a glass tube. Tubes were incubated at 37°C for 3 hours in a shaking water bath. The steroids could then be extracted, and TLC was performed as described previously (section 2.7.2) with cold 11-DHC and corticosterone standards also added to the TLC plate for reference. The plate could then be scanned under UV light to determine the position of ^{3}H-11-DHC. Once established, the silica containing the ^{3}H-11-DHC was scraped into a glass tube with 1 ml ethanol at 4°C overnight to elute the steroid. The steroid was separated from the silica by centrifugation at 2500 rpm for 5 minutes. 5 µl of the resulting supernatant containing ^{3}H-11-DHC was spotted onto a TLC plate and ran on the bioscanner to determine the radioactivity. The solution could be diluted in ethanol to give a radioactivity of 1000 counts/µl. The resulting ^{3}H-11-DHC solution was stored in a fresh glass tube at -20°C when not in use.

2.8 Histology

Tissues were dissected and fixed in 4% formalin before being stored in 70% ethanol at 4°C. Elbows were decalcified in EDTA (0.5 M) prior to embedding. All histology was performed on paraffin embedded sections cut and processed courtesy of the Department of Musculoskeletal Pathology at the Royal Orthopaedic Hospital (ROH). After staining, all sections were stored in the dark to avoid bleaching of stain.

2.8.1 Pannus analysis

Haematoxylin and Eosin (H&E) staining of sections was carried out by the Department of Musculoskeletal Pathology at the ROH. Briefly, liver and elbow joint sections were dewaxed in two changes of xylene (2x 5 minutes) before being rehydrated through graded alcohol concentrations (100%, 100%, 95%, 70%). Sections were then washed in running tap water before being immersed in Mayer's Haematoxylin solution for 1 minute to stain the nuclei of cells, followed by a wash in running tap water. Upon addition of the alkaline solution Scott's tap water substitute, the nuclei will turn a blue colour. Following a further wash in running tap water, sections were stained in eosin solution for 2 minutes, which stains the cytoplasm pink. After a final wash in running tap water, sections were dehydrated through graded alcohol concentrations (70%, 95%, 100%, 100%) and cleared in xylene (2x 5 minutes). DPX was used to mount the slides. To quantify the degree of pannus invasion in the elbow joints, ImageJ software was used. Using the freehand selection tool a line was drawn around the pannus and the area was measured. This was then repeated to get the total area of the joint. Pannus invasion was calculated as the ratio of pannus area to total area and expressed as arbitrary units (AU).

2.8.2 TRAP staining of osteoclasts

TRAP is a commonly used histochemical marker to stain for the presence of osteoclasts. In order to visualise osteoclasts in the pannus of elbow joints, the sections were first dewaxed in two changes of xylene for 5 minutes each and rehydrated through decreasing concentrations of alcohol (100%, 100%, 90% and 70%) for 1 minute each. After a thorough wash in distilled water, sections were incubated in pre-warmed TRAP staining solution consisting of TRAP buffer (pH4.7-5.0, Table 2.6), Fast Red Violet LB Salt (0.5

mg/ml), and Naphthol AS-MX phosphate substrate mix (0.5 ml per 100 ml buffer, Table 2.7) at 37°C for 2 hours. Sections were rinsed in distilled water and dehydrated quickly through increasing concentrations of alcohol (70%, 90% and 100%) for no more than 5 seconds each. Sections were cleared in xylene for 1 minute before being mounted using Immu-Mount (ThermoScientific, Pittsburgh, USA) aqueous mounting medium. Osteoclasts can then be visualised under a microscope stained red. Osteoclast numbers at the head of the joint were counted and an average was taken amongst the different genotypes.

Table 2. 6: Components used to make up 1L TRAP buffer

TRAP buffer components	Amount per litre
Sodium Acetate Anhydrous	9.2 g
L+ Tartaric Acid	11.4 g
Glacial Acetic Acid	2.8 ml
Distilled water	997 ml

Table 2. 7: Components used to make up 1ml Naphthol AS-MX phosphate substrate mix

Naphthol AS-MX Phosphate Substrate Mix	Amount per ml
Naphthol AS-MX phosphate	20 mg
Ethylene glycol monoethyl ether	1 ml

2.8.3 Safranin O staining of cartilage

Safranin O is a stain which binds proteoglycans and thus can be used to detect articular depletion of collagen in tissues. Elbow sections were first dewaxed in two changes of xylene for 5 minutes each and rehydrated in decreasing alcohol concentrations; two changes of 100% alcohol for 3 minutes each, followed by 3 minutes in 95% and 2 minutes in 70%. Sections were rinsed in running water before being counterstained with Lillie Mayer's Haematoxylin (Sigma, Gillingham, UK) for 1 minute to stain nuclei present in the tissue. Excess haematoxylin was washed off in running water. Sections were then counterstained in 0.02% Fast Green (FCF) solution (Sigma, Gillingham, UK) for 3 minutes to stain the surrounding bones. After a quick rinse in 1% acetic acid solution (10 – 30 seconds), sections were incubated in 0.1% Safranin O solution (Sigma, Gillingham) for 5 minutes. Sections were then rinsed in running water to remove excess stain and dehydrated through increasing concentrations of alcohol, specifically 2 minutes in 70%, and two changes in 100% for 3 minutes each. Finally, sections were cleared in two changes of xylene (5 minutes each) prior to mounting in DPX (Sigma, Gillingham, UK). Cartilage was stained red, with the intensity of the staining being proportional to the amount of proteoglycan present in the cartilage. Analysis of cartilage stain was performed using ImageJ software. To determine the total cartilage volume of the joint, the freehand selection tool was used to draw around the total area of the joint and the cartilage area (Fig 2.10 A and B, respectively). Area measurements from these regions of interest were used to calculate the percentage of cartilage area in relation to the total area. An area of cartilage beside the neck of the joint was selected for proteoglycan content measurements, collected by calculating the percentage of intense stain (Fig 2.10 E) to

total stain area (Fig 2.10 D), and proteoglycan loss measurements by calculating the percentage of unstained cartilage (Fig 2.10 F) to total cartilage area.

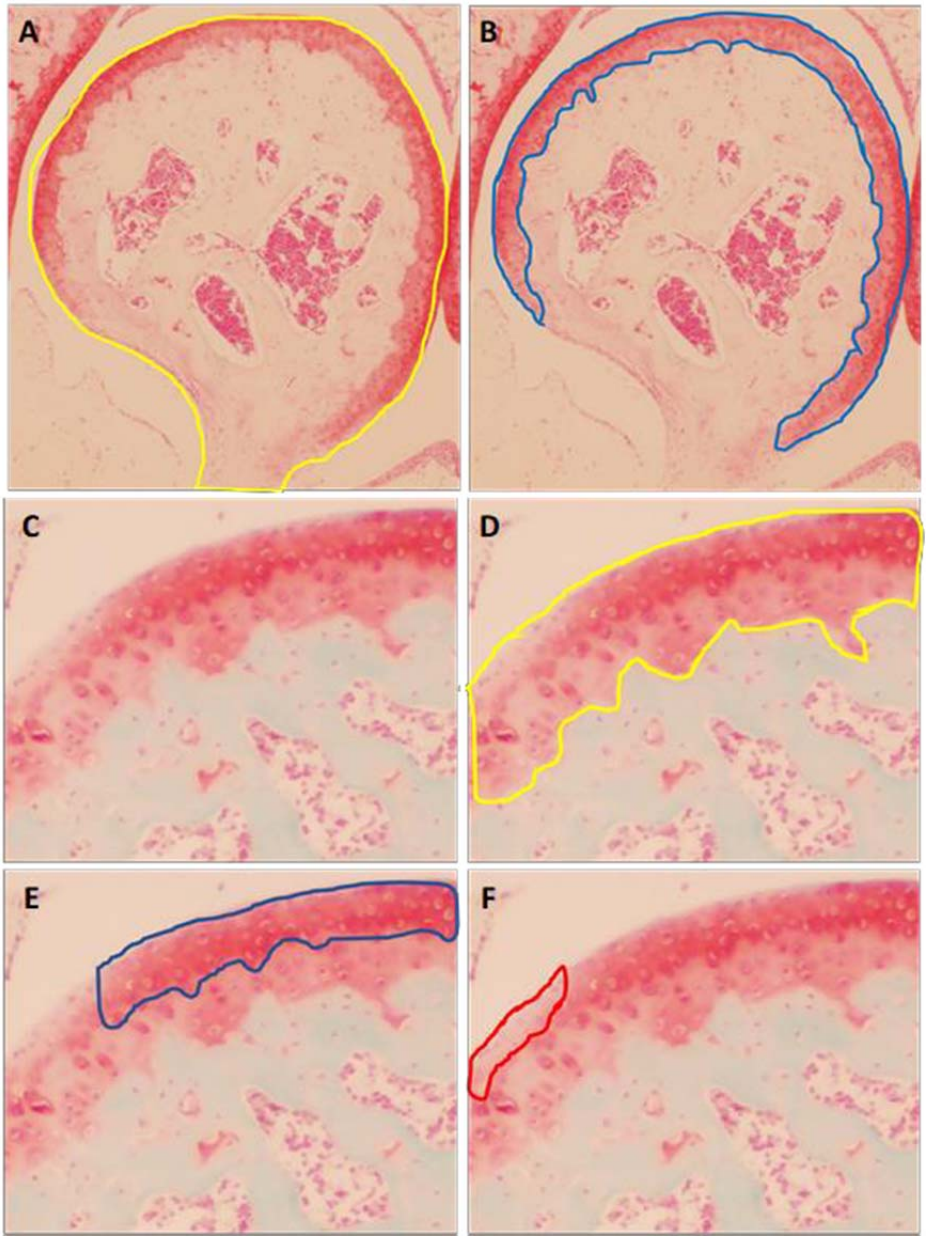

Figure 2. 10: Representative images of safranin O analysis of cartilage

Area of interest drawn around A. total joint area and B. cartilage area. C. the area of cartilage selected for analysis with areas of interest drawn on for D. total cartilage area, E. area of intense stain and F. area of stain loss.

2.8.4 Static histomorphometry

Static histomorphometry was carried out by the skelet.AL Skeletal Analysis Laboratories (Sheffield, UK). In brief, spines were dissected from mice post mortem and fixed in 4% formalin before being stored in 70% ethanol at 4°C prior to use. Lumbar 3 and 4 were decalcified in EDTA and paraffin embedded. A Leica Microsystems microtome (Leica Microsystems, Milton Keynes, UK) was used to cut 3 μm sections of the vertebrae, which were then stained for the presence of the osteoblasts and osteoclasts with either H&E or TRAP and counterstained with Gill's haematoxylin. The Osteomeasure analysis software (Osteometrics, Decatur, GA, USA) was used to measure the number of osteoblasts and osteoclasts per millimetre on 6.5 mm of the corticoendosteal surfaces, beginning 0.25 mm from the growth plate.

2.9 Statistical analysis

All statistical analysis was performed using GraphPad Prism software (GraphPad, San Diego, USA). All variables were tested for a gaussian distribution and shown to be normally distributed using a Shapiro-Wilk test. To compare between both treatment groups and mouse genotypes a two-way ANOVA was used with a Tukey post hoc analysis. One-way ANOVA with a Tukey's test was used to test for significance between different treatment groups in cell culture experiments when more than two groups were present. When only two treatment groups were being compared an unpaired student t test was conducted. All cell culture experiments had an n=3 and mouse experiments n=6 unless otherwise stated. When the n number was less than 3, statistical analysis was not performed due to the small sample size. * denotes $P \leq 0.05$, ** denotes $P \leq 0.01$ and *** denotes $P \leq 0.001$.

Chapter 3: Examining the interaction between GCs, inflammation and the bone

Sections of the literature review from this chapter have been previously published (2). Data from this chapter have been previously published (281).

3.1 Introduction

Chronic inflammatory polyarthritis is characterised by progressive destruction of the joint, leading to deformity and disability. In addition to the juxta-articular problems associated with chronic inflammatory polyarthritis, systemic inflammation also results in extra-articular complications such as osteoporosis. A longitudinal study showed that at a two year follow up, RA patients had decreased BMD of 0.64%, 0.77% and 0.29% in the femoral neck, hip and spine, respectively (285). However, the contribution of disease to bone loss is often confounded by the heterogenicity of treatment regimes in patients.

3.1.1 The interaction of GCs with inflammation and bone

The impact of GC treatment on the bone in patients with chronic inflammation can be difficult to separate from the effects of inflammatory bone loss due to the anti-anabolic, catabolic action of GCs on bone metabolism (286). Glucocorticoids induce osteoblast apoptosis and decrease their differentiation, whilst simultaneously increasing the RANKL/OPG ratio favouring osteoclast maturation and activation (see section 1.5.5) (235, 287, 288). The mechanisms of inflammatory bone loss (reviewed in greater detail in section 1.5.7) are mediated by the influence of pro-inflammatory cytokines on the activity of osteoclasts and, to a lesser extent, osteoblasts (252-255, 260). However, GCs potently suppress the production of pro-inflammatory cytokines via the inhibition of transcription factors such as NF-κB and AP-1 (124). Therefore, GCs can have both detrimental actions on the bone by inducing GIO, but also beneficial actions by suppressing inflammatory bone loss (Fig 3.1). Currently, whether the beneficial effects outweigh the negative, or vice versa, is poorly understood.

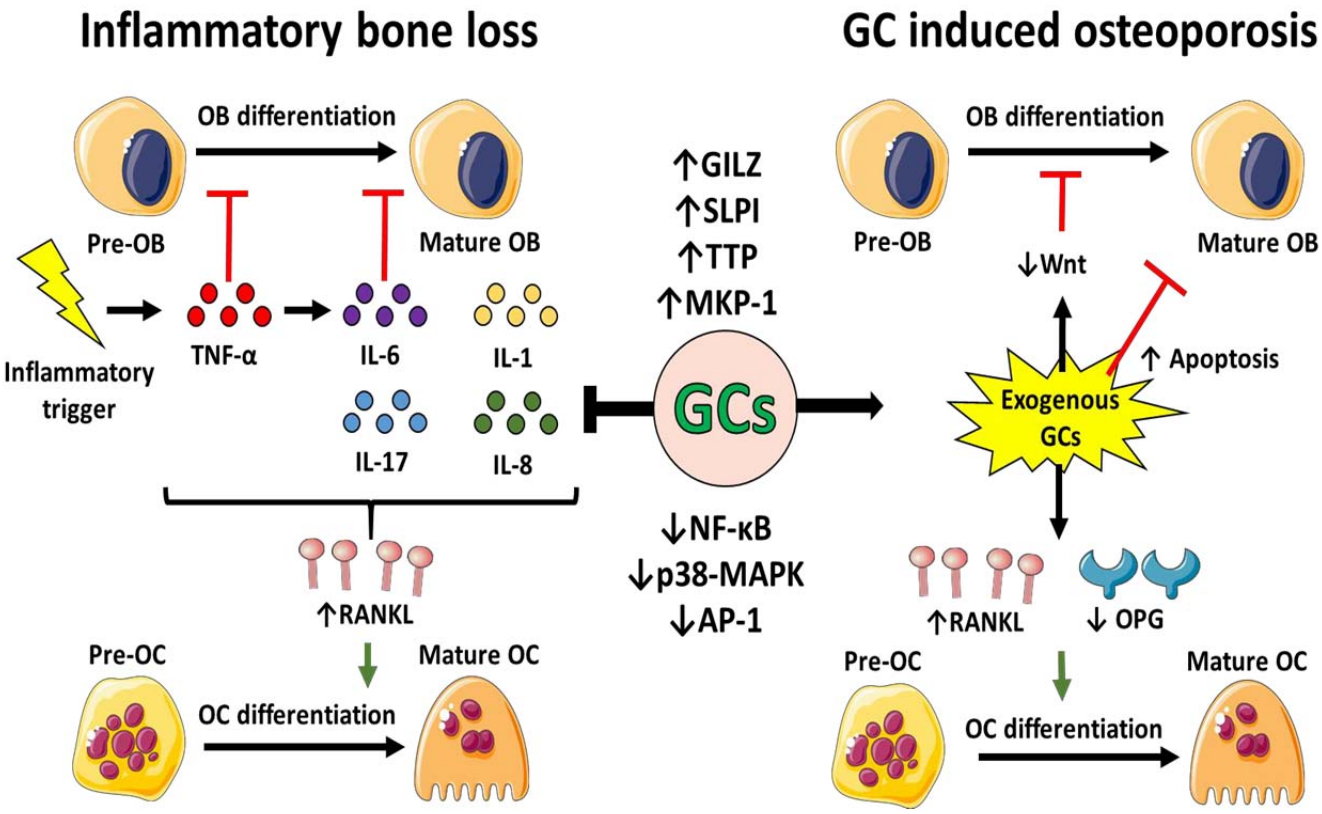

Figure 3. 1: Effects of inflammation and GC therapy on bone remodelling

During inflammation, elevated levels of pro-inflammatory cytokines, such as TNF-α and IL-6, inhibit the differentiation of bone forming osteoblasts from their precursors. These cytokines, along with other pro-inflammatory mediators including IL-1, IL-17 and IL-8, also upregulate the expression of RANKL which binds to RANK on pre-osteoclasts and triggers their differentiation into mature bone resorbing osteoclasts. Overall, bone formation is decreased while bone resorption is increased leading to a net loss of bone. Although GCs suppress inflammation via suppression of pro-inflammatory factors and induction of anti-inflammatory mediators, they can also independently drive bone loss by inhibiting differentiation and inducing apoptosis of osteoblasts whilst increasing osteoclast differentiation by stimulating expression of RANKL and decreasing its decoy receptor OPG.

3.1.2 Clinical studies examining the effects of inflammation and GCs on the bone

Several clinical studies have explored the balance between the beneficial and detrimental effects of GCs on the bone during chronic inflammation, with varying outcomes reported. Güler et al identified no differences in BMD loss in RA patients treated with high dose

GCs for one year compared to other therapies, such as anti-TNF treatment (5). Similarly, Sambrook et al showed that low dose GC therapy in RA did not increase the risk of generalised osteoporosis at the spine and hip (289, 290). Interestingly, Wijbrandts et al reported that patients receiving GCs in combination with anti-TNF therapy had a 2.5% increase in BMD at the femoral neck compared to a 0.7% decrease in BMD in those using anti-TNF alone (291). Taken together, these results suggest that controlling inflammation with GCs may prevent the progression of inflammatory bone loss in RA patients. In contrast, studies by Pereira et al and Varonos et al reported opposing results in juvenile chronic arthritis (JCA) and found that GC treated patients had significantly less trabecular bone and higher risk of vertebral collapse (292, 293). One of these studies revealed that the patients who developed sustained vertebral fractures received a 2.3 times higher dose of daily GCs than those who did not. In addition, vertebral collapse only occurred after a cumulative dose of at least 5 g of prednisolone was administered, suggesting that the effects of GCs on the bone depend upon the dose received (293). Further studies found that GC use was associated with decreased BMD in patients with RA (285, 294). The conflicting results obtained from these studies may stem from a variety of issues. These include differences in severity of inflammation between individuals, differences in disease duration, variations in delivery and dose of GC therapy, and concomitant use of DMARDs. To help address these confounding factors, we utilised the TNF-tg mouse model of chronic inflammatory arthritis to establish the effect of GCs on the bone during chronic inflammation.

3.2 Hypothesis

The therapeutic anti-inflammatory actions of GCs will outweigh their catabolic effects on the bone during chronic inflammation.

3.3 Materials and Methods

3.3.1 Animal experiments

TNF-tg animals were bred as previously mentioned in section 2.1.1. An initial dose response experiment was set up in TNF-tg animals using 50 mg/L or 100 mg/L corticosterone (Cort) drinking water to determine the optimum GC treatment for inflammatory suppression. For the main experiments, four-week old WT and TNF-tg mice were treated with 100 mg/L corticosterone drinking water for three weeks, during which time clinical and arthritic paw scores were evaluated as described in section 2.1.4. Following the treatment period, mice were culled by cervical dislocation following exsanguination by cardiac puncture and tissues were fixed and stored as previously mentioned (section 2.1.4). Adrenals were excised and weighed.

3.3.2 Micro-CT analysis

Formalin fixed tibias and front paws were stored in 70% ethanol prior to being scanned on a Skyscanner 1172 (Bruker Micro-CT, Belgium) (see section 2.2). Tibias were analysed as described in section 2.2.1, whilst front paws were analysed according to section 2.2.2.

3.3.3 ELISA analysis

Blood was isolated from mice by cardiac puncture and allowed to clot for 30 minutes at room temperature. For serum corticosterone analysis 150 µl of 200 mg/L corticosterone was administered to mice via oral gavage 20 minutes before cardiac puncture in order to reduce variability due to the rapid excretion of GCs in the urine. 20 minutes was chosen

as an appropriate time before corticosterone levels started to decline according to Supplementary Fig 1. Serum was separated by centrifuging at 13,000 rpm for 30 minutes and aspirated into a fresh tube to be stored at -80°C until required. Serum levels of corticosterone, IL-6, P1NP and CTX-1 were assessed by ELISA assays as outlined in sections 2.6.2.2, 2.6.1.1, 2.6.2.1 and 2.6.3.2, respectively.

3.3.4 Gene expression analysis

Tibias were excised post mortem and homogenised in a pestle and mortar using liquid nitrogen. RNA was isolated using the innuPREP RNA Mini Kit 2.0 (AnalytikJena, Jena, Germany) as described in section 2.5.1. RNA purity and concentration was assessed using a NanoDrop^{TM} 1000 Spectrophotometer (ThermoFisher, Paisley, UK) and 700 ng RNA was used for the synthesis of cDNA with the High-Capacity cDNA Reverse Transcription Kit (ThermoFisher, Paisley, UK) as outlined in section 2.5.2. Quantitative real time PCR was utilised to measure the expression of genes in the tibias from different mouse groups (see section 2.5.3) using the Taqman probes listed in Supplementary Table 1 (Applied Biosystems).

3.3.5 Histological staining

Livers and front paws for histology were formalin fixed following dissection and stored in 70% ethanol at 4°C. Front paws required decalcification in EDTA (0.5 M) prior to embedding. Samples were embedded and cut courtesy of the Department of Musculoskeletal Pathology at the Royal Orthopaedic Hospital. Haematoxylin and Eosin (H&E) staining of sections was carried out by the Department of Musculoskeletal

Pathology at the ROH as described in section 2.8.1. Pannus invasion into the joint was measured using ImageJ software (see section 2.8.1). The presence of osteoclasts in the joint was detected using TRAP staining solution (section 2.8.2) and the degree of cartilage degradation was assessed using safranin O proteoglycan staining (section 2.8.3).

3.3.6 Statistical analysis

GraphPad Prism software (GraphPad, San Diego, USA) was used to determine statistical significance. Two-way ANOVA analysis was used with a Tukey post hoc analysis to compare between treatment groups and genotypes unless otherwise stated in the figure legend. N numbers are recorded in the relevant figure legend. Statistical significance was determined as $P \leq 0.05$. * denotes $P \leq 0.05$, ** denotes $P \leq 0.01$ and *** denotes $P \leq 0.001$.

3.4 Results

3.4.1 GCs suppress inflammation in the TNF-tg mouse

In order to determine the appropriate dose necessary for the GC corticosterone to suppress inflammation, TNF-tg mice received oral delivery in drinking water at 50 mg/L or 100 mg/L for three weeks, during which time clinical and arthritic paw scores were assessed. Whilst TNF-tg animals treated with 50 mg/L corticosterone showed no difference in either clinical or arthritic paw scores when compared to untreated animals, those treated with 100 mg/L had significant decreases in both scoring parameters. Consequently, corticosterone at 100 mg/L was chosen for further experiments (Fig 3.2).

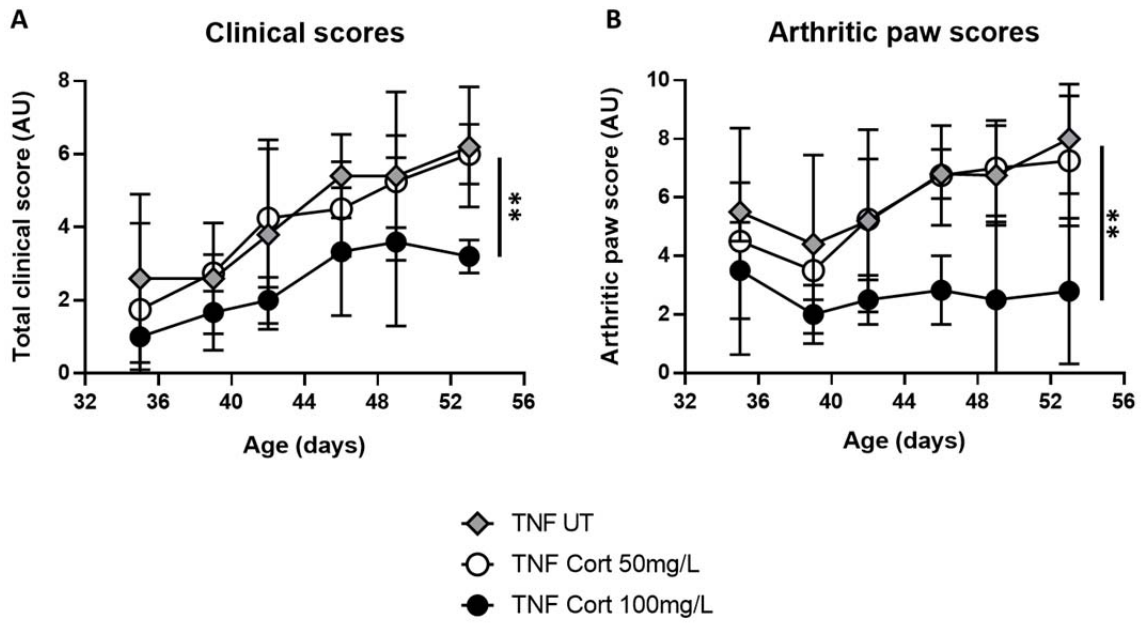

Figure 3. 2: Disease activity with varying doses of GC treatment

(A) Clinical and (B) arthritic paw scores (AU) in TNF-tg mice treated with either 50 mg/L (n=4) or 100 mg/L (n=4) corticosterone drinking water for three weeks compared to untreated TNF-tg (n=5). Scoring data is presented as mean ± SEM and statistical significance was determined using one-way ANOVA with Tukey's multiple comparisons test (** denotes P≤0.01).

In addition to suppressing inflammation, oral delivery of corticosterone at 100 mg/L was sufficient to potently induce parameters characteristic of therapeutic GC use. Namely, serum corticosterone levels were significantly higher (Fig 3.3 A), adrenal weights were suppressed (Fig 3.3 B), mRNA expression of *Gilz* was induced (Fig 3.3 C), and liver histology revealed higher adiposity (Fig 3.3 D) in animals receiving oral corticosterone compared to their untreated counterparts.

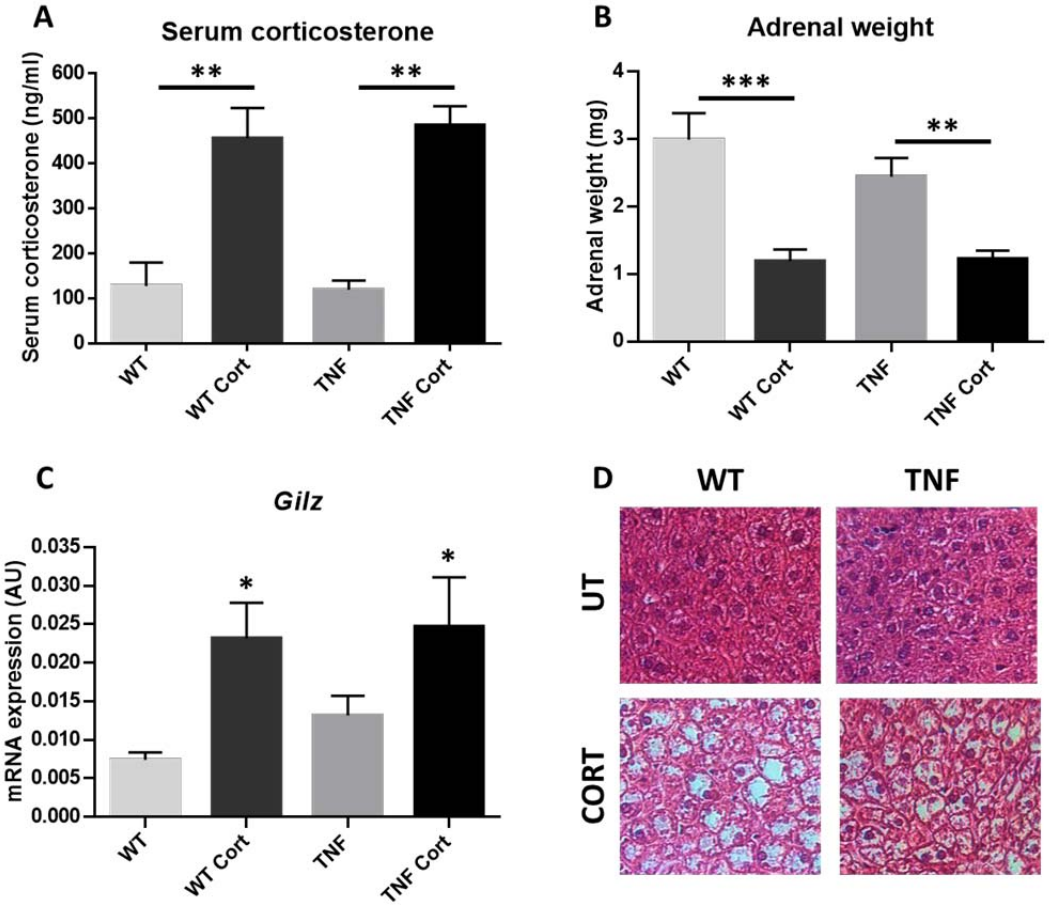

Figure 3. 3: Corticosterone treatment induces parameters characteristic of GC use in WT and TNF-tg animals

(A) Serum corticosterone levels (ng/ml) in WT and TNF-tg mice following oral gavage with 150 µl 200 mg/L corticosterone (n=3 per group) determined by ELISA analysis. (B) Adrenal weights (mg) in WT (n=6) and TNF-tg (n=5) animals treated with control or 100 mg/L corticosterone WT (n=8) and TNF-tg (n=13) in the drinking water for three weeks. (C) mRNA expression of *Gilz* (AU) in control (n=6 per group) and 100 mg/L corticosterone treated (n=5 per group) WT and TNF-tg tibias. (D) Representative images of H&E stains of WT and TNF-tg livers treated with control or 100 mg/L corticosterone in the drinking water for three weeks. Data is presented as mean ± SEM and statistical significance was determined using two-way ANOVA with Tukey's multiple comparisons test (* denotes P≤0.05, ** denotes P≤0.01 and *** denotes P≤0.001).

Having established 100 mg/L as an effective dose to suppress inflammation, we fully assessed their anti-inflammatory properties at this dose relative to animals receiving

vehicle control. WT and TNF-tg animals were treated with 100 mg/L corticosterone or vehicle for three weeks and clinical and arthritic paw scores were recorded. TNF-tg animals exhibited significant swelling and deformity of the paws compared to WT animals. At 53 days a significant decrease in both clinical and arthritic paw scores was observed between untreated and TNF-tg animals receiving oral corticosterone treatment (Clinical scores: TNF-tg 6.33 AU ± 0.5 vs TNF-tg Cort 3.60 AU ± 0.9, P≤0.001; Arthritic paw scores: TNF-tg 7.17 AU ± 0.8 vs TNF-tg Cort 2.20 AU ± 0.8, P≤0.0001) (Fig 3.4).

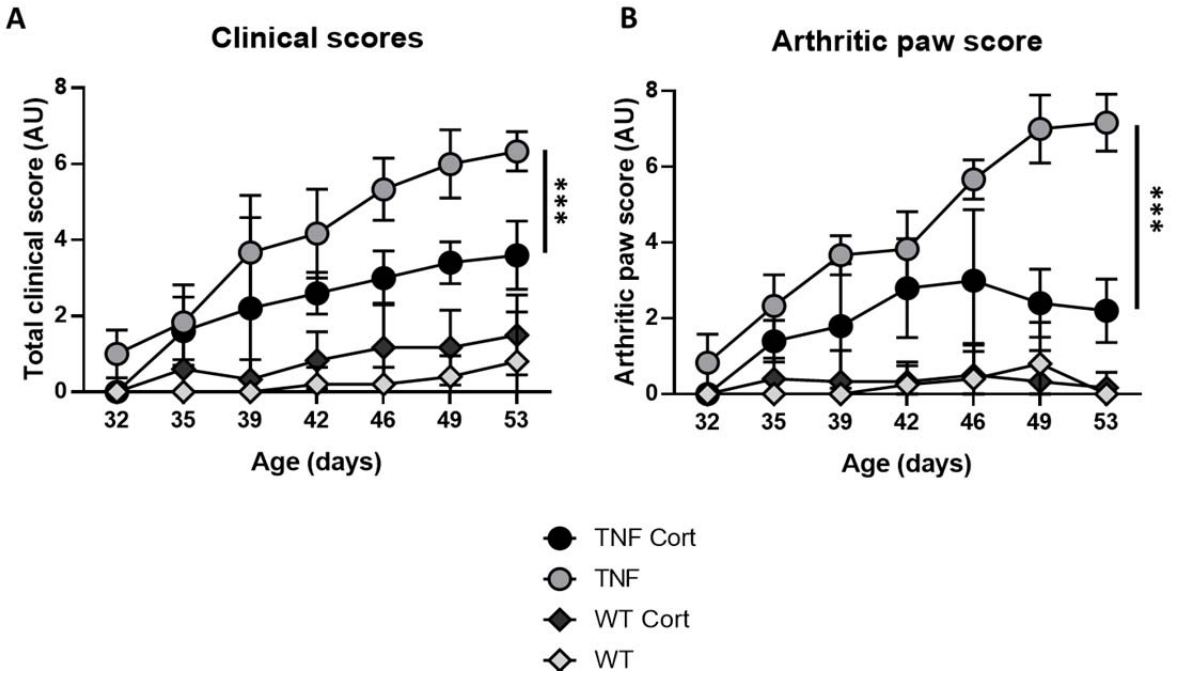

Figure 3. 4: GCs potently suppress markers of disease activity in TNF-tg animals

(A) Clinical scores and (B) arthritic paw scores (AU) of WT and TNF-tg mice receiving vehicle control or 100 mg/L corticosterone in the drinking water for three weeks (n=6 per group). Data is presented as mean ± SEM and statistical significance was determined using two-way ANOVA with Tukey's multiple comparisons test (*** denotes P≤0.001).

The mRNA expression levels of both *mTNF* and *hTNF* were also examined. A non-significant increase in *mTNF* levels was observed in untreated TNF-tg mice, accompanied by a trend towards decreased levels in TNF-tg animals receiving oral corticosterone (Fig

3.5 A). The changes observed in *hTNF* levels appeared more robust, with a significant increase in untreated TNF-tg animals compared to WT mice, and a significant decrease in TNF-tg animals receiving oral corticosterone relative to untreated controls (TNF-tg 0.00007 AU ± 0.00001 vs TNF-tg Cort 0.00002 AU ± 0.00001, P≤0.0001) (Fig 3.5 B). Serum levels of IL-6 showed a significantly higher amount of the pro-inflammatory cytokine in untreated TNF-tg animals compared to WT controls, which was no longer apparent in the TNF-tg mice receiving oral corticosterone (TNF-tg 5.46 ng/ml ± 1.5 vs TNF-tg Cort -2.77 ng/ml ± 0.3, P≤0.001) (Fig 3.5 C). Gene expression levels of *il1* were suppressed to a similar extent in both WT animals and TNF-tg animals receiving oral corticosterone compared to their untreated counterparts (Fig 3.5 D).

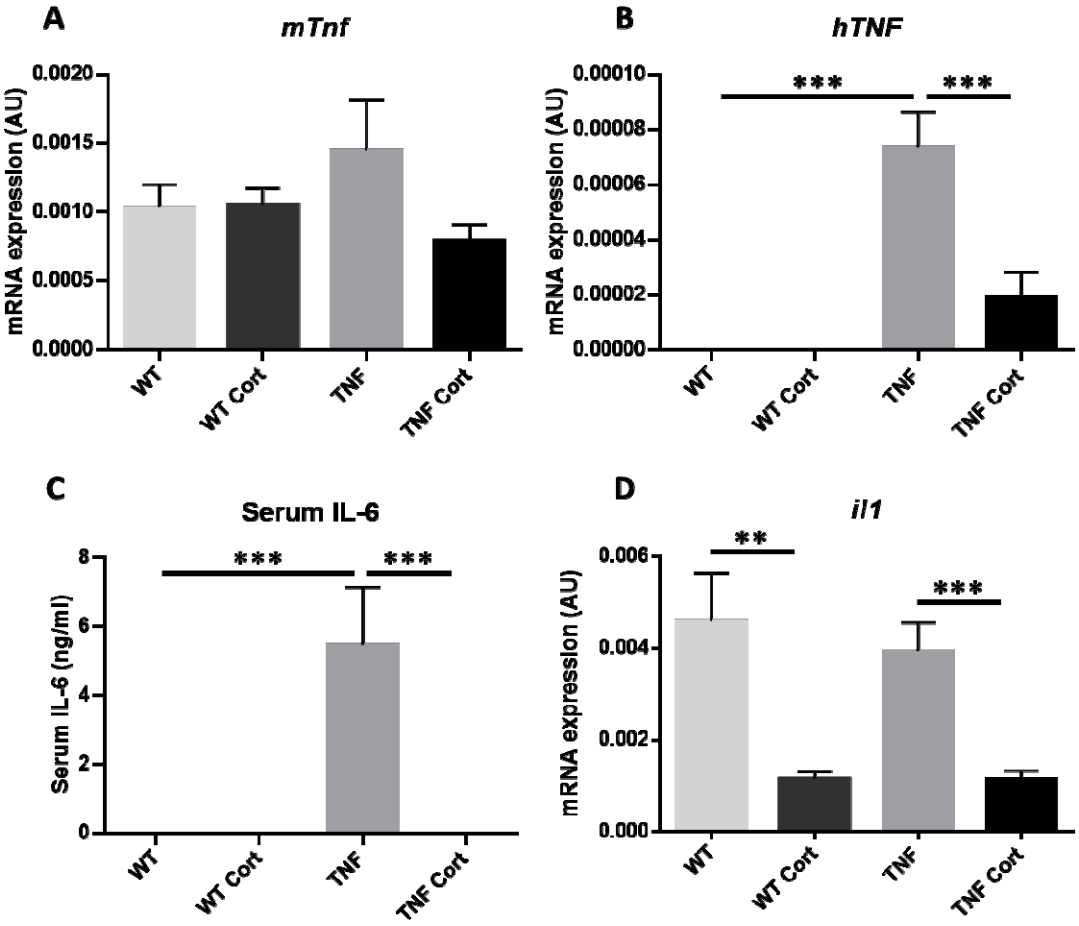

Figure 3. 5: GCs suppress pro-inflammatory cytokines in TNF-tg mice

Gene expression analysis (AU) of (A) *mTnf*, (B) *hTNF* and (D) *il1* in tibias from WT and TNF-tg animals treated with vehicle or 100 mg/L corticosterone water for three weeks (n=6 per group) determined by qPCR. (C) ELISA analysis of serum IL-6 (ng/ml) in WT (n=6) and TNF-tg (n=5) animals receiving vehicle or 100 mg/L corticosterone WT (n=6) and TNF-tg (n=6) in drinking water for three weeks. Data is presented as mean ± SEM and statistical significance was determined using two-way ANOVA with Tukey's multiple comparisons test (** denotes P≤0.01, *** denotes P≤0.001).

Collectively, these data indicate that the treatment regime is sufficient to effectively reduce disease parameters and pro-inflammatory mediators in the TNF-tg model of inflammatory arthritis.

3.4.2 Effects of GCs on joint erosion and synovitis

For a more in-depth analysis of the interaction between GCs and inflammation at the joint, front paws were excised post mortem following GC treatment for μCT and histological analysis. Micro-CT analysis of front paws showed a significant increase in bone erosions in untreated TNF-tg animals compared to WT animals (WT 0.93 AU ± 0.4 vs TNF-tg 13.56 AU ± 1.6, P≤0.0001), indicative of inflammatory bone loss. Following GC treatment TNF-tg mice exhibited a significant decrease in bone erosions compared to their untreated controls (TNF-tg 13.56 AU ± 1.6 vs TNF-tg 5.19 AU ± 1.9, P≤0.0001) (Fig 3.6).

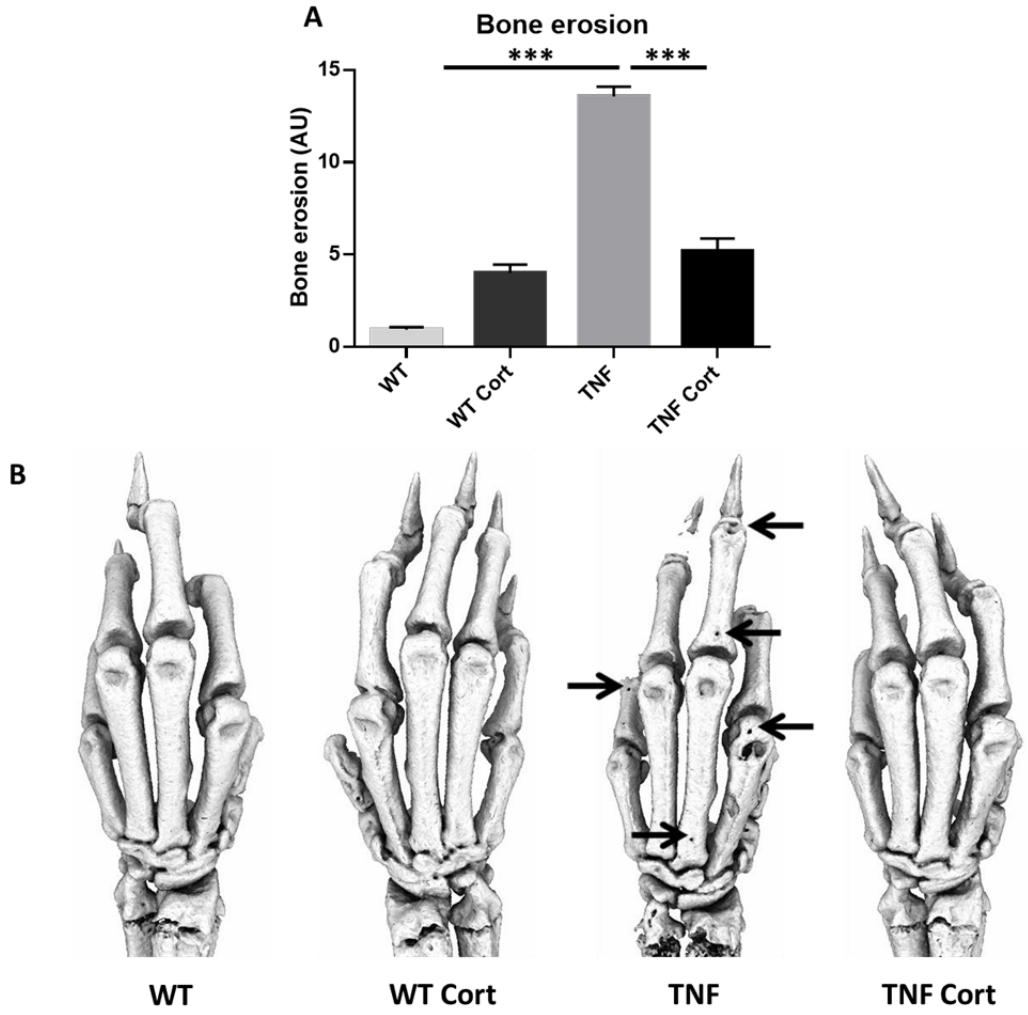

Figure 3. 6: Analysis of bone erosions in WT and TNF-tg animals treated with GCs

(A) Quantification of degree of bone erosions (AU) by micro-CT analysis in WT (n=7) and TNF-tg (n=8) animals receiving vehicle control or 100 mg/L corticosterone WT (n=6) and TNF-tg (n=8) in drinking water for three weeks. (B) Representative images of reconstructed front paw micro-CT scans. Arrows indicate bone erosions. Data is presented as mean ± SEM and statistical significance was determined using two-way ANOVA with Tukey's multiple comparisons test (*** denotes $P \leq 0.001$).

For a more in depth analysis of the mechanism behind the reduction in juxta-articular joint erosions, histological analysis of elbow joints was performed. First, the degree of pannus invasion relative to the total joint area was measured. As predicted a significantly higher degree of pannus invasion was reported in untreated TNF-tg mice compared to WT

animals (WT 0.007 AU ± 0.004 vs TNF-tg 0.146 AU ± 0.03, P≤0.0001), and this was dramatically suppressed upon GC treatment (TNF-tg 0.146 AU ± 0.03 vs TNF-tg Cort 0.021 AU ± 0.01, P≤0.001) (Fig 3.7).

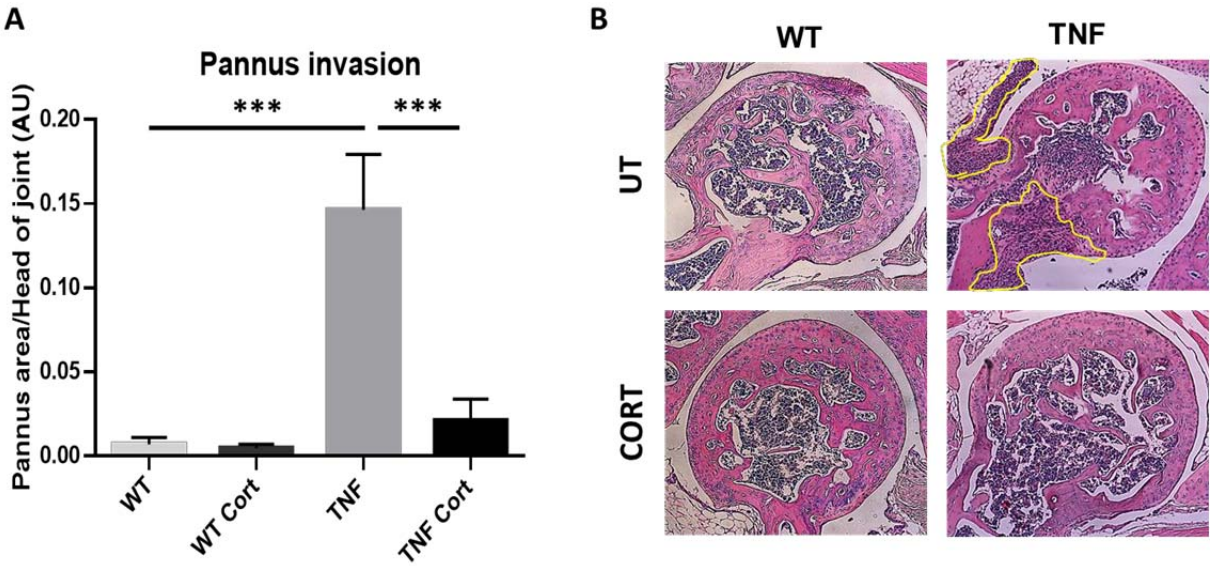

Figure 3. 7: Analysis of pannus formation in WT and TNF-tg animals receiving GCs

(A) ImageJ analysis of pannus invasion (AU) in the elbow joints of WT and TNF-tg mice receiving vehicle or corticosterone drinking water for three weeks (n=6 per group). (B) Representative images of H&E stained elbow sections of vehicle and 100 mg/L corticosterone treated WT and TNF-tg animals. Pannus invasion is highlighted in yellow. Data is presented as mean ± SEM and statistical significance was determined using two-way ANOVA with Tukey's multiple comparisons test (*** denotes P≤0.001).

Gene expression levels of pro-inflammatory chemokines were also assessed in TNF-tg mice. *Ccl2,* which is associated with the recruitment of monocytes and macrophages, was potently upregulated in TNF-tg animals compared to WT controls (WT 0.0003 AU ± 0.00009 vs TNF-tg 0.0024 ± 0.0004, P≤0.001). This upregulation was significantly repressed upon treatment with corticosterone (TNF-tg 0.0024 AU ± 0.0004 vs TNF-tg Cort 0.0004 AU ± 0.0001, P≤0.001), to levels comparable to WT animals (Fig 3.8 A). An

additional monocyte/macrophage chemokine *Cxcl10* was also significantly downregulated in response to GC treatment, in both the WT and TNF-tg groups compared to untreated controls (TNF-tg 0.0009 AU ± 0.0002 vs TNF-tg Cort 0.0002 AU ± 0.00002, P≤0.001) (Fig 3.8 B). *Cxcl2*, a chemokine secreted by macrophages which recruits neutrophils, showed similar trends to *Ccl2*, with an increase in untreated TNF-tg animals compared to WT and a decrease in TNF-tg animals receiving oral corticosterone compared to untreated TNF-tg mice (Fig 3.8 C). These data suggest that the decreased synovitis present in animals receiving oral corticosterone may be in part mediated by a reduction in pro-inflammatory chemokine expression and a subsequent suppression of inflammatory cell infiltration into the joint.

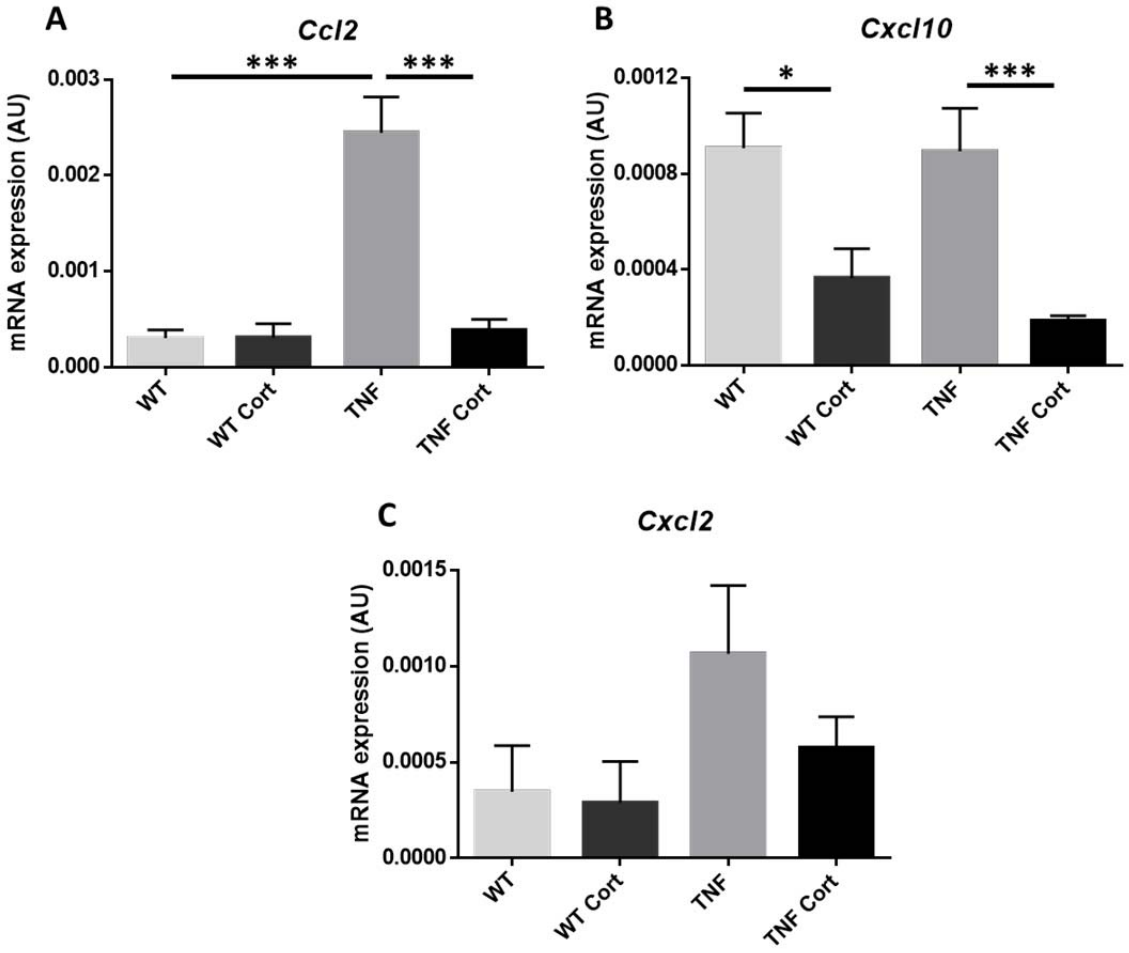

Figure 3. 8: GCs suppress pro-inflammatory chemokines in TNF-tg mice

Gene expression analysis (AU) of (A) *Ccl2,* (B) *Cxcl10* and (C) *Cxcl2* determined by quantitative PCR in tibias from WT (n=4) and TNF-tg (n=6) mice receiving vehicle control or 100 mg/L corticosterone WT (n=5) and TNF-tg (n=6) in drinking water for three weeks. Data is presented as mean ± SEM and statistical significance was determined using two-way ANOVA with Tukey's multiple comparisons test (* denotes P≤0.05, *** denotes P≤0.001).

Parallel to results examining synovitis, osteoclast numbers at the joint exhibited a similar pattern, with increased osteoclast numbers in untreated TNF-tg animals compared to WT mice, and a dramatic reduction in osteoclast numbers in GC treated TNF-tg animals compared to their untreated counterparts (TNF-tg 18 AU ± 3.1 vs TNF-tg Cort 1.5 AU ±

0.3, P≤0.001) (Fig 3.9). Taken together, these data indicate a protective effect of exogenous GC treatment on juxta-articular erosions during chronic inflammation.

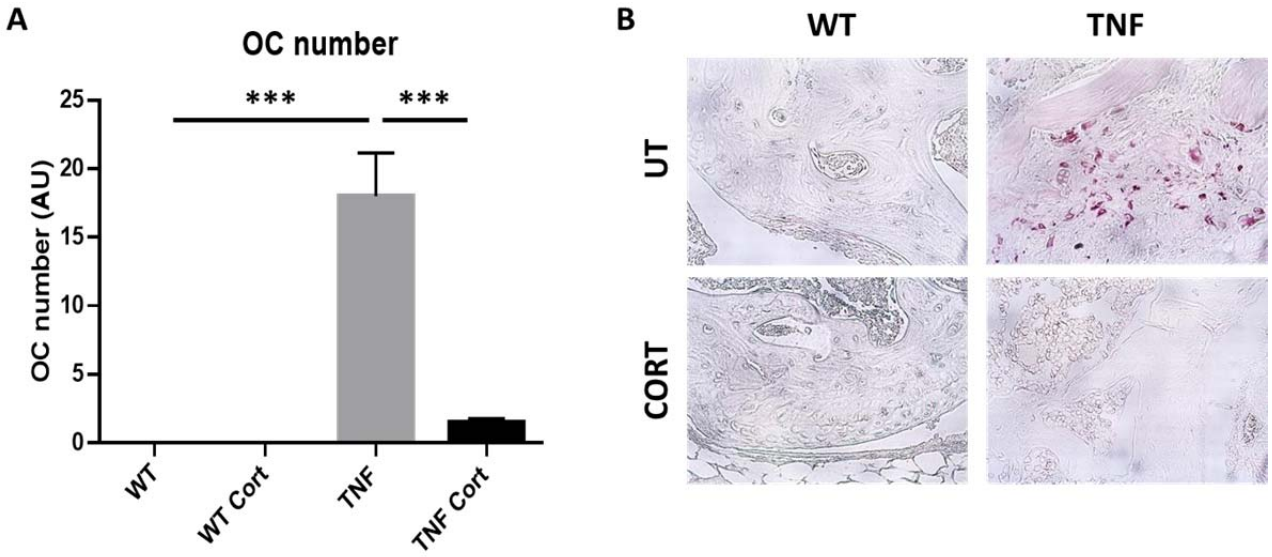

Figure 3. 9: Osteoclast counts at the elbow joints of WT and TNF-tg animals receiving GCs

(A) Osteoclast numbers (AU) at the head of the elbow joints in WT (n=3) and TNF-tg (n=5) mice receiving vehicle or 100 mg/L corticosterone WT (n=3) and TNF-tg (n=4) in drinking water for three weeks determined by TRAP stains. (B) Representative images of TRAP stains in vehicle and 100 mg/L corticosterone treated WT and TNF-tg animals with osteoclasts stained red. Data is presented as mean ± SEM and statistical significance was determined using two-way ANOVA with Tukey's multiple comparisons test (*** denotes P≤0.001).

After investigating the juxta-articular bone phenotype associated with GC treatment in chronic inflammation, examination of the surrounding joint cartilage was performed. Histological analysis of the cartilage with safranin O stain revealed a trend towards decreased total cartilage area in TNF-tg mice compared to the WT group. Although inflammation appeared to reduce the total cartilage area of the joint, corticosterone treatment seemed to have no effect in either WT or TNF-tg animals (Fig 3.10 B). Safranin O staining intensity is directionally proportional to the proteoglycan content of cartilage

(295). Thus, stain intensity was analysed to assess the proportion of proteoglycan-rich areas of the joint by calculating intense stain as a percentage of the total cartilage area. WT animals receiving oral corticosterone showed a significant decrease in intense stain compared to untreated WT animals, indicating that GC treatment has a negative effect on the production of proteoglycan-rich areas of cartilage. Untreated TNF-tg animals also showed a significant decrease in intense staining areas which suggests that inflammation also has a negative impact on proteoglycan content. Interestingly, corticosterone treatment of TNF-tg animals did not produce a protective effect on proteoglycan content, with TNF-tg mice receiving oral corticosterone showing no significant difference in intense stain relative to untreated TNF-tg mice (Fig 3.10 C). Proteoglycan loss was also measured by analysing the areas of total loss of stain compared to total cartilage area. WT animals treated with GCs and untreated TNF-tg animals both showed a trend towards increased areas of proteoglycan loss when compared to WT controls, reinforcing the idea that both GCs and inflammation have a negative impact on proteoglycan levels. Again, TNF-tg animals receiving oral corticosterone showed no protection from proteoglycan loss when compared to untreated controls (Fig 3.10 D). Overall, these results indicate that contrary to the protective effect of GC treatment on juxta-articular bone loss in chronic inflammation, GCs do not rescue the destructive effects of inflammation on the cartilage in the TNF-tg mouse model.

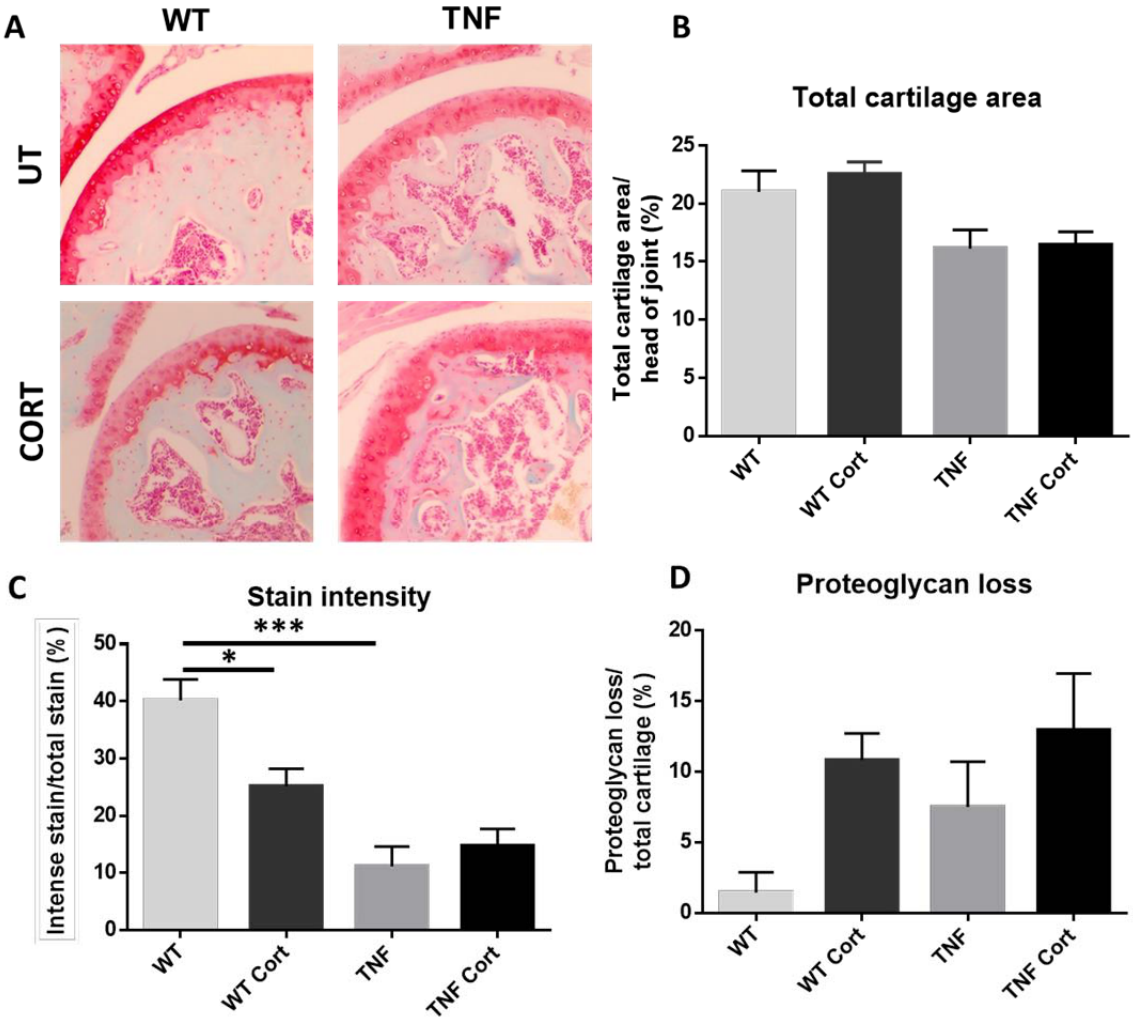

Figure 3. 10: Analysis of the interaction between GCs and inflammation on the cartilage.

(A) Representative images of safranin O stained cartilage in the elbows of vehicle and three weeks of 100 mg/L corticosterone treated WT and TNF-tg animals. (B) Total cartilage area (%) relative to the head of the joint, (C) stain intensity (%) relative to total stain and (D) proteoglycan loss (%) relative to total cartilage in WT (n=5) and TNF-tg (n=6) animals receiving vehicle or 100 mg/L corticosterone WT (n=6) and TNF-tg (n=5) in drinking water for three weeks. Data is presented as mean ± SEM and statistical significance was determined using two-way ANOVA with Tukey's multiple comparisons test (* denotes P≤0.05, *** denotes P≤0.001).

3.4.3 Effects of GCs on systemic bone

Inflammatory arthritis is not just associated with juxta-articular bone loss, but also systemic bone loss at sites distant to inflammation (4). Thus, tibias were excised post mortem from mice following GC treatment and micro-CT was performed to assess trabecular bone parameters. Analysis of bone volume relative to total volume of the trabecular compartment of the tibia revealed a significantly lower percentage of trabecular bone in the tibias of untreated TNF-tg animals compared to WT controls, characteristic of inflammatory bone loss. Interestingly, GC treatment in TNF-tg animals resulted in an abrogation of this reduction in bone loss (TNF-tg 2.19% ± 0.2 vs TNF-tg Cort 4.25% ± 0.2, P≤0.001) (Fig 3.11 B). In regards to trabecular thickness, untreated TNF-tg animals again exhibited a significant reduction in this parameter relative to untreated WT animals. However, GC treatment in TNF-tg mice did not rescue this effect and trabecular thickness remained at a level comparable to untreated TNF-tg mice (Fig 3.11 C). Trabecular number followed a similar pattern to that of the bone volume measurements, with untreated TNF-tg animals having significantly lower numbers of trabeculae compared to WT controls, and GC treatment of TNF-tg mice significantly abrogated this decrease (TNF-tg 0.0004 1/μm ± 0.00004 vs TNF-tg Cort 0.0008 1/μm ± 0.00003, P≤0.001) (Fig 3.11 D). Analysis of trabecular separation showed no significant changes (Fig 3.11 E). Corticosterone treatment did not induce any changes in bone parameters of WT animals after a three week treatment period. These data indicate that GCs have a partial protective effect on systemic bone during chronic inflammation, with increases in bone volume being reflective of increased trabecular number.

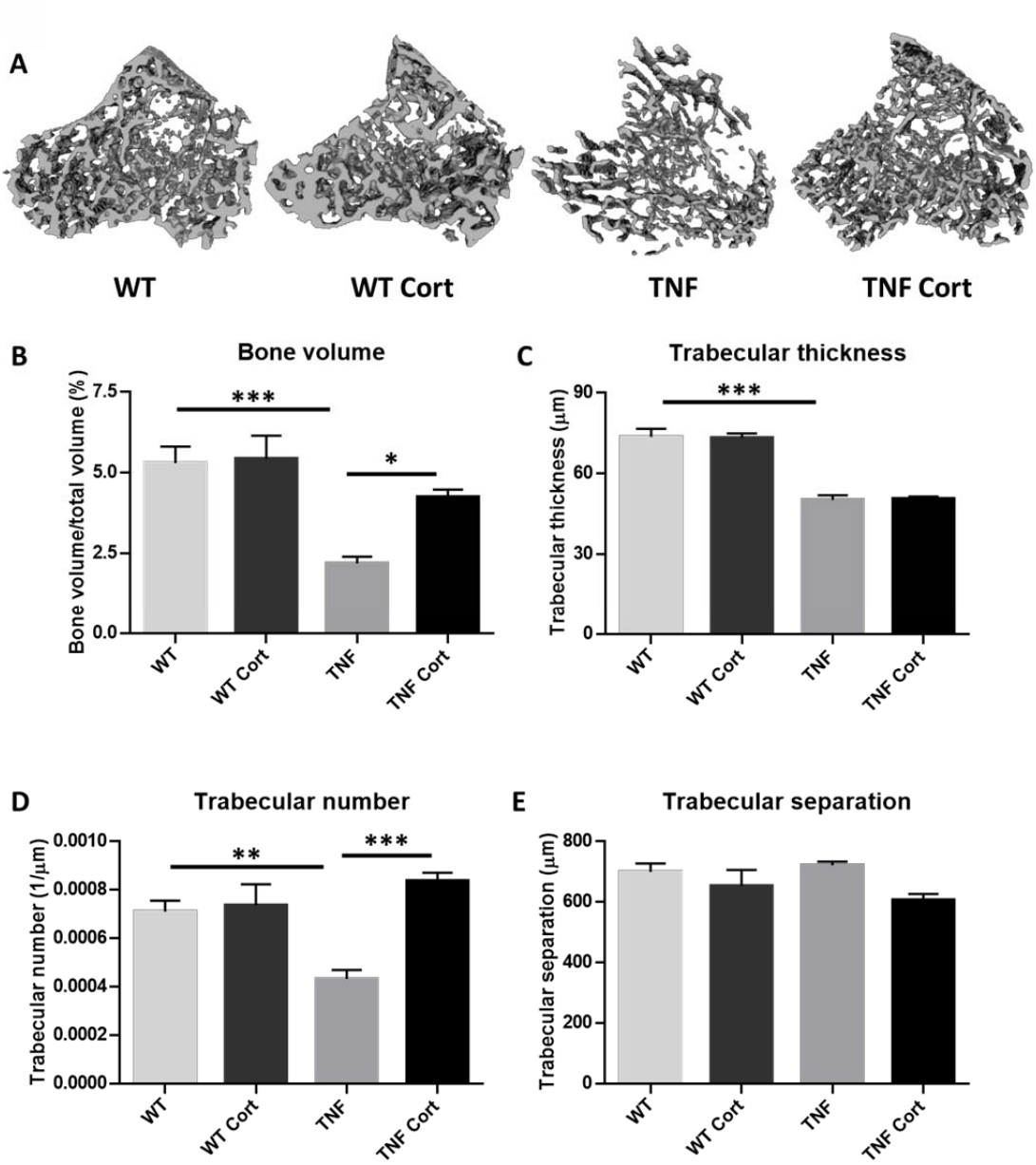

Figure 3. 11: Systemic bone parameters in WT and TNF-tg animals receiving GCs.

(A) Representative images of reconstructed trabecular bone from tibia scans of WT and TNF-tg animals treated for three weeks with vehicle or 100 mg/L corticosterone drinking water. Micro-CT analysis of (B) bone volume (%) relative to total volume, (C) trabecular thickness (µm), (D) trabecular number (1/µm) and (E) trabecular separation (µm) of WT (n=8) and TNF-tg (n=6) animals receiving vehicle or 100 mg/L corticosterone WT (n=6) and TNF-tg (n=6) in drinking water for three weeks. Data is presented as mean ± SEM and statistical significance was determined using two-way ANOVA with Tukey's multiple comparisons test (* denotes P≤0.05, ** denotes P≤0.01 and *** denotes P≤0.001).

Serum was isolated and RNA was extracted from tibias for further analysis of bone formation and resorption markers in WT and TNF-tg animals receiving corticosterone treatment. ELISA analysis of the bone formation marker P1NP in the serum of mice demonstrated that whilst untreated TNF-tg animals had significantly lower levels in relation to untreated WT animals, both groups receiving oral corticosterone had a similar level of suppression of P1NP (WT 494.2 ng/ml ± 61.1 vs WT CORT 31.4 ng/ml ± 7.4, P≤0.001; TNF 269.7 ng/ml ± 38.4 vs TNF-tg CORT 32.3 ng/ml ± 4.2, P≤0.001) (Fig 3.12 A). Gene expression of mature osteoblast markers *Bglap* and *Alpl* showed a similar pattern. Gene expression levels of *Bglap* showed a trend towards reduction in untreated TNF-tg animals and were significantly reduced in both WT animals and TNF-tg animals receiving oral corticosterone compared to their relevant controls, with no significant difference between the corticosterone treatment groups (Fig 3.12 B). *Alpl* levels were significantly reduced in untreated TNF-tg animals compared to WT controls, and WT animals receiving oral corticosterone had dramatically reduced *Alpl* levels compared to controls. No significant difference was noted between untreated TNF-tg animals and TNF-tg animals receiving oral corticosterone, however this is likely due to the marked suppressions in untreated TNF-tg mice already present. Animals administered oral corticosterone had similar levels of *Alpl* suppression in both WT and TNF-tg groups (Fig 3.12 C). Subsequently, expression of genes relating to osteoblast differentiation were examined. Analysis of the major transcription factor associated with osteoblast differentiation *Runx2* and the negative regulator of osteoblast differentiation *Dkk1* showed no significant differences amongst the groups (Fig 3.12 D-E). Analysis of the negative regulator of osteoblast differentiation *Sost* showed a significant upregulation in TNF-tg animals receiving oral corticosterone compared to untreated TNF-tg animals Fig 3.12F).

However, this was not significantly different from WT controls. Together these data suggest that GC suppress numbers of mature osteoblasts and bone formation by osteoblasts. Changes in markers of differentiation remained unchanged, suggesting that this is not mediated by reduced maturation. Despite this, the negative action of GCs on osteoblasts does not appear to mediate bone loss over three weeks in this model.

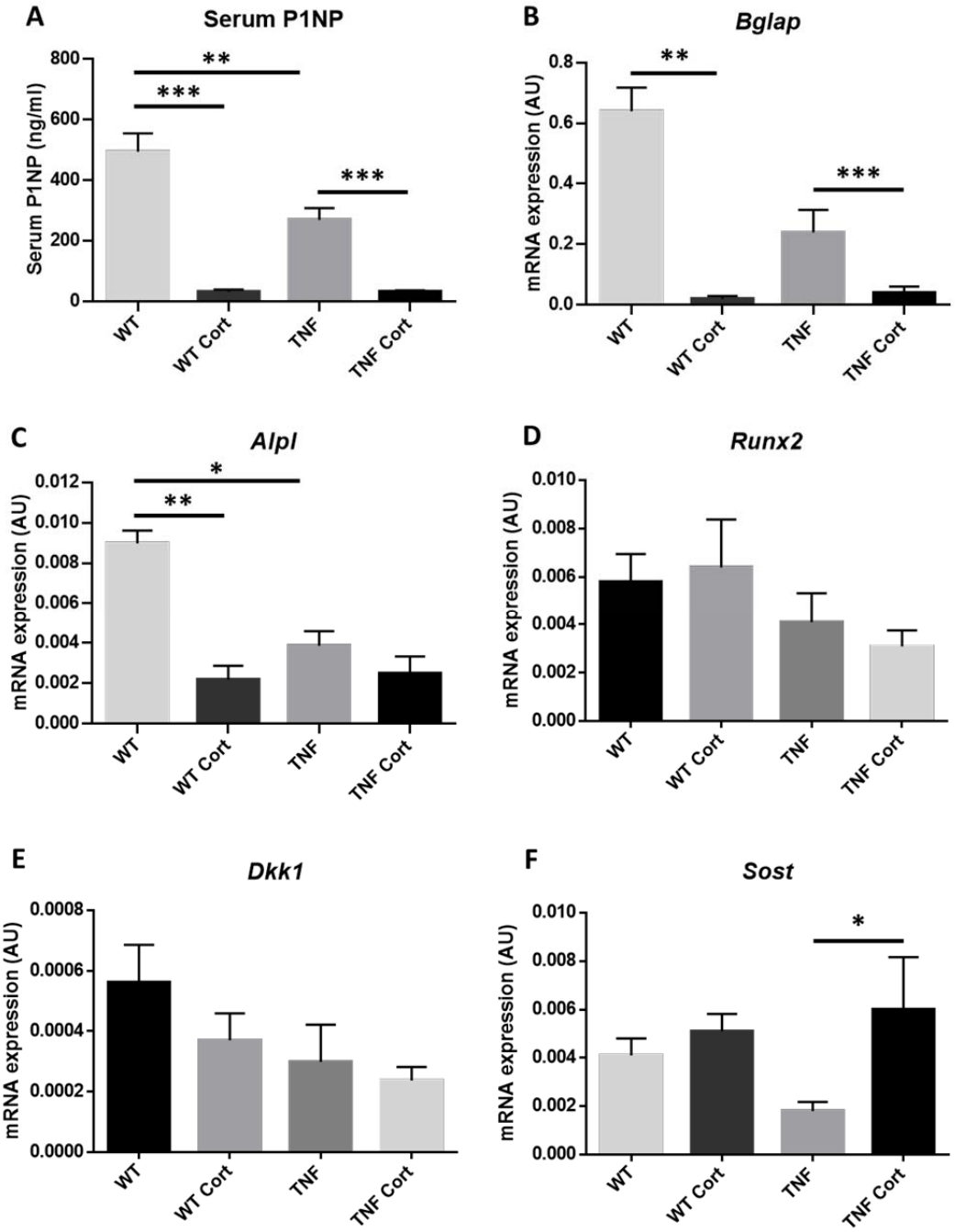

Figure 3. 12: Osteoblast markers in WT and TNF-tg animals receiving GCs.

(A) ELISA analysis of serum P1NP (ng/ml) (n=6 per group) and gene expression analysis (AU) determined by qPCR of (B) *Bglap,* (C) *Alpl,* (D) *Runx2,* (E) *Dkk1* and (F) *Sost* in tibias from WT (n=6) and TNF-tg (n=6) mice receiving vehicle or 100 mg/L corticosterone WT (n=5) and TNF-tg (n=6) in drinking water for three weeks. Data is presented as mean ± SEM and statistical significance was determined using two-way ANOVA with Tukey's multiple comparisons test (* denotes P≤0.05, ** denotes P≤0.01 and *** denotes P≤0.001).

To examine the impact of GCs on bone resorption, serum and mRNA analysis of osteoclast markers was performed. Serum levels of the osteoclast resorption marker CTX-1 were analysed and showed a non-significant increase in untreated TNF-tg animals compared to WT mice, which was significantly abrogated in TNF-tg animals treated with oral corticosterone (TNF-tg 81.6 ng/ml ± 10.7 vs TNF-tg Cort 36.0 ng/ml ± 2.7, P≤0.01) (Fig 3.13 A). The gene expression levels of the osteoclast marker *Ctsk* showed no differences between groups (Fig 3.13 B). The ratio of the inducer of osteoclast activation RANKL (*Tnfsf11*) to its decoy receptor OPG (*Tnfrsf11b*) was assessed due to their well-established roles in regulating osteoclast differentiation and activity. Both WT animals and TNF-tg animals treated with corticosterone showed a significant increase in the RANKL/OPG ratio compared to untreated WT controls (Fig 3.13 C). Gene expression levels of *Csf1* a factor essential for the differentiation and survival of osteoclasts, remained unchanged between groups (Fig 3.13 D). These data suggest that GCs exert their protective effects on the bone via a suppression of osteoclast resorption activity. However, this does not seem to be dependent on RANKL/OPG mediated differentiation of osteoclasts.

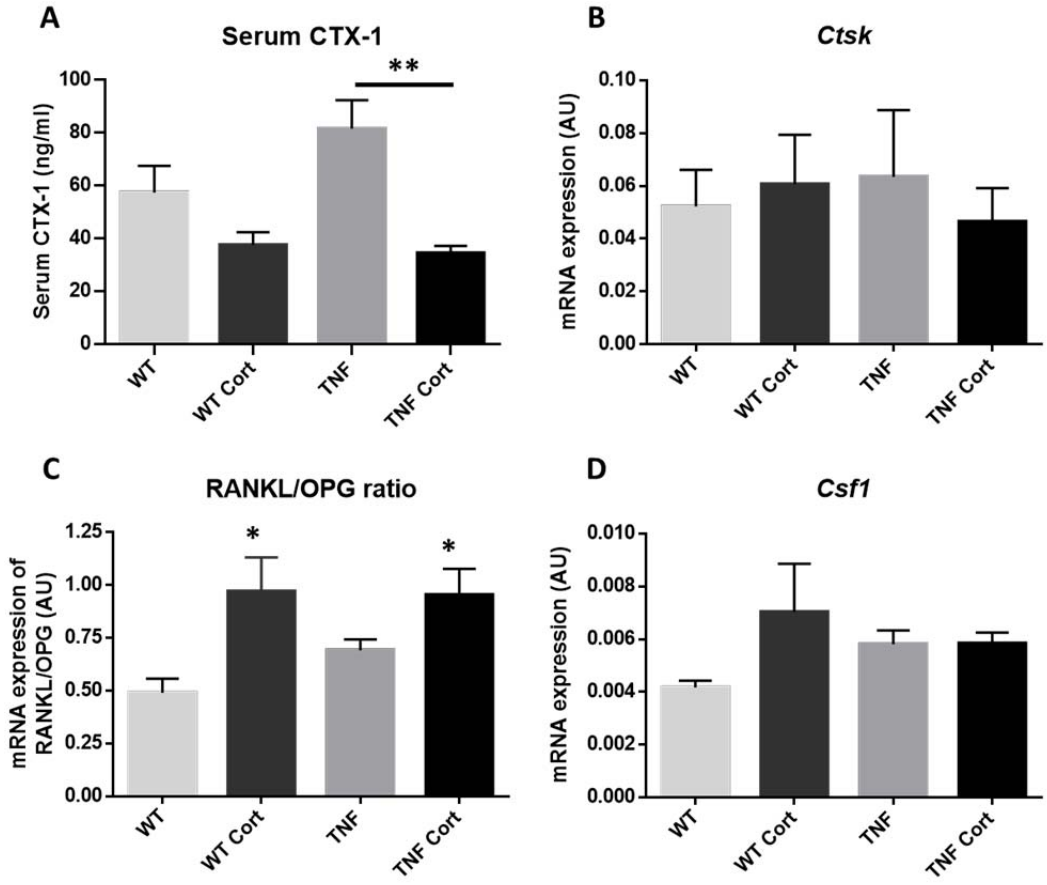

Figure 3. 13: Osteoclast markers in WT and TNF-tg animals receiving GCs.

(A) ELISA analysis of serum CTX-1 (ng/ml) in WT (n=5) and TNF-tg (n=6) animals receiving vehicle or 100 mg/L corticosterone WT (n=5) and TNF-tg (n=6) in drinking water for three weeks. Gene expression analysis (AU) determined by qPCR of (B) *Ctsk*, (C) the Rankl/Opg ratio and (D) *Csf1* in tibias of WT (n=6) and TNF-tg (n=6) mice receiving vehicle or 100 mg/L corticosterone WT (n=5) and TNF-tg (n=6) in drinking water for three weeks. Data is presented as mean ± SEM and statistical significance was determined using two-way ANOVA with Tukey's multiple comparisons test (* denotes P≤0.05, ** denotes P≤0.01).

3.5 Discussion

Chronic inflammation and GC use independently drive systemic bone loss (285, 286). However, GCs are also often used in the treatment of chronic inflammatory diseases due to their potent immunosuppressant properties to suppress the detrimental actions of inflammation on the bone (124). Clinical studies remain inconclusive as to the overall outcome of GC treatment on the bone during inflammation. Thus, we utilised the TNF-tg model of chronic inflammatory polyarthritis with exogenous oral GC administration to examine the net effects of GCs on the bone during inflammation. The TNF-tg model exhibits a disease progression similar to that of human RA and develops substantial local juxta-articular and systemic inflammatory bone loss, making it an effective *in vivo* model for studying the effects of GCs on the bone in the context of inflammation (157).

In order to determine the dose required to obtain effective suppression of disease parameters, a dose response experiment was set up in which TNF-tg animals were treated with 50 mg/L or 100 mg/L corticosterone in the drinking water and clinical and arthritic paw scores were assessed to monitor the progression of the disease. Whilst the 50 mg/L treatment group showed no change in disease scores compared to untreated controls, 100 mg/L resulted in significant declines in both disease scores (Fig 3.2). Upon further examination of this dose, 100 mg/L induced significant adrenal atrophy and hepatic steatosis, which are characteristic of GC use (Fig 3.3 B & D) (296). 100 mg/L corticosterone also potently upregulated the classical GC-responsive and anti-inflammatory gene *Gilz* in both groups (Fig 3.3 C). Additionally, both WT and TNF-tg animals had increased levels of serum corticosterone in corticosterone treatment groups (Fig 3.3 A). Thus, these data suggest that the effects of 100 mg/L corticosterone in the drinking water appears to closely resemble those of pharmacological GC interventions,

in terms of reductions in clinical disease parameters and development of systemic adverse effects. A previous study has shown that corticosterone administration via the drinking water results in a consistent diurnal variation which closely resembles that of clinical GC treatment. Additionally, this method is non-invasive and prevents unnecessary stress of animals, which would otherwise lead to an undesirable stress response that would skew the results (297). The drawback of this approach is the inability to administer a specific amount of treatment. However, all mice in the present study exhibited features of GC use (Fig 3.3), thus it can be concluded that they received an appropriate dose.

Once an appropriate dose was chosen, WT and TNF-tg animals were treated with 100 mg/L corticosterone drinking water for three weeks. This resulted in a significant decrease in disease activity in terms of clinical and arthritic paw scores (Fig 3.4). Consistent with this, significant reductions in the pro-inflammatory cytokines TNFα, IL-6 and IL-1 were observed in TNF-tg animals receiving oral corticosterone (Fig 3.5). Thus, this treatment regime was able to achieve the potent suppression of inflammation which is a well-established GC action (124, 159).

The TNF-tg mouse developed the characteristic juxta-articular destruction associated with chronic inflammatory arthritis, in terms of prevalent bone erosions, florid synovitis leading to pannus formation and invasion into the subchondral bone, and cartilage damage (Fig 3.6, 3.7 & 3.10). Cartilage volume and proteoglycan content was not improved with corticosterone treatment (Fig 3.10), however bone erosions and synovitis were almost completely reversed to baseline upon treatment with GCs (Fig 3.6 & 3.7). Furthermore, GC treatment led to a dramatic decrease in pro-inflammatory chemokines CCL2, CXCL10 and CXCL2 (Fig 3.8). These cytokines have previously been shown to be significantly elevated in the synovium and synovial fluid of RA patients (298-300).

Injection of CCL2 into the joints of rabbits induces infiltration of macrophages to the site and inhibition of CCL2 in antigen-induced arthritis reduced joint inflammation, bone erosions and monocyte migration, thus CCL2 is highly implicated as an important mediator of immune cell infiltration into the joint during chronic inflammatory arthritis (298, 301). The expression of CCL2 and CXCL10 at the joint leads to the recruitment of monocytes and macrophages, whilst CXCL2 induces the migration of neutrophils (298-300). This infiltration of immune cells leads to synovitis, characterised as synovial hyperplasia and pannus formation, in the joints of RA patients and thus the suppression of these chemokines in the TNF-tg mouse upon GC treatment is likely to explain the reduction in pannus invasion observed here.

Once in the synovium, the high levels of pro-inflammatory cytokines and RANKL can induce the differentiation of the infiltrating monocytes into osteoclasts which drive bone destruction (302). The TNF-tg mouse had a significantly higher number of osteoclasts in the pannus of the joints in this study. This was dramatically suppressed upon GC treatment (Fig 3.9). Additionally, serum CTX-1, a marker of osteoclast activity, was also significantly suppressed upon GC treatment (Fig 3.13 A). These decreases in osteoclast number and activity likely mediate the protection against both juxta-articular and systemic bone loss observed in TNF-tg animals treated with oral corticosterone (Fig 3.6 & 3.11). RANKL has been shown to be increased in tissues from RA patients compared to healthy controls, and it is the expression of this osteoclast differentiation factor that has been implicated in the development of bone erosions in inflammatory disease (303). However, in this study the RANKL/OPG ratio showed no increase in the TNF-tg animals compared to WT mice (Fig 3.13 C). In contrast, the RANKL/OPG ratio was increased upon GC treatment, despite the decrease in osteoclast number observed. Previous studies have

shown that TNFα in combination with M-CSF can induce osteoclastogenesis via a RANKL-independent mechanism (304-306). M-CSF (*Csf1*) levels did not change in this study (Fig 3.13 D), however potent suppression of TNFα was observed upon GC treatment (Fig 3.5 B). An additional study has demonstrated the ability to prevent the development of inflammatory induced local and systemic bone loss by controlling inflammation, thus it is likely that the protection against bone loss upon GC treatment is mediated directly by the downregulation of pro-inflammatory cytokines (Fig 3.5) (265). Moreover, gene expression levels of the osteoclast activity marker cathepsin K (*Ctsk*) did not change amongst the groups (Fig 3.13 B).

Inflammatory induced systemic bone loss was only partially protected against by GC therapy, with percentage bone volume and trabecular number being rescued to approximately WT levels, whilst trabecular thickness remained significantly lower than controls (Fig 3.11). A potential explanation for this is that thickness of trabeculae may depend more on osteoblast activity than osteoclasts. Both RA and GCs have been shown to independently decrease osteoblast markers (307, 308). In keeping with this, TNF-tg animals had significant decreases in serum P1NP, a marker of osteoblast activity, and the mature osteoblast markers osteocalcin (*Bglap*) and alklaline phosphatase (*Alpl*) compared to WT animals (Fig 3.12 A-C). However, GC treatment exacerbated the reduction of these osteoblast markers to comparable levels between WT and TNF-tg groups. This dramatic suppression of osteoblast activity may impact on the ability to build up the thickness of trabeculae. Factors which influence osteoblast differentiation, such as the master transcription factor Runx2 and the wnt inhibitors sclerostin (*Sost*) and Dkk1, remained largely unchanged indicating a reduction in functionality of osteoblasts or an increase in osteoblast apoptosis as opposed to an inhibition of differentiation. The pro-

apoptotic nature of both TNFα and therapeutic GCs has been previously reported (237, 261). Further research could utilise apoptosis assays such as TUNEL staining to test for this.

In conclusion, GC treatment in the TNF-tg model of chronic inflammatory arthritis revealed that GCs had an overall beneficial effect on both local and systemic bone despite potent suppression of osteoblast markers. This beneficial effect appeared to be mediated by the suppression of pro-inflammatory cytokine induced osteoclast differentiation and activity. In collaboration with the Goodyear lab, we have identified that TNFα-stimulated primary osteoclast cultures suppressed osteoclast numbers and resorption of calcified matrix in response to treatment with cortisol which supports this hypothesis (309). Currently, RA patients are often administered bone sparing agents which inhibit the actions of osteoclasts, such as bisphosphonates or denosumab, alongside GC treatment to reduce potential side effects on the bone (19, 310). Overall, our research suggests the use of therapies which stimulate the anabolic actions of osteoblasts on bone would be more important to be administered in combination with GC therapy. Further research is needed to establish whether the finding that GCs have a net positive effect on the bone still holds true with varying doses and durations of treatment.

Chapter 4: Investigating the role of 11β-HSD1 metabolism in GC-induced osteoporosis

Data from this chapter have been previously published (311).

4.1 Introduction

GCs are highly effective at suppressing inflammation, therefore synthetic GCs such as dexamethasone, prednisolone and hydrocortisone are often given therapeutically to treat inflammatory diseases. A community based cross-sectional study found that approximately 0.5% of 65,786 patients were currently prescribed oral GC therapy for at least three months, with that figure increasing to 1.4% in patients over 55 years of age. Among the various reasons for GC administration, rheumatoid arthritis was the disease most frequently prescribed GCs (accounting for 23% of GC users) (312). Unfortunately, despite the potent anti-inflammatory effects of therapeutic GCs, their use is limited by the occurrence of adverse metabolic effects, such as GC-induced osteoporosis (GIO), muscle wasting, skin thinning, hepatic steatosis and insulin resistance (313). In particular, therapeutic GCs have detrimental effects on bone, through the suppression of anabolic bone formation as a result of increased osteoblast apoptosis and decreased differentiation (237). The mechanisms behind GIO have been discussed in further detail in section 1.5.5. BMD measurements of the lumbar spine and hips of patients receiving GC treatment were found to be approximately 10% lower than that of aged matched controls (21). Additionally, fracture risk was significantly greater in GC treated patients, with a 33% and 61% increase in the rate of nonvertebral and hip fractures, respectively. Vertebral fractures were of particular concern, with the risk increasing over 2-fold in patients receiving GC treatment compared to age matched controls (314). Thus, preventing the development of GIO is crucial in optimising GC therapy.

4.1.1 11β-HSD1 expression in bone cells

As previously mentioned in section 1.4.4, one study by Morgan et al used 11β-HSD1 KO mice treated with corticosterone to show that activation of GCs at the local tissue level by 11β-HSD1 was responsible for many of the metabolic side effects associated with GC excess, including muscle wasting, hepatic steatosis, glucose intolerance, hypertension and increased adiposity (70). However, the contribution of 11β-HSD1 to GIO had not been investigated in this study.

Previously, glucocorticoid activation by 11β-HSD1 was shown to be present in human ex vivo bone chips (71). Immunohistochemical analysis of bone sections confirmed that 11β-HSD1 was present in the cytoplasm of bone cells, predominantly expressed in the osteoblasts, with lower expression in osteoclasts and variable expression in osteocytes. In contrast, 11β-HSD2 was not present in osteoclasts and osteocytes, and only low levels were detected in osteoblasts (71). A separate study investigated the link between activity of 11β-HSD1 and susceptibility to changes in bone remodelling in response to GCs. Volunteers were treated for one week with 5 mg oral prednisolone twice daily before analysis of the bone formation markers osteocalcin and P1NP. Although decreases in bone formation markers were observed in all subjects, those with higher 11β-HSD1 activity, determined by urinary metabolite measures, showed substantially greater reductions in these parameters. Therefore, it was concluded that 11β-HSD1 activity could predict the sensitivity of the bone to therapeutic GCs. Furthermore, subjects with higher 11β-HSD1 activity did not have higher levels of circulating prednisolone, thus it was suggested that local 11β-HSD1 activity within osteoblasts determines the magnitude of response to GCs in terms of bone formation markers, as opposed to systemic 11β-HSD1 activity. Thus, this study proposed that this information could be used to formulate bone-

sparing GC therapies (315). Moreover, another study used primary human osteoblasts to show that 11β-HSD1 reductase activity was positively correlated with age of the donor and was significantly increased by treatment with prednisone (352). Thus, 11β-HSD1 activity within osteoblasts has been shown to increase with age and in response to pro-inflammatory cytokines, which may explain the increased susceptibility to bone loss in aged patients and those with chronic inflammatory conditions (154). Therefore, 11β-HSD1 activity appears to play an important role in mediating the detrimental effects of GCs on the bone.

4.2 Hypothesis

11β-HSD1 metabolism of GCs is necessary to mediate glucocorticoid-induced osteoporosis.

4.3 Materials and Methods

4.3.1 Animal experiments

Global (11βKO), mesenchymal-specific (Twist2) and myeloid-specific (LysM) 11β-HSD1 mice were bred as previously described in sections 2.1.2 and 2.1.3. Animals were treated with 100 mg/L corticosterone water for either three or four weeks. At seven weeks, mice were culled by cervical dislocation following exsanguination by cardiac puncture and tissues were fixed and stored as previously outlined (section 2.1.4). Adrenals were excised and weighed.

4.3.2 Micro-CT analysis

Tibias and spines were fixed in formalin and stored in 70% ethanol prior to being scanned on a Skyscanner 1172 (Bruker Micro-CT, Belgium) (see section 2.2). Tibias and spines were analysed according to section 2.2.2. A further analysis of the spine was performed on ImageJ software as described in section 2.2.3.

4.3.3 ELISA analysis

Following cardiac puncture, blood was allowed to clot for 30 minutes at room temperature before being centrifuged at 13,000 rpm for 30 minutes. Serum was aspirated and stored at -80°C prior to use. For serum corticosterone analysis, cardiac puncture was performed between 11.00 p.m to 1.00 a.m during the active phase of the animals when they will be consuming most corticosterone water. Serum levels of corticosterone, P1NP and CTX-1 were analysed by ELISA as previously described in sections 2.6.2.2, 2.6.2.1 and 2.6.3.2, respectively.

4.3.4 Gene expression analysis

Tibias were isolated and homogenised with liquid nitrogen in a pestle and mortar before extracting RNA using the innuPREP RNA Mini Kit 2.0 (AnalytikJena, Jena, Germany) as described in section 2.5.1. The yield of RNA was measured using a NanoDrop^{TM} 1000 Spectrophotometer (ThermoFisher, Paisley, UK) and cDNA was synthesised from 700 ng RNA using the High-Capacity cDNA Reverse Transcription Kit (ThermoFisher, Paisley, UK) as outlined in section 2.5.2. Gene expression levels in the tibias were measured using quantitative real time PCR (see section 2.5.3) using the Taqman probes listed in Supplementary Table 1 (Applied Biosystems).

4.3.5 H&E staining

Livers were extracted post mortem and formalin fixed before being stored in 70% ethanol at 4°C. Samples were embedded, cut and H&E stained courtesy of the Department of Musculoskeletal Pathology at the Royal Orthopaedic Hospital (as described in section 2.8.1).

4.3.6 Static histomorphometry

Spines were formalin fixed and stored in 70% ethanol at 4°C prior to use. Histomorphometry of the spine was carried out by the skelet.AL Skeletal Analysis Laboratories (Sheffield, UK) as outlined in section 2.8.4.

4.3.7 Statistical analysis

GraphPad Prism software (GraphPad, San Diego, USA) was used to determine statistical significance. Two-way ANOVA analysis was used with a Tukey post hoc analysis to compare between treatment groups and genotypes unless otherwise stated in the figure legend. When only two treatment groups were being compared an unpaired student t test was conducted. N numbers are recorded in the relevant figure legend. Statistical significance was determined as $P \leq 0.05$. * denotes $P \leq 0.05$, ** denotes $P \leq 0.01$ and *** denotes $P \leq 0.001$.

4.4 Results

4.4.1 Characterisation of the global 11βKO mouse phenotype

To establish the response to oral GCs in mice lacking 11β-HSD1, characteristic features of GC excess were assessed. 100 mg/L corticosterone treatment was sufficient to potently induce parameters characteristic of therapeutic GC use. Significant adrenal atrophy occurred in both WT and 11βKO animals (Fig 4.1 A). Whilst liver histology of WT animals receiving oral corticosterone revealed lipid deposition, this was not apparent in 11βKO GC treated animals (Fig 4.1 B). Gene expression levels of the GC-responsive gene *Gilz* was induced in both groups administered corticosterone treatment, although to a lesser extent in 11βKO mice (Fig 4.1 C). Serum corticosterone levels were significantly higher in animals receiving corticosterone treatment compared to their untreated counterparts (Fig 4.1 D). In addition, *ex vivo* osteoblast cultures isolated from 11βKO mice had significantly lower activity of 11β-HSD1, confirming the efficient disruption of this enzyme (Fig 4.1 E).

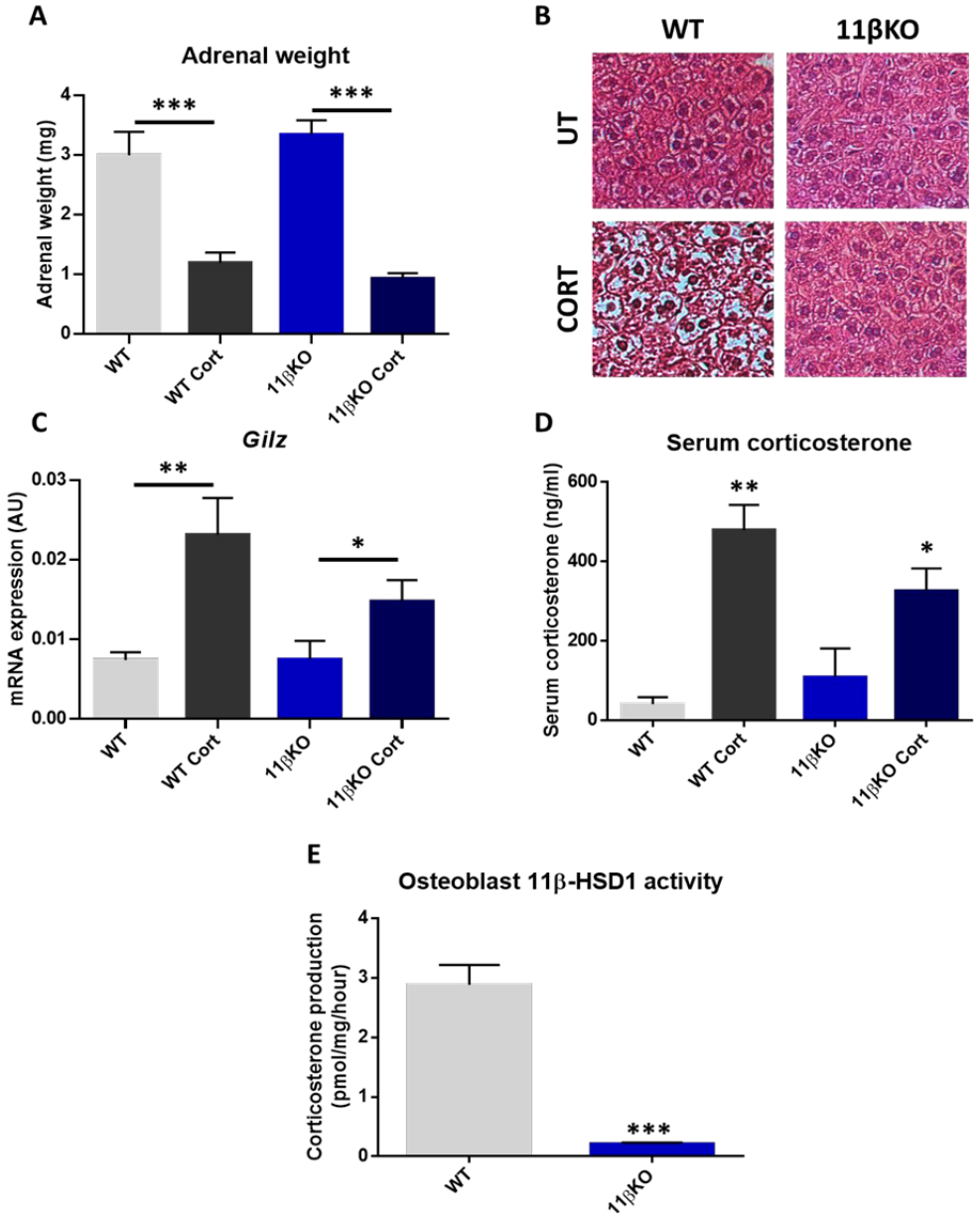

Figure 4. 1: Characterisation of GC response in WT and 11βKO animals

(A) Adrenal weights (mg) of WT (n=6) and 11βKO (n=9) animals receiving vehicle control or 100 mg/L corticosterone WT (n=8) and 11βKO (n=9) in the drinking water for three weeks. (B) Representative images of untreated and three weeks of 100 mg/L corticosterone drinking water treated H&E stains of WT and 11βKO livers. (C) qPCR analysis of mRNA expression of *Gilz* (AU) in tibias of mice receiving vehicle WT (n=6) and 11βKO (n=6) or 100 mg/L oral corticosterone WT (n=5) and 11βKO (n=6) for three weeks. (D) Serum corticosterone levels (ng/ml) determined by ELISA in WT and 11βKO mice following three weeks of oral 100 mg/L corticosterone treatment (n=3 per group, n=5 11βKO Cort). (E) 11β-HSD1 activity (pmol/mg/hour) in osteoblasts isolated from WT and 11βKO mice (n=5 per group) determined by TLC. Data is presented as mean ± SEM and statistical significance was determined using two-way ANOVA with Tukey's multiple comparisons test and unpaired t test (* denotes P≤0.05, ** denotes P≤0.01 and *** denotes P≤0.001).

4.4.2 11βKO mice are protected from GC-induced trabecular bone loss

In order to investigate the contribution of 11β-HSD1 to GIO, WT and 11βKO animals were treated with corticosterone drinking water, after which their tibias were excised and micro-CT analysis was performed. Bone loss was measured after three and four weeks of corticosterone treatment. Whilst no significant changes in WT trabecular bone parameters were reported at three weeks (Supplementary Fig 2), significant reductions were apparent at four weeks (Fig 4.2). Analysis of the percentage of bone volume to total volume of the inner space of the bone revealed that WT animals receiving oral corticosterone developed significant reductions in bone volume compared to untreated WT animals (WT 8.54% ± 0.7 vs WT Cort 4.12% ± 0.4, P≤0.001). In contrast, a significant protection from GC induced bone loss was apparent in 11βKO mice treated with oral corticosterone relative to WT mice (WT Cort 4.12% ± 0.4 vs 11βKO Cort 7.16% ± 0.7, P≤0.05) (Fig 4.2 B). However, measurement of trabecular thickness showed significant decreases in both groups receiving oral corticosterone compared to their relative controls (Fig 4.2 C). WT animals receiving oral corticosterone demonstrated significantly less trabeculae compared to their untreated counterparts (WT 0.0009 1/μm ± 0.00004 vs WT Cort 0.0006 1/μm ± 0.00004, P≤0.01), whilst 11βKO mice treated with corticosterone showed a marked protection against this decrease, again with 11βKO numbers being significantly higher than WT numbers in corticosterone treatment groups (WT Cort 0.0006 1/μm ± 0.00004 vs 11βKO Cort 0.0009 1/μm ± 0.00008, P≤0.01) (Fig 4.2 D). Trabecular separation analysis reflected these results with significantly more separation between the trabeculae in WT animals receiving oral corticosterone compared to control (WT 664.96 μm ± 26.3 vs WT Cort 959.05 μm ± 41.1, P≤0.01), which was abrogated in 11βKO groups (Fig 4.2 E). Taken together, these data indicate that 100 mg/L corticosterone treatment

for four weeks is sufficient to induce GIO in WT animals, however 11βKO animals appear to be partially protected from this effect. Additionally, the protection in bone volume appears to be reflective of a protection against a loss of trabecular number rather than a loss of trabecular thickness.

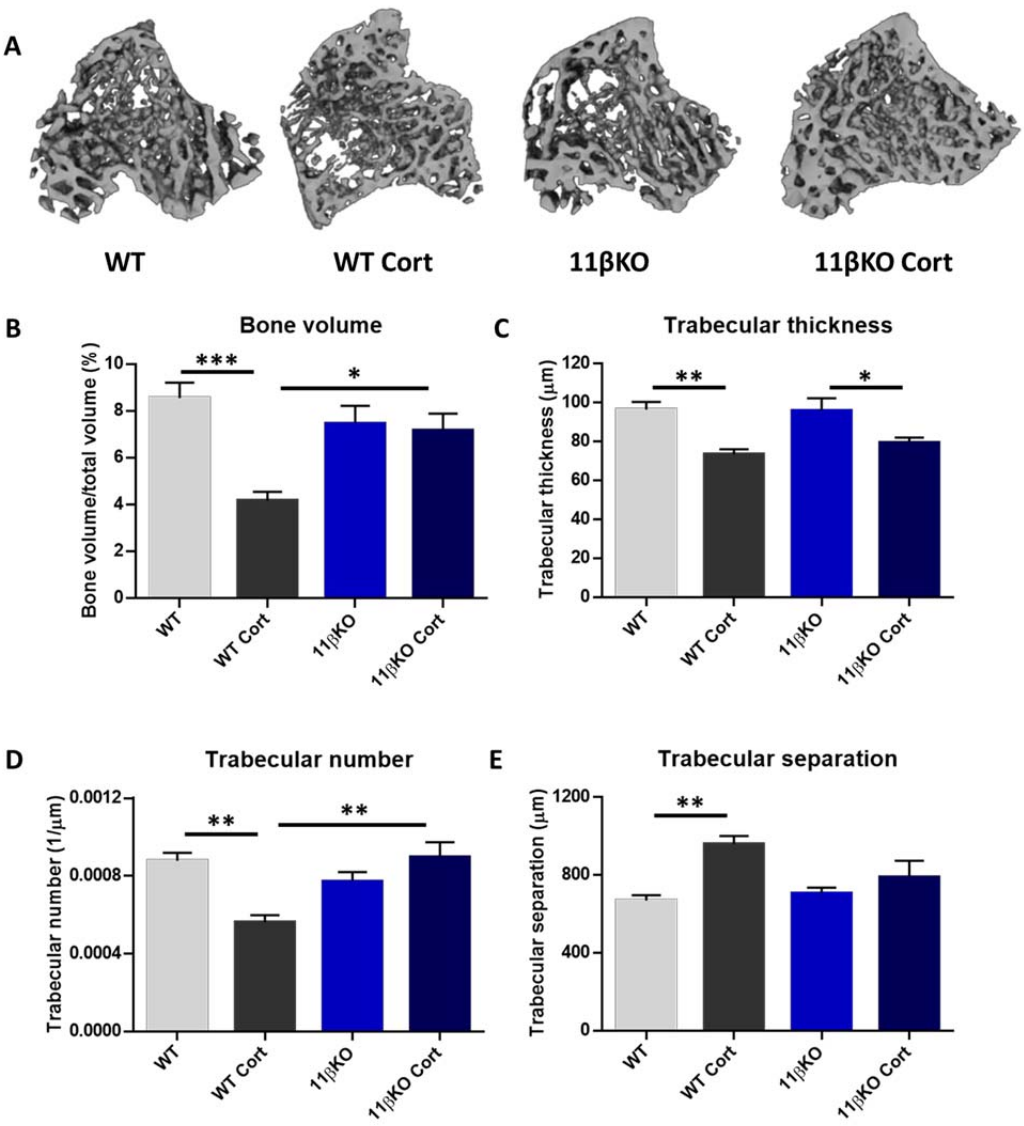

Figure 4. 2: Trabecular bone parameters of tibias from WT and 11βKO animals after four weeks corticosterone treatment

(A) Representative images of reconstructed trabecular bone from tibia scans of WT and 11βKO animals receiving vehicle control or 100 mg/L corticosterone in the drinking water for four weeks. Micro-CT analysis of (B) bone volume (%) relative to total volume, (C) trabecular thickness (µm), (D) trabecular number (1/µm) and trabecular separation (µm) of WT and 11βKO animals receiving vehicle control or 100 mg/L corticosterone in the drinking water for four weeks (n=6 per group). Data is presented as mean ± SEM and statistical significance was determined using two-way ANOVA with Tukey's multiple comparisons test (* denotes P≤0.05, ** denotes P≤0.01 and *** denotes P≤0.001).

4.4.3 11βKO animals are partially protected against GC-induced changes at the spine

GIO also affects the vertebral bones of the spine, with the relative risk of vertebral fractures significantly increasing in patients using GCs (21). In order to examine the contribution of 11β-HSD1 metabolism to bone loss at the vertebrae, spines were dissected from seven-week old mice post mortem following three week corticosterone treatment, and micro-CT analysis was performed on the vertebral body of lumbar 6. Modest changes in bone parameters were observed in WT corticosterone treated animals. Bone volume in WT mice receiving oral corticosterone was decreased compared to untreated 11βKO animals, however this decrease did not reach significance when compared to untreated WT animals (Fig 4.3 B). Trabeculae were significantly thinner in WT GC treated animals compared to their untreated counterparts (WT 92.3 μm ± 2.4 vs WT Cort 83.1 μm ± 2.6, P≤0.01), whilst no differences were observed in 11βKO GC treated mice relative to controls (Fig 4.3 C). No changes were observed in trabecular number or trabecular separation parameters amongst the groups (Fig 4.3 D-E).

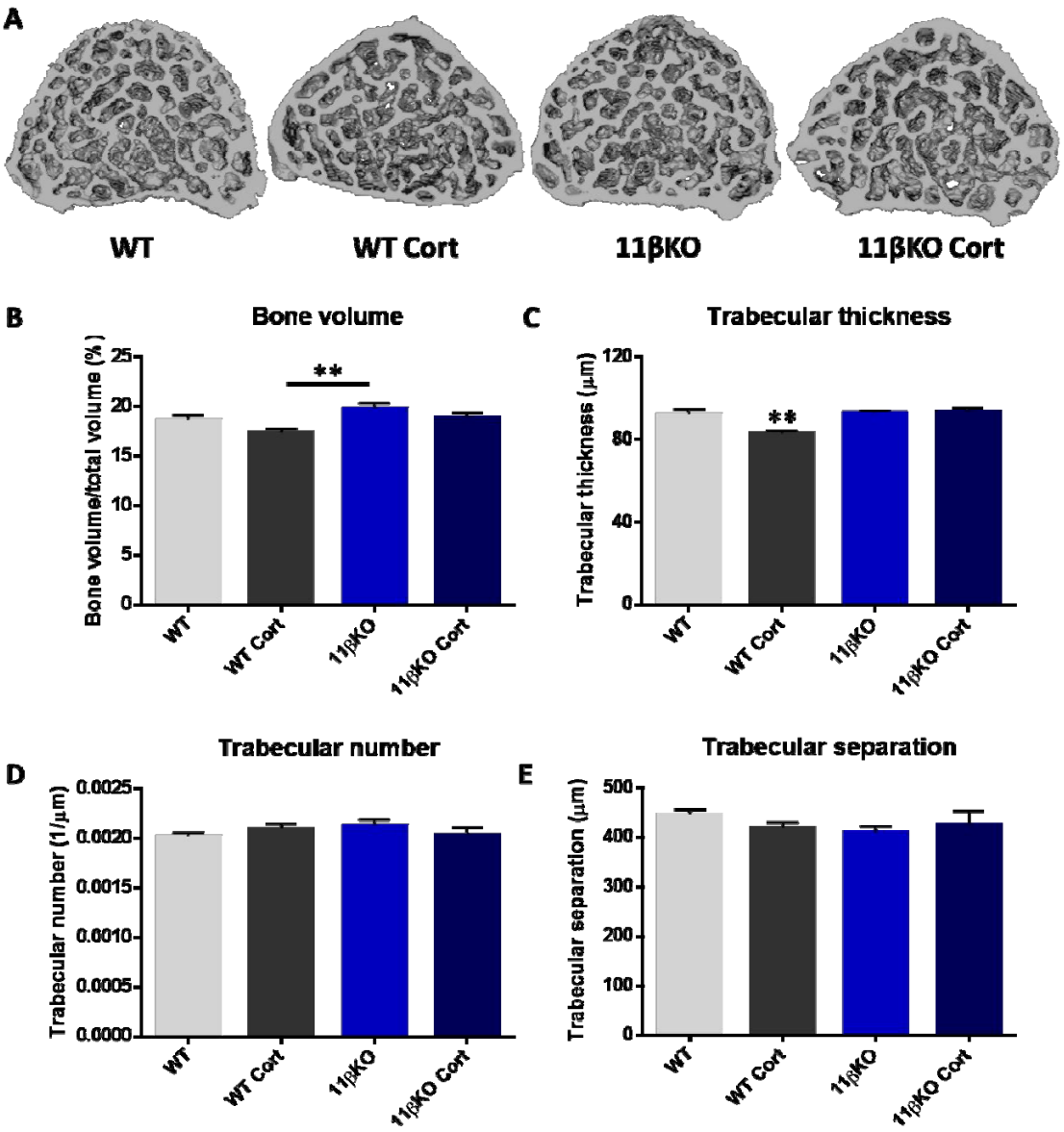

Figure 4. 3: Bone parameters from lumbar 6 of GC treated WT and 11βKO animals

(A) Representative images of reconstructed lumbar vertebrae of WT and 11βKO animals receiving vehicle control or 100 mg/L corticosterone in the drinking water for three weeks. Micro-CT analysis of (B) bone volume (%) relative to total volume, (C) trabecular thickness (µm), (D) trabecular number (1/µm) and trabecular separation (µm) of WT (n=6) and 11βKO (n=6) animals receiving control or 100 mg/L corticosterone WT (n=6) and 11βKO (n=5) in the drinking water for three weeks. Data is presented as mean ± SEM and statistical significance was determined using two-way ANOVA with Tukey's multiple comparisons test (** denotes $P \leq 0.01$)

ImageJ analysis of lumbar 6 was also performed to further assess the phenotype of 11βKO animals receiving oral corticosterone. WT corticosterone treated animals had significantly less cortical area compared to untreated WT mice (WT 0.68 mm^2 ± 0.1 vs WT Cort 0.44 mm^2 ± 0.06, P≤0.001), whilst 11βKO animals receiving oral corticosterone were protected from this decrease (Fig 4.4 B). Both periosteal and endosteal perimeters of GC treated WT animals were significantly smaller than their relative controls (periosteal perimeter: WT 7.2 mm ± 0.17 vs WT Cort 6.38 mm ± 0.17, P≤0.001; endosteal perimeter: WT 6.38 mm ± 0.14 vs WT Cort 5.75 mm ± 0.11, P≤0.01), suggesting an overall smaller vertebra in the WT group administered corticosterone. Again, GC treated 11βKO animals were resistant to this effect (Fig 4.4 C-D).

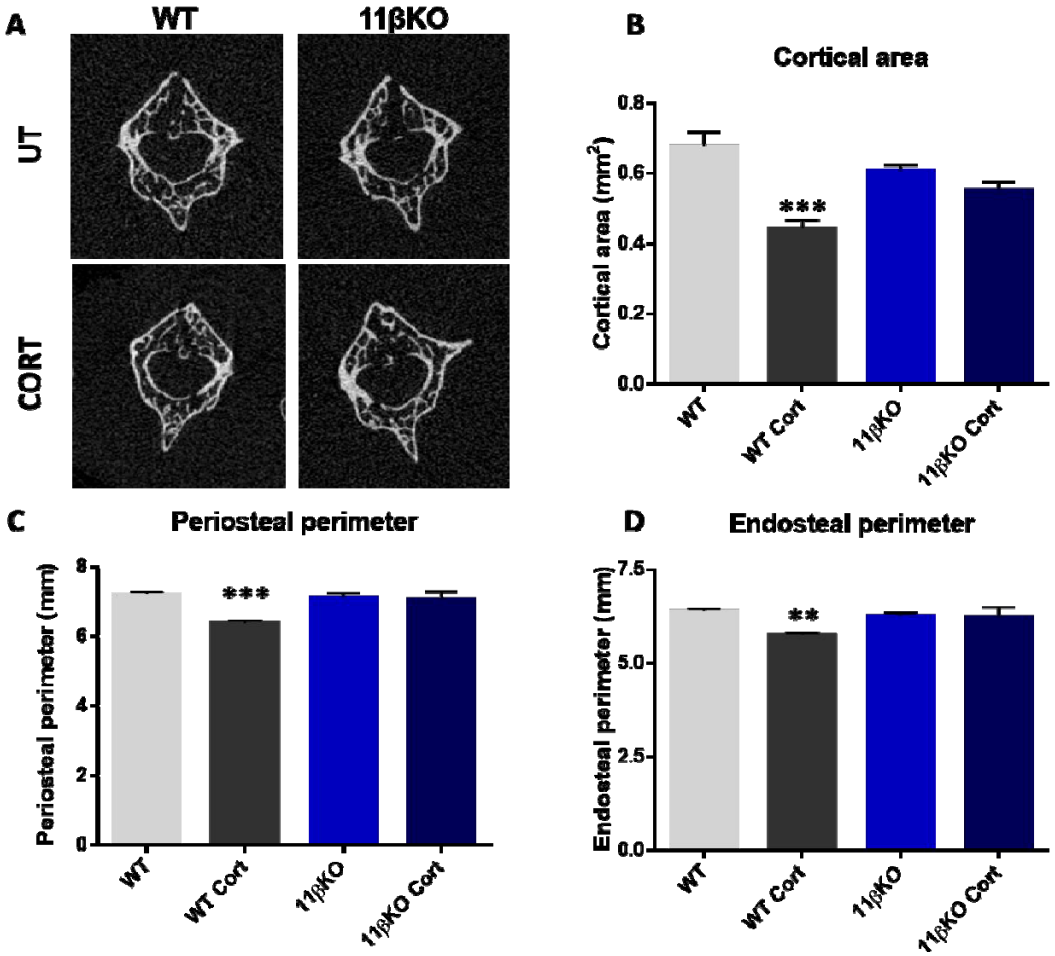

Figure 4. 4: ImageJ analysis of GC treated WT and 11βKO spines

(A) Representative images of lumbar vertebrae of WT and 11βKO animals receiving vehicle control or 100 mg/L corticosterone in the drinking water for three weeks. ImageJ analysis of (B) cortical area (mm^2), (C) periosteal perimeter (mm), and (D) endosteal perimeter (mm) of WT (n=6) and 11βKO (n=6) animals receiving control or 100 mg/L corticosterone WT (n=6) and 11βKO (n=5) in the drinking water for three weeks. Data is presented as mean ± SEM and statistical significance was determined using two-way ANOVA with Tukey's multiple comparisons test (** denotes P≤0.01, *** denotes P≤0.001)

4.4.4 11βKO animals are protected from GC induced suppression of bone formation markers

To examine the mechanisms driving 11β-HSD1 mediated bone loss at the onset of GIO, osteoblast markers were assessed in the serum and tibia mRNA of three week GC treated WT and 11βKO mice. Serum levels of the bone formation marker P1NP were significantly reduced in WT animals treated with GCs compared to untreated. GC treated 11βKO animals also showed a significant reduction in P1NP levels compared to untreated controls, however there was a trend towards increased P1NP levels in GC treated 11βKO mice compared to GC treated WT mice (WT 494.2 ng/ml ± 61.1 vs WT Cort 31.3 ng/ml± 7.4, P≤0.001; 11βKO 405.7 ng/ml ± 58.4 vs 11βKO Cort 158.6 ng/ml ± 53.1, P≤0.05) (Fig 4.5 A). Expression levels of genes relating to mature osteoblasts *Bglap* and *Alpl* were analysed from mRNA extracted from the tibias of mice. *Bglap* showed a dramatic suppression in GC treated WT animals compared to their untreated counterparts (WT 0.64 AU ± 0.08 vs WT Cort 0.02 AU ± 0.01, P≤0.001). However, there was no significant difference in *Bglap* levels in GC treated 11βKO mice relative to untreated 11βKO controls. Interestingly, a marked increase in *Bglap* levels in 11βKO animals receiving oral corticosterone was noted when compared to WT mice treated with corticosterone (WT Cort 0.02 AU ± 0.01 vs 11βKO Cort 0.27 AU ± 0.04, P≤0.001) (Fig 4.5 B). This pattern was mimicked in the expression levels of *Alpl*, with a significant suppression in WT animals receiving oral corticosterone compared to their untreated group and no difference amongst the 11βKO groups. Again, a significant increase in expression levels was noted between 11βKO GC treated mice and WT GC treated animals (WT Cort 0.002 AU ± 0.0006 vs 11βKO Cort 0.008 AU ± 0.002, P≤0.01) (Fig 4.5 C). The master regulator of osteoblast differentiation *Runx2* and the inhibitor of wnt signalling *DKK1* showed no

significant differences amongst the groups (Fig 4.5 D and F). Another inhibitor of wnt signalling *Sost* showed a significantly higher level in 11βKO animals receiving corticosterone treatment compared to their respective controls, however there was no significant difference between the GC treated groups (Fig 4.5 E). Collectively, these data indicate that GCs suppress markers of mature osteoblasts and bone formation but do not inhibit markers of osteoblast differentiation. These data indicate that reduced osteoblast survival rather than reduced differentiation may underpin this phenotype. Interestingly, this appears to be partially mediated by 11β-HSD1 metabolism as 11βKO animals are somewhat protected from these effects.

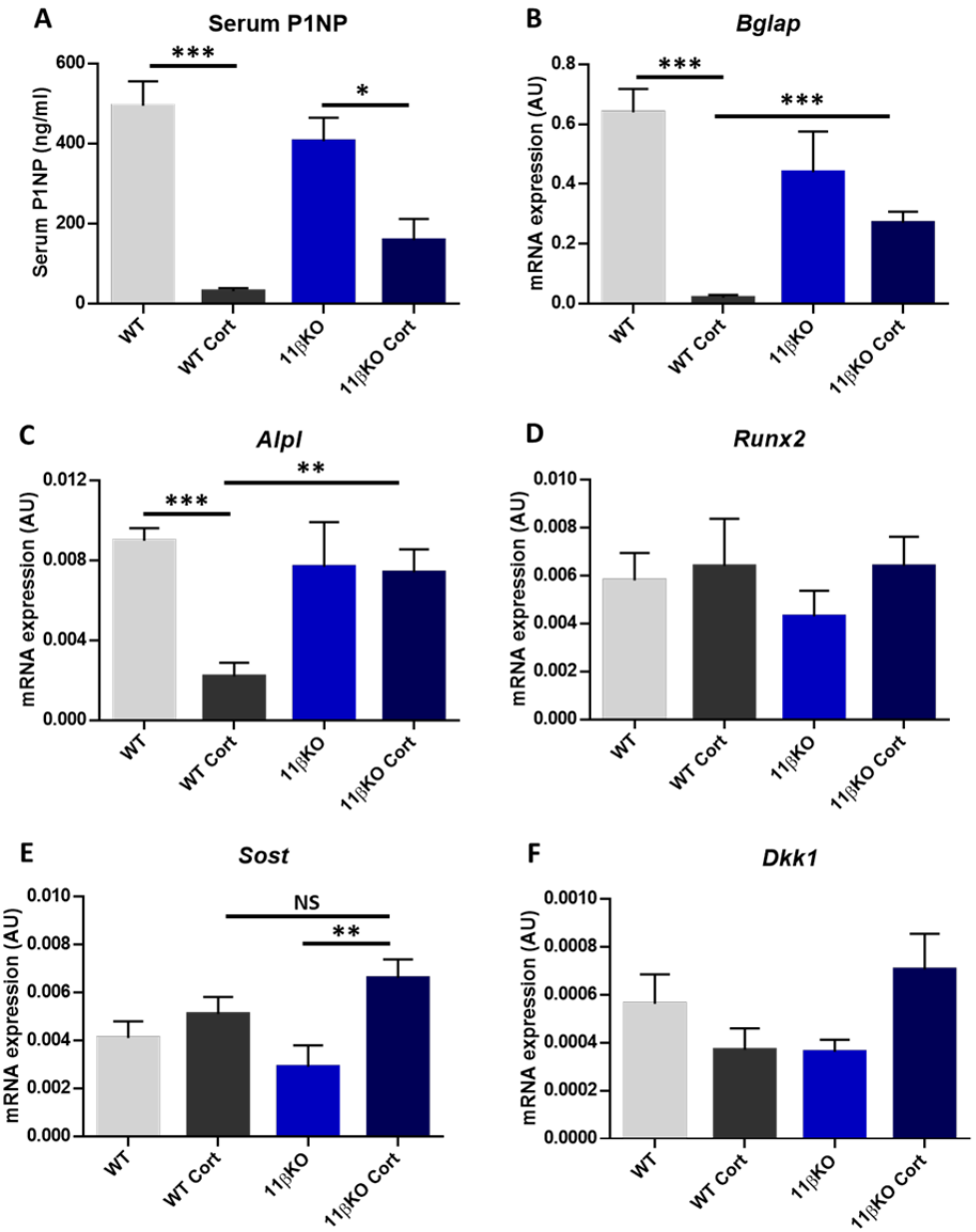

Figure 4. 5: Osteoblast markers in GC treated WT and 11βKO animals

(A) ELISA analysis of serum P1NP (ng/ml) (n=6 per group) and qPCR analysis (AU) of (B) *Bglap,* (C) *Alpl,* (D) *Runx2,* (E) *Dkk1* and (F) *Sost* in tibias of WT (n=6) and 11βKO (n=6) animals receiving control or 100 mg/L corticosterone WT (n=5) and 11βKO (n=6) in the drinking water for three weeks. Data is presented as mean ± SEM and statistical significance was determined using two-way ANOVA with Tukey's multiple comparisons test (* denotes P≤0.05, ** denotes P≤0.01 and *** denotes P≤0.001).

4.4.5 Osteoclast markers are comparable in WT and 11βKO animals receiving corticosterone

Serum and mRNA markers of osteoclasts were also assessed in WT and 11βKO animals. ELISA analysis of the bone resorption marker CTX-1 showed no significant changes across the groups, however a non-significant trend towards decreased resorption was observed in both groups receiving oral corticosterone treatment (Fig 4.6 A). The ratio of the inducer of osteoclast differentiation RANKL (*Tnfsf11*) to its inhibitor OPG (*Tnfrsf11b*) was measured by gene expression analysis from tibia mRNA. While a significant upregulation of the RANKL/OPG ratio was observed in corticosterone treated WT animals compared to untreated WT animals, this upregulation was not apparent in corticosterone treated 11βKO animals compared to the relative controls (Fig 4.6 B). However, no change was detected in gene expression levels of the marker of osteoclast activity *Ctsk* or the differentiation factor *Csf1* between groups (Fig 4.6 C-D). These data indicate that while a protection against RANKL/OPG mediated induction of osteoclastogenesis was observed, this was not reflected in serum or mRNA markers of resorption. Together, these data suggest that the bone protective phenotype in the 11β-HSD1 KO in response to GCs is not mediated through a reduction in GC induced osteoclast resorption.

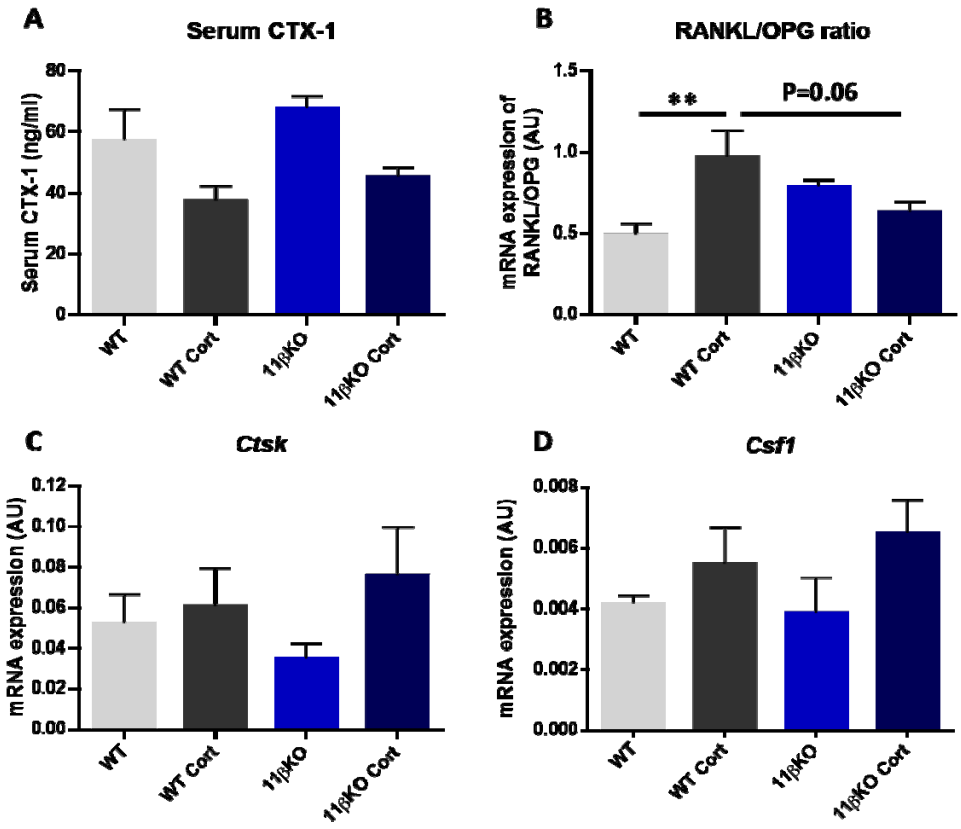

Figure 4. 6: Osteoclast markers in GC treated WT and 11βKO animals

(A) ELISA analysis of serum CTX-1 (ng/ml) (n=5 per group) and qPCR analysis of gene expression (AU) of (B) the Rankl/Opg ratio, (C) *Ctsk* and (D) *Csf1* in tibias from WT (n=6) and 11βKO (n=6) animals receiving control or 100 mg/L corticosterone WT (n=5) and 11βKO (n=6) in the drinking water for three weeks. Data is presented as mean ± SEM and statistical significance was determined using two-way ANOVA with Tukey's multiple comparisons test (** denotes P≤0.01).

4.4.6 Histomorphometric analysis of osteoblasts and osteoclasts in WT and 11βKO animals receiving corticosterone

Finally, histomorphometry was performed on the spines to examine the effects of GCs on the numbers of osteoblasts and osteoclasts on the surface of the bone. The surface covered by osteoblasts was significantly reduced in WT animals receiving oral corticosterone treatment compared to untreated WT (WT 10.5% ± 2.66 vs WT Cort 0.17%

± 2.43, P≤0.01). In corticosterone treated 11βKO animals a significant decrease in osteoblast surface was observed compared to their untreated controls (11βKO 11.2% ± 5.92 vs 11βKO Cort 4.2% ± 4.55, P≤0.05), however this appeared to be to a lesser extent than in WT animals (Fig 4.7 A). No significant difference in osteoclast surface was observed amongst the groups, however trends towards decreased osteoclasts were seen in both GC treated groups compared to their relevant controls (Fig 4.7 B). Taken together, these results suggest that 11β-HSD1 metabolism of steroids is responsible for driving cortical and trabecular bone thinning and reduced vertebra size in WT animals after GC treatment via a reduction of osteoblast number.

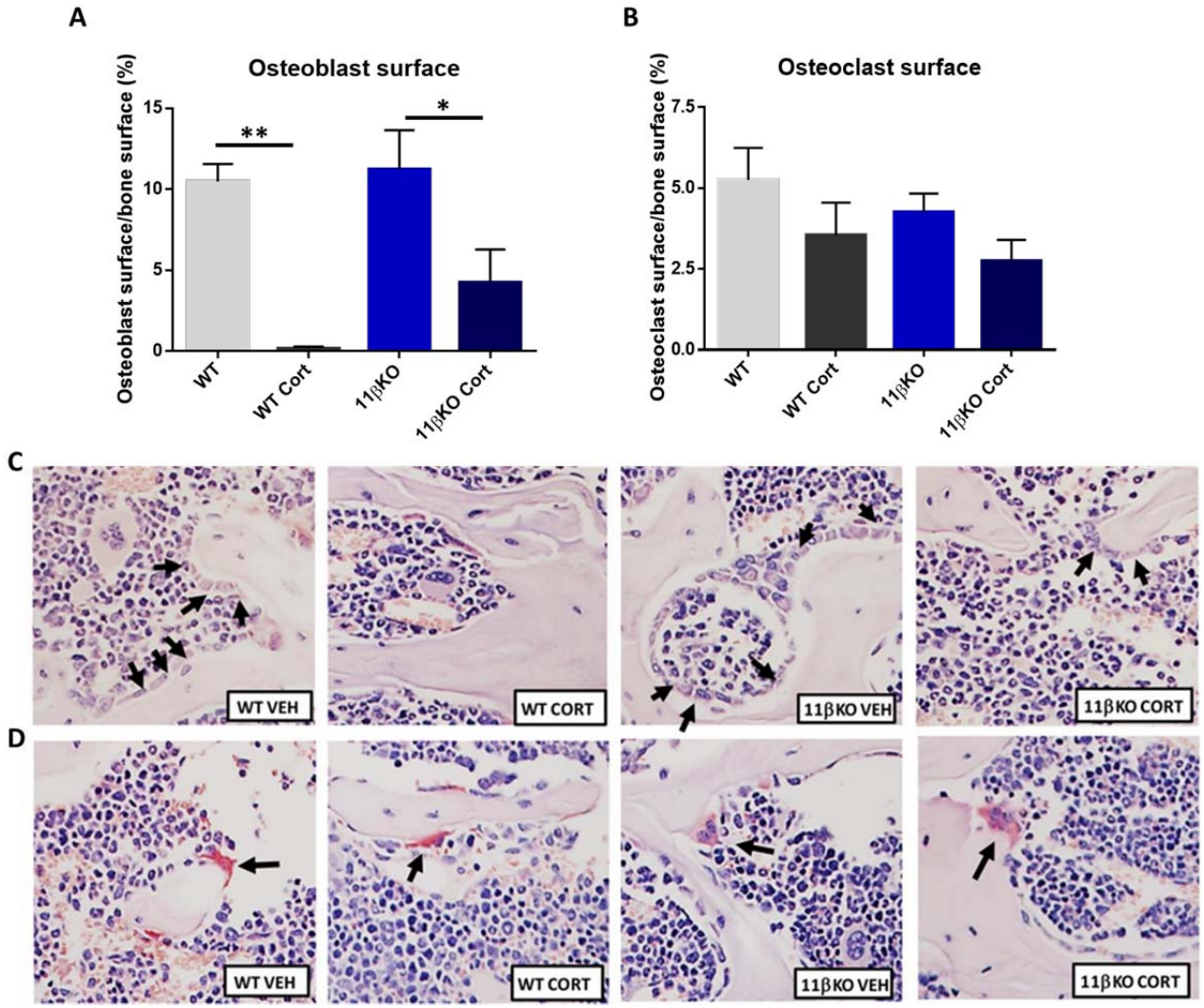

Figure 4. 7: Effect of GCs on bone cells at the spine of WT and 11βKO animals

Percentage of bone surface covered by (A) osteoblasts and (B) osteoclasts of WT (n=6) and 11βKO (n=6) animals receiving control or 100 mg/L corticosterone WT (n=6) and 11βKO (n=5) in the drinking water for three weeks determined by static histomorphometry. (C) Representative images of osteoblasts (indicated by arrows) and (D) osteoclasts (indicated by arrows) in the spine by H&E and TRAP staining. Data is presented as mean ± SEM and statistical significance was determined using two-way ANOVA with Tukey's multiple comparisons test (* denotes P≤0.05, ** denotes P≤0.01)

4.4.7 Characterisation of the mesenchymal specific 11βKO mouse phenotype

In an attempt to decipher the contribution of cell specific 11β-HSD1 to GIO, a mesenchymal specific 11βKO mouse (WT-Twist2) was generated. Four-week old WT-Twist2 mice were treated with 100 mg/L corticosterone for three weeks and tissues were collected post mortem at seven weeks of age. 100 mg/L corticosterone in the drinking water was sufficient to induce the characteristic effects of therapeutic GC use. Adrenal weights were significantly suppressed and *Gilz* gene expression was elevated in GC treated animals compared to their untreated controls (Fig 4.8 A-B). The mesenchymal-derived osteoblasts were isolated from these mice and 11β-HSD1 activity was found to be significantly suppressed in WT-Twist2 animals compared to WT (Fig 4.8 C).

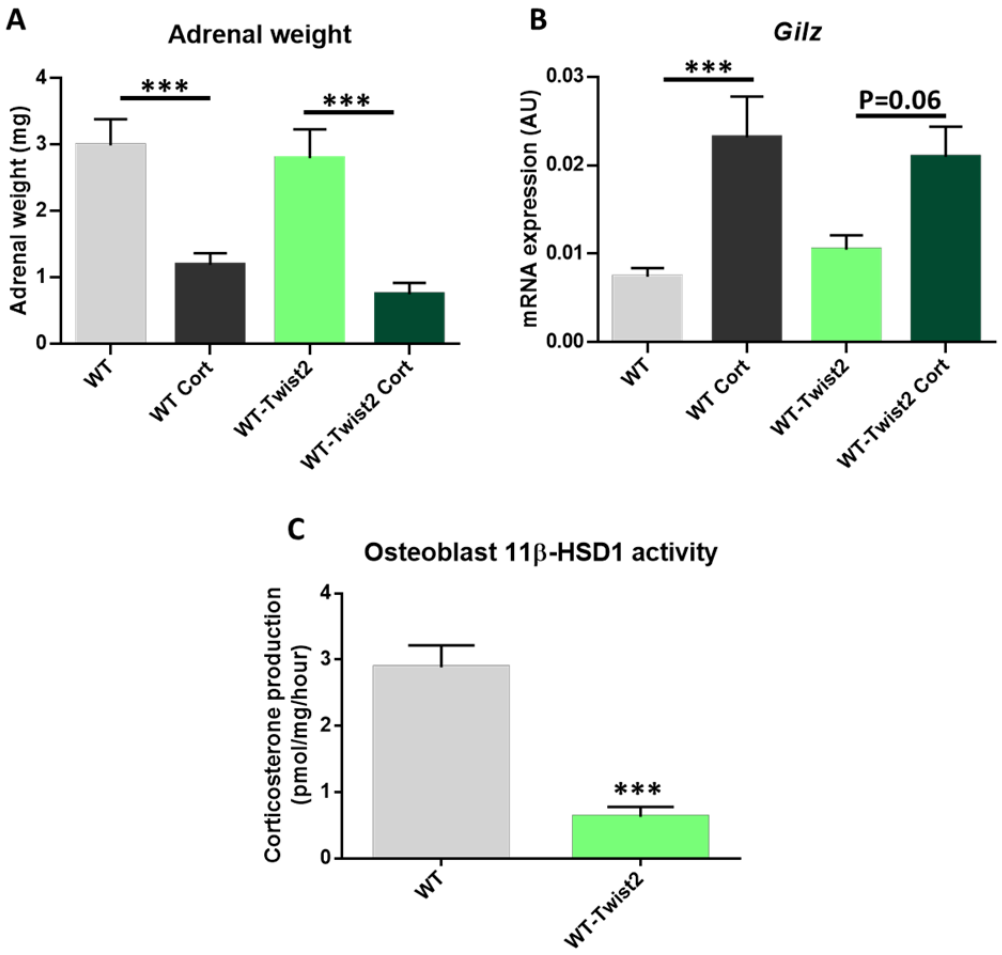

Figure 4. 8: Analysis of GC response parameters in WT and WT-Twist2 mice

(A) Adrenal weights (mg) in WT (n=6) and WT-Twist2 (n=3) animals receiving control or 100 mg/L corticosterone WT (n=8) and WT-Twist2 (n=6) in the drinking water for three weeks. (B) Gene expression of *Gilz* (AU) determined by qPCR in tibias of WT (n=6) and WT-Twist2 (n=4) mice receiving control or 100 mg/L corticosterone WT (n=5) and WT-Twist2 (n=4) in the drinking water for three weeks. (C) 11β-HSD1 activity (pmol/mg/hour) determined by TLC analysis in osteoblasts isolated from WT (n=6) and WT-Twist2 (n=7) mice. Data is presented as mean ± SEM and statistical significance was determined using two-way ANOVA with Tukey's multiple comparisons test and unpaired t test (*** denotes P≤0.001).

4.4.8 WT and WT-Twist2 mice exhibit comparable signs of GC-induced changes in bone remodelling at three weeks

As previously reported, corticosterone effects on bone are not apparent in animals at three weeks. However, to assess the impact of mesenchymal 11β-HSD1 deletion on bone

metabolism in WT-Twist2 Cre animals, tibias were excised post mortem and micro-CT used to assess trabecular bone parameters. Unlike WT animals receiving GCs over four weeks, no significant differences in bone volume, trabecular number or trabecular separation were detected amongst the groups (Fig 4.9 B, D, E). Thickness of trabeculae was significantly increased in the WT-Twist2 groups compared to WT controls (Fig 4.9 C). Non-significant decreases were observed in trabecular separation of WT-Twist2 groups, likely reflecting the increase in trabecular thickness (Fig 4.9 E). These data indicate that in mice receiving vehicle and corticosterone in drinking water for three weeks, mesenchymal deletion of 11β-HSD1 does not elicit a trabecular bone phenotype relative to WT control animals.

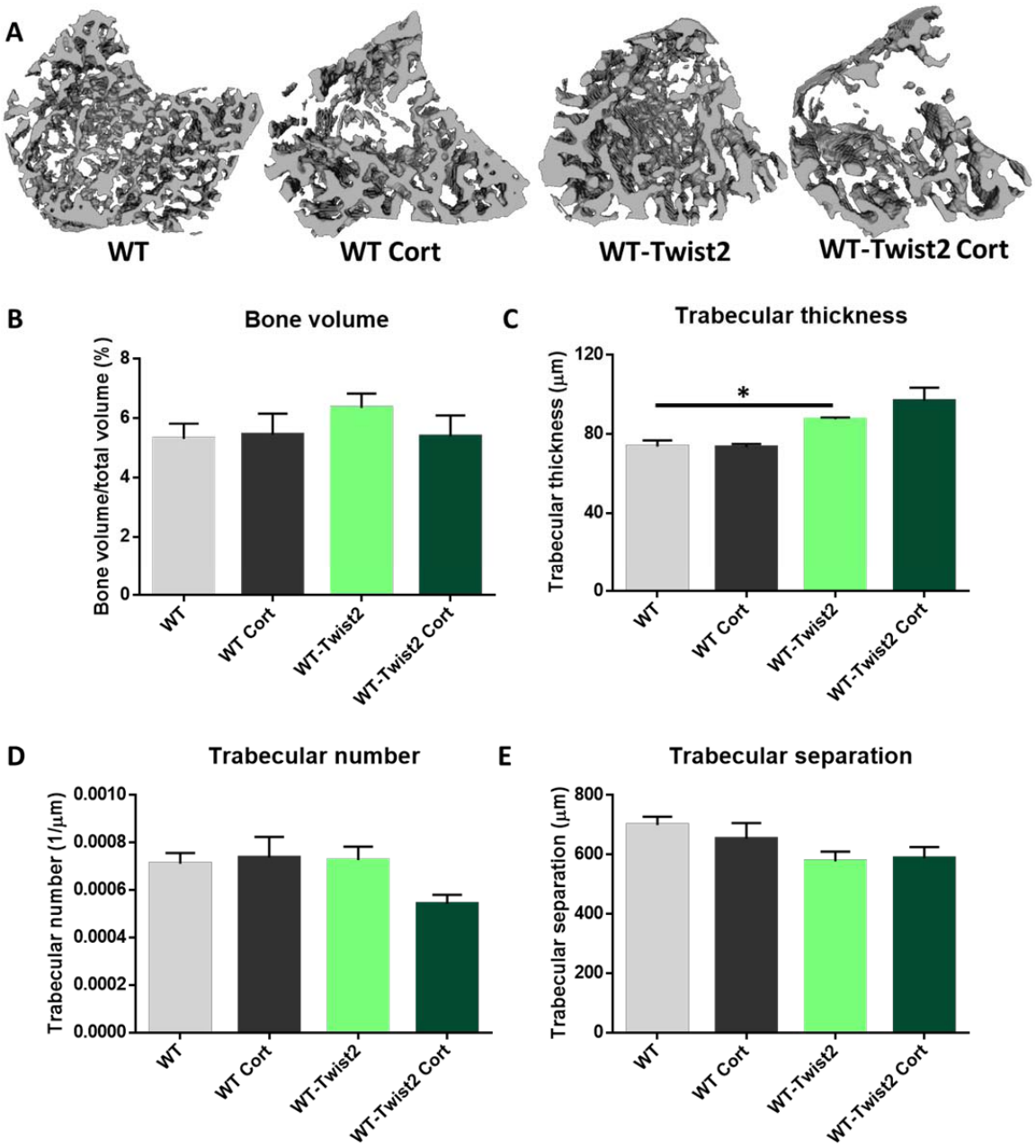

Figure 4. 9: Trabecular bone parameters of corticosterone treated WT and WT-Twist2 mice

(A) Representative images of reconstructed trabecular bone from tibia scans of WT and WT-Twist2 animals receiving vehicle control or 100 mg/L corticosterone in the drinking water for three weeks. Micro-CT analysis of (B) bone volume (%) relative to total volume, (C) trabecular thickness (µm), (D) trabecular number (1/µm) and trabecular separation (µm) of WT (n=8) and WT-Twist2 (n=5) animals receiving control or 100 mg/L corticosterone WT (n=6) and WT-Twist2 (n=6) in the drinking water for three weeks Data is presented as mean ± SEM and statistical significance was determined using two-way ANOVA with Tukey's multiple comparisons test (* denotes P≤0.05)

Whilst bone phenotypes are not apparent at three weeks of exposure to corticosterone, we previously demonstrated that biochemical and gene markers of bone turnover were significantly regulated at this early timepoint in WT animals. Consequently, we examined osteoblast markers in WT-Twist2 animals receiving either vehicle or corticosterone relative to WT controls. Serum levels of the bone formation marker P1NP were significantly lower in untreated WT-Twist2 animals compared to WT controls (WT 494.2 ng/ml ± 61.1 vs WT-Twist2 260.5 ng/ml ± 49.9, P≤0.01). A significant reduction was also observed in both groups receiving oral corticosterone compared to their relevant untreated controls (WT-Twist2 260.5 ng/ml ± 49.9 vs WT-Twist2 Cort 22.9 ng/ml ± 2.3, P≤0.01). Levels of P1NP in both WT and WT-Twist2 mice treated with corticosterone were suppressed to a comparable level (Fig 4.10 A). WT GC treated animals exhibited a significantly lower amount of *Bglap* and *Alpl* than their untreated counterparts. A significant decrease in *Bglap* was also observed between GC treated WT-Twist2 animals relative to untreated controls (WT-Twist2 0.39 AU ± 0.06 vs WT-Twist2 Cort 0.03 AU ± 0.01, P≤0.001), whilst a trend towards decreased levels of *Alpl* was identified. Again, GC treatment groups had suppressed mature osteoblast markers to a comparable level (Fig 4.10 B-C). Gene levels of *Runx2*, the key transcription factor in osteoblast differentiation, showed no significant decreases, however a trend towards decreased levels in WT-Twist2 groups was noted (Fig 4.10 D). Analysis of both inhibitors of wnt signalling *Sost* and *Dkk1* revealed no significant changes amongst the groups (Fig 4.10 E-F).

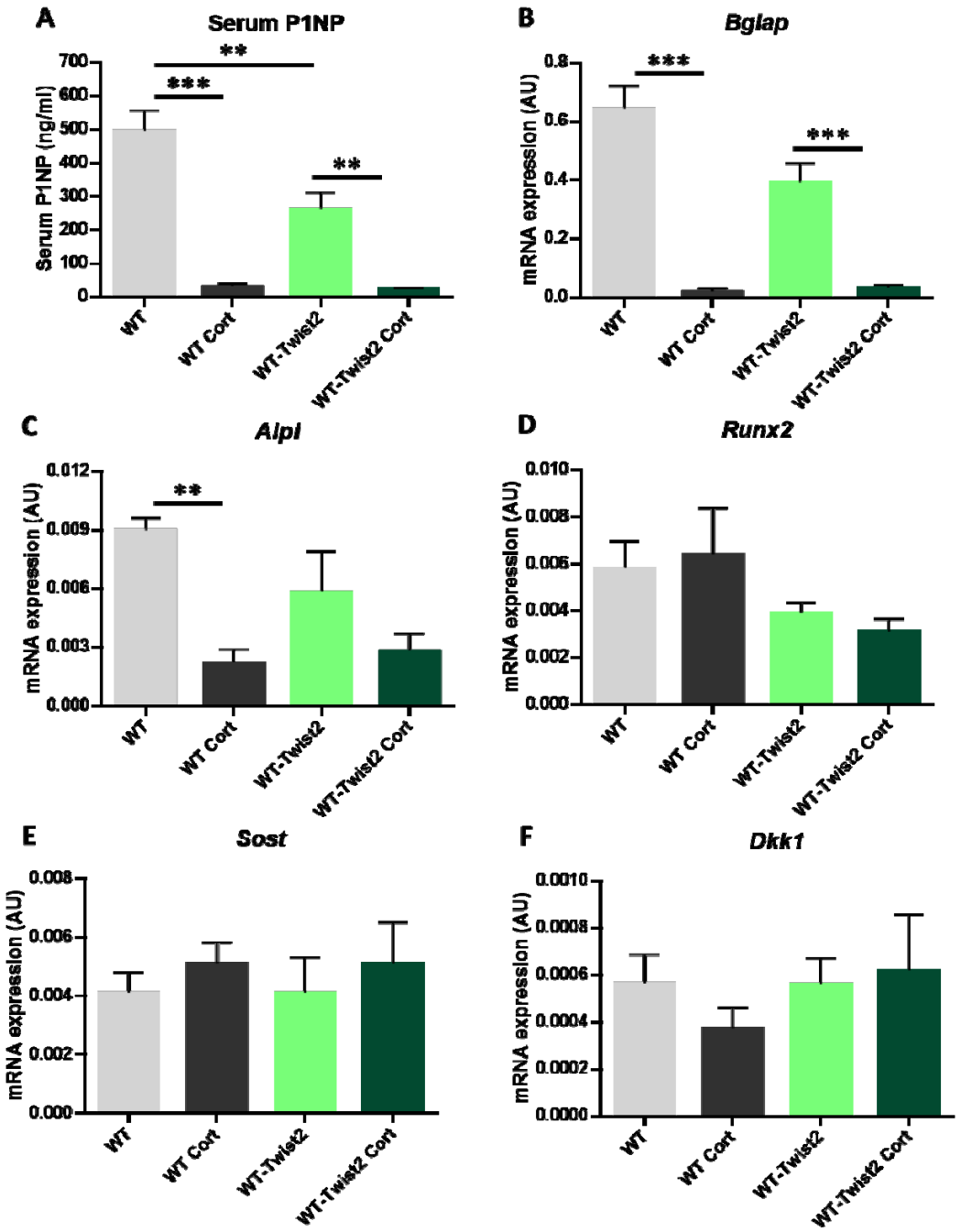

Figure 4. 10: Osteoblast markers in GC treated WT and WT-Twist2 animals

(A) ELISA analysis of serum P1NP (ng/ml) (n=6 per group) and gene expression analysis (AU) of (B) *Bglap,* (C) *Alpl,* (D) *Runx2,* (E) *Sost* and (F) *Dkk1* determined by qPCR analysis in tibias from WT (n=6) and WT-Twist2 (n=5) mice receiving control or 100 mg/L corticosterone WT (n=5) and WT-Twist2 (n=6) in the drinking water for three weeks. Data is presented as mean ± SEM and statistical significance was determined using two-way ANOVA with Tukey's multiple comparisons test (** denotes P≤0.01 and *** denotes P≤0.001).

Analysis of osteoclast markers from mRNA isolated from tibias of WT-Twist2 mice revealed no significant changes in the RANKL/OPG ratio or the marker of osteoclast activity *Ctsk* (Fig 4.11 A-B). The osteoclast survival factor *Csf1* was significantly increased in WT-Twist2 animals receiving oral corticosterone compared to their untreated counterparts, however gene expression between corticosterone treatment groups was comparable (Fig 4.11 C).

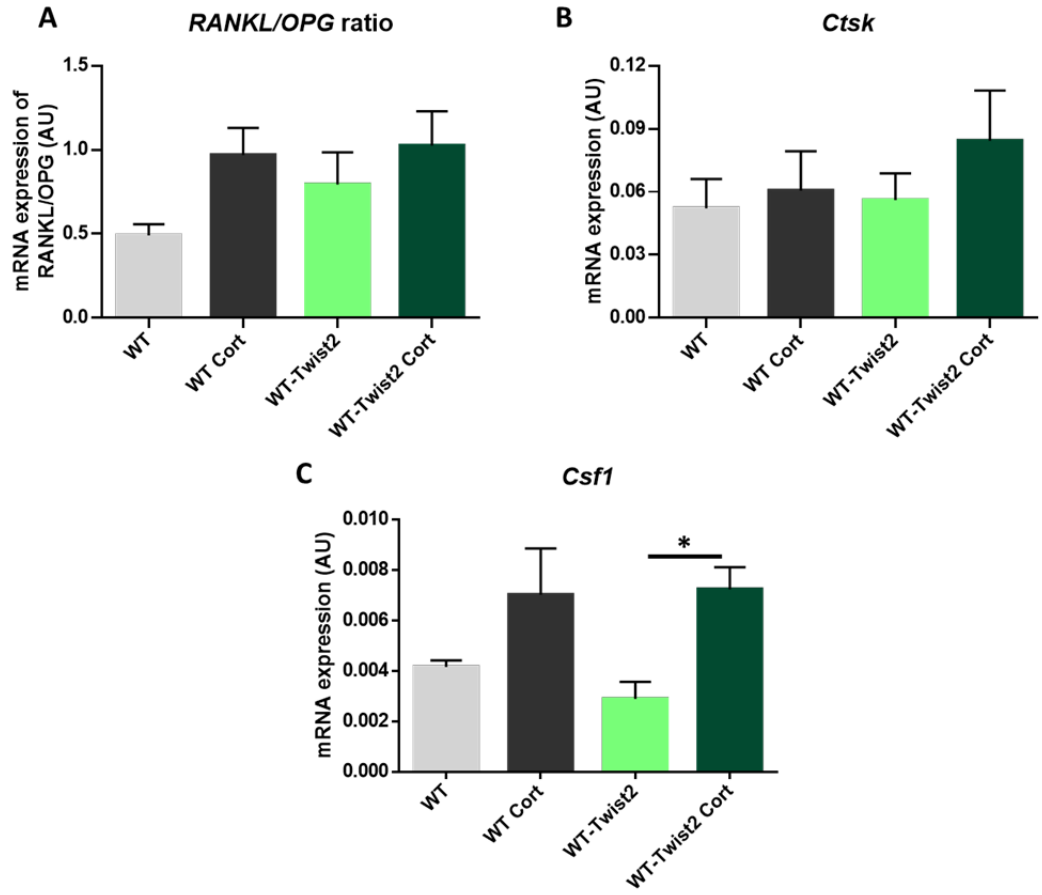

Figure 4. 11: Osteoclast markers in GC treated WT and WT-Twist2 animals

Gene expression analysis (AU) of (A) the Rankl/Opg ratio, (B) *Ctsk* and (C) *Csf1* determined by qPCR analysis from tibias of WT (n=6) and WT-Twist2 (n=5) animals receiving control or 100 mg/L corticosterone WT (n=5) and WT-Twist2 (n=6) in the drinking water for three weeks. Data is presented as mean ± SEM and statistical significance was determined using two-way ANOVA with Tukey's multiple comparisons test (* denotes P≤0.05).

Overall, these data show no major differences in osteoblast markers between WT and WT-Twist2 animals receiving oral corticosterone treatment, indicating that mesenchymal 11β-HSD1 does not appear to mediate changes in bone metabolism in GIO. Interestingly, a decrease in osteoblast markers in untreated WT-Twist2 animals seems to be apparent, indicating changes in bone remodelling at a basal level associated with this genotype. Osteoclasts do not appear to be as sensitive to the effects of GC treatment in terms of osteoclast RNA markers in these mouse models. However, examining bone loss at longer GC exposure to drive a bone loss phenotype is required, to better delineate the contribution of mesenchymal 11β-HSD1 to GIO.

4.4.9 Characterisation of the myeloid specific 11βKO mouse phenotype

In order to determine the contribution of myeloid-derived 11β-HSD1 activity to the development of GIO, a myeloid-specific 11βKO mouse (WT-LysM) was utilised and subjected to three weeks treatment with 100 mg/L corticosterone drinking water. GC treatment suppressed adrenal weights and induced *Gilz* expression to similar levels between corticosterone treated groups (Fig 4.12 A & B). 11β-HSD1 activity was significantly suppressed in macrophages isolated by peritoneal lavage from WT-LysM mice compared to WT animals, confirming disruption of 11β-HSD1 action in these myeloid cells (Fig 4.12 C). Tibialis anterior, fat tissue and liver possessed comparable levels of 11β-HSD1 activity between WT-LysM and WT mice, indicating that no off target effects were observed in these compartments (Fig 4.12 D-F).

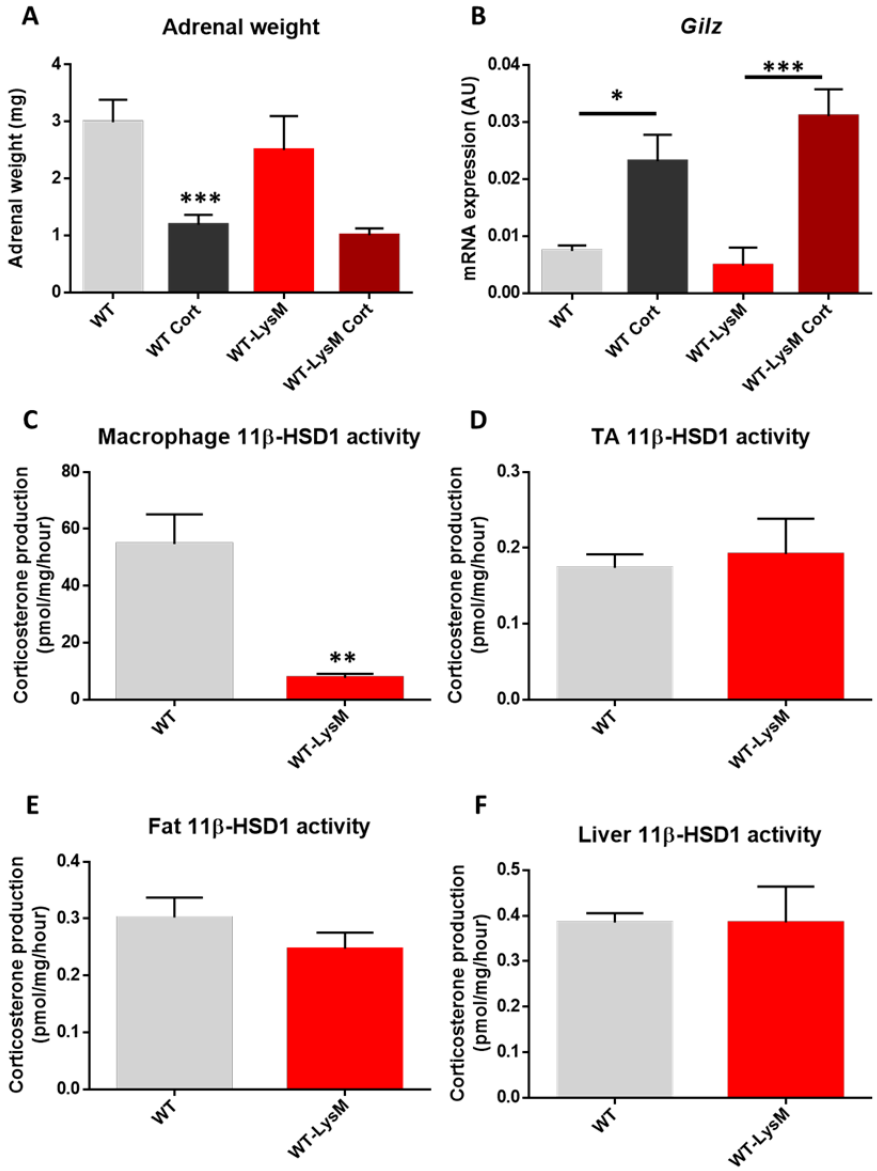

Figure 4. 12: Analysis of GC response parameters in WT and WT-LysM mice

(A) Adrenal weights (mg) in WT (n=6) and WT-LysM (n=2) animals receiving control or 100 mg/L corticosterone WT (n=8) and WT-LysM (n=5) in the drinking water for three weeks. (B) Gene expression of *Gilz* (AU) determined by qPCR analysis of WT (n=6) and WT-LysM (n=4) animals receiving control or 100 mg/L corticosterone WT (n=5) and WT-LysM (n=5) in the drinking water for three weeks 11β-HSD1 activity (pmol/mg/hour) determined by TLC assays in (C) macrophages isolated from WT (n=3) and WT-LysM (n=5) mice and (D) tibialis anterior muscles, (E) fat tissue and (F) liver tissue (WT n=3 and WT-LysM (n=2). Data is presented as mean ± SEM and statistical significance was determined using two-way ANOVA with Tukey's multiple comparisons test and unpaired t test (* denotes P≤0.05, ** denotes P≤0.01 and *** denotes P≤0.001).

4.4.10 WT-LysM have an overall reduction in trabecular bone compared to WT animals

As previously reported, corticosterone effects are not apparent in animals at three weeks. However, to assess the impact of myeloid 11β-HSD1 deletion on bone metabolism in WT-LysM cre animals tibias were formalin fixed post mortem and stored at 4°C in 70% ethanol prior to micro-CT analysis. No difference in bone parameters was observed between corticosterone treated groups and their untreated counterparts, however WT-LysM animals had significantly lower bone volume and trabecular thickness compared to WT controls (BV/TV: WT 5.3% ± 0.5 vs WT-LysM 3.0% ± 0.4, P≤0.05; Tb.Th: WT 73.7 μm ± 3.1 vs WT-LysM 58.8 μm ± 1.4, P≤0.01) (Fig 4.13 B-C). Trabecular number showed a trend towards reductions in WT-LysM animals compared to WT mice (Fig 4.13 D). Trabecular separation revealed no significant differences amongst the groups (Fig 4.13 E). These data indicate that in mice receiving vehicle and corticosterone in drinking water for three weeks, myeloid deletion of 11β-HSD1 may elicit a trabecular bone loss phenotype relative to WT control animals.

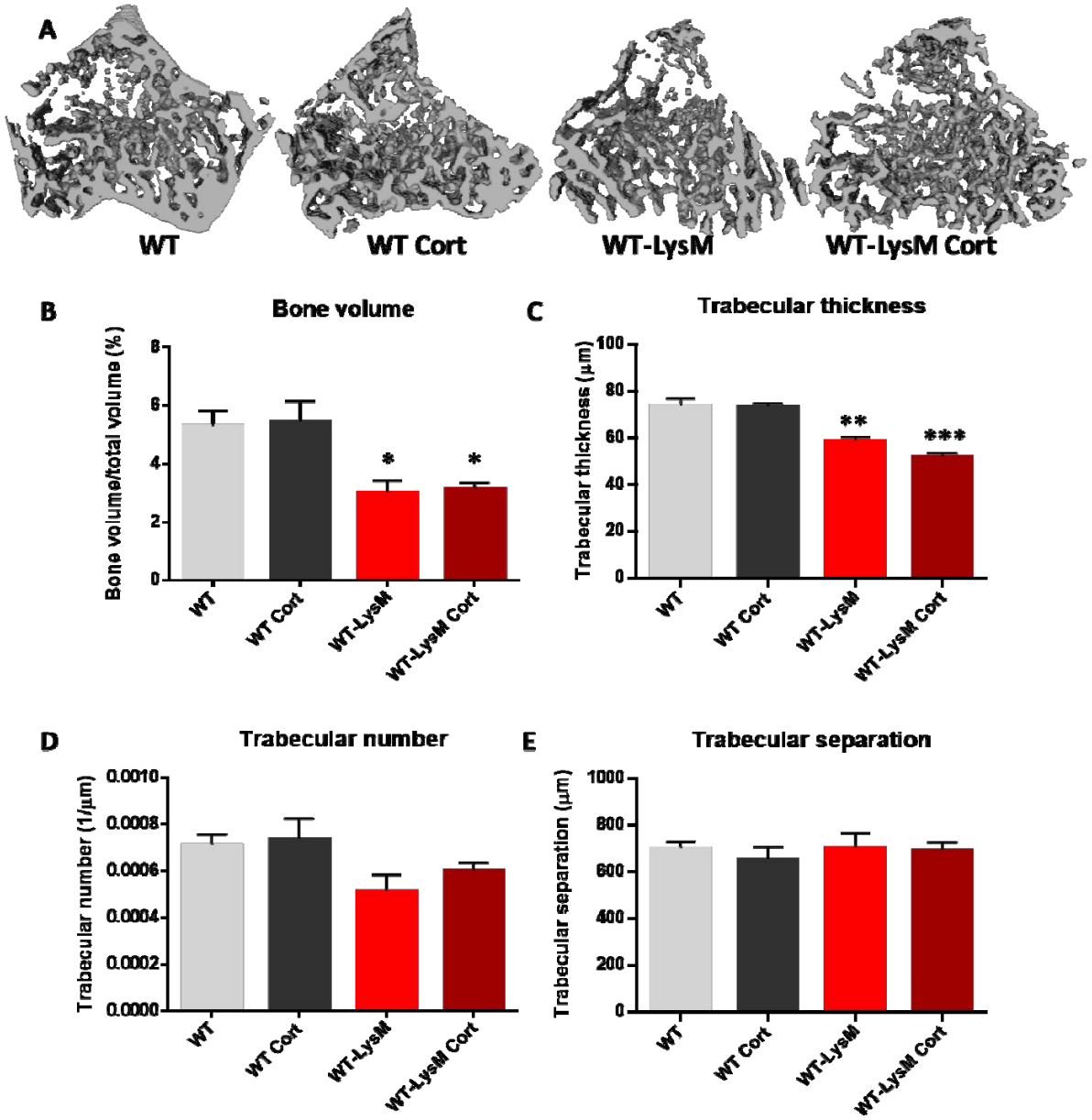

Figure 4. 13: Trabecular bone parameters of tibias from WT and WT-LysM animals

(A) Representative images of reconstructed trabecular bone from tibia scans of WT and WT-LysM animals receiving vehicle control water or 100 mg/L corticosterone drinking water for three weeks. Micro-CT analysis of (B) bone volume (%) relative to total volume, (C) trabecular thickness (µm), (D) trabecular number (1/µm) and trabecular separation (µm) of WT (n=8) and WT-LysM (n=5) animals receiving control or 100 mg/L corticosterone WT (n=6) and WT-LysM (n=5) in the drinking water for three weeks Data is presented as mean ± SEM and statistical significance was determined using two-way ANOVA with Tukey's multiple comparisons test (* denotes P≤0.05, ** denotes P≤0.01 and *** denotes P≤0.001).

4.4.11 WT-LysM mice exhibit changes in bone remodelling markers similarly to WT animals

As reported previously, whilst bone phenotypes are not apparent at three weeks of exposure to corticosterone, changes in biochemical and gene markers of bone turnover are apparent at three weeks. Consequently, we examined bone turnover markers at this timepoint in WT-LysM cre animals receiving either vehicle or corticosterone relative to WT controls. Serum levels of the osteoblast activity marker P1NP were significantly lower in both WT-LysM animals and WT animals receiving oral corticosterone compared to their untreated counterparts (WT-LysM 445.8 ng/ml ± 42.0 vs WT-LysM Cort 28.4 ng/ml ± 9.4, P≤0.001), with no significant difference between genotypes (Fig 4.14 A). Similar patterns were observed with gene expression levels of the mature osteoblast markers *Bglap* and *Alpl*, with significant suppressions in both corticosterone treated groups relative to their untreated controls. Again, no differences were identified between the different genotypes (Fig 4.14 B-C). Analysis of factors involved in osteoblast differentiation, *Runx2*, *Sost* and *Dkk1*, revealed no significant differences amongst the groups (Fig 4.14 D-F). These data indicate that mice with myeloid deletion of 11β-HSD1 are not protected from anti-anabolic bone loss in response to oral delivery of corticosterone over three weeks, with markers of mature osteoblasts and osteoblast activity suppressed in these animals in a similar manner to WT animals.

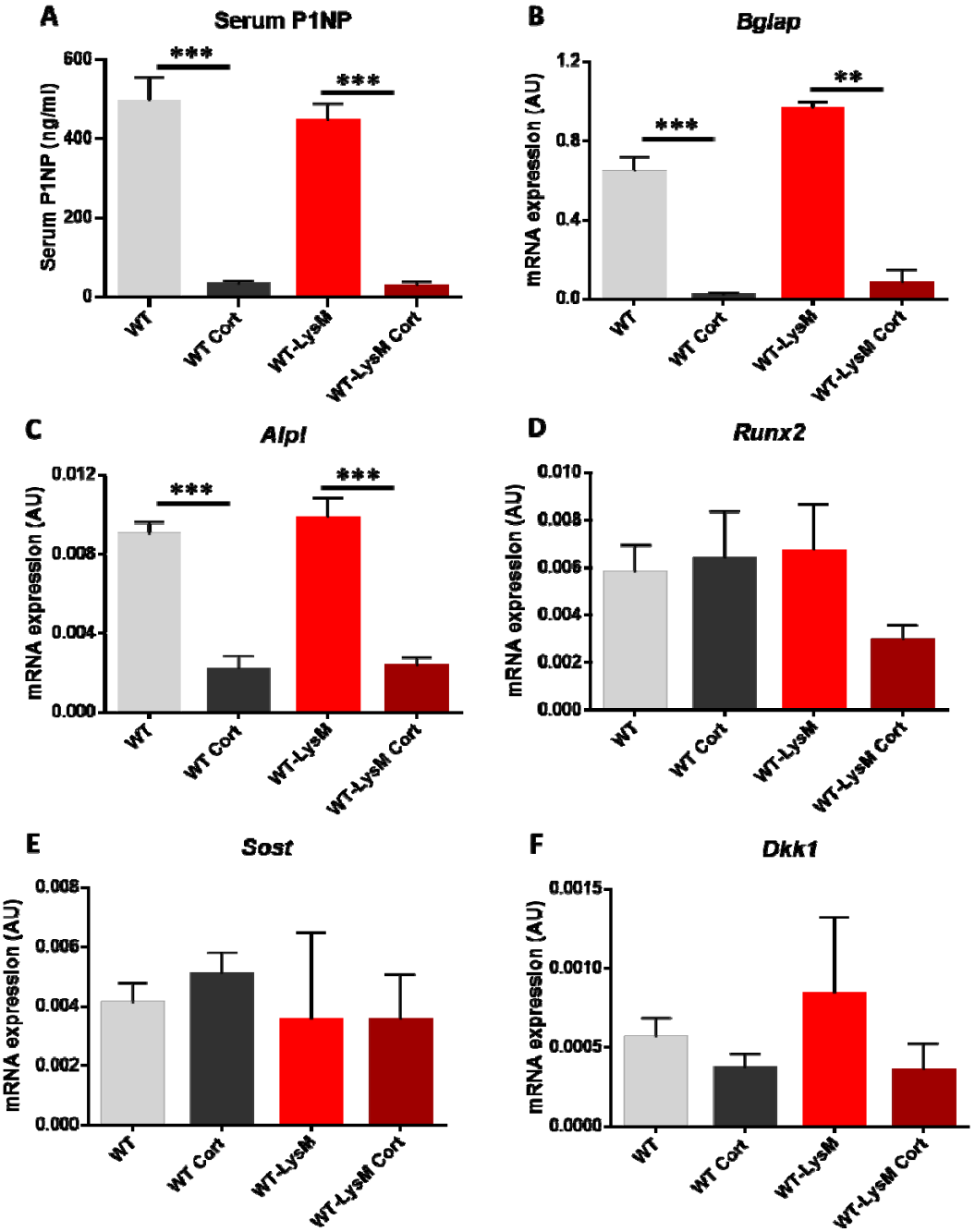

Figure 4. 14: Osteoblast markers in GC treated WT and WT-LysM animals

(A) ELISA analysis of serum P1NP (ng/ml) of WT (n=6) and WT-LysM (n=5) animals receiving control or 100 mg/L corticosterone WT (n=6) and WT-LysM (n=5) in the drinking water for three weeks. qPCR gene expression analysis (AU) of (B) *Bglap,* (C) *Alpl,* (D) *Runx2,* (E) *Sost* and (F) *Dkk1* in tibias from WT (n=6) and WT-LysM (n=4) animals receiving control or 100 mg/L corticosterone WT (n=5) and WT-LysM (n=5) in the drinking water for three weeks. Data is presented as mean ± SEM and statistical significance was determined using two-way ANOVA with Tukey's multiple comparisons test (** denotes P≤0.01 and *** denotes P≤0.001).

Finally, osteoclasts markers in the serum and mRNA generated from the tibias of WT-LysM mice were analysed. Serum levels of the osteoclast activity marker, CTX-1, were significantly reduced in WT-LysM animals treated with oral corticosterone compared to their untreated counterparts. A trend towards decreased CTX-1 levels was observed between WT animals receiving corticosterone compared to untreated WT mice. GC treated WT mice relative to GC treated WT-LysM mice showed no significant differences (Fig 4.15 A). No significant differences were observed in gene expression levels of osteoclast differentiation factors, Rankl/Opg ratio and *Csf1*, or the osteoclast activity marker, *Ctsk*, amongst the groups (Fig 4.15 B-D). These data indicate that mice lacking 11β-HSD1 specifically within the myeloid compartment are not resistant to decreases in osteoclast activity in response to corticosterone in the drinking water for three weeks.

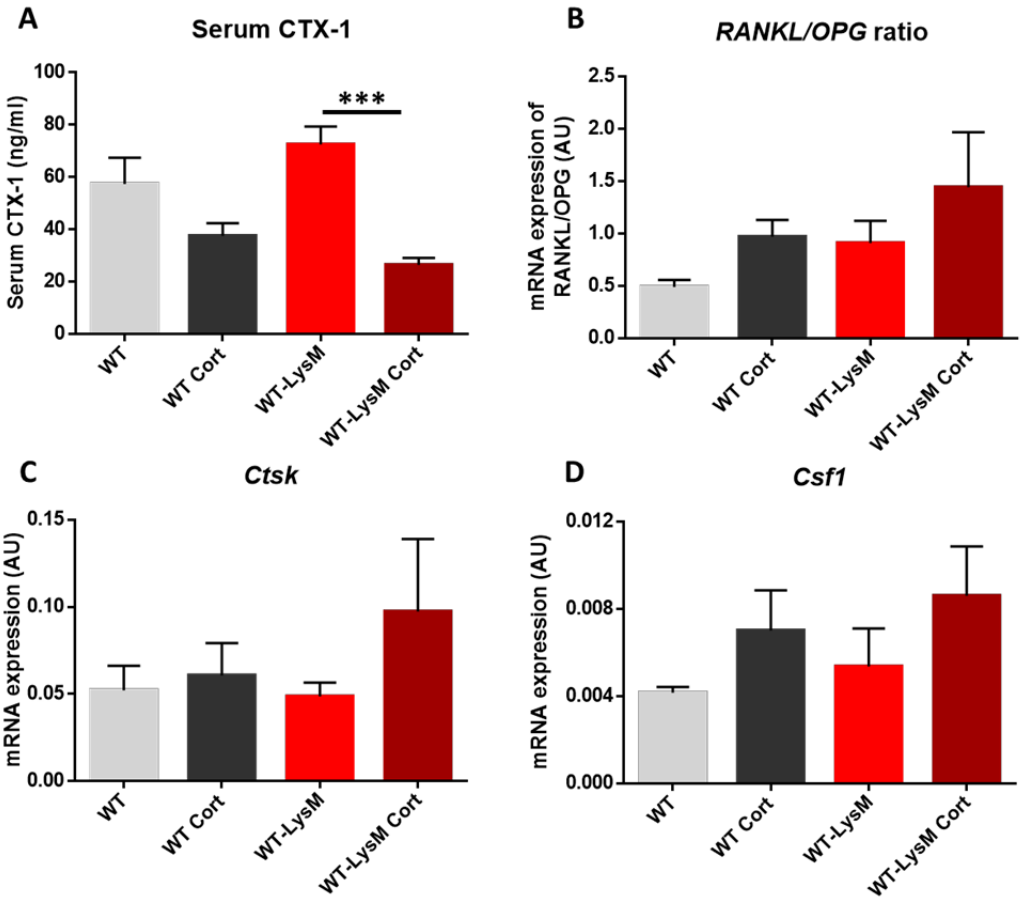

Figure 4. 15: Osteoclast markers in GC treated WT and WT-LysM animals

(A) ELISA analysis of serum CTX-1 (ng/ml) (n=5 per group) and qPCR gene expression analysis (AU) of (B) the Rankl/Opg ratio, (C) *Ctsk* and (D) *Csf1* of tibias from WT (n=6) and WT-LysM (n=4) animals receiving control or 100 mg/L corticosterone WT (n=5) and WT-LysM (n=4) in the drinking water for three weeks. Data is presented as mean ± SEM and statistical significance was determined using two-way ANOVA with Tukey's multiple comparisons test (*** denotes P≤0.001).

4.5 Discussion

Local activation of GCs by 11β-HSD1 has been shown to mediate many of the adverse metabolic effects of therapeutic GCs, such as muscle wasting, visceral obesity and glucose intolerance (70). However, less is known about the contribution of 11β-HSD1 metabolism to GIO. To address this question, we used the 11β-HSD1 KO mouse and treated with 100 mg/L corticosterone in the drinking water prior to examination of measures of systemic bone loss and markers of bone metabolism.

Typical features of GC excess were examined in the 11βKO animals to determine how their GC metabolism differs from WT animals. 100 mg/L corticosterone in the drinking water has been previously shown to induce many of the characteristic features of GC excess (70). 100 mg/L corticosterone treatment induced adrenal atrophy and increased serum corticosterone levels in both WT and 11βKO animals (Fig 4.1 A & D). Additionally, lipid deposition was observed in the liver of WT animals receiving oral corticosterone treatment, but 11βKO animals were protected from this, as previously reported by Morgan et al (70) (Fig 4.1 B). Local 11β-HSD1 GC activation within the osteoblasts of 11βKO animals was significantly ablated and induction of the GC-responsive gene *Gilz* in the tibia was blunted supporting this (Fig 4.1 C & E).

Four weeks of corticosterone treatment sufficiently induced a significant bone loss in the tibia of WT animals, characterised by significant reductions in bone volume, trabecular thickness and trabecular number and increases in separation between trabeculae. Previous studies examining bone loss in this strain reported that the C57BL/6J strain was resistant to GIO using slow release prednisolone pellets (2.5 mg/60 days for 56 days) (316). Our data indicate that timing is critical here, with limited bone loss apparent at three weeks. Similarly, the diurnal delivery and dosing may influence these processes

and may be responsible for the differences between these studies. Regardless, in our study, the reduced bone volume in spine and tibia was strongly supported by a suppression in osteoblast markers and numbers. Deletion of 11β-HSD1 protected against detrimental actions of GCs on bone volume, trabecular number and trabecular separation (Fig 4.2). Thus, 11β-HSD1 metabolism of exogenous GCs plays a significant role in the development of GIO.

Whilst reducing the exposure of GCs to three weeks resulted in no apparent trabecular bone loss in tibias, analysis of spines indicated that there was a significant reduction in cortical bone. Despite this, metabolic and gene markers of bone metabolism were readily detectable at this time point and were taken forward for further analysis. The bone formation marker P1NP and the mature osteoblast markers osteocalcin and alkaline phosphatase were markedly suppressed in WT animals upon treatment with GCs, similarly to what is reported in human patients receiving GC therapy (317). However, 11βKO animals showed partial protection from the suppression of osteoblast markers. Factors influencing osteoblast differentiation, *Runx2, Sost* and *Dkk1* showed no differences between WT and 11βKO animals treated with corticosterone, indicating a reduction in mature osteoblast numbers rather than a decrease in osteoblast differentiation. Further research could examine changes in other anabolic regulatory factors such as wnt ligands, TGF-β or androgens to investigate whether they mediate the suppression of osteoblasts observed here. A previous study showed that exogenous treatment with GCs induced osteoblast and osteocyte apoptosis and overexpressing the GC-inactivating enzyme 11β-HSD2 specifically in mature osteoblasts protected these cells from steroid-induced apoptosis (237). Thus, it is possible that 11β-HSD1 metabolism mediates apoptosis of osteoblasts in response to exogenous GC treatment and this

subsequently leads to reductions in bone formation. In contrast, osteoclasts appeared less susceptible to changes in response to GCs, with trends towards decreased bone resorption in both WT and 11βKO animals treated with corticosterone. GCs did however increase the RANKL/OPG ratio in WT animals consistent with what is reported in the literature but failed to do so in 11βKO animals, indicating that 11β-HSD1 metabolism of GCs may influence differentiation and activation of osteoclasts (242).

The spine is particularly susceptible to GIO, with patients on GC therapy having an approximate 10% decrease in BMD at the lumbar spine and upwards of double the risk of vertebral fracture (21, 314). Therefore, the spine of WT and 11βKO mice were also analysed for response to GC treatments. Micro-CT analysis of the sixth lumbar vertebrae revealed modest changes in trabecular bone, with reductions in bone volume and trabecular thickness in WT animals treated with GCs, which were not present in 11βKO animals (Fig 4.3). However, more robust changes were reported by ImageJ analyses of the cortical bone of lumber 6. Cortical area, periosteal perimeter and endosteal perimeter were all markedly reduced in WT animals receiving corticosterone. In contrast, these reductions were not apparent in 11βKO animals receiving corticosterone, suggesting that 11β-HSD1 metabolism of GCs also mediates the destruction of vertebral bone in GIO (Fig 4.4). GC therapy in children often results in a retardation of bone growth and subsequent reduced height (318). Given that both periosteal perimeter and endosteal perimeter were reduced in WT animals may suggest that bone growth is affected in this setting, rather than changing homeostatic metabolism alone. The effects on the spines of WT animals receiving corticosterone were shown to coincide with a dramatic suppression of osteoblast numbers. As with the levels of anabolic bone markers, this was partially abrogated in GC treated 11βKO animals (Fig 4.5).

Overall, 11β-HSD1 metabolism of therapeutic GCs appears to play an important role in the development of GIO. The main bone cells are the mesenchymal-derived bone forming osteoblasts and the myeloid-derived bone resorbing osteoclasts. The next aim was to try to ascertain which cells expressing 11β-HSD1 were responsible for mediating the negative effects of GCs on the bone. Both the mesenchymal specific 11β-HSD1 KO (WT-Twist2) mouse and the myeloid specific 11β-HSD1 KO (WT-LysM) mouse developed adrenal suppression upon corticosterone treatment similar to WT animals and exhibited upregulated *Gilz* expression demonstrating a normal response to GCs in these animals. Reduced activity of 11β-HSD1 in osteoblasts was confirmed in the WT-Twist2 animals (Fig 4.8). We have previously shown that Twist2 animals have retained activity in the spleen and bone marrow cells, whilst activity is reduced in the front paws and tibialis anterior, and 11β-HSD1 activity is completely absent in FLS isolated from these animals (157). Reduced activity of 11β-HSD1 in peritoneal macrophages was reported in WT-LysM mice (Fig 4.12). Importantly, 11β-HSD1 activity was retained in the tibialis anterior muscle, adipose tissue and liver of the myeloid specific KO animals (Fig 4.12). Further validation may be necessary to characterise these mice via methods such as immunohistochemistry or western blot to confirm KO in specific tissues and cells. However, 11β-HSD1 activity assays are advantageous in that they provide functional readouts of the activity of the enzyme.

Unsurprisingly, corticosterone-induced changes in tibial trabecular bone phenotypes were not apparent in either cre KO at three weeks, in line with previous findings in WT and global 11β-HSD1 KO animals. The three week time points were originally selected for examination of metabolic markers and changes in gene expression markers of bone metabolism. Future work would need to examine this at a later time point such as 4-5

weeks to confirm our findings. However, whilst no changes were observed in WT-LysM mice receiving corticosterone compared to untreated controls, these animals had significantly reduced bone volume and trabecular thickness compared to WT animals, suggesting there may be altered bone metabolism at a basal level when 11β-HSD1 is deleted from myeloid cells (Fig 4.13). A recently identified subtype of resident macrophage in the bone, known as osteomacs, have been shown to be closely associated with osteoblasts and are required for efficient osteoblastic mineralisation (319). This raises the possibility that disruption of GC amplification in osteoclasts or osteomacs may inhibit the capacity to facilitate osteoblast function at a basal level.

In contrast to global 11β-HSD1 KO mice, both mesenchymal specific KOs and myeloid specific KOs treated with GCs had reduced P1NP, osteocalcin and alkaline phosphatase to a similar extent as corticosterone treated WT animals (Fig 4.10 & 4.14). Osteoclast markers were also similar in WT-Twist2 and WT-LysM animals receiving oral corticosterone compared to corticosterone treated WT mice (Fig 4.11 & 4.15). Consequently, these data indicate that 11β-HSD1 within either osteoclasts or osteoblasts are not sufficient to mediate the effects of therapeutic GCs on bone as observed in the global HSD1 KO animal. This may indicate that another cell type expressing 11β-HSD1 is responsible, or that deletion in only one cell population is insufficient to mediate GC effects. It may be that paracrine signalling of GCs via 11β-HSD1 may compensate for this, or that a failure to initiate 100% deletion using these cre mice is not sufficient to reproduce the global KO protective phenotype. Further validation of the cell specific KO mice may be required to address this.

In conclusion, 11β-HSD1 metabolism of therapeutic GCs significantly contributes to the manifestation of GIO by suppressing bone formation via reducing the numbers of mature

osteoblasts present. This would suggest 11β-HSD1 inhibitors may be beneficial to prevent GIO, as well as muscle wasting, obesity and hypertension in patients receiving therapeutic GCs (70). However, before 11β-HSD1 inhibitors can be utilised for the prevention of GC-induced side effects, research should first be performed, to assess whether the anti-inflammatory immunomodulatory effects of GCs are also dependent on 11β-HSD1.

Chapter 5: The role of 11β-HSD1 in the anti-inflammatory properties of therapeutic glucocorticoids

5.1 Introduction

GCs are effective in the treatment of many chronic inflammatory diseases, however the development of metabolic side effects remains a substantial problem associated with their application (320). Thus, a better understanding of the precise mechanisms of GC actions is required to overcome this. Initially, efforts centred on investigating the functions of the monomeric GR versus the dimeric GR, with the view that the anti-inflammatory properties of GCs were mediated by transrepression by monomeric GRs, whilst the adverse metabolic side effects were dependent on transactivation by dimeric GR complexes (132). However, this was shown to be an oversimplified view of the mechanisms of GC action (see section 1.4.2) (138). More recently, research has focussed on developing a better understanding of the cell-specific actions of GCs to develop targeted GC treatments capable of bypassing their detrimental side effects.

5.1.1 Cell specific anti-inflammatory responses to therapeutic GCs

Various papers have investigated the contribution of specific cell types in the suppression of inflammation in response to GC therapy using various cell specific GR KO models.

In 2007, Tuckermann *et al* examined the role of different cell types in the therapeutic response to GCs in a mouse model of contact hypersensitivity (CHS) (321). Despite the fact that T cells have been shown to play an important role in CHS, with T cell depleted mice having significantly less disease activity, a T cell specific GR KO (GR^{lckCre}) mouse retained the ability to strongly suppress inflammation in response to treatment with dexamethasone (322). Similarly, whilst keratinocytes drive pathogenesis of CHS by producing pro-inflammatory cytokines and chemokines, keratinocyte specific GR KO

(GR^{K14Cre}) mice could also potently suppress inflammation upon dexamethasone treatment. The myeloid specific GR KO ($GR^{LysMCre}$) mouse which predominantly targets macrophages and neutrophils, on the other hand, could no longer suppress inflammation by GC treatment. In these mice, macrophage and neutrophil activity persisted at the sites of inflammation in the skin following dexamethasone treatment. Thus, the authors concluded that macrophages and neutrophils mediate the therapeutic actions of GCs in CHS (321).

Additional studies have investigated the cell types mediating the anti-inflammatory response to therapeutic GCs in mouse models of inflammatory arthritis. One study found that a T cell specific GR deletion inhibited the therapeutic response to dexamethasone in an antigen-induced arthritis model, whilst macrophage, B cell and dendritic cell specific KOs had a normal response to GC treatment, indicating that T cell GC signalling mediates the anti-inflammatory actions of GC in this model (323). Conversely, another study showed that the GR in stromal cells, such as FLS, was required to polarise macrophages towards the pro-resolution phenotype and suppress disease activity in the serum transfer-induced arthritis model (138). These discrepancies could be due to differences in inflammatory models, which have different pathogeneses and may require alternative resolution pathways.

5.1.2 The role of 11β-HSD1 in inflammation

As previously discussed in section 1.4.7, 11β-HSD1 metabolism of endogenous GCs plays an important role in the suppression and resolution of inflammation. Coutinho *et al* showed the progression of inflammation in animals deficient in 11β-HSD1 in three distinct

mouse models of acute inflammation. 11β-HSD1 KO mice developed earlier onset and more severe inflammation in the STIA model, in addition to a significant impairment in resolution. In the thioglycolate-induced sterile peritonitis mouse model, 11β-HSD1 KO animals had a significantly greater inflammatory infiltrate into the peritoneum. Similarly, in the carrageenan-induced pleurisy model, inflammatory cell infiltration was significantly greater in the 11β-HSD1 KO mouse with significantly higher cell numbers in pleural lavages and delayed resolution (324). These studies indicated that 11β-HSD1 acts to restrain inflammation in acute diseases and support resolution. Additionally, we have previously shown that 11β-HSD1 metabolism of endogenous GCs plays a fundamental role in suppressing inflammation in chronic inflammation. Moreover, a stromal cell specific 11β-HSD1 KO mouse crossed with the TNF-tg animal did not show the same exacerbation of disease and in fact had a modest protection from joint inflammation and local juxta-articular bone loss, indicating that stromal 11β-HSD1 metabolism of GCs worsens inflammation (157).

Overall, 11β-HSD1 appears to mediate the endogenous anti-inflammatory and pro-resolution pathways associated with GC production. However, whether metabolism by 11β-HSD1 is necessary to produce the therapeutic immunosuppressive properties of GCs during chronic inflammation remains unknown. Thus, this chapter utilises GC treatment in the global 11β-HSD1 KO mouse, in addition to the mesenchymal and myeloid specific KOs, crossed with the TNF-tg model of chronic inflammatory polyarthritis to determine how GCs mediate their therapeutic effects.

5.2 Hypothesis

The therapeutic anti-inflammatory action of GCs in chronic inflammatory polyarthritis is mediated by their local activation by 11β-HSD1.

5.3 Materials and Methods

5.3.1 Animal experiments

Heterozygous TNF-tg mice (section 2.1.1) were crossed with global 11β-HSD1 KO mice (section 2.1.2) to generate the TNF11βKO mouse. TNF-tg animals were also crossed with a mesenchymal specific 11β-HSD1 KO mouse and a myeloid specific 11β-HSD1 KO mouse to generate TNF-Twist2 and TNF-LysM animals, respectively (section 2.1.3). Four-week old mice were treated with 100 mg/L corticosterone in the drinking water for three weeks and scored for clinical and arthritic paw scores as described in section 2.1.4. At seven weeks, animals were sacrificed by cervical dislocation after exsanguination by cardiac puncture. Tissues were dissected and stored prior to use as previously described (section 2.1.4). Adrenals were removed and weighed immediately.

5.3.2 Micro-CT analysis

Front paws were formalin fixed prior to being stored in 70% ethanol at 4°C. Samples were scanned on a Skyscanner 1172 (Bruker Micro-CT, Belgium) and reconstructed using NRecon (section 2.2). Front paws were scored for bone erosions as described in section 2.2.2.

5.3.3 Cell culture

Synovial fibroblasts and peritoneal macrophages were isolated from WT and KO mice as described in sections 2.4.1 and 2.4.2, respectively. Co-culture and conditioned media experiments were set up according to sections 2.4.3 and 2.4.4, respectively. Following

the experiments, media was collected and RNA was isolated and stored at -80°C prior to use.

5.3.4 ELISA analysis

Following cardiac punctures, blood was left to clot for 30 minutes at room temperature before being centrifuged at 13,000 rpm for 30 minutes to separate out the serum. Serum was aspirated into a fresh tube and stored at -80°C prior to use. Levels of IL-6 in the serum of animals or the media from cell cultures was assessed according to section 2.6.1.1.

5.3.5 Gene expression analysis

Following dissection, one tibia from each mouse was homogenised in a pestle and mortar with liquid nitrogen. RNA was isolated from the resulting homogenate or from primary cells using the innuPREP RNA Mini Kit 2.0 (AnalytikJena, Jena, Germany) as outlined in section 2.5.1. Purity and concentration of RNA was assessed using a NanoDrop™ 1000 Spectrophotometer (ThermoFisher, Paisley, UK). 700 ng RNA was reverse transcribed to make cDNA using the High-Capacity cDNA Reverse Transcription Kit (ThermoFisher, Paisley, UK) (see section 2.5.2). Gene expression could then be measured by quantitative real time PCR (section 2.5.3) using the Taqman probes listed in Supplementary Table 1 (Applied Biosystems).

5.3.6 Histological staining

Front paws were excised and formalin fixed before being stored in 70% ethanol at 4°C prior to histological staining and analysis. Bones were decalcified in EDTA (0.5 M) and embedded courtesy of the Department of Musculoskeletal Pathology at the ROH. H&E staining was carried out by the Department of Musculoskeletal Pathology as outlined in section 2.8.1. Pannus invasion into the joint was assessed using ImageJ software according to section 2.8.1. Osteoclasts were stained for TRAP as described in section 2.8.2 and cartilage degradation was assessed using safranin O proteoglycan staining (section 2.8.3).

5.3.7 Statistical analysis

GraphPad Prism software (GraphPad, San Diego, USA) was used to determine statistical significance. Two-way ANOVA analysis was used with a Tukey post hoc analysis to compare between treatment groups and genotypes unless otherwise stated in the figure legend. One-way ANOVA analysis was used with a Tukey post hoc analysis to compare between different conditions in cell culture assays. N numbers are recorded in the relevant figure legend. Statistical significance was determined as $P \leq 0.05$. * denotes $P \leq 0.05$, ** denotes $P \leq 0.01$ and *** denotes $P \leq 0.001$.

5.4 Results

5.4.1 GCs do not suppress inflammation in the TNF11βKO mouse

GCs have been shown to have potent immunosuppressant properties when administered during chronic inflammatory disease. In order to determine the contribution of 11β-HSD1 metabolism to the therapeutic actions of GCs, TNF-tg animals were crossed with global 11β-HSD1 KO animals and treated with 100 mg/L corticosterone in the drinking water for three weeks. Three weeks of 100 mg/L corticosterone caused significant adrenal atrophy in both genotypes (Fig 5.1).

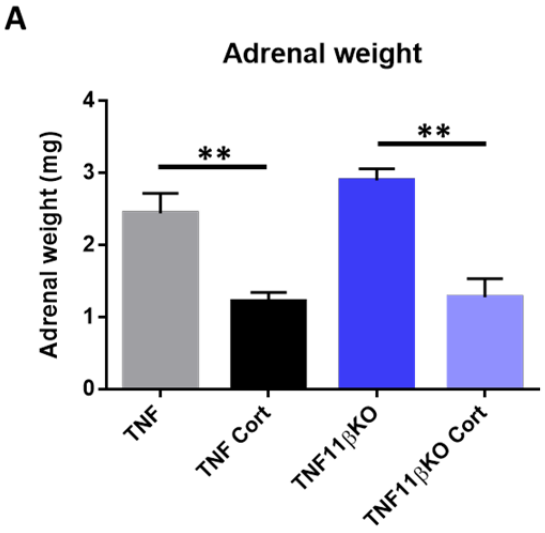

Figure 5. 1: Adrenal weights of TNF-tg and TNF11βKO animals receiving GCs

Adrenal weights (mg) of TNF-tg (n=5) and TNF11βKO (n=3) animals receiving control or 100 mg/L corticosterone TNF-tg (n=13) and TNF11βKO (n=8) in the drinking water for three weeks. Data is presented as mean ± SEM and statistical significance was determined using two-way ANOVA with Tukey's multiple comparisons test (** denotes P≤0.01)

Clinical and arthritic paw scores were recorded from GC treatment commencement at four weeks old until seven weeks old, after which mice were culled by cervical dislocation.

As previously reported in 11β-HSD1 KO animals, arthritic paws scores of TNF11βKO animals were significantly higher than TNF-tg animals, indicating that the level of arthritis is more severe in the absence of 11β-HSD1 (Fig 5.2 B) (157). Whilst both the clinical and arthritic paw scores of TNF-tg mice were significantly suppressed upon GC treatment (Clinical scores: TNF-tg 6.33 AU ± 0.5 vs TNF-tg Cort 3.60 AU ± 0.9, P≤0.001; Arthritic paw scores: TNF-tg 7.17 AU ± 0.8 vs TNF-tg Cort 2.20 AU ± 0.8, P≤0.0001), TNF11βKO animals were resistant to these effects and scoring parameters remained elevated following corticosterone administration (Clinical scores: TNF11βKO 7.33 AU ± 0.5 vs TNF11βKO Cort 7.50 AU ± 1.1, P=0.9999; Arthritic paw scores: TNF11βKO 9.17 AU ± 1.3 vs TNF11βKO Cort 9.75 AU ± 0.9, P>0.9999) (Fig 5.2).

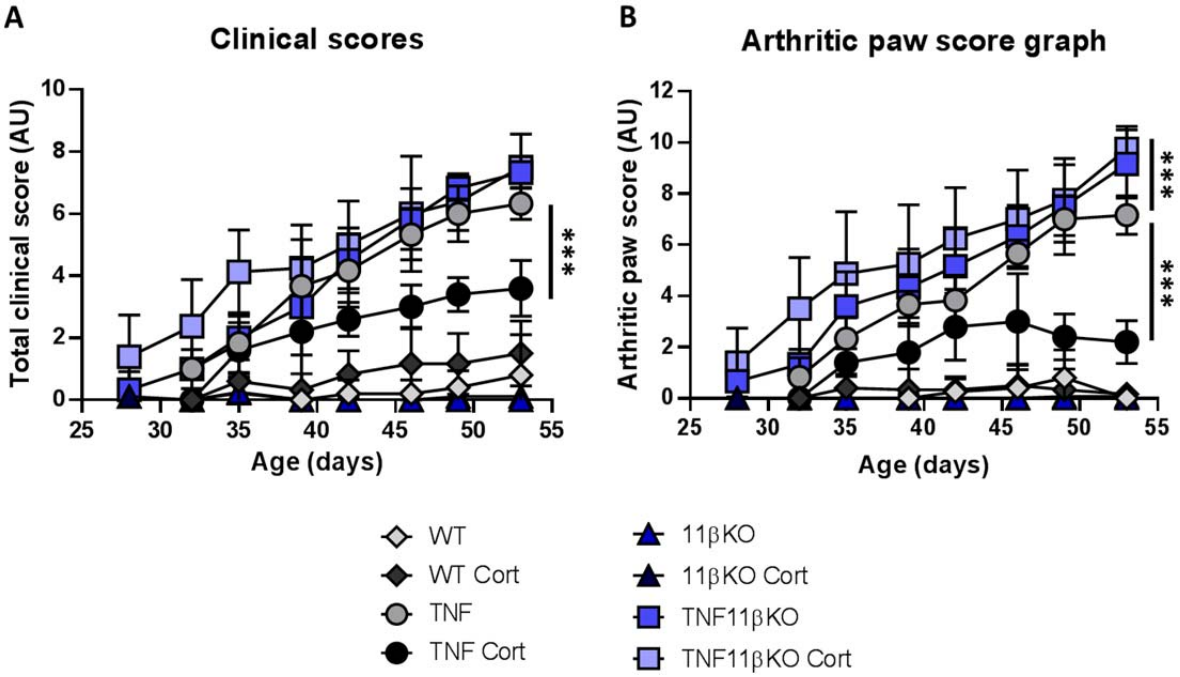

Figure 5. 2: Clinical and arthritis paw scores of TNF11βKO animals with or without GC treatment

(A) Clinical scores and (B) arthritic paw scores (AU) in WT, TNF-tg, 11βKO and TNF11βKO mice receiving control or 100 mg/L corticosterone in the drinking water for three weeks (n=6 per group). Data is presented as mean ± SEM and statistical significance was determined using two-way ANOVA with Tukey's multiple comparisons test (*** denotes P≤0.001).

To examine the regulation of inflammatory mediators in the synovium, pro-inflammatory cytokines were analysed by qPCR analysis of tibia RNA and ELISA analysis of isolated serum. In TNF-tg mice, murine *Tnf* showed no significant difference between untreated animals and mice receiving GC treatment. In TNF11βKO animals, *mTnf* was not suppressed by corticosterone treatment and was significantly higher in TNF11βKO mice receiving oral corticosterone compared to TNF-tg mice receiving corticosterone (TNF-tg Cort 0.0008 AU ± 0.0001 vs TNF11βKO Cort 0.002 AU ± 0.0003, P≤0.01) (Fig 5.3 A). Analysis of the human TNF transgene expression (*hTNF)* was also analysed in these mice. Corticosterone treatment significantly suppressed *hTNF* levels in TNF-tg mice,

whilst no suppression was observed in TNF11βKO animals. TNF11βKO animals treated with GCs had significantly higher levels of *hTNF* relative to GC treated TNF-tg animals (TNF-tg Cort 0.00002 AU ± 0.000009 vs TNF11βKO Cort 0.0002 AU ± 0.00007, P≤0.001) (Fig 5.3 B). Analysis of serum levels of IL-6 revealed a near complete inhibition of IL-6 in TNF-tg animals receiving oral corticosterone compared to their untreated counterparts, whilst levels of IL-6 persisted in the serum of corticosterone treated TNF11βKO animals (Fig 5.3 C). Finally, *il-1* expression levels showed significant decreases in both WT and TNF-tg animals receiving oral corticosterone compared to their untreated controls. This suppression was not apparent in 11βKO and TNF11βKO mice and TNF11βKO animals receiving GCs had significantly higher levels of *il-1* expression than TNF-tg animals receiving GC treatment (TNF-tg Cort 0.001 AU ± 0.0002 vs TNF11βKO Cort 0.005 AU ± 0.0009, P≤0.01) (Fig 5.3 D). These data suggest that the resistance of TNF11βKO animals to the therapeutic effects of GCs is mediated at least in part by a failure to suppress pro-inflammatory cytokines.

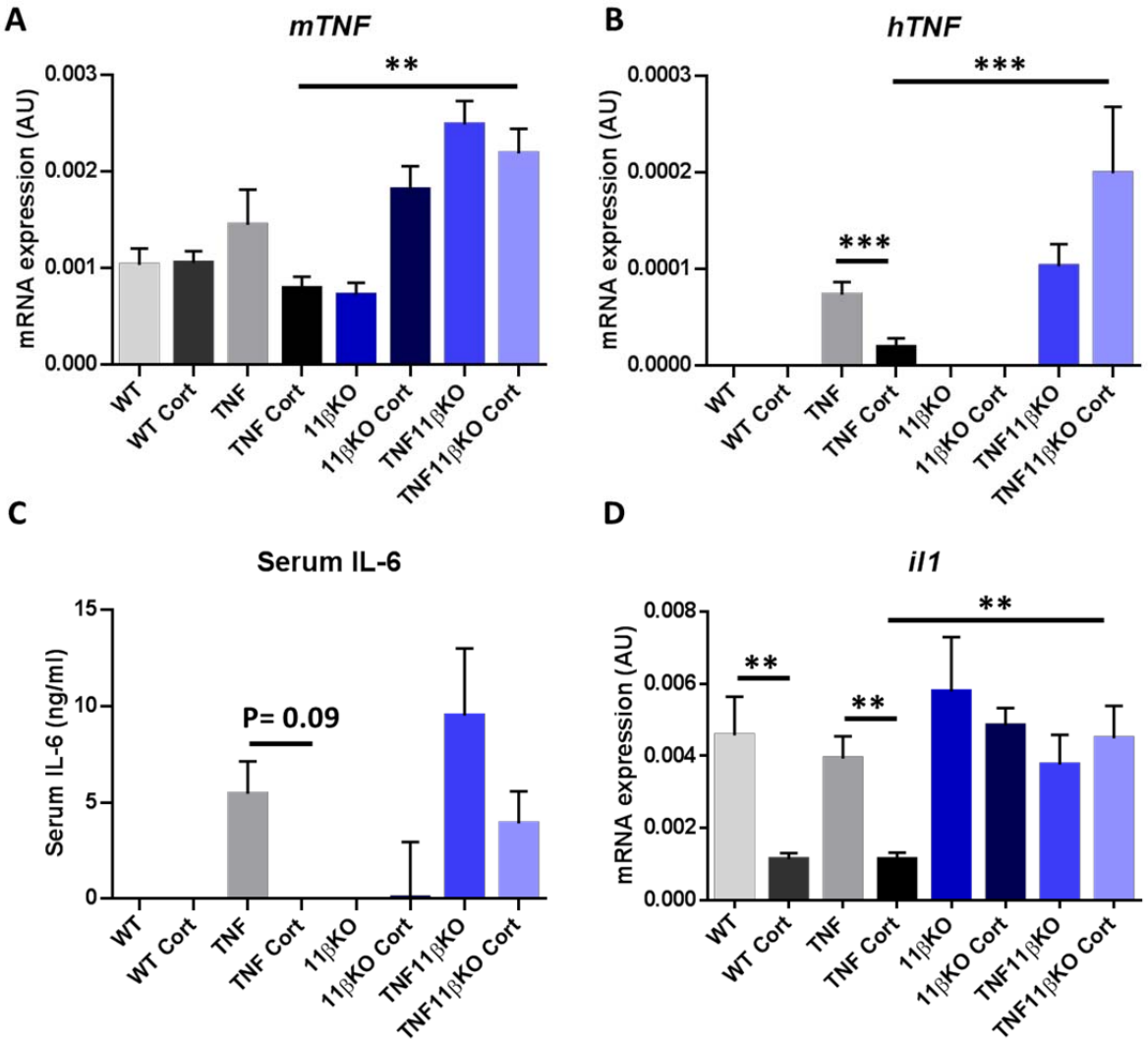

Figure 5. 3: Pro-inflammatory cytokine analysis in TNF11βKO animals

qPCR analysis of gene expression (AU) of (A) *mTnf*, (B) *hTNF* and (D) *il1* in tibias from WT (n=6), TNF-tg (n=6), 11βKO (n=5) and TNF11βKO (n=6) animals receiving control or 100 mg/L corticosterone WT (n=5), TNF-tg (n=6), 11βKO (n=6) and TNF11βKO (n=6) in the drinking water for three weeks. (C) ELISA analysis of serum IL-6 (ng/ml) in WT (n=6), TNF-tg (n=5), 11βKO (n=6) and TNF11βKO (n=6) animals receiving control or 100 mg/L corticosterone (n=6 per group) in the drinking water for three weeks. Data is presented as mean ± SEM and statistical significance was determined using two-way ANOVA with Tukey's multiple comparisons test (** denotes P≤0.01, *** denotes P≤0.001).

5.4.2 Impact of GC treatment on the joints of TNF11βKO animals

We have previously shown that GCs have an overall protective effect on the joint when administered during chronic inflammation. Therefore, to investigate the role of 11β-HSD1 activation of GCs in mediating these effects, front paws of TNF-tg and TNF11βKO animals receiving 100 mg/L corticosterone treatment were excised post mortem for micro-CT and histological analysis. Micro-CT analysis of front paws revealed that whilst corticosterone treatment significantly reduced bone erosions in the TNF-tg group compared to untreated controls, erosions persisted in the TNF11βKO corticosterone treatment group comparable to their untreated controls. Erosion scores were significantly higher in TNF11βKO animals receiving oral corticosterone compared to corticosterone treated TNF-tg mice (TNF-tg Cort 5.2 AU ± 1.93 vs TNF11βKO 16.4 AU ± 1.44, P≤0.001) (Fig 5.4). Thus, this indicates that the protective effect of GCs on juxta-articular bone erosions in chronic inflammation that I have previously reported (Chapter 3) is mediated through the activation of GCs by 11β-HSD1 metabolism.

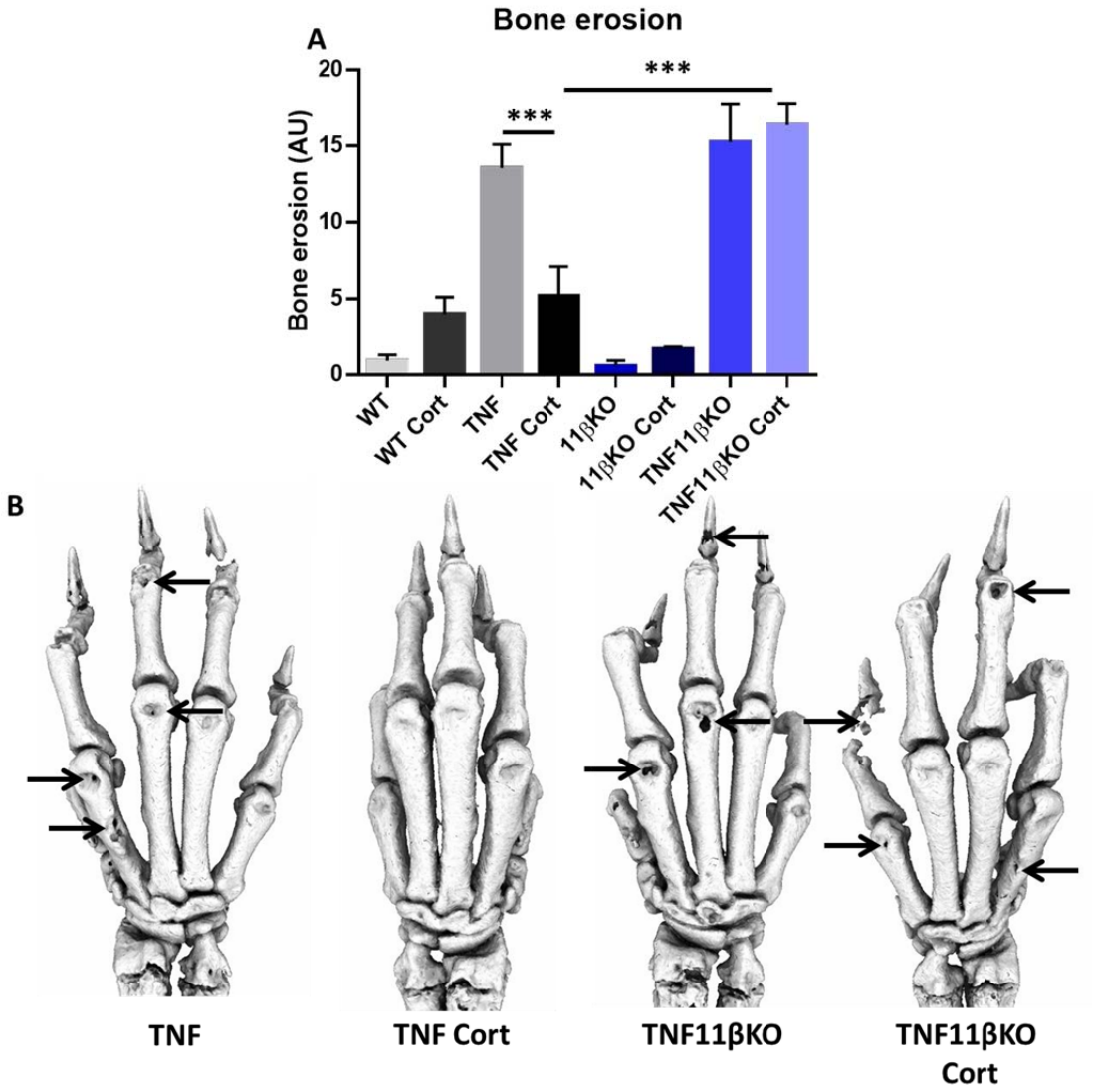

Figure 5. 4: Analysis of bone erosions in TNF-tg and TNF11βKO animals treated with GCs

(A) Quantification of degree of bone erosions (AU) by micro-CT analysis in WT (n=7), TNF-tg (n=8), 11βKO (n=7) and TNF11βKO (n=6) animals receiving control or 100 mg/L corticosterone WT (n=6), TNF-tg (n=8), 11βKO (n=8) and TNF11βKO (n=8) in the drinking water for three weeks. (B) Representative images of reconstructed front paw micro-CT scans. Arrows indicate bone erosions. Data is presented as mean ± SEM and statistical significance was determined using two-way ANOVA with Tukey's multiple comparisons test (*** denotes P≤0.001).

To examine joint histology, elbow joint sections were H&E stained, prior to quantification of pannus invasion using ImageJ software. Pannus invasion (highlighted in yellow) was apparent in untreated TNF-tg animals and significantly suppressed with GC treatment (Fig 5.5 A). In TNF11βKO animals, pannus invasion was not significantly suppressed in the GC treatment group. TNF11βKO mice receiving oral corticosterone showed significantly higher levels of pannus formation compared to corticosterone treated TNF-tg animals (TNF-tg Cort 0.02 AU ± 0.01 vs TNF11βKO Cort 0.15 AU ± 0.03, $P \leq 0.001$) (Fig 5.5 A). Therefore, GC activation by 11β-HSD1 is required for GC-induced suppression of pannus formation.

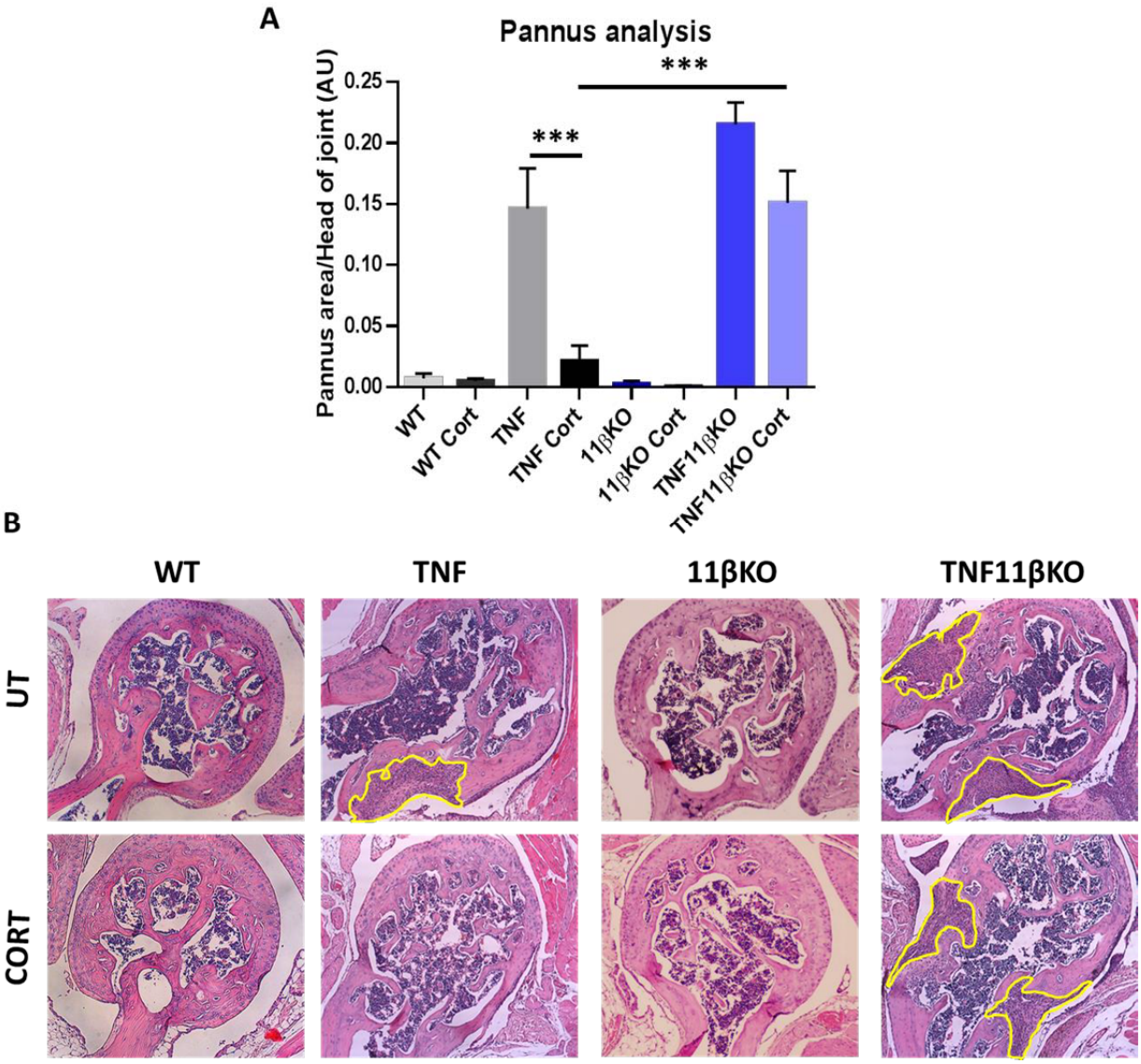

Figure 5. 5: Analysis of pannus formation in TNF-tg and TNF11βKO animals

(A) ImageJ analysis of pannus invasion (AU) in the elbow joints of WT (n=6), TNF-tg (n=6), 11βKO (n=5) and TNF11βKO (n=3) mice receiving control or 100 mg/L corticosterone (n=6 per group) in the drinking water for three weeks by H&E staining. (B) Representative images of H&E stained elbow sections of WT, TNF-tg, 11βKO and TNF11βKO animals receiving control or 100 mg/L corticosterone drinking water for three weeks. Pannus invasion is highlighted in yellow. Data is presented as mean ± SEM and statistical significance was determined using two-way ANOVA with Tukey's multiple comparisons test (*** denotes P≤0.001).

Chemokine expression was also analysed by qPCR analysis of tibia RNA. The monocyte chemoattractant *Ccl2* was potently suppressed with GC treatment in TNF-tg animals. In TNF11βKO mice GC treatment failed to suppress *Ccl2* levels and levels were significantly higher in TNF11βKO animals receiving oral corticosterone compared to corticosterone treated TNF-tg animals (TNF-tg Cort 0.0004 AU ± 0.0001 vs TNF11βKO Cort 0.0018AU ± 0.0004, P≤0.001) (Fig 5.6 A). Another monocyte/macrophage chemoattractant *Cxcl10* was assessed and showed a significant decrease in TNF-tg mice receiving GC treatment compared to their controls. This was not apparent in TNF11βKO animals receiving corticosterone compared to untreated TNF11βKO animals, with a significant increase being observed between TNF11βKO and TNF-tg GC treatment groups (TNF-tg Cort 0.0002 AU ± 0.00002 vs TNF11βKO Cort 0.0007 AU ± 0.00011, P≤0.05) (Fig 5.6 B). Analysis of the neutrophil chemoattractant *Cxcl2* revealed no significant changes amongst the groups, however untreated TNF-tg animals had a trend towards suppressed levels of the chemokine upon GC treatment. Levels of *Cxcl10* did not appear to be upregulated in TNF11βKO compared to non-inflammatory controls (Fig 5.6 C). Overall, these data indicate that the loss of GC activation by 11β-HSD1 in TNF11βKO animals results in them being unable to suppress chemokines in response to GC treatment.

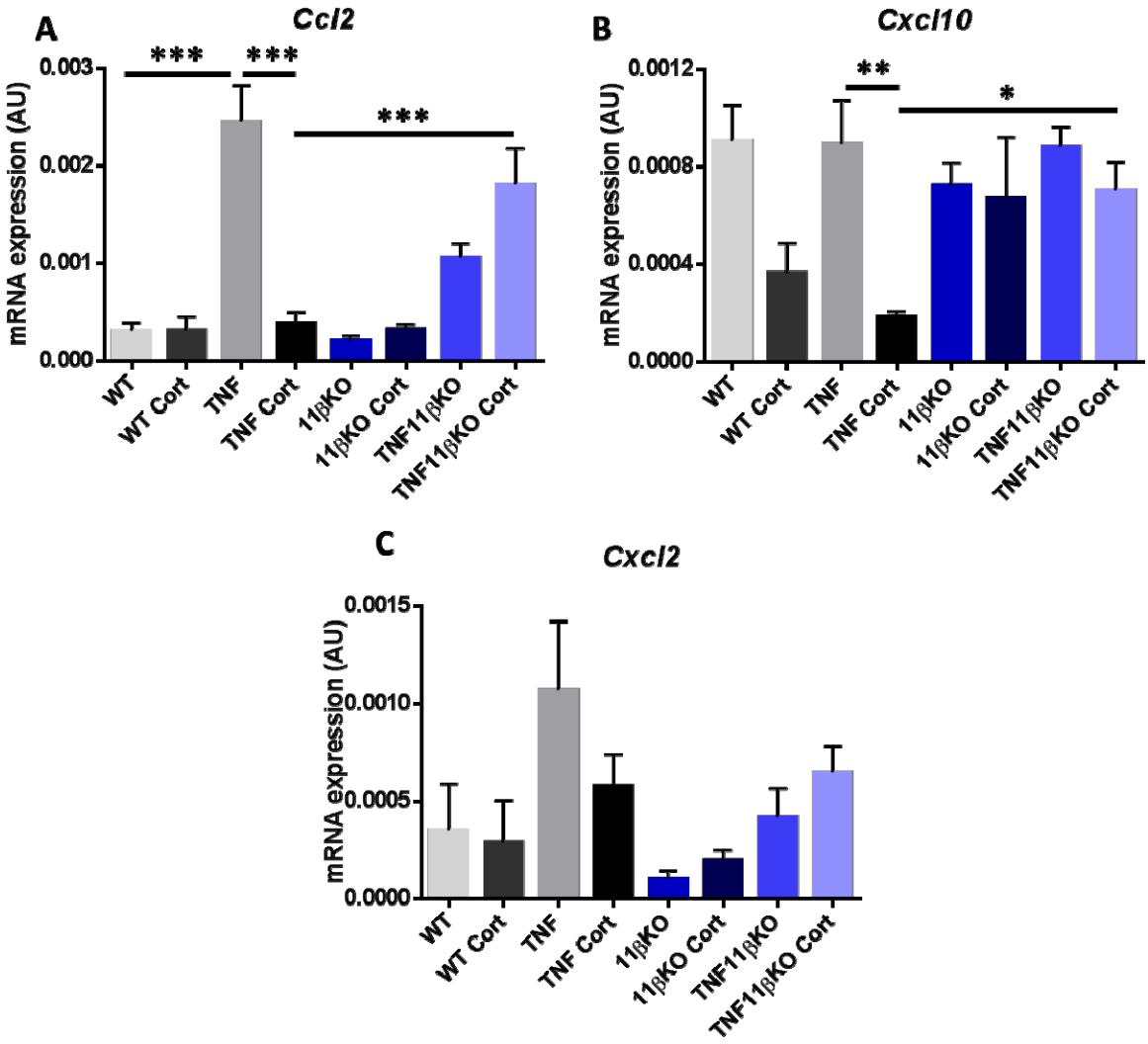

Figure 5. 6: GCs fail to suppress pro-inflammatory chemokines in TNF11βKO animals

qPCR analysis of gene expression (AU) of (A) *Ccl2*, (B) *Cxcl10* and (C) *Cxcl2* in tibias from WT (n=4), TNF-tg (n=6), 11βKO (n=4) and TNF11βKO (n=6) mice receiving vehicle control or 100 mg/L corticosterone WT (n=5), TNF-tg (n=6), 11βKO (n=5) and TNF11βKO (n=5) in the drinking water for three weeks. Data is presented as mean ± SEM and statistical significance was determined using two-way ANOVA with Tukey's multiple comparisons test (* denotes P≤0.05, ** denotes P≤0.01 *** denotes P≤0.001).

TRAP +ve osteoclast numbers were examined at the pannus/bone interface to assess their role in inflammatory bone loss in TNF-tg and TNF11βKO animals receiving corticosterone. At the humerus-ulna joint interface GC treatment potently reduced osteoclast number in TNF-tg animals but failed to suppress osteoclast numbers in

TNF11βKO animals. TNF11βKO animals treated with corticosterone had a significantly higher number of juxta-articular osteoclasts relative to TNF-tg mice receiving corticosterone treatment (TNF-tg Cort 1.5 AU ± 0.3 vs TNF11βKO Cort 19.8 AU ± 3.8, P≤0.001) (Fig 5.7). This suggests that GC activation by 11β-HSD1 is required for the suppression of osteoclasts at sites of joint inflammation in animals receiving corticosterone.

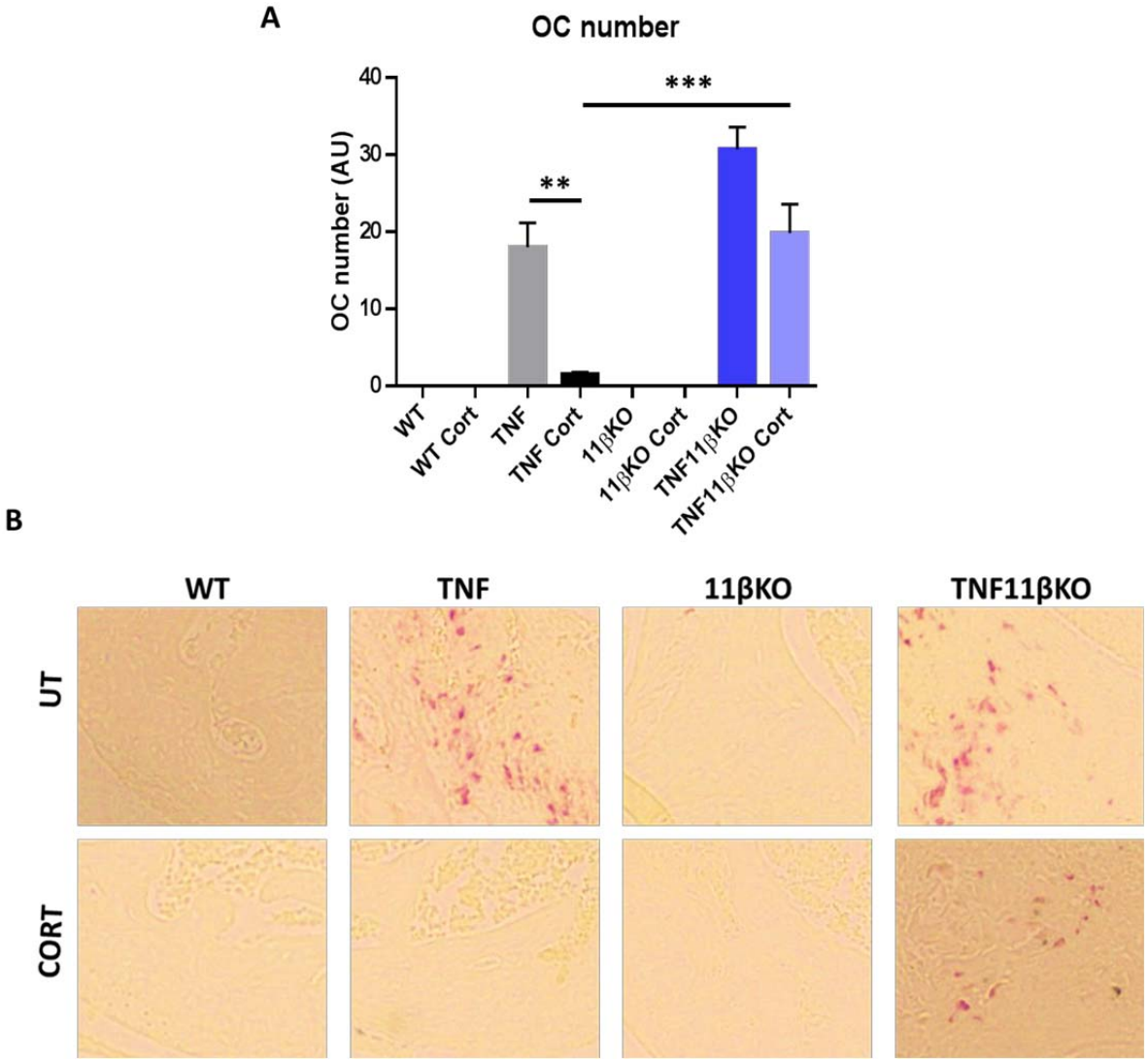

Figure 5. 7: Osteoclast counts at the elbow joints of TNF-tg and TNF11βKO corticosterone treated animals

(A) Osteoclast numbers (AU) at the head of the elbow joints determined by TRAP stains in WT (n=3), TNF-tg (n=5), 11βKO (n=3) and TNF11βKO (n=3) mice receiving control or 100 mg/L corticosterone WT (n=3), TNF-tg (n=4), 11βKO (n=3) and TNF11βKO (n=6) in the drinking water for three weeks. (B) Representative images of TRAP stains in WT, TNF-tg, 11βKO and TNF11βKO animals receiving control or 100 mg/L corticosterone drinking water for three weeks, with osteoclasts stained red. Data is presented as mean ± SEM and statistical significance was determined using two-way ANOVA with Tukey's multiple comparisons test (** denotes P≤0.01, *** denotes P≤0.001).

Further analysis of the joint was performed by investigating the role of 11β-HSD1 in cartilage damage. Safranin O staining of cartilage at the elbow joints of mice showed a trend towards decreased total cartilage area in both TNF-tg and TNF11βKO mice, compared to their non-inflammatory control groups, WT and 11βKO animals. This decrease was not ameliorated by corticosterone treatment in either TNF-tg or TNF11βKO animals (Fig 5.8 B). As previously mentioned, safranin O stain intensity is proportional to proteoglycan content of cartilage, therefore the percentage of intense staining areas were determined to assess the proportion of proteoglycan-rich areas of the joints (295). WT animals treated with corticosterone showed a trend towards decreased stain intensity compared to untreated controls. This was reduced further in the untreated TNF-tg group compared to WT mice. TNF11βKO animals showed a similar trend towards decreased intensity compared to 11βKO animals, indicating a detrimental effect of inflammation on proteoglycan content. However, corticosterone treatment had no beneficial effect on the staining intensity of TNF-tg or TNF11βKO mice (Fig 5.8 C). Finally, proteoglycan loss was analysed by measuring areas of the cartilage where stain was completely lost relative to total cartilage area. WT animals receiving oral corticosterone demonstrated a trend towards increased areas of proteoglycan loss compared to their untreated counterparts. TNF-tg animals also exhibited a trend towards increased proteoglycan loss compared to WT animals, thus further indicating potential negative effects of GCs and inflammation on proteoglycans. Again, corticosterone treatment in TNF-tg animals did not ameliorate the negative effects of inflammation on proteoglycan loss and, in fact, showed a trend towards increased loss of proteoglycans compared to untreated controls. In contrast, corticosterone treated 11βKO animals did not display an increase in proteoglycan loss compared to their relative controls. A trend towards increased proteoglycan loss was

apparent in TNF11βKO animals compared to 11βKO controls, however, contrary to TNF-tg animals, this was not exacerbated by GC treatment (Fig 5.8 D). These data therefore indicate that the negative effect of GCs on proteoglycan loss is mediated by GCs activated by 11β-HSD1 in TNF-tg animals receiving corticosterone.

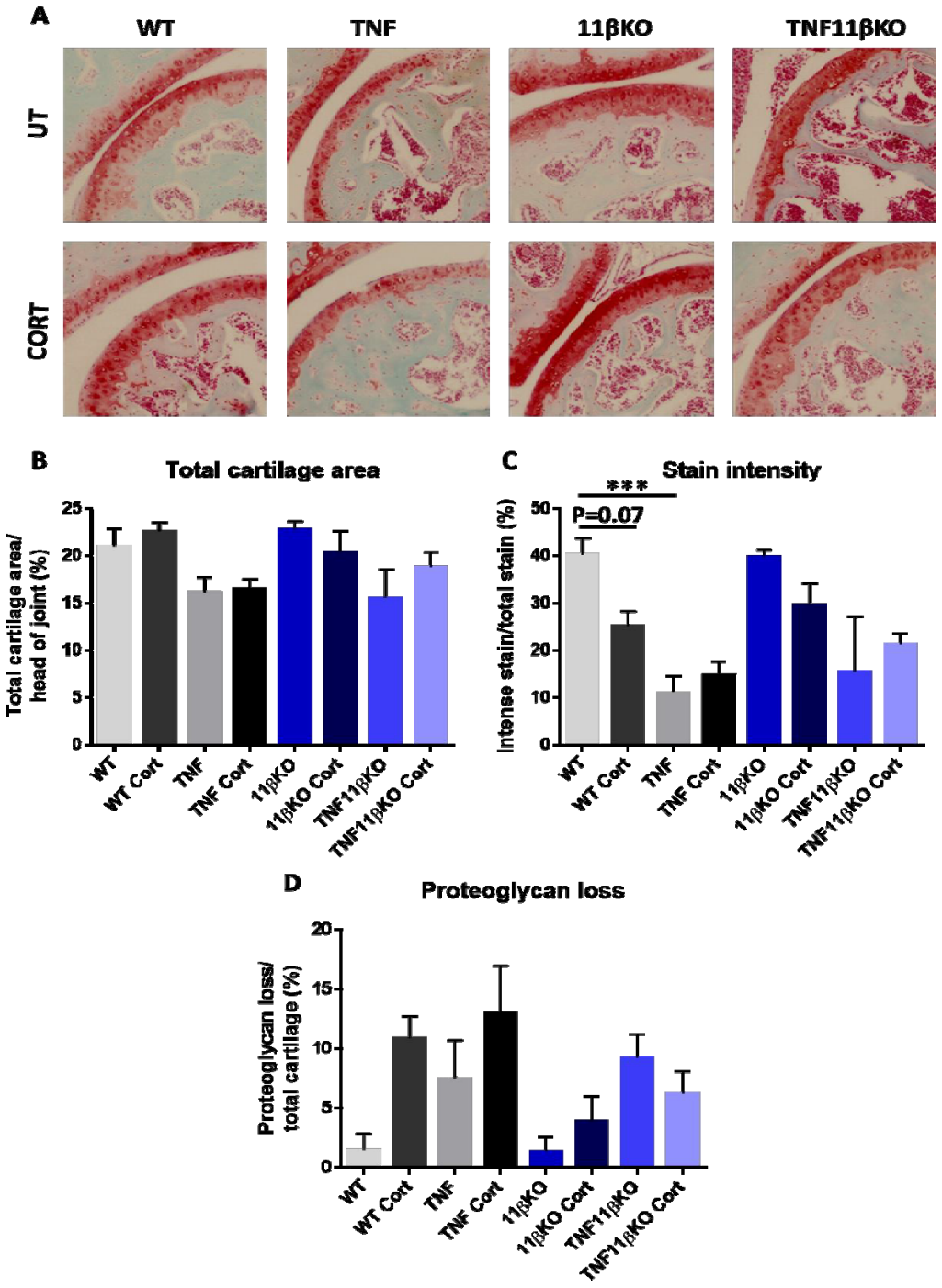

Figure 5. 8: Analysis of cartilage damage in GC treated TNF-tg and TNF11βKO animals

(A) Representative images of safranin O stained cartilage in elbows of WT, TNF-tg, 11βKO and TNF11βKO mice receiving control or 100 mg/L corticosterone in the drinking water for three weeks. (B) Total cartilage area (%) relative to head of joint, (C) stain intensity (%) relative to total stain and (D) proteoglycan loss (%) relative to total cartilage in WT (n=5), TNF-tg (n=6), 11βKO (n=5) and TNF11βKO (n=3) mice receiving control or 100 mg/L corticosterone WT (n=6), TNF-tg (n=5), 11βKO (n=6) and TNF11βKO (n=6) in the drinking water for three weeks. Data is presented as mean ± SEM and statistical significance was determined using two-way ANOVA with Tukey's multiple comparisons test (*** denotes P≤0.001).

Overall, the data collected from the global 11β-HSD1 KO mouse crossed with the TNF-tg model of chronic inflammation suggest that the therapeutic effects of GCs in RA, namely reductions in clinical parameters, pro-inflammatory cytokine production, juxta-articular bone erosions and synovitis, are mediated via GC activation by 11β-HSD1 metabolism.

5.4.3 GCs suppress inflammation in a mesenchymal specific 11β-HSD1 KO mouse

In order to determine which cell populations expressing 11β-HSD1 are responsible for mediating the 11β-HSD1 dependent therapeutic effects of GC treatment, cell specific 11β-HSD1 KO mice were utilised. Fibroblasts have been heavily implicated as drivers of the inflammatory response in RA (325). Thus, the mesenchymal-specific 11β-HSD1 KO mouse was generated and crossed with the TNF-tg model to produce the TNF-Twist2 mouse. These mice were subjected to the same corticosterone treatment as previously reported with the global TNF11βKO animals which resulted in adrenal atrophy (Fig 5.9).

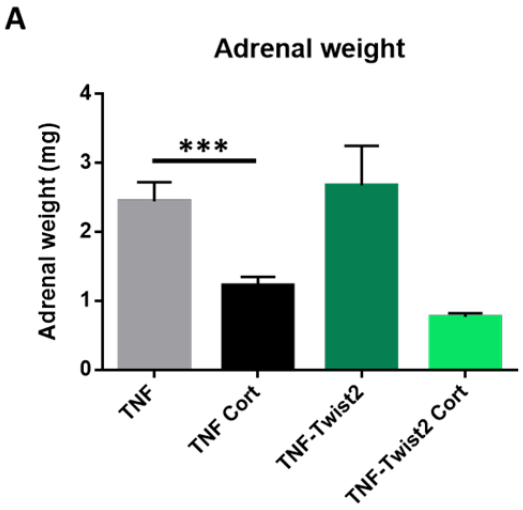

Figure 5. 9: Adrenal weights of TNF-tg and TNF-Twist2 animals receiving GC treatment

Adrenal weights (mg) of TNF-tg (n=5) and TNF-Twist2 (n=2) receiving control or corticosterone TNF-tg (n=13) and TNF-Twist2 (n=6) in the drinking water for three weeks. Data is presented as mean ± SEM and statistical significance was determined using two-way ANOVA with Tukey's multiple comparisons test (*** denotes P≤0.001).

TNF-Twist2 animals responded remarkably similarly to TNF-tg mice, with similar clinical and arthritic paw scores in untreated animals, and a comparable suppression of these scores in both corticosterone treated groups (Clinical scores: TNF-Twist2 6.25 AU ± 0.5 vs TNF-Twist2 Cort 3.20 AU ± 1.9, P≤0.05; Arthritic paw scores: TNF-Twist2 7.25 AU ± 0.5 vs TNF-Twist2 Cort 3.20 ± 1.92, P≤0.001) (Fig 5.10). These data suggest that activation of GCs by mesenchymal derived 11β-HSD1 is not necessary for suppression of clinical signs of disease activity.

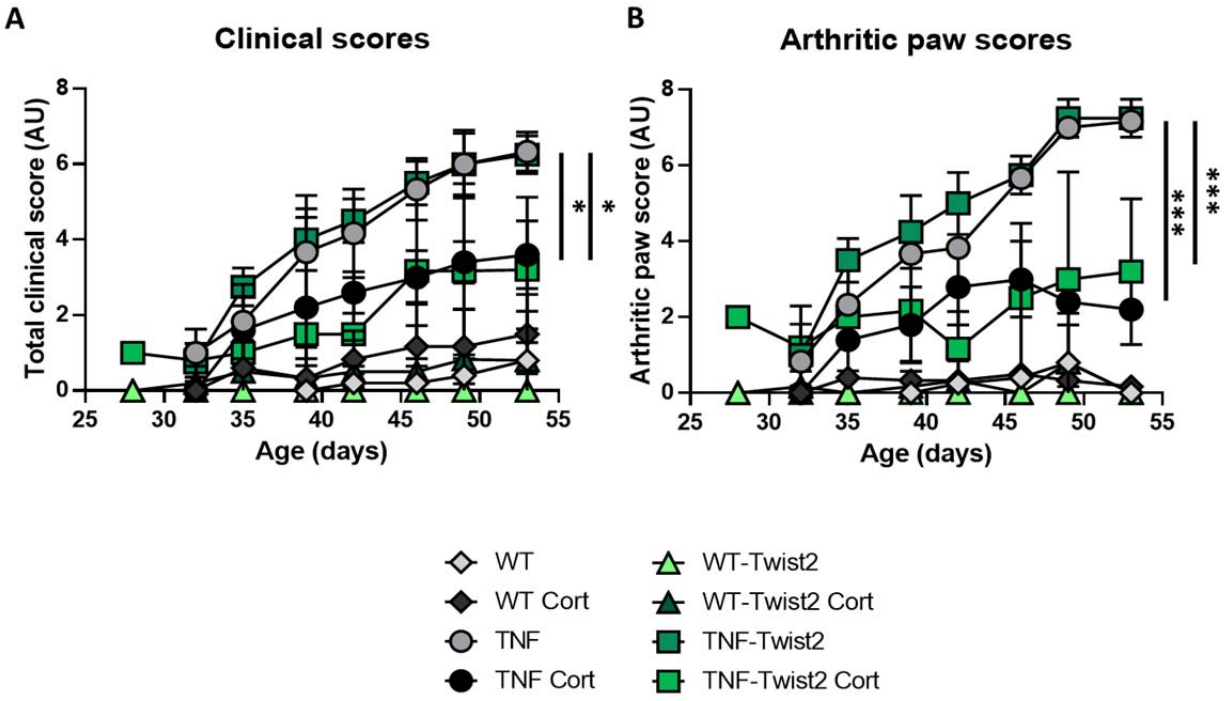

Figure 5. 10: GCs potently suppress markers of disease activity in TNF-Twist2 animals comparable to TNF-tg animals

(A) Clinical scores and (B) arthritic paw scores (AU) of WT (n=5), TNF-tg (n=5), WT-Twist2 (n=3) and TNF-Twist2 (n=4) mice receiving control or 100 mg/L corticosterone (n=5 per group) in the drinking water for three weeks. Data is presented as mean ± SEM and statistical significance was determined using two-way ANOVA with Tukey's multiple comparisons test (* denotes P≤0.05, *** denotes P≤0.001).

Gene expression and serum ELISA analysis of pro-inflammatory cytokines was also performed to determine the effect of GCs on inflammation in these mouse genotypes. Gene expression of *mTnf* revealed a non-significant trend towards decreased levels in TNF-tg mice receiving oral corticosterone compared to untreated controls. Expression levels of *mTnf* were significantly suppressed in TNF-Twist2 animals treated with corticosterone relative to their untreated controls, whilst no significant differences were observed between both GC treatment groups (Fig 5.11 A). Gene expression levels of *hTNF* followed a similar pattern, with a significant decrease in *hTNF* in TNF-tg animals

receiving oral corticosterone and a non-significant decrease in *hTNF* levels in corticosterone treated TNF-Twist2 mice compared to their respective controls. Again, no difference was observed between GC treatment groups (Fig 5.11 B). Thus, GC treatment decreases both *mTnf* and *hTNF* gene expression levels to a similar extent in TNF-tg and TNF-Twist2 animals. Serum levels of IL-6 were also analysed. Whilst serum IL-6 levels were completely suppressed in response to corticosterone treatment in TNF-tg animals, IL-6 persisted in the serum of TNF-Twist2 animals receiving corticosterone (Fig 5.11 C). Gene expression analysis of *il1* revealed significant suppression in both GC treatment groups compared to their relevant untreated controls, with no difference observed between the two treatment groups (Fig 5.11 D). Overall, these data suggest that activation of GCs by mesenchymal-derived 11β-HSD1 may be partially responsible for suppressing IL-6 during inflammation but does not appear to affect other pro-inflammatory cytokines.

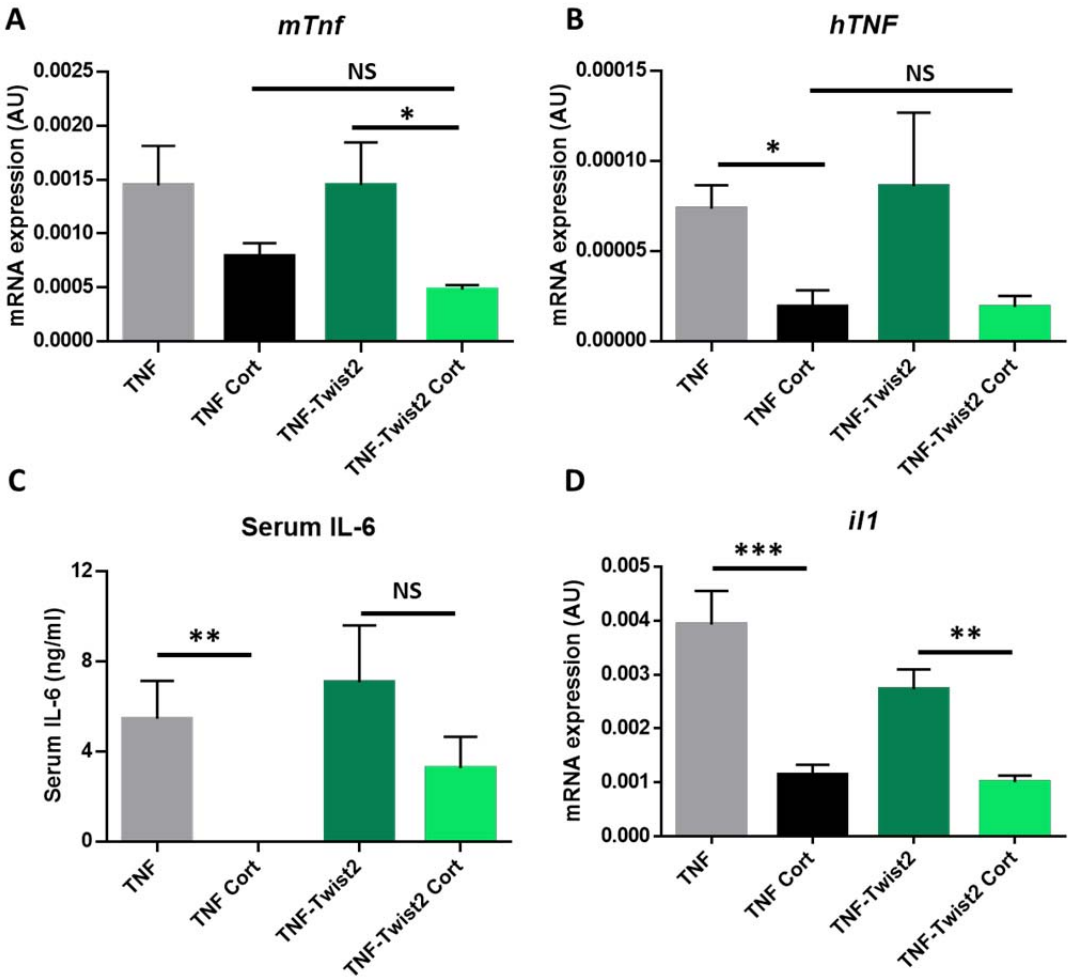

Figure 5. 11: Pro-inflammatory cytokine analysis in TNF-tg and TNF-Twist2 animals

qPCR analysis of gene expression (AU) of (A) *mTnf*, (B) *hTNF* and (D) *il1* in tibias from TNF-tg (n=6) and TNF-Twist2 (n=6) animals receiving vehicle control or 100 mg/L corticosterone TNF-tg (n=6) and TNF-Twist2 (n=5) in the drinking water for three weeks. (C) ELISA analysis of serum IL-6 (ng/ml) in TNF-tg (n=5) and TNF-Twist2 (n=4) animals receiving control or 100 mg/L corticosterone TNF-tg (n=6) and TNF-Twist2 (n=6) in the drinking water for three weeks. Data is presented as mean ± SEM and statistical significance was determined using two-way ANOVA with Tukey's multiple comparisons test (* denotes P≤0.05, ** denotes P≤0.01, *** denotes P≤0.001).

5.4.4 Impact of GC treatment on the joints of TNF-Twist2 mice

To analyse the impact of mesenchymal-derived 11β-HSD1 metabolism on the therapeutic effects of GCs at the joint, front paws of TNF-Twist2 animals were excised post mortem for micro-CT and histological analysis. Following micro-CT scanning and reconstruction, front paws were scored for the prevalence and severity of bone erosions. Corticosterone treatment induced a significant reduction in bone erosions in the TNF-tg animals compared to their untreated counterparts. TNF-Twist2 mice appeared to show a trend towards less bone erosions than untreated TNF-tg mice. Corticosterone treatment did not reduce erosions compared to untreated TNF-Twist2 animals, however no difference was observed between GC treatment groups (Fig 5.12).

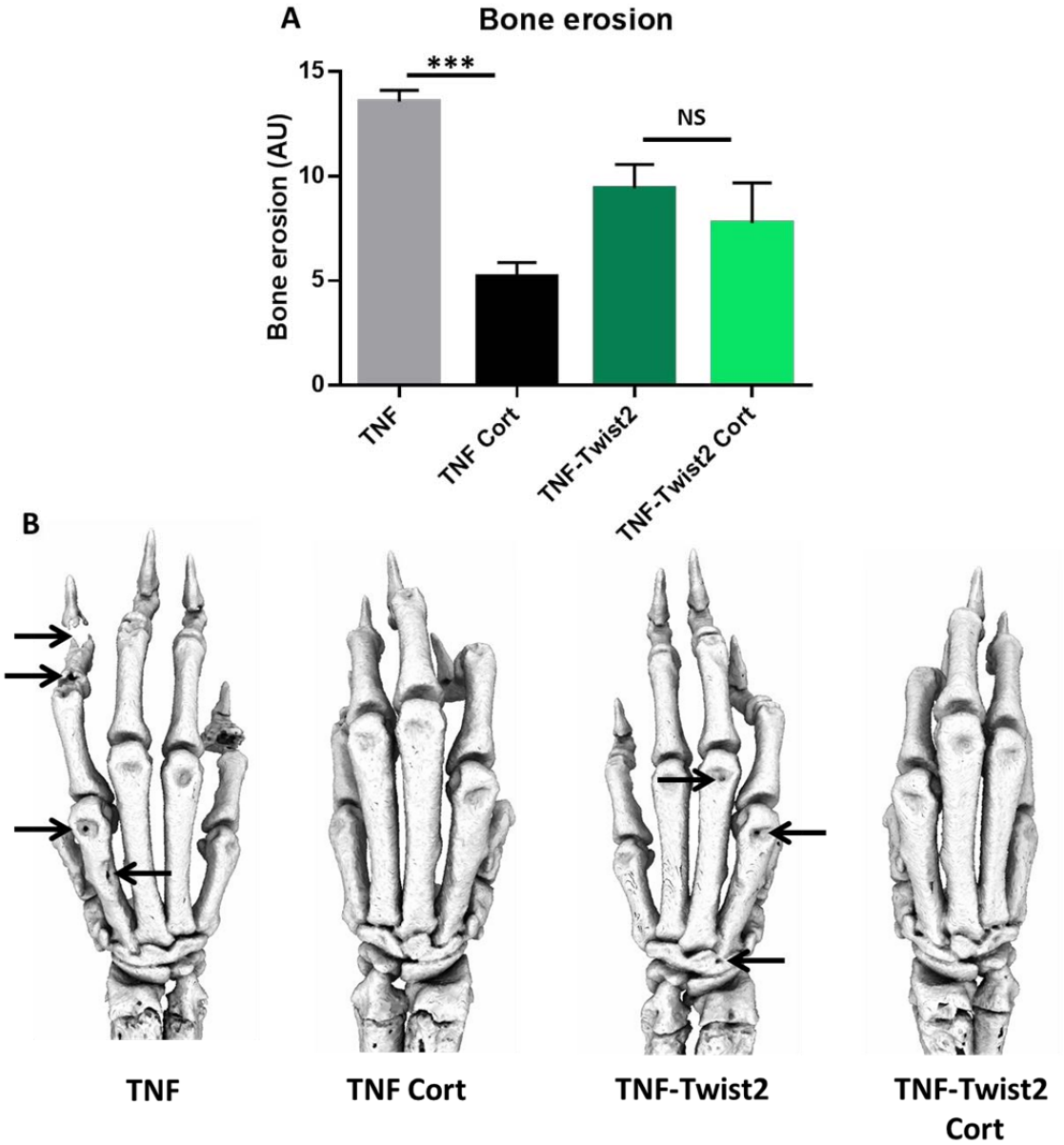

Figure 5. 12: Analysis of bone erosions in TNF-tg and TNF-Twist2 animals treated with GCs

(A) Quantification of degree of bone erosions (AU) by micro-CT analysis in TNF-tg (n=8) and TNF-Twist2 (n=6) animals receiving control or 100 mg/L corticosterone TNF-tg (n=8) and TNF-Twist2 (n=6) in the drinking water for three weeks. (B) Representative images of reconstructed front paw micro-CT scans from TNF-tg and TNF-Twist2 animals receiving control or 100 mg/L corticosterone in the drinking water for three weeks. Arrows indicate bone erosions. Data is presented as mean ± SEM and statistical significance was determined using two-way ANOVA with Tukey's multiple comparisons test (*** denotes P≤0.001).

Further analysis of the joint was performed by H&E staining of elbow joints from TNF-Twist2 animals in order to assess the degree of synovitis and pannus invasion among the different genotypes and treatments. Untreated TNF-Twist2 animals had comparable levels of pannus invasion compared to untreated TNF-tg animals, and both these genotypes were able to potently suppress synovitis upon GC treatment (TNF-Twist2 0.16 AU ± 0.03 vs TNF-Twist2 Cort 0.05 AU ± 0.01, P≤0.05) (Fig 5.13). This suggests that GC activation by 11β-HSD1 within the mesenchyme is not necessary for suppression of synovitis and pannus invasion into the joint.

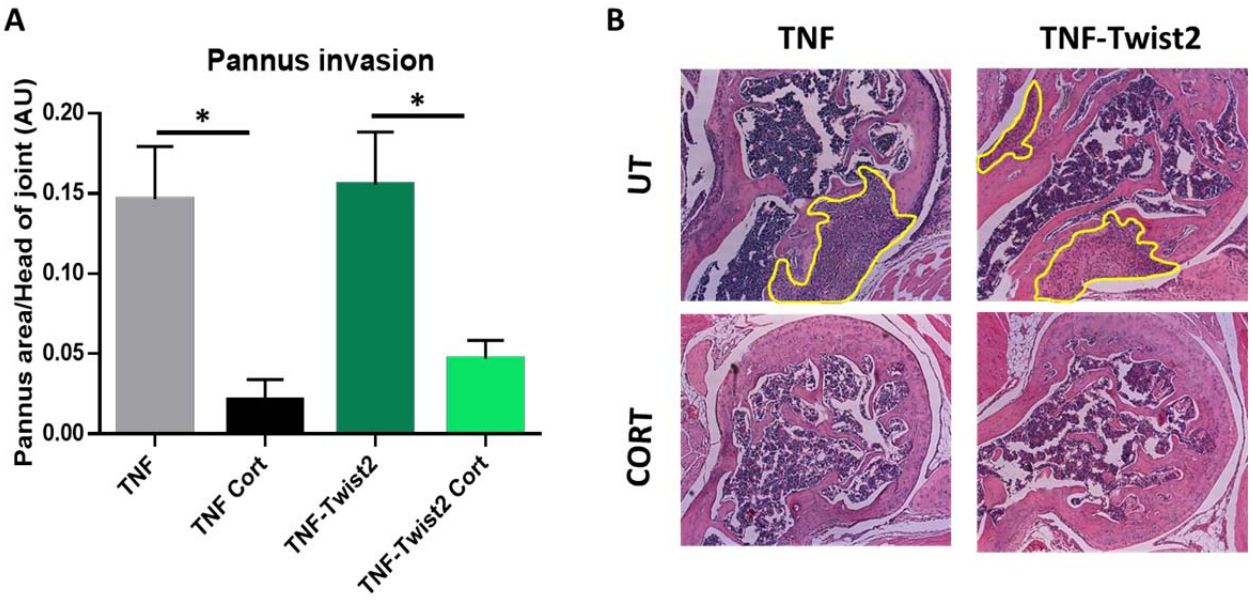

Figure 5. 13: Analysis of pannus formation in TNF-tg and TNF-Twist2 corticosterone treated animals

(A) ImageJ analysis of pannus invasion (AU) in the elbow joints of TNF-tg and TNF-Twist2 mice (n=6 per group) receiving control or 100 mg/L corticosterone in the drinking water for three weeks. (B) Representative images of H&E stained elbow sections of TNF-tg and TNF-Twist2 animals receiving control or 100 mg/L corticosterone in the drinking water for three weeks. Pannus invasion is highlighted in yellow. Data is presented as mean ± SEM and statistical significance was determined using two-way ANOVA with Tukey's multiple comparisons test (* denotes P≤0.05).

The expression of pro-inflammatory chemokines was also assessed from the tibia RNA of these mice. The monocyte/macrophage chemoattractant *Ccl2* was significantly suppressed upon corticosterone treatment in both TNF-tg and TNF-Twist2 animals (TNF-Twist2 0.0013 AU ± 0.0004 vs TNF-Twist2 Cort 0.0003 AU ± 0.00005, P≤0.01). Additionally, untreated TNF-Twist2 animals showed a non-significant trend towards decreased expression of this chemokine in comparison to untreated TNF-tg mice (Fig 5.14 A). Another monocyte/macrophage chemoattractant *Cxcl10* showed a similar trend towards decreased levels in untreated TNF-Twist2 animals compared to untreated TNF-tg animals. However, whilst a significant decrease in *Cxcl10* levels was observed in TNF-tg mice in response to GC treatment, this was not the case in TNF-Twist2 animals which exhibited comparable levels between the untreated and corticosterone treated groups (TNF-Twist2 0.0005 AU ± 0.00008 vs TNF-Twist2 Cort 0.0004 AU ± 0.00007, P=0.4) (Fig 5.14 B). The neutrophil chemoattractant *Cxcl2* exhibited no significant changes amongst the groups, however both genotypes displayed a trend towards decreased *Cxcl2* levels when treated with GCs (Fig 5.14 C). Overall, these data indicate that activation of GCs by mesenchymal-derived 11β-HSD1 contributes to decreases in *Cxcl10* expression in response to GC treatment, but does not affect the expression of *Ccl2* or *Cxcl2* in TNF-tg mice.

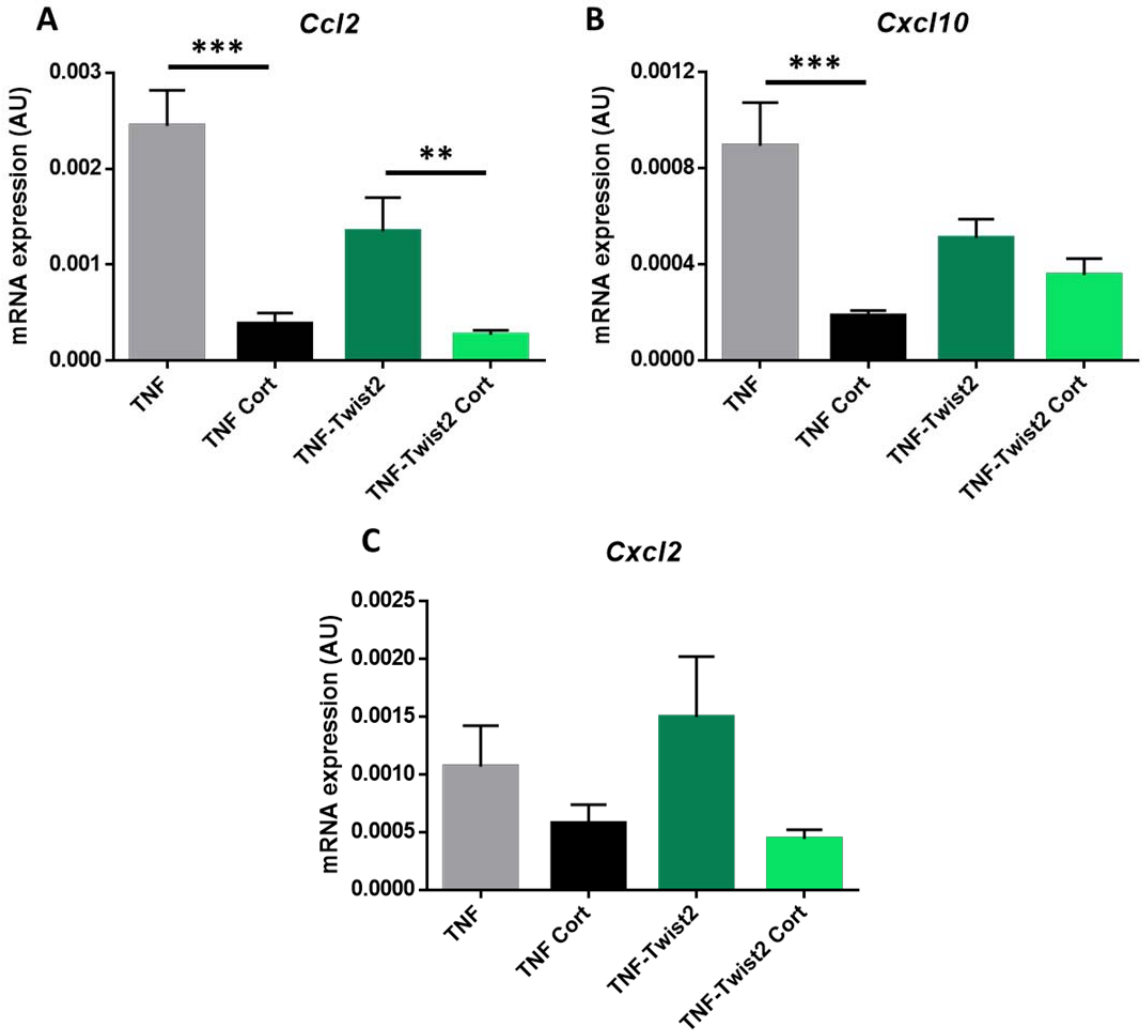

Figure 5. 14: GCs suppress pro-inflammatory chemokines in TNF-tg and TNF-Twist2 mice

qPCR analysis of gene expression (AU) of (A) *Ccl2,* (B) *Cxcl10* and (C) *Cxcl2* in tibias from TNF-tg (n=6) and TNF-Twist2 (n=6) mice receiving vehicle control or 100 mg/L corticosterone TNF-tg (n=6) and TNF-Twist2 (n=5) in the drinking water for three weeks. Data is presented as mean ± SEM and statistical significance was determined using two-way ANOVA with Tukey's multiple comparisons test (** denotes P≤0.01, *** denotes P≤0.001).

TRAP +ve osteoclast numbers were assessed at the pannus to examine their role in inflammatory bone loss in TNF-tg and TNF-Twist2 animals receiving corticosterone. Analysis of osteoclasts at these joints revealed that corticosterone treatment induced significant reductions in osteoclast numbers in both TNF-tg and TNF-Twist2 animals

(TNF-Twist2 16.5 AU ± 4.5 vs TNF-Twist2 Cort 3.8 AU ± 1.4, P≤0.05) (Fig 5.15). Therefore, these data indicate that activation of GCs by mesenchymal 11β-HSD1 is not necessary to reduce osteoclast numbers at the joint in TNF-tg animals.

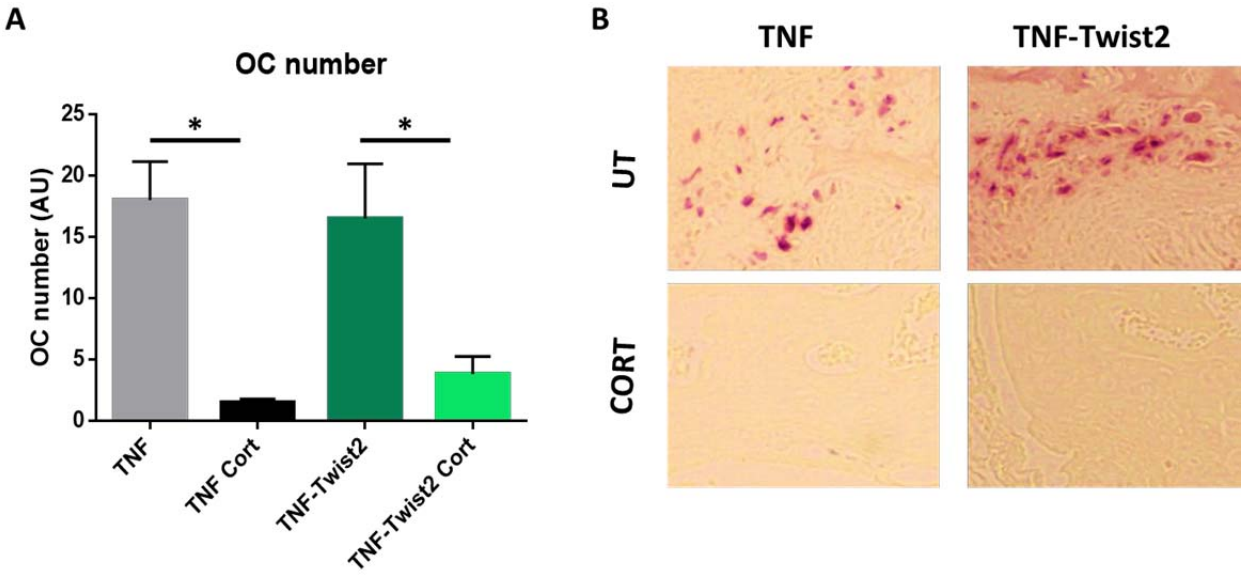

Figure 5. 15: Osteoclast counts at the elbow joints of TNF-tg and TNF-Twist2 corticosterone treated animals

(A) Osteoclast numbers (AU) at the head of elbow joints determined by TRAP stains of TNF-tg (n=5) and TNF-Twist2 (n=6) mice receiving control or 100 mg/L corticosterone TNF-tg (n=4) and TNF-Twist2 (n=6) in the drinking water for three weeks. (B) Representative images of TRAP stains in TNF-tg and TNF-Twist2 animals receiving control or 100 mg/L corticosterone in the drinking water for three weeks, with osteoclasts stained red. Data is presented as mean ± SEM and statistical significance was determined using two-way ANOVA with Tukey's multiple comparisons test (* denotes P≤0.05).

Finally, analysis of the cartilage was performed by safranin O staining to investigate the contribution of GC activation by mesenchymal 11β-HSD1 to cartilage destruction. Both total cartilage area and staining intensity showed no significant differences amongst the groups, with TNF-Twist2 animals responding to GC treatment similarly to TNF-tg animals

(Fig 5.16 B-C). Proteoglycan loss also showed no significant differences, however whilst a trend towards increased proteoglycan loss was observed in TNF-tg animals treated with GCs, this was not observed in TNF-Twist2 animals. TNF-Twist2 animals receiving oral corticosterone appeared to have less proteoglycan loss than corticosterone treated TNF-tg animals (Fig 5.16 C). This suggests that GC activation by 11β-HSD1 within mesenchymal cell populations may play a role in proteoglycan loss in the cartilage in response to therapeutic GCs.

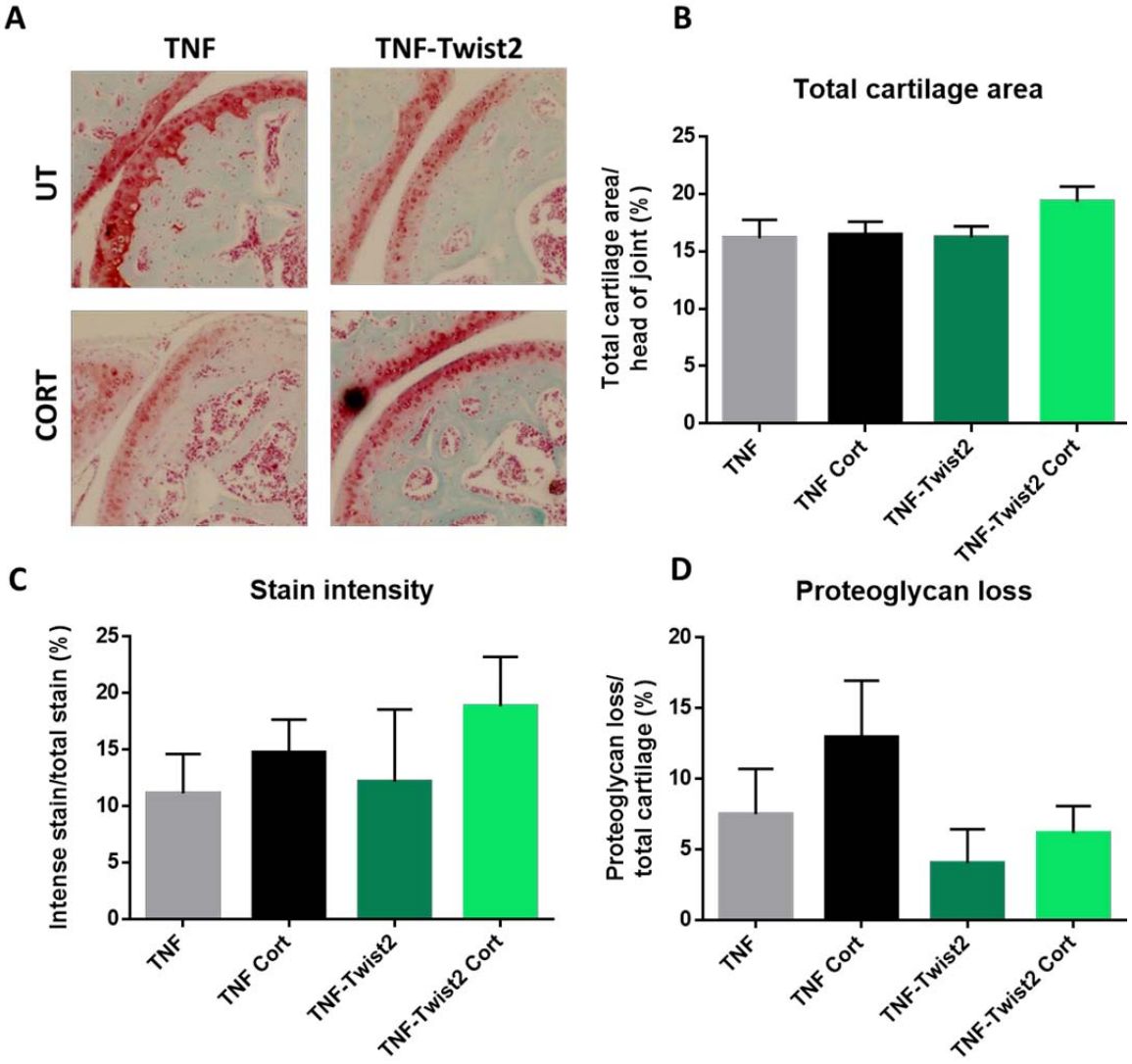

Figure 5. 16: Analysis of the cartilage of TNF-tg and TNF-Twist2 animals following GC treatment

(A) Representative images of safranin O stained cartilage in the elbows of TNF-tg and TNF-Twist2 animals receiving control or 100 mg/L corticosterone in the drinking water for three weeks. (B) Total cartilage area (%) relative to the head of the joint, (B) stain intensity (%) relative to total stain and (D) proteoglycan loss (%) relative to total cartilage in TNF-tg (n=6) and TNF-Twist2 (n=5) animals receiving control or 100 mg/L corticosterone TNF-tg (n=5) and TNF-Twist2 (n=6) in the drinking water for three weeks. Data is presented as mean ± SEM and statistical significance was determined using two-way ANOVA with Tukey's multiple comparisons test.

Taken together, the TNF-tg mouse with a mesenchymal specific 11β-HSD1 knockout responds to GC treatment in a largely similar fashion as the TNF-tg animals, in terms of

reduced clinical disease parameters, pro-inflammatory cytokines, synovitis and osteoclast numbers. However, some differences are observed in the TNF-Twist2 animals treated with corticosterone, specifically a persistence of certain pro-inflammatory factors; IL-6 and *Cxcl10*, an inability to reduce bone erosions and a potential decrease in cartilage destruction.

5.4.5 GCs suppress inflammation in a myeloid specific 11β-HSD1 mouse

Since 11β-HSD1 within mesenchymal cell populations did not appear to mediate the therapeutic effects of GCs, the contribution of 11β-HSD1 in myeloid cells to the therapeutic actions of GCs was investigated. 11β-HSD1 metabolism of GCs within macrophages has been shown to drive the cells towards the pro-resolution M2 phenotype, and may represent a mechanism whereby GCs mediate their therapeutic effects in chronic polyarthritis where inflammatory macrophages play a role in disease pathophysiology (158). Therefore, a myeloid-specific 11β-HSD1 KO mouse was crossed with the TNF-tg animals (TNF-LysM) and administered 100 mg/L corticosterone in the drinking water for three weeks. This treatment induced significant adrenal atrophy in both TNF-tg and TNF-LysM animals (Fig 5.17).

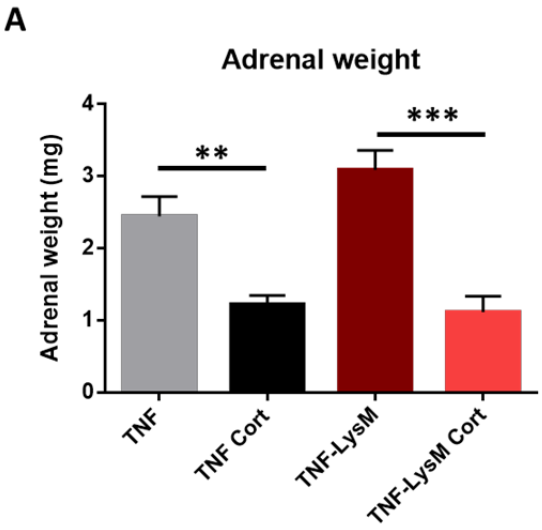

Figure 5. 17: Adrenal weights of TNF-tg and TNF-LysM animals receiving GC treatment

Adrenal weights (mg) of TNF-tg (n=5) and TNF-LysM (n=6) receiving control or corticosterone TNF-tg (n=13) and TNF-LysM (n=6) in the drinking water for three weeks. Data is presented as mean ± SEM and statistical significance was determined using two-way ANOVA with Tukey's multiple comparisons test (** denotes P≤0.01, *** denotes P≤0.001).

As previously reported, corticosterone treatment induced a significant reduction in clinical scores in TNF-tg mice. However, the clinical scores of TNF-LysM animals were not reduced at day 55 upon corticosterone treatment, and TNF-LysM animals receiving oral corticosterone had significantly higher clinical scores than corticosterone treated TNF-tg mice (TNF-tg Cort 3.6 AU ± 0.9 vs TNF-LysM Cort 5.5 AU ± 1.6, P≤0.05) (Fig 5.18 A). The arthritic paw scores of untreated TNF-LysM mice were significantly higher than untreated TNF-tg animals (TNF-tg 7.3 AU ± 0.8 vs TNF-LysM 9.4 AU ± 1.0, P≤0.05), indicating a worsened basal arthritis in mice lacking myeloid 11β-HSD1. Upon corticosterone treatment, both groups demonstrated a significant reduction in arthritic paw scores. However, TNF-LysM mice treated with corticosterone retained significantly higher arthritic paw scores than corticosterone treated TNF-tg animals (TNF-tg Cort 2.2 AU ±

0.8 vs TNF-LysM Cort 4.7 AU ± 1.6, P≤0.01) (Fig 5.18 B). Overall, these data indicate that mice lacking myeloid 11β-HSD1 may possess a partial resistance to the therapeutic effects of exogenous GC treatment.

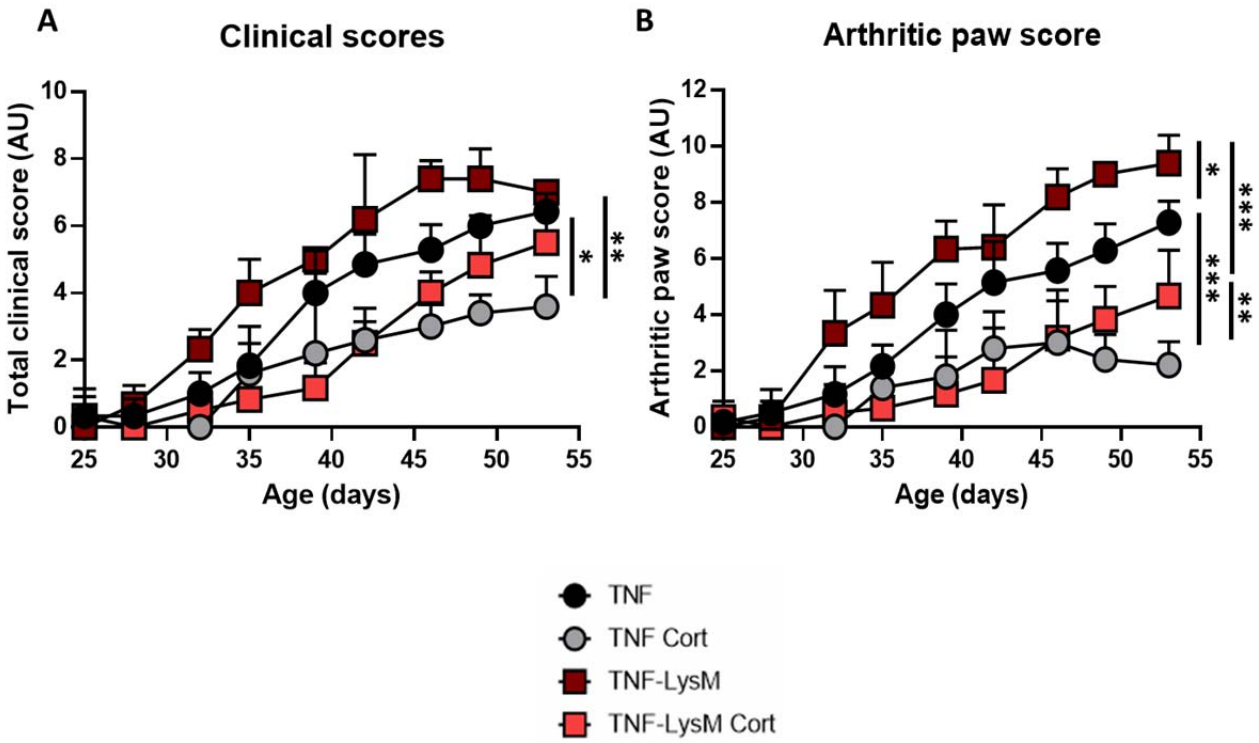

Figure 5. 18: Clinical and arthritic paw scores of TNF-tg and TNF-LysM mice with or without GC treatment

(A) Clinical scores and (B) arthritic paw scores (AU) in TNF-tg and TNF-LysM mice receiving control or 100 mg/L corticosterone in the drinking water for three weeks (n=6 per group). Data is presented as mean ± SEM and statistical significance was determined using two-way ANOVA with Tukey's multiple comparisons test (* denotes P≤0.05, ** denotes P≤0.01, *** denotes P≤0.001).

Analysis of pro-inflammatory cytokines revealed a trend towards decreased levels of *mTnf* in both TNF-tg and TNF-LysM animals treated with GCs (Fig 5.19 A). Similarly, a non-significant trend towards decreased levels of *hTNF* was observed in TNF-tg animals receiving corticosterone treatment compared to their untreated controls, and a significant

decrease was recorded in GC treated TNF-LysM relative to untreated counterparts (Fig 5.19 B). Additionally, serum levels of IL-6 and gene expression levels of *il1* were significantly suppressed upon GC treatment in both genotypes (TNF-LysM 6.03 ng/ml ± 1.98 vs TNF-LysM -2.10 ng/ml ± 0.80, $P \leq 0.05$) (Fig 5.19 C-D). Thus, despite the significantly higher arthritic paw scores associated with the GC treated TNF-LysM mice compared to GC treated TNF-tg mice, pro-inflammatory cytokines are effectively suppressed by GC treatment to a similar level.

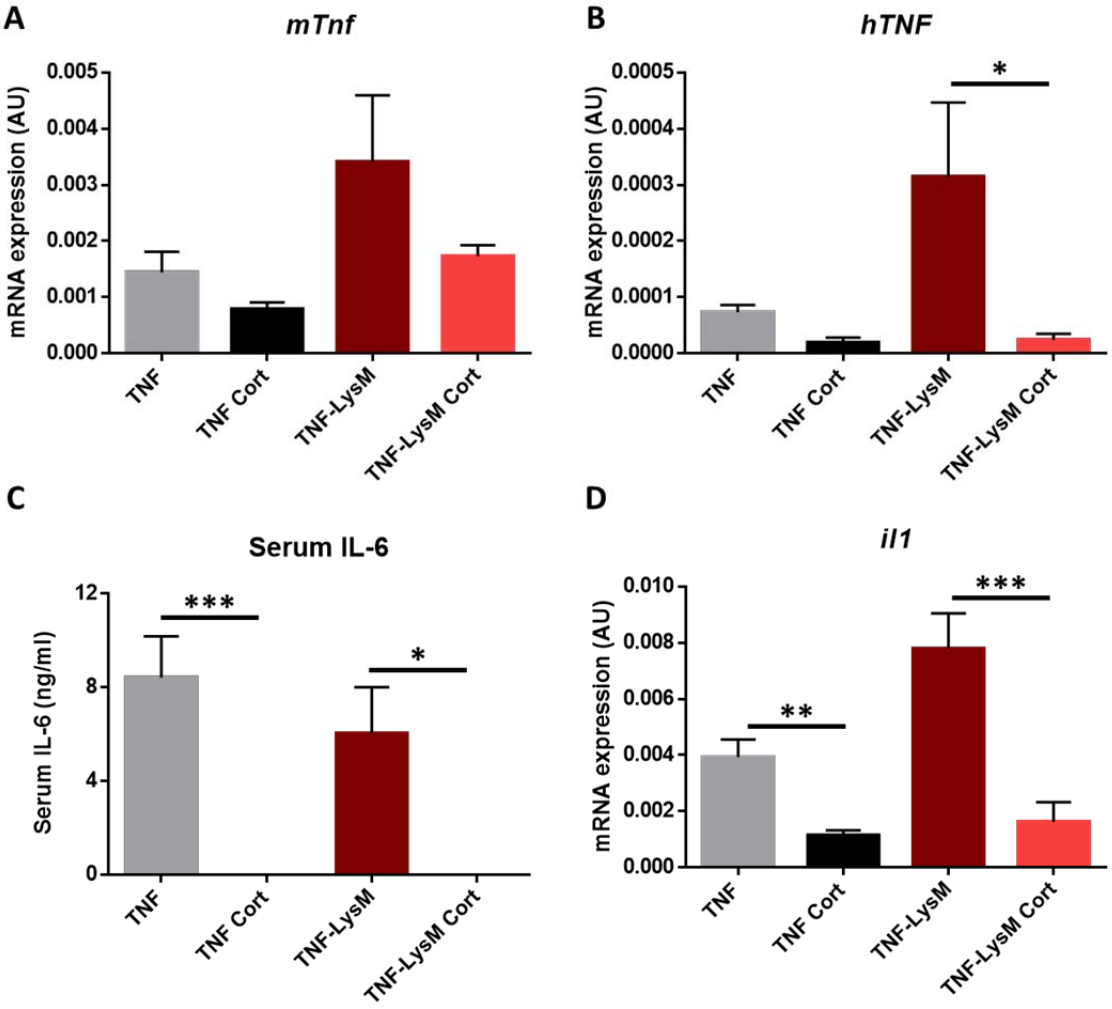

Figure 5. 19: Analysis of pro-inflammatory cytokines in corticosterone treated TNF-tg and TNF-LysM animals

qPCR analysis of gene expression (AU) of (A) *mTnf*, (B) *hTNF* and (D) *il1* in tibias from TNF-tg and TNF-LysM animals receiving control or 100 mg/L corticosterone in the drinking water for three weeks (n=6 per group). (C) ELISA analysis of serum IL-6 (ng/ml) in TNF-tg (n=8) and TNF-LysM (n=5) animals receiving control or 100 mg/L corticosterone TNF-tg (n=7) and TNF-LysM (n=4) in the drinking water for three weeks. Data is presented as mean ± SEM and statistical significance was determined using two-way ANOVA with Tukey's multiple comparisons test (* denotes P≤0.05, ** denotes P≤0.01, *** denotes P≤0.001).

5.4.6 Impact of GC treatment on the joints of TNF-LysM mice

To analyse the contribution of GC activation by myeloid derived 11β-HSD1 to the specific therapeutic actions of GCs at the joint, front paws were collected for both micro-CT and histological analysis. Micro-CT analysis of bone erosions revealed a significant decrease in erosion scores upon treatment with corticosterone in TNF-tg animals, whilst TNF-LysM animals receiving GCs were resistant to these effects. TNF-LysM animals receiving GCs had a significantly increased severity of bone erosions compared to TNF-tg animals treated with GCs (TNF-tg Cort 5.19 AU ± 1.93 vs TNF-LysM Cort 14.83 AU ± 1.87, $P \leq 0.001$) (Fig 5.20).

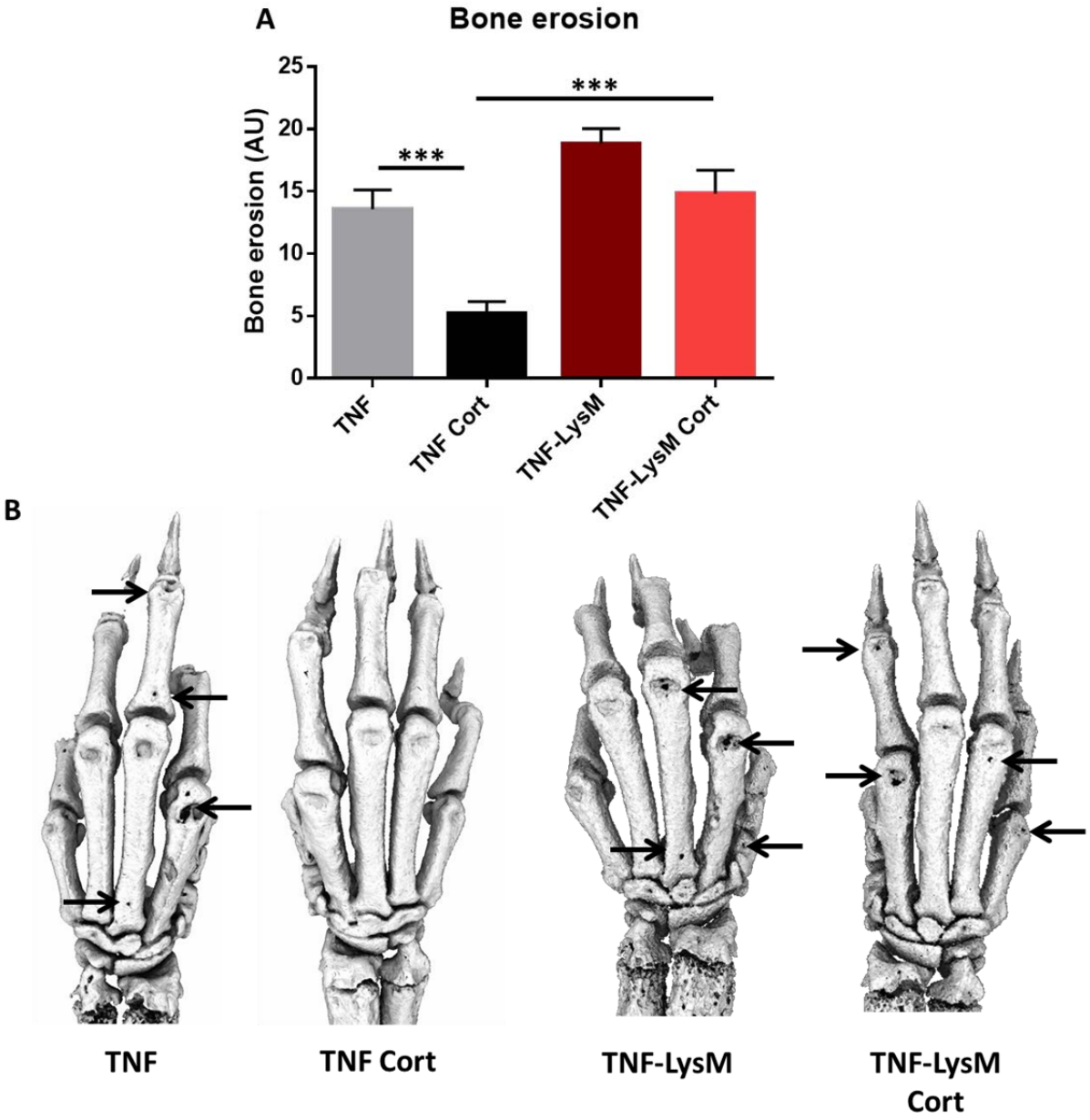

Figure 5. 20: Analysis of bone erosions in TNF-tg and TNF-LysM animals treated with GCs

(A) Quantification of degree of bone erosions (AU) by micro-CT analysis in TNF-tg (n=8) and TNF-LysM (n=5) animals receiving control or 100 mg/L corticosterone TNF-tg (n=8) and TNF-LysM (n=6) in the drinking water for three weeks. (B) Representative images of reconstructed front paw micro-CT scans of TNF-tg and TNF-LysM animals receiving control or 100 mg/L corticosterone in the drinking water for three weeks. Arrows indicate bone erosions. Data is presented as mean ± SEM and statistical significance was determined using two-way ANOVA with Tukey's multiple comparisons test (*** denotes P≤0.001).

The degree of inflammatory infiltrate and pannus invasion into the underlying bone was assessed by ImageJ analysis of H&E stained elbow joints. Synovitis was significantly suppressed in both TNF-tg and TNF-LysM animals in response to corticosterone treatment (TNF-LysM 0.19 AU ± 0.03 vs TNF-LysM Cort 0.06 AU ± 0.02, P≤0.05) (Fig 5.21).

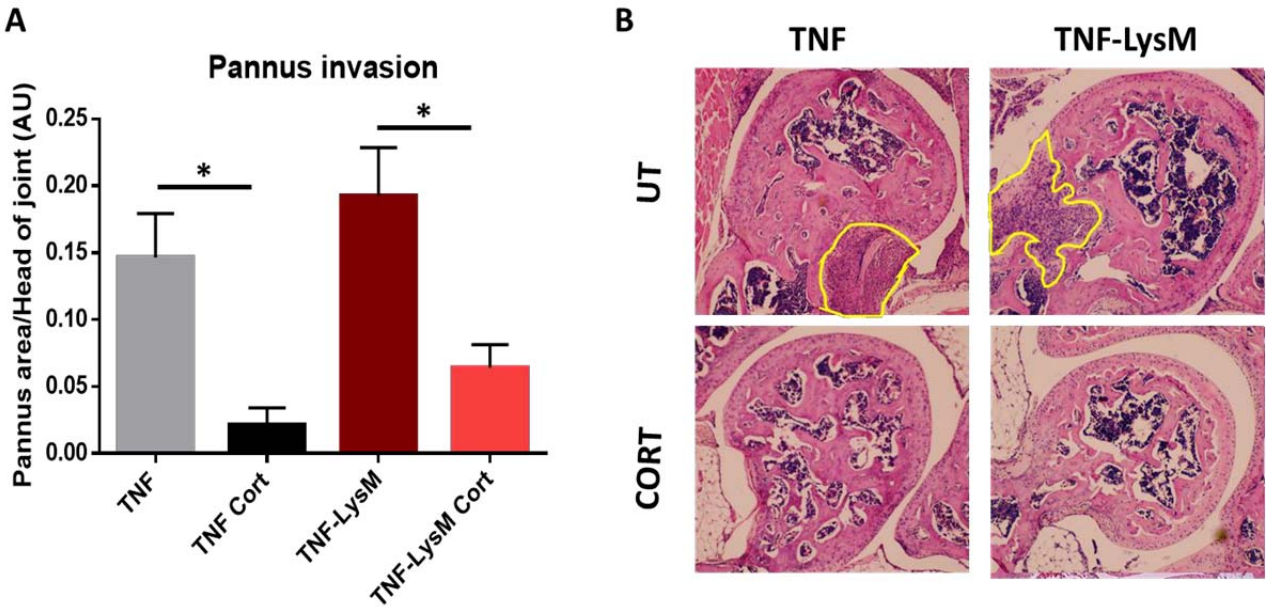

Figure 5. 21: Analysis of pannus formation in TNF-tg and TNF-LysM corticosterone treated animals

(A) ImageJ analysis of pannus invasion (AU) in the elbow joints of TNF-tg (n=6) and TNF-LysM (n=5) mice receiving control or 100 mg/L corticosterone TNF-tg (n=6) and TNF-LysM (n=5) in the drinking water for three weeks. (B) Representative images of H&E stained elbow sections of control and three weeks of 100 mg/L oral corticosterone treated TNF-tg and TNF-LysM animals. Pannus invasion is highlighted in yellow. Data is presented as mean ± SEM and statistical significance was determined using two-way ANOVA with Tukey's multiple comparisons test (* denotes P≤0.05).

Gene expression levels of pro-inflammatory chemokines were analysed from RNA isolated from the tibia of these mice. The macrophage/monocyte chemoattractant molecules, *Ccl2* and *Cxcl10*, were significantly suppressed in response to GC treatment in both TNF-tg and TNF-LysM animals (*Ccl2*: TNF-LysM 0.0049 AU ± 0.001 vs TNF-LysM

Cort 0.0002 AU ± 0.00005, P≤0.001; *Cxcl10*: TNF-LysM 0.0011 AU ± 0.0002 vs TNF-LysM Cort 0.0002 AU ± 0.00003, P≤0.001) (Fig 5.22 A-B). The neutrophil chemoattractant, *Cxcl2*, exhibited a trend towards decreased levels in TNF-tg mice treated with corticosterone compared to their untreated controls. Untreated TNF-LysM mice also demonstrated a non significant decrease compared to untreated TNF-tg mice and corticosterone treatment in TNF-LysM animals further decreased *Cxcl2* levels (Fig 5.22 C). Therefore, GC activation by myeloid 11β-HSD1 is not required to suppress pro-inflammatory chemokines in response to GC treatment.

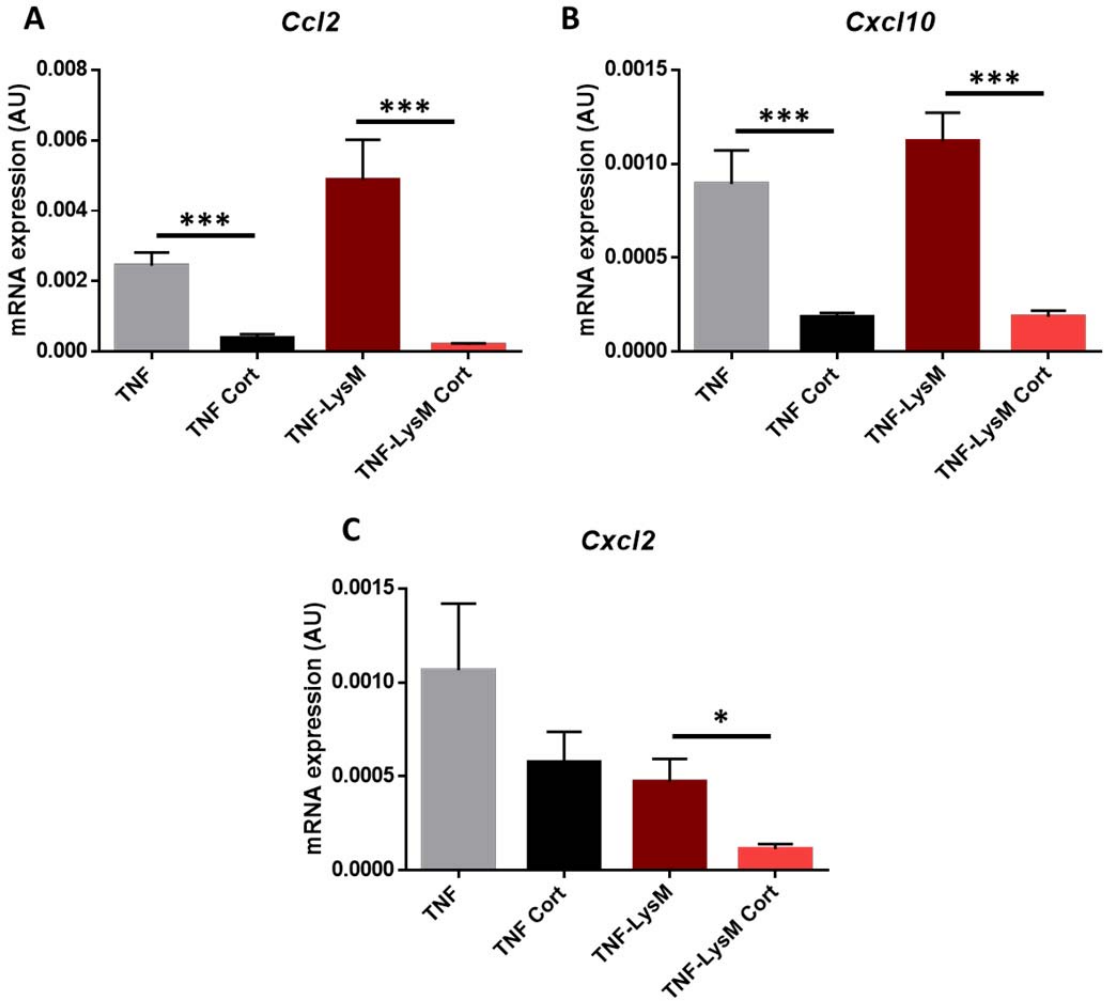

Figure 5. 22: Analysis of pro-inflammatory chemokines in TNF-tg and TNF-LysM mice

qPCR analysis of gene expression (AU) of (A) *Ccl2,* (B) *Cxcl10* and (C) *Cxcl2* in tibias from TNF-tg (n=6) and TNF-LysM (n=5) animals receiving control or 100 mg/L corticosterone TNF-tg (n=6) and TNF-LysM (n=6) in the drinking water for three weeks. Data is presented as mean ± SEM and statistical significance was determined using two-way ANOVA with Tukey's multiple comparisons test (* denotes P≤0.05, *** denotes P≤0.001).

Analysis of osteoclast numbers at the elbow joints of the mice demonstrated a significant increase in osteoclasts in untreated TNF-LysM animals compared to untreated TNF-tg mice (TNF-tg 18 AU ± 3.15 vs TNF-LysM 35.8 AU ± 6.55, P≤0.05). Corticosterone treatment significantly suppressed the numbers of osteoclasts at the joints in both TNF-

tg and TNF-LysM animals (TNF-LysM 35.8 AU ± 6.55 vs TNF-LysM Cort 7.4 AU ± 1.69, P≤0.001) (Fig 5.23). These data suggest that GC activation by myeloid 11β-HSD1 is not required for the suppression of osteoclast numbers associated with GC treatment.

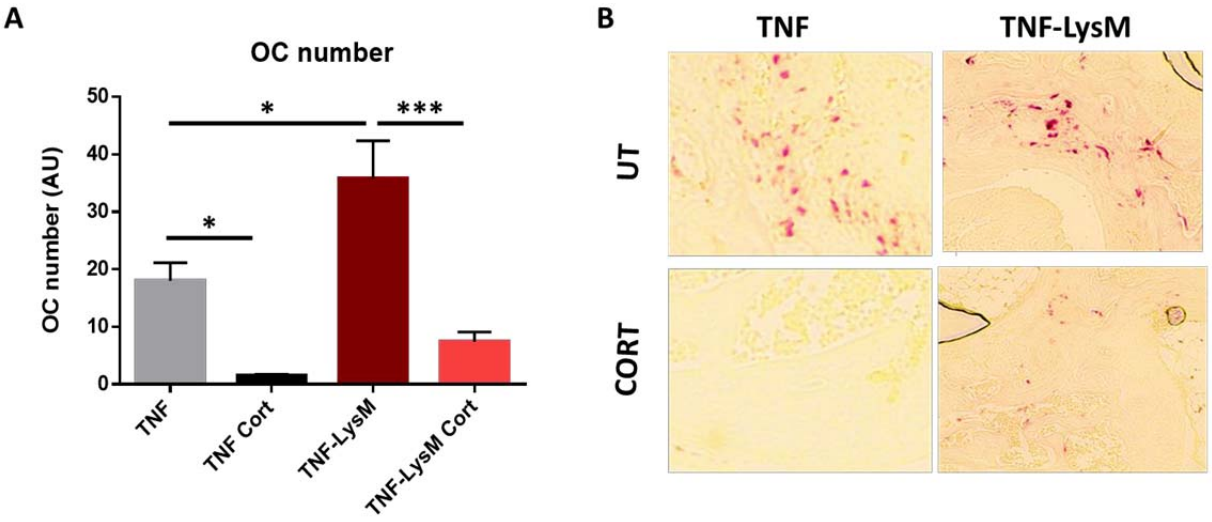

Figure 5. 23: Osteoclast counts at the elbow joints of TNF-tg and TNF-LysM corticosterone treated animals

(A) Osteoclast numbers (AU) at the head of the elbow joints determined by TRAP stains in TNF-tg (n=5) and TNF-LysM (n=5) mice receiving control or 100 mg/L corticosterone TNF-tg (n=4) and TNF-LysM (n=5) in the drinking water for three weeks. (B) Representative images of TRAP stains in control and three weeks of 100 mg/L corticosterone treated TNF-tg and TNF-LysM animals, with osteoclasts stained red. Data is presented as mean ± SEM and statistical significance was determined using two-way ANOVA with Tukey's multiple comparisons test (* denotes P≤0.05, *** denotes P≤0.001).

Lastly, safranin O staining of the elbow joints was performed to assess the degree of cartilage destruction in the mice. No significant changes were observed in terms of total cartilage area, stain intensity or proteoglycan loss amongst the genotypes or treatments (Fig 5.24).

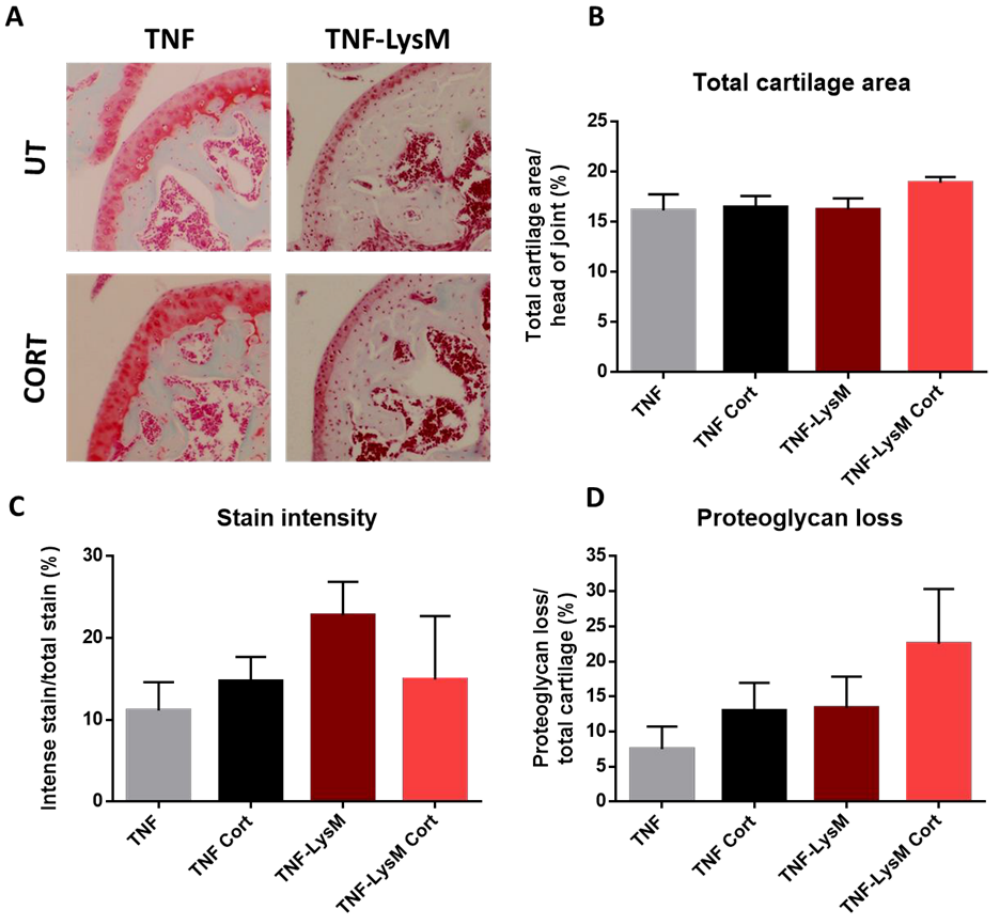

Figure 5. 24: Analysis of the cartilage of TNF-tg and TNF-LysM animals following GC treatment

(A) Representative images of safranin O stained cartilage in the elbows of TNF-tg and TNF-LysM animals receiving control or 100 mg/L corticosterone in the drinking water for three weeks. (B) Total cartilage area (%) relative to the head of the joint, (B) stain intensity (%) relative to total stain and (D) proteoglycan loss (%) relative to total cartilage in TNF-tg (n=6) and TNF-LysM (n=5) animals receiving control or 100 mg/L corticosterone TNF-tg (n=5) and TNF-LysM (n=6) in the drinking water for three weeks. Data is presented as mean ± SEM and statistical significance was determined using two-way ANOVA with Tukey's multiple comparisons test.

Overall, the TNF-tg mouse lacking myeloid derived 11β-HSD1 can still respond to GC treatment similarly to the TNF-tg animals by reducing synovitis, pro-inflammatory cytokines and pro-inflammatory chemokines, despite a reduced response in terms of clinical and arthritic paws scores and an inability to inhibit juxta-articular bone erosions.

Thus, since neither myeloid specific or mesenchymal specific 11β-HSD1 KO animals replicate the phenotype of the global KO mouse, it appears likely that a compensatory mechanism by which neighbouring cells can communicate GC signals exists.

5.4.7 Interaction between fibroblasts and macrophages

To investigate whether GCs can be activated by 11β-HSD1 in one cell and secreted to exert their effects on a neighbouring cell via paracrine signalling, conditioned media experiments were set up (Fig 5.25).

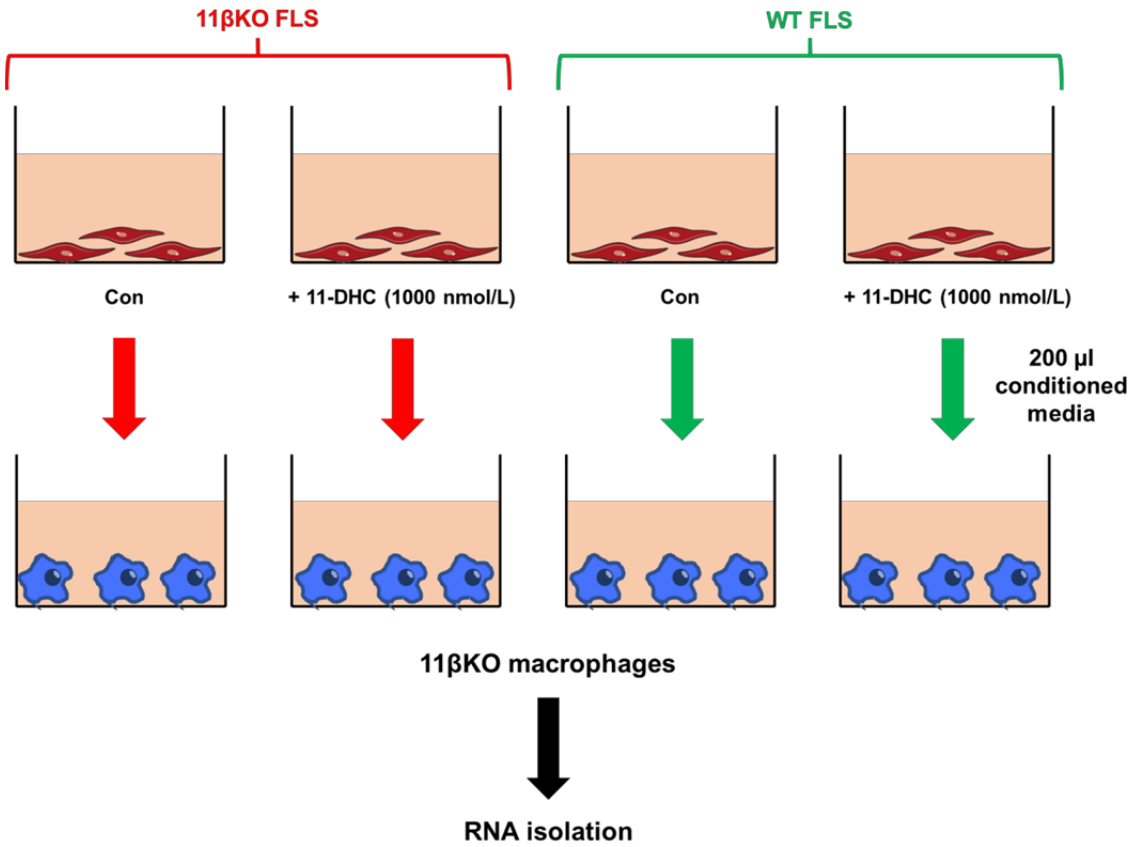

Figure 5. 25: Set up of conditioned media experiments

WT and 11βKO fibroblasts were cultured in the absence or presence of 11-DHC. Media was collected and used to treat 11βKO macrophages. Experiments were also performed in reverse with macrophages providing the conditioned media and FLS being treated.

First, macrophages isolated from both WT and 11β-HSD1 KO mice were treated in the absence or presence of the inactive murine GC 11-DHC (1000 nmol/L) and media collected from these cultures was used to treat fibroblasts isolated from 11β-HSD1 KO mice. Following this treatment, gene expression and media ELISA analysis were used to assess the response of the KO fibroblasts to GCs in the macrophage conditioned media. Gene expression levels of *Gilz* was significantly increased in KO fibroblasts treated with media from DHC treated WT macrophages, whilst this induction of *Gilz* was lost in KO fibroblasts treated with media from DHC treated KO macrophages (Fig 5.26 A). Similarly, both gene expression and protein levels of IL-6 were significantly suppressed when KO fibroblasts were treated with media from DHC treated WT macrophages, and this effect again was lost when KO fibroblasts were treated with media from DHC treated KO macrophages (Fig 5.26 B-C). Thus, these data indicate that macrophages are able to translate GC signals to the fibroblasts.

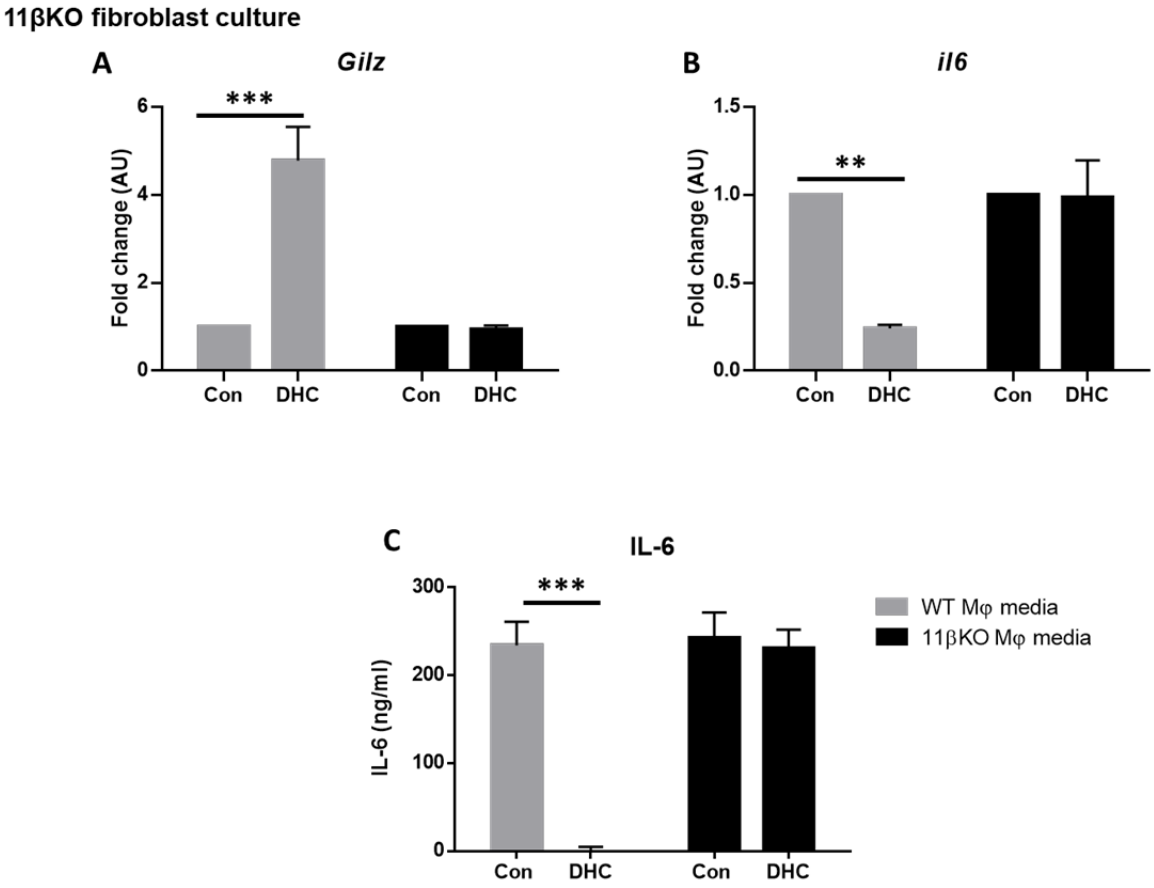

Figure 5. 26: Response of KO fibroblasts to GCs metabolised by WT & 11βKO macrophages

Gene expression analysis (AU) by qPCR of (A) *Gilz* and (B) *il6* and ELISA analysis (ng/ml) of (C) IL-6 in the media of 11β-HSD1 KO fibroblasts treated with media from either WT or 11β-HSD1 KO macrophages treated in the absence or presence of 11-DHC (n=3). Data is presented as mean ± SEM and statistical significance was determined using one-way ANOVA with Tukey's multiple comparisons test. (** denotes P≤0.01, *** denotes P≤0.001).

In order to investigate whether fibroblasts can communicate GC signals to macrophages, WT and KO fibroblasts were treated with or without 11-DHC and this media was used to treat KO macrophages. Gene expression levels of *Gilz* were significantly increased in KO macrophages treated with media from 11-DHC treated WT fibroblasts, but again this induction was lost in KO macrophages treated with media from DHC treated KO

fibroblasts (Fig 5.27 A). Additionally, gene expression of *il6* showed a trend towards decreased levels in KO macrophages treated with media from DHC treated WT fibroblasts, an effect which was not present when KO macrophages were treated with media from 11-DHC treated KO fibroblasts (Fig 5.27 B). Therefore, these data suggest that fibroblasts can also communicate GC signals to the macrophage.

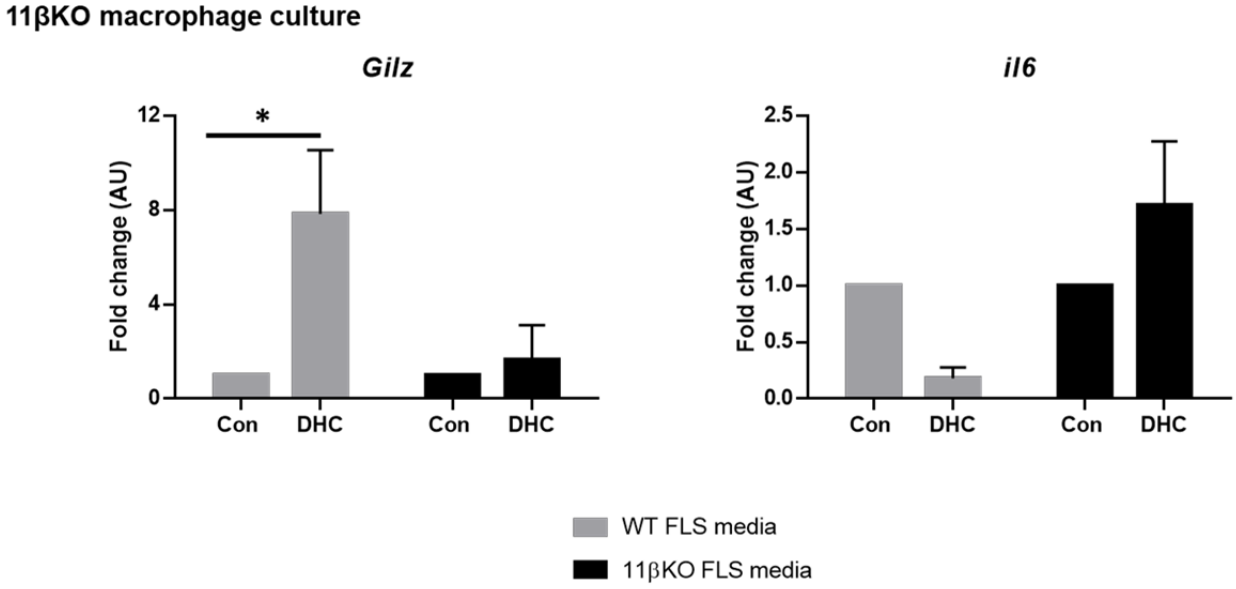

Figure 5. 27: Response of KO macrophages to GCs metabolised by WT & 11βKO fibroblasts

Gene expression analysis (AU) by qPCR of (A) *Gilz* and (B) *il6* of 11β-HSD1 KO macrophages treated with media from either WT or 11β-HSD1 KO fibroblasts treated in the absence or presence of 11-DHC (n=3). Data is presented as mean ± SEM and statistical significance was determined using one-way ANOVA with Tukey's multiple comparisons test. (* denotes P≤0.05)

Finally, co-culture experiments were utilised in which KO fibroblasts were cultured on a plate and treated with active and inactive GCs either in the absence or presence of WT macrophages on an insert. In both KO fibroblast only and KO fibroblast with WT macrophage cultures, treatment with the active GC corticosterone could potently upregulate the GC-responsive gene *Gilz*. However, treatment with the inactive GC 11-

DHC was unable to upregulate *Gilz* in the KO fibroblast only cultures, and could only upregulate *Gilz* in the presence of WT macrophages (Fig 5.28). Thus, GCs can be activated by 11β-HSD1 within macrophages and secreted into the surrounding environment to exert effects on neighbouring fibroblasts.

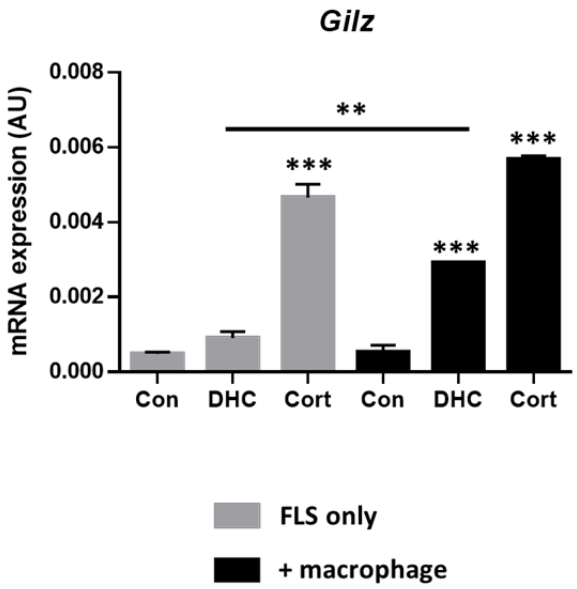

Figure 5. 28: Gilz expression in KO fibroblasts treated with DHC in the absence or presence of WT macrophages

Gene expression analysis (AU) by qPCR of *Gilz* in 11β-HSD1 KO fibroblasts co-cultured with macrophages from either WT or 11β-HSD1 KO mice and treated in the absence or presence of 11-DHC (n=3). Data is presented as mean ± SEM and statistical significance was determined using one-way ANOVA with Tukey's multiple comparisons test. (* denotes P≤0.05)

5.5 Discussion

Therapeutic GCs are frequently used to treat chronic inflammatory diseases such as RA because of their potent anti-inflammatory properties. However, their long term use is limited, in part due to their detrimental metabolic adverse effects, such as osteoporosis, muscle wasting and obesity (159, 320). Therefore, it is important to fully understand the mechanisms that mediate GC signalling in response to therapeutic GCs to identify novel strategies to better target the beneficial anti-inflammatory effects whilst avoiding unwanted side effects. This chapter uses therapeutic GC treatment in the global 11β-HSD1 KO mouse crossed with the TNF-tg model of chronic inflammatory polyarthritis to determine the contribution of 11β-HSD1 activation of GCs to their therapeutic anti-inflammatory effects. Furthermore, myeloid specific and mesenchymal specific 11β-HSD1 KO mice were also utilised in an attempt to delineate the cell specific contributions of GC activation by 11β-HSD1 to their therapeutic effects.

Clinical and arthritic paw scores were significantly reduced in response to GC treatment in TNF-tg animals, whilst TNF11βKO animals showed no response to GC treatment in terms of disease activity scores (Fig 5.2). In keeping with this, whilst TNF-tg animals potently suppressed pro-inflammatory cytokines such as TNF, IL-6 and IL-1 in response to corticosterone treatment, levels of pro-inflammatory cytokines in TNF11βKO mice remained persistently elevated with corticosterone treatment (Fig 5.3). Overall, TNF11βKO animals appear to be resistant to the anti-inflammatory effects of GCs suggesting that 11β-HSD1 amplification of exogenous GCs is a critical step required to mediate their beneficial effects. In patients with ANCA-associated vasculitis, a group of autoimmune diseases characterised by inflammation of the blood vessels, polymorphisms in the gene encoding 11β-HSD1 have been associated with an increased

risk of relapse after prednisolone treatment due to a pro-inflammatory phenotype, suggesting that defects in 11β-HSD1 in humans affects the efficacy of GC treatment (326).

Additionally, previous studies have demonstrated the requirement for 11β-HSD1 when mediating anti-inflammatory effects to endogenous GCs. When STIA is induced in 11β-HSD1 KO mice, arthritis is significantly exacerbated (324). Similarly, 9-week old TNF11βKO animals have previously been shown to have significantly higher levels of arthritis and inflammation under basal conditions (157). In keeping with this, the results of the present study show that seven-week old TNF11βKO animals have significantly elevated arthritic paw scores (Fig 5.2 B). However, no significant increases were observed in pro-inflammatory cytokines at this time point (Fig 5.3).

Chronic inflammatory arthritis is frequently associated with juxta-articular bone erosions (327). TNF-tg animals also develop significant local bone loss, which is significantly suppressed upon treatment with GCs. In contrast, TNF11βKO animals show no improvement of local bone erosions in response to GC treatment (Fig 5.4). Studies have shown the extent of synovitis strongly correlates with the development of bone erosions and thus controlling inflammation in RA patients can vastly improve the radiographic damage associated with the disease (327-331). The inability of TNF11βKO animals to suppress the pro-inflammatory chemokines CCL2, CXCL10 and CXCL2, responsible for attracting cells such as monocytes, macrophages and neutrophils, in response to GCs lead to the persistent accumulation of inflammatory infiltrate into the synovium (Fig 5.6 & 5.5). Previously, 11β-HSD1 deficiency in both carrageenan-induced pleurisy and peritonitis resulted in increased recruitment of inflammatory cells (324).

TNFα has been shown to induce the release of osteoclast precursors into the circulation, which then migrate to sites of inflammation where the presence of osteoclastogenic cytokines triggers their maturation into mature bone resorbing osteoclasts (332). Whilst the TNF-tg animals could potently suppress osteoclasts in response to GCs, TNF11βKO animals were unable to do so, and osteoclast numbers remained unchanged in response to corticosterone treatment (Fig 5.7). The exact chemoattractant responsible for the migration of osteoclast precursors to the site of inflammation remains unknown, however CCL2 has been suggested as a possible mediator and has also been shown to promote osteoclast fusion and differentiation (333, 334). Overall, the inability of GCs to reduce bone erosions in the absence of 11β-HSD1 activity is likely due to the persistent pro-inflammatory cytokines and chemokines observed in the TNF11βKO mouse.

Mesenchymal derived cells such as fibroblasts and osteoblasts potently upregulate 11β-HSD1 expression in response to treatment with pro-inflammatory cytokines (154). Additionally, fibroblasts have been implicated in the pathogenesis of RA. FLS recruit immune cells through expression of pro-inflammatory chemokines and cytokines, and prolong the survival of activated T cells (95). Thus, the mesenchymal specific 11β-HSD1 KO mouse was used to investigate whether stromal 11β-HSD1 plays an important role in mediating the anti-inflammatory actions of GCs in chronic inflammatory polyarthritis. Interestingly, the TNF-Twist2 animals were almost identical to TNF-tg animals, in terms of both basal levels of inflammation in the untreated group and suppression of disease activity in response to GC treatment (Fig 5.9). These data indicate that GC activation by mesenchymal derived 11β-HSD1 is not required for suppression of inflammation by endogenous or exogenous GCs. We have previously observed that TNF-Twist2 animals have abrogated inflammation compared to TNF-tg animals at 9 weeks old, suggesting

that 11β-HSD1 in stromal populations plays a destructive role in inflammation (153). This reduced inflammation was not observed in the present study, however this is potentially due to the earlier time point chosen to study.

Additionally, TNF-Twist2 animals retained the ability to suppress the pro-inflammatory cytokines TNFα and IL-1 in response to GC treatment. However, GC treatment was unable to suppress serum IL-6 in mice lacking mesenchymal 11β-HSD1 (Fig 5.11). Stromal cell populations have been shown to produce high levels of IL-6 during inflammation (335-338). Thus, 11β-HSD1 may be required to amplify the anti-inflammatory actions of GCs in mesenchymal cell populations to sufficiently inhibit this source of IL-6.

Whilst TNF-tg animals have been shown to significantly reduce juxta-articular bone erosions in response to GCs, bone loss was not significantly reduced between GC treated and untreated TNF-Twist2 animals. However, bone erosions appeared to be reduced in TNF-Twist2 animals compared to TNF-tg mice under basal conditions and no difference was observed between the GC treatment groups (Fig 5.12). In support of this, we have previously found that the TNF-Twist2 animals have significantly less juxta-articular bone erosions than TNF-tg controls (339). Therefore, it is possible that mesenchymal 11β-HSD1 KO animals are still able to reduce bone erosions in response to corticosterone treatment, but statistical significance is not achieved due to the reduced severity of bone erosions in the untreated controls. Synovitis was also significantly reduced upon treatment with GCs in mice with mesenchymal 11β-HSD1, indicating that mesenchymal GC activation does not mediate the GC induced protection of the joint (Fig 5.13). Additionally, levels of the pro-inflammatory chemokines CCL2, CXCL10 and CXCL2 were

equally suppressed in TNF-Twist2 animals receiving oral corticosterone compared to TNF-tg animals. Furthermore, osteoclast numbers were suppressed in TNF-Twist2 to a similar extent as TNF-tg animals upon GC treatment (Fig 5.14). Whilst no significant changes were observed in the cartilage of the animals, TNF-tg mice showed a trend towards increased proteoglycan loss in response to GC treatment, while TNF-Twist2 animals appeared to be somewhat protected from this (Fig 5.16). Overall, activation of GCs by mesenchymal 11β-HSD1 does not appear to be necessary for their therapeutic effects during chronic inflammation.

11β-HSD1 metabolism of GCs within myeloid derived macrophages during inflammation has been shown to play an important role in the polarisation of macrophages towards a pro-resolution phenotype (158). Thus, since deletion of mesenchymal derived 11β-HSD1 was not sufficient to replicate the phenotype of the global KO mouse, we hypothesised that myeloid derived 11β-HSD1 would be important in mediating this GC resistance phenotype. Therefore, the myeloid specific 11β-HSD1 KO mouse was crossed with the TNF-tg and utilised to examine the role that GC activation by myeloid 11β-HSD1 metabolism plays in mediating the anti-inflammatory effects of GCs in chronic inflammatory polyarthritis.

Arthritic paw scores were exacerbated, and osteoclast numbers were elevated in untreated TNF-LysM animals compared to TNF-tg counterparts, suggesting a role for myeloid derived 11β-HSD1 metabolism of endogenous GCs in resolving inflammation (Fig 5.18 and 5.23). A previous study showed that myeloid derived 11β-HSD1 KO mouse had a similar impairment of resolution of inflammation as global KO animals in a K/BxN STIA model of inflammatory arthritis (340). Additionally, 11β-HSD1 deficient macrophages have been shown to produce significantly higher levels of pro-inflammatory

cytokines in response to LPS stimulation (341). Whilst no significant changes were observed in pro-inflammatory cytokines expression between untreated TNF-LysM animals and TNF-tg controls, trends towards increased TNF and IL-1 were observed (Fig 5.19).

Interestingly, whilst TNF-LysM mice still exhibited significant suppression of arthritic paw scores in response to therapeutic GCs, this genotype had a blunted response to therapeutic GCs in terms of both clinical and arthritic paw scores compared to TNF-tg animals, suggesting an important contribution of myeloid derived 11β-HSD1 to the therapeutic effects of GCs (Fig 5.18). In contrast, TNF-LysM animals maintained the ability to potently suppress pro-inflammatory cytokines and chemokines, in addition to synovitis and osteoclast numbers at the elbow joints (Fig 5.19, 5.22, 5.21 and 5.23). However, despite significant reductions in pro-inflammatory factors and osteoclast numbers, TNF-LysM animals failed to suppress juxta-articular bone erosions in response to GC treatment (Fig 5.20). Further research could investigate whether synovitis and osteoclast numbers are reduced at the metacarpal and phalange bones of the front paw where the erosions are present, as there could be a differential response to GCs at different joint regions. No changes were observed in terms of cartilage destruction amongst the genotypes indicating that GC activation by myeloid derived 11β-HSD1 has no impact on proteoglycan production and cartilage damage (Fig 5.24).

Previously, GC signalling in myeloid derived macrophages and neutrophils has been shown to be necessary for the therapeutic actions of GCs during contact hypersensitivity, whilst a separate study ruled out myeloid cells as the mediators of the therapeutic effects of GCs in antigen-induced arthritis (321, 323). Our data reveal a partial GC resistance phenotype in TNF-LysM mice, pointing towards a contribution of GC activation by myeloid

derived 11β-HSD1 metabolism to the therapeutic effects of GCs. We have previously shown that global 11β-HSD1 KO mice have impaired polarisation of macrophages towards the pro-resolution phenotype and another study showed that this was mediated by 11β-HSD1 within macrophage populations, thus indicating that the blunted response of the TNF-LysM mouse in the current study may be due to impaired polarisation of macrophages (157, 158). Further research could investigate the ratio of M1/M2 macrophages in response to GCs in the different genotypes.

However, since neither mesenchymal nor myeloid derived 11β-HSD1 KO mice completely recapitulated the phenotype of the global KO mouse, this suggests a compensatory mechanism by which neighbouring cells can communicate GC signals in a paracrine manner. In order to address this, conditioned media and co-culture experiments were implemented. 11β-HSD1 KO FLS cultures exposed to media from 11-DHC treated WT macrophages were able to potently upregulate the GC-responsive gene *Gilz* and suppress both gene expression and protein levels of the pro-inflammatory IL-6, despite lacking the ability to activate 11-DHC themselves. In contrast, this robust response to GCs was lost when 11β-HSD1 KO FLS were exposed to media from 11-DHC treated 11β-HSD1 KO macrophages (Fig 5.26). These data indicate that GCs can be activated by 11β-HSD1 in macrophages and transmitted to a neighbouring FLS to exert its effects. This was confirmed in co-culture experiments where KO FLS could respond to GCs in terms of increased *Gilz* expression in the presence of WT macrophages only (Fig 5.28). Similarly, the same result was observed when KO macrophages were treated with conditioned media from WT and KO FLS, indicating that FLS can also activate and transmit GC signals to macrophages (Fig 5.27). Thus, paracrine signalling between cell types may explain the failure of cell specific 11β-HSD1 KO animals to fully replicate the

global KO mouse. Alternatively, this could be due to incomplete penetrance of the cre targeted deletion in these animals or the therapeutic effects of GCs could be driven by other 11β-HSD1 expressing cells such as T cells or B cells. Further research could use T and B cell specific 11β-HSD1 KO animals to address this.

Overall, these data show that 11β-HSD1 is necessary to mediate the therapeutic effects of GCs during chronic inflammatory diseases. Previously, 11β-HSD1 inhibitors have been suggested to be used alongside GC treatment in an attempt to reduce their adverse side effects (70). However, our data suggest that this would severely interfere with the efficacy of the treatment. Furthermore, we have demonstrated that neighbouring cells can communicate GC signals. This information will prove important when attempting to target GCs to specific cell types in order to achieve the beneficial anti-inflammatory effects whilst avoiding the metabolic side effects.

Chapter 6: The role of 11β-HSD1 in mediating glucocorticoid induced osteoporosis during chronic inflammatory polyarthritis

6.1 Introduction

As previously reported in Chapter 3, GCs have an initial net beneficial effect on bone when administered during chronic inflammation, through their suppression of inflammatory osteoclast differentiation and resorption. However, whilst 11β-HSD1 mediates the detrimental actions of GCs in glucocorticoid induced osteoporosis (GIO) by suppressing osteoblastic bone formation (Chapter 4), the therapeutic actions of GCs, such as suppression of pro-inflammatory mediators, reduction of synovitis and reduction of joint erosions, have been shown to be dependent on GC activation by 11β-HSD1 metabolism (Chapter 5). Thus, the question remains as to whether 11β-HSD1 mediates the protective effects of GCs on systemic bone during chronic inflammation.

As described previously in section 1.4.7, 11β-HSD1 plays an important role in suppressing inflammation by the activation of endogenous GCs. Deletion of 11β-HSD1 in the TNF-tg mouse leads to significantly exacerbated inflammation and disease activity. In addition, the TNF11βKO mouse had significantly reduced systemic bone parameters, such as bone volume, trabecular thickness and trabecular number, compared to age matched TNF-tg animals. This was caused by a reduction in osteoblast differentiation, via suppression in Runx2, and an increase in osteoclastogenesis, via a suppression of OPG and an increase in M-CSF, likely driven by the increase in pro-inflammatory cytokines, such as TNFα and IL-6, observed in the TNF11βKO mouse (157).

Osteoblasts have been shown to upregulate 11β-HSD1 in response to pro-inflammatory cytokines, thus osteoblasts may play an important role in responding to therapeutic GCs during inflammation (154). Disrupting GC signalling by overexpression of the GC-inactivating enzyme 11β-HSD2 specifically in mature osteoblasts and osteocytes has been shown to significantly ameliorate joint swelling, synovitis and cartilage destruction

in the STIA mouse model of chronic inflammatory arthritis (342). Furthermore, histomorphometry revealed that transgenic mice were protected from decreases in osteoblast and increases in osteoclast numbers in response to induction of arthritis. In keeping with this, bone volume and trabecular number were unchanged in transgenic mice upon arthritis induction, whilst these parameters were significantly reduced in WT K/BxN mice (342). We generated a mesenchymal specific 11β-HSD1 KO mouse, which targets cells such as osteoblasts, fibroblasts and chondrocytes, and crossed it with a TNF-tg mouse. Although no significant differences were observed in the systemic bone phenotype, TNF-tg animals lacking mesenchymal 11β-HSD1 had attenuated inflammation and less local bone erosions compared to normal TNF-tg mice (157). Currently, data investigating the effects of osteoclast derived 11β-HSD1 metabolism of GCs on inflammation and inflammatory bone loss are poorly defined.

A clear link exists between inflammation and bone destruction, and controlling inflammation has been shown to have beneficial effects on the progression of bone erosions in patients with RA (343). Since 11β-HSD1 plays a profound role in the therapeutic effects associated with GC therapy, we wished to examine whether this enzyme also mediates the protective effects of GCs on the bone during chronic inflammation. Thus, this chapter utilises the global, mesenchymal and myeloid specific 11β-HSD1 KO mice crossed with TNF-tg animals to examine the effect of therapeutic GCs on the bone in a chronic inflammatory environment in the absence of 11β-HSD1.

6.2 Hypothesis

The protective effects of therapeutic GCs on the bone during chronic inflammation are mediated by activation via 11β-HSD1 metabolism.

6.3 Materials and Methods

6.3.1 Animal experiments

Heterozygous TNF-tg animals were bred according to section 2.1.1 and crossed with global (TNF11βKO), mesenchymal (TNF-Twist2) or myeloid (TNF-LysM) 11β-HSD1 KO mice (section 2.1.2 and 2.1.3). Four-week old mice were administered 100 mg/L corticosterone via the drinking water for three weeks (section 2.1.4). At seven weeks, animals were culled by cervical dislocation after exsanguination by cardiac puncture. Tissues were dissected and stored prior to use as previously described (section 2.1.4).

6.3.2 Micro-CT analysis

Formalin fixed tibias were stored in 70% ethanol at 4°C prior to scanning on a Skyscanner 1172 (Bruker Micro-CT, Belgium) (see section 2.2). Tibias were reconstructed and analysed as described in section 2.2.1.

6.3.3 ELISA analysis

Blood was isolated from mice by cardiac puncture and allowed to clot for 30 minutes at room temperature prior to being centrifuged at 13,000 rpm for 30 minutes. Serum was aspirated into a fresh tube to be stored at -80°C until required. Serum levels of P1NP and CTX-1 were assessed by ELISA assays as outlined in sections 2.6.2.1 and 2.6.3.2, respectively.

6.3.4 Gene expression analysis

Tibias were excised post mortem and homogenised in a pestle and mortar using liquid nitrogen. RNA was isolated using the innuPREP RNA Mini Kit 2.0 (AnalytikJena, Jena, Germany) as described in section 2.5.1. RNA purity and concentration were assessed using a NanoDrop™ 1000 Spectrophotometer (ThermoFisher, Paisley, UK) and 700 ng RNA was used for the synthesis of cDNA with the High-Capacity cDNA Reverse Transcription Kit (ThermoFisher, Paisley, UK) as outlined in section 2.5.2. Quantitative real time PCR was utilised to measure the expression of genes in the tibias from different mouse groups (see section 2.5.3) using the Taqman probes listed in Supplementary Table 1 (Applied Biosystems).

6.3.5 Statistical analysis

GraphPad Prism software (GraphPad, San Diego, USA) was used to determine statistical significance. Two-way ANOVA analysis was used with a Tukey post hoc analysis to compare between treatment groups and genotypes unless otherwise stated in the figure legend. N numbers are recorded in the relevant figure legend. Statistical significance was determined as $P \leq 0.05$. * denotes $P \leq 0.05$, ** denotes $P \leq 0.01$ and *** denotes $P \leq 0.001$.

6.4 Results

6.4.1 Impact of GC treatment on the bone of TNF11βKO animals

To examine the contribution of activation of GCs by 11β-HSD1 to the bone protective effect of GCs in chronic inflammation observed in Chapter 3, global 11β-HSD1 KO

animals were crossed with the TNF-tg mouse to generate the TNF11βKO mouse. After three weeks of treatment with corticosterone drinking water, tibias were scanned for micro-CT analysis. TNF-tg animals treated with GCs had a significant improvement in bone volume, trabecular number and trabecular separation compared to untreated controls (Fig 6.1 B, D & E). TNF11βKO animals also showed significant increases in bone volume and trabecular number upon corticosterone treatment, however the bone phenotype had not improved to the same extent as with TNF-tg animals treated with corticosterone, with GC treated TNF11βKO animals still having significantly lower bone volume and trabecular number compared to GC treated TNF-tg animals (BV/TV: TNF-tg Cort 4.25% ± 0.22 vs TNF11βKO Cort 2.83% ± 0.25, P≤0.01; Tb.N: TNF-tg Cort 0.0008 1/μm ± 0.00003 vs TNF11βKO Cort 0.0006 1/μm ± 0.00004, P≤0.01) (Fig 6.1 B & D). Trabecular separation showed no improvements in TNF11βKO animals compared to their untreated controls (Fig 6.1 E). No significant differences were observed amongst the different groups in terms of trabecular thickness (Fig 6.1 C). Thus, 11β-HSD1 activation of GCs is at least partially responsible for their beneficial effects on the trabecular bone during chronic inflammation.

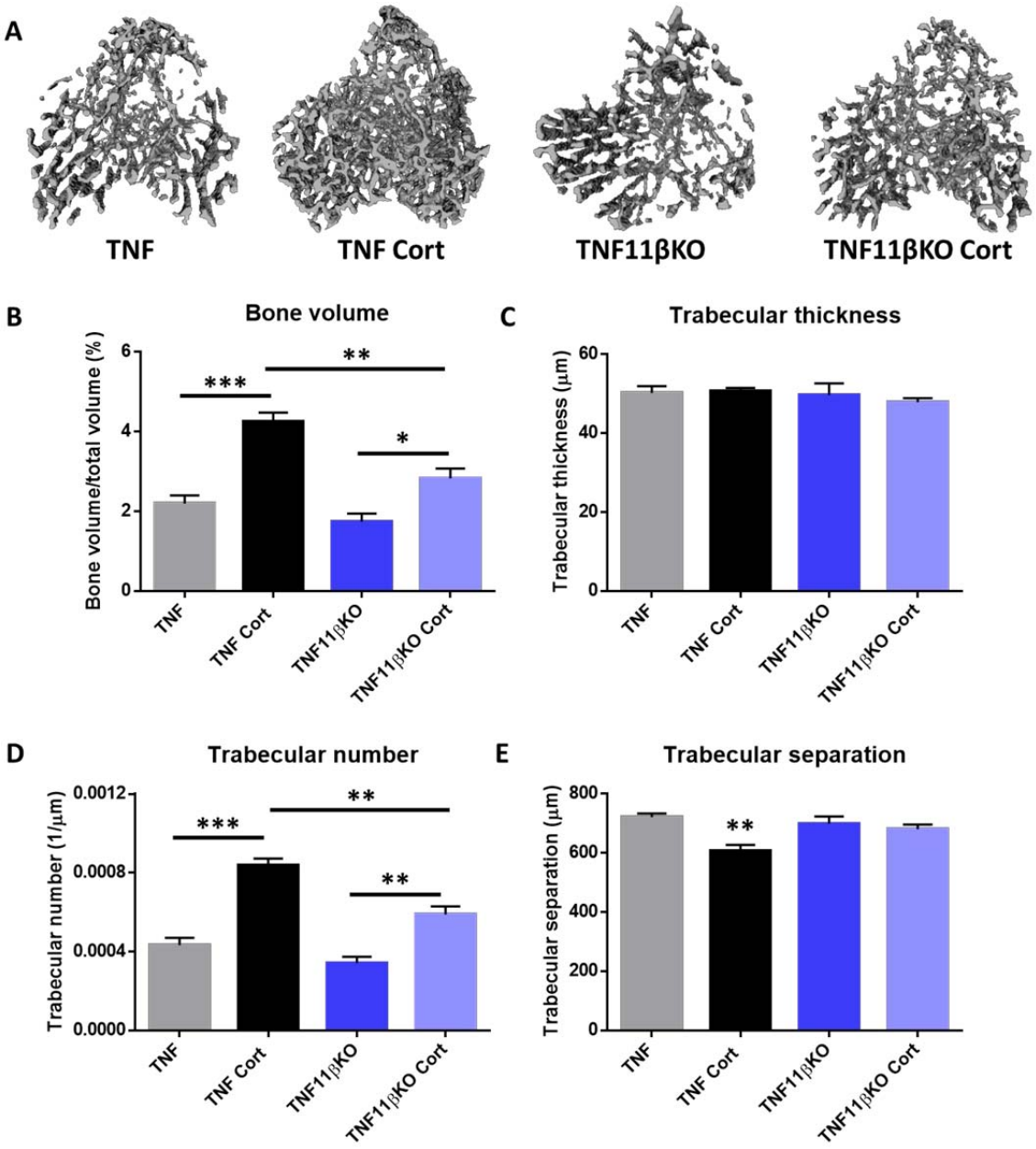

Figure 6. 1: Systemic bone parameters in TNF-tg and TNF11βKO animals treated with GCs

(A) Representative images of reconstructed trabecular bone from tibia scans of TNF-tg and TNF11βKO animals receiving vehicle control or 100 mg/L corticosterone in the drinking water for three weeks. Micro-CT analysis of (B) bone volume (%) relative to total volume, (C) trabecular thickness (µm), (D) trabecular number (1/µm) and (E) trabecular separation (µm) of TNF-tg and TNF11βKO animals receiving vehicle control or 100 mg/L corticosterone in the drinking water for three weeks (n=6 per group). Data is presented as mean ± SEM and statistical significance was determined using two-way ANOVA with Tukey's multiple comparisons test (* denotes P≤0.05, ** denotes P≤0.01 and *** denotes P≤0.001).

ELISA analysis of serum and gene expression analysis of RNA from tibias of these mice were then performed to assess alterations in bone remodelling markers. Firstly, osteoblast markers were examined. The serum bone formation marker P1NP showed a non-significant decrease in levels in TNF-tg animals receiving oral corticosterone compared to their untreated counterparts, however, no difference was determined between GC treated TNF11βKO P1NP levels compared to their relevant controls (Fig 6.2 A). A similar pattern was seen with the mature osteoblast marker *Bglap*, which was significantly suppressed upon corticosterone treatment in TNF-tg animals, but GC treated TNF11βKO animals were protected from this suppression (TNF-tg Cort 0.04 AU ± 0.02 vs TNF11βKO Cort 0.41 AU ± 0.07, P≤0.001) (Fig 6.2 B). A second mature osteoblast marker *Alpl* showed a modest trend towards decreased levels in TNF-tg animals receiving oral corticosterone compared to untreated TNF-tg animals, which was no longer apparent in the TNF11βKO untreated and corticosterone treated groups. In fact, TNF11βKO animals receiving GC treatment had significantly higher levels of *Alpl* than TNF-tg mice receiving GC treatment (TNF-tg Cort 0.002 AU ± 0.0007 vs TNF11βKO Cort 0.007 AU ± 0.0016, P≤0.05) (Fig 6.2 C). No corticosterone induced changes were observed in the expression levels of the osteoblast differentiation marker *Runx2*, however significantly higher levels were observed in untreated TNF11βKO animals compared to untreated TNF-tg animals (Fig 6.2 D). The wnt inhibitor *Sost* showed a trend towards increased levels in both TNF-tg and TNF11βKO GC treated groups compared to their untreated controls, whilst TNF11βKO animals were protected from the corticosterone induced decreases in *Dkk1* observed in TNF-tg animals (Fig 6.2 E-F). Overall, these data suggest that GC activation by 11β-HSD1 largely protects against corticosterone induced

suppression of osteoblasts in chronic inflammation in a similar manner reported in 11βKO animals receiving corticosterone (Chapter 4).

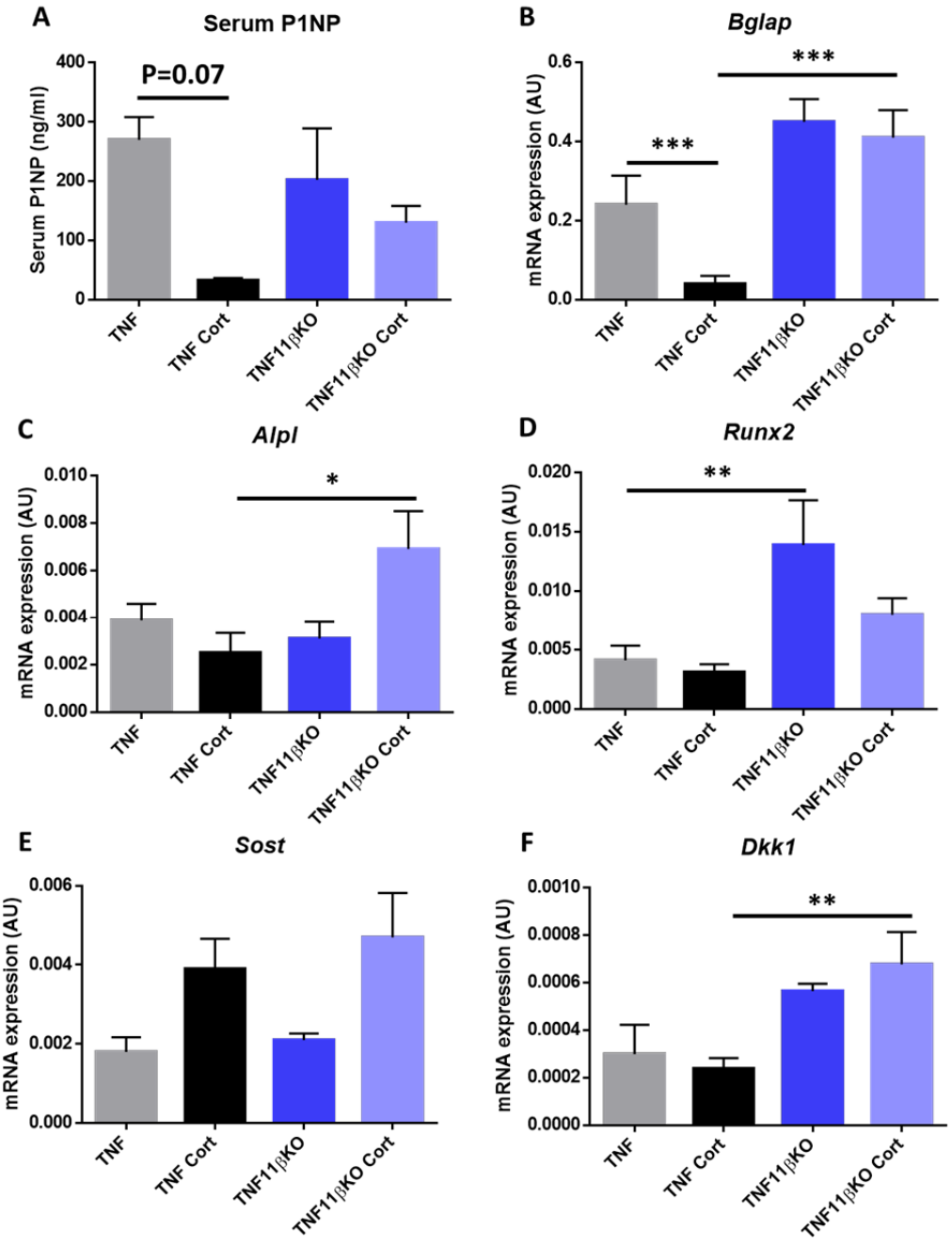

Figure 6. 2: Osteoblast markers in TNF-tg and TNF11βKO animals treated with GCs

(A) ELISA analysis of serum P1NP (ng/ml) (n=6 per group) and qPCR analysis (AU) of (B) *Bglap,* (C) *Alpl,* (D) *Runx2,* (E) *Sost* and (F) *Dkk1* in tibias from TNF-tg and TNF11βKO (n=6 per group) animals receiving control or 100 mg/L corticosterone in the drinking water for three weeks. Data is presented as mean ± SEM and statistical significance was determined using two-way ANOVA with Tukey's multiple comparisons test (* denotes P≤0.05, ** denotes P≤0.01 and *** denotes P≤0.001).

Following this, osteoclast markers were assessed. Serum levels of the bone resorption marker CTX-1 showed a significant decrease in TNF-tg animals receiving oral corticosterone compared to untreated controls, however TNF11βKO animals were again protected from these changes (TNF11βKO 62.67 ng/ml ± 2.09 vs TNF11βKO Cort 52.04 ng/ml ± 4.25, P=0.36) (Fig 6.3 A). In contrast, the RANKL/OPG ratio showed trends towards increases in both corticosterone treated groups compared to their controls (Fig 6.3 B). The osteoclast activity and survival factors, *Ctsk* and *Csf1*, showed no significant changes amongst the groups (Fig 6.3 C-D). Thus, the systemic osteoclast activity marker is protected from corticosterone induced decreases in TNF11βKO animals, but 11β-HSD1 does not appear to affect local differentiation markers in the tibia.

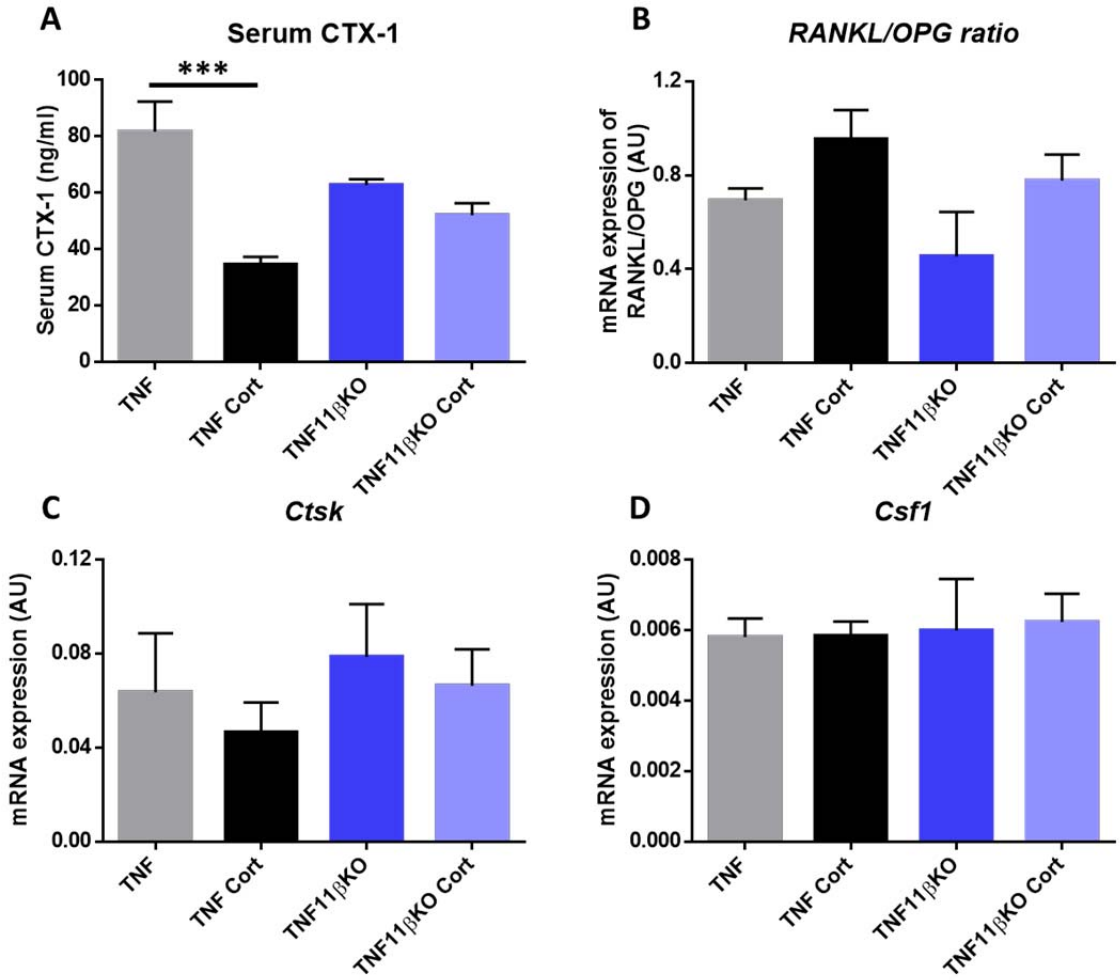

Figure 6. 3: Osteoclast markers in TNF-tg and TNF11βKO animals treated with GCs

(A) ELISA analysis of serum CTX-1 (ng/ml) in TNF-tg (n=6) and TNF11βKO (n=5) mice receiving vehicle control or 100 mg/L corticosterone TNF-tg (n=6) and TNF11βKO (n=5) in the drinking water for three weeks. qPCR analysis of gene expression (AU) of (B) the Rankl/Opg ratio, (C) *Ctsk* and (D) *Csf1* from tibias of TNF-tg and TNF11βKO animals receiving control or 100 mg/L corticosterone drinking water for three weeks (n=6 per group). Data is presented as mean ± SEM and statistical significance was determined using two-way ANOVA with Tukey's multiple comparisons test (*** denotes P≤0.001).

Taken together, these data suggest that the protective effects of GCs on the bone of TNF-tg animals is at least partially dependent on 11β-HSD1 mediated suppression of osteoclastic bone resorption during chronic inflammation.

6.4.2 Impact of GC treatment on the bone of TNF-Twist2 mice

In order to determine the specific cell type responsible for the protective effects of GCs on the bone during chronic inflammation, the mesenchymal specific 11β-HSD1 KO TNF-Twist2 mouse with effective deletion in OBs (characterised in Chapter 4), was utilised to examine the actions of therapeutic GCs on bone. After three weeks of corticosterone drinking water, mice were sacrificed and tibias collected for micro-CT analysis. Bone volume was significantly increased in TNF-tg animals receiving oral corticosterone compared to untreated TNF-tg mice (Fig 6.4 B). A comparable trend towards an increase was seen in the TNF-Twist2 mice receiving corticosterone relative to vehicle treated controls (TNF-Twist2 2.66% ± 0.44 vs TNF-Twist2 Cort 3.97% ± 0.42, P=0.06). This induction was comparable with GC treated TNF-tg mice (Fig 6.4 B). No corticosterone induced changes were observed in terms of trabecular thickness, however under basal conditions TNF-Twist2 animals had significantly thicker trabecular than TNF-tg mice (Fig 6.4 C). Corticosterone treatment increased the number of trabeculae in TNF-tg mice, however this was not as apparent in TNF-Twist2 animals which had significantly fewer trabeculae in the GC treated group compared to GC treated TNF-tg mice (TNF-tg Cort 0.0008 1/μm ± 0.00003 vs TNF-Twist2 Cort 0.0003 1/μm ± 0.00003, P≤0.001) (Fig 6.4 D). Trabecular separation significantly lessened in both genotypes in response to GC treatment (Fig 6.4 E). Overall, the beneficial effects of GCs on bone volume and trabecular separation during chronic inflammation persist in the absence of mesenchymal derived 11β-HSD1.

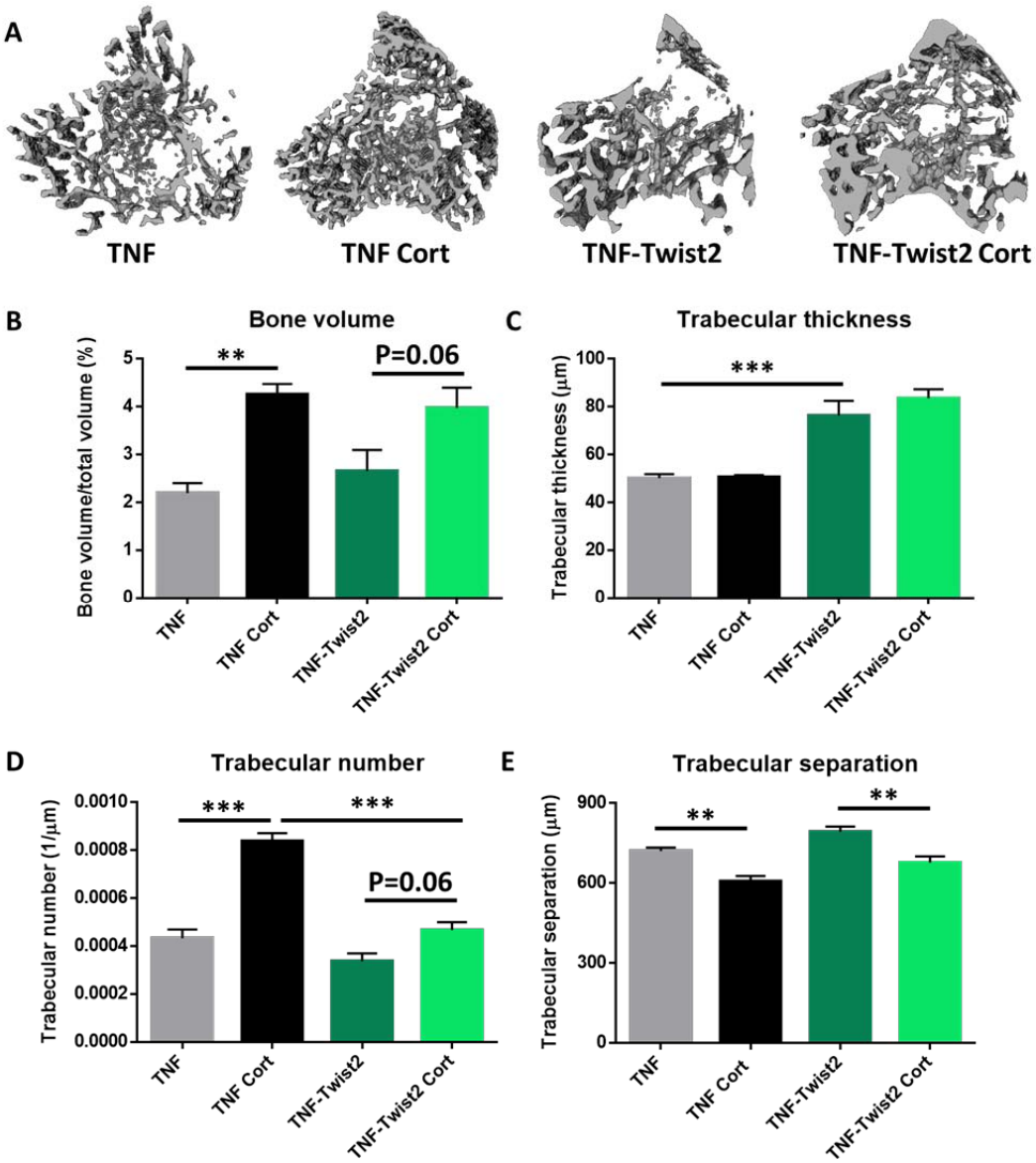

Figure 6. 4: Systemic bone parameters in TNF-tg and TNF-Twist2 animals receiving GCs

(A) Representative images of reconstructed trabecular bone from tibia scans of TNF-tg and TNF-Twist2 animals receiving vehicle control or 100 mg/L corticosterone in the drinking water for three weeks. Micro-CT analysis of (B) bone volume (%) relative to total volume, (C) trabecular thickness (µm), (D) trabecular number (1/µm) and (E) trabecular separation (µm) of TNF-tg and TNF-Twist2 animals receiving vehicle control or 100 mg/L corticosterone in the drinking water for three weeks (n=6 per group). Data is presented as mean ± SEM and statistical significance was determined using two-way ANOVA with Tukey's multiple comparisons test (** denotes P≤0.01 and *** denotes P≤0.001).

Bone formation markers were examined from the serum and tibia RNA of these mice. Whilst levels of the bone formation marker P1NP were significantly decreased in untreated TNF-Twist2 animals compared to untreated TNF-tg mice, a comparable suppression of P1NP was apparent in both groups in response to GCs (TNF-Twist2 145.34 ng/ml ± 36.1 vs TNF-Twist2 Cort 30.79 ng/ml ± 3.6, P≤0.05) (Fig 6.5 A). The osteoblast marker *Bglap* was also significantly reduced in both genotypes in response to GC treatment (TNF-Twist2 0.29 AU ± 0.091 vs TNF-Twist2 Cort 0.02 AU ± 0.003, P≤0.001) (Fig 6.5 B). No significant differences in *Alpl* and *Runx2* were apparent between the groups, (Fig 6.5 C-D). *Sost* levels demonstrated a trend towards an increase in TNF-tg animals receiving oral corticosterone compared to their untreated controls, which was lost in the GC treated TNF-Twist2 group (Fig 6.5 E). Corticosterone treated TNF-Twist2 animals also showed significantly higher levels of *Dkk1* than corticosterone treated TNF-tg mice (Fig 6.5 F). Therefore, TNF-Twist2 mice exhibit largely similar changes in osteoblast markers in response to GC treatment as TNF-tg mice, despite lacking 11β-HSD1 in the mesenchyme.

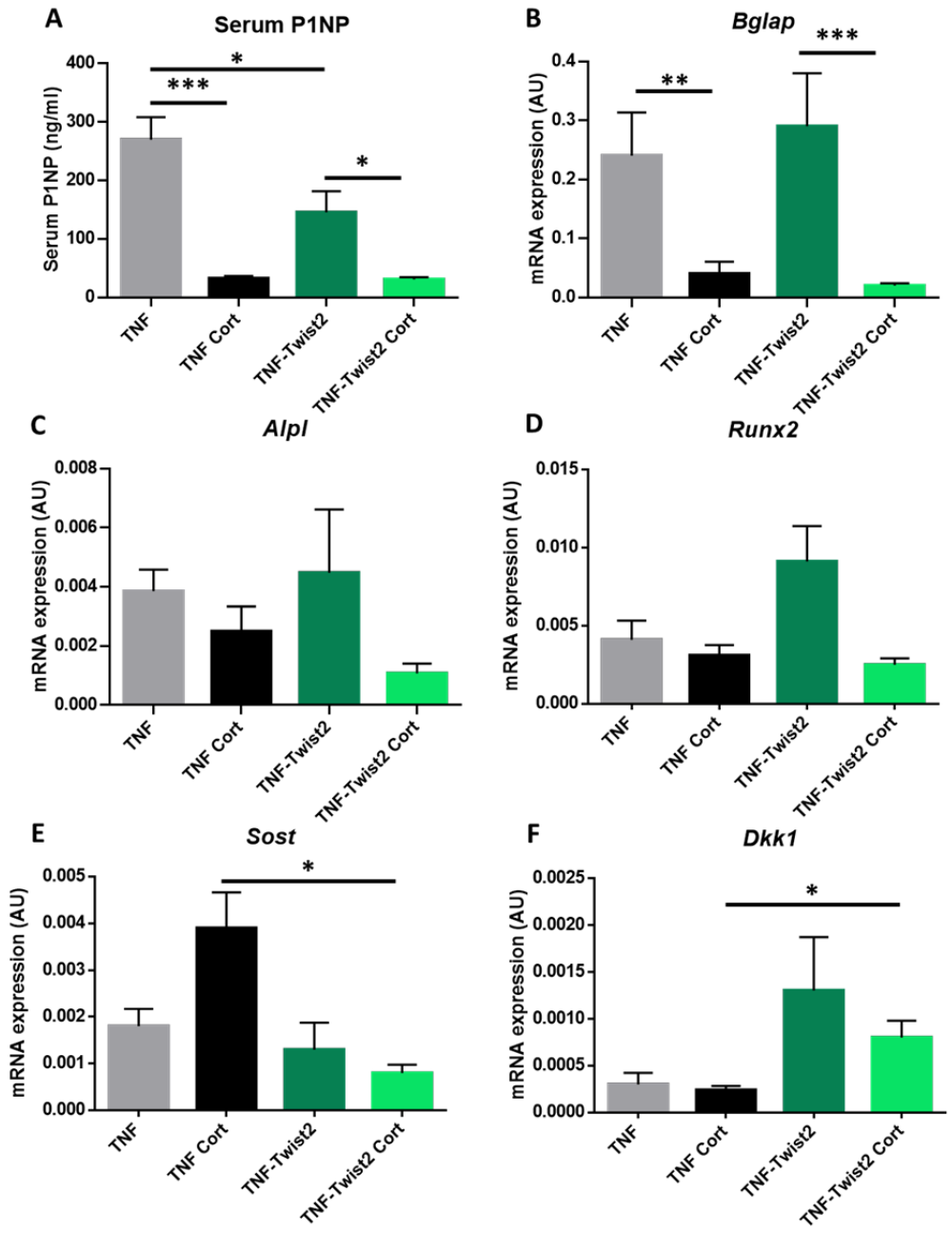

Figure 6. 5: Osteoblast markers in TNF-tg and TNF-Twist2 animals receiving GCs

(A) ELISA analysis of serum P1NP (ng/ml) (n=6 per group) and qPCR analysis (AU) of (B) *Bglap,* (C) *Alpl,* (D) *Runx2,* (E) *Sost* and (F) *Dkk1* in tibias from TNF-tg and TNF-Twist2 (n=6 per group) animals receiving control or 100 mg/L corticosterone in the drinking water for three weeks. Data is presented as mean ± SEM and statistical significance was determined using two-way ANOVA with Tukey's multiple comparisons test (* denotes P≤0.05, ** denotes P≤0.01 and *** denotes P≤0.001).

Next, gene expression levels of osteoclast markers were assessed from RNA isolated from the tibia. The RANKL/OPG ratio was increased in TNF-Twist2 mice receiving oral corticosterone compared to their untreated controls (Fig 6.6 A). The osteoclast activity marker *Ctsk* showed no significant changes between the groups, whilst the osteoclast survival marker *Csf1* showed decreased levels in untreated TNF-Twist2 animals compared to untreated TNF-tg mice. However, no corticosterone induced changes were observed in these markers (Fig 6.6 B-C). Thus, corticosterone treatment does not appear to significantly affect these osteoclast markers in either TNF-tg or TNF-Twist2 animals.

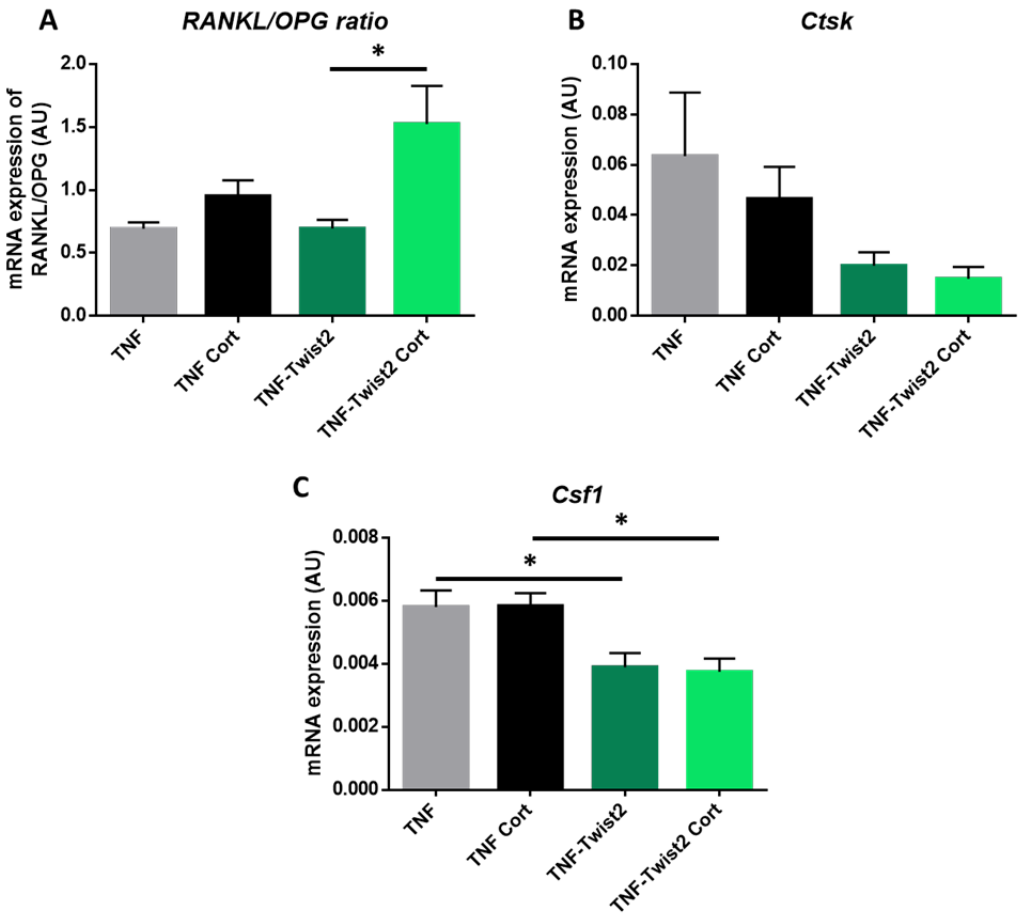

Figure 6. 6: Osteoclast markers in TNF-tg and TNF-Twist2 animals treated with GCs

qPCR analysis of gene expression (AU) of (A) the Rankl/Opg ratio, (B) *Ctsk* and (C) *Csf1* in tibias of TNF-tg and TNF-Twist2 animals receiving control or 100 mg/L corticosterone drinking water for three weeks (n=6 per group). Data is presented as mean ± SEM and statistical significance was determined using two-way ANOVA with Tukey's multiple comparisons test (* denotes P≤0.05).

6.4.3 Impact of GC treatment on the bone of TNF-LysM mice

Finally, to determine the impact of myeloid derived 11β-HSD1 on the protective effect of GCs on the bone observed during chronic inflammation, a myeloid specific 11β-HSD1 KO mouse was crossed with the TNF-tg animals to yield the TNF-LysM mouse. After three weeks of GC treatment, tibias were removed and scanned for micro-CT analysis. Whilst

TNF-tg mice responded to GC treatment with an increase in bone volume and trabecular number, TNF-LysM animals receiving oral corticosterone showed no difference in bone volume or trabecular number to their untreated controls. GC treated TNF-tg animals had significantly higher bone volume and trabecular number than GC treated TNF-LysM animals (BV/TV: TNF-tg Cort 4.25% ±0.22 vs TNF-LysM Cort 2.95% ± 0.24, P≤0.01; Tb.N: TNF-tg Cort 0.0008 1/μm ± 0.00003 vs TNF-LysM Cort 0.0006 1/μm ± 0.00004, P≤0.001) (Fig 6.7 B & D). Additionally, whilst TNF-tg animals had significantly less separation between trabeculae when treated with GCs, TNF-LysM animals showed no difference in trabecular separation between untreated and corticosterone treated groups (TNF-LysM 622.35 μm ± 25.71 vs TNF-LysM Cort 694.85 μm ± 31.20, P=0.19) (Fig 6.7 E). Thus, TNF-tg mice with myeloid deletion of 11β-HSD1 have an attenuated bone protective response to GCs.

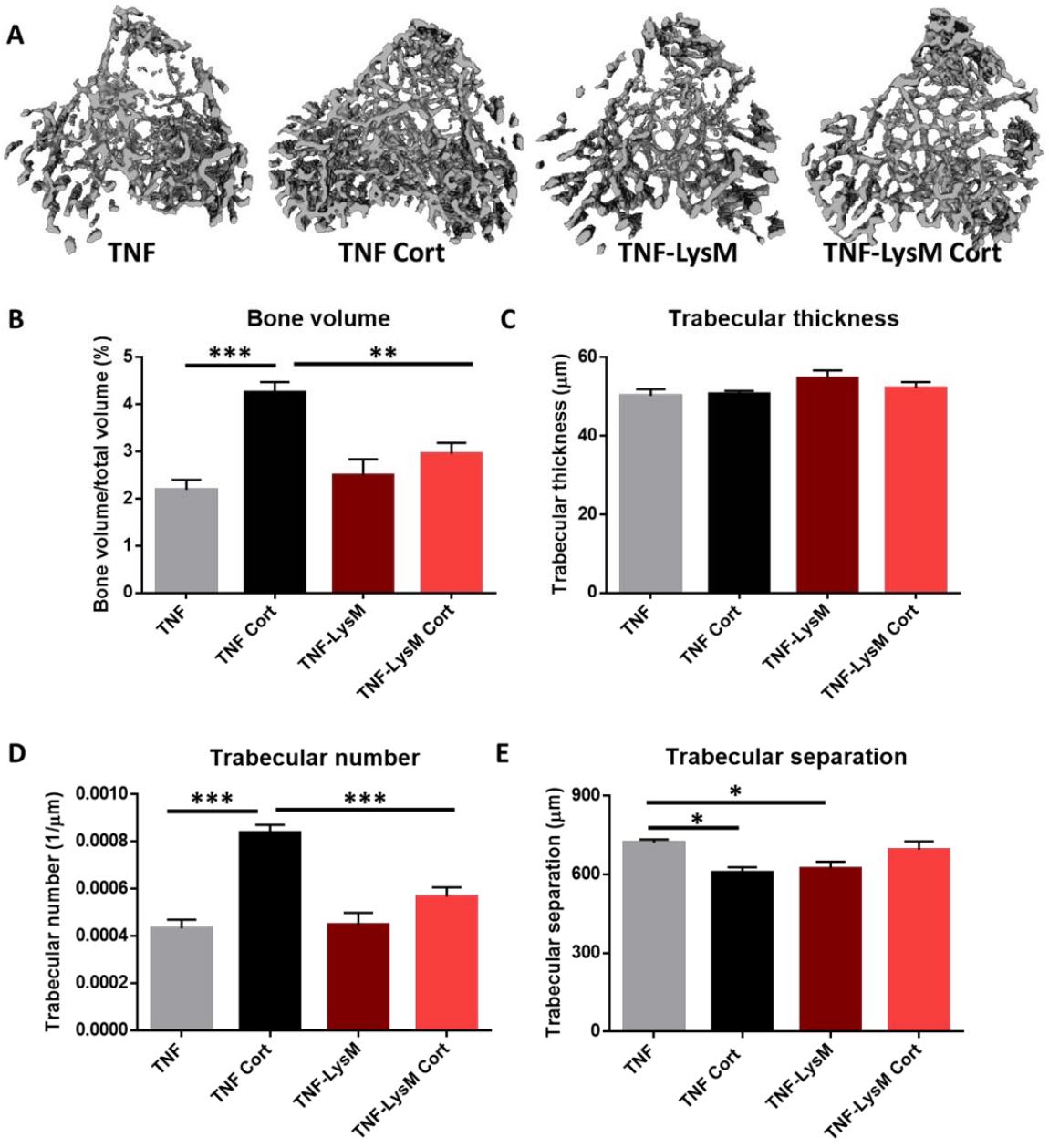

Figure 6. 7: Systemic bone parameters in TNF-tg and TNF-LysM animals treated with GCs

(A) Representative images of reconstructed trabecular bone from tibia scans of TNF-tg and TNF-LysM animals receiving vehicle control or 100 mg/L corticosterone in the drinking water for three weeks. Micro-CT analysis of (B) bone volume (%) relative to total volume, (C) trabecular thickness (µm), (D) trabecular number (1/µm) and (E) trabecular separation (µm) of TNF-tg (n=6) and TNF-LysM (n=5) animals receiving vehicle control or 100 mg/L corticosterone TNF-tg (n=6) and TNF-LysM (n=6) in the drinking water for three weeks. Data is presented as mean ± SEM and statistical significance was determined using two-way ANOVA with Tukey's multiple comparisons test (* denotes P≤0.05, ** denotes P≤0.01 and *** denotes P≤0.001).

Analysis of serum P1NP showed that both TNF-tg and TNF-LysM animals had significantly suppressed bone formation in response to GC treatment to similar levels (TNF-LysM 260.60 ng/ml ± 22.82 vs TNF-LysM Cort 67.00 ng/ml ± 28.45, P≤0.001) (Fig 6.8 A). Similarly, both genotypes significantly suppressed *Bglap* in response to corticosterone treatment (TNF-LysM 1.46 AU ± 0.21 vs TNF-LysM Cort 0.18 AU ± 0.08, P≤0.001). However, untreated TNF-LysM animals exhibited significantly higher levels of *Bglap* than untreated TNF-tg mice (Fig 6.8 B). *Alpl* levels showed a trend towards decrease in TNF-tg animals receiving oral corticosterone and a significant decrease in corticosterone treated TNF-LysM animals compared to their relevant untreated controls. Again, the levels of *Alpl* were significantly higher in untreated TNF-LysM animals compared to untreated TNF-tg mice (Fig 6.8 C). *Runx2* and *Dkk1* exhibited no corticosterone induced changes, however levels were again higher in untreated TNF-LysM animals compared to untreated TNF-tg mice (Fig 6.8 D & F). *Sost* demonstrated no significant changes amongst the groups (Fig 6.8 E). Taken together, these data suggest that myeloid derived 11β-HSD1 is not required for the changes in osteoblast markers in response to GCs during chronic inflammation.

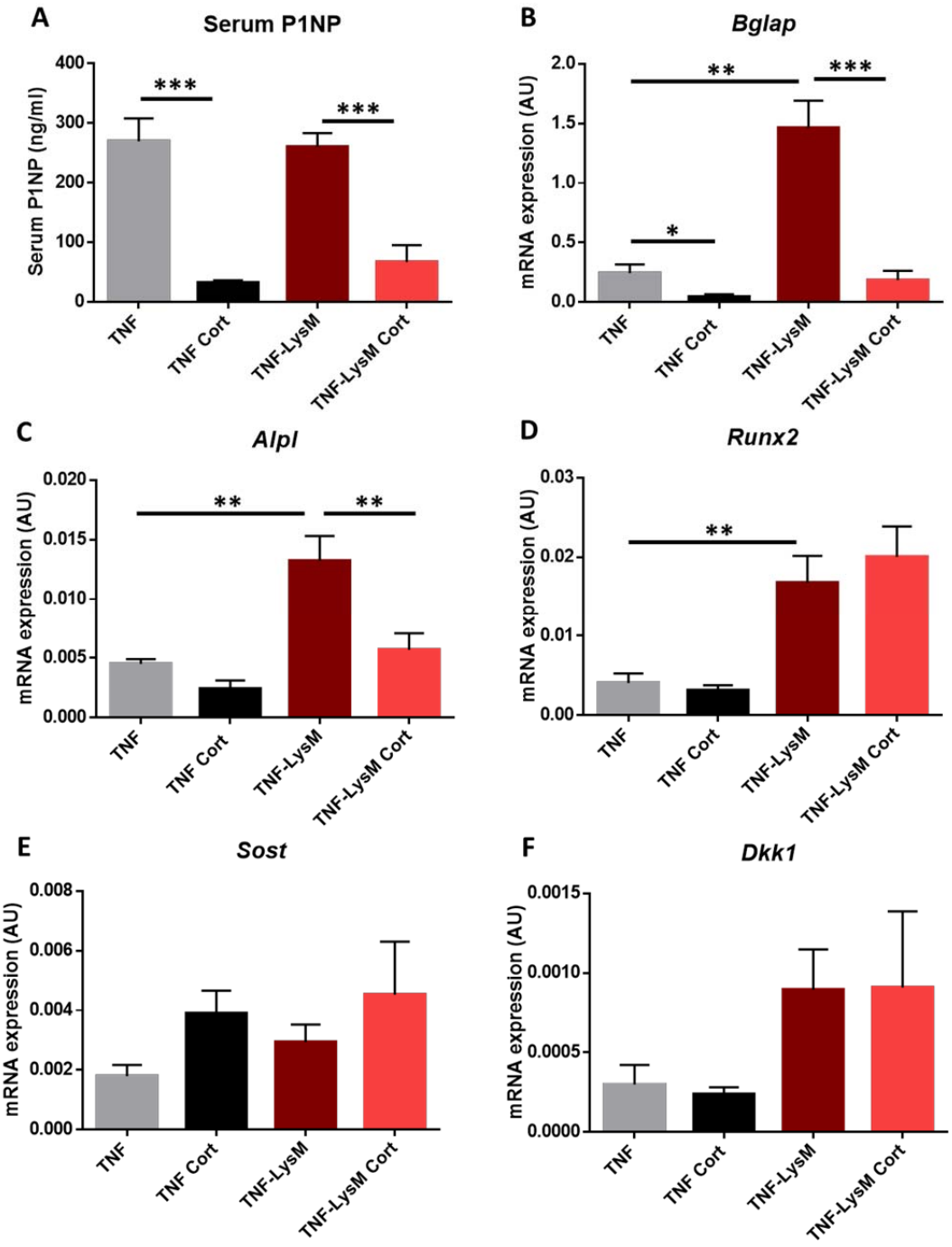

Figure 6. 8: Osteoblast markers in TNF-tg and TNF-LysM animals receiving GCs

(A) ELISA analysis of serum P1NP (ng/ml) in TNF-tg (n=6) and TNF-LysM (n=5) animals receiving vehicle or 100 mg/L corticosterone TNF-tg (n=6) and TNF-LysM (n=5) in the drinking water for three weeks. qPCR analysis (AU) of (B) *Bglap,* (C) *Alpl,* (D) *Runx2,* (E) *Sost* and (F) *Dkk1* in tibias from TNF-tg and TNF-LysM (n=6 per group) animals receiving control or 100 mg/L corticosterone in the drinking water for three weeks. Data is presented as mean ± SEM and statistical significance was determined using two-way ANOVA with Tukey's multiple comparisons test (* denotes P≤0.05, ** denotes P≤0.01 and *** denotes P≤0.001).

Lastly, changes in osteoclast markers were assessed by analysis of serum and gene expression markers in the tibia. Serum levels of the bone resorption marker CTX-1 were significantly suppressed in both TNF-tg and TNF-LysM animals in response to GC treatment (TNF-LysM 86.7 ng/ml ± 5.58 vs TNF-LysM Cort 41.7 ng/ml ± 7.13, P≤0.01) (Fig 6.9 A). No corticosterone induced changes were observed with *Ctsk* or *Csf1*, however there was a significant increase in levels in the untreated TNF-LysM group compared to untreated TNF-tg animals (Fig 6.9 C-D). No significant changes were detected in the RANKL/OPG ratio between the groups (Fig 6.9 B). Thus, CTX-1 is significantly suppressed by therapeutic GCs in TNF-LysM animals in a similar fashion as seen in TNF-tg mice, despite lacking myeloid derived 11β-HSD1.

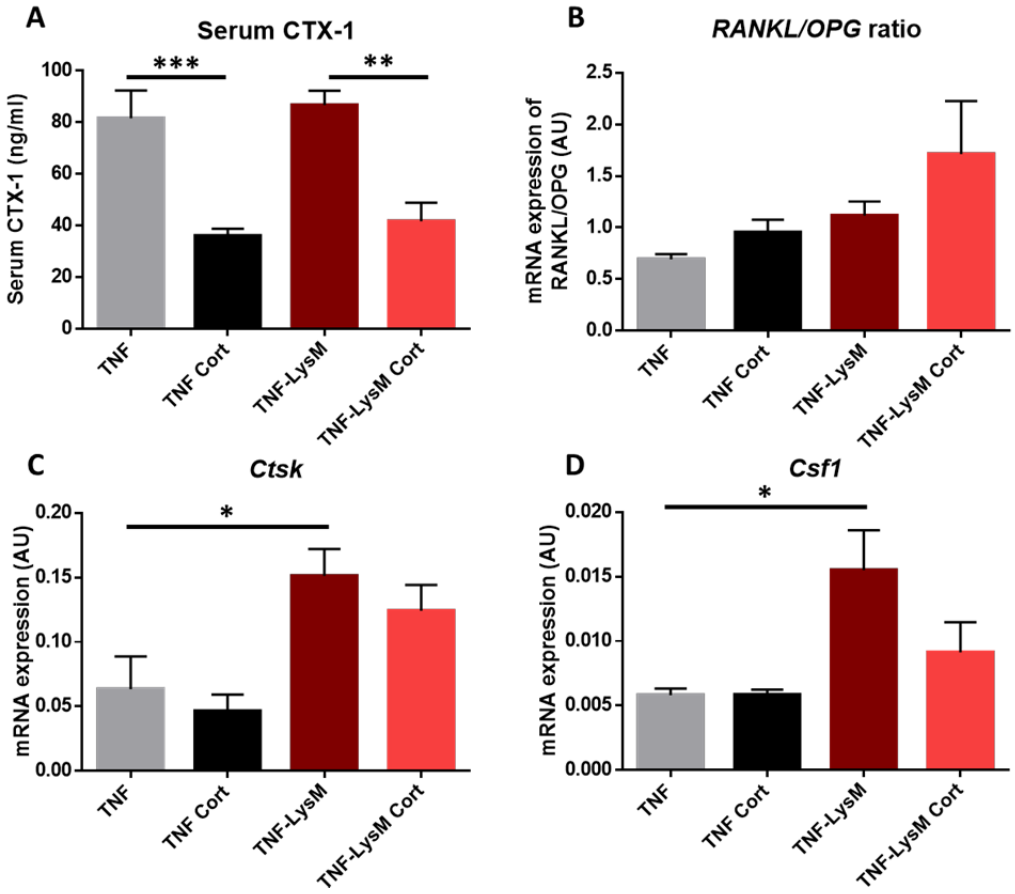

Figure 6. 9: Osteoclast markers in TNF-tg and TNF-LysM animals receiving GCs

(A) ELISA analysis of serum CTX-1 (ng/ml) and qPCR analysis of gene expression (AU) of (B) the Rankl/Opg ratio, (C) *Ctsk* and (D) *Csf1* in tibias of TNF-tg (n=6) and TNF-LysM (n=5) animals receiving control or 100 mg/L corticosterone TNF-tg (n=6) and TNF-LysM (n=5) drinking water for three weeks (n=6 per group). Data is presented as mean ± SEM and statistical significance was determined using two-way ANOVA with Tukey's multiple comparisons test (* denotes P≤0.05, ** denotes P≤0.01 and *** denotes P≤0.001).

6.5 Discussion

Elevated levels of pro-inflammatory cytokines during chronic inflammatory polyarthritis lead to juxta-articular problems, such as bone and cartilage loss, in addition to systemic complications such as inflammatory osteoporosis (285). Therapeutic GCs are often used to treat chronic inflammatory disease due to their potent anti-inflammatory actions. Despite the fact that GCs are often associated with generalised bone loss themselves we have previously shown that GCs have an overall beneficial effect on the bone when administered during chronic inflammation by suppressing pro-inflammatory cytokines and subsequently inhibiting the development of juxta-articular and systemic bone loss driven by osteoclastic bone resorption (Chapter 3) (21). Additionally, the results of Chapter 5 indicate that suppression of inflammation by GCs is mediated via activation by 11β-HSD1. Thus, this chapter aimed to investigate whether the beneficial actions of therapeutic GCs on the bone during chronic inflammation were dependent on reactivation by 11β-HSD1. Consequently, TNF-tg animals were crossed with global, mesenchymal and myeloid specific 11β-HSD1 KO mice, treated with 100 mg/L corticosterone in the drinking water for three weeks before serum was isolated for ELISA analysis of bone remodelling markers and tibias were excised for micro-CT analysis and gene expression assays.

Micro-CT analysis of tibias from TNF11βKO animals revealed that the protective effect of GCs observed in TNF-tg animals, in terms of increased bone volume, trabecular number and decreased trabecular separation, was blunted in TNF11βKO mice, suggesting a significant role for 11β-HSD1 activation of GCs in their beneficial effects on the bone. Some degree of protection was still observed in TNF11βKO animals however, suggesting a partial role of systemic levels of active drug in protecting the bone from inflammatory bone loss (Fig 6.1). This lack of protection by GCs on the bone in global KO mice was in

spite of the fact that osteoblast markers such as P1NP and osteocalcin were protected from the GC-induced suppressions seen in TNF-tg mice, indicating that osteoblasts are not driving the increased systemic bone in response to GCs (Fig 6.2). Instead, this phenotype appeared to be mediated through a loss of suppression of inflammatory osteoclast bone resorption, where CTX-1 failed to be suppressed in TNF11βKO mice receiving corticosterone. This may be secondary to a failure of therapeutic GCs to suppress pro-inflammatory cytokines in response to GCs such as mTNF and IL-6 and osteoclast precursor chemokines such as CCL2, CXCL2 and CXCL10 (Chapter 5). The RANKL/OPG ratio was comparable between the different genotypes, suggesting that this mRNA marker may not be fully informative in regard to interpreting osteoclast metabolism in this setting. However, TNFα has previously been shown to induce osteoclast differentiation independently of RANKL expression, thus persistently elevated levels of TNFα may drive the diminished response to GCs on the bone (304-306). Overall, therapeutic GCs appear to mediate their beneficial effects on the bone during chronic inflammation via suppression of inflammatory cytokines and subsequent reduction in osteoclast differentiation secondary to the activation of GCs by 11β-HSD1.

Mesenchymal derived osteoblasts have been shown to potently upregulate 11β-HSD1 in response to pro-inflammatory cytokines, indicating a potential role for osteoblasts in modulating inflammation (154). In this study, the mesenchymal specific 11β-HSD1 KO mouse was used to determine the contribution of mesenchymal cell populations to the protective effect of GCs on the bone. Micro-CT analysis of the tibias of TNF-Twist2 mice showed that whilst GCs induced an increase in bone volume and decrease in trabecular separation similar to that of TNF-tg animals receiving oral corticosterone, this appeared to be due to an overall increase in trabecular thickness in the TNF-Twist2 groups, with

only modest increases observed in trabecular number in response to GCs (Fig 6.4). Thus, mesenchymal 11β-HSD1 may play a role in the beneficial effects of GCs on trabecular number during chronic inflammation.

In mice lacking 11β-HSD1 in the mesenchyme, GC treatment retained its ability to potently reduce the anabolic osteoblast markers P1NP and osteocalcin. Conflicting results were obtained upon analysis of the wnt inhibitors sclerostin (*Sost*) and *Dkk1*, with sclerostin levels being protected from GC-induced increases in TNF-Twist2 mice, whilst *Dkk1* levels were significantly higher in GC treated TNF-Twist2 mice compared to GC treated TNF-tg animals (Fig 6.5). IL-6 has previously been shown to inhibit wnt signalling in osteoblasts, thus the increased levels of *Dkk1* in corticosterone treated TNF-Twist2 animals compared to corticosterone treated TNF-tg mice could be due to the persistently elevated levels of serum IL-6 observed in the TNF-Twist2 GC treated group (Fig 5.11) (344). A separate study has reported that deletion of Dkk1 increased bone volume and formation in mice despite an increase in sclerostin expression levels, potentially indicating that sclerostin is not an ideal marker for bone formation (345). Future research could examine any changes in wnt ligands to better understand if these anabolic pro-osteoblastic factors are impacted.

The osteoclast activity marker, cathepsin K (*Ctsk*), and the osteoclast differentiation factor, M-CSF (*Csf1*), were reduced in both untreated and corticosterone treated TNF-Twist2 animals compared to untreated and corticosterone treated TNF-tg mice, indicating a baseline reduction in osteoclast activity in mice lacking mesenchymal derived 11β-HSD1. Previously, we have found that at 9 weeks TNF-Twist2 mice have significantly less disease activity and inflammation compared to TNF-tg mice (157). Although, at seven weeks no changes in mRNA levels of pro-inflammatory cytokines or inflammatory scores

were recorded between TNF-Twist2 and TNF-tg animals, subtle decreases could already exist in protein levels of pro-inflammatory cytokines at this time point in TNF-Twist2 animals which could reduce the inflammatory induced differentiation of osteoclasts. Decreases in osteoclast markers could also explain the increased trabecular thickness of TNF-Twist2 animals (Fig 6.4). Serum levels of CTX-1 were not measured in the TNF-Twist2 animals thus a suppression of osteoclast activity cannot be confirmed, however a potential reduction of resorption is likely, due to the GC induced suppression of pro-inflammatory cytokines observed in the TNF-Twist2 mouse (Fig 5.11). Further analysis is necessary to confirm this. Overall, mesenchymal 11β-HSD1 KO mice exhibit a partial protection from inflammatory bone loss in response to GC treatment.

The other key cell type in the bone is the myeloid derived osteoclast, however a lot less is known about 11β-HSD1 in this cell type. 11β-HSD1 is expressed in osteoclasts, however it is unknown how this expression is regulated in response to pro-inflammatory cytokines (71). Therefore, to investigate the contribution of 11β-HSD1 within myeloid cell populations to the protective effects of therapeutic GCs on inflammatory bone loss, a myeloid specific 11β-HSD1 KO mouse was crossed with the TNF-tg and treated with corticosterone in the drinking water for three weeks. Micro-CT analysis of tibias showed that whilst TNF-tg animals responded to GC treatment with increased bone volume and trabecular number, TNF-LysM animals exhibited no changes between the GC treated and untreated groups (Fig 6.7). These data suggest that GC activation by 11β-HSD1 within myeloid derived cell populations may mediate some of the protective effects of GCs through the suppression of inflammatory bone resorption. However, this was not supported by CTX-1 data which was significantly suppressed in response to GC treatment. WT-LysM animals showed significantly lower bone parameters than WT

controls (Chapter 4), suggesting that animals lacking myeloid 11β-HSD1 have a developmental bone phenotype. Therefore, it is also possible that inflammatory bone loss is not significantly induced in these animals due to low bone volume at baseline and thus corticosterone treatment has no effect on the trabecular parameters of this genotype. Static histomorphometry of the bones from these mice could help clarify the effects of corticosterone treatment on osteoclasts in the absence of myeloid 11β-HSD1. Additionally, further characterisation of this model is required to confirm cre penetrance to the osteoclasts.

Previously, myeloid specific GR KO mice were found to be protected from suppression of bone formation by dexamethasone treatment, indicating that osteoclasts are necessary to mediate GC-induced changes in bone formation (243). However, in the current study, significant decreases were still observed in the osteoblast markers P1NP, osteocalcin (*Bglap*) and alkaline phosphatase (*Alpl*) in TNF-LysM animals in response to corticosterone treatment (Fig 6.8). Since corticosterone treated TNF-LysM animals had significantly increased arthritic paw scores compared to corticosterone treated TNF-tg mice (Fig 5.20), the lack of a beneficial response to GCs on the bone may be due to residual inflammation and a longer duration of treatment or higher dose may be required to overcome this. Untreated TNF-LysM animals had significantly higher levels of the osteoblast markers osteocalcin, alkaline phosphatase and runx2 than TNF-tg controls (Fig 6.8), however the osteoclast markers cathepsin K (*Ctsk*) and M-CSF (*Csf1*) were similarly elevated in TNF-LysM animals compared to TNF-tg (Fig 6.9) suggesting that the overall balance between formation and resorption remains unchanged.

Overall, these data suggest that 11β-HSD1 is required to mediate the protective effect of GCs on the bone during chronic inflammation, due to the ability of 11β-HSD1 metabolised

GCs to suppress pro-inflammatory mediators and thus suppress osteoclast activation. Both the mesenchymal and the myeloid cell specific 11β-HSD1 KO mice fail to effectively replicate the resistance to the anti-inflammatory actions of GCs observed in the TNF11βKO animals (Chapter 5), thus with only partial suppression of their anti-inflammatory actions, GCs retain the capacity to prevent bone loss in the cell specific 11β-HSD1 KO animals.

Chapter 7: General discussion

Rheumatoid arthritis is a chronic inflammatory disease affecting around 1% of the adult population characterised by systemic inflammation, polyarthritis, joint deformity and increased mortality (81, 83). Glucocorticoids potently suppress disease activity and inflammation associated with RA and as a consequence of their anti-inflammatory and immunomodulatory effects are frequently used in disease management (159). Unfortunately, long term use of GCs results in adverse metabolic side effects such as osteoporosis, muscle wasting, hypertension, diabetes and obesity, severely limiting their application (22). Consequently, understanding the precise mechanisms of actions of GCs in order to delineate the beneficial anti-inflammatory actions from the detrimental metabolic side effects of therapeutic GC use remains paramount. The overarching aim of this thesis was to gain a better understanding of how pre-receptor metabolism of therapeutic GCs mediate both their positive and negative effects.

Glucocorticoid induced osteoporosis represents a severe side effect of therapeutic GCs in many patients. Consequently, the net effect of GCs on the bone during chronic inflammation was investigated using the TNF-tg mouse on a three week corticosterone drinking water treatment regime to fully characterise GC induced bone loss in this setting and to inform our experimental design for examining pre-receptor metabolism. At high doses, GCs inhibit differentiation and promote apoptosis of the bone forming osteoblasts (235, 287, 288). However, GCs suppress inflammation which, if left untreated, can induce osteoclast differentiation and inhibit osteoblast differentiation, ultimately promoting inflammatory bone loss (252-255, 260). Thus, we wished to understand whether the beneficial anti-inflammatory effects of GCs on the bone outweigh their negative anti-anabolic actions. Here, we demonstrate that oral GC monotherapy protected against the development of both juxta-articular and systemic inflammatory bone loss when

administered early in chronic inflammatory diseases. This coincided with a reduction in pro-inflammatory pro-osteoclastogenic cytokines such as TNFα, IL-6 and IL-1, which have previously been shown to stimulate osteoclast differentiation (256). TNFα in particular is implicated as a potent regulator of osteoclasts, with the ability to induce osteoclastogenesis independently of RANKL signalling, which may explain why the RANKL/OPG ratio is elevated in TNF-tg animals receiving oral corticosterone, despite substantial reductions in osteoclast numbers and activity (304-306). Additionally, TNFα can trigger the release of osteoclast precursors from the spleen into the circulation, where they can then travel to sites of inflammation where pro-inflammatory cytokines trigger their differentiation into mature bone resorbing osteoclasts (332). The monocyte chemoattractant CCL2, produced by cells such as macrophages, fibroblasts and osteoblasts, has been suggested as the chemokine responsible for recruitment of osteoclast precursors to sites of inflammation, and can promote osteoclast fusion and differentiation (333, 334). Thus, in the TNF-tg mouse treated with GCs, the downregulation of factors such as TNFα and CCL2 could simultaneously prevent the release and migration of osteoclast precursors, whilst a local suppression of pro-inflammatory mediators could inhibit their differentiation, subsequently suppressing bone resorption. Future research could cross the TNF-tg mouse with RANKL or OPG KO models in order to determine if the effects of GCs are completely mediated by TNFα or if the RANKL/OPG ratio is contributing in some way. Furthermore, mRNA levels do not always correlate with protein levels, thus analysis of RANKL and OPG protein levels by western blot or ELISA assays would prove useful in this model (346).

In support of our study, several clinical studies investigating GC therapy in RA patients have found no increased risk of osteoporosis compared to other disease controlling

therapies and even an increase in BMD in patients receiving GC and anti-TNF combination therapies as opposed to anti-TNF alone (289-291). However, these findings are not unanimous with further studies showing that GC therapy is associated with decreased BMD in RA (285, 294). The difference in conclusion from these studies may be due to differences in the treatment regime implemented, specifically dose and duration of treatment. Our study models the use of GCs as a bridging therapy to control inflammation before slow-acting DMARDS take effect at the onset of disease (109). Here, we show markers of osteoblast activity, P1NP, osteocalcin and alkaline phosphatase, were suppressed upon treatment with GCs, however no decrease in bone parameters was observed in the WT group treated with GCs, indicating that 100 mg/L corticosterone in the drinking water for three weeks is sufficient to induce early changes in bone metabolism but not phenotypic changes. In Chapter 4, we show that WT mice treated with 100 mg/L corticosterone for four weeks have significant decreases in bone parameters as determined by micro-CT. Timing is likely paramount, therefore it would be interesting to investigate a longer treatment period in the TNF-tg animals. It is likely that over longer durations bone loss would occur secondary to reduced formation, whilst with shorter timeframes GCs support increased BMD due to suppressed osteoclast activity. Thus, we predict that long-term use of GCs is limited in this setting, but GCs are beneficial as a bridging therapy since bone formation is rapidly recovered following cessation of therapy (21).

Previous work from our group investigated the interaction between GCs and inflammation in the muscles of these mice and concluded that therapeutic GCs do not protect against inflammatory muscle wasting and drive GC induced muscle atrophy (309). The catabolic effect of GCs on the bone is often focused on when administering therapeutic GCs and

bone sparing agents such as bisphosphonates are often given alongside GC treatment (19, 310). However, our data suggest that in the setting of new onset disease, when GCs are given as a bridging therapy, priority should be given to the development of muscle sparing therapies in addition to bone sparing.

Despite their efficacy in suppressing inflammation, the use of long term GCs is limited due to the prevalence of metabolic side effects. Osteoporosis is of particular concern, with an approximate 10% decrease in BMD in patients receiving GCs and a dramatic increase in fracture risk within the first 3 to 6 months of starting GC treatment (21). In approximately 30-50% of patients on GC therapy changes in bone metabolism lead to osteoporotic fractures (347). The enzyme 11β-HSD1, which predominantly converts inactive GCs to their active counterparts, has been heavily implicated in the development of many of the metabolic side effects associated with GC use. Morgan *et al* demonstrated that mice lacking 11β-HSD1 were protected from the development of Cushingoid features in response to GC excess, such as myopathy, hepatic steatosis, glucose intolerance and increased adiposity (348). However, the bone phenotype of these mice was not examined, despite GIO being a significant issue associated with GC therapy.

Here, we identified that 11β-HSD1 metabolism of exogenous GCs plays a major role in the development of GIO. After four weeks of corticosterone in the drinking water, WT animals developed significant reductions in tibial bone parameters, such as bone volume, trabecular thickness, trabecular number, and an increase in trabecular separation. In contrast, 11β-HSD1 KO animals were protected from changes in bone volume, trabecular number and trabecular separation. This appeared to be predominantly mediated by a protection of mature osteoblasts and their bone forming activity. This may be explained by the higher expression of 11β-HSD1 in osteoblasts compared to osteoclasts, rendering

the osteoblasts more susceptible to GC effects (71). GCs have been shown to act directly on osteoblasts to trigger their apoptosis (237). Further analysis of this model could utilise apoptotic analysis, such as TUNEL staining, to confirm whether 11β-HSD1 KO animals are protected from GIO via inhibition of osteoblast apoptosis. Vertebral fractures are particularly common in patient receiving GC therapy, with the risk of fracture reaching over double that of age matched controls (314). Modest changes in spine architecture were observed in WT animals treated with three week corticosterone in the drinking water, which were not observed in 11βKO GC treated animals. Again, this appeared to be mediated by protection of osteoblast numbers at the spine. A previous study indicated that C57BL/6 mice were resistant to the bone loss associated with administration of GC by subcutaneously implanted slow release pellets (349). However, we observed significant bone loss in C57BL/6 mice after four weeks of corticosterone drinking water. This may be due to greater dosing and exposure in the oral delivery method compared to the subcutaneously implanted GC pellets.

Overall, these data suggest that 11β-HSD1 plays a role in the inhibition of osteoblast activity in response to GCs. Previous studies have differed when attempting to determine which cells specifically mediate the bone destructive effects of GCs. One study showed that disruption of GC signalling in mature osteoblasts and osteocytes prevented their apoptosis and resulted in mice being resistant to the decreases in osteoid area, bone formation rate and compression strength observed in WT animals receiving prednisolone (237). In contrast, studies using 11β-HSD2 overexpression to disrupt GC signalling specifically in osteoclasts, showed that osteoblast apoptosis and reductions in bone formation still occurred in response to GC treatment, revealing that GC action in osteoclasts was not mediating changes in osteoblasts in response to GCs (238).

Conversely, another study using mice lacking the GR in osteoclasts showed that these mice were protected from decreases in bone formation induced by dexamethasone treatment, indicating that anti-anabolic actions of GCs can act indirectly on the osteoblast via the osteoclast (243). Our study used a mesenchymal and myeloid specific 11β-HSD1 KO mouse in an attempt to delineate in which cell type GC activation by 11β-HSD1 was responsible for mediating GIO. However, both genotypes responded to GCs in terms of potent suppression of bone formation and mature osteoblast markers, indicating that 11β-HSD1 activation of GCs is not required in either the osteoblasts or the osteoclasts. This may be due to a similar mechanism as determined in Chapter 5, where our study demonstrated that paracrine GC signalling could overcome deletion in cell specific cre models. The use of co-culture and conditioned media experiments, as outlined with the FLS and macrophage cells, could be performed using WT and KO osteoblasts and osteoclasts to determine if they can also participate in paracrine signalling of GCs to compensate for loss of 11β-HSD1 in one cell type.

Since 11β-HSD1 metabolism has been shown to play a major role in many of the metabolic side effects of GC use, 11β-HSD1 inhibitors have been suggested as an adjunctive therapy given alongside GCs in order to reduce their side effects (348). However, in order for this approach to be feasible, GC activation by 11β-HSD1 metabolism must mediate the detrimental actions of therapeutic GCs, but not the beneficial therapeutic effects of GCs. This is particularly relevant where the most widely prescribed GC in the US, prednisone, is readily metabolised and activated by 11β-HSD1 (19, 118). Consequently, we wished to determine whether the therapeutic anti-inflammatory actions of GCs depend on their activation by 11β-HSD1. Using the TNF-tg murine model of polyarthritis on a global 11β-HSD1 KO background we identified that the

anti-inflammatory effects of GCs in chronic inflammatory polyarthritis are dependent on 11β-HSD1 activation. TNF-tg mice lacking 11β-HSD1 were unable to suppress clinical and arthritic paw scores in response to GC treatment. Additionally, despite GC treatment, mRNA levels of pro-inflammatory cytokines and chemokines and serum levels of IL-6 remained elevated in TNF11βKO mice, leading to the persistence of synovitis and osteoclast numbers, inhibiting the protective effect of GCs on juxta-articular bone erosions. Ideally, analysis of pro-inflammatory cytokines and chemokines would be performed by serum ELISA to quantify protein concentrations, however due to the limited amount of serum obtained from each mouse, mRNA analysis was used as a surrogate. Alternatively, ELISA analysis of synovial fluid of synovial tissue homogenate could be used to gain a more accurate representation of local inflammation at the joint.

Similarly, TNF11βKO animals do not show the same protective effects of GCs on systemic trabecular parameters at the tibia, despite being protected from GC induced reductions in osteoblast markers. Together, these findings reinforce the idea that osteoclasts are the more important cell type in inflammatory bone loss. Thus, mice deficient in 11β-HSD1 are resistant to the therapeutic effects of GCs. Consistent with this, 11β-HSD1 has previously been shown to be required for the immunosuppressive effects of endogenous GCs, as mice lacking 11β-HSD1 have significantly exacerbated inflammation and worsened resolution (157, 324). Previously, we have shown that the exacerbation of inflammation in TNF-tg mice lacking 11β-HSD1 is due to the inability of macrophages to polarise towards the M2 pro-resolution phenotype (157). It would therefore be interesting to investigate whether this is the case in response to exogenous GCs and thus whether the persistence of inflammation upon treatment with therapeutic GCs in the TNF11βKO mouse results from the failure of macrophages to polarise towards

the M2 phenotype in the absence of 11β-HSD1 activation of GCs. Flow cytometry analysis of cells stained for M1 or M2 markers (such as CD68 and MHCII, and CD163, respectively) from synovial tissue digests of KO and control mice treated with vehicle or corticosterone could be performed to address this. Alternatively, histological staining for M1 and M2 markers could be performed on sections of the synovium from these animals in order to assess the proportion of M1 or M2 macrophages in response to GC treatment.

Several studies have focused on delineating the exact cell type responsible for the therapeutic effects of GCs with varying results. In a mouse model of chronic hypersensitivity, macrophages were pinpointed as the mediators of the anti-inflammatory effects, whilst in inflammatory arthritis stromal cells have been implicated in STIA model, and T cells in the AIA model (129, 138, 350). This variation in different mouse models indicates the need to validate our findings in alternative models. The CIA model would be of particular interest due to the involvement of the adaptive immune system and the production of auto-antibodies, which could provide a more representative image of rheumatoid arthritis on which to investigate the contribution of 11β-HSD1 metabolism of therapeutic and endogenous GCs (267).

The mesenchymal specific 11β-HSD1 KO mouse responded to GCs similarly to normal TNF-tg animals, by reducing disease activity, pro-inflammatory cytokines and chemokines, synovitis and osteoclast numbers. TNF-Twist2 animals also showed increased bone volume in response to GC treatment, however this appeared to be mainly due to an overall increase in trabecular thickness more so than the increases in trabecular number. Additionally, TNF-Twist2 animals exhibited some modest decreases in basal levels of pro-inflammatory chemokines and bone erosions, consistent with the decreased inflammation previously noted in this mouse aged 9 weeks (157). The myeloid specific

11β-HSD1 KO animal presented with some signs of GC resistance in terms of persistent bone erosions and elevated clinical and arthritic paw scores, however these mice still retained the ability to respond to GCs by reducing pro-inflammatory mediators, synovitis and osteoclast number. This indicates that myeloid derived 11β-HSD1 activation of GCs is at least partially required for their therapeutic actions. LysM animals also appeared to be resistant to corticosterone induced improvements in systemic trabecular bone parameters. However, a developmental bone phenotype in mice lacking myeloid 11β-HSD1 cannot be entirely ruled out, as WT-LysM animals exhibited significantly less trabecular bone than WT mice in the absence of inflammation. Inducible cre deletion models could be utilised to examine whether myeloid 11β-HSD1 mediates the protective effects of GCs on systemic bone without the added complication of a developmental phenotype.

Further assessment of LysM cre penetrance is required to fully interpret these findings. Here, a failure to mediate 100% deletion in macrophages may result in residual responsiveness to GCs that could account for the partial suppression of disease activity and bone loss observed in the TNF-LysM animals. Our preliminary findings in peritoneal macrophages suggested 11β-HSD1 deletion was significant (approximately 85%) but not complete. Published studies indicate in vivo deletion at around 70% in macrophages (129). Therefore, the retention of 11β-HSD1 activity in a small proportion of the macrophages may be sufficient to produce the anti-inflammatory effects of GCs. Further research could be done to examine the efficacy of the cre targeting in greater detail. Crossing the LysM animals with cre-reporter mice such as LacZ or GFP expressing mice, which undergo a colour change or produce a fluorescent signal in cells with cre activity, would allow identification of cre expression in a broader range of myeloid cell populations.

Of particular interest due to the persistence of bone erosions in the LysM animals, would be determining whether 11β-HSD1 is deleted within the osteoclasts.

Given that both cre models retained some GC responsiveness, we wished to test the hypothesis that paracrine signalling may compensate for cell specific knockout of 11β-HSD1. It was determined that GC activation by 11β-HSD1 in fibroblasts can compensate for 11β-HSD1 deletion in neighbouring macrophages in a paracrine fashion, and vice versa. Whether this is a mechanism isolated to stromal and myeloid cells is unknown. Paracrine signalling of 11β-HSD1 metabolised GCs between fibroblasts and macrophages could promote the polarisation of macrophages towards the M2 phenotype, thus stimulating the production of anti-inflammatory cytokines, such as IL-10, and reducing the production of pro-inflammatory cytokines, such as TNFα, subsequently suppressing the activation and differentiation of pro-inflammatory T and B cells. This would make effective deletion of GC signalling in macrophages using a targeted cre ineffective, with neighbouring stromal populations compensating through local amplification and paracrine GC signalling. One of the limitations of the TNF-tg mouse model is the lack of involvement of the adaptive immune system, thus the use of an alternative model, such as the CIA model, would allow the assessment of whether cells such as T and B cells are also affected by this compensatory paracrine GC signalling.

Complete disruption of GC signalling in specific cells is likely to be necessary to determine which cell types mediate the anti-inflammatory effects of GCs. The utilisation of a macrophage specific GR KO TNF-tg mice would help establish whether GC signalling within the macrophage mediates the therapeutic effects of GCs in this model and investigate the partial GC resistance phenotype in the LysM animals without the complication of paracrine signalling.

11β-HSD1 metabolism can determine both the systemic levels of GCs, by hepatic reactivation of GCs following renal inactivation by 11β-HSD2, and also the local tissue levels of GCs, by tissue specific expression of 11β-HSD1 (76). It is possible that the GC resistance of 11β-HSD1 KO animals is due to the inactivation of GCs by renal 11β-HSD2 and an inability of hepatic type 1 enzymes to reactivate GCs, thus altering the systemic levels of GCs available. However, we show that 11β-HSD1 KO animals exhibit adrenal atrophy and increased systemic corticosterone concentrations in response to GC treatment, which would indicate that systemic metabolism is unaltered and effects are mediated by local metabolism of GCs. However, we have shown by administering corticosterone via oral gavage that GCs are rapidly excreted from the body, and we cannot control for when the mice last intake corticosterone drinking water prior to cardiac puncture, which introduces significant variability. Thus, further analysis could use oral gavage of corticosterone to produce less variable results. Furthermore, the use of LC-MS analysis to determine the levels of the inactive GC 11-DHC in the serum of corticosterone treated KO animals is required to provide a more detailed kinetics analysis of whether systemic metabolism is affected. It is also possible that the deletion of 11β-HSD1 may have indirect effects on other endocrine systems, such as impacting on the level of androgen and mineralocorticoid production, in addition to the direct effects on glucocorticoid metabolism. Thus, further LC-MS analysis of the levels of different steroid classes could prove to be important in this model.

In summary, we have identified a novel step in mediating the action of therapeutic GCs via 11β-HSD1 activation. This mechanism is likely to apply to GCs such as prednisone which is frequently used in the treatment of chronic inflammatory diseases, whilst dexamethasone is not readily metabolised by 11β-HSD1 and thus is unlikely to be

affected in the same way by 11β-HSD1 inhibition (67). We provide further knowledge of the mechanism of GC actions in showing that neighbouring cells can exchange locally generated active GCs in a paracrine manner, which will prove important when attempting to selectively target cell types to harness the beneficial effects of GCs whilst avoiding their detrimental effects.

7.1 Future directions

We have shown that whilst inhibition of 11β-HSD1 was beneficial to prevent glucocorticoid-induced osteoporosis, it also resulted in detrimental effects such as the exacerbation of inflammatory arthritis and resistance to the anti-inflammatory GC actions in the TNF-tg model. These data raise concern over the use of 11β-HSD1 inhibitors to prevent the development of metabolic side effects in patients with chronic inflammation. However, some anti-inflammatory actions of GCs are retained in the TNF11β-HSD1 KO mouse, for example, mild decreases in serum IL-6, as well as decreases in B cell and CD8+ T cell populations (unpublished data from Hardy lab). Therefore, understanding whether these results translate to other inflammatory diseases where GCs are widely prescribed will be a key step in the progression of this research, therefore the 11β-HSD1 KO mouse could be crossed with mouse models of diseases such as inflammatory bowel disease (IBD) and chronic obstructive pulmonary disease (COPD), for the examination of GC resistance in these settings.

Myeloid specific 11β-HSD1 KO animals showed some evidence of reduced responses to therapeutic GCs, thus future experiments could attempt to directly target GC preparations to the juxta-articular macrophages, for example, with the use of liposomes. We have

demonstrated that cells can communicate GCs in a paracrine fashion, thus experiments would also need to focus on the most efficient dose and delivery of GCs in these preparations to avoid saturation of the GR in macrophages and the subsequent leakage of GCs into the surrounding cells.

7.2 Limitations

One potential limitation of the study is with the use of male mice. Male animals were chosen to reduce potential changes in metabolism or the immune response based on the different stages of the estrous cycle, however, as previously stated, rheumatoid arthritis is a disease which predominantly effects women, thus the use of female mice would be more representative of human patients. Additionally, the mouse model used is not fully representative of human RA due to the lack of involvement of the adaptive immune system. As a result of this, the study would benefit from the use of a secondary RA model in which the adaptive response plays a larger role. Moreover, the sample size was limited in some cases thus increasing the number of mice per group would improve the study.

Another limitation with regards to the mice, is the use of young mice (seven-week old) for the study of GIO and changes in bone remodelling. At this age, bone is not yet fully formed and thus may be more susceptible to alterations by inflammatory mediators or GC treatment. Additionally, in human RA and osteoporosis are typically observed in the adult population. Therefore, the use of mature animals with fully developed bone would strengthen the findings of this study.

The use of a three week corticosterone treatment period was insufficient to induce macroscopic changes in the bone phenotype of WT animals, thus a longer duration of

treatment would maximise the impact of the results in the GIO study. In addition, with the use of the drinking water method of GC administration it was not possible to accurately determine the dose of corticosterone ingested by each individual animal, therefore variations in dose are a possibility.

Supplementary

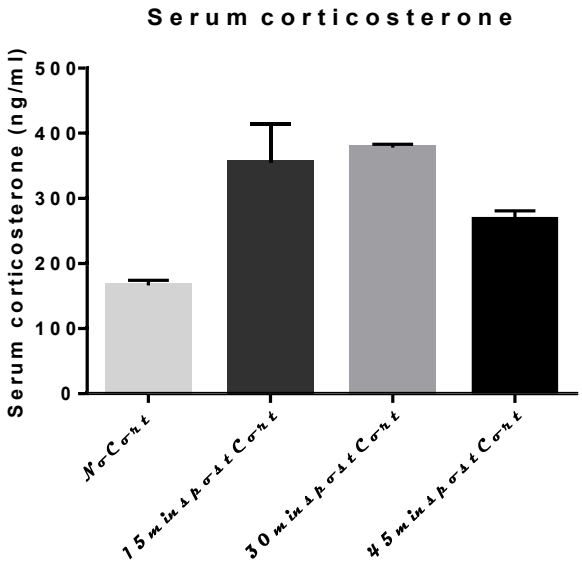

Supplementary Figure 1: Serum levels of corticosterone following oral gavage

Serum levels of corticosterone (ng/ml) in TNF-tg animals (n=1 per group) 15, 30 or 45 minutes following oral gavage with 200 mg/L corticosterone drinking water. Data is presented as mean ± SEM and statistical significance was determined using one-way ANOVA with Tukey's multiple comparisons test (* denotes P≤0.05).

Supplementary Table 1: Taqman primers used for real time PCR analysis

Primer	Assay ID
Tsc22d3 (Gilz)	Mm00726417_s1
mTnf	Mm00443258_m1
hTNF	Hs00174128_m1
Il1	Mm00434228_m1
Ccl2	Mm00441242_m1
Cxcl10	Mm00445235_m1
Cxcl2	Mm00436450_m1
Bglap	Mm03413826_mH
Alpl	Mm00475834_m1
Runx2	Mm00501584_m1
Dkk1	Mm00438422_m1
Sost	Mm00470479_m1
Ctsk	Mm00484039_m1
Tnfsf11 (Rankl)	Mm00441906_m1
Tnfrsf1 (Opg)	Mm00435454_m1
Csf1 (M-csf)	Mm00432686_m1

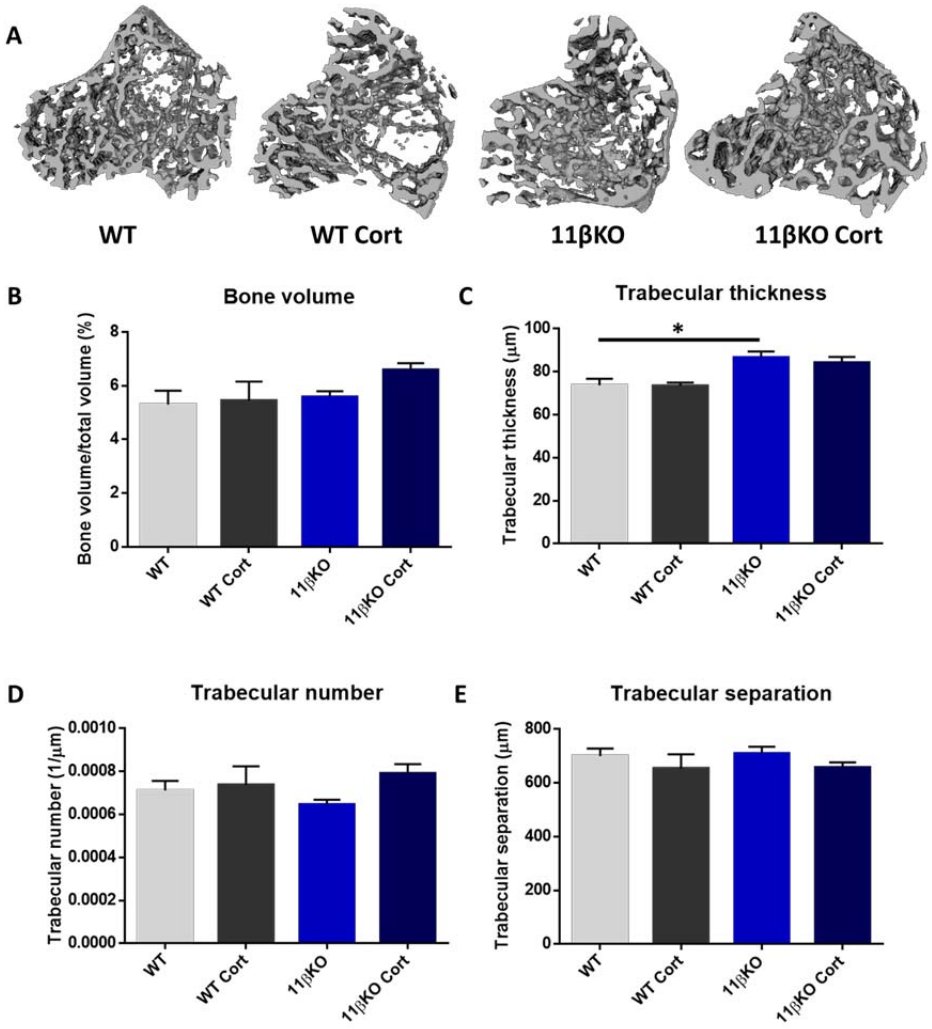

Supplementary Figure 2: Trabecular bone parameters of tibias from WT and 11βKO animals after three weeks corticosterone treatment

(A) Representative images of reconstructed trabecular bone from tibia scans of untreated and three weeks 100 mg/L corticosterone drinking water WT and 11βKO animals. Micro-CT analysis of (B) bone volume (%) relative to total volume, (C) trabecular thickness (µm), (D) trabecular number (1/µm) and trabecular separation (µm) of WT and 11βKO animals with or without 100 mg/L corticosterone treatment for three weeks (WT n=8, WT Cort n=6, 11βKO n=7, 11βKO Cort n=7). Data is presented as mean ± SEM and statistical significance was determined using two-way ANOVA with Tukey's multiple comparisons test (* denotes $P \leq 0.05$)

References

1. Han TS, Walker BR, Arlt W, Ross RJ. Treatment and health outcomes in adults with congenital adrenal hyperplasia. Nature Reviews Endocrinology. 2013;10:115.
2. Webster JM, Fenton CG, Langen R, Hardy RS. Exploring the Interface between Inflammatory and Therapeutic Glucocorticoid Induced Bone and Muscle Loss. Int J Mol Sci. 2019;20(22).
3. Orstavik RE, Haugeberg G, Mowinckel P, Hoiseth A, Uhlig T, Falch JA, et al. Vertebral deformities in rheumatoid arthritis: a comparison with population-based controls. Arch Intern Med. 2004;164(4):420-5.
4. van Staa TP, Geusens P, Bijlsma JW, Leufkens HG, Cooper C. Clinical assessment of the long-term risk of fracture in patients with rheumatoid arthritis. Arthritis Rheum. 2006;54(10):3104-12.
5. Guler-Yuksel M, Bijsterbosch J, Goekoop-Ruiterman YP, de Vries-Bouwstra JK, Hulsmans HM, de Beus WM, et al. Changes in bone mineral density in patients with recent onset, active rheumatoid arthritis. Ann Rheum Dis. 2008;67(6):823-8.
6. Walsmith J, Roubenoff R. Cachexia in rheumatoid arthritis. Int J Cardiol. 2002;85(1):89-99.
7. Calabrese LH, Calabrese C, Kirchner E. The 2015 American College of Rheumatology Guideline for the Treatment of Rheumatoid Arthritis Should Include New Standards for Hepatitis B Screening: Comment on the Article by Singh et al. Arthritis Rheumatol. 2016;68(5):1314-5.
8. Smolen JS, Landewe R, Bijlsma J, Burmester G, Chatzidionysiou K, Dougados M, et al. EULAR recommendations for the management of rheumatoid arthritis with synthetic and biological disease-modifying antirheumatic drugs: 2016 update. Ann Rheum Dis. 2017;76(6):960-77.
9. Sassoon CS, Zhu E, Pham HT, Nelson RS, Fang L, Baker MJ, et al. Acute effects of high-dose methylprednisolone on diaphragm muscle function. Muscle Nerve. 2008;38(3):1161-72.
10. Angeli A, Guglielmi G, Dovio A, Capelli G, de Feo D, Giannini S, et al. High prevalence of asymptomatic vertebral fractures in post-menopausal women receiving chronic glucocorticoid therapy: a cross-sectional outpatient study. Bone. 2006;39(2):253-9.
11. Feldstein AC, Elmer PJ, Nichols GA, Herson M. Practice patterns in patients at risk for glucocorticoid-induced osteoporosis. Osteoporos Int. 2005;16(12):2168-74.
12. Strehl C, Bijlsma JW, de Wit M, Boers M, Caeyers N, Cutolo M, et al. Defining conditions where long-term glucocorticoid treatment has an acceptably low level of harm to facilitate implementation of existing recommendations: viewpoints from an EULAR task force. Ann Rheum Dis. 2016;75(6):952-7.
13. Lofberg E, Gutierrez A, Wernerman J, Anderstam B, Mitch WE, Price SR, et al. Effects of high doses of glucocorticoids on free amino acids, ribosomes and protein turnover in human muscle. Eur J Clin Invest. 2002;32(5):345-53.
14. Schakman O, Gilson H, de Coninck V, Lause P, Verniers J, Havaux X, et al. Insulin-like growth factor-I gene transfer by electroporation prevents skeletal muscle atrophy in glucocorticoid-treated rats. Endocrinology. 2005;146(4):1789-97.
15. Tomas FM, Munro HN, Young VR. Effect of glucocorticoid administration on the rate of muscle protein breakdown in vivo in rats, as measured by urinary excretion of N tau-methylhistidine. Biochem J. 1979;178(1):139-46.
16. Glyn J. The discovery and early use of cortisone. Journal of the Royal Society of Medicine. 1998;91(10):513-7.
17. Barnes PJ, Adcock IM. Glucocorticoid resistance in inflammatory diseases. Lancet. 2009;373(9678):1905-17.
18. van Staa TP, Leufkens HG, Abenhaim L, Begaud B, Zhang B, Cooper C. Use of oral corticosteroids in the United Kingdom. Qjm. 2000;93(2):105-11.
19. Overman RA, Yeh JY, Deal CL. Prevalence of oral glucocorticoid usage in the United States: a general population perspective. Arthritis Care Res (Hoboken). 2013;65(2):294-8.

20. Fardet L, Flahault A, Kettaneh A, Tiev KP, Genereau T, Toledano C, et al. Corticosteroid-induced clinical adverse events: frequency, risk factors and patient's opinion. Br J Dermatol. 2007;157(1):142-8.
21. van Staa TP, Leufkens HG, Cooper C. The epidemiology of corticosteroid-induced osteoporosis: a meta-analysis. Osteoporos Int. 2002;13(10):777-87.
22. Curtis JR, Westfall AO, Allison J, Bijlsma JW, Freeman A, George V, et al. Population-based assessment of adverse events associated with long-term glucocorticoid use. Arthritis Rheum. 2006;55(3):420-6.
23. Exton JH, Miller TB, Harper SC, Park CR. Carbohydrate metabolism in perfused livers of adrenalectomized and steroid-replaced rats. Am J Physiol. 1976;230(1):163-70.
24. Exton JH, Friedmann N, Wong EH, Brineaux JP, Corbin JD, Park CR. Interaction of glucocorticoids with glucagon and epinephrine in the control of gluconeogenesis and glycogenolysis in liver and of lipolysis in adipose tissue. J Biol Chem. 1972;247(11):3579-88.
25. Bloom SR, Edwards AV, Hardy RN, Malinowska KW, Silver M. Endocrine responses to insulin hypoglycaemia in the young calf. J Physiol. 1975;244(3):783-803.
26. Cole TJ, Blendy JA, Monaghan AP, Krieglstein K, Schmid W, Aguzzi A, et al. Targeted disruption of the glucocorticoid receptor gene blocks adrenergic chromaffin cell development and severely retards lung maturation. Genes Dev. 1995;9(13):1608-21.
27. Crowley PA. Antenatal corticosteroid therapy: a meta-analysis of the randomized trials, 1972 to 1994. Am J Obstet Gynecol. 1995;173(1):322-35.
28. McDevitt TM, Gonzales LW, Savani RC, Ballard PL. Role of endogenous TGF-beta in glucocorticoid-induced lung type II cell differentiation. Am J Physiol Lung Cell Mol Physiol. 2007;292(1):L249-57.
29. Rog-Zielinska EA, Thomson A, Kenyon CJ, Brownstein DG, Moran CM, Szumska D, et al. Glucocorticoid receptor is required for foetal heart maturation. Human Molecular Genetics. 2013;22(16):3269-82.
30. Wust S, van den Brandt J, Tischner D, Kleiman A, Tuckermann JP, Gold R, et al. Peripheral T cells are the therapeutic targets of glucocorticoids in experimental autoimmune encephalomyelitis. J Immunol. 2008;180(12):8434-43.
31. Tu J, Stoner S, Fromm PD, Wang T, Chen D, Tuckermann J, et al. Endogenous glucocorticoid signaling in chondrocytes attenuates joint inflammation and damage. Faseb j. 2018;32(1):478-87.
32. Kizaki T, Ookawara T, Oh-Ishi S, Itoh Y, Iwabuchi K, Onoe K, et al. An increase in basal glucocorticoid concentration with age induces suppressor macrophages with high-density Fc gamma RII/III. Immunology. 1998;93(3):409-14.
33. Vale W, Spiess J, Rivier C, Rivier J. Characterization of a 41-residue ovine hypothalamic peptide that stimulates secretion of corticotropin and beta-endorphin. Science. 1981;213(4514):1394-7.
34. Karalis KP, Venihaki M, Zhao J, van Vlerken LE, Chandras C. NF-kappaB participates in the corticotropin-releasing, hormone-induced regulation of the pituitary proopiomelanocortin gene. J Biol Chem. 2004;279(12):10837-40.
35. Jefcoate C. High-flux mitochondrial cholesterol trafficking, a specialized function of the adrenal cortex. J Clin Invest. 2002;110(7):881-90.
36. Nader N, Chrousos GP, Kino T. Interactions of the circadian CLOCK system and the HPA axis. Trends Endocrinol Metab. 2010;21(5):277-86.
37. Ulrich-Lai YM, Arnhold MM, Engeland WC. Adrenal splanchnic innervation contributes to the diurnal rhythm of plasma corticosterone in rats by modulating adrenal sensitivity to ACTH. Am J Physiol Regul Integr Comp Physiol. 2006;290(4):R1128-35.
38. Berkenbosch F, van Oers J, del Rey A, Tilders F, Besedovsky H. Corticotropin-releasing factor-producing neurons in the rat activated by interleukin-1. Science. 1987;238(4826):524-6.
39. Bernardini R, Kamilaris TC, Calogero AE, Johnson EO, Gomez MT, Gold PW, et al. Interactions between tumor necrosis factor-alpha, hypothalamic corticotropin-releasing hormone, and adrenocorticotropin secretion in the rat. Endocrinology. 1990;126(6):2876-81.

40. Spinedi E, Hadid R, Daneva T, Gaillard RC. Cytokines stimulate the CRH but not the vasopressin neuronal system: evidence for a median eminence site of interleukin-6 action. Neuroendocrinology. 1992;56(1):46-53.
41. Fukata J, Usui T, Naitoh Y, Nakai Y, Imura H. Effects of recombinant human interleukin-1 alpha, -1 beta, 2 and 6 on ACTH synthesis and release in the mouse pituitary tumour cell line AtT-20. J Endocrinol. 1989;122(1):33-9.
42. Brown SL, Smith LR, Blalock JE. Interleukin 1 and interleukin 2 enhance proopiomelanocortin gene expression in pituitary cells. J Immunol. 1987;139(10):3181-3.
43. O'Connell NA, Kumar A, Chatzipanteli K, Mohan A, Agarwal RK, Head C, et al. Interleukin-1 regulates corticosterone secretion from the rat adrenal gland through a catecholamine-dependent and prostaglandin E2-independent mechanism. Endocrinology. 1994;135(1):460-7.
44. Salas MA, Evans SW, Levell MJ, Whicher JT. Interleukin-6 and ACTH act synergistically to stimulate the release of corticosterone from adrenal gland cells. Clin Exp Immunol. 1990;79(3):470-3.
45. Tominaga T, Fukata J, Naito Y, Usui T, Murakami N, Fukushima M, et al. Prostaglandin-dependent in vitro stimulation of adrenocortical steroidogenesis by interleukins. Endocrinology. 1991;128(1):526-31.
46. Evanson NK, Tasker JG, Hill MN, Hillard CJ, Herman JP. Fast feedback inhibition of the HPA axis by glucocorticoids is mediated by endocannabinoid signaling. Endocrinology. 2010;151(10):4811-9.
47. Erkut ZA, Pool C, Swaab DF. Glucocorticoids suppress corticotropin-releasing hormone and vasopressin expression in human hypothalamic neurons. J Clin Endocrinol Metab. 1998;83(6):2066-73.
48. Parvin R, Saito-Hakoda A, Shimada H, Shimizu K, Noro E, Iwasaki Y, et al. Role of NeuroD1 on the negative regulation of Pomc expression by glucocorticoid. PLoS One. 2017;12(4):e0175435.
49. Lewis JG, Bagley CJ, Elder PA, Bachmann AW, Torpy DJ. Plasma free cortisol fraction reflects levels of functioning corticosteroid-binding globulin. Clinica Chimica Acta. 2005;359(1):189-94.
50. HAMMOND GL, SMITH CL, PATERSON NAM, SIBBALD WJ. A Role for Corticosteroid-Binding Globulin in Delivery of Cortisol to Activated Neutrophils*. The Journal of Clinical Endocrinology & Metabolism. 1990;71(1):34-9.
51. Dunn JF, Nisula BC, Rodbard D. Transport of steroid hormones: binding of 21 endogenous steroids to both testosterone-binding globulin and corticosteroid-binding globulin in human plasma. J Clin Endocrinol Metab. 1981;53(1):58-68.
52. Danielian PS, White R, Lees JA, Parker MG. Identification of a conserved region required for hormone dependent transcriptional activation by steroid hormone receptors. Embo j. 1992;11(3):1025-33.
53. Hard T, Kellenbach E, Boelens R, Maler BA, Dahlman K, Freedman LP, et al. Solution structure of the glucocorticoid receptor DNA-binding domain. Science. 1990;249(4965):157-60.
54. Renaud J-P, Rochel N, Ruff M, Vivat V, Chambon P, Gronemeyer H, et al. Crystal structure of the RAR-γ ligand-binding domain bound to all-trans retinoic acid. Nature. 1995;378(6558):681-9.
55. Ding XF, Anderson CM, Ma H, Hong H, Uht RM, Kushner PJ, et al. Nuclear Receptor-Binding Sites of Coactivators Glucocorticoid Receptor Interacting Protein 1 (GRIP1) and Steroid Receptor Coactivator 1 (SRC-1): Multiple Motifs with Different Binding Specificities. Molecular Endocrinology. 1998;12(2):302-13.
56. Chung CC, Shimmin L, Natarajan S, Hanis CL, Boerwinkle E, Hixson JE. Glucocorticoid receptor gene variant in the 3' untranslated region is associated with multiple measures of blood pressure. J Clin Endocrinol Metab. 2009;94(1):268-76.
57. Leung DY, Hamid Q, Vottero A, Szefler SJ, Surs W, Minshall E, et al. Association of glucocorticoid insensitivity with increased expressionof glucocorticoid receptor beta. J Exp Med. 1997;186(9):1567-74.
58. van Steensel B, Jenster G, Damm K, Brinkmann AO, van Driel R. Domains of the human androgen receptor and glucocorticoid receptor involved in binding to the nuclear matrix. J Cell Biochem. 1995;57(3):465-78.
59. Wu B, Li P, Liu Y, Lou Z, Ding Y, Shu C, et al. 3D structure of human FK506-binding protein 52: implications for the assembly of the glucocorticoid receptor/Hsp90/immunophilin heterocomplex. Proc Natl Acad Sci U S A. 2004;101(22):8348-53.

60. Barnes PJ. How corticosteroids control inflammation: Quintiles Prize Lecture 2005. Br J Pharmacol. 2006;148(3):245-54.
61. Govindan MV. Recruitment of cAMP-response element-binding protein and histone deacetylase has opposite effects on glucocorticoid receptor gene transcription. J Biol Chem. 2010;285(7):4489-510.
62. La Noce M, Mele L, Laino L, Iolascon G, Pieretti G, Papaccio G, et al. Cytoplasmic Interactions between the Glucocorticoid Receptor and HDAC2 Regulate Osteocalcin Expression in VPA-Treated MSCs. Cells. 2019;8(3).
63. Surjit M, Ganti KP, Mukherji A, Ye T, Hua G, Metzger D, et al. Widespread negative response elements mediate direct repression by agonist-liganded glucocorticoid receptor. Cell. 2011;145(2):224-41.
64. Ito K, Barnes PJ, Adcock IM. Glucocorticoid receptor recruitment of histone deacetylase 2 inhibits interleukin-1beta-induced histone H4 acetylation on lysines 8 and 12. Mol Cell Biol. 2000;20(18):6891-903.
65. Brem AS, Bina RB, King T, Morris DJ. Bidirectional activity of 11 beta-hydroxysteroid dehydrogenase in vascular smooth muscle cells. Steroids. 1995;60(5):406-10.
66. Lavery GG, Walker EA, Draper N, Jeyasuria P, Marcos J, Shackleton CH, et al. Hexose-6-phosphate dehydrogenase knock-out mice lack 11 beta-hydroxysteroid dehydrogenase type 1-mediated glucocorticoid generation. J Biol Chem. 2006;281(10):6546-51.
67. Homma M, Oka K, Niitsuma T, Itoh H. A novel 11 beta-hydroxysteroid dehydrogenase inhibitor contained in saiboku-to, a herbal remedy for steroid-dependent bronchial asthma. J Pharm Pharmacol. 1994;46(4):305-9.
68. Lakshmi V, Monder C. Evidence for independent 11-oxidase and 11-reductase activities of 11 beta-hydroxysteroid dehydrogenase: enzyme latency, phase transitions, and lipid requirements. Endocrinology. 1985;116(2):552-60.
69. Bocchi B, Fagart J, Cluzeaud F, Fay M, Rafestin-Oblin ME, Farman N. Glucocorticoid metabolism by 11-beta hydroxysteroid dehydrogenase type 2 modulates human mineralocorticoid receptor transactivation activity. J Steroid Biochem Mol Biol. 2003;84(2-3):239-44.
70. Morgan SA, McCabe EL, Gathercole LL, Hassan-Smith ZK, Larner DP, Bujalska IJ, et al. 11beta-HSD1 is the major regulator of the tissue-specific effects of circulating glucocorticoid excess. Proc Natl Acad Sci U S A. 2014;111(24):E2482-91.
71. Cooper MS, Walker EA, Bland R, Fraser WD, Hewison M, Stewart PM. Expression and functional consequences of 11beta-hydroxysteroid dehydrogenase activity in human bone. Bone. 2000;27(3):375-81.
72. Hardy RS, Filer A, Cooper MS, Parsonage G, Raza K, Hardie DL, et al. Differential expression, function and response to inflammatory stimuli of 11beta-hydroxysteroid dehydrogenase type 1 in human fibroblasts: a mechanism for tissue-specific regulation of inflammation. Arthritis Res Ther. 2006;8(4):R108.
73. Agarwal AK, Mune T, Monder C, White PC. NAD(+)-dependent isoform of 11 beta-hydroxysteroid dehydrogenase. Cloning and characterization of cDNA from sheep kidney. J Biol Chem. 1994;269(42):25959-62.
74. Whorwood CB, Ricketts ML, Stewart PM. Epithelial cell localization of type 2 11 beta-hydroxysteroid dehydrogenase in rat and human colon. Endocrinology. 1994;135(6):2533-41.
75. Roland BL, Funder JW. Localization of 11beta-hydroxysteroid dehydrogenase type 2 in rat tissues: in situ studies. Endocrinology. 1996;137(3):1123-8.
76. Hardy RS, Raza K, Cooper MS. Glucocorticoid metabolism in rheumatoid arthritis. Annals of the New York Academy of Sciences. 2014;1318(1):18-26.
77. Nahoum V, Gangloff A, Legrand P, Zhu DW, Cantin L, Zhorov BS, et al. Structure of the human 3alpha-hydroxysteroid dehydrogenase type 3 in complex with testosterone and NADP at 1.25-A resolution. J Biol Chem. 2001;276(45):42091-8.
78. Penning TM, Chen M, Jin Y. Promiscuity and diversity in 3-ketosteroid reductases. J Steroid Biochem Mol Biol. 2015;151:93-101.

79. Mueller JW, Gilligan LC, Idkowiak J, Arlt W, Foster PA. The Regulation of Steroid Action by Sulfation and Desulfation. Endocr Rev. 2015;36(5):526-63.
80. Vassiliadi DA, Barber TM, Hughes BA, McCarthy MI, Wass JAH, Franks S, et al. Increased 5α-Reductase Activity and Adrenocortical Drive in Women with Polycystic Ovary Syndrome. The Journal of Clinical Endocrinology & Metabolism. 2009;94(9):3558-66.
81. Plenge RM. Rheumatoid arthritis genetics: 2009 update. Curr Rheumatol Rep. 2009;11(5):351-6.
82. Cross M, Smith E, Hoy D, Carmona L, Wolfe F, Vos T, et al. The global burden of rheumatoid arthritis: estimates from the global burden of disease 2010 study. Ann Rheum Dis. 2014;73(7):1316-22.
83. Campbell IK, Hamilton JA, Wicks IP. Collagen-induced arthritis in C57BL/6 (H-2b) mice: new insights into an important disease model of rheumatoid arthritis. Eur J Immunol. 2000;30(6):1568-75.
84. Clarke B. Normal Bone Anatomy and Physiology. Clinical Journal of the American Society of Nephrology : CJASN. 2008;3(Suppl 3):S131-S9.
85. Archer CW, Francis-West P. The chondrocyte. Int J Biochem Cell Biol. 2003;35(4):401-4.
86. Sophia Fox AJ, Bedi A, Rodeo SA. The basic science of articular cartilage: structure, composition, and function. Sports Health. 2009;1(6):461-8.
87. Jay GD, Britt DE, Cha CJ. Lubricin is a product of megakaryocyte stimulating factor gene expression by human synovial fibroblasts. J Rheumatol. 2000;27(3):594-600.
88. Haubeck HD, Kock R, Fischer DC, Van de Leur E, Hoffmeister K, Greiling H. Transforming growth factor beta 1, a major stimulator of hyaluronan synthesis in human synovial lining cells. Arthritis Rheum. 1995;38(5):669-77.
89. Tamer TM. Hyaluronan and synovial joint: function, distribution and healing. Interdiscip Toxicol. 2013;6(3):111-25.
90. Guo Q, Wang Y, Xu D, Nossent J, Pavlos NJ, Xu J. Rheumatoid arthritis: pathological mechanisms and modern pharmacologic therapies. Bone Res. 2018;6:15.
91. Hayer S, Redlich K, Korb A, Hermann S, Smolen J, Schett G. Tenosynovitis and osteoclast formation as the initial preclinical changes in a murine model of inflammatory arthritis. Arthritis Rheum. 2007;56(1):79-88.
92. MacGregor AJ, Snieder H, Rigby AS, Koskenvuo M, Kaprio J, Aho K, et al. Characterizing the quantitative genetic contribution to rheumatoid arthritis using data from twins. Arthritis Rheum. 2000;43(1):30-7.
93. Huang Q, Ma Y, Adebayo A, Pope RM. Increased macrophage activation mediated through toll-like receptors in rheumatoid arthritis. Arthritis Rheum. 2007;56(7):2192-201.
94. Kim KW, Cho ML, Lee SH, Oh HJ, Kang CM, Ju JH, et al. Human rheumatoid synovial fibroblasts promote osteoclastogenic activity by activating RANKL via TLR-2 and TLR-4 activation. Immunol Lett. 2007;110(1):54-64.
95. Bradfield PF, Amft N, Vernon-Wilson E, Exley AE, Parsonage G, Rainger GE, et al. Rheumatoid fibroblast-like synoviocytes overexpress the chemokine stromal cell-derived factor 1 (CXCL12), which supports distinct patterns and rates of CD4+ and CD8+ T cell migration within synovial tissue. Arthritis Rheum. 2003;48(9):2472-82.
96. Pilling D, Akbar AN, Girdlestone J, Orteu CH, Borthwick NJ, Amft N, et al. Interferon-beta mediates stromal cell rescue of T cells from apoptosis. Eur J Immunol. 1999;29(3):1041-50.
97. Buckley CD, Amft N, Bradfield PF, Pilling D, Ross E, Arenzana-Seisdedos F, et al. Persistent induction of the chemokine receptor CXCR4 by TGF-beta 1 on synovial T cells contributes to their accumulation within the rheumatoid synovium. J Immunol. 2000;165(6):3423-9.
98. Pettipher ER, Higgs GA, Henderson B. Interleukin 1 induces leukocyte infiltration and cartilage proteoglycan degradation in the synovial joint. Proc Natl Acad Sci U S A. 1986;83(22):8749-53.
99. Schett G. Cells of the synovium in rheumatoid arthritis. Osteoclasts. Arthritis Res Ther. 2007;9(1):203.
100. Pap T, Aupperle KR, Gay S, Firestein GS, Gay RE. Invasiveness of synovial fibroblasts is regulated by p53 in the SCID mouse in vivo model of cartilage invasion. Arthritis Rheum. 2001;44(3):676-81.

101. Hummel KM, Petrow PK, Franz JK, Muller-Ladner U, Aicher WK, Gay RE, et al. Cysteine proteinase cathepsin K mRNA is expressed in synovium of patients with rheumatoid arthritis and is detected at sites of synovial bone destruction. J Rheumatol. 1998;25(10):1887-94.
102. Unemori EN, Hibbs MS, Amento EP. Constitutive expression of a 92-kD gelatinase (type V collagenase) by rheumatoid synovial fibroblasts and its induction in normal human fibroblasts by inflammatory cytokines. J Clin Invest. 1991;88(5):1656-62.
103. Shultz LD, Schweitzer PA, Christianson SW, Gott B, Schweitzer IB, Tennent B, et al. Multiple defects in innate and adaptive immunologic function in NOD/LtSz-scid mice. J Immunol. 1995;154(1):180-91.
104. Muller-Ladner U, Kriegsmann J, Franklin BN, Matsumoto S, Geiler T, Gay RE, et al. Synovial fibroblasts of patients with rheumatoid arthritis attach to and invade normal human cartilage when engrafted into SCID mice. Am J Pathol. 1996;149(5):1607-15.
105. Finckh A, Liang MH, van Herckenrode CM, de Pablo P. Long-term impact of early treatment on radiographic progression in rheumatoid arthritis: A meta-analysis. Arthritis Rheum. 2006;55(6):864-72.
106. Quan L-d, Thiele GM, Tian J, Wang D. The Development of Novel Therapies for Rheumatoid Arthritis. Expert opinion on therapeutic patents. 2008;18(7):723-38.
107. Hazlewood GS, Barnabe C, Tomlinson G, Marshall D, Devoe D, Bombardier C. Methotrexate monotherapy and methotrexate combination therapy with traditional and biologic disease modifying antirheumatic drugs for rheumatoid arthritis: abridged Cochrane systematic review and network meta-analysis. Bmj. 2016;353:i1777.
108. Galloway JB, Hyrich KL, Mercer LK, Dixon WG, Fu B, Ustianowski AP, et al. Anti-TNF therapy is associated with an increased risk of serious infections in patients with rheumatoid arthritis especially in the first 6 months of treatment: updated results from the British Society for Rheumatology Biologics Register with special emphasis on risks in the elderly. Rheumatology (Oxford). 2011;50(1):124-31.
109. Crofford LJ. Use of NSAIDs in treating patients with arthritis. Arthritis Res Ther. 2013;15 Suppl 3(Suppl 3):S2.
110. Smolen JS, Landewe R, Breedveld FC, Dougados M, Emery P, Gaujoux-Viala C, et al. EULAR recommendations for the management of rheumatoid arthritis with synthetic and biological disease-modifying antirheumatic drugs. Ann Rheum Dis. 2010;69(6):964-75.
111. Kirwan JR, Bijlsma JW, Boers M, Shea BJ. Effects of glucocorticoids on radiological progression in rheumatoid arthritis. Cochrane Database Syst Rev. 2007;2007(1):Cd006356.
112. af Klint E, Grundtman C, Engstrom M, Catrina AI, Makrygiannakis D, Klareskog L, et al. Intraarticular glucocorticoid treatment reduces inflammation in synovial cell infiltrations more efficiently than in synovial blood vessels. Arthritis Rheum. 2005;52(12):3880-9.
113. Kirwan JR, Hallgren R, Mielants H, Wollheim F, Bjorck E, Persson T, et al. A randomised placebo controlled 12 week trial of budesonide and prednisolone in rheumatoid arthritis. Ann Rheum Dis. 2004;63(6):688-95.
114. Suponitskaia EV, Smirnov AV, Aleksandrova EN, Novikov AA, Nasonov EL. [Effect of small-dose glucocorticoids on the course of early rheumatic arthritis]. Klin Med (Mosk). 2004;82(9):39-42.
115. Wolf J, Kapral T, Grisar J, Stamm T, Koeller M, Smolen JS, et al. Glucocorticoid treatment in rheumatoid arthritis: low-dose therapy does not reduce responsiveness to higher doses. Clin Exp Rheumatol. 2008;26(1):113-6.
116. Liu D, Ahmet A, Ward L, Krishnamoorthy P, Mandelcorn ED, Leigh R, et al. A practical guide to the monitoring and management of the complications of systemic corticosteroid therapy. Allergy Asthma Clin Immunol. 2013;9(1):30.
117. Hong D, Heiman AS, Kwon T, Lee HL. Synthesis of 6-(methoxycarbonyl)prednisolone and its derivatives as new antiinflammatory steroidal antedrugs. J Pharm Sci. 1994;83(3):357-61.
118. Diederich S, Eigendorff E, Burkhardt P, Quinkler M, Bumke-Vogt C, Rochel M, et al. 11β-Hydroxysteroid Dehydrogenase Types 1 and 2: An Important Pharmacokinetic Determinant for the Activity of Synthetic Mineralo- and Glucocorticoids. The Journal of Clinical Endocrinology & Metabolism. 2002;87(12):5695-701.

119. Abbinante-Nissen JM, Simpson LG, Leikauf GD. Corticosteroids increase secretory leukocyte protease inhibitor transcript levels in airway epithelial cells. Am J Physiol. 1995;268(4 Pt1):L601-6.
120. Manetsch M, Ramsay EE, King EM, Seidel P, Che W, Ge Q, et al. Corticosteroids and β_2-agonists upregulate mitogen-activated protein kinase phosphatase 1: in vitro mechanisms. Br J Pharmacol. 2012;166(7):2049-59.
121. Wang JC, Derynck MK, Nonaka DF, Khodabakhsh DB, Haqq C, Yamamoto KR. Chromatin immunoprecipitation (ChIP) scanning identifies primary glucocorticoid receptor target genes. Proc Natl Acad Sci U S A. 2004;101(44):15603-8.
122. Smoak K, Cidlowski JA. Glucocorticoids regulate tristetraprolin synthesis and posttranscriptionally regulate tumor necrosis factor alpha inflammatory signaling. Mol Cell Biol. 2006;26(23):9126-35.
123. Terrando N, Monaco C, Ma D, Foxwell BM, Feldmann M, Maze M. Tumor necrosis factor-alpha triggers a cytokine cascade yielding postoperative cognitive decline. Proc Natl Acad Sci U S A. 2010;107(47):20518-22.
124. Liu T, Zhang L, Joo D, Sun S-C. NF-κB signaling in inflammation. Signal Transduction And Targeted Therapy. 2017;2:17023.
125. Auphan N, DiDonato JA, Rosette C, Helmberg A, Karin M. Immunosuppression by glucocorticoids: inhibition of NF-kappa B activity through induction of I kappa B synthesis. Science. 1995;270(5234):286-90.
126. Matyszak MK, Citterio S, Rescigno M, Ricciardi-Castagnoli P. Differential effects of corticosteroids during different stages of dendritic cell maturation. Eur J Immunol. 2000;30(4):1233-42.
127. Chen X, Murakami T, Oppenheim JJ, Howard OMZ. Differential response of murine CD4+CD25+ and CD4+CD25- T cells to dexamethasone-induced cell death. Eur J Immunol. 2004;34(3):859-69.
128. Cronstein BN, Kimmel SC, Levin RI, Martiniuk F, Weissmann G. A mechanism for the antiinflammatory effects of corticosteroids: the glucocorticoid receptor regulates leukocyte adhesion to endothelial cells and expression of endothelial-leukocyte adhesion molecule 1 and intercellular adhesion molecule 1. Proceedings of the National Academy of Sciences. 1992;89(21):9991-5.
129. Tuckermann JP, Kleiman A, Moriggl R, Spanbroek R, Neumann A, Illing A, et al. Macrophages and neutrophils are the targets for immune suppression by glucocorticoids in contact allergy. J Clin Invest. 2007;117(5):1381-90.
130. Lombardi L, Forte N, Paradisi F. Effect of pretreatment with prednisolone on the phagocytic activity of mouse peritoneal macrophages in vitro. Experientia. 1978;34(11):1503-4.
131. Ehrchen J, Steinmuller L, Barczyk K, Tenbrock K, Nacken W, Eisenacher M, et al. Glucocorticoids induce differentiation of a specifically activated, anti-inflammatory subtype of human monocytes. Blood. 2007;109(3):1265-74.
132. Schäcke H, Schottelius A, Döcke WD, Strehlke P, Jaroch S, Schmees N, et al. Dissociation of transactivation from transrepression by a selective glucocorticoid receptor agonist leads to separation of therapeutic effects from side effects. Proc Natl Acad Sci U S A. 2004;101(1):227-32.
133. Reichardt HM, Kaestner KH, Tuckermann J, Kretz O, Wessely O, Bock R, et al. DNA Binding of the Glucocorticoid Receptor Is Not Essential for Survival. Cell. 1998;93(4):531-41.
134. Tuckermann JP, Reichardt HM, Arribas R, Richter KH, Schutz G, Angel P. The DNA binding-independent function of the glucocorticoid receptor mediates repression of AP-1-dependent genes in skin. J Cell Biol. 1999;147(7):1365-70.
135. Reichardt HM, Tuckermann JP, Göttlicher M, Vujic M, Weih F, Angel P, et al. Repression of inflammatory responses in the absence of DNA binding by the glucocorticoid receptor. Embo j. 2001;20(24):7168-73.
136. Frijters R, Fleuren W, Toonen EJ, Tuckermann JP, Reichardt HM, van der Maaden H, et al. Prednisolone-induced differential gene expression in mouse liver carrying wild type or a dimerization-defective glucocorticoid receptor. BMC Genomics. 2010;11:359.

137. Patel GC, Millar JC, Clark AF. Glucocorticoid Receptor Transactivation Is Required for Glucocorticoid-Induced Ocular Hypertension and Glaucoma. Invest Ophthalmol Vis Sci. 2019;60(6):1967-78.
138. Koenen M, Culemann S, Vettorazzi S, Caratti G, Frappart L, Baum W, et al. Glucocorticoid receptor in stromal cells is essential for glucocorticoid-mediated suppression of inflammation in arthritis. Ann Rheum Dis. 2018;77(11):1610-8.
139. Ballegeer M, Van Looveren K, Timmermans S, Eggermont M, Vandevyver S, Thery F, et al. Glucocorticoid receptor dimers control intestinal STAT1 and TNF-induced inflammation in mice. J Clin Invest. 2018;128(8):3265-79.
140. Rauch A, Seitz S, Baschant U, Schilling AF, Illing A, Stride B, et al. Glucocorticoids suppress bone formation by attenuating osteoblast differentiation via the monomeric glucocorticoid receptor. Cell Metab. 2010;11(6):517-31.
141. Watson ML, Baehr L, Brandt Jvd, Reichardt H, Tuckermann J, Bodine S, et al. Analysis of glucocorticoid regulated gene expression and skeletal muscle atrophy in glucocorticoid receptor mutant mice. The FASEB Journal. 2010;24(1_supplement):989.6-.6.
142. Lonard DM, O'Malley BW. Nuclear receptor coregulators: modulators of pathology and therapeutic targets. Nature Reviews Endocrinology. 2012;8:598.
143. Meijer OC, Koorneef LL, Kroon J. Glucocorticoid receptor modulators. Annales d'Endocrinologie. 2018;79(3):107-11.
144. Coghlan MJ, Jacobson PB, Lane B, Nakane M, Lin CW, Elmore SW, et al. A Novel Antiinflammatory Maintains Glucocorticoid Efficacy with Reduced Side Effects. Molecular Endocrinology. 2003;17(5):860-9.
145. Mantero F, Terzolo M, Arnaldi G, Osella G, Masini AM, Ali A, et al. A survey on adrenal incidentaloma in Italy. Study Group on Adrenal Tumors of the Italian Society of Endocrinology. J Clin Endocrinol Metab. 2000;85(2):637-44.
146. Sharma ST, Nieman LK, Feelders RA. Cushing's syndrome: epidemiology and developments in disease management. Clin Epidemiol. 2015;7:281-93.
147. Andrews RC, Rooyackers O, Walker BR. Effects of the 11 beta-hydroxysteroid dehydrogenase inhibitor carbenoxolone on insulin sensitivity in men with type 2 diabetes. J Clin Endocrinol Metab. 2003;88(1):285-91.
148. Rosenstock J, Banarer S, Fonseca VA, Inzucchi SE, Sun W, Yao W, et al. The 11-beta-hydroxysteroid dehydrogenase type 1 inhibitor INCB13739 improves hyperglycemia in patients with type 2 diabetes inadequately controlled by metformin monotherapy. Diabetes Care. 2010;33(7):1516-22.
149. Feig PU, Shah S, Hermanowski-Vosatka A, Plotkin D, Springer MS, Donahue S, et al. Effects of an 11beta-hydroxysteroid dehydrogenase type 1 inhibitor, MK-0916, in patients with type 2 diabetes mellitus and metabolic syndrome. Diabetes Obes Metab. 2011;13(6):498-504.
150. Hardy R, Rabbitt EH, Filer A, Emery P, Hewison M, Stewart PM, et al. Local and systemic glucocorticoid metabolism in inflammatory arthritis. Ann Rheum Dis. 2008;67(9):1204-10.
151. Cooper MS, Bujalska I, Rabbitt E, Walker EA, Bland R, Sheppard MC, et al. Modulation of 11beta-hydroxysteroid dehydrogenase isozymes by proinflammatory cytokines in osteoblasts: an autocrine switch from glucocorticoid inactivation to activation. J Bone Miner Res. 2001;16(6):1037-44.
152. Tomlinson JW, Moore J, Cooper MS, Bujalska I, Shahmanesh M, Burt C, et al. Regulation of expression of 11beta-hydroxysteroid dehydrogenase type 1 in adipose tissue: tissue-specific induction by cytokines. Endocrinology. 2001;142(5):1982-9.
153. Hardy RS, Doig CL, Hussain Z, O'Leary M, Morgan SA, Pearson MJ, et al. 11β-Hydroxysteroid dehydrogenase type 1 within muscle protects against the adverse effects of local inflammation. The Journal of Pathology. 2016;240(4):472-83.
154. Kaur K, Hardy R, Ahasan MM, Eijken M, van Leeuwen JP, Filer A, et al. Synergistic induction of local glucocorticoid generation by inflammatory cytokines and glucocorticoids: implications for inflammation associated bone loss. Ann Rheum Dis. 2010;69(6):1185-90.

155. Thieringer R, Le Grand CB, Carbin L, Cai T-Q, Wong B, Wright SD, et al. 11β-Hydroxysteroid Dehydrogenase Type 1 Is Induced in Human Monocytes upon Differentiation to Macrophages. The Journal of Immunology. 2001;167(1):30-5.
156. Martinez FO, Gordon S, Locati M, Mantovani A. Transcriptional Profiling of the Human Monocyte-to-Macrophage Differentiation and Polarization: New Molecules and Patterns of Gene Expression. The Journal of Immunology. 2006;177(10):7303-11.
157. Hardy RS, Fenton C, Croft AP, Naylor AJ, Begum R, Desanti G, et al. 11 Beta-hydroxysteroid dehydrogenase type 1 regulates synovitis, joint destruction, and systemic bone loss in chronic polyarthritis. J Autoimmun. 2018;92:104-13.
158. Gilmour JS, Coutinho AE, Cailhier J-F, Man TY, Clay M, Thomas G, et al. Local Amplification of Glucocorticoids by 11β-Hydroxysteroid Dehydrogenase Type 1 Promotes Macrophage Phagocytosis of Apoptotic Leukocytes. The Journal of Immunology. 2006;176(12):7605-11.
159. Straub RH, Cutolo M. Glucocorticoids and chronic inflammation. Rheumatology. 2016;55(suppl_2):ii6-ii14.
160. Joseph RM, Hunter AL, Ray DW, Dixon WG. Systemic glucocorticoid therapy and adrenal insufficiency in adults: A systematic review. Semin Arthritis Rheum. 2016;46(1):133-41.
161. Manolagas SC. Birth and Death of Bone Cells: Basic Regulatory Mechanisms and Implications for the Pathogenesis and Treatment of Osteoporosis*. Endocrine Reviews. 2000;21(2):115-37.
162. Hadjidakis DJ, Androulakis, II. Bone remodeling. Ann N Y Acad Sci. 2006;1092:385-96.
163. Taichman RS. Blood and bone: two tissues whose fates are intertwined to create the hematopoietic stem-cell niche. Blood. 2005;105(7):2631-9.
164. Kenkre JS, Bassett J. The bone remodelling cycle. Ann Clin Biochem. 2018;55(3):308-27.
165. Moore SG, Dawson KL. Red and yellow marrow in the femur: age-related changes in appearance at MR imaging. Radiology. 1990;175(1):219-23.
166. McCreadie BR, Hollister SJ, Schaffler MB, Goldstein SA. Osteocyte lacuna size and shape in women with and without osteoporotic fracture. Journal of biomechanics. 2004;37(4):563-72.
167. Nakamura Y, Arai F, Iwasaki H, Hosokawa K, Kobayashi I, Gomei Y, et al. Isolation and characterization of endosteal niche cell populations that regulate hematopoietic stem cells. Blood. 2010;116(9):1422-32.
168. Colnot C. Skeletal cell fate decisions within periosteum and bone marrow during bone regeneration. J Bone Miner Res. 2009;24(2):274-82.
169. Frost HM. Skeletal structural adaptations to mechanical usage (SATMU): 2. Redefining Wolff's law: the remodeling problem. Anat Rec. 1990;226(4):414-22.
170. van Oers RF, Ruimerman R, Tanck E, Hilbers PA, Huiskes R. A unified theory for osteonal and hemi-osteonal remodeling. Bone. 2008;42(2):250-9.
171. Burra S, Nicolella DP, Francis WL, Freitas CJ, Mueschke NJ, Poole K, et al. Dendritic processes of osteocytes are mechanotransducers that induce the opening of hemichannels. Proc Natl Acad Sci U S A. 2010;107(31):13648-53.
172. Verborgt O, Tatton NA, Majeska RJ, Schaffler MB. Spatial distribution of Bax and Bcl-2 in osteocytes after bone fatigue: complementary roles in bone remodeling regulation? J Bone Miner Res. 2002;17(5):907-14.
173. Aguirre JI, Plotkin LI, Stewart SA, Weinstein RS, Parfitt AM, Manolagas SC, et al. Osteocyte apoptosis is induced by weightlessness in mice and precedes osteoclast recruitment and bone loss. J Bone Miner Res. 2006;21(4):605-15.
174. Al-Dujaili SA, Lau E, Al-Dujaili H, Tsang K, Guenther A, You L. Apoptotic osteocytes regulate osteoclast precursor recruitment and differentiation in vitro. J Cell Biochem. 2011;112(9):2412-23.
175. Destaing O, Saltel F, Geminard JC, Jurdic P, Bard F. Podosomes display actin turnover and dynamic self-organization in osteoclasts expressing actin-green fluorescent protein. Mol Biol Cell. 2003;14(2):407-16.

176. Luxenburg C, Geblinger D, Klein E, Anderson K, Hanein D, Geiger B, et al. The architecture of the adhesive apparatus of cultured osteoclasts: from podosome formation to sealing zone assembly. PLoS One. 2007;2(1):e179.
177. Kanehisa J, Yamanaka T, Doi S, Turksen K, Heersche JN, Aubin JE, et al. A band of F-actin containing podosomes is involved in bone resorption by osteoclasts. Bone. 1990;11(4):287-93.
178. Faccio R, Novack DV, Zallone A, Ross FP, Teitelbaum SL. Dynamic changes in the osteoclast cytoskeleton in response to growth factors and cell attachment are controlled by beta3 integrin. J Cell Biol. 2003;162(3):499-509.
179. Gay CV, Mueller WJ. Carbonic Anhydrase and Osteoclasts: Localization by Labeled Inhibitor Autoradiography. Science. 1974;183(4123):432-4.
180. Väänänen HK, Karhukorpi EK, Sundquist K, Wallmark B, Roininen I, Hentunen T, et al. Evidence for the presence of a proton pump of the vacuolar H(+)-ATPase type in the ruffled borders of osteoclasts. The Journal of Cell Biology. 1990;111(3):1305-11.
181. Blair HC, Schlesinger PH. Purification of a stilbene sensitive chloride channel and reconstitution of chloride conductivity into phospholipid vesicles. Biochem Biophys Res Commun. 1990;171(3):920-5.
182. Teti A, Blair HC, Teitelbaum SL, Kahn AJ, Koziol C, Konsek J, et al. Cytoplasmic pH regulation and chloride/bicarbonate exchange in avian osteoclasts. The Journal of Clinical Investigation. 1989;83(1):227-33.
183. Bossard MJ, Tomaszek TA, Thompson SK, Amegadzie BY, Hanning CR, Jones C, et al. Proteolytic activity of human osteoclast cathepsin K. Expression, purification, activation, and substrate identification. J Biol Chem. 1996;271(21):12517-24.
184. Cleiren E, Benichou O, Van Hul E, Gram J, Bollerslev J, Singer FR, et al. Albers-Schonberg disease (autosomal dominant osteopetrosis, type II) results from mutations in the ClCN7 chloride channel gene. Hum Mol Genet. 2001;10(25):2861-7.
185. Ljusberg J, Wang Y, Lang P, Norgard M, Dodds R, Hultenby K, et al. Proteolytic excision of a repressive loop domain in tartrate-resistant acid phosphatase by cathepsin K in osteoclasts. J Biol Chem. 2005;280(31):28370-81.
186. Reinholt FP, Widholm SM, Ek-Rylander B, Andersson G. Ultrastructural localization of a tartrate-resistant acid ATPase in bone. J Bone Miner Res. 1990;5(10):1055-61.
187. Halleen JM, Raisanen S, Salo JJ, Reddy SV, Roodman GD, Hentunen TA, et al. Intracellular fragmentation of bone resorption products by reactive oxygen species generated by osteoclastic tartrate-resistant acid phosphatase. J Biol Chem. 1999;274(33):22907-10.
188. Tang Y, Wu X, Lei W, Pang L, Wan C, Shi Z, et al. TGF-beta1-induced migration of bone mesenchymal stem cells couples bone resorption with formation. Nat Med. 2009;15(7):757-65.
189. Xian L, Wu X, Pang L, Lou M, Rosen CJ, Qiu T, et al. Matrix IGF-1 maintains bone mass by activation of mTOR in mesenchymal stem cells. Nat Med. 2012;18(7):1095-101.
190. Zhao C, Irie N, Takada Y, Shimoda K, Miyamoto T, Nishiwaki T, et al. Bidirectional ephrinB2-EphB4 signaling controls bone homeostasis. Cell Metab. 2006;4(2):111-21.
191. Cowles EA, DeRome ME, Pastizzo G, Brailey LL, Gronowicz GA. Mineralization and the expression of matrix proteins during in vivo bone development. Calcif Tissue Int. 1998;62(1):74-82.
192. Weiner S. Organization of extracellularly mineralized tissues: a comparative study of biological crystal growth. CRC Crit Rev Biochem. 1986;20(4):365-408.
193. Orimo H. The mechanism of mineralization and the role of alkaline phosphatase in health and disease. J Nippon Med Sch. 2010;77(1):4-12.
194. Yuan Q, Jiang Y, Zhao X, Sato T, Densmore M, Schüler C, et al. Increased osteopontin contributes to inhibition of bone mineralization in FGF23-deficient mice. J Bone Miner Res. 2014;29(3):693-704.
195. Poole KE, van Bezooijen RL, Loveridge N, Hamersma H, Papapoulos SE, Lowik CW, et al. Sclerostin is a delayed secreted product of osteocytes that inhibits bone formation. Faseb j. 2005;19(13):1842-4.

196. Eriksen EF, Hodgson SF, Eastell R, Cedel SL, O'Fallon WM, Riggs BL. Cancellous bone remodeling in type I (postmenopausal) osteoporosis: quantitative assessment of rates of formation, resorption, and bone loss at tissue and cellular levels. J Bone Miner Res. 1990;5(4):311-9.
197. Guerrini MM, Sobacchi C, Cassani B, Abinun M, Kilic SS, Pangrazio A, et al. Human osteoclast-poor osteopetrosis with hypogammaglobulinemia due to TNFRSF11A (RANK) mutations. Am J Hum Genet. 2008;83(1):64-76.
198. Ducy P, Zhang R, Geoffroy V, Ridall AL, Karsenty G. Osf2/Cbfa1: a transcriptional activator of osteoblast differentiation. Cell. 1997;89(5):747-54.
199. Roca H, Phimphilai M, Gopalakrishnan R, Xiao G, Franceschi RT. Cooperative interactions between RUNX2 and homeodomain protein-binding sites are critical for the osteoblast-specific expression of the bone sialoprotein gene. J Biol Chem. 2005;280(35):30845-55.
200. Dowling AH, Fleming GJP, McGinley EL, Addison O. Improving the standard of the standard for glass ionomers: An alternative to the compressive fracture strength test for consideration? Journal of Dentistry. 2012;40(3):189-201.
201. Gutierrez S, Javed A, Tennant DK, van Rees M, Montecino M, Stein GS, et al. CCAAT/enhancer-binding proteins (C/EBP) beta and delta activate osteocalcin gene transcription and synergize with Runx2 at the C/EBP element to regulate bone-specific expression. J Biol Chem. 2002;277(2):1316-23.
202. Villagra A, Cruzat F, Carvallo L, Paredes R, Olate J, van Wijnen AJ, et al. Chromatin remodeling and transcriptional activity of the bone-specific osteocalcin gene require CCAAT/enhancer-binding protein beta-dependent recruitment of SWI/SNF activity. J Biol Chem. 2006;281(32):22695-706.
203. Day TF, Guo X, Garrett-Beal L, Yang Y. Wnt/beta-catenin signaling in mesenchymal progenitors controls osteoblast and chondrocyte differentiation during vertebrate skeletogenesis. Dev Cell. 2005;8(5):739-50.
204. Mao J, Wang J, Liu B, Pan W, Farr GH, 3rd, Flynn C, et al. Low-density lipoprotein receptor-related protein-5 binds to Axin and regulates the canonical Wnt signaling pathway. Mol Cell. 2001;7(4):801-9.
205. Gaur T, Lengner CJ, Hovhannisyan H, Bhat RA, Bodine PV, Komm BS, et al. Canonical WNT signaling promotes osteogenesis by directly stimulating Runx2 gene expression. J Biol Chem. 2005;280(39):33132-40.
206. Li J, Sarosi I, Cattley RC, Pretorius J, Asuncion F, Grisanti M, et al. Dkk1-mediated inhibition of Wnt signaling in bone results in osteopenia. Bone. 2006;39(4):754-66.
207. van Lierop AH, Hamdy NA, Hamersma H, van Bezooijen RL, Power J, Loveridge N, et al. Patients with sclerosteosis and disease carriers: human models of the effect of sclerostin on bone turnover. J Bone Miner Res. 2011;26(12):2804-11.
208. Schwarz P. Dose response dependency in regulation of acute PTH (1-84) release and suppression in normal humans: a citrate and calcium infusion study. Scand J Clin Lab Invest. 1993;53(6):601-5.
209. Brown EM, Gamba G, Riccardi D, Lombardi M, Butters R, Kifor O, et al. Cloning and characterization of an extracellular Ca(2+)-sensing receptor from bovine parathyroid. Nature. 1993;366(6455):575-80.
210. ROULEAU MF, MITCHELL J, GOLTZMAN D. In Vivo Distribution of Parathyroid Hormone Receptors in Bone: Evidence that a Predominant Osseous Target Cell Is Not the Mature Osteoblast*. Endocrinology. 1988;123(1):187-91.
211. Bringhurst FR, Juppner H, Guo J, Urena P, Potts JT, Jr., Kronenberg HM, et al. Cloned, stably expressed parathyroid hormone (PTH)/PTH-related peptide receptors activate multiple messenger signals and biological responses in LLC-PK1 kidney cells. Endocrinology. 1993;132(5):2090-8.
212. Schiller PC, D'Ippolito G, Roos BA, Howard GA. Anabolic or catabolic responses of MC3T3-E1 osteoblastic cells to parathyroid hormone depend on time and duration of treatment. J Bone Miner Res. 1999;14(9):1504-12.
213. Horwitz MJ, Tedesco MB, Sereika SM, Syed MA, Garcia-Ocana A, Bisello A, et al. Continuous PTH and PTHrP infusion causes suppression of bone formation and discordant effects on 1,25(OH)2 vitamin D. J Bone Miner Res. 2005;20(10):1792-803.

214. Datta NS, Pettway GJ, Chen C, Koh AJ, McCauley LK. Cyclin D1 as a target for the proliferative effects of PTH and PTHrP in early osteoblastic cells. J Bone Miner Res. 2007;22(7):951-64.
215. Nishida S, Yamaguchi A, Tanizawa T, Endo N, Mashiba T, Uchiyama Y, et al. Increased bone formation by intermittent parathyroid hormone administration is due to the stimulation of proliferation and differentiation of osteoprogenitor cells in bone marrow. Bone. 1994;15(6):717-23.
216. Canalis E, Centrella M, Burch W, McCarthy TL. Insulin-like growth factor I mediates selective anabolic effects of parathyroid hormone in bone cultures. J Clin Invest. 1989;83(1):60-5.
217. Kulkarni NH, Halladay DL, Miles RR, Gilbert LM, Frolik CA, Galvin RJ, et al. Effects of parathyroid hormone on Wnt signaling pathway in bone. J Cell Biochem. 2005;95(6):1178-90.
218. Fretz JA, Zella LA, Kim S, Shevde NK, Pike JW. 1,25-Dihydroxyvitamin D3 induces expression of the Wnt signaling co-regulator LRP5 via regulatory elements located significantly downstream of the gene's transcriptional start site. J Steroid Biochem Mol Biol. 2007;103(3-5):440-5.
219. Haussler MR, Haussler CA, Whitfield GK, Hsieh JC, Thompson PD, Barthel TK, et al. The nuclear vitamin D receptor controls the expression of genes encoding factors which feed the "Fountain of Youth" to mediate healthful aging. J Steroid Biochem Mol Biol. 2010;121(1-2):88-97.
220. Paredes R, Arriagada G, Cruzat F, Olate J, Van Wijnen A, Lian J, et al. The Runx2 transcription factor plays a key role in the 1alpha,25-dihydroxy Vitamin D3-dependent upregulation of the rat osteocalcin (OC) gene expression in osteoblastic cells. J Steroid Biochem Mol Biol. 2004;89-90(1-5):269-71.
221. Hodge JM, Collier FM, Pavlos NJ, Kirkland MA, Nicholson GC. M-CSF potently augments RANKL-induced resorption activation in mature human osteoclasts. PLoS One. 2011;6(6):e21462.
222. Nakashima T, Hayashi M, Fukunaga T, Kurata K, Oh-Hora M, Feng JQ, et al. Evidence for osteocyte regulation of bone homeostasis through RANKL expression. Nat Med. 2011;17(10):1231-4.
223. Wei X, Zhang X, Zuscik MJ, Drissi MH, Schwarz EM, O'Keefe RJ. Fibroblasts express RANKL and support osteoclastogenesis in a COX-2-dependent manner after stimulation with titanium particles. J Bone Miner Res. 2005;20(7):1136-48.
224. Kawai T, Matsuyama T, Hosokawa Y, Makihira S, Seki M, Karimbux NY, et al. B and T lymphocytes are the primary sources of RANKL in the bone resorptive lesion of periodontal disease. Am J Pathol. 2006;169(3):987-98.
225. Page G, Miossec P. RANK and RANKL expression as markers of dendritic cell-T cell interactions in paired samples of rheumatoid synovium and lymph nodes. Arthritis Rheum. 2005;52(8):2307-12.
226. Atkins GJ, Kostakis P, Vincent C, Farrugia AN, Houchins JP, Findlay DM, et al. RANK Expression as a cell surface marker of human osteoclast precursors in peripheral blood, bone marrow, and giant cell tumors of bone. J Bone Miner Res. 2006;21(9):1339-49.
227. Naito A, Azuma S, Tanaka S, Miyazaki T, Takaki S, Takatsu K, et al. Severe osteopetrosis, defective interleukin-1 signalling and lymph node organogenesis in TRAF6-deficient mice. Genes Cells. 1999;4(6):353-62.
228. Takayanagi H, Kim S, Koga T, Nishina H, Isshiki M, Yoshida H, et al. Induction and activation of the transcription factor NFATc1 (NFAT2) integrate RANKL signaling in terminal differentiation of osteoclasts. Dev Cell. 2002;3(6):889-901.
229. Kukita T, Wada N, Kukita A, Kakimoto T, Sandra F, Toh K, et al. RANKL-induced DC-STAMP is essential for osteoclastogenesis. J Exp Med. 2004;200(7):941-6.
230. Wu H, Xu G, Li YP. Atp6v0d2 is an essential component of the osteoclast-specific proton pump that mediates extracellular acidification in bone resorption. J Bone Miner Res. 2009;24(5):871-85.
231. Mizuno A, Kanno T, Hoshi M, Shibata O, Yano K, Fujise N, et al. Transgenic mice overexpressing soluble osteoclast differentiation factor (sODF) exhibit severe osteoporosis. J Bone Miner Metab. 2002;20(6):337-44.
232. Cao J, Venton L, Sakata T, Halloran BP. Expression of RANKL and OPG correlates with age-related bone loss in male C57BL/6 mice. J Bone Miner Res. 2003;18(2):270-7.
233. Huang JC, Sakata T, Pfleger LL, Bencsik M, Halloran BP, Bikle DD, et al. PTH differentially regulates expression of RANKL and OPG. J Bone Miner Res. 2004;19(2):235-44.

234. Zhou H, Mak W, Zheng Y, Dunstan CR, Seibel MJ. Osteoblasts directly control lineage commitment of mesenchymal progenitor cells through Wnt signaling. J Biol Chem. 2008;283(4):1936-45.
235. Mak W, Shao X, Dunstan CR, Seibel MJ, Zhou H. Biphasic glucocorticoid-dependent regulation of Wnt expression and its inhibitors in mature osteoblastic cells. Calcif Tissue Int. 2009;85(6):538-45.
236. Weinstein RS, Jilka RL, Parfitt AM, Manolagas SC. Inhibition of osteoblastogenesis and promotion of apoptosis of osteoblasts and osteocytes by glucocorticoids. Potential mechanisms of their deleterious effects on bone. J Clin Invest. 1998;102(2):274-82.
237. O'Brien CA, Jia D, Plotkin LI, Bellido T, Powers CC, Stewart SA, et al. Glucocorticoids act directly on osteoblasts and osteocytes to induce their apoptosis and reduce bone formation and strength. Endocrinology. 2004;145(4):1835-41.
238. Jia D, O'Brien CA, Stewart SA, Manolagas SC, Weinstein RS. Glucocorticoids act directly on osteoclasts to increase their life span and reduce bone density. Endocrinology. 2006;147(12):5592-9.
239. Rubin J, Biskobing DM, Jadhav L, Fan D, Nanes MS, Perkins S, et al. Dexamethasone promotes expression of membrane-bound macrophage colony-stimulating factor in murine osteoblast-like cells. Endocrinology. 1998;139(3):1006-12.
240. Swanson C, Lorentzon M, Conaway HH, Lerner UH. Glucocorticoid regulation of osteoclast differentiation and expression of receptor activator of nuclear factor-kappaB (NF-kappaB) ligand, osteoprotegerin, and receptor activator of NF-kappaB in mouse calvarial bones. Endocrinology. 2006;147(7):3613-22.
241. Hofbauer LC, Gori F, Riggs BL, Lacey DL, Dunstan CR, Spelsberg TC, et al. Stimulation of osteoprotegerin ligand and inhibition of osteoprotegerin production by glucocorticoids in human osteoblastic lineage cells: potential paracrine mechanisms of glucocorticoid-induced osteoporosis. Endocrinology. 1999;140(10):4382-9.
242. Humphrey EL, Williams JH, Davie MW, Marshall MJ. Effects of dissociated glucocorticoids on OPG and RANKL in osteoblastic cells. Bone. 2006;38(5):652-61.
243. Kim HJ, Zhao H, Kitaura H, Bhattacharyya S, Brewer JA, Muglia LJ, et al. Glucocorticoids suppress bone formation via the osteoclast. J Clin Invest. 2006;116(8):2152-60.
244. Gough AK, Lilley J, Eyre S, Holder RL, Emery P. Generalised bone loss in patients with early rheumatoid arthritis. Lancet. 1994;344(8914):23-7.
245. Roubenoff R, Roubenoff RA, Ward LM, Holland SM, Hellmann DB. Rheumatoid cachexia: depletion of lean body mass in rheumatoid arthritis. Possible association with tumor necrosis factor. J Rheumatol. 1992;19(10):1505-10.
246. Ekdahl C, Broman G. Muscle strength, endurance, and aerobic capacity in rheumatoid arthritis: a comparative study with healthy subjects. Ann Rheum Dis. 1992;51(1):35-40.
247. Helliwell PS, Jackson S. Relationship between weakness and muscle wasting in rheumatoid arthritis. Ann Rheum Dis. 1994;53(11):726-8.
248. Minetti GC, Feige JN, Rosenstiel A, Bombard F, Meier V, Werner A, et al. Galphai2 signaling promotes skeletal muscle hypertrophy, myoblast differentiation, and muscle regeneration. Sci Signal. 2011;4(201):ra80.
249. Crossland H, Constantin-Teodosiu D, Gardiner SM, Constantin D, Greenhaff PL. A potential role for Akt/FOXO signalling in both protein loss and the impairment of muscle carbohydrate oxidation during sepsis in rodent skeletal muscle. J Physiol. 2008;586(22):5589-600.
250. Lodder MC, de Jong Z, Kostense PJ, Molenaar ETH, Staal K, Voskuyl AE, et al. Bone mineral density in patients with rheumatoid arthritis: relation between disease severity and low bone mineral density. Annals of the Rheumatic Diseases. 2004;63(12):1576-80.
251. Spector TD, Hall GM, McCloskey EV, Kanis JA. Risk of vertebral fracture in women with rheumatoid arthritis. Bmj. 1993;306(6877):558.
252. Wei S, Kitaura H, Zhou P, Ross FP, Teitelbaum SL. IL-1 mediates TNF-induced osteoclastogenesis. J Clin Invest. 2005;115(2):282-90.

253. Palmqvist P, Persson E, Conaway HH, Lerner UH. IL-6, leukemia inhibitory factor, and oncostatin M stimulate bone resorption and regulate the expression of receptor activator of NF-kappa B ligand, osteoprotegerin, and receptor activator of NF-kappa B in mouse calvariae. J Immunol. 2002;169(6):3353-62.
254. Yoshitake F, Itoh S, Narita H, Ishihara K, Ebisu S. Interleukin-6 directly inhibits osteoclast differentiation by suppressing receptor activator of NF-kappaB signaling pathways. J Biol Chem. 2008;283(17):11535-40.
255. Kotake S, Udagawa N, Takahashi N, Matsuzaki K, Itoh K, Ishiyama S, et al. IL-17 in synovial fluids from patients with rheumatoid arthritis is a potent stimulator of osteoclastogenesis. J Clin Invest. 1999;103(9):1345-52.
256. Ragab AA, Nalepka JL, Bi Y, Greenfield EM. Cytokines synergistically induce osteoclast differentiation: support by immortalized or normal calvarial cells. Am J Physiol Cell Physiol. 2002;283(3):C679-87.
257. Sato K, Suematsu A, Okamoto K, Yamaguchi A, Morishita Y, Kadono Y, et al. Th17 functions as an osteoclastogenic helper T cell subset that links T cell activation and bone destruction. J Exp Med. 2006;203(12):2673-82.
258. Takayanagi H, Ogasawara K, Hida S, Chiba T, Murata S, Sato K, et al. T-cell-mediated regulation of osteoclastogenesis by signalling cross-talk between RANKL and IFN-gamma. Nature. 2000;408(6812):600-5.
259. Cheng J, Liu J, Shi Z, Xu D, Luo S, Siegal GP, et al. Interleukin-4 inhibits RANKL-induced NFATc1 expression via STAT6: a novel mechanism mediating its blockade of osteoclastogenesis. J Cell Biochem. 2011;112(11):3385-92.
260. Abbas S, Zhang YH, Clohisy JC, Abu-Amer Y. Tumor necrosis factor-alpha inhibits pre-osteoblast differentiation through its type-1 receptor. Cytokine. 2003;22(1-2):33-41.
261. Jilka RL, Weinstein RS, Bellido T, Parfitt AM, Manolagas SC. Osteoblast Programmed Cell Death (Apoptosis): Modulation by Growth Factors and Cytokines. Journal of Bone and Mineral Research. 1998;13(5):793-802.
262. Kaneshiro S, Ebina K, Shi K, Higuchi C, Hirao M, Okamoto M, et al. IL-6 negatively regulates osteoblast differentiation through the SHP2/MEK2 and SHP2/Akt2 pathways in vitro. J Bone Miner Metab. 2014;32(4):378-92.
263. Itoh S, Udagawa N, Takahashi N, Yoshitake F, Narita H, Ebisu S, et al. A critical role for interleukin-6 family-mediated Stat3 activation in osteoblast differentiation and bone formation. Bone. 2006;39(3):505-12.
264. Hardy R, Cooper MS. Bone loss in inflammatory disorders. 2009;201(3):309.
265. Redlich K, Görtz B, Hayer S, Zwerina J, Doerr N, Kostenuik P, et al. Repair of local bone erosions and reversal of systemic bone loss upon therapy with anti-tumor necrosis factor in combination with osteoprotegerin or parathyroid hormone in tumor necrosis factor-mediated arthritis. Am J Pathol. 2004;164(2):543-55.
266. Asquith DL, Miller AM, McInnes IB, Liew FY. Animal models of rheumatoid arthritis. European Journal of Immunology. 2009;39(8):2040-4.
267. . !!! INVALID CITATION !!! (282, 283).
268. Pan M, Kang I, Craft J, Yin Z. Resistance to development of collagen-induced arthritis in C57BL/6 mice is due to a defect in secondary, but not in primary, immune response. J Clin Immunol. 2004;24(5):481-91.
269. Inglis JJ, Simelyte E, McCann FE, Criado G, Williams RO. Protocol for the induction of arthritis in C57BL/6 mice. Nat Protoc. 2008;3(4):612-8.
270. Stuart JM, Dixon FJ. Serum transfer of collagen-induced arthritis in mice. J Exp Med. 1983;158(2):378-92.

271. Nandakumar KS, Backlund J, Vestberg M, Holmdahl R. Collagen type II (CII)-specific antibodies induce arthritis in the absence of T or B cells but the arthritis progression is enhanced by CII-reactive T cells. Arthritis Res Ther. 2004;6(6):R544-50.
272. Kouskoff V, Korganow AS, Duchatelle V, Degott C, Benoist C, Mathis D. Organ-specific disease provoked by systemic autoimmunity. Cell. 1996;87(5):811-22.
273. Christianson CA, Corr M, Yaksh TL, Svensson CI. K/BxN serum transfer arthritis as a model of inflammatory joint pain. Methods Mol Biol. 2012;851:249-60.
274. Matsumoto I, Lee DM, Goldbach-Mansky R, Sumida T, Hitchon CA, Schur PH, et al. Low prevalence of antibodies to glucose-6-phosphate isomerase in patients with rheumatoid arthritis and a spectrum of other chronic autoimmune disorders. Arthritis Rheum. 2003;48(4):944-54.
275. van Gaalen FA, Toes RE, Ditzel HJ, Schaller M, Breedveld FC, Verweij CL, et al. Association of autoantibodies to glucose-6-phosphate isomerase with extraarticular complications in rheumatoid arthritis. Arthritis Rheum. 2004;50(2):395-9.
276. Keffer J, Probert L, Cazlaris H, Georgopoulos S, Kaslaris E, Kioussis D, et al. Transgenic mice expressing human tumour necrosis factor: a predictive genetic model of arthritis. Embo j. 1991;10(13):4025-31.
277. Li P, Schwarz EM. The TNF-α transgenic mouse modelof inflammatory arthritis. Springer Seminars in Immunopathology. 2003;25(1):19-33.
278. Douni E, Akassoglou K, Alexopoulou L, Georgopoulos S, Haralambous S, Hill S, et al. Transgenic and knockout analyses of the role of TNF in immune regulation and disease pathogenesis. J Inflamm. 1995;47(1-2):27-38.
279. Luo G, Li F, Li X, Wang ZG, Zhang B. TNF-α and RANKL promote osteoclastogenesis by upregulating RANK via the NF-κB pathway. Mol Med Rep. 2018;17(5):6605-11.
280. Wang D-T, Yin Y, Yang Y-J, Lv P-J, Shi Y, Lu L, et al. Resveratrol prevents TNF-α-induced muscle atrophy via regulation of Akt/mTOR/FoxO1 signaling in C2C12 myotubes. International Immunopharmacology. 2014;19(2):206-13.
281. Fenton CG, Webster JM, Martin CS, Fareed S, Wehmeyer C, Mackie H, et al. Therapeutic glucocorticoids prevent bone loss but drive muscle wasting when administered in chronic polyarthritis. Arthritis Res Ther. 2019;21(1):182.
282. Naylor AJ, Desanti G, Saghir AN, Hardy RS. TNFα depleting therapy improves fertility and animal welfare in TNFα-driven transgenic models of polyarthritis when administered in their routine breeding. Laboratory animals. 2018;52(1):59-68.
283. Sternberg N, Sauer B, Hoess R, Abremski K. Bacteriophage P1 cre gene and its regulatory region. Evidence for multiple promoters and for regulation by DNA methylation. Journal of molecular biology. 1986;187(2):197-212.
284. Semjonous NM, Sherlock M, Jeyasuria P, Parker KL, Walker EA, Stewart PM, et al. Hexose-6-phosphate dehydrogenase contributes to skeletal muscle homeostasis independent of 11beta-hydroxysteroid dehydrogenase type 1. Endocrinology. 2011;152(1):93-102.
285. Haugeberg G, Orstavik RE, Uhlig T, Falch JA, Halse JI, Kvien TK. Bone loss in patients with rheumatoid arthritis: results from a population-based cohort of 366 patients followed up for two years. Arthritis Rheum. 2002;46(7):1720-8.
286. LoCascio V, Bonucci E, Imbimbo B, Ballanti P, Adami S, Milani S, et al. Bone loss in response to long-term glucocorticoid therapy. Bone Miner. 1990;8(1):39-51.
287. Chen F, Zhang L, OuYang Y, Guan H, Liu Q, Ni B. Glucocorticoid induced osteoblast apoptosis by increasing E4BP4 expression via up-regulation of Bim. Calcif Tissue Int. 2014;94(6):640-7.
288. Swanson C, Lorentzon M, Conaway HH, Lerner UH. Glucocorticoid regulation of osteoclast differentiation and expression of receptor activator of nuclear factor-kappaB (NF-kappaB) ligand, osteoprotegerin, and receptor activator of NF-kappaB in mouse calvarial bones. Endocrinology. 2006;147(7):3613-22.

289. Sambrook PN, Cohen ML, Eisman JA, Pocock NA, Champion GD, Yeates MG. Effects of low dose corticosteroids on bone mass in rheumatoid arthritis: a longitudinal study. Annals of the Rheumatic Diseases. 1989;48(7):535-8.
290. Sambrook PN, Eisman JA, Yeates MG, Pocock NA, Eberl S, Champion GD. Osteoporosis in rheumatoid arthritis: safety of low dose corticosteroids. Annals of the Rheumatic Diseases. 1986;45(11):950-3.
291. Wijbrandts CA, Klaasen R, Dijkgraaf MGW, Gerlag DM, van Eck-Smit BLF, Tak PP. Bone mineral density in rheumatoid arthritis patients 1 year after adalimumab therapy: arrest of bone loss. Annals of the Rheumatic Diseases. 2009;68(3):373-6.
292. Pereira RM, Corrente JE, Chahade WH, Yoshinari NH. Evaluation by dual X-ray absorptiometry (DXA) of bone mineral density in children with juvenile chronic arthritis. Clin Exp Rheumatol. 1998;16(4):495-501.
293. Varonos S, Ansell BM, Reeve J. Vertebral collapse in juvenile chronic arthritis: its relationship with glucocorticoid therapy. Calcif Tissue Int. 1987;41(2):75-8.
294. Haugeberg G, Uhlig T, Falch JA, Halse JI, Kvien TK. Bone mineral density and frequency of osteoporosis in female patients with rheumatoid arthritis: Results from 394 patients in the Oslo County rheumatoid arthritis register. Arthritis & Rheumatism. 2000;43(3):522-30.
295. Camplejohn KL, Allard SA. Limitations of safranin 'O' staining in proteoglycan-depleted cartilage demonstrated with monoclonal antibodies. Histochemistry. 1988;89(2):185-8.
296. Raff H, Sharma ST, Nieman LK. Physiological basis for the etiology, diagnosis, and treatment of adrenal disorders: Cushing's syndrome, adrenal insufficiency, and congenital adrenal hyperplasia. Compr Physiol. 2014;4(2):739-69.
297. Gasparini SJ, Weber MC, Henneicke H, Kim S, Zhou H, Seibel MJ. Continuous corticosterone delivery via the drinking water or pellet implantation: A comparative study in mice. Steroids. 2016;116:76-82.
298. Akahoshi T, Wada C, Endo H, Hirota K, Hosaka S, Takagishi K, et al. Expression of monocyte chemotactic and activating factor in rheumatoid arthritis. Regulation of its production in synovial cells by interleukin-1 and tumor necrosis factor. Arthritis Rheum. 1993;36(6):762-71.
299. Hanaoka R, Kasama T, Muramatsu M, Yajima N, Shiozawa F, Miwa Y, et al. A novel mechanism for the regulation of IFN-gamma inducible protein-10 expression in rheumatoid arthritis. Arthritis Res Ther. 2003;5(2):R74-81.
300. Ha J, Choi HS, Lee Y, Kwon HJ, Song YW, Kim HH. CXC chemokine ligand 2 induced by receptor activator of NF-kappa B ligand enhances osteoclastogenesis. J Immunol. 2010;184(9):4717-24.
301. Shahrara S, Proudfoot AE, Park CC, Volin MV, Haines GK, Woods JM, et al. Inhibition of monocyte chemoattractant protein-1 ameliorates rat adjuvant-induced arthritis. J Immunol. 2008;180(5):3447-56.
302. Komano Y, Nanki T, Hayashida K, Taniguchi K, Miyasaka N. Identification of a human peripheral blood monocyte subset that differentiates into osteoclasts. Arthritis Research & Therapy. 2006;8(5):R152.
303. Gravallese EM, Manning C, Tsay A, Naito A, Pan C, Amento E, et al. Synovial tissue in rheumatoid arthritis is a source of osteoclast differentiation factor. Arthritis Rheum. 2000;43(2):250-8.
304. Adamopoulos I, Sabokbar A, Wordsworth B, Carr A, Ferguson D, Athanasou N. Synovial fluid macrophages are capable of osteoclast formation and resorption. The Journal of Pathology. 2006;208(1):35-43.
305. Kudo O, Fujikawa Y, Itonaga I, Sabokbar A, Torisu T, Athanasou NA. Proinflammatory cytokine (TNFalpha/IL-1alpha) induction of human osteoclast formation. J Pathol. 2002;198(2):220-7.
306. Kim N, Kadono Y, Takami M, Lee J, Lee S-H, Okada F, et al. Osteoclast differentiation independent of the TRANCE–RANK–TRAF6 axis. The Journal of Experimental Medicine. 2005;202(5):589-95.
307. Kroger H, Risteli J, Risteli L, Penttila I, Alhava E. Serum osteocalcin and carboxyterminal propeptide of type I procollagen in rheumatoid arthritis. Ann Rheum Dis. 1993;52(5):338-42.
308. Ton FN, Gunawardene SC, Lee H, Neer RM. Effects of Low-Dose Prednisone on Bone Metabolism. Journal of Bone and Mineral Research. 2005;20(3):464-70.

309. Fenton CG, Webster JM, Martin CS, Fareed S, Wehmeyer C, Mackie H, et al. Therapeutic glucocorticoids prevent bone loss but drive muscle wasting when administered in chronic polyarthritis. Arthritis Research & Therapy. 2019;21(1):182.
310. Hsu E, Nanes M. Advances in treatment of glucocorticoid-induced osteoporosis. Curr Opin Endocrinol Diabetes Obes. 2017;24(6):411-7.
311. Fenton CG, Doig CL, Fareed S, Naylor A, Morrell AP, Addison O, et al. 11β-HSD1 plays a critical role in trabecular bone loss associated with systemic glucocorticoid therapy. Arthritis Research & Therapy. 2019;21(1):188.
312. Walsh LJ, Wong CA, Pringle M, Tattersfield AE. Use of oral corticosteroids in the community and the prevention of secondary osteoporosis: a cross sectional study. Bmj. 1996;313(7053):344-6.
313. McDonough AK, Curtis JR, Saag KG. The epidemiology of glucocorticoid-associated adverse events. Curr Opin Rheumatol. 2008;20(2):131-7.
314. Van Staa TP, Leufkens HG, Abenhaim L, Zhang B, Cooper C. Use of oral corticosteroids and risk of fractures. June, 2000. J Bone Miner Res. 2005;20(8):1487-94; discussion 6.
315. Cooper MS, Blumsohn A, Goddard PE, Bartlett WA, Shackleton CH, Eastell R, et al. 11β-Hydroxysteroid Dehydrogenase Type 1 Activity Predicts the Effects of Glucocorticoids on Bone. The Journal of Clinical Endocrinology & Metabolism. 2003;88(8):3874-7.
316. Ersek A, Santo AI, Vattakuzhi Y, George S, Clark AR, Horwood NJ. Strain dependent differences in glucocorticoid-induced bone loss between C57BL/6J and CD-1 mice. Sci Rep. 2016;6:36513.
317. Dovio A, Perazzolo L, Osella G, Ventura M, Termine A, Milano E, et al. Immediate fall of bone formation and transient increase of bone resorption in the course of high-dose, short-term glucocorticoid therapy in young patients with multiple sclerosis. J Clin Endocrinol Metab. 2004;89(10):4923-8.
318. Ma J, Siminoski K, Alos N, Halton J, Ho J, Cummings EA, et al. Impact of Vertebral Fractures and Glucocorticoid Exposure on Height Deficits in Children During Treatment of Leukemia. The Journal of clinical endocrinology and metabolism. 2019;104(2):213-22.
319. Chang MK, Raggatt LJ, Alexander KA, Kuliwaba JS, Fazzalari NL, Schroder K, et al. Osteal tissue macrophages are intercalated throughout human and mouse bone lining tissues and regulate osteoblast function in vitro and in vivo. J Immunol. 2008;181(2):1232-44.
320. Buchman AL. Side effects of corticosteroid therapy. J Clin Gastroenterol. 2001;33(4):289-94.
321. Tuckermann JP, Kleiman A, Moriggl R, Spanbroek R, Neumann A, Illing A, et al. Macrophages and neutrophils are the targets for immune suppression by glucocorticoids in contact allergy. The Journal of Clinical Investigation. 2007;117(5):1381-90.
322. Wang B, Fujisawa H, Zhuang L, Freed I, Howell BG, Shahid S, et al. CD4+ Th1 and CD8+ type 1 cytotoxic T cells both play a crucial role in the full development of contact hypersensitivity. J Immunol. 2000;165(12):6783-90.
323. Baschant U, Frappart L, Rauchhaus U, Bruns L, Reichardt HM, Kamradt T, et al. Glucocorticoid therapy of antigen-induced arthritis depends on the dimerized glucocorticoid receptor in T cells. Proc Natl Acad Sci U S A. 2011;108(48):19317-22.
324. Coutinho AE, Gray M, Brownstein DG, Salter DM, Sawatzky DA, Clay S, et al. 11β-Hydroxysteroid dehydrogenase type 1, but not type 2, deficiency worsens acute inflammation and experimental arthritis in mice. Endocrinology. 2012;153(1):234-40.
325. Turner JD, Filer A. The role of the synovial fibroblast in rheumatoid arthritis pathogenesis. Curr Opin Rheumatol. 2015;27(2):175-82.
326. Hessels AC, Tuin J, Sanders JSF, Huitema MG, van Rossum EFC, Koper JW, et al. Clinical outcome in anti-neutrophil cytoplasmic antibody-associated vasculitis and gene variants of 11beta-hydroxysteroid dehydrogenase type 1 and the glucocorticoid receptor. Rheumatology (Oxford). 2019;58(3):447-54.
327. van der Heijde D. Radiographic progression in rheumatoid arthritis: does it reflect outcome? Does it reflect treatment? Ann Rheum Dis. 2001;60 Suppl 3(Suppl 3):iii47-iii50.

328. Boers M, Verhoeven AC, Markusse HM, van de Laar MA, Westhovens R, van Denderen JC, et al. Randomised comparison of combined step-down prednisolone, methotrexate and sulphasalazine with sulphasalazine alone in early rheumatoid arthritis. Lancet. 1997;350(9074):309-18.
329. van Gestel AM, Anderson JJ, van Riel PL, Boers M, Haagsma CJ, Rich B, et al. ACR and EULAR improvement criteria have comparable validity in rheumatoid arthritis trials. American College of Rheumatology European League of Associations for Rheumatology. J Rheumatol. 1999;26(3):705-11.
330. Conaghan PG, O'Connor P, McGonagle D, Astin P, Wakefield RJ, Gibbon WW, et al. Elucidation of the relationship between synovitis and bone damage: a randomized magnetic resonance imaging study of individual joints in patients with early rheumatoid arthritis. Arthritis Rheum. 2003;48(1):64-71.
331. Haavardsholm EA, Boyesen P, Ostergaard M, Schildvold A, Kvien TK. Magnetic resonance imaging findings in 84 patients with early rheumatoid arthritis: bone marrow oedema predicts erosive progression. Ann Rheum Dis. 2008;67(6):794-800.
332. Li P, Schwarz EM, O'Keefe RJ, Ma L, Boyce BF, Xing L. RANK signaling is not required for TNFalpha-mediated increase in CD11(hi) osteoclast precursors but is essential for mature osteoclast formation in TNFalpha-mediated inflammatory arthritis. J Bone Miner Res. 2004;19(2):207-13.
333. Rahimi P, Wang CY, Stashenko P, Lee SK, Lorenzo JA, Graves DT. Monocyte chemoattractant protein-1 expression and monocyte recruitment in osseous inflammation in the mouse. Endocrinology. 1995;136(6):2752-9.
334. Kim MS, Day CJ, Morrison NA. MCP-1 is induced by receptor activator of nuclear factor-{kappa}B ligand, promotes human osteoclast fusion, and rescues granulocyte macrophage colony-stimulating factor suppression of osteoclast formation. J Biol Chem. 2005;280(16):16163-9.
335. Huynh PT, Beswick EJ, Coronado YA, Johnson P, O'Connell MR, Watts T, et al. CD90(+) stromal cells are the major source of IL-6, which supports cancer stem-like cells and inflammation in colorectal cancer. Int J Cancer. 2016;138(8):1971-81.
336. Rogler G, Gelbmann CM, Vogl D, Brunner M, Scholmerich J, Falk W, et al. Differential activation of cytokine secretion in primary human colonic fibroblast/myofibroblast cultures. Scand J Gastroenterol. 2001;36(4):389-98.
337. Rougier F, Cornu E, Praloran V, Denizot Y. IL-6 and IL-8 production by human bone marrow stromal cells. Cytokine. 1998;10(2):93-7.
338. Huh J-E, Lee SY. IL-6 is produced by adipose-derived stromal cells and promotes osteogenesis. Biochimica et Biophysica Acta (BBA) - Molecular Cell Research. 2013;1833(12):2608-16.
339. Hardy RS, Doig CL, Hussain Z, O'Leary M, Morgan SA, Pearson MJ, et al. 11beta-Hydroxysteroid dehydrogenase type 1 within muscle protects against the adverse effects of local inflammation. J Pathol. 2016;240(4):472-83.
340. Zhang Z, Coutinho AE, Man TY, Kipari TMJ, Hadoke PWF, Salter DM, et al. Macrophage 11β-HSD-1 deficiency promotes inflammatory angiogenesis. J Endocrinol. 2017;234(3):291-9.
341. Zhang TY, Daynes RA. Macrophages from 11beta-hydroxysteroid dehydrogenase type 1-deficient mice exhibit an increased sensitivity to lipopolysaccharide stimulation due to TGF-beta-mediated up-regulation of SHIP1 expression. J Immunol. 2007;179(9):6325-35.
342. Buttgereit F, Zhou H, Kalak R, Gaber T, Spies CM, Huscher D, et al. Transgenic disruption of glucocorticoid signaling in mature osteoblasts and osteocytes attenuates K/BxN mouse serum–induced arthritis in vivo. Arthritis & Rheumatism. 2009;60(7):1998-2007.
343. Schett G, Gravallese E. Bone erosion in rheumatoid arthritis: mechanisms, diagnosis and treatment. Nat Rev Rheumatol. 2012;8(11):656-64.
344. Malysheva K, de Rooij K, Lowik CW, Baeten DL, Rose-John S, Stoika R, et al. Interleukin 6/Wnt interactions in rheumatoid arthritis: interleukin 6 inhibits Wnt signaling in synovial fibroblasts and osteoblasts. Croat Med J. 2016;57(2):89-98.
345. Colditz J, Thiele S, Baschant U, Niehrs C, Bonewald LF, Hofbauer LC, et al. Postnatal Skeletal Deletion of Dickkopf-1 Increases Bone Formation and Bone Volume in Male and Female Mice, Despite Increased Sclerostin Expression. Journal of Bone and Mineral Research. 2018;33(9):1698-707.

346. de Sousa Abreu R, Penalva LO, Marcotte EM, Vogel C. Global signatures of protein and mRNA expression levels. Mol Biosyst. 2009;5(12):1512-26.
347. Fraser LA, Adachi JD. Glucocorticoid-induced osteoporosis: treatment update and review. Ther Adv Musculoskelet Dis. 2009;1(2):71-85.
348. Morgan SA, McCabe EL, Gathercole LL, Hassan-Smith ZK, Larner DP, Bujalska IJ, et al. 11β-HSD1 is the major regulator of the tissue-specific effects of circulating glucocorticoid excess. Proceedings of the National Academy of Sciences. 2014;111(24):E2482-E91.
349. Ersek A, Santo AIE, Vattakuzhi Y, George S, Clark AR, Horwood NJ. Strain dependent differences in glucocorticoid-induced bone loss between C57BL/6J and CD-1 mice. Scientific Reports. 2016;6:36513.
350. Baschant U, Frappart L, Rauchhaus U, Bruns L, Reichardt HM, Kamradt T, et al. Glucocorticoid therapy of antigen-induced arthritis depends on the dimerized glucocorticoid receptor in T cells. Proceedings of the National Academy of Sciences. 2011;108(48):19317-22.
351. Kocijan R, Finzel S, Englbrecht M, Engelke K, Rech J, Schett G. Decreased quantity and quality of the periarticular and nonperiarticular bone in patients with rheumatoid arthritis: a cross-sectional HR-pQCT study. J Bone Miner Res. 2014;29(4):1005-14.
352. Cooper MS, Rabbitt EH, Goddard PE, Bartlett WA, Hewison M, Stewart PM. Osteoblastic 11β-Hydroxysteroid Dehydrogenase Type 1 Activity Increases With Age and Glucocorticoid Exposure. Journal of Bone and Mineral Research. 2002;17(6):979-86.
353. Khan D, Ansar Ahmed S. The Immune System Is a Natural Target for Estrogen Action: Opposing Effects of Estrogen in Two Prototypical Autoimmune Diseases. *Front Immunol*. 2016;6:635. Published 2016 Jan 6. doi:10.3389/fimmu.2015.00635
354. Morgan, R.A., Beck, K.R., Nixon, M. *et al.* Carbonyl reductase 1 catalyzes 20β-reduction of glucocorticoids, modulating receptor activation and metabolic complications of obesity. *Sci Rep* **7,** 10633 (2017). https://doi.org/10.1038/s41598-017-10410-1
355. Pal SB. 6-Hydroxylation of cortisol and urinary 6β-hydroxycortisol. Metabolism. 1978 Aug 1;27(8):1003-11.

Publications

Arthritis Research & Therapy

RESEARCH ARTICLE Open Access

Therapeutic glucocorticoids prevent bone loss but drive muscle wasting when administered in chronic polyarthritis

C. G. Fenton[1,2†], J. M. Webster[2,4†], C. S. Martin[2], S. Fareed[2], C. Wehmeyer[1], H. Mackie[7], R. Jones[3], A. P. Seabright[9], J. W. Lewis[1,3], Y. C. Lai[2,3,9], C. S. Goodyear[7], S. W Jones[1], M. S. Cooper[5], G. G. Lavery[2,4], R. Langen[8], K. Raza[1,6] and R. S. Hardy[1,2,3,10*]

Abstract

Background: Patients with rheumatoid arthritis (RA) experience extra-articular manifestations including osteoporosis and muscle wasting, which closely associate with severity of disease. Whilst therapeutic glucocorticoids (GCs) reduce inflammation in RA, their actions on muscle and bone metabolism in the context of chronic inflammation remain unclear. We utilised the TNF-tg model of chronic polyarthritis to ascertain the impact of therapeutic GCs on bone and muscle homeostasis in the context of systemic inflammation.

Methods: TNF-tg and wild-type (WT) animals received either vehicle or the GC corticosterone (100 μg/ml) in drinking water at onset of arthritis. Arthritis severity and clinical parameters were measured, serum collected for ELISA and muscle and bone biopsies collected for μCT, histology and mRNA analysis. In vivo findings were examined in primary cultures of osteoblasts, osteoclasts and myotubes.

Results: TNF-tg mice receiving GCs showed protection from inflammatory bone loss, characterised by a reduction in serum markers of bone resorption, osteoclast numbers and osteoclast activity. In contrast, muscle wasting was markedly increased in WT and TNF-tg animals receiving GCs, independently of inflammation. This was characterised by a reduction in muscle weight and fibre size, and an induction in anti-anabolic and catabolic signalling.

Conclusions: This study demonstrates that when given in early onset chronic polyarthritis, oral GCs partially protect against inflammatory bone loss, but induce marked muscle wasting. These results suggest that in patients with inflammatory arthritis receiving GCs, the development of interventions to manage deleterious side effects in muscle should be prioritised.

Keywords: Polyarthritis, Glucocorticoids, Muscle wasting, Osteoporosis

Introduction

Patients with inflammatory arthritis experience extra-articular manifestations, including osteoporosis and muscle wasting, which closely correlate with measures of disease activity [1–4]. Glucocorticoids (GCs) are effective at controlling inflammation in rheumatoid arthritis (RA) and are recommended as an initial line of therapy for the rapid control of disease [5–7]. However, long-term GC use is associated with osteoporosis and systemic muscle wasting, resulting in increased fracture risk and mortality in patients with RA [8–13].

It remains unclear what the effects of GCs on bone and muscle are, when used to treat new onset inflammatory arthritis, in particular, whether the beneficial effects of controlling articular and systemic inflammation on bone and muscle outweigh their direct catabolic actions in these tissues.

Murine models of polyarthritis have proven a powerful tool in examining the pathophysiology of inflammatory diseases, such as RA. The TNF-tg mouse is a murine

* Correspondence: r.hardy@bham.ac.uk
Fenton CG and Webster JM shared joint authorship.
[1]Institute of Inflammation and Ageing, University of Birmingham, Birmingham, UK
[2]Institute of Metabolism and Systems Research, University of Birmingham, Birmingham, UK
Full list of author information is available at the end of the article

model of polyarthritis driven by the transgenic overexpression of the pro-inflammatory cytokine TNFα that proved valuable in the initial validation of anti-TNFα biologicals [14]. We have previously shown that this animal model develops systemic bone loss and muscle wasting in a manner consistent with human disease [15, 16]. In this study, we use the TNF-tg model of polyarthritis and wild-type (WT) counterparts to examine the effects of orally administered anti-inflammatory GCs on bone and muscle metabolism in the context of systemic inflammation. We demonstrate that during active polyarthritis, therapeutic GCs are effective at suppressing synovitis, joint destruction and systemic bone loss, but markedly promote systemic muscle wasting.

Materials and methods

TNF-transgenic mouse model

Procedures on animals were performed under guidelines by the Animal (Scientific Procedures) Act 1986 in accordance with the project licence (P51102987) and approved by the Birmingham Ethical Review Subcommittee (BERSC). The TNF-tg model of chronic inflammatory polyarthritis, obtained courtesy of Dr. George Kollias (BSRC Fleming, Athens), were maintained on a C57BL/6 background and compared to WT littermates [17]. At day 32 of age, at the first onset of measurable polyarthritis, male TNF-tg mice received drinking water supplemented with either corticosterone (Cort) (100 μg/mL, 0.66% ethanol), or vehicle (0.66% ethanol) for 3 weeks. Interventions were designed to model initial preventative bridging therapeutic glucocorticoid treatments in early onset disease. Following the administration of vehicle and corticosterone, mice were scored twice weekly for clinical scores of disease activity and arthritic paw scores as previously described [18, 19]. Mobility of animals within cages was assessed by measuring numbers of rotations walked by animals in a 3-min period and normalised to rotations per minute to get an activity score. At day 53, serum was collected by cardiac puncture under terminal anaesthesia, and tissues excised for analysis. Wet tissue weights (mg) of tibialis anterior, quadriceps and tibia were recorded, normalised to total body weights and either snap frozen of fixed in 4% formalin (mg).

Primary human osteoblast culture

Following ethical approval (UK National Research Ethics Committee 14/ES/1044), patients with hip osteoarthritis (OA) (age 69±3 years, Kellgren Lawrence grade 3/4; $n = 4$) were recruited prior to elective joint replacement surgery. Trabecular chips of approximately 400–600 mg were excised and placed in PBS prior to culturing. Reagents were obtained from Sigma (Gillingham, UK) unless otherwise stated. Trabecular bone chips from patient samples were cultured in osteoclast growth media to facilitate release of osteoblasts (Additional file 1: Table S1). Osteoblasts were allowed to grow and once confluent bone chips were removed. Osteoblasts were then differentiated in media containing TNFα (10 ng/ml) and/or cortisol (1000 ng/ml). Treatments were replaced three times per week. Cultures were stained with 0.5% alizarin red S to confirm differentiation into mature osteoblasts.

Primary human osteoclast culture

Peripheral blood mononuclear cells (PBMCs) from healthy donors, obtained from the Scottish National Blood Transfusion Service (approved by Glasgow NHS Trust-East Ethics Committee), were isolated via Ficoll-paque PLUS (GE Healthcare) density gradient centrifugation and $CD14^+$ monocytes isolated using positive selection (Miltenyi). Monocytes were cultured in selective survival media (Additional file 1: Table S1). Osteoclasts were generated using supplementation with 1 ng/ml RANKL over 72 h before stimulation with vehicle, 10 ng/ml TNFα or 1000 ng/ml corticosterone (or DMSO vehicle) as appropriate. Osteoclast numbers were assessed by staining with tartrate-resistant acid phosphatase (TRAP) kit (Sigma-Aldrich). Osteoclast activity was assessed on mineral-coated plates (Corning) at day 14. Images were acquired using EVOS FL Auto Cell Imaging System (Life Technologies). Osteoclasts were identified as TRAP +ve multinucleated cells (nuclei ≥ 3). Resorption area was calculated using Fiji software (ImageJ) and defined as % resorbed area of entire well.

Primary murine muscle cell culture

Primary myotubes were generated from tibialis anterior as previously described [20]. In brief, whole tibialis anterior muscle was removed from WT C57/Bl6 animals at 9 weeks and digested in type 1 collagenase at 37 °C for 2 h before isolation of individual fibres. Fibres were plated in 2 ml of muscle expansion medium (Additional file 1: Table S1) and grown in plates coated with Matrigel™ (Corning Life Sciences, Flintshire, UK) (diluted 1/40 in DMEM High Glucose). Satellite cells migrating from muscle fibres were removed and cultured in maintenance medium until confluent, prior to differentiation in selective media for 5 days (Additional file 1: Table S1).

Gene expression analysis

Gene expression in cells and tissues was assessed using TaqMan® Gene Expression Assays (ThermoFisher Scientific). Tissues were homogenised in liquid nitrogen with a sterile pestle and mortar. mRNA was isolated using an innuPREP RNA Mini Kit (Analytikjena, Cambridge) as per the manufacturer's instructions. One microgramme of RNA per sample was reverse transcribed using Multiscribe™ using the manufacturer's

protocol (ThermoFisher Scientific) to generate cDNA. Alp, Bglap, Redd1, Foxo1, Trim63 and Fbxo32 were determined using species-specific probe sets by real-time PCR on an ABI7500 system (Applied Biosystems, Warrington, UK). Final reactions are listed in Additional file 1: Table S2. mRNA abundance was normalised to that of 18S or GAPDH. Data were obtained as Ct values and ΔCt determined (Ct target − Ct 18S/GAPDH). Data were expressed as arbitrary units (AU) using the following transformation: [arbitrary units (AU) = $1000 \times (2^{-\Delta ct})$].

ELISA analysis

Serum IL-6 (R&D Systems, Abingdon, UK), P1NP and CTX-1 (Immunodiagnostic Systems, Tyne & Wear, UK) and conditioned media pro-collagen I α1 (R&D Systems, Abingdon, UK) were determined using a commercially available ELISA assays in accordance with the manufacturer's instructions.

Histological analysis of joints and muscle

Histochemistry was performed on paraffin-embedded 10-μm sections of hind paws and quadriceps of WT and TNF-Tg animals following staining with haematoxylin and eosin. Pannus size at the metatarsal-phalangeal joint interface was determined using Image J software as previously reported [18]. Sections were deparaffinised and incubated in TRAP buffer (Additional file 1: Table S3) for 1 h at 37 °C to detect osteoclasts. Quantification of osteoclast numbers on the bone surface pannus interface of the ulna/humerus joint interface were normalised to bone surface area determined by image J analysis of TRAP-stained paraffin-embedded sections. Sections were stained with H&E prior to quantitative analysis in order to visualise pannus formation at the ankle joints and CSA of fibres. For all quantifications, the mean of data from three adjacent 10-μm sections cut from the centre of the joint or from the vastus medialis from six animals was utilised and assessed using Image J software.

MicroCT morphometry analysis

Front paws and tibias from mice were imaged using a Skyscan 1172 micro-CT scanner (Bruker) using X-ray beam settings of 60 kV/167 μA with a 0.5-mm aluminium filter. Projections were taken every 0.45° at 580-ms exposure. Image volumes were reconstructed using the Feldkamp algorithm (NRecon 1.6.1.5, Bruker) having applied beam hardening correction. Trabecular bone parameters (bone volume to tissue volume (BV/TV), trabecular thickness (Tb.Th) and trabecular number (Tb.N)) of the tibia were analysed using CTAn software. One millimetre of bone (150 sections) in the metaphyseal region beneath the growth plate was analysed, and regions of interest (ROI) were selected by drawing around the trabecular network for each cross-sectional slice. Front paws were reconstructed, and MeshLab 1.3.2 was used to generate meshes which could then be scored for bone erosions as described previously [18].

Immunoblot analysis

Briefly, muscle were homogenised in 10-fold volume excess of ice-cold sucrose lysis buffer (Additional file 1: Table S3). Protein concentration was determined using the Bradford protein assay (ThermoScientific). Forty microgrammes of protein was loaded into 4–12% Bis-Tris midi protein gels (Invitrogen) prior to electrophoresis. Proteins were transferred and blocked in blocking buffer (Additional file 1: Table S3) before incubation with primary antibodies (Additional file 1: Table S4) overnight at 4 °C. Membranes were then incubated in horseradish peroxidase-conjugated secondary antibody (1/10,000) at room temperature for 1 h. Antibody detection was performed via enhanced chemiluminescence horseradish peroxidase substrate detection kit (Millipore). Imaging was undertaken using a G:Box Chemi-XR5 (Syngene) and band quantification via (ImageJ). All data were corrected for protein loading as determined after Ponceau S staining (Sigma-Aldrich).

Statistical analysis

Statistical significance was defined as $P < 0.05$ (*$P < 0.05$; **$P < 0.01$; ***$P < 0.001$) using either an unpaired Student's t test or two way ANOVA with a Bonferroni correction Tukey post hoc analysis where a Gaussian distribution is identified.

Results

Oral GCs suppress disease activity in TNF-tg animals

TNF-tg mice received drinking water containing vehicle or corticosterone at 100 μg/ml for 3 weeks. Daily oral water intake of corticosterone was calculated per mouse and was shown to be 22.0 ± 0.83 and 23.2 ± 2.0 μg/g body weight/day and did not vary significantly between groups (Additional file 2: Figure S1a). Serum corticosterone was shown to be significantly elevated in both WT and TNF-tg animals receiving corticosterone following oral intake relative to vehicle-treated controls (WT vehicle, 128.3 ± 66.7, WT CORT, 456.2 ± 82.5 ng/ml; $P < 0.005$; TNF-tg vehicle, 119.8 ± 29.9, TNF-tg CORT, 485.1 ± 43.7 ng/ml; $P < 0.005$) (Additional file 2: Figure S1b). Body weights did not vary significantly between groups (Additional file 2: Figure S1c). TNF-tg mice developed significant joint inflammation by day 53, characterised by increased joint deformity, redness and reduced mobility (clinical score, wild type, 0.6 ± 0.004 vs TNF-tg, 6.2 ± 0.3; $P < 0.005$; joint inflammation, wild type, 0.16 ± 0.0001 vs TNF-tg, 7.2 ± 0.7; $P < 0.0001$) (Fig. 1a, b). Corticosterone significantly reduced joint inflammation in TNF-tg animals (clinical

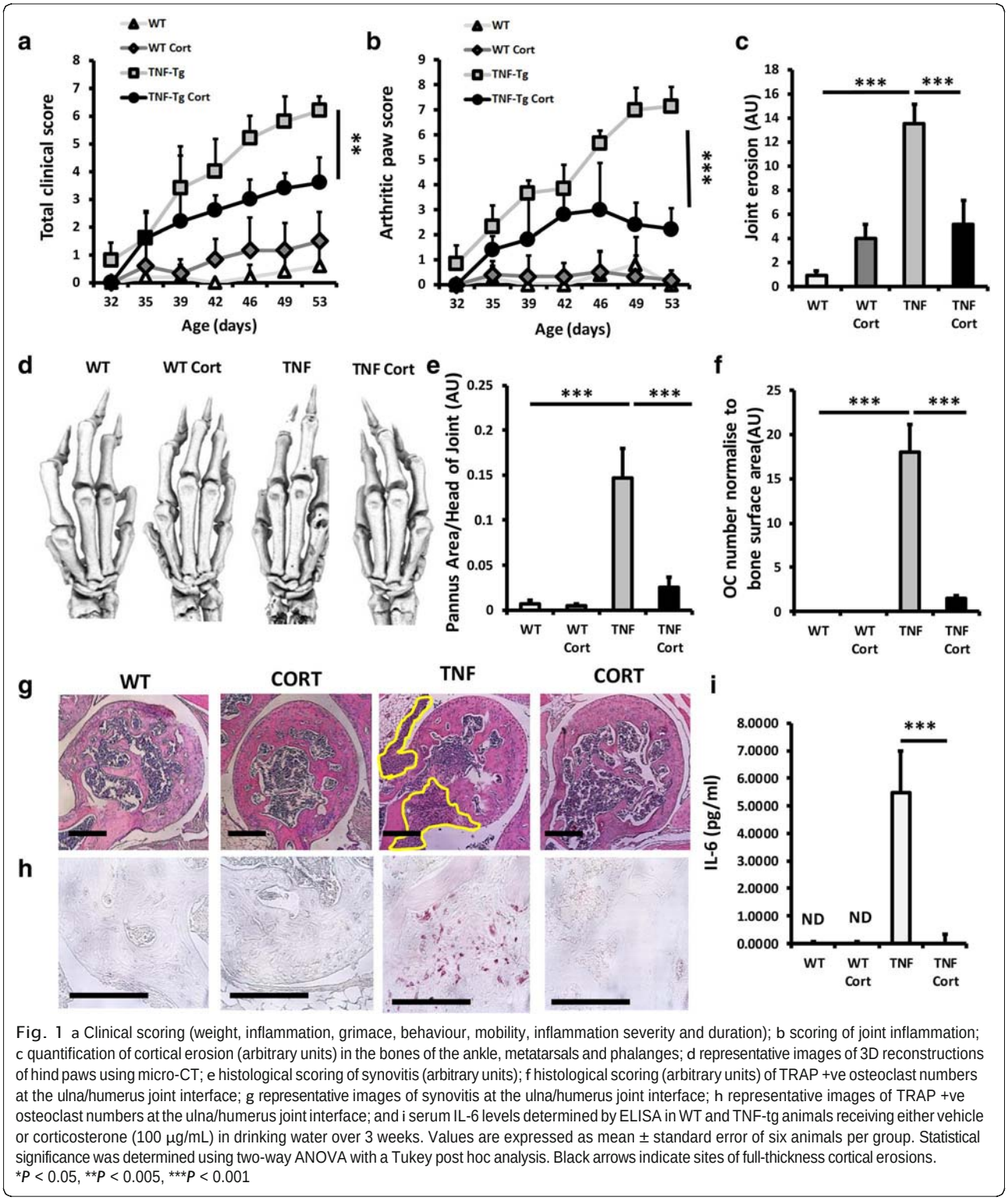

Fig. 1 a Clinical scoring (weight, inflammation, grimace, behaviour, mobility, inflammation severity and duration); b scoring of joint inflammation; c quantification of cortical erosion (arbitrary units) in the bones of the ankle, metatarsals and phalanges; d representative images of 3D reconstructions of hind paws using micro-CT; e histological scoring of synovitis (arbitrary units); f histological scoring (arbitrary units) of TRAP +ve osteoclast numbers at the ulna/humerus joint interface; g representative images of synovitis at the ulna/humerus joint interface; h representative images of TRAP +ve osteoclast numbers at the ulna/humerus joint interface; and i serum IL-6 levels determined by ELISA in WT and TNF-tg animals receiving either vehicle or corticosterone (100 μg/mL) in drinking water over 3 weeks. Values are expressed as mean ± standard error of six animals per group. Statistical significance was determined using two-way ANOVA with a Tukey post hoc analysis. Black arrows indicate sites of full-thickness cortical erosions. *P < 0.05, **P < 0.005, ***P < 0.001

score, TNF-tg/vehicle, 6.2 ± 0.3 vs TNF-tg/cort, 3.3 ± 0.9; P < 0.005; joint inflammation, TNF-tg/vehicle, 6.2 ± 0.3 vs TNF-tg/cort, 2.2 ± 0.4; P < 0.0005) (Fig. 1a, b) [21]. Scoring of synovitis and joint erosions by histology and micro-CT revealed a marked increase in vehicle-treated TNF-tg mice relative to WT controls (Fig. 1c, d, e, g). These were significantly abrogated in TNF-tg animals receiving corticosterone (joint erosion score, TNF-tg/vehicle, 13.6 ± 1.3 vs TNF-tg/cort, 5.3 ± 2.1; P < 0.0005, Pannus area, TNF-tg/vehicle, 0.14 ± 3.9 vs TNF-tg/cort, 0.025 ± 0.004;

$P < 0.0005$) (Fig. 1c, d, e, g). Juxta articular bone loss was characterised by increased osteoclast numbers at the pannus/subchondral bone interface (Fig 1f, h). Corticosterone treatment reversed this, dramatically reducing osteoclast numbers (TNF-tg/vehicle, 18 ± 3.3 vs TNF-tg/cort, 1.5 ± 0.2; $P < 0.0005$). Serum IL-6 was potently upregulated in vehicle-treated TNF-tg animals and strongly suppressed in animals receiving corticosterone. These data demonstrate that corticosterone administered at 100 μg/ml in drinking water over 3 weeks is sufficient to markedly suppress disease activity and joint destruction.

Oral GCs prevent trabecular bone loss during polyarthritis

In vehicle-treated TNF-tg animals, significant trabecular bone loss was apparent at day 53 (Fig. 2a). This appeared to be partially abrogated in TNF-tg animal receiving corticosterone. Analysis of trabecular bone volume to tissue volume (BV/TV), trabecular thickness (Tb.Th) and trabecular number (Tb.N) was performed in all groups. In vehicle-treated TNF-tg animals, a significant reduction in all parameters was apparent. Treatment with corticosterone partially protected from the loss in BV/TV (BV/TV: TNF-tg/vehicle, 2.1% ± 0.21 vs TNF-tg/corticosterone, 4.3%±0.23, $P < 0.05$) (Fig. 2b). Analysis of Tb.Th in TNF-tg animals revealed a similar loss of trabecular thickness in those treated with either vehicle or corticosterone (Tb.Th: TNF-tg/vehicle, 50.2 μm ± 3.7 vs TNF-tg/corticosterone, 50.6 μm ± 2.7, NS) (Fig. 2c). In contrast, corticosterone was able to protect against the reduction in trabecular number in this model of inflammatory polyarthritis (Tb.N: TNF-tg/vehicle, 0.0004 1/μm ± 0.00002 vs TNF-tg/corticosterone, 0.00083 1/μm± 0.00002, $P < 0.0001$) (Fig. 2d). Together these data demonstrate that oral administration of corticosterone provides partial protection from inflammatory bone loss in TNF-tg mice, characterised by preservation of trabecular number but not thickness.

GCs suppress both bone formation and resorption during inflammation

To delineate the actions of corticosterone on bone turnover in TNF-tg mice, we examined systemic markers of bone formation (P1NP) and resorption (CTX-1) and modelled therapeutic GC treatments in human cultures of osteoblasts and osteoclasts in combination with TNFα. Whilst TNF-tg animals had significantly lower P1NP levels at day 53 relative to WT counterparts, both groups developed a comparable suppression of P1NP in response

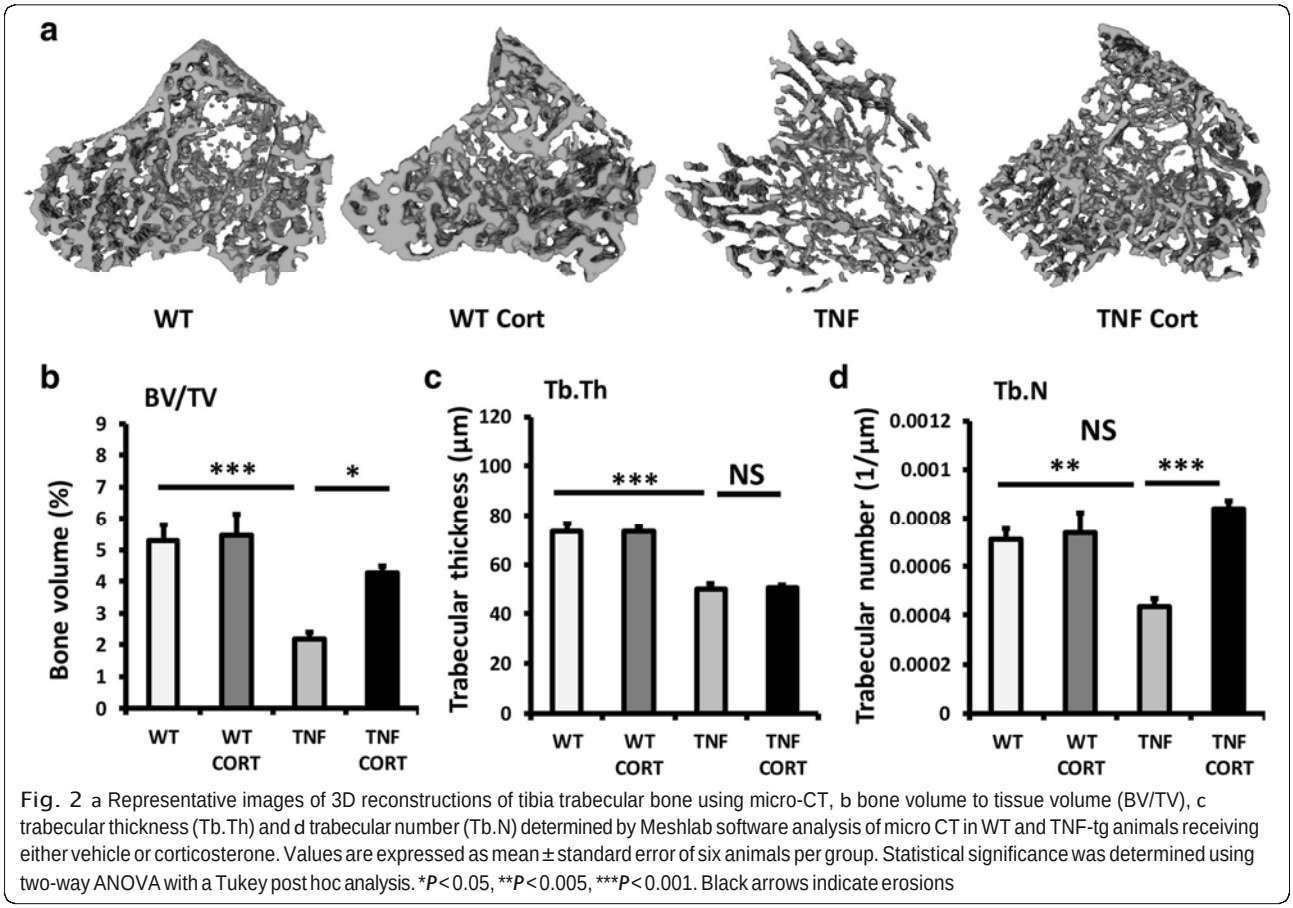

Fig. 2 a Representative images of 3D reconstructions of tibia trabecular bone using micro-CT, b bone volume to tissue volume (BV/TV), c trabecular thickness (Tb.Th) and d trabecular number (Tb.N) determined by Meshlab software analysis of micro CT in WT and TNF-tg animals receiving either vehicle or corticosterone. Values are expressed as mean ± standard error of six animals per group. Statistical significance was determined using two-way ANOVA with a Tukey post hoc analysis. *$P < 0.05$, **$P < 0.005$, ***$P < 0.001$. Black arrows indicate erosions

to corticosterone (wild type/vehicle, 494 ng/ml ± 46.3 vs wild type/corticosterone, 31.3 ng/ml ± 8.2; $P < 0.0001$, TNF-tg/vehicle, 269.7 ng/ml ± 27.2 vs TNF-tg/corticosterone, 32.3 ng/ml ± 7.5; $P < 0.0001$) (Fig. 3a). Analysis of mature osteoblast markers in tibia homogenates supported these data. Here, whilst gene expression of alkaline phosphatase (Alp) and osteocalcin (Bglap) were significantly reduced in TNF-tg animals at day 53 relative to WT counterparts (Alp, 2.2-fold; Bglap, 2.6-fold; $P < 0.0001$), a comparable suppression of gene expression was apparent in both groups receiving corticosterone relative to vehicle (wild type, 32-fold; $P < 0.0001$, TNF-tg, 6-fold; $P < 0.0001$) (Fig. 3b, c). In mature primary human osteoblasts, incubation with the pro-inflammatory cytokine TNFα resulted in a significant reduction in both pro-collagen production and osteocalcin mRNA (Fig. 3d, f).

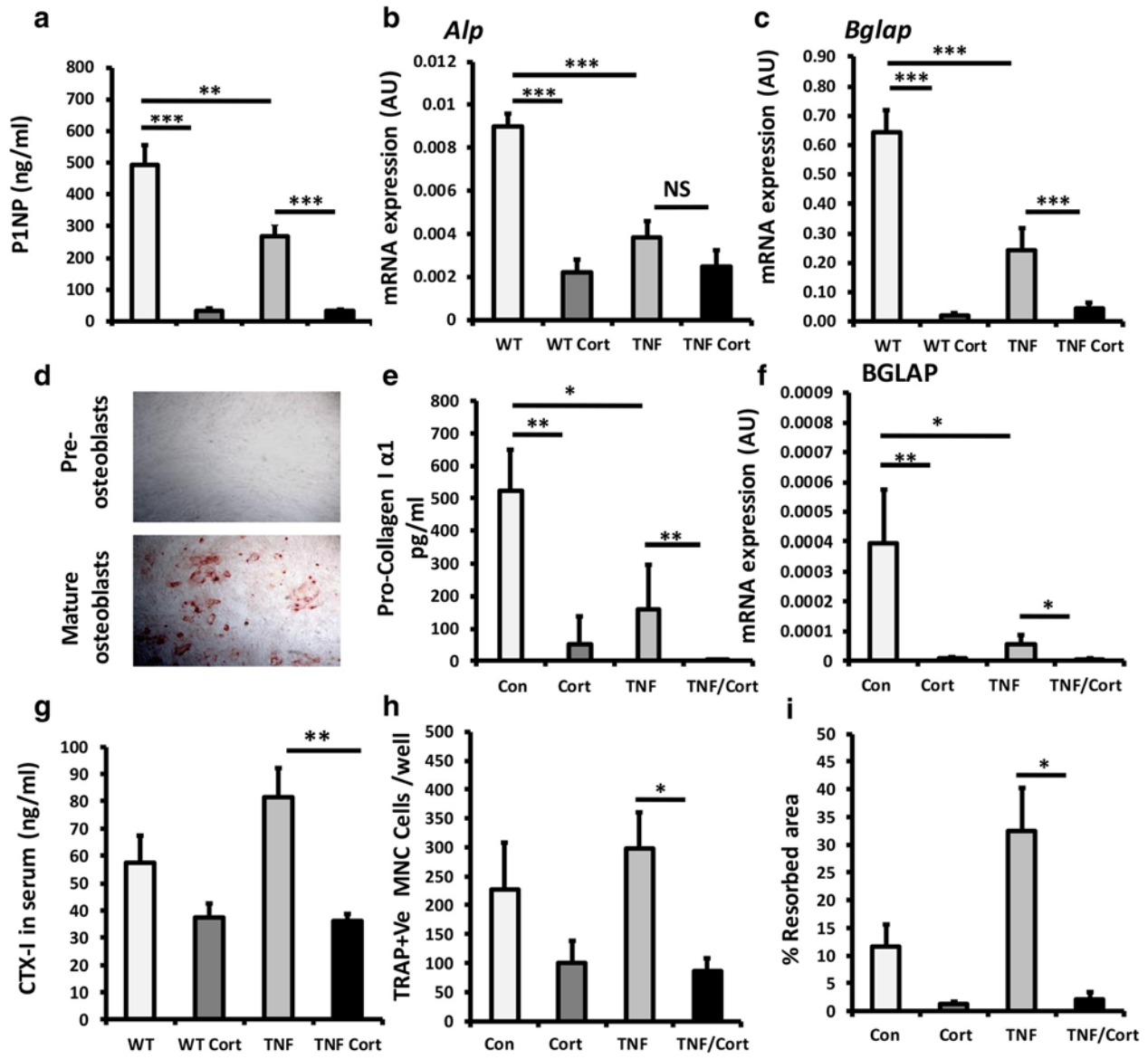

Fig. 3 a Serum P1NP (ng/ml) determined by ELISA. b, c Gene expression (AU) of Alp and Bglap, determined by RT qPCR in tibia homogenates, in WT and TNF-tg animals receiving either vehicle or corticosterone (100 μg/mL) in drinking water over 3 weeks. d Representative image of primary human pre-osteoblasts and mature nodule forming osteoblasts in vitro stained with alizarin red. e Pro-collagen 1 α1 formation determined by ELISA and f quantification of gene expression (arbitrary units) of Bglap, determined by RT qPCR in primary cultures of mature osteoblasts treated with either vehicle, TNFα (10 ng/ml), corticosterone (1 μmol/l) or a combination of TNF and corticosterone for 48 h. g Serum CTX-1 (ng/ml) determined by ELISA in WT and TNF-tg animals receiving either vehicle or corticosterone. h TRAP +ve cells per well and i % calcified matrix resorption in primary human osteoclasts cultures treated with either vehicle, TNFα (10 ng/ml), corticosterone (1 μmol/l) or a combination of TNFα and corticosterone over differentiation from mononuclear cells. Values are expressed as mean ± standard error of six animals or primary cultures derived from six separate individuals. Statistical significance was determined using either two-way or one-way ANOVA with Tukey post hoc analysis. *$P < 0.05$, **$P < 0.005$, ***$P < 0.001$

Here, the addition of the GC cortisol resulted in a comparable and dramatic suppression of osteoblast matrix formation and mRNA expression in control and TNFα-treated osteoblasts (pro-collagen Iα1, control, 524 ng/ml ± 128.9 vs cortisol, 50.0 ng/ml ± 93.1, $P < 0.001$, TNFα, 158.2 ng/ml ± 131.4 vs TNFα/cortisol, 11.3 ng/ml ± 6.8; $P < 0.001$; BGLAP, control vs cortisol, 43-fold suppression; $P < 0.001$, TNFα vs TNFα/cortisol; 10-fold suppression; $P < 0.05$).

Serum CTX-1 levels were determined as a measure of osteoclastic bone resorption. TNF-tg animals receiving corticosterone had a significant suppression of CTX-1 at day 53 (TNF-tg/vehicle, 87.6 ng/ml ± 11.3 vs TNF-tg/corticosterone, 36.3 ng/ml ± 3.1; $P < 0.05$) (Fig. 3g). In primary human osteoclasts, the addition of cortisol to TNFα-stimulated cultures resulted in a significant suppression of both osteoclast numbers and calcified matrix resorption in vitro (osteoclast no., TNFα, 297.5 cells per well ± 53.7 vs TNFα/cortisol, 85.6 cells per well ± 17.8; $P < 0.05$; resorbed area, TNFα, 32.5% ± 7.0 vs TNFα/cortisol, 2.1% ± 0.8; $P < 0.05$) (Fig. 3h, i). The resorption pits in wells treated with cortisol were characterised by a reduction in both number and size (Additional file 3: Figure S2a). These data indicate that GCs suppress both osteoblast bone formation and osteoclast maturation and activity.

Oral GCs drive severe muscle wasting and reduce mobility in TNF-tg animals

We examined muscle weights and morphology in WT and TNF-tg animals receiving corticosterone. Corticosterone significantly reduced quadriceps and tibialis anterior weights in WT and TNF-tg animals relative to vehicle controls (quadriceps, wild type/vehicle, 0.0029 mg/body weight ± 0.00024 vs wild type/corticosterone, 0.0019 mg/body weight ± 0.00021; $P < 0.0001$; TNF-tg/vehicle, 0.0025.7 mg/body weight ± 0.00025 vs TNF-tg/corticosterone, 0.0017 mg/body weight ± 0.00028; $P < 0.001$) (Fig. 4a, b). Analysis of animal mobility with cages was assessed at day 53 to determine the effects of polyarthritis and corticosterone treatment (Fig. 4c). Here, a significant reduction in movement was apparent in TNF-tg animals relative to WT counterparts. This was mirrored by a comparable reduction in movement seen in both WT and TNF-tg animals receiving corticosterone relative to vehicle-treated WT counterparts. Analysis of average muscle fibre cross-sectional area (CSA) indicated that this was underpinned by a reduction in muscle fibre size in WT and TNF-tg animals receiving corticosterone (fibre size, wild type/vehicle, 2064 μm^2 ± 144 vs wild type/corticosterone, 1636 μm^2 ± 96; $P < 0.05$; TNF-tg/vehicle, 1767 μm^2 ± 76 vs TNF-tg/corticosterone, 1559 μm^2 ± 88; $P < 0.05$) (Fig. 4c–e). Further analysis of fibre CSA distribution identified a significant shift towards increased small diameter fibres in TNF-tg animals relative to WT counterparts (Fig. 4e). In response to corticosterone, both WT and TNF-tg animals demonstrated a further shift in fibre CSA distribution, favouring a significant increase in small fibres (800–1800 μm^2) and significant reduction in large fibres (2200–2600 μm^2) relative to vehicle-treated controls (Fig. 4f, g). In contrast, no significant shift was observed between WT and TNF-tg animals receiving corticosterone (Fig 4h). These data demonstrate that during active polyarthritis, administration of oral corticosterone promotes muscle wasting independent of inflammation.

During inflammation, oral GCs drive catabolic and anti-anabolic muscle wasting

To ascertain the pathways that underpin increased muscle wasting in TNF-tg mice treated with GCs, we examined well-defined catabolic and anti-anabolic signalling pathways in tibialis anterior muscle homogenates and in primary muscle cultures. In wild-type animals, corticosterone resulted in a comparable induction in expression of the anti-anabolic gene Redd1 and the catabolic genes Foxo1, Trim63 and Fbxo32 (Redd1, 7.7-fold; $P < 0.005$; Foxo1, 10.3-fold; $P < 0.0005$; Trim63, 7.8-fold; $P < 0.05$; Fbxo32, 8.9-fold; $P < 0.0005$) (Fig. 5a–d). Comparable inductions in gene expression of Foxo1, Trim63 and Fxo32 were also apparent in TNF-tg animals receiving corticosterone (Foxo1, 3.1; $P < 0.005$, Trim63, 3.2-fold; $P < 0.05$; Fbxo32, 5.2-fold; $P < 0.0005$) (Fig. 5b–d, Additional file 4: Figure S3). These results were supported by a marked increase in protein expression of both phosphorylated and total Foxo1 in WT and TNF-tg animals in response to corticosterone (Fig. 5j). In contrast, expression of anabolic factors such as EF2 did not differ between groups. A deeper analysis of muscle gene expression was performed examining catabolic signalling and E3 ligases (*Foxo1, Fbxo32, Trim63, Ube3a*), anabolic and anti-anabolic myokines and signalling (*Igf1, Igf2, Mstn, Redd1*), muscle differentiation (*Myog, MyoD, Myf5, Myf6*) and inflammatory myokines and signalling (*Tnfa, Il6, Cxcl1, IkBa*) (Additional file 3: Figure S2a-p). In addition to the upregulation of all atrogenes examined, gene expression of the inflammatory myokines *Il6* and *Cxcl1* showed evidence of suppression in response to corticosterone in line with expected anti-inflammatory action. Similar observations were apparent in primary cultures of murine muscle cells treated with corticosterone. Here, a significant upregulation was observed in Trim63 and Fbxo32 regardless of inflammatory stimulation with TNFα (Fig. 5e–i). These data demonstrate that at therapeutic doses, GCs result in a significant induction in anti-anabolic and catabolic gene expression in muscle.

Discussion

We employed a murine model of polyarthritis treated with oral corticosterone to examine the effects of GCs

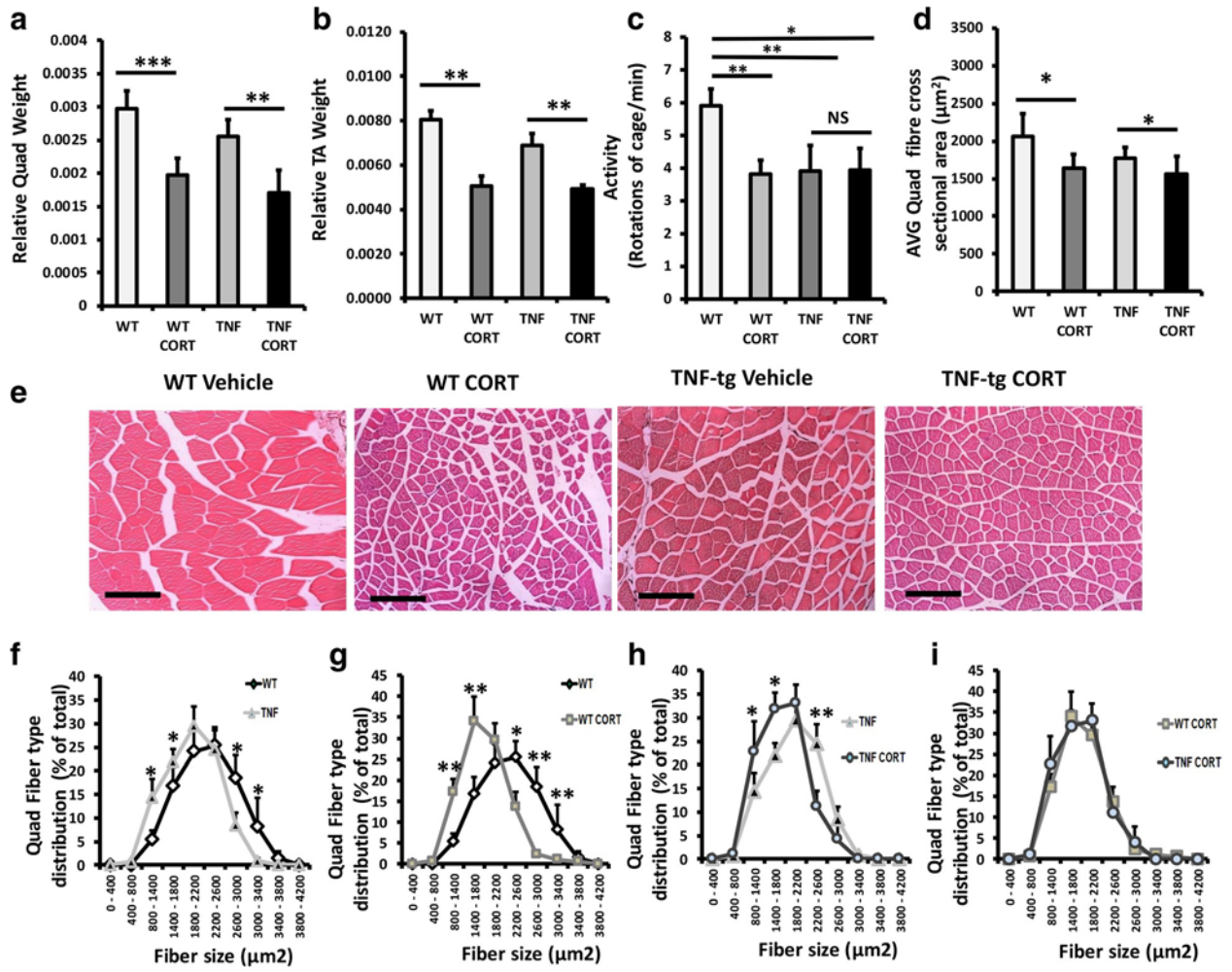

Fig. 4 a, b Total quadriceps and tibialis anterior muscle weights relative to total bodyweight, c mouse activity determined by rotations of cage per minute, d average quadriceps muscle fibre cross sectional area (μm^2), e representative images of quadriceps muscle sections, f–i distribution of quadriceps muscle fibre cross-sectional area determined using Image J in paraffin embedded sections in WT and TNF-Tg animals receiving either vehicle or corticosterone (100 μg/mL) in drinking water over 3 weeks. Values are expressed as mean ± standard error of six animals per group. Statistical significance was determined using two-way ANOVA with a Tukey post hoc analysis. *P < 0.05, **P < 0.005, ***P < 0.001 (scale bars, 50 μm)

on bone and muscle in the context of initial preventative bridging therapy in early-onset polyarthritis. This approach was effective at suppressing disease activity and joint destruction and has previously been demonstrated to mimic the kinetics of oral GC therapy [22]. Clinically, GCs suppress disease activity, joint destruction and systemic inflammation, which are drivers of bone and muscle loss in RA [1, 23–26]. However, whilst effective in controlling disease activity, they are independently associated with GC-induced osteoporosis and muscle wasting through direct anti-anabolic and catabolic pathways [8–13, 27, 28]. Currently, their impact on bone and muscle when used to treat new-onset inflammatory arthritis remains unclear.

The anti-inflammatory properties of oral GC administration were evidenced by a marked suppression in disease activity, joint inflammation and joint destruction in the TNF-tg model. We observed a marked decrease in trabecular bone volume at day 53 in TNF-tg mice, characterised by an increase in osteoclast activity and numbers. Administration of oral GCs resulted in a significant protection from this inflammatory bone loss.

Increased osteoclast numbers and activity are recognised mediators of inflammatory bone loss in RA, whilst therapeutic control of inflammation abrogates this [29–31]. Our study mirrors these findings, where TRAP +ve osteoclast numbers and bone resorption determined by serum CTX1 were significantly reduced in animals receiving corticosterone. In vitro data supported these findings where osteoclast numbers and activity were markedly reduced by GCs in TNFα-stimulated osteoclasts. These data indicate that the protection from

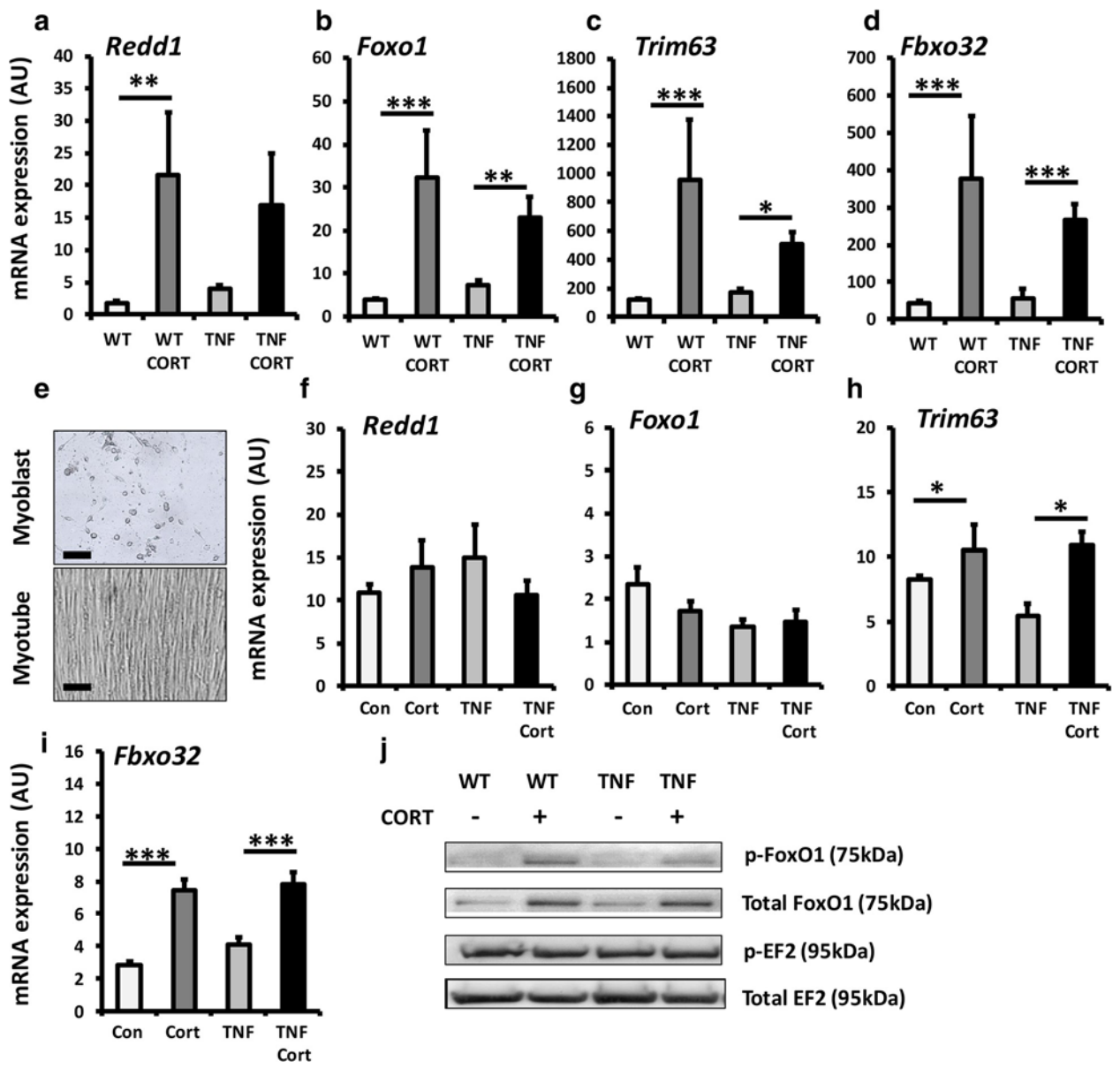

Fig. 5 a–d Quantification of gene expression (arbitrary units) of Redd1, Foxo1, Trim63 and Fbxo32, determined by RT qPCR, in ex vivo quadriceps biopsies. e–h Representative images of primary murine myoblast and myotubes and quantification of gene expression of Redd1, Foxo1, Trim63 and Fbxo32, determined by RT qPCR and j representative western blot staining for p-Foxo1, total Foxo1, pEF2 and p-EF2 after loading of 20 μg of protein and normalisation to ponso staining in quadriceps for either WT mice and TNF-Tg animals receiving either vehicle or corticosterone (100 μg/mL) in drinking water over 3 weeks or in primary myotubes treated with either vehicle, TNFα (10 ng/ml), corticosterone (1 μmol/l) or a combination of TNF and corticosterone for 48 h. Values are expressed as mean ± standard error of six animals or primary cultures derived from four separate animals. Statistical significance was determined using two-way ANOVA with a Tukey post hoc analysis. *$P < 0.05$, **$P < 0.005$, ***$P < 0.001$

inflammatory bone loss in TNF-tg animals receiving corticosterone are mediated through the suppression of osteoclastic bone resorption.

Both inflammation and GCs are reported to be negative regulators of bone formation and osteoblastogenesis [32–34]. Here, the anti-anabolic actions of GCs on bone formation are associated with a rapid suppression of P1NP and reduction in trabecular bone in patients [34].

In our study, whilst markers of mature osteoblasts and bone formation were suppressed in TNF-tg animals, therapeutic GCs dramatically exacerbated this and mirror observations in patient studies. These data suggest that the direct anti-anabolic actions of GCs outweigh

positive effects of suppressing inflammation on bone formation in vivo.

Several studies have explored the effects of therapeutic GCs on bone metabolism in RA. These yielded conflicting outcomes and are complicated by differences in disease severity, parallel DMARD therapy and dosing of GCs. Several reported increased fracture risk, with complications more apparent at higher doses [23, 35–37]. Others reported no worsening of bone mineral density or fracture risk when given at low doses in combination with DMARDS [3, 38, 39].

In contrast to bone loss, oral GCs increased muscle wasting and did not restore animal mobility in the TNF-tg model of polyarthritis, despite effective suppression of disease activity. This was characterised by a comparable decrease in muscle wet weights and fibre size in WT and TNF-tg animals suggesting that these changes occur independent of inflammatory muscle wasting and that GC-driven muscle wasting impacts on animal mobility.

In patients receiving therapeutic GCs, muscle wasting is characterised by increased protein breakdown driven through the ubiquitin proteasome and the lysosomal systems [11–13, 28]. Our results mirror this with an upregulation of anti-anabolic and catabolic pathway activation in animals receiving corticosterone.

Similar results were observed in primary muscle cultures, where regardless of pro-inflammatory stimulation with TNFα, a direct induction of catabolic gene expression was observed in response to GCs. Additive or synergistic catabolic actions in muscle by oral GCs in combination with inflammation were not observed in this study. This is most likely attributed to the effective suppression of well-defined inflammatory mediators of muscle wasting that are themselves suppressed by GCs [40–42].

Few studies address therapeutic GC use on muscle wasting in RA. However, of note, a recent study by Lemmey et al. reported a rapid loss of muscle mass in RA patients receiving a single intramuscular injection of GCs to treat disease flares [43]. Unfortunately, this study was not able to address the impact of disease activity (itself a significant driver of muscle wasting) and DMARD use on muscle wasting independent of corticosterone use. However, our study supports the author's conclusions that muscle wasting is an immediate and severe complication in RA patients receiving GCs, independent of inflammation. Indeed, the marked increase in fracture risk upon initiation of GCs in RA may be primarily driven by GC-induced muscle wasting, rather than secondary to GC-induced osteoporosis [44].

Conclusions

Using an animal model of chronic polyarthritis, this study examined how controlling disease activity with oral GCs as a monotherapy influenced inflammatory osteoporosis and muscle wasting. We demonstrate that when given in early disease, oral GCs protect against inflammatory bone loss, but induce marked systemic muscle wasting. These results suggest that the development of interventions to manage deleterious side effects in muscle should be prioritised in patients with inflammatory arthritis receiving GCs.

Additional files

Additional file 1: Table S1. Media for primary culture. Tables S2. Real-time PCR Master mix. Table S3. Buffers. Table S4. IgGs used in Immunoblotting. (DOCX 17 kb)

Additional file 2: Figure S1. (a) body weights (g), (b) daily corticosterone intake (μg/g body weight/day) and (c) serum corticosterone determined by ELISA (ng/ml) in in WT and TNF-Tg animals receiving either vehicle or corticosterone (100 μg/mL) in drinking water over 3 weeks. Values are expressed as mean ± standard error of six per group for weight and at least three animals per group for steroid intake and serum measurement. Statistical significance was determined using two-way ANOVA with a Tukey post hoc analysis. *P < 0.05, **P < 0.005, ***P < 0.001. (TIF 435 kb)

Additional file 3: Figure S2. Representative images of human primary culture osteoclast activity assessed on mineral-coated plates at day 14 treated with vehicle, cortisol (1000 nmol/l), TNFa 10 ng/ml) or a combination of both. Images were acquired using EVOS FL Auto Cell Imaging System (Life Technologies). (TIF 1090 kb)

Additional file 4: Figure S3. (a-p) Gene expression of *Foxo1*, *Fbxo32*, *Trim63*, *Ube3a*, *Igf1*, *Igf2*, *Mstn*, *Redd1*, *Myog*, *MyoD*, *Myf5*, *Myf6*, *Tnfa*, *Il6*, *Cxcl1* and *IkBa* were determined by RT qPCR in quadriceps for either WT mice and TNF-Tg animals receiving either vehicle or corticosterone (100 μg/mL) in drinking water over 3 weeks. Values are expressed as mean ± standard error of six animals or primary cultures derived from four separate animals. Statistical significance was determined using two-way ANOVA with a Tukey post hoc analysis. *P < 0.05, **P < 0.005, ***P < 0.001. (TIF 1454 kb)

Acknowledgements

We would like to thank Professor George Kollias (Hellenic Pasteur Institute, Athens, Greece) for providing the hTNFtg mice, the Biomedical Services Unit (University of Birmingham) for supporting animal experiments and the Department of Musculoskeletal Pathology (Robert Aitken Institute, University of Birmingham) for embedding and cutting tissue for histology. JWL was funded by MRC Arthritis Research UK Centre for Musculoskeletal Ageing Research PhD Studentship (MR/P021220/1). Analysis performed by CJM was supported by the Wellcome Trust MIDAS programme. We would also like to acknowledge the Arthritis Research UK Centre of Excellence for the Pathogenesis of Rheumatoid Arthritis in supporting this work. This research was supported by the Arthritis Research UK Centre of Excellence for the Pathogenesis of Rheumatoid Arthritis and the MRC Arthritis Research UK Centre for Musculoskeletal Ageing Research.

Authors' contributions

Animal experiments and analysis of in vivo and ex vivo data were performed by FCG, and WJM carried out the experiments with support from MCS, SAP and LYC. In vitro experiments were performed and analysed by FCM, WC, FS and LJW and designed by RSH, GCS and JS. RSH, KR, LR and LGG designed and supervised the project with support from MSC. All authors discussed the results and contributed to the final manuscript. All authors read and approved the final manuscript.

Funding

Collaboration. This research was supported by the Arthritis Research UK grants (Reference: 19859 & 20843) and Wellcome Trust Senior Fellowship (GGL-104612/Z/14/Z).

Availability of data and materials
All data generated or analysed during this study are included in this published article [and its supplementary information files].

Ethics approval and consent to participate
Experiments were carried out at the University of Birmingham, UK (project licence number P51102987), following strict guidelines governed by the UK Animal (Scientific Procedures) Act 1986 and were approved by the local ethics committee (BERSC: Birmingham Ethical Review Subcommittee).

Consent for publication
Not applicable.

Competing interests
The authors declare that they have no competing interests.

Author details
[1]Institute of Inflammation and Ageing, University of Birmingham, Birmingham, UK. [2]Institute of Metabolism and Systems Research, University of Birmingham, Birmingham, UK. [3]MRC Arthritis Research UK Centre for Musculoskeletal Ageing Research, University of Birmingham, Birmingham, UK. [4]Centre for Endocrinology, Diabetes and Metabolism, Birmingham Health Partners, Birmingham, UK. [5]ANZAC Research Institute, University of Sydney, Sydney, Australia. [6]Sandwell and West Birmingham Hospitals NHS Trust, Birmingham, UK. [7]Centre of Immunobiology, Institute of Infection, Immunity and Inflammation, College of Medical, Veterinary and Life Sciences, University of Glasgow, Glasgow, UK. [8]Department of Respiratory Medicine, NUTRIM School of Nutrition and Translational Research in Metabolism, Faculty of Health, Medicine and Life Sciences, Maastricht University, Maastricht, Netherlands. [9]School of Sport, Exercise and Rehabilitation Sciences, University of Birmingham, Birmingham, UK. [10]Institute of Clinical Sciences, University of Birmingham, Birmingham, UK.

Received: 25 April 2019 Accepted: 22 July 2019
Published online: 01 August 2019

References

1. Orstavik RE, Haugeberg G, Mowinckel P, Hoiseth A, Uhlig T, Falch JA, et al. Vertebral deformities in rheumatoid arthritis: a comparison with population-based controls. Arch Intern Med. 2004;164(4):420–5.
2. van Staa TP, Geusens P, Bijlsma JW, Leufkens HG, Cooper C. Clinical assessment of the long-term risk of fracture in patients with rheumatoid arthritis. Arthritis Rheum. 2006;54(10):3104–12.
3. Guler-Yuksel M, Bijsterbosch J, Goekoop-Ruiterman YP, de Vries-Bouwstra JK, Hulsmans HM, de Beus WM, et al. Changes in bone mineral density in patients with recent onset, active rheumatoid arthritis. Ann Rheum Dis. 2008;67(6):823–8.
4. Walsmith J, Roubenoff R. Cachexia in rheumatoid arthritis. Int J Cardiol. 2002;85(1):89–99.
5. Calabrese LH, Calabrese C, Kirchner E. The 2015 American College of Rheumatology guideline for the treatment of rheumatoid arthritis should include new standards for hepatitis B screening: comment on the article by Singh et al. Arthritis Rheumatol. 2016;68(5):1314–5.
6. Smolen JS, Landewe R, Bijlsma J, Burmester G, Chatzidionysiou K, Dougados M, et al. EULAR recommendations for the management of rheumatoid arthritis with synthetic and biological disease-modifying antirheumatic drugs: 2016 update. Ann Rheum Dis. 2017;76(6):960–77.
7. Sassoon CS, Zhu E, Pham HT, Nelson RS, Fang L, Baker MJ, et al. Acute effects of high-dose methylprednisolone on diaphragm muscle function. Muscle Nerve. 2008;38(3):1161–72.
8. Angeli A, Guglielmi G, Dovio A, Capelli G, de Feo D, Giannini S, et al. High prevalence of asymptomatic vertebral fractures in post-menopausal women receiving chronic glucocorticoid therapy: a cross-sectional outpatient study. Bone. 2006;39(2):253–9.
9. Feldstein AC, Elmer PJ, Nichols GA, Herson M. Practice patterns in patients at risk for glucocorticoid-induced osteoporosis. Osteoporos Int. 2005;16(12): 2168–74.
10. Strehl C, Bijlsma JW, de Wit M, Boers M, Caeyers N, Cutolo M, et al. Defining conditions where long-term glucocorticoid treatment has an acceptably low level of harm to facilitate implementation of existing recommendations: viewpoints from an EULAR task force. Ann Rheum Dis. 2016;75(6):952–7.
11. Lofberg E, Gutierrez A, Wernerman J, Anderstam B, Mitch WE, Price SR, et al. Effects of high doses of glucocorticoids on free amino acids, ribosomes and protein turnover in human muscle. Eur J Clin Investig. 2002;32(5):345–53.
12. Schakman O, Gilson H, de Coninck V, Lause P, Verniers J, Havaux X, et al. Insulin-like growth factor-I gene transfer by electroporation prevents skeletal muscle atrophy in glucocorticoid-treated rats. Endocrinology. 2005;146(4):1789–97.
13. Tomas FM, Munro HN, Young VR. Effect of glucocorticoid administration on the rate of muscle protein breakdown in vivo in rats, as measured by urinary excretion of N tau-methylhistidine. Biochem J. 1979;178(1):139–46.
14. Shealy DJ, Wooley PH, Emmell E, Volk A, Rosenberg A, Treacy G, et al. Anti-TNF-α antibody allows healing of joint damage in polyarthritic transgenic mice. Arthritis Res. 2002; 4(5): R7. https://doi.org/10.1186/ar430.
15. Hardy R, Rabbitt EH, Filer A, Emery P, Hewison M, Stewart PM, et al. Local and systemic glucocorticoid metabolism in inflammatory arthritis. Ann Rheum Dis. 2008;67(9):1204–10.
16. Hardy RS, Doig CL, Hussain Z, Leary MO, Morgan SA, Pearson MJ, et al. 11beta-hydroxysteroid dehydrogenase type 1 within muscle protects against the adverse effects of local inflammation. J Pathol. 2016;240(4):472–83.
17. Keffer J, Probert L, Cazlaris H, Georgopoulos S, Kaslaris E, Kioussis D, et al. Transgenic mice expressing human tumour necrosis factor: a predictive genetic model of arthritis. EMBO J. 1991;10(13):4025–31.
18. Naylor AJ, Desanti G, Saghir AN, Hardy RS. TNFalpha depleting therapy improves fertility and animal welfare in TNFalpha-driven transgenic models of polyarthritis when administered in their routine breeding. Lab Anim. 2018;52(1):59–68.
19. Naylor AJ, Desanti G, Saghir AN, Hardy RS. TNFa Depleting Therapy Improves Fertility and Animal Welfare in TNFa Driven Transgenic Models of Polyarthritis When Administered in their Routine Breeding. Laboratory Animals, Lab Anim. 2017;52(1):59-68.
20. Rosenblatt JD, Lunt AI, Parry DJ, Partridge TA. Culturing satellite cells from living single muscle fiber explants. In Vitro Cell Dev Biol Anim. 1995;31(10):773–9.
21. Morgan SA, McCabe EL, Gathercole LL, Hassan-Smith ZK, Larner DP, Bujalska IJ, et al. 11beta-HSD1 is the major regulator of the tissue-specific effects of circulating glucocorticoid excess. Proc Natl Acad Sci U S A. 2014;111(24):E2482–91.
22. Gasparini SJ, Weber MC, Henneicke H, Kim S, Zhou H, Seibel MJ. Continuous corticosterone delivery via the drinking water or pellet implantation: a comparative study in mice. Steroids. 2016;116:76–82.
23. Haugeberg G, Uhlig T, Falch JA, Halse JI, Kvien TK. Bone mineral density and frequency of osteoporosis in female patients with rheumatoid arthritis: results from 394 patients in the Oslo County Rheumatoid Arthritis register. Arthritis Rheum. 2000;43(3):522–30.
24. Gough AK, Lilley J, Eyre S, Holder RL, Emery P. Generalised bone loss in patients with early rheumatoid arthritis. Lancet. 1994;344(8914):23–7.
25. van der Goes MC, Jacobs JW, Boers M, Andrews T, Blom-Bakkers MA, Buttgereit F, et al. Patient and rheumatologist perspectives on glucocorticoids: an exercise to improve the implementation of the European League Against Rheumatism (EULAR) recommendations on the management of systemic glucocorticoid therapy in rheumatic diseases. Ann Rheum Dis. 2010;69(6):1015–21.
26. Roubenoff R, Roubenoff RA, Cannon JG, Kehayias JJ, Zhuang H, Dawson-Hughes B, et al. Rheumatoid cachexia: cytokine-driven hypermetabolism accompanying reduced body cell mass in chronic inflammation. J Clin Invest. 1994;93(6):2379–86.
27. Schakman O, Kalista S, Barbe C, Loumaye A, Thissen JP. Glucocorticoid-induced skeletal muscle atrophy. Int J Biochem Cell Biol. 2013;45(10):2163–72.
28. Hilton-Jones D. Diagnosis and treatment of inflammatory muscle diseases. J Neurol Neurosurg Psychiatry. 2003;74(Suppl 2):ii25–31.
29. Bromley M, Woolley DE. Chondroclasts and osteoclasts at subchondral sites of erosion in the rheumatoid joint. Arthritis Rheum. 1984;27(9):968–75.
30. Moller Dohn U, Boonen A, Hetland ML, Hansen MS, Knudsen LS, Hansen A, et al. Erosive progression is minimal, but erosion healing rare, in patients with rheumatoid arthritis treated with adalimumab. A 1 year investigator-initiated follow-up study using high-resolution computed tomography as the primary outcome measure. Ann Rheum Dis. 2009;68(10):1585–90.
31. Kotake S, Udagawa N, Takahashi N, Matsuzaki K, Itoh K, Ishiyama S, et al. IL-17 in synovial fluids from patients with rheumatoid arthritis is a potent stimulator of osteoclastogenesis. J Clin Invest. 1999;103(9):1345–52.
32. Gilbert L, He X, Farmer P, Rubin J, Drissi H, van Wijnen AJ, et al. Expression of the osteoblast differentiation factor RUNX2 (Cbfa1/AML3/Pebp2alpha a) is inhibited by tumor necrosis factor-alpha. J Biol Chem. 2002;277(4):2695–701.

33. Wei S, Kitaura H, Zhou P, Ross FP, Teitelbaum SL. IL-1 mediates TNF-induced osteoclastogenesis. J Clin Invest. 2005;115(2):282–90.
34. Ton FN, Gunawardene SC, Lee H, Neer RM. Effects of low-dose prednisone on bone metabolism. J Bone Miner Res. 2005;20(3):464–70.
35. Varonos S, Ansell BM, Reeve J. Vertebral collapse in juvenile chronic arthritis: its relationship with glucocorticoid therapy. Calcif Tissue Int. 1987;41(2):75–8.
36. Pereira RM, Corrente JE, Chahade WH, Yoshinari NH. Evaluation by dual X-ray absorptiometry (DXA) of bone mineral density in children with juvenile chronic arthritis. Clin Exp Rheumatol. 1998;16(4):495–501.
37. de Nijs RN, Jacobs JW, Bijlsma JW, Lems WF, Laan RF, Houben HH, et al. Prevalence of vertebral deformities and symptomatic vertebral fractures in corticosteroid treated patients with rheumatoid arthritis. Rheumatology (Oxford). 2001;40(12):1375–83.
38. Sambrook PN, Cohen ML, Eisman JA, Pocock NA, Champion GD, Yeates MG. Effects of low dose corticosteroids on bone mass in rheumatoid arthritis: a longitudinal study. Ann Rheum Dis. 1989;48(7):535–8.
39. Sambrook PN, Eisman JA, Yeates MG, Pocock NA, Eberl S, Champion GD. Osteoporosis in rheumatoid arthritis: safety of low dose corticosteroids. Ann Rheum Dis. 1986;45(11):950–3.
40. Yamaki T, Wu CL, Gustin M, Lim J, Jackman RW, Kandarian SC. Rel a/p65 is required for cytokine-induced myotube atrophy. Am J Physiol Cell Physiol. 2012;303(2):C135–42.
41. Ladner KJ, Caligiuri MA, Guttridge DC. Tumor necrosis factor-regulated biphasic activation of NF-kappa B is required for cytokine-induced loss of skeletal muscle gene products. J Biol Chem. 2003;278(4):2294–303.
42. Schakman O, Dehoux M, Bouchuari S, Delaere S, Lause P, Decroly N, et al. Role of IGF-I and the TNFalpha/NF-kappaB pathway in the induction of muscle atrogenes by acute inflammation. Am J Physiol Endocrinol Metab. 2012;303(6):E729–39.
43. Lemmey AB, Wilkinson TJ, Perkins CM, Nixon LA, Sheikh F, Jones JG, et al. Muscle loss following a single high-dose intramuscular injection of corticosteroids to treat disease flare in patients with rheumatoid arthritis. Eur J Rheumatol. 2018;5(3):160–4.
44. Stanmore EK, Oldham J, Skelton DA, O'Neill T, Pilling M, Campbell AJ, et al. Risk factors for falls in adults with rheumatoid arthritis: a prospective study. Arthritis Care Res (Hoboken). 2013;65(8):1251–8.

Publisher's Note

Arthritis Research & Therapy

RESEARCH ARTICLE Open Access

11β-HSD1 plays a critical role in trabecular bone loss associated with systemic glucocorticoid therapy

C. G. Fenton[1,2], C. L. Doig[1], S. Fareed[2], A. Naylor[1], A. P. Morrell[3], O. Addison[4,5], C. Wehmeyer[1], C. D. Buckley[1], M. S. Cooper[6], G. G. Lavery[2], K. Raza[1,7] and R. S. Hardy[1,2*]

Abstract

Background: Despite their efficacy in the treatment of chronic inflammation, the prolonged application of therapeutic glucocorticoids (GCs) is limited by significant systemic side effects including glucocorticoid-induced osteoporosis (GIOP). 11β-Hydroxysteroid dehydrogenase type 1 (11β-HSD1) is a bi-directional enzyme that primarily activates GCs in vivo, regulating tissue-specific exposure to active GC. We aimed to determine the contribution of 11β-HSD1 to GIOP.

Methods: Wild type (WT) and 11β-HSD1 knockout (KO) mice were treated with corticosterone (100 μg/ml, 0.66% ethanol) or vehicle (0.66% ethanol) in drinking water over 4 weeks (six animals per group). Bone parameters were assessed by micro-CT, sub-micron absorption tomography and serum markers of bone metabolism. Osteoblast and osteoclast gene expression was assessed by quantitative RT-PCR.

Results: Wild type mice receiving corticosterone developed marked trabecular bone loss with reduced bone volume to tissue volume (BV/TV), trabecular thickness (Tb.Th) and trabecular number (Tb.N). Histomorphometric analysis revealed a dramatic reduction in osteoblast numbers. This was matched by a significant reduction in the serum marker of osteoblast bone formation P1NP and gene expression of the osteoblast markers *Alp* and *Bglap*. In contrast, 11β-HSD1 KO mice receiving corticosterone demonstrated almost complete protection from trabecular bone loss, with partial protection from the decrease in osteoblast numbers and markers of bone formation relative to WT counterparts receiving corticosterone.

Conclusions: This study demonstrates that 11β-HSD1 plays a critical role in GIOP, mediating GC suppression of anabolic bone formation and reduced bone volume secondary to a decrease in osteoblast numbers. This raises the intriguing possibility that therapeutic inhibitors of 11β-HSD1 may be effective in preventing GIOP in patients receiving therapeutic steroids.

Keywords: Glucocorticoids, Osteoporosis, 11β-HSD1, Trabecular bone

Introduction

Therapeutic glucocorticoids (GCs) show marked efficacy in the treatment of chronic inflammatory conditions. Unfortunately, prolonged exposure to GCs results in severe adverse metabolic side effects including osteoporosis, insulin resistance and obesity, severely limiting their long-term therapeutic application [1–3]. Glucocorticoid-induced osteoporosis (GIOP) is common in patients receiving therapeutic GCs with 30–50% of patients developing decreased bone mineral density and increased fracture risk within 6 months [4–6]. Several mechanisms have been proposed whereby GCs cause loss of bone mineral density and deterioration in bone architecture. Chief amongst these is the direct inhibition of the osteoid-forming osteoblasts within bone, as evidenced by a marked and rapid suppression of serum P1NP and osteocalcin in patients receiving the therapeutic GC prednisolone [7]. In addition, GCs cause increased

* Correspondence: r.hardy@bham.ac.uk
[1]Institute of Inflammation and Ageing, University of Birmingham, Birmingham, UK
[2]Institute of Metabolism and Systems Research, University of Birmingham, Birmingham, UK
Full list of author information is available at the end of the article

bone resorption by supporting the survival, differentiation and activation of osteoclasts in vivo [8–12]. Additional mechanisms whereby GCs drive bone loss include the suppression of anabolic sex steroids as well as calcium and vitamin D metabolism and induction of myopathy that collectively contribute to systemic bone loss [13, 14].

11β-Hydroxysteroid dehydrogenase type 1 (11β-HSD1) is a bi-directional enzyme that, in the presence of the NADPH-generating enzyme H6PDH, primarily activates GCs (cortisone to cortisol in humans, 11-dehydrocorticosterone to corticosterone in mice) in vivo and determines their tissue-specific exposure [15]. In response to therapeutic glucocorticoids, such as hydrocortisol and prednisolone, renal inactivation competes with hepatic reactivation of steroids, providing both active and inactive glucocorticoid substrates in the circulation for tissue-specific metabolism by 11β-HSD1 [16, 17]. Pre-receptor metabolism of GCs by this enzyme has been shown to be critical in mediating insulin resistance, obesity, skin thinning and hepatic steatosis in mice following exposure to both active and inactive GCs [18]. This is in part mediated through renal inactivation of active GCs by 11β-hydroxysteroid dehydrogenase type 2 (11β-HSD2), which are then recycled within peripheral target tissues expressing 11β-HSD1.

Currently, the contribution of 11β-HSD1 to GIOP is poorly understood despite its expression being reported in primary osteoblasts and bone, where it is potently upregulated by inflammation [19–23]. In this study, we employed a murine model of exogenous oral corticosterone delivery, known to closely mimic the kinetics of clinical GC therapy, in wild type (WT) and global 11β-HSD1 knockout (KO) mice to delineate the contribution of 11β-HSD1 to GIOP, and demonstrate its critical role in mediating the effects of therapeutic GCs on bone [24].

Materials and methods

11β-HSD1 KO mouse model

Experiments were carried out at the University of Birmingham, UK (project licence number P51102987), following strict guidelines governed by the UK Animal (Scientific Procedures) Act 1986 and were approved by the local ethics committee (BERSC: Birmingham Ethical Review Subcommittee). 11β-HSD1 KO mice were generated as previously described through crossing HSD11B1 floxed mice with the ZP3-Cre expressing strain to achieve germline deletion of 11β-HSD1 [25]. Nine-week-old male WT or 11β-HSD1 KO littermate mice on a C57BL/6J background had ad libitum access to standard chow and drinking water supplemented with either corticosterone (Cort) (100 μg/mL, 0.66% ethanol), or vehicle (0.66% ethanol) for 4 weeks (six animals per group, 24 animals in total). Treatments were replaced twice weekly. At the end of the experiment, 13-week-old animals were culled by cervical dislocation following a cardiac bleed under terminal anaesthetic and tissues excised, weighed and fixed in 4% formalin or snap-frozen in liquid nitrogen for later analyses.

Analysis of mRNA abundance

Expression of specific mRNAs was determined using TaqMan® Gene Expression Assays (Thermo Fisher Scientific, Loughborough, UK). RNA was extracted from homogenised tibia. Briefly, whole tibias were removed from the hind limb ensuring complete removal of soft tissue under a dissection microscope. The heads of bone were removed at the metaphysis, and the bone marrow was flushed with a syringe. The diaphysis of the tibia was powdered in liquid nitrogen in a sterilised pestle and mortar. mRNA isolation was then performed on the resulting homogenate using an innuPREP RNA Mini Kit (Analytikjena, Cambridge, UK) as per the manufacturer's instructions. Aliquots containing 1 μg of RNA were then reverse transcribed using random hexamers according to the manufacturer's protocol (4311235, Multiscribe™, Thermo Fisher Scientific) to generate cDNA. The levels of murine 11β-HSD1 (*Hsd11b1*), RUNX2 (*Runx2*), OPG (*Tnfrsf11b*), RANKL (*Tnfsf11*), osteocalcin (*Bglap*), cathepsin K (*Ctsk*), alkaline phosphatase (*Alp*) and sclerostin (*Sost*) were assessed to determine expression of genes that define osteoblasts and osteoclasts and contribute to the balance of bone metabolism. Gene expression was determined using species-specific probe sets for real-time PCR on an ABI7500 system (Applied Biosystems, Warrington, UK). Final reactions contained 2X TaqMan PCR mastermix (Life Technologies), 200 nmol TaqMan probe and 25–50 ng cDNA. The abundance of specific mRNAs in a sample was normalised to that of 18S RNA. Data were obtained as Ct values and used to determine ΔCt values (Ct target – Ct 18S). Data were expressed as arbitrary units using the following transformation: [arbitrary units (AU) = $1000 \times (2^{-\Delta Ct})$].

11β-HSD1 activity of tibia tissue

Ex vivo tibia biopsies were placed in a culture medium containing 100 nmol/l of 11-dehydrocorticosterone (11-DHC) (to measure oxo-reductase/activation activity) along with tritiated [^{3}H] tracer amounts of 11-DHC. Steroids were extracted using dichloromethane and separated by thin-layer chromatography using ethanol:chloroform (8:92) as the mobile phase. Thin-layer chromatography plates were analysed by a Bioscan imager (Bioscan, Washington, DC, USA) and the fractional conversion of steroids was calculated. The protein concentration was assessed by a 96-well assay kit (Bio-Rad). Results were expressed as picomole product/per milligramme of protein/hour, and experiments were performed in triplicate.

Analysis of corticosterone, P1NP and CTX by ELISA

Serum was collected from mice by cardiac puncture under terminal anaesthetic. Briefly, whole blood was left at room temperature for 30 min prior to centrifugation for 20 min at 12,000 rpm. Serum was aspirated and stored at −80 °C prior to analysis. Unbound, serum-free corticosterone levels were measured using a commercially available sandwich ELISA designed to specifically detect active (but not inactive 11DHC) steroid (cat no: KGE009, R&D systems, Abingdon, UK). Serum was analysed in accordance with the manufacturer's instructions and data expressed as nanogrammes per millilitre (ng/ml). Serum P1NP was determined using a commercially available sandwich ELISA (cat no: AC-33F1, Immunodiagnostic Systems, Tyne & Wear, UK) in accordance with the manufacturer's instructions and data expressed as ng/ml. Serum CTX-1 was determined using a commercially available sandwich ELISA (cat no: AC-06F1, Immunodiagnostic Systems, Tyne & Wear, UK) in accordance with the manufacturer's instructions and data expressed as units per microlitre.

Static histomorphometry

Static histomorphometry was performed by the skelet.AL Skeletal Analysis Laboratories. Briefly, lumbar vertebrae 3 and 4 were fixed in 10% neutral buffered formalin, decalcified in EDTA and embedded in paraffin, and 3-μm sections were cut using a Leica Microsystems microtome (Leica Microsystems, Milton Keynes, UK). The sections were stained with either haematoxylin and eosin or tartrate-resistant acid phosphatise (TRAP) to identify osteoclasts and counterstained with Gill's haematoxylin. The sections were examined by light microscopy (Leica Microsystems). The number of osteoblasts and osteoclasts per millimetre were measured on 6.5 mm of the corticoendosteal surfaces, starting 0.25 mm from the growth plate using the Osteomeasure analysis software (Osteometrics, Decatur, GA, USA).

Micro-CT morphometry analysis

Formalin-fixed tibiae from 13-week-old mice were scanned using a Skyscan 1172 X-ray microtomograph at 60 kV/167 μA with a 0.5-mm aluminium filter. Images were obtained at a 5-μm resolution with a rotation step of 0.45°. NRecon software was used to reconstruct the images. Trabecular and cortical bone parameters were analysed using CTAn Skyscan software: regions of interest (ROI) were selected by drawing around trabecular or cortical bone regions for each cross-sectional slice; the tibia and bone architecture was determined by quantifying trabecular and cortical bone parameters using CTAn software. Trabecular bones 1.35 mm in length (200 sections) were selected for trabecular bone analysis at the metaphyseal region near the growth plate. Extent was determined by the length of trabecular bone growth in each sample, which was calculated by multiplying slice number by pixel size of scanned image (13.5 μm). Meshlab software was used to process 3D meshes of tibiae and calculate trabecular bone volume to tissue volume (BV/TV), trabecular number (Tb.N), trabecular separation (Tb.Sp) and trabecular thickness (Tb.Th).

Synchrotron sub-micron absorption tomography

Mice tibiae were examined on the Diamond Manchester Imaging Branch I13-2 beamline at the UK's national synchrotron facility, Diamond Light Source (Harwell, UK). Whole bones were centrally mounted on a rotation-translation stage. A defocused polychromatic incident X-ray source (pink beam) was used to irradiate the entire sample. A PCO.edge 5.5 camera system containing a sCMOS sensor was positioned behind the sample to collect an X-ray absorption image. A ×4 objective lens was positioned in front of the camera sensor to provide a resolution of 0.81 μm and a total field of view of 2.1 mm horizontally and 1.8 mm vertically. Each measurement consisted of 2500 projections, recorded over an angular range of 360° with an irradiation time of 100 ms per projection. Full 3D reconstruction was performed using in house I-13 software following identification of the centre of rotation in a single orthogonal image from the mid-diaphysis to the region immediately below the proximal epiphysis line. The reconstructed volumes were analysed in software package Aviso®, where osteocyte lacunae were rendered and thresholded consistently for analysis of pore volume and morphology.

Statistical analysis

Statistical significance was defined as $p < 0.05$ ($^{*}p < 0.05$; $^{**}p < 0.01$; $^{***}p < 0.001$) using either an unpaired Student *t* test or two-way ANOVA with a Bonferroni correction where a Gaussian distribution is identified (determined by both Kolmogorov-Smirnov and Shapiro-Wilk test), or a non-parametric Kruskal-Wallis test with Dunn's Multiple Comparison where it is absent.

Results

Oral corticosterone induces GC excess in wild type and 11β-HSD1 KO animals

Nine-week-old C57BL/6 WT and global 11β-HSD1 KO mice received drinking water containing either vehicle or corticosterone at 100 μg/ml for 4 weeks. Deletion of 11β-HSD1 and inhibition of corticosterone generation in the bones of 11β-HSD1 KO mice was confirmed in ex vivo tibia biopsies, where corticosterone generation from DHC was significantly abrogated in 11β-HSD1 KO mice compared to WT animals (Fig. 1a). Expression of *H6pd* (the gene encoding the NADPH cofactor-generating enzyme H6PDH) required for 11β-HSD1 steroid activation

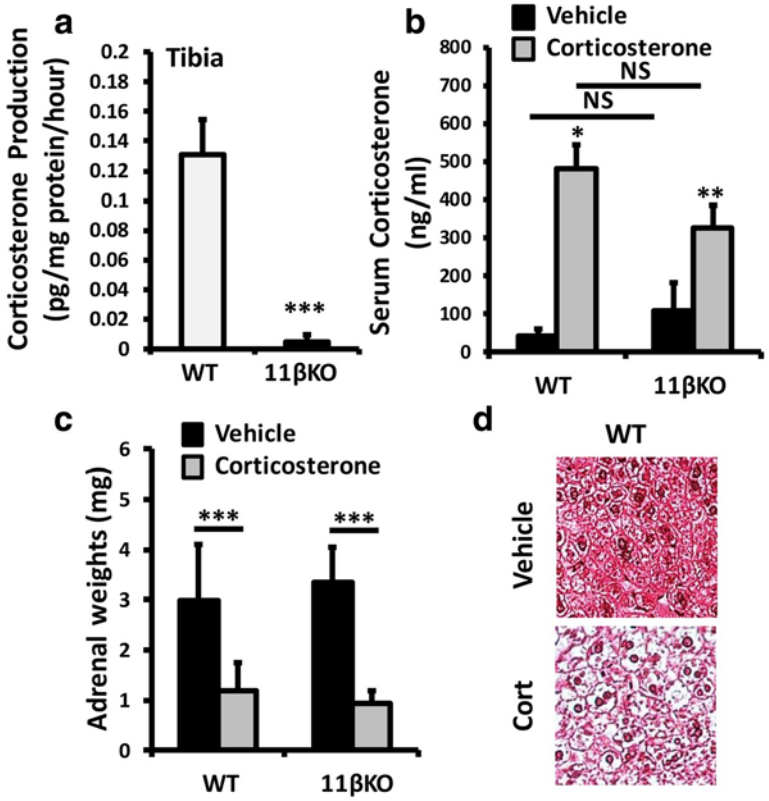

Fig. 1 a Corticosterone generation in tibia ex vivo biopsies isolated from WT and 11β-HSD1 KO mice determined by scanning thin-layer chromatography. b Serum corticosterone levels determined by ELISA in WT and 11β-HSD1 KO receiving either vehicle or oral corticosterone (100 μg/ml). c Adrenal weights (mg) from WT and 11β-HSD1 KO mice receiving either vehicle or oral corticosterone (100 μg/ml) and d representative paraffin-embedded sections of the liver taken from WT mice receiving either vehicle or oral corticosterone (100 μg/ml) (×20), stained with haematoxylin and eosin. Values are expressed as mean ± standard error of six animals per group. Statistical significance was determined using two-way ANOVA with a Bonferroni correction. *$p < 0.05$, **$p < 0.01$, ***$p < 0.001$

was highly expressed and did not change in tibiae, across groups (Additional file 1: Figure S1a).

Evidence of circulating GC excess was determined by measuring midnight (within normal active phase) serum corticosterone levels. Serum levels of corticosterone were significantly increased in both WT and 11β-HSD1 KO animals receiving corticosterone in drinking water relative to those receiving vehicle (WT, 41.2 ± 12.3 ng/ml versus WT + Cort, 479.6 ± 76.1 ng/ml, $p < 0.01$; 11β-HSD1 KO, 108.2 ± 72.2 ng/ml versus 11β-HSD1 KO + Cort, 329.5 ± 51.6 ng/ml, $p < 0.05$) (Fig. 1b) (Additional file 2). Serum levels were not significantly different between WT and 11β-HSD1 KO animals receiving corticosterone. Increased systemic exposure to corticosterone was evidenced by the marked suppression of adrenal weights in both WT and 11β-HSD1 KO animals receiving corticosterone and the onset of hepatic steatosis in WT animals (Fig. 1c, d). These data confirm that oral administration of corticosterone in drinking water at 100 μg/ml is sufficient to induce circulating GC excess in both WT and 11β-HSD1 KO animals.

11β-HSD1 KO showed protection from corticosterone-induced trabecular bone

To determine the role of 11β-HSD1 in GIOP, we generated 3D trabecular meshes from the tibia following micro-CT using Meshlab software (Fig. 2a). Analysis of 3D trabecular meshes demonstrated that trabecular bone volume to tissue volume (BV/TV), trabecular number (Tb.N), trabecular separation (Tb.Sp) and trabecular thickness (Tb.Th) were identical between vehicle-treated WT and 11β-HSD1 KO animals (Fig. 2b–e). Following oral corticosterone administration over 4 weeks, a significant reduction in trabecular bone parameters was identified in WT animals (BV/TV: WT, 8.5% ± 0.66 vs WT + Cort, 4.2% ± 0.38, $p < 0.001$; Tb.N: WT, 0.0009 1/μm ± 0.00004 vs WT + Cort, 0.0006 1/μm ± 0.00004, $p < 0.01$; Tb.Th: WT, 96.5 μm ± 3.8 vs WT + Cort, 73.5 μm ± 3.5, $p < 0.01$; Tb.Sp: WT, 664 μm ± 27 vs WT + Cort, 959 μm ± 31, $p < 0.01$) (Fig. 2b–e). In contrast, 11β-HSD1 KO mice receiving corticosterone were protected from this reduction in trabecular BV/TV, Tb.N and Tb.Sp relative to vehicle-treated controls (BV/TV: 11β-HSD1 KO, 7.5% ± 0.76 vs 11β-HSD1 KO + Cort, 7.2% ± 0.71, NS; Tb.N: 11β-HSD1 KO, 0.0008

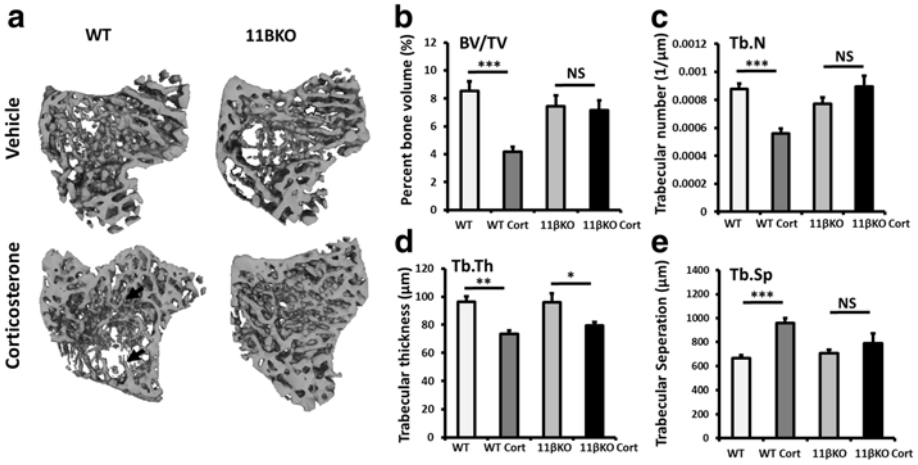

Fig. 2 a Representative images of 3D reconstructions of tibia trabecular bone using micro-CT from WT and 11β-HSD1 KO receiving either vehicle or oral corticosterone (100 μg/ml). b Bone volume to tissue volume (BV/TV), c trabecular number (Tb.N), d trabecular thickness (Tb.Th) and e trabecular separation (Tb.Sp) determined by Meshlab software analysis of micro-CT in WT and 11β-HSD1 KO receiving either vehicle or oral corticosterone (100 μg/ml). Values are expressed as mean ± standard error of six animals per group. Statistical significance was determined using two-way ANOVA with a Bonferroni correction. *$p < 0.05$, **$p < 0.01$, ***$p < 0.001$. Black arrows represent regions of mesh surface trabecular thinning

1/μm ± 0.00004 vs 11β-HSD1 KO + Cort, 0.0009 1/μm ± 0.00008, NS; Tb.Sp: 11β-HSD1 KO, 706.9 μm ± 28, NS vs 11β-HSD1 KO + Cort, 789 μm ± 61, NS) (Fig. 2b, c). In contrast, 11β-HSD1 KO animals were not protected from suppressed Tb.Th in response to corticosterone with a significant reduction identified in these animals relative to vehicle-treated controls (Tb.Th: 11β-HSD1 KO 95.8 μm ± 5.2 vs 11β-HSD1 KO + Cort, 79.4 μm ± 3.1, $p < 0.05$) (Fig. 2d). Micro-CT analysis of cortical bone from 3D cortical bone reconstructions revealed no significant differences in cortical thickness (Crt.T), cortical cross-sectional area (Crt.A), endosteal medullary area (Med.A), periosteal perimeter (Per.P) or cortical lacunae properties between WT and 11β-HSD1 KO animals (Additional file 1: Figure S1a-g).

These data indicate that treatment with oral corticosterone at 100 μg/ml in drinking water for 4 weeks is sufficient to induce marked trabecular bone loss at the tibia of WT C57BL/6 animals. In contrast, animals with deletion of 11β-HSD1 demonstrate significant protection against the bone-wasting effects of oral corticosterone in trabecular bone.

GC-induced suppression of osteoblast numbers and bone formation markers was blunted in 11β-HSD1-KO mice

Bone metabolism is tightly regulated by the balance between osteoblast-mediated bone formations and osteoclast bone resorption. Analysis of bone osteoblast and osteoclast numbers and serum biomarkers of bone formation (procollagen type 1 amino-terminal propeptide (P1NP)) and bone resorption (degradation products from C-terminal telopeptides of type I collagen (CTX-1)) was performed by histomorphometry and ELISA respectively to ascertain the impact of oral corticosterone on these cell populations. A dramatic decrease in osteoblast numbers per bone perimeter (Ob.N./B.pm) was readily apparent in WT mice receiving oral corticosterone relative to controls, with an almost total absence of osteoblasts (WT, 8.5 + 1.7 mm, versus WT + Cort, 0.1 ± 0.07 mm; $p < 0.001$)(Fig. 3a, e). This was partially abrogated in 11β-HSD1 KO mice receiving corticosterone, where osteoblast numbers were detectable, despite a significant suppression (11β-HSD1 KO, 10.3 ± 2.9, versus 11β-HSD1 KO + Cort, 3.3 ± 2.1 ng/ml; $p < 0.05$). These results were closely mirrored by a comparable dramatic decrease in serum P1NP in WT mice receiving oral corticosterone (WT, 494.2 + 67, versus WT + Cort, 31.3 + 2.1 ng/ml; $p < 0.00$) that was also partially abrogated in 11β-HSD1 KO mice (11β-HSD1 KO, 405.7 ± 69.4, versus 11β-HSD1 KO + Cort, 158.6 + 55.1 ng/ml; $p < 0.01$) (Fig. 3c). Serum levels of P1NP were significantly higher in 11β-HSD1 KO mice receiving corticosterone than in WT counterparts (WT + Cort, 31.3 + 2.1, versus 11β-HSD1 KO + Cort, 158.6 + 55.1 ng/ml; $p < 0.05$).

In contrast to osteoblasts, no significant changes in osteoclast numbers per bone perimeter (Oc.N./B.pm) or in serum measures of osteoclast activity determined by CTX-1 were observed in WT and 11β-HSD1 KO mice receiving GCs (Fig. 3b, d, f). The ratio of RANKL/OPG gene expression was examined as a critical regulator of osteoclast formation and activation in ex vivo tibia biopsies (Fig. 3). A significant increase in the RANKL/OPG ratio was apparent in WT mice receiving oral corticosterone (1.9-fold; $p < 0.01$). 11β-HSD1 KO mice were protected from this increased ratio in response to oral corticosterone with no significant change in expression

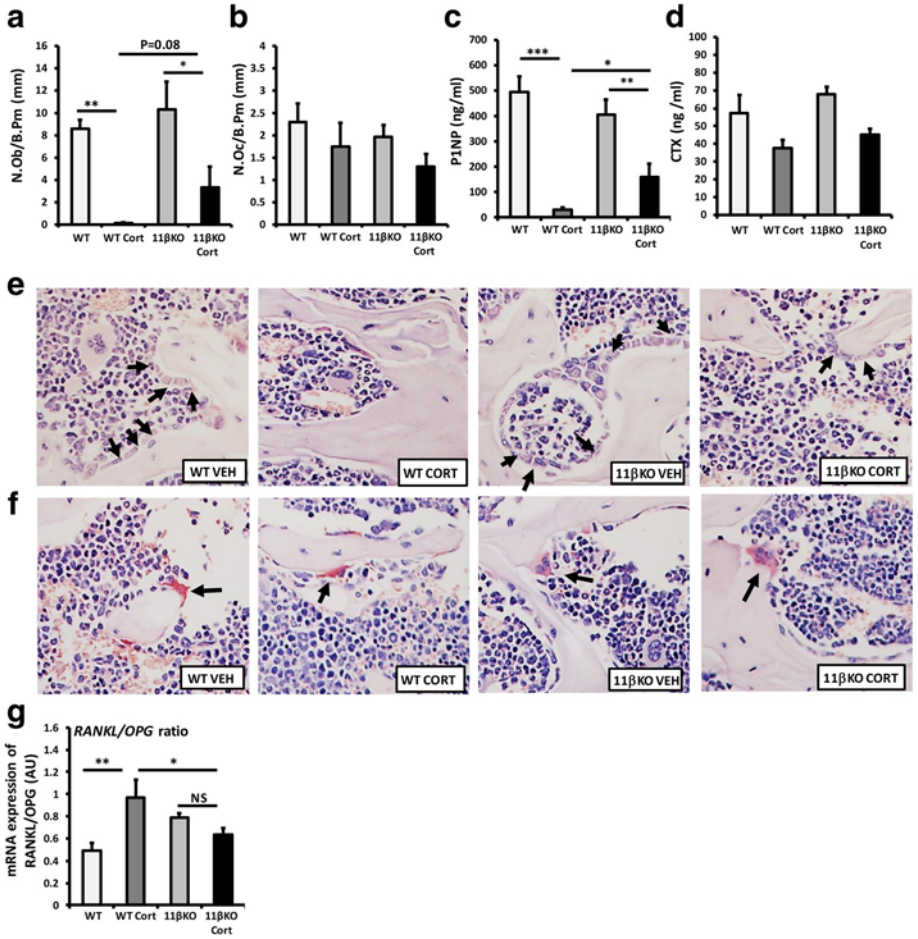

Fig. 3 Histomorphometric analysis of numbers of (a) osteoblasts (N.Ob/B.Pm) and (b) osteoclasts (N.Oc/B.Pm) at the bone perimeter per square millimetre from vertebrae L3 and L4. c Serum P1NP (ng/ml) (d) and serum CTX-1 (ng/ml) were determined by ELISA in WT and 11β-HSD1 KO mice receiving either vehicle or oral corticosterone (100 μg/ml). e Representative images of osteoblasts and f representative images of osteoclasts on trabecular bone surface. g The ratio of RANKL/OPG gene expression in the tibia from WT and 11β-HSD1 KO mice receiving either vehicle or oral corticosterone (100 μg/ml) was determined by quantitative RT-PCR. Values are expressed as mean ± standard error of six animals per group. Statistical significance was determined using two-way ANOVA with a Bonferroni correction. *$p < 0.05$, **$p < 0.01$, ***$p < 0.001$. Black arrows indicate osteoblasts and osteoclasts

relative to 11β-HSD1 KO mice receiving vehicle and a significantly lower ratio compared to WT animals receiving GCs (Fig. 3e).

Analysis of markers of mature osteoblast gene expression in whole ex vivo biopsies of tibia was determined by quantitative RT-PCR. In WT mice, the osteoblast markers *Bglap* and *Alp* were significantly reduced following administration of oral corticosterone (*Bglap*, 33-fold; $p < 0.0001$, *Alp*, 4-fold; $p < 0.01$) (Fig. 4a, b). In contrast, 11β-HSD1 KO mice showed significant protection from the suppression of *Bglap* with no significant change in expression, whilst the suppression of *Alp* was completely abrogated following administration of oral corticosterone (Fig. 4b). mRNA expression of the osteoclast marker *Ctsk*, the master regulator of osteoblast differentiation *Runx2* and the negative regulators of osteoblast differentiation, *Sost* and *Dkk1*, were not altered in either WT or 11β-HSD1 KO mice receiving oral corticosteroids (Fig. 4c–f).

Taken together, these data strongly indicate that the bone loss identified in WT mice receiving corticosterone is characterised by a profound suppression in osteoblast numbers and bone formation, and a shift in the resorption/formation ratio that would favour net bone loss. This appears to be partially dependant on 11β-HSD1 activity, where 11β-HSD1 KO animals show significant, but not complete protection from the suppression in osteoblast activity.

Discussion

Despite important systemic side effect, GCs continue to be routinely employed in the management of chronic

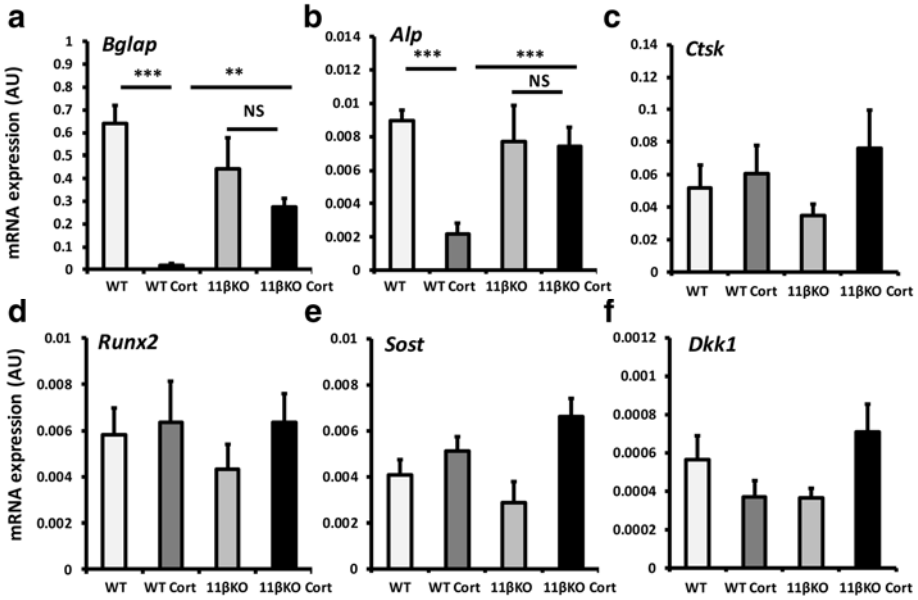

Fig. 4 a–f Gene expression (AU) of *Bglap*, *Alp*, *Ctsk*, *Runx2*, *Sost* and *Dkk1* in tibias taken from WT and 11β-HSD1 KO receiving either vehicle or oral corticosterone (100 μg/ml) determined by quantitative RT-PCR. Values are expressed as mean ± standard error of six animals per group. Statistical significance was determined using two-way ANOVA with a Bonferroni correction. *$p < 0.05$, **$p < 0.01$, ***$p < 0.001$

inflammatory diseases such as rheumatoid arthritis. In this study, we show for the first time that pre-receptor metabolism of exogenously administered GCs by the enzyme 11β-HSD1 is a key component mediating bone loss in a murine model of GIOP. Here, following administration of active glucocorticoids such as corticosterone, renal and hepatic metabolism ensures an equilibrium between active and inactive glucocorticoid substrates, which are then available for tissue-specific pre-receptor activation by the 11β-HSD enzymes [17, 18]. Previously, the GC receptor (GR) has been shown to be critical in mediating GIOP in mouse models of GC excess with the targeted deletion of GR in both osteoblasts and osteoclasts being shown to be protective [26, 27].

We used a model of oral administration of corticosterone in drinking water to delineate the precise contribution of pre-receptor GC metabolism by 11β-HSD1 to GIOP using a global KO model. Previously, this model of exogenous GC excess has been shown to result in a consistent diurnal exposure pattern, closely mimicking the kinetics of clinical GC therapy [24]. Of note, systemic and renal inactivation of glucocorticoid by 11β-HSD2 has been shown to be unaffected in the global 11β-HSD1 KO mouse in response to corticosterone [28].

Both WT and 11β-HSD1 KO mice treated with exogenous corticosterone showed signs of corticosterone excess with significantly elevated levels of the serum-free steroid and marked suppression of adrenal weights relative to untreated controls. Furthermore, WT mice developed hepatic steatosis in response to corticosterone treatments in line with classical presentations of GC excess previously reposted in human and mouse models [18, 29].

Analysis of trabecular bone in the tibias of WT animals revealed a significant reduction in all trabecular bone parameters following addition of corticosterone. These data are supportive of a systemic GC-induced bone loss in WT C57BL/6 mice in response to corticosterone in drinking water at 100 μg/ml for 4 weeks.

Similar studies have reported a robust decrease in bone mass in response to therapeutic GCs such as prednisolone in C57BL/6 mice [30, 31]. These studies identify a significant decrease in trabecular and cortical content at the tibia in response to subcutaneous prednisolone pellets over 28 days. The bone loss phenotype observed in our model is less marked, but is broadly consistent with this, with evidence of early trabecular bone loss at the tibia.

In vivo, GCs have been shown to potently suppress osteoblast-mediated bone formation by increasing both apoptosis and autophagy [32–35]. Certainly in this model, we observed a dramatic suppression of osteoblast numbers in trabecular bone of wild type mice treated with corticosterone, with a robust suppression of P1NP as a marker of systemic bone formation and a marked suppression of mature osteoblast markers including osteocalcin and alkaline phosphatase. Together, these data suggest that this model of GC excess is comparable to those previously reported and suitable to examine the role of 11β-HSD1.

Importantly, mice with a global deletion of 11β-HSD1 demonstrated a significant protection from trabecular bone loss at the tibia following administration of exogenous corticosterone in drinking water. This approached full protection from reductions in BV/TV, trabecular number and trabecular separation and conferred a partial protection from reduced trabecular thickness. This protective effect appeared to be mediated through a resistance to GC-induced suppression of bone formation in osteoblasts, with a partial preservation of trabecular osteoblast numbers, increased serum P1NP levels and elevated expression of the mature osteoblast markers, osteocalcin and alkaline phosphatase in 11β-HSD1 KO animals relative to WT counterparts receiving corticosterone. Further experiments in these animals might utilise delivery of inactive steroid metabolites such as DHC to assess 11β-HSD1-mediated activation and tissue-specific targeting without interference from residual active corticosterone to examine its role in vivo.

Previous studies examining the overexpression of 11β-HSD2 targeted to osteoblasts and osteocytes in mice, mediating complete GC signalling blockade in these cells, have identified a phenotype characterised by reduced cranial ossification and bone mineral density [36, 37]. These studies demonstrate that GC signalling is required for normal osteoblast and osteocyte maturation and function. Deletion of 11β-HSD1 did not reproduce these findings in our study, suggesting that basal GC signalling mediated by free circulating active GCs is sufficient to mediate normal bone development.

In contrast, targeted blockade of GC signalling in osteoblasts and osteocytes using either the overexpression of 11β-HSD2 or the inhibition of GR dimerization is able to prevent GIOP in murine models of GC excess [26, 32]. We see similar findings in the 11β-HSD1 KO mouse suggesting that, whilst total levels of the active steroid are increased in our model, they are insufficient to induce trabecular bone loss in the absence of 11β-HSD1 GC activation.

These prior studies provide compelling evidence that the deleterious actions of GCs are mediated directly through osteoblasts via an increase in osteoblast apoptosis and autophagy. Whilst our studies do not address in which cell type deletion of 11β-HSD1 is mediating protection from GIOP, previous studies demonstrating robust expression of 11β-HSD1 in vivo and vitro strongly indicate that 11β-HSD1 expression within osteoblasts is likely to mediate the protection reported in our global 11β-HSD1 KO mice [20, 22, 26, 32]. However, the possibility that 11β-HSD1 within alternative cell populations such as osteoclasts cannot be discounted. Regardless, better characterisation of the 11β-HSD1-expressing cell subtypes that mediate protection may prove beneficial in the future where targeting of therapeutic inhibitors of 11β-HSD1 may be of interest to more effectively prevent GIOP.

In this model, we chose oral administration of corticosterone at 100 μg/ml to initiate GC excess in male C57BL/6 mice and so cannot extrapolate these findings to female animals. This dose of corticosterone was selected due to the strong evidence of diurnal exposure patterns, which closely mimic that seen in patients following oral therapeutic GC administration [24]. Other methods such as subcutaneous pellets result in a continuous steady delivery of GC. Whilst this allows for the better control of drug release, it may be less representative of delivery regimes in patients.

Conclusions

`For the first time, this study demonstrates that 11β-HSD1 plays a critical role in mediating the detrimental actions of exogenous therapeutic corticosterone administration on bone and that its targeted deletion is able to ameliorate GIOP in this murine model. This raises the intriguing possibility that therapeutic inhibitors of 11β-HSD1 may be effective in preventing GIOP in patients receiving therapeutic steroids.

Additional files

Additional file 1: Figure S1. (a), Representative images of 3D reconstructions of tibia cortical bone using micro-CT from WT and 11β-HSD1 KO receiving either vehicle or oral corticosterone (100 μg/ml). (b), Cortical cross-sectional thickness (Crt.Cs.T), (c), cortical cross-sectional area (Crt.Cs.A), (d) endosteal medullary area (Med.A) and (e) periosteal perimeter (Per.P) determined by Meshlab software analysis of micro-CT in WT and 11β-HSD1 KO receiving either vehicle or oral corticosterone (100 μg/ml). (f), Quantification of osteoblast lacunae in murine cortical bone collected at I-13 using pink beam, count time 100 ms, rotations 2500. Full 3D reconstruction was performed using in house I-13 script following identification of centre of rotation in a single orthogonal slice. Volume rendering of osteocyte lacunae was performed in Aviso® prior to pore analysis of Volume3d and Area^{3}d. (f), Average pore area (μm^3), (g) lacunae number within a 100μm^3 region of interest in WT and 11β-HSD1 KO receiving either vehicle or oral corticosterone (100 μg/ml). Values are expressed as mean ± standard error of three animals per group. Statistical significance was determined using one way ANOVA with a Tukey's post hoc analysis. Values are expressed as mean ± standard error of six animals per group. Statistical significance was determined using two way ANOVA with a Bonferroni correction. (TIFF 1190 kb)

Additional file 2: Figure S2. (a), Gene expression (AU) of H6pd determined by quantitative RT-PCR in WT and 11β-HSD1 KO receiving either vehicle or oral corticosterone (100 mg/ml). Values are expressed as mean ± standard error of six animals per group. Statistical significance was determined using two way ANOVA with a Bonferroni correction. (TIFF 316 kb)

Abbreviations

11-DHC: 11-Dehydrocorticosterone; 11β-HSD1: 11β-Hydroxysteroid dehydrogenase type 1; BV/TV: Trabecular bone volume to tissue volume; Cort: Corticosterone; Crt.CS.A: Cortical cross-sectional area; Crt.Cs.T: Cortical cross-sectional thickness; GCs: Glucocorticoids; GIOP: Glucocorticoid-induced osteoporosis; KO: Knockout; Med.A: Endosteal medullary area; P1NP: Procollagen type 1 amino-terminal propeptide; Per.P: Periosteal perimeter; Tb.N: Trabecular number; Tb.Th: Trabecular thickness; WT: Wild type

Acknowledgements
We would like to acknowledge the Arthritis Research UK funded Rheumatoid Arthritis Pathogenesis Centre of Excellence at the University of Birmingham. We would like to thank the Biomedical Services Unit (University of Birmingham) for supporting animal experiments and the Department of Musculoskeletal Pathology (Robert Aitken Institute, University of Birmingham) for embedding and cutting tissue for histology.

Authors' contributions
CF carried out the experiments with support from CD, AN, SF, AM, OA and CW. RSH, KR and GGL supervised the project with support from MSC. RSH wrote the manuscript. All authors discussed the results and contributed to the final manuscript. All authors read and approved the final manuscript.

Funding
This work was carried out with the support of the Diamond Light Source (proposal MT16654-1) on beamline I13-2 with beamtime awarded through the Diamond Birmingham Collaboration. This research was supported by the Arthritis Research UK grants (Reference: 19859 & 20843) and Wellcome Trust Senior Fellowship (GGL-104612/Z/14/Z).

Availability of data and materials
All data generated or analysed during this study are included in this published article [and its supplementary information files].

Ethics approval and consent to participate
Experiments were carried out at the University of Birmingham, UK (project licence number P51102987) following strict guidelines governed by the UK Animal (Scientific Procedures) Act 1986 and were approved by the local ethics committee (BERSC: Birmingham Ethical Review Subcommittee).

Consent for publication
Not applicable.

Competing interests
The authors declare that they have no competing interests.

Author details
[1]Institute of Inflammation and Ageing, University of Birmingham, Birmingham, UK. [2]Institute of Metabolism and Systems Research, University of Birmingham, Birmingham, UK. [3]Aston Institute of Materials Research, Aston University, Birmingham, UK. [4]Institute of Clinical Sciences, University of Birmingham, Birmingham, UK. [5]Faculty of Medicine and Dentistry, University of Alberta, Edmonton, Canada. [6]ANZAC Research Institute, University of Sydney, Sydney, Australia. [7]Sandwell and West Birmingham Hospitals NHS Trust, Birmingham, UK.

Received: 17 December 2018 Accepted: 7 August 2019
Published online: 16 August 2019

References
1. Sury MR, Russell GN, Heaf DP. Hydrocortisone myopathy. Lancet. 1988; 2(8609):515.
2. LoCascio V, Bonucci E, Imbimbo B, Ballanti P, Adami S, Milani S, et al. Bone loss in response to long-term glucocorticoid therapy. Bone Miner. 1990;8(1): 39–51.
3. Arner P, Gunnarsson R, Blomdahl S, Groth CG. Some characteristics of steroid diabetes: a study in renal-transplant recipients receiving high-dose corticosteroid therapy. Diabetes Care. 1983;6(1):23–5.
4. Angeli A, Guglielmi G, Dovio A, Capelli G, de Feo D, Giannini S, et al. High prevalence of asymptomatic vertebral fractures in post-menopausal women receiving chronic glucocorticoid therapy: a cross-sectional outpatient study. Bone. 2006;39(2):253–9.
5. Feldstein AC, Elmer PJ, Nichols GA, Herson M. Practice patterns in patients at risk for glucocorticoid-induced osteoporosis. Osteoporos Int. 2005;16(12): 2168–74.
6. Strehl C, Bijlsma JW, de Wit M, Boers M, Caeyers N, Cutolo M, et al. Defining conditions where long-term glucocorticoid treatment has an acceptably low level of harm to facilitate implementation of existing recommendations: viewpoints from an EULAR task force. Ann Rheum Dis. 2016;75(6):952–7.
7. Ton FN, Gunawardene SC, Lee H, Neer RM. Effects of low-dose prednisone on bone metabolism. J Bone Miner Res. 2005;20(3):464–70.
8. Swanson C, Lorentzon M, Conaway HH, Lerner UH. Glucocorticoid regulation of osteoclast differentiation and expression of receptor activator of nuclear factor-kappaB (NF-kappaB) ligand, osteoprotegerin, and receptor activator of NF-kappaB in mouse calvarial bones. Endocrinology. 2006; 147(7):3613–22.
9. Jia D, O'Brien CA, Stewart SA, Manolagas SC, Weinstein RS. Glucocorticoids act directly on osteoclasts to increase their life span and reduce bone density. Endocrinology. 2006;147(12):5592–9.
10. Weinstein RS, Chen JR, Powers CC, Stewart SA, Landes RD, Bellido T, et al. Promotion of osteoclast survival and antagonism of bisphosphonate-induced osteoclast apoptosis by glucocorticoids. J Clin Invest. 2002;109(8): 1041–8.
11. Hofbauer LC, Zeitz U, Schoppet M, Skalicky M, Schuler C, Stolina M, et al. Prevention of glucocorticoid-induced bone loss in mice by inhibition of RANKL. Arthritis Rheum. 2009;60(5):1427–37.
12. Yao W, Cheng Z, Busse C, Pham A, Nakamura MC, Lane NE. Glucocorticoid excess in mice results in early activation of osteoclastogenesis and adipogenesis and prolonged suppression of osteogenesis: a longitudinal study of gene expression in bone tissue from glucocorticoid-treated mice. Arthritis Rheum. 2008;58(6):1674–86.
13. Snow-Harter C, Bouxsein M, Lewis B, Charette S, Weinstein P, Marcus R. Muscle strength as a predictor of bone mineral density in young women. J Bone Miner Res. 1990;5(6):589–95.
14. Calogero AE, Burrello N, Bosboom AM, Garofalo MR, Weber RF, D'Agata R. Glucocorticoids inhibit gonadotropin-releasing hormone by acting directly at the hypothalamic level. J Endocrinol Investig. 1999;22(9):666–70.
15. Lavery GG, Walker EA, Draper N, Jeyasuria P, Marcos J, Shackleton CH, et al. Hexose-6-phosphate dehydrogenase knock-out mice lack 11 beta-hydroxysteroid dehydrogenase type 1-mediated glucocorticoid generation. J Biol Chem. 2006;281(10):6546–51.
16. Frerichs VA, Tornatore KM. Determination of the glucocorticoids prednisone, prednisolone, dexamethasone, and cortisol in human serum using liquid chromatography coupled to tandem mass spectrometry. J Chromatogr B Analyt Technol Biomed Life Sci. 2004;802(2):329–38.
17. Johnson TN, Whitaker MJ, Keevil B, Ross RJ. Bioavailability of oral hydrocortisone corrected for binding proteins and measured by LC-MS/MS using serum cortisol and salivary cortisone. J Bioequivalence Bioavailab. 2018;10(1):001–3.
18. Morgan SA, McCabe EL, Gathercole LL, Hassan-Smith ZK, Larner DP, Bujalska IJ, et al. 11beta-HSD1 is the major regulator of the tissue-specific effects of circulating glucocorticoid excess. Proc Natl Acad Sci U S A. 2014;111(24): E2482–91.
19. Bland R, Worker CA, Noble BS, Eyre LJ, Bujalska IJ, Sheppard MC, et al. Characterization of 11β-hydroxysteroid dehydrogenase activity and corticosteroid receptor expression in human osteosarcoma cell lines. JEndocrinol. 1999;161(3):455–64.
20. Cooper MS, Walker EA, Bland R, Fraser WD, Hewison M, Stewart PM. Expression and functional consequences of 11β-hydroxysteroid dehydrogenase activity in human bone. Bone. 2000;27(3):375–81.
21. Woitge H, Harrison J, Ivkosic A, Krozowski Z, Kream B. Cloning and in vitro characterization of alpha 1(I)-collagen 11 beta-hydroxysteroid dehydrogenase type 2 transgenes as models for osteoblast-selective inactivation of natural glucocorticoids. Endocrinology. 2001;142(3):1341–8.
22. Kaur K, Hardy R, Ahasan MM, Eijken M, van Leeuwen JP, Filer A, et al. Synergistic induction of local glucocorticoid generation by inflammatory cytokines and glucocorticoids: implications for inflammation associated bone loss. Ann Rheum Dis. 2010;69(6):1185–90.
23. Ahasan MM, Hardy R, Jones C, Kaur K, Nanus D, Juarez M, et al. Inflammatory regulation of glucocorticoid metabolism in mesenchymal stromal cells. Arthritis Rheum. 2012;64(7):2404–13.
24. Gasparini SJ, Weber MC, Henneicke H, Kim S, Zhou H, Seibel MJ. Continuous corticosterone delivery via the drinking water or pellet implantation: a comparative study in mice. Steroids. 2016;116:76–82.
25. Semjonous NM, Sherlock M, Jeyasuria P, Parker KL, Walker EA, Stewart PM, et al. Hexose-6-phosphate dehydrogenase contributes to skeletal muscle homeostasis independent of 11beta-hydroxysteroid dehydrogenase type 1. Endocrinology. 2011;152(1):93–102.
26. Rauch A, Seitz S, Baschant U, Schilling AF, Illing A, Stride B, et al. Glucocorticoids suppress bone formation by attenuating osteoblast

differentiation via the monomeric glucocorticoid receptor. Cell Metab. 2010; 11:517–31.
27. Kim HJ, Zhao H, Kitaura H, Bhattacharyya S, Brewer JA, Muglia LJ, et al. Glucocorticoids suppress bone formation via the osteoclast. J Clin Invest. 2006;116(8):2152–60.
28. Kotelevtsev Y, Holmes MC, Burchell A, Houston PM, Schmoll D, Jamieson P, et al. 11beta-hydroxysteroid dehydrogenase type 1 knockout mice show attenuated glucocorticoid-inducible responses and resist hyperglycemia on obesity or stress. Proc Natl Acad Sci U S A. 1997;94(26):14924–9.
29. Dourakis SP, Sevastianos VA, Kaliopi P. Acute severe steatohepatitis related to prednisolone therapy. Am J Gastroenterol. 2002;97(4):1074–5.
30. Sato AY, Richardson D, Cregor M, Davis HM, Au ED, McAndrews K, et al. Glucocorticoids induce bone and muscle atrophy by tissue-specific mechanisms upstream of E3 ubiquitin ligases. Endocrinology. 2017;158(3): 664–77.
31. Thiele S, Baschant U, Rauch A, Rauner M. Instructions for producing a mouse model of glucocorticoid-induced osteoporosis. Bonekey Rep. 2014;3:552.
32. O'Brien CA, Jia D, Plotkin LI, Bellido T, Powers CC, Stewart SA, et al. Glucocorticoids act directly on osteoblasts and osteocytes to induce their apoptosis and reduce bone formation and strength. Endocrinology. 2004; 145:1835–41.
33. Plotkin LI, Manolagas SC, Bellido T. Glucocorticoids induce osteocyte apoptosis by blocking focal adhesion kinase-mediated survival. Evidence for inside-out signaling leading to anoikis. J Biol Chem. 2007;282(33):24120–30.
34. Xia X, Kar R, Gluhak-Heinrich J, Yao W, Lane NE, Bonewald LF, et al. Glucocorticoid-induced autophagy in osteocytes. J Bone Miner Res. 2010; 25(11):2479–88.
35. Weinstein RS, Hogan EA, Borrelli MJ, Liachenko S, O'Brien CA, Manolagas SC. The pathophysiological sequence of glucocorticoid-induced osteonecrosis of the femoral head in male mice. Endocrinology. 2017;158(11):3817–31.
36. Kalak R, Zhou H, Street J, Day RE, Modzelewski JRK, Spies CM, et al. Endogenous glucocorticoid signalling in osteoblasts is necessary to maintain normal bone structure in mice. Bone. 2009;45(1):61–7.
37. Sher LB, Woitge HW, Adams DJ, Gronowicz GA, Krozowski Z, Harrison JR, et al. Transgenic expression of 11beta-hydroxysteroid dehydrogenase type 2 in osteoblasts reveals an anabolic role for endogenous glucocorticoids in bone. Endocrinology. 2004;145(2):922–9.

Publisher's Note

International Journal of
Molecular Sciences

MDPI

Review

Exploring the Interface between Inflammatory and Therapeutic Glucocorticoid Induced Bone and Muscle Loss

Justine M. Webster [1,2,†], Chloe G. Fenton [1,3,†], Ramon Langen [4] and Rowan S. Hardy [1,3,5,*]

1 Institute of Metabolism and Systems Research, University of Birmingham, Birmingham B15 2TT, UK; JMW801@student.bham.ac.uk (J.M.W.); CXF637@student.bham.ac.uk (C.G.F.)
2 Centre for Endocrinology, Diabetes and Metabolism, Birmingham Health Partners, Birmingham B15 2TT, UK
3 Institute of Inflammation and Ageing, University of Birmingham, Birmingham B15 2TT, UK
4 Department of Respiratory Medicine, NUTRIM School of Nutrition and Translational Research in Metabolism, Faculty of Health, Medicine and Life Sciences, Maastricht University, 6211 LK Maastricht, The Netherlands; r.langen@maastrichtuniversity.nl
5 MRC Arthritis Research UK Centre for Musculoskeletal Ageing Research, University of Birmingham, Birmingham B15 2TT, UK
* Correspondence: r.hardy@bham.ac.uk; Tel.: +44-0121-414-3776
† These authors contributed equally.

Received: 30 October 2019; Accepted: 14 November 2019; Published: 16 November 2019

Abstract: Due to their potent immunomodulatory anti-inflammatory properties, synthetic glucocorticoids (GCs) are widely utilized in the treatment of chronic inflammatory disease. In this review, we examine our current understanding of how chronic inflammation and commonly used therapeutic GCs interact to regulate bone and muscle metabolism. Whilst both inflammation and therapeutic GCs directly promote systemic osteoporosis and muscle wasting, the mechanisms whereby they achieve this are distinct. Importantly, their interactions in vivo are greatly complicated secondary to the directly opposing actions of GCs on a wide array of pro-inflammatory signalling pathways that underpin catabolic and anti-anabolic metabolism. Several clinical studies have attempted to address the net effects of therapeutic glucocorticoids on inflammatory bone loss and muscle wasting using a range of approaches. These have yielded a wide array of results further complicated by the nature of inflammatory disease, underlying the disease management and regimen of GC therapy. Here, we report the latest findings related to these pathway interactions and explore the latest insights from murine models of disease aimed at modelling these processes and delineating the contribution of pre-receptor steroid metabolism. Understanding these processes remains paramount in the effective management of patients with chronic inflammatory disease.

Keywords: glucocorticoid; muscle wasting; osteoporosis

1. Glucocorticoids and Therapeutic Glucocorticoid Excess

Synthetic glucocorticoids (GCs), such as dexamethasone, prednisolone and hydrocortisone, are widely utilized in the treatment of chronic inflammatory diseases such as chronic obstructive pulmonary disease (COPD), inflammatory bowel disease (IBD) and rheumatoid arthritis (RA), with approximately 1% of the adult population in the U.K. and U.S. receiving this class of drugs. Their mechanisms of action are diverse, with GCs suppressing a range of pro-inflammatory pathways including p38-mitogen

activated protein kinases (p38-MAPK), nuclear factor kappa-light-chain-enhancer (NF-κB) and activator protein (AP-1), in addition to inducing pro-resolving factors such as glucocorticoid induced leucine zipper (GILZ) and annexin-1 [1–3]. These significantly reduce leukocyte infiltration at sites of inflammation, suppress the production of pro-inflammatory cytokines and chemokines and support resolution of inflammation and tissue remodelling [4,5]. Despite the potent immune-modulatory anti-inflammatory actions of therapeutic GCs, their clinical application is limited due to severe systemic side effects. These occur in up to 70% of patients and can include muscle wasting and GC induced osteoporosis (GIO) [6–10]. The actions of GCs on bone and muscle metabolism are well established, but themselves complicated in the backdrop of chronic inflammation by separate inflammatory driven muscle wasting and bone loss. The inflammatory pathways that mediate bone and muscle loss in chronic inflammation are in turn suppressed by the anti-inflammatory actions of GCs, further complicating the prediction of their outcome on the musculoskeletal system. Understanding the complex interactions between GC and inflammatory regulation of bone and muscle metabolism remains paramount in the effective management of patients with chronic inflammatory disease. In this review, we explore how inflammatory drivers and therapeutic GCs interact to regulate bone and muscle metabolism and consider the role of local steroid metabolism in shaping these processes.

2. Glucocorticoid Signalling and Regulation of Inflammation

Lipophilic GCs readily diffuse across cell membranes, signalling through the cytoplasmic GC receptor (GR) superfamily, encoded by the NR3C1 gene. Classically, GC signalling and GR transactivation occur through ligand binding of the GRα homodimer. In its unbound state, GRα forms a multi-protein complex with chaperone proteins such as heat shock proteins (HSPs), HSPp-70, HSP90 and FK506 binding protein 52 that block their nuclear localization signal (NLS) and prevent translocation to the nucleus from the cytoplasm [11]. Upon GC binding, the GRα undergoes a conformational change, allowing dissociation of chaperone proteins. Homo-dimerization and exposure of the NLS are required for nuclear translocation of the ligand bound GR, where it can influence gene expression [12] (Figure1). This is an oversimplified view of GC signalling, as several studies utilizing the GR^{dim} mouse (possessing a mutation preventing GR dimerization) reveal that the anti-inflammatory properties of therapeutic GCs are mediated by both homo-dimeric GRα complexes and monomeric GRα to facilitate transactivation or transrepression of pro-inflammatory genes [5,13–16]. Whilst the mechanisms that underpin GR signalling have been reviewed extensively elsewhere, several key pathways are prominent in mediating the anti-inflammatory actions of GCs [17]. These include the direct GRα homodimer transactivation of anti-inflammatory genes such as secretory leukocyte protease inhibitor (*SLPI*), *MAKP-1*, *GILZ* and tristetraprolin (*TTP*), which suppress the NF-kB and p38-MAPK inflammatory pathways, in addition to the inhibition of pro-inflammatory transcription factors via their tethering to the GC bound GR [18–21]. In particular, GCs act via the GR to suppress the NF-κB and p38-MAPK inflammatory pathways and AP-1 pro-inflammatory pathways, which regulate the transcription of various genes relating to inflammation such as tumour necrosis factor-alpha (TNF-α) and interleukin-1 (IL-1β) and -6 [22]. Many of these inflammatory pathways considered are direct contributors to the process of inflammatory bone and muscle wasting and are themselves opposed by the actions of therapeutic GCs. This review will now consider how inflammation and GCs influence bone and muscle metabolism, both in isolation and in concert with one another.

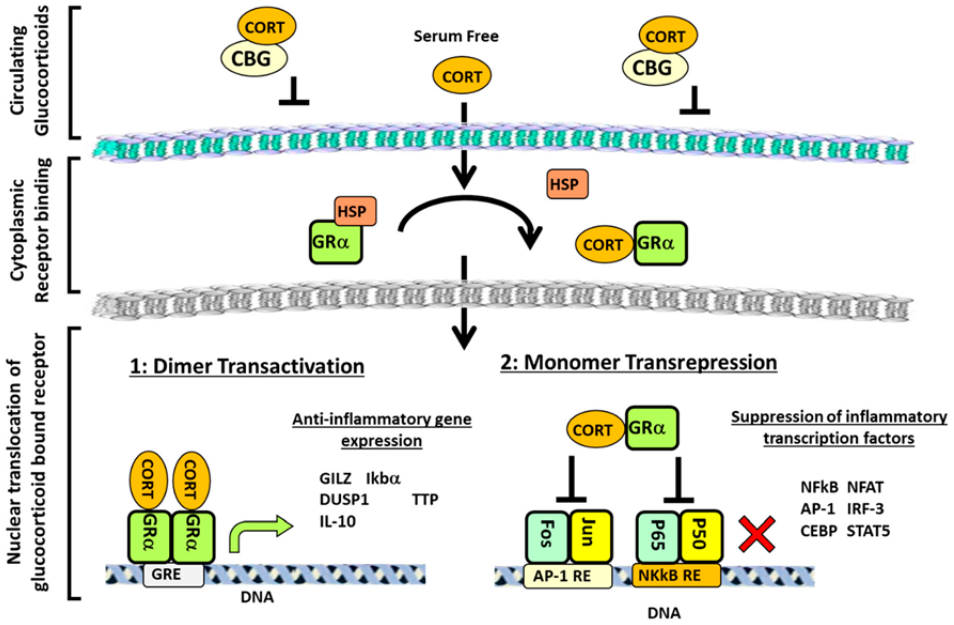

Figure 1. Overview of glucocorticoid (GC) signalling pathways. The majority of glucocorticoids (GCs) in the circulation are bound by corticosteroid-binding globulin (CBG), which prevents diffusion across the membrane. However, free GCs can readily enter the cell, where they bind to the GR in the cytoplasm. This induces a conformational change in the glucocorticoid receptor (GR), which causes the dissociation of chaperone molecules, such as heat shock proteins (HSPs), to expose the nuclear localisation signal (NLS) and allow translocation of the GC/GR complex to the nucleus. Here, the GR can either dimerise to transactivate anti-inflammatory genes or signal as a monomer to inhibit pro-inflammatory transcription factors. Cortisol (CORT), nuclear factor of activated T-cells (NFAT), CCAAT-enhancer-binding proteins (or C/EBPs), nuclear factor kappa-light-chain-enhancer of activated B cells (NF-κB), p38 mitogen-activated protein kinases (p-38-MAPK), glucocorticoid induced leucine zipper (GILZ), secretory leukocyte protease inhibitor (SLPI), tristetraprolin (TTP), mitogen-activated protein kinase-1 (MKP-1), activator protein 1 (AP-1), signal transducer and activator of transcription 5 (STAT5), and response element (RE).

3. Bone Metabolism

Bone metabolism is a tightly regulated process that ensures homeostasis between bone resorption and bone formation. This process maintains a balance in calcium and phosphate mineral homeostasis, as well as allowing constant healthy remodelling to compensate for external loading stress and damage and requires the close interaction between osteocytes, bone lining cells, bone forming osteoblasts and bone resorbing osteoclasts [23]. Here, in quiescent bone, osteocytes produce factors such as transforming growth factor-β (TGF-β), sclerostin and dickkopf WNT signaling pathway inhibitor 1 (DKK-1), which inhibits osteoclast and osteoblast maturation and differentiation [24]. Signals such as bone matrix damage or immobilization result in osteocyte apoptosis, leading to a removal of the inhibitory signals and increases in factors that promote osteoclastogenesis, such as macrophage colony stimulating factor (M-CSF) and receptor activator of nuclear factor kappa-β ligand (RANKL) [25–27]. Together, these promote osteoclast differentiation from hematopoietic precursors and increase receptor activator of nuclear factor kappa-β (RANK) pathway activation, driving multinuclear polykaryon formation and the formation of mature osteoclasts that express osteoclast specific genes including tartrate-resistant acid phosphatase (*TRAP*) and cathepsin K [28–30]. Mature osteoclasts form tight integrin junctions on mineralized bone matrix, forming an acidified resorption compartment that facilitates the degradation of the inorganic hydroxyapatite component of the bone [31,32]. The organic component of bone can then be degraded by lysosomal enzymes, such as cathepsin K. In parallel to this process, a reduction in factors that suppress osteoblast differentiation (such as sclerostin and DKK-1)

and an increase in factors that induce osteoblast differentiation (such as WNT, TGFβ and insulin-like growth factor 1 (IGF-1)) promote the formation of osteoblast pre-cursors from mesenchymal derived progenitors [33–35]. This process is tightly regulated through the master transcriptional regulator runt-related transcription factor 2 (RUNX2), mediating the expression of osteoblast specific genes such as osteocalcin, osteopontin and bone sialoprotein [36,37]. As osteoblasts continue to mature, RANKL levels (which maintain osteoclasts) decrease, whilst osteoprotegerin (OPG) (the dummy receptor for RANKL that suppresses RANK signalling) increases. Together with increasing TGFβ signalling, the decrease in RANK/RANKL signalling leads to reduced osteoclast differentiation, activity and survival [38]. The transition toward the reversal phase is characterised by an increase in mature osteoblasts at the vacated osteoclast lacunae site of bone resorption. One key cell type that appears to facilitate this transition appears to be a unique cell population known as reversal cells, which cover the eroded bone surface. Here, one study has revealed that the disruption of these cells results in a loss of the initiation of bone resorption, highlighting their importance in this process [39]. Mature osteoblasts then secrete factors required for osteoid formation including organic matrix rich in type 1 collagen, osteocalcin and bone sialoprotein (BSP) [40]. This is then mineralized via the deposition of hydroxyapatite crystals, created by the flux of calcium and phosphate ions within vesicles that are deposited as a mineralized nodule, in a process that has been shown to require the enzyme alkaline phosphatase to release phosphate ions [41,42]. Ultimately, bone formation ceases as osteoblasts undergo apoptosis or are incorporated into the osteocyte network.

4. Regulation of Bone Metabolism by Inflammation

In diseases such as RA, IBD and COPD, ongoing systemic inflammation results in inflammatory osteoporosis, with localized destruction of bone at sites of inflammation in diseases such as RA [43–47]. Systemic bone loss is characterized by a general decrease in bone mineral density (BMD) at the femoral neck, hip and spine in patients, resulting in increased fracture rates [47–50]. It is widely accepted that this inflammatory bone loss results from an imbalance in the bone remodelling cycle, shifting towards resorption and away from formation [51]. Studies exploring inflammatory bone loss are complicated by immobility in patients and the impact of concurrent anti-inflammatory drugs that can influence bone metabolism. However, significant insights have been derived from in vitro studies and clinical studies.

A prominent mechanism associated with a shift toward inflammatory bone loss is the interaction of the activated immune system with bone resorbing osteoclasts. Here, changes in the inflammatory cytokine profiles in patients with chronic inflammation result in increased levels of pro-osteoclastogenic mediators and a decrease in anti-osteoclastogenic mediators. Many of the pro-osteoclastogenic cytokines upregulated in chronic inflammation, including TNF-α, IL-1, IL-6, IL-8 and IL-17, mediate their actions via an upregulation of RANKL on fibroblasts and osteoblasts, which in turn promotes osteoclastic bone resorption [52–55]. In particular, combinations of cytokines including TNF-α, IL-1 and IL-6, act synergistically to increase RANKL in inflammation [56]. Activated Th17 and B cells also upregulate *RANKL* expression promoting resorptive bone lesions in patients and in vitro in a RANKL dependent manner [57–59]. A recent study identified a novel cytokine induced in response to TNF-α in T cells, known as secreted osteoclastogenic factor of activated T cells (SOFAT), which has the ability to cause osteoclastogenesis in a RANKL independent manner and may have implications in bone loss induced by chronic inflammatory disease [60].

Of particular interest, TNF-α also has effects on the bone forming ability of osteoblasts in inflammation. TNF-α treatment of osteoblasts' precursors inhibits their differentiation by suppressing the DNA binding ability of RUNX2, leading to inhibition of alkaline phosphatase expression and matrix deposition [61]. The pro-apoptotic properties of TNF-α on osteoblasts has also been observed [62]. Similarly, IL-6 treatment of osteoblasts leads to reductions in alkaline phosphatase activity and in the expression of RUNX2 and osteocalcin, with mineralisation dramatically reduced in a dose dependent manner [63]. The prominent role of the inflammatory activation of osteoclastogenesis was derived from murine models using the TNF-tg mouse of chronic polyarthritis and inflammatory bone loss.

Here, blockade of both the TNF-α and the RANKL/RANK signalling pathways using anti-TNF therapy in combination with anti-osteoclastic (OPG) was able to prevent inflammatory bone erosions [64]. Bone repair was then augmented through the addition of the pro-osteoblastic hormone parathyroid hormone (PTH). These results highlight the importance of bot inflammatory activation of osteoclasts and suppression of osteoblasts in mediating systemic and localized bone loss in chronic inflammation. Consequently, these results indicate that repair of bone erosions requires a therapy that simultaneously controls inflammation while also impacting both osteoclastic bone resorption and osteoblastic bone formation to shift the balance in bone homeostasis and promote normal repair and recovery of bone.

5. Effects of Glucocorticoids on Bone Metabolism

Whilst GCs are widely used in the treatment of chronic inflammation, they are themselves associated with an increased risk of fractures and osteoporosis at therapeutic doses resulting in GIO. GIO is the most common form of secondary osteoporosis with risk of fracture increasing dramatically within three to six months of starting GC therapy [65]. Interestingly, these changes are reversed rapidly upon cessation of GCs, indicating a rapid and acute nature of action at the cellular level. The mechanism that underpins this appears to be primarily mediated by a substantial inhibition of osteoblastic bone formation [66]. Under physiological conditions, GCs promote osteoblast maturation. However, at higher therapeutic doses, GCs downregulate WNT agonists and upregulate WNT inhibitors, which induce apoptosis and suppress osteoblast differentiating [67–69]. In one clinical study examining children receiving exogenous glucocorticoids, serum levels of the WNT signalling inhibitor DKK-1 were shown to be significantly elevated, suggesting it may play a key role in reduced bone formation in GIO [70]. In studies using transgenic mice with osteoblast targeted disruption of glucocorticoid signalling, GC signalling via the GR was shown to mediate reduced bone formation through the suppression of osteoblast differentiation via the WNT pathway and through inducing osteoblast apoptosis, with animals with GR signaling disruption being protected from GC induced bone loss [67,71].

The impact of GCs on osteoclasts is less clear. Studies have reported that GC treatment results in a decrease in osteoclast number, but an increase in osteoclast longevity, potentially mediated via a GC induced increase in M-CSF production [66,72,73]. In addition, studies have shown conflicting results on the expression of osteoclastic genes in response to GCs. One study showed that dexamethasone treatment of murine calvarial bones resulted in increased mRNA levels of *Rank* and *Rankl*, leading to increased markers of osteoclast activation [74]. Other studies showed that OPG levels are suppressed or reported no change at all in RANKL and OPG levels [72,75,76]. Some insight comes from one study in children receiving exogenous GCs, where serum levels of RANKL were elevated and OPG suppressed [77]. In these patients, spontaneous osteoclastogenesis in vitro was apparent in monocytic cell precursors. Certainly, one study utilizing a murine model of therapeutic GC delivery revealed that the targeting of osteoclasts using bisphosphonates was an effective strategy to prevent both cortical and trabecular bone loss [78]. There is some evidence to indicate that the responsiveness of osteoclasts to GCs is highly dependent on the stage of cell differentiation, but these findings require further investigation [79]. The variation in GC dose, the method of administration and the models employed may explain the variation in the results reported to date, whilst their interactions with inflammatory mediators in patients with chronic inflammation should also be taken into account when investigating their bone related effects.

6. Glucocorticoids, Inflammation and Bone Homeostasis

Glucocorticoids directly oppose a wide array of the pathways that drive inflammatory bone loss. Amongst these, their suppression of pro-inflammatory factors such as RANKL, TNF-α and IL-6 appears to be prominent in mediating their bone sparing effects in chronic inflammatory joint destruction, through the direct suppression of osteoclastogenesis and osteoclast activation [80] (Figure2). In contrast, their potent suppression of anabolic bone formation by osteoblasts may synergize with the deleterious

actions of inflammation on osteoblasts. Consequently, the net balance of GCs on bone metabolism in the context of chronic inflammation is less clear. Several clinical studies shed light on the balance between beneficial and detrimental actions of GCs on bone metabolism in chronic inflammation. These include a study reporting no differences in BMD loss in RA patients receiving therapeutic GCs in combination with traditional disease modifying anti-rheumatic drugs (DMARDS), relative to a matched control cohort [81]. Of particular interest were studies exploring whether GCs at lower therapeutic doses might promote positive anti-inflammatory actions without eliciting detrimental bone loss. These studies reported that low dose GC therapy in RA did not increase the risk of generalized osteoporosis at the spine and hip [82,83]. Another study found that patients receiving GCs in combination with anti-TNF therapy had a 2.5% increase in BMD at the femoral neck compared to a 0.7% decrease in BMD in those using anti-TNF alone, suggesting that GCs may increase bone metabolism in this context [84]. In contrast, two further studies found that GCs' use was associated with decreased BMD in RA patients [43,85]. Similarly, in juvenile chronic arthritis (JCA), two studies found that GC treated patients had significantly less trabecular bone and higher risk of vertebral collapse than a matched control cohort [86,87]. These studies found strong links with the dose of steroid applied, but were further complicated by the application of GCs in the developing skeleton of younger patients, who may be more vulnerable to the anti-anabolic actions of GCs than adults. The conflicting nature of these results may stem from a variety of issues, including differences in disease pathophysiology, disease activity, duration and variations in the delivery and dose of GC therapy. In addition, concomitant use of alternative therapies such as anti-TNF treatments causes further complications, making it difficult to dissect the contribution of GCs to changes in bone metabolism in chronic inflammatory disease.

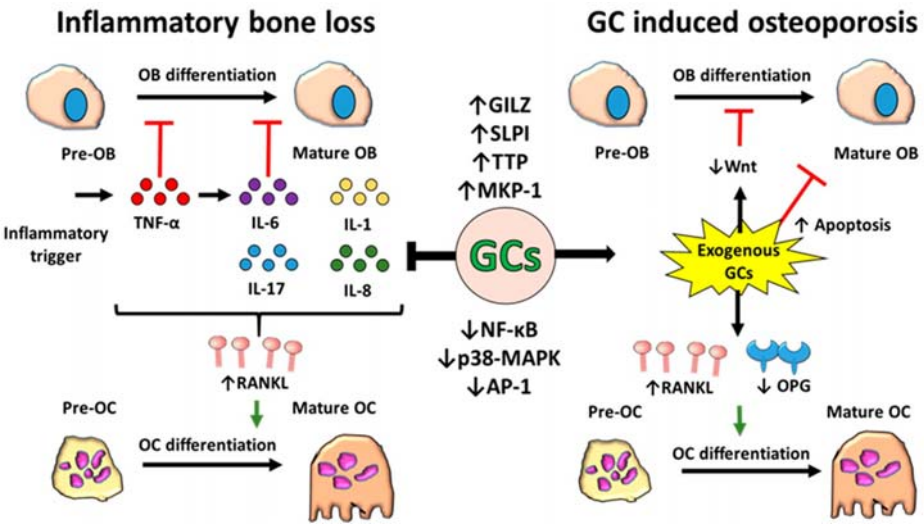

Figure 2. Schematic representation of the effects of inflammation and glucocorticoids (GCs) on bone remodelling. During inflammation, elevated levels of pro-inflammatory cytokines, such as TNF-α and IL-6, inhibit the differentiation of bone forming osteoblasts from their precursors. These cytokines, along with other pro-inflammatory mediators including IL-1, IL-17 and IL-8, also upregulate the expression of receptor activator of nuclear factor kappa-B ligand (RANKL), which binds to receptor activator of nuclear factor kappa-B (RANK) on pre-osteoclasts and triggers their differentiation into mature bone resorbing osteoclasts. Overall, bone formation is decreased while bone resorption is increased, leading to a net loss of bone. Although GCs suppress inflammation via suppression of pro-inflammatory factors and induction of anti-inflammatory mediators, they can also independently drive bone loss by inhibiting differentiation and inducing apoptosis of osteoblasts whilst increasing osteoclast differentiation by stimulating expression of RANKL and decreasing its decoy receptor osteoprotegerin (OPG). Osteoblasts (OBs), p38 mitogen-activated protein kinases (p-38-MAPK), glucocorticoid-induced leucine zipper (GILZ), secretory leukocyte protease inhibitor (SLPI), tristetraprolin (TTP), mitogen-activated protein kinase-1 (MKP-1), activator protein 1 (AP-1), OC (osteoclast), canonical WNT signalling (WNT), and nuclear factor kappa-light-chain-enhancer of activated B cells (NF-κB).

7. Muscle Mass Related Metabolism

Similar to bone, muscle metabolism is tightly regulated to ensure a balance between anabolic and catabolic processes governing muscle mass. Its regulation is critical not only to facilitate mechanical locomotion, but also as a key site for whole body energy metabolism and homeostasis [88]. Several critical anabolic and catabolic signalling pathways determine muscle protein synthesis, muscle proteolysis and myogenesis as cellular processes in control of muscle mass.

IGF-1 has been identified as a critical factor mediating the regulation of anabolic and catabolic muscle homeostasis in adult myofibers. Produced primarily in the liver, its binding to the IGF-1 receptor (IGF1R) in skeletal muscle allows recruitment of the insulin receptor substrate 1 (IRS-1) and activation of phosphatidylinositol-3-kinase (PI3K) and phosphorylation of protein kinase B (nnown as AKT), [89,90]. Together, these result in the activation of the mammalian target of rapamycin (mTOR) signalling pathway, which results in suppression of proteolysis and activation of muscle protein synthesis. mTOR activation suppresses proteolytic, forkhead box class O family member proteins (FOXOs) and glycogen synthase kinase-3 beta (GSK-3β) pathways [91,92]. The activation of mTOR signalling promotes muscle protein synthesis through the downstream phosphorylation and inactivation of eIF4E-binding protein 1 (4E-BP1) and activation of the ribosomal protein S6 kinase beta-1 (p70S6K) [93–95]. When active, 4E-BP1 operates by suppressing the eukaryotic translation initiation factors (eIF), which are a central rate limiting step in the regulation of protein synthesis in muscle. Here, eIF4F (a complex of initiation factors, eIF4e, eIF4G and eIF4A), promotes the translation of mRNA coding for muscle proteins by facilitating the cap dependent binding of messenger RNA to the 40S ribosomal subunit [96]. The repressor protein 4E-BP1 is a powerful negative regulator of eIF4F mediated protein translation, whilst its phosphorylation causes its dissociation from eIF4E and enables mRNA translation of anabolic muscle proteins. A second key stage in the regulation of anabolic protein metabolism in muscle occurs through the regulation of phosphorylated p70S6K by mTOR, which facilitates ribosomal biogenesis and translation capacity required for muscle protein anabolism [97]. An additional modulator of skeletal muscle mass downstream of the IGF-1/AKT pathway is GSK-3β. This protein kinase is a negative regulator of the translation initiation factor eIF2B and is phosphorylated and inactivated by AKT, allowing initiation of mRNA translation [98–100]. Together, the activation of these pathways by IGF-1 or insulin promote protein synthesis in muscle, favouring increased muscle mass.

The regulation of muscle catabolism shares many of these pathways and involves their inverse activation state. Proteolysis of skeletal muscle proteins through their targeted degradation by the ubiquitin-proteasome system (UPS) and autophagy pathways is under stringent control of the PI3K/AKT and mTOR signalling pathways [101]. Here, a reduction in anabolic factors such as IGF-1 or an increase in negative regulators such as myostatin, TGFβ or FGF results in a decrease of the PI3K/AKT and mTOR signalling. As AKT and mTOR kinase activity is responsible for inhibitory phosphorylation of the FOXOs, including FOXO1, FOXO3 and FOXO4 [102,103], the lack thereof allows their nuclear translocation. FOXO transcription factors bind to promoter and enhancer regions of target genes such as the E3 ligases, Atrogin-1 and muscle RING-Finger protein-1 (MURF-1) and the autophagy-related genes *LC3* and *Bnip3* [104–107]. In addition to FOXO, increased GSK-3β secondary to reduced IGF-1/AKT signalling has also been implicated in upregulating Atrogin-1 and MURF-1 [108].

The E3 ligases are the largest family of ubiquitination factors targeting muscle proteins for degradation by the UPS [109,110] and can be highly upregulated in catabolic conditions. These include the muscle specific F-box protein Atrogin-1 encoded by the *FBXO32* gene and MURF-1 encoded by the *TRIM63* gene [111,112]. Their expression is elevated in a plethora of skeletal muscle atrophy models, including immobilisation, denervation, cancer, starvation and diabetes [111–113]. Atrogin-1 has been shown to ubiquitinate desmin and vimentin, muscle proteins essential to sarcomere Z-disk architecture [114]. In addition, Atrogin-1 stimulates the degradation of transcription factor EIF3F,

leading to impaired muscle protein synthesis [115]. This E3 ligase has also been shown to play a pivotal role in repressing myogenesis through the ubiquitination of myoblast determination protein 1 (MYOD) [116].

MURF-1 encodes a protein containing a RING finger domain, which is responsible for its ubiquitin-ligase activity [112,117]. MURF-1 ubiquitinates and catalyses the degradation of contractile proteins and thick filaments, such as myosin and troponin I, with the sparing of thin filaments such as actin [118,119]. Besides a role in the UPS, increased FOXO activation also upregulates protein degradation and clearance through the autophagy pathways [106]. In muscle, this appears to be mediated through the direct upregulation of autophagy genes such as *LC3, BNIP3* and *ATG* through the FOXO pathway during muscular atrophy [120–122].

Postnatal myogenesis is an anabolic process important to the maintenance of muscle mass and integrity. Insulin-like growth factor 1 (IGF-1) has been shown to be a positive driver of myogenesis, whilst fibroblast growth factor (FGF), transforming growth factor β (TGF- β) and myostatin are potent inhibitors [123–126]. In addition, various secreted WNT signalling factors positively influence myogenesis. These are regulated by an array of stimuli, including exercise, nerve innervation and dietary protein intake, and are mediated through various gene regulatory networks including the T-box family, tbx6, ripply1 and mesp-ba in mesenchymal stem cell populations [127–129]. Ultimately, this drives the expression of myogenic regulatory factors (MRFs) such as myogenic differentiation 1 (MYOD), myogenic factor 5 (MYF5) and myogenin (MYOG), this process being in mesenchymal derived muscle progenitor cells called satellite cells [130–133]. Although some redundancy exists in their cellular function, MYF5 is mostly implicated in mediating the proliferation of satellite cells and MYOD in their differentiation into myoblasts, whilst downstream factors, including myogenin, initiate further differentiation of mature myocytes followed by the fusion and formation of mature myotubes [130–132] or mostly relevant for adult muscle, fusion with myofibers.

Below, we will describe how inflammation and glucocorticoids impact these regulatory processes of muscle mass metabolism, driving a shift towards anti-anabolic and catabolic protein metabolism, resulting in muscle wasting.

8. Effects of Inflammation of Muscle Metabolism

Inflammation is a well established driver of muscle wasting in preclinical models and strongly relates to poor prognostic outcome and increased morbidity and mortality in patients with chronic inflammatory diseases [134]. Pro-inflammatory cytokines such as TNFβα, IL-1β and IL-6, which are elevated in chronic inflammation, are themselves reported to drive proteolysis and autophagy and suppress myogenesis and protein synthesis in muscle [135–138]. Of these, TNF-α, at the apex of the inflammatory cytokine cascade in many chronic inflammatory diseases, is critical in regulating inflammatory muscle wasting. Here, its activation of the NF-kB and p-38 MAPK pathways directly induces muscle wasting through the increased expression of the E3 ligases, atrogin-1 and MURF-1 and activation of the UPS system [139–143]. In models of chronic inflammation, TNF-α also downregulates circulating levels of IGF-1 and the downstream PI3K/AKT/mTOR signalling pathways, whilst upregulating the catabolic FOXO pathway to suppress protein synthesis and myogenesis in muscle [141,142,144,145]. Another factor implicated in inflammatory muscle wasting is myostatin. This is also reported to be increased in chronic inflammation, where it positively correlates with markers of disease severity. Elevated myostatin downregulates PI3K/AKT/mTOR signalling, promoting muscle atrophy [146,147]. Of interest, several studies have reported elevated endogenous GC levels as being central mediators of inflammatory muscle wasting. Here, the inflammatory activation of the hypothalamic/pituitary/adrenal (HPA) axis in response results in an elevation of circulating cortisol to mediate muscle wasting [148–151]. Of note, the blockade of endogenous GC production or muscle GR signalling could reverse muscle wasting in some experimental

models [152,153]. This indicates that in addition to a direct impact of inflammation on intra-cellular muscle mass regulatory processes, activation of the HPA axis as an evolutionarily conserved response to suppress systemic inflammation can result in GC driven muscle wasting as an indirect effect of inflammation on skeletal muscle.

9. Effects of Glucocorticoids on Muscle Metabolism

Extended exposure to therapeutic GCs results in the rapid onset of a GC induced muscle atrophy, characterised by a decrease in myogenesis and protein synthesis and an increase in proteolysis and atrophy of muscle fibres [9,154–157]. This leads to a significant decrease in muscle fibre size, with a greater degree of wasting apparent in fast-twitch or type II muscle fibres [158]. The shift towards greater catabolic loss of protein and decreased anabolic synthesis in muscle is elicited by GCs through a number of pathways, including a decrease in IGF-1 signalling and an increase in negative regulators of the mTOR pathways such as myostatin and the protein regulated in development and DNA damage response 1 (REDD1) [157,159]. Similarly, as with inflammatory pathway activation, GCs also activate the UPS and autophagy secondary to upregulation of the FOXO1 pathway [80,154,160]. In particular, the marked increase in degradation of contractile skeletal muscle proteins through the UPS system is believed to be central in GC induced muscle wasting in vivo. This is supported by several studies demonstrating the downregulation of the PI3K/AKT/mTOR signalling pathways and the upregulation of the E3 ligases Atrogin-1 and MURF-1 in response to GCs [112]. Several studies have also demonstrated a significant increase in 4E-BP1 and suppression of p70S6K in GC induced muscle atrophy, demonstrating a role for reduced protein synthesis and regeneration [157,159]. Of interest, the restoration of IGF-1 signalling can rescue GC induced myopathy in mice, demonstrating a crucial role for this growth factor in the process of GC-induced myopathy [9,154–156]. Glucocorticoid mediated muscle wasting has also been shown to be rescued through the in vivo deletion of myostatin, indicating that the negative regulation of the IGF-1 pathway may also be a crucial step in this process [161–163].

10. Interaction between Inflammation and Glucocorticoids in Muscle

As with bone, many of the central inflammatory pathways that induce muscle wasting, including the NF-kB and p38-MAPK pathways, are themselves suppressed by GC signalling, suggesting that therapeutic application may protect against the process of inflammatory muscle wasting. However, other elements of inflammatory muscle wasting such as the suppression of IGF-1 and induction of myostatin and FOXO1 pathway activation are common components in both inflammatory and GC induced muscle wasting (Figure3). Understanding how these interact in vivo remains paramount in our understanding of how therapeutic GCs should be applied in the setting of chronic inflammatory disease. Some insights arise from clinical studies exploring these processes in patients with inflammatory disease receiving GCs. Of note, in inflammatory myopathies arising directly from muscle inflammation, such as with polymyositis and dermatomyositis, GCs are effective in controlling inflammation and protecting against inflammatory muscle wasting and associated weakness [164]. Similarly, therapeutic GCs are effective in preventing muscle wasting in patients with Duchenne muscular dystrophy (DMD), where progressive muscle necrosis mediates loss of muscle [165–169]. However, in other inflammatory diseases, where muscle wasting occurs secondarily to inflammation at a non-muscle site, the application of therapeutic GCs is strongly associated with rapid loss of muscle mass [170,171]. These findings may suggest that GCs can oppose the process of inflammatory muscle wasting when the active inflammation is confined to the muscle, but promote muscle wasting when used to manage other systemic chronic inflammatory diseases such as RA. As with GC induced osteoporosis in patients with chronic inflammatory disease, the interpretation of these findings in relation to muscle wasting is complicated by disease severity and duration and by concurrent DMARD therapies.

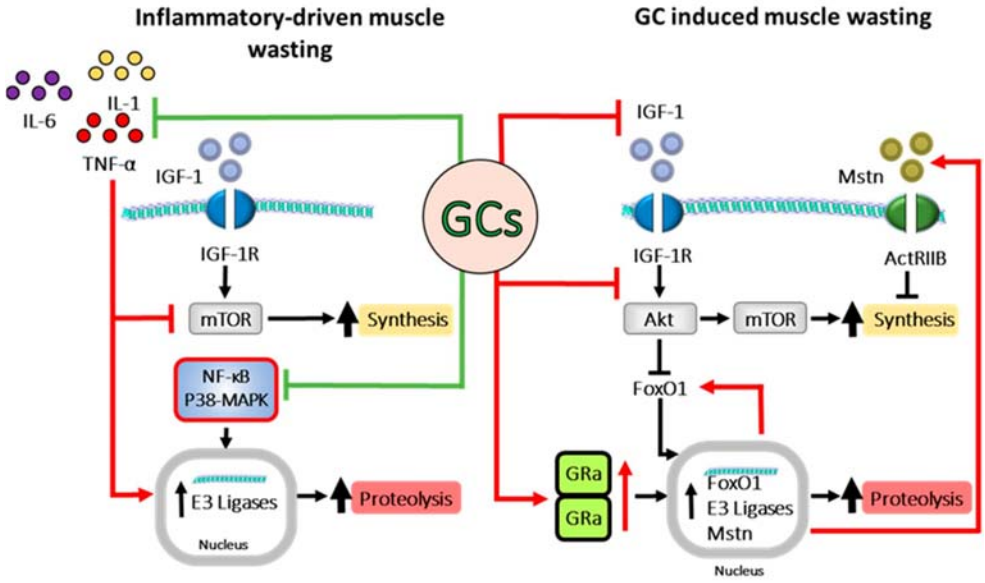

Figure 3. Schematic representation of signalling pathways involved in both inflammatory driven and GC induced muscle wasting and their interactions. Inflammatory cytokines such as TNF-α and IL-1 inhibit mammalian target of rapamycin (mTOR) signalling, dampening muscle protein synthesis, whilst simultaneously inducing transcription of E3 ligases, leading to muscle proteolysis. Glucocorticoids (GCs) inhibit inflammatory signalling, including nuclear factor kappa-light-chain-enhancer of activated B cells (NF-κB) signalling, and therefore decrease inflammatory driven muscle wasting. Despite this, GCs also drive muscle wasting through several pathways themselves, including suppression of the IGF-1/AKT/mTOR signalling cascade, leading to decreased protein synthesis and increased FOXO1 transcription. GR activation and dimerization induce the transcription of myostatin (MSTN), FOXO1 and other E3 ligases, leading to increased proteolysis and diminished protein synthesis. Forkhead box protein O1 (FOXO1), mammalian target of rapamycin (mTOR), insulin like growth factor (IGF-1), (p-38-MAPK), glucocorticoid induced leucine zipper (GILZ), secretory leukocyte protease inhibitor (SLPI), tristetraprolin (TTP), nuclear factor kappa-light-chain-enhancer of activated B cells (NF-κB), glucocorticoid receptor (GR), myostatin (MSTN), and IGF-1 receptor (IGF-1 R).

11. Insights from Murine Models of Chronic Inflammation Receiving Therapeutic Glucocorticoids

Additional insight has come from murine models of polyarthritis receiving therapeutic GCs. These are able to circumvent issues related to differences in disease activity between patients and complications arising from the various alternative anti-inflammatory drugs used to manage disease in patients. In one such study, we examined the role of the GC corticosterone, delivered as a monotherapy in the TNF-tg murine model of polyarthritis, on net bone and muscle metabolism [80]. This revealed that therapeutic doses of GCs, whilst effective at suppressing disease activity, also potently suppressed inflammatory osteoporosis and juxta articular bone loss. This confirmed that their capacity to suppress inflammatory pathways that mediate inflammatory bone loss outweighed their deleterious effects on bone metabolism. These bone sparing effects of GCs were mediated through the suppression of pro-inflammatory osteoclasts' activation, both systemically and at sites of inflammation. However, whilst these treatments protected from inflammatory bone loss, we still observed a suppression of anabolic bone formation in all mice receiving GCs, suggesting that long term administration may still ultimately result in GIO.

Unlike bone, therapeutic GCs markedly exacerbated muscle wasting in mice with chronic inflammation. This was characterized by a marked activation of the catabolic FOXO1 and UPS pathways [80]. Similar findings had been reported in rats, where dexamethasone exacerbated inflammatory muscle wasting in models of sepsis [172]. These data indicate that the beneficial effects of inflammatory suppression by GCs in muscle were not sufficient to outweigh their deleterious actions on muscle metabolism. Whilst further

work is required to better elucidate the actions of therapeutic GCs in the context of chronic inflammation, these data shed light on the potential strengths and weaknesses of their application in muscle and bone. In particular, they indicate that the management of side effects in muscle may need to be prioritised over those in bone, in patients with chronic inflammatory diseases receiving therapeutic GCs.

12. Pre-Receptor Regulation of Therapeutic GC Action to Protect against Side Effects

The pre-receptor metabolism of GCs by the 11β-hydroxysteroid dehydrogenase (11β-HSD) enzymes is recognised as a critical step in mediating GC signalling in many peripheral tissues. These are the 11β-HSD type 1 (11β-HSD1) and type 2 (11β-HSD2). 11β-HSD1 is expressed in many tissues, including the liver, bone, muscle and fat, where it converts inactive endogenous and therapeutic GCs (such as corticosterone and prednisone) to their active counterparts (such as cortisol and prednisolone), leading to a local accumulation and concentration of active GCs [173–175] (Figure4). In contrast, 11β-HSD2 solely inactivates endogenous and therapeutic GCs within the kidney, providing circulating inactive GC substrate for the peripheral 11β-HSD1 enzyme and supporting renal clearance of GCs [175]. Several key studies have demonstrated a critical role for the pre-receptor activation of GCs by 11β-HSD1 in mediating the deleterious actions of therapeutic GCs in muscle and bone [176,177]. Here, animals with transgenic deletion of 11β-HSD1 are resistant to both exogenous GC induced muscle wasting and osteoporosis. This raises the exciting possibility that therapeutic 11β-HSD1 inhibitors, widely explored in the management of metabolic disease, may prevent bone loss and muscle wasting in patients with chronic inflammatory diseases receiving GCs [178,179]. Further studies lend strength to this concept, showing that 11β-HSD1 is potently upregulated within muscle cells and osteoblasts, where it is potently upregulated by circulating inflammatory cytokines such as TNF-α and IL-1β [174,180,181]. Despite this, caution should be applied in this context, given that systemic deletion of 11β-HSD1 can exacerbate disease activity in murine models of inflammation, secondary to a reduction in reactivation of endogenous GC at sites of inflammation [182,183]. Consequently, further studies are required to delineate the potential benefits and risks of 11β-HSD1 inhibition in chronic inflammatory disease.

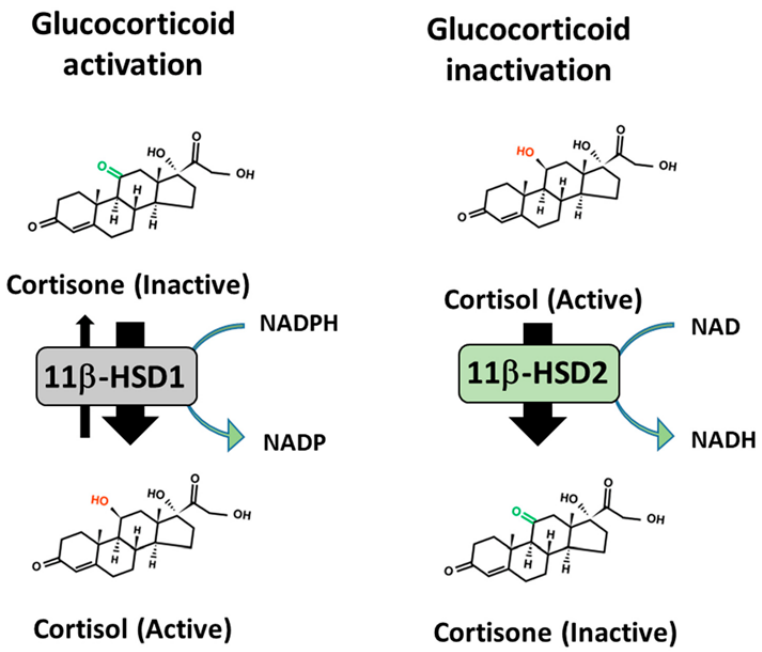

Figure 4. Pre-receptor metabolism of GCs by 11β-HSD1. 11β-hydroxysteroid dehydrogenase (11β-HSD) type 1 is a bidirectional enzyme that predominantly reduces inactive GCs to their active counterparts in an NADPH dependent manner, whilst 11β-HSD type 2 is an NAD+ dependent unidirectional enzyme that converts active GCs to their inactive counterparts.

13. Conclusions

Both chronic inflammation and therapeutic GCs are potent drivers for systemic bone and muscle wasting resulting from an imbalance between anabolic and catabolic homeostasis. Whilst therapeutic GCs oppose many of the inflammatory pathways that drive bone and muscle wasting, they share common pathways that promote anti-anabolic and catabolic metabolism of bone and muscle and can drive or exacerbate these deleterious processes in chronic inflammatory disease. However, these relationships are invariably complicated by the nature of the inflammatory disease in which therapeutic GCs are utilized. Intriguingly, 11β-HSD1 inhibitors may possess the potential to prevent the deleterious actions of therapeutic GCs in the backdrop of chronic inflammation. However, further studies are required to assess their efficacy and safety in this context.

Acknowledgments: This review was supported by the Arthritis Research UK grant, Versus Arthritis: 20843.

Conflicts of Interest: The authors declare no conflict of interest.

References

1. Clayton, S.A.; Jones, S.W.; Kurowska-Stolarska, M.; Clark, A.R. The role of microRNAs in glucocorticoid action. *J. Biol. Chem.* **2018**, *293*, 1865–1874. [CrossRef] [PubMed]
2. Abraham, S.M.; Lawrence, T.; Kleiman, A.; Warden, P.; Medghalchi, M.; Tuckermann, J.; Saklatvala, J.; Clark, A.R. Antiinflammatory effects of dexamethasone are partly dependent on induction of dual specificity phosphatase 1. *J. Exp. Med.* **2006**, *203*, 1883–1889. [CrossRef] [PubMed]
3. Marco, B.D.; Massetti, M.; Bruscoli, S.; Macchiarulo, A.; Virgilio, R.D.; Velardi, E.; Donato, V.; Migliorati, G.; Riccardi, C. Glucocorticoid-induced leucine zipper (GILZ)/NF-kappaB interaction: Role of GILZ homo-dimerization and C-terminal domain. *Nucleic Acids Res.* **2007**, *35*, 517–528. [CrossRef] [PubMed]
4. Klint, E.A.; Grundtman, C.; Engström, M.; Catrina, A.I.; Makrygiannakis, D.; Klareskog, L.; Andersson, U.; Ulfgren, A.K. Intraarticular glucocorticoid treatment reduces inflammation in synovial cell infiltrations more efficiently than in synovial blood vessels. *Arthritis Rheum.* **2005**, *52*, 3880–3889. [CrossRef] [PubMed]
5. Gilmour, J.S.; Coutinho, A.E.; Cailhier, J.F.; Man, T.Y.; Clay, M.; Thomas, G.; Harris, H.J.; Mullins, J.J.; Seckl, J.R.; Savill, J.S.; et al. Local amplification of glucocorticoids by 11 beta-hydroxysteroid dehydrogenase type 1 promotes macrophage phagocytosis of apoptotic leukocytes. *J. Immunol.* **2006**, *176*, 7605–7611. [CrossRef]
6. Fardet, L.; Flahault, A.; Kettaneh, A.; Tiev, K.P.; Généreau, T.; Tolédano, C.; Lebbé, C.; Cabane, J. Corticosteroid-induced clinical adverse events: Frequency, risk factors and patient's opinion. *Br. J. Dermatol.* **2007**, *157*, 142–148. [CrossRef]
7. Feldstein, A.C.; Elmer, P.J.; Nichols, G.A.; Herson, M. Practice patterns in patients at risk for glucocorticoid-induced osteoporosis. *Osteoporos. Int.* **2005**, *16*, 2168–2174. [CrossRef]
8. Strehl, C.; Bijlsma, J.W.; de Wit, M.; Boers, M.; Caeyers, N.; Cutolo, M.; Dasgupta, B.; Dixon, W.G.; Geenen, R.; Huizinga, T.W.; et al. Defining conditions where long-term glucocorticoid treatment has an acceptably low level of harm to facilitate implementation of existing recommendations: Viewpoints from an EULAR task force. *Ann. Rheum. Dis.* **2016**, *75*, 952–957. [CrossRef]
9. Löfberg, E.; Gutierrez, A.; Wernerman, J.; Anderstam, B.; Mitch, W.E.; Price, S.R.; Bergström, J.; Alvestrand, A. Effects of high doses of glucocorticoids on free amino acids, ribosomes and protein turnover in human muscle. *Eur. J. Clin. Investig.* **2002**, *32*, 345–353. [CrossRef]
10. Qi, D.; Pulinilkunnil, T.; An, D.; Ghosh, S.; Abrahani, A.; Pospisilik, J.A.; Brownsey, R.; Wambolt, R.; Allard, M.; Rodrigues, B. Single-dose dexamethasone induces whole-body insulin resistance and alters both cardiac fatty acid and carbohydrate metabolism. *Diabetes* **2004**, *53*, 1790–1797. [CrossRef]
11. Wu, B.; Li, P.; Liu, Y.; Lou, Z.; Ding, Y.; Shu, C.; Ye, S.; Bartlam, M.; Shen, B.; Rao, Z. 3D structure of human FK506-binding protein 52: Implications for the assembly of the glucocorticoid receptor/Hsp90/immunophilin heterocomplex. *Proc. Natl. Acad. Sci. USA* **2004**, *101*, 8348–8353. [CrossRef] [PubMed]
12. Barnes, P.J. How corticosteroids control inflammation: Quintiles Prize Lecture 2005. *Br. J. Pharmacol.* **2006**, *148*, 245–254. [CrossRef] [PubMed]

13. Reichardt, H.M.; Tuckermann, J.P.; Göttlicher, M.; Vujic, M.; Weih, F.; Angel, P.; Herrlich, P.; Schütz, G. Repression of inflammatory responses in the absence of DNA binding by the glucocorticoid receptor. *EMBO J.* **2001**, *20*, 7168–7173. [CrossRef] [PubMed]
14. Schäcke, H.; Schottelius, A.; Döcke, W.D.; Strehlke, P.; Jaroch, S.; Schmees, N.; Rehwinkel, H.; Hennekes, H.; Asadullah, K. Dissociation of transactivation from transrepression by a selective glucocorticoid receptor agonist leads to separation of therapeutic effects from side effects. *Proc. Natl. Acad. Sci. USA* **2004**, *101*, 227–232. [CrossRef]
15. Reichardt, H.M.; Kaestner, K.H.; Tuckermann, J.; Kretz, O.; Wessely, O.; Bock, R.; Gass, P.; Schmid, W.; Herrlich, P.; Angel, P.; et al. DNA Binding of the Glucocorticoid Receptor Is Not Essential for Survival. *Cell* **1998**, *93*, 531–541. [CrossRef]
16. Koenen, M.; Culemann, S.; Vettorazzi, S.; Caratti, G.; Frappart, L.; Baum, W.; Krönke, G.; Baschant, U.; Tuckermann, J.P. Glucocorticoid receptor in stromal cells is essential for glucocorticoid-mediated suppression of inflammation in arthritis. *Ann. Rheum. Dis.* **2018**, *77*, 1610–1618. [CrossRef]
17. Scheschowitsch, K.; Leite, J.A.; Assreuy, J. New Insights in Glucocorticoid Receptor Signaling-More Than Just a Ligand-Binding Receptor. *Front. Endocrinol.* **2017**, *8*, 16. [CrossRef]
18. Abbinante-Nissen, J.M.; Simpson, L.G.; Leikauf, G.D. Corticosteroids increase secretory leukocyte protease inhibitor transcript levels in airway epithelial cells. *Am. J. Physiol.* **1995**, *268 Pt 1*, L601–L606. [CrossRef]
19. Manetsch, M.; Ramsay, E.E.; King, E.M.; Seidel, P.; Che, W.; Ge, Q.; Hibbs, D.E.; Newton, R.; Ammit, A.J. Corticosteroids and β_2-agonists upregulate mitogen-activated protein kinase phosphatase 1: In vitro mechanisms. *Br. J. Pharmacol.* **2012**, *166*, 2049–2059. [CrossRef]
20. Wang, J.C.; Derynck, M.K.; Nonaka, D.F.; Khodabakhsh, D.B.; Haqq, C.; Yamamoto, K.R. Chromatin immunoprecipitation (ChIP) scanning identifies primary glucocorticoid receptor target genes. *Proc. Natl. Acad. Sci. USA* **2004**, *101*, 15603–15608. [CrossRef]
21. Smoak, K.; Cidlowski, J.A. Glucocorticoids regulate tristetraprolin synthesis and posttranscriptionally regulate tumor necrosis factor alpha inflammatory signaling. *Mol. Cell. Biol.* **2006**, *26*, 9126–9135. [CrossRef] [PubMed]
22. Liu, T.; Zhang, L.; Joo, D.; Sun, S.-C. NF-κB signaling in inflammation. *Signal Transduct. Target. Ther.* **2017**, *2*, 17023. [CrossRef] [PubMed]
23. Frost, H.M. Skeletal structural adaptations to mechanical usage (SATMU): 2. Redefining Wolff's law: The remodeling problem. *Anat. Rec.* **1990**, *226*, 414–422. [CrossRef] [PubMed]
24. Burra, S.; Nicolella, D.P.; Francis, W.L.; Freitas, C.J.; Mueschke, N.J.; Poole, K.; Jiang, J.X. Dendritic processes of osteocytes are mechanotransducers that induce the opening of hemichannels. *Proc. Natl. Acad. Sci. USA* **2010**, *107*, 13648–13653. [CrossRef] [PubMed]
25. Verborgt, O.; Tatton, N.A.; Majeska, R.J.; Schaffler, M.B. Spatial distribution of Bax and Bcl-2 in osteocytes after bone fatigue: Complementary roles in bone remodeling regulation? *J. Bone Miner. Res.* **2002**, *17*, 907–914. [CrossRef]
26. Aguirre, J.I.; Plotkin, L.I.; Stewart, S.A.; Weinstein, R.S.; Parfitt, A.M.; Manolagas, S.C.; Bellido, T. Osteocyte apoptosis is induced by weightlessness in mice and precedes osteoclast recruitment and bone loss. *J. Bone Miner. Res.* **2006**, *21*, 605–615. [CrossRef]
27. Al-Dujaili, S.A.; Lau, E.; Al-Dujaili, H.; Tsang, K.; Guenther, A.; You, L. Apoptotic osteocytes regulate osteoclast precursor recruitment and differentiation in vitro. *J. Cell. Biochem.* **2011**, *112*, 2412–2423. [CrossRef]
28. Takayanagi, H.; Kim, S.; Koga, T.; Nishina, H.; Isshiki, M.; Yoshida, H.; Saiura, A.; Isobe, M.; Yokochi, T.; Inoue, J.I.; et al. Induction and activation of the transcription factor NFATc1 (NFAT2) integrate RANKL signaling in terminal differentiation of osteoclasts. *Dev. Cell.* **2002**, *3*, 889–901. [CrossRef]
29. Kukita, T.; Wada, N.; Kukita, A.; Kakimoto, T.; Sandra, F.; Toh, K.; Nagata, K.; Iijima, T.; Horiuchi, M.; Matsusaki, H.; et al. RANKL-induced DC-STAMP is essential for osteoclastogenesis. *J. Exp. Med.* **2004**, *200*, 941–946. [CrossRef]
30. Wu, H.; Xu, G.; Li, Y.P. Atp6v0d2 is an essential component of the osteoclast-specific proton pump that mediates extracellular acidification in bone resorption. *J. Bone Miner. Res.* **2009**, *24*, 871–885. [CrossRef]

31. Väänänen, H.K.; Karhukorpi, E.K.; Sundquist, K.; Wallmark, B.; Roininen, I.; Hentunen, T.; Tuukkanen, J.; Lakkakorpi, P. Evidence for the presence of a proton pump of the vacuolar H(+)-ATPase type in the ruffled borders of osteoclasts. *J. Cell Biol.* **1990**, *111*, 1305–1311. [CrossRef] [PubMed]
32. Blair, H.C.; Schlesinger, P.H. Purification of a stilbene sensitive chloride channel and reconstitution of chloride conductivity into phospholipid vesicles. *Biochem. Biophys. Res. Commun.* **1990**, *171*, 920–925. [CrossRef]
33. Tang, Y.; Wu, X.; Lei, W.; Pang, L.; Wan, C.; Shi, Z.; Zhao, L.; Nagy, T.R.; Peng, X.; Hu, J.; et al. TGF-beta1-induced migration of bone mesenchymal stem cells couples bone resorption with formation. *Nat. Med.* **2009**, *15*, 757–765. [CrossRef] [PubMed]
34. Xian, L.; Wu, X.; Pang, L.; Lou, M.; Rosen, C.J.; Qiu, T.; Crane, J.; Frassica, F.; Zhang, L.; Rodriguez, J.P.; et al. Matrix IGF-1 maintains bone mass by activation of mTOR in mesenchymal stem cells. *Nat. Med.* **2012**, *18*, 1095–1101. [CrossRef]
35. Poole, K.E.; van Bezooijen, R.L.; Loveridge, N.; Hamersma, H.; Papapoulos, S.E.; Löwik, C.W.; Reeve, J. Sclerostin is a delayed secreted product of osteocytes that inhibits bone formation. *FASEB J.* **2005**, *19*, 1842–1844. [CrossRef]
36. Ducy, P.; Zhang, R.; Geoffroy, V.; Ridall, A.L.; Karsenty, G. Osf2/Cbfa1: A transcriptional activator of osteoblast differentiation. *Cell* **1997**, *89*, 747–754. [CrossRef]
37. Roca, H.; Phimphilai, M.; Gopalakrishnan, R.; Xiao, G.; Franceschi, R.T. Cooperative interactions between RUNX2 and homeodomain protein-binding sites are critical for the osteoblast-specific expression of the bone sialoprotein gene. *J. Biol. Chem.* **2005**, *280*, 30845–30855. [CrossRef]
38. Cao, J.; Venton, L.; Sakata, T.; Halloran, B.P. Expression of RANKL and OPG correlates with age-related bone loss in male C57BL/6 mice. *J. Bone Miner. Res.* **2003**, *18*, 270–277. [CrossRef]
39. Andersen, T.L.; Abdelgawad, M.E.; Kristensen, H.B.; Hauge, E.M.; Rolighed, L.; Bollerslev, J.; Kjærsgaard-Andersen, P.; Delaisse, J.M. Understanding coupling between bone resorption and formation: Are reversal cells the missing link? *Am. J. Pathol.* **2013**, *183*, 235–246. [CrossRef]
40. Cowles, E.A.; DeRome, M.E.; Pastizzo, G.; Brailey, L.L.; Gronowicz, G.A. Mineralization and the expression of matrix proteins during in vivo bone development. *Calcif. Tissue Int.* **1998**, *62*, 74–82. [CrossRef]
41. Weiner, S. Organization of extracellularly mineralized tissues: A comparative study of biological crystal growth. *CRC Crit. Rev. Biochem.* **1986**, *20*, 365–408. [CrossRef] [PubMed]
42. Orimo, H. The mechanism of mineralization and the role of alkaline phosphatase in health and disease. *J. Nippon Med. Sch.* **2010**, *77*, 4–12. [CrossRef] [PubMed]
43. Haugeberg, G.; Orstavik, R.E.; Uhlig, T.; Falch, J.A.; Halse, J.I.; Kvien, T.K. Bone loss in patients with rheumatoid arthritis: Results from a population-based cohort of 366 patients followed up for two years. *Arthritis Rheum.* **2002**, *46*, 1720–1728. [CrossRef] [PubMed]
44. Walker-Bone, K. Recognizing and treating secondary osteoporosis. *Nat. Rev. Rheumatol.* **2012**, *8*, 480–492. [CrossRef]
45. Tack, G.J.; Verbeek, W.H.; Schreurs, M.W.; Mulder, C.J. The spectrum of celiac disease: Epidemiology, clinical aspects and treatment. *Nat. Rev. Gastroenterol. Hepatol.* **2010**, *7*, 204–213. [CrossRef]
46. Graat-Verboom, L.; Spruit, M.A.; van den Borne, B.E.; Smeenk, F.W.; Martens, E.J.; Lunde, R.; Wouters, E.F. Correlates of osteoporosis in chronic obstructive pulmonary disease: An underestimated systemic component. *Respir. Med.* **2009**, *103*, 1143–1151. [CrossRef]
47. Ding, C.; Parameswaran, V.; Udayan, R.; Burgess, J.; Jones, G. Circulating levels of inflammatory markers predict change in bone mineral density and resorption in older adults: A longitudinal study. *J. Clin. Endocrinol. Metab.* **2008**, *93*, 1952–1958. [CrossRef]
48. Barbour, K.E.; Lui, L.Y.; Ensrud, K.E.; Hillier, T.A.; LeBlanc, E.S.; Ing, S.W.; Hochberg, M.C.; Cauley, J.A. Study of Osteoporotic Fractures (SOF) Research Group. Inflammatory markers and risk of hip fracture in older white women: The study of osteoporotic fractures. *J. Bone Miner. Res.* **2014**, *29*, 2057–2064. [CrossRef]
49. Barbour, K.E.; Boudreau, R.; Danielson, M.E.; Youk, A.O.; Wactawski-Wende, J.; Greep, N.C.; LaCroix, A.Z.; Jackson, R.D.; Wallace, R.B.; Bauer, D.C.; et al. Inflammatory markers and the risk of hip fracture: The Women's Health Initiative. *J. Bone Miner. Res.* **2012**, *27*, 1167–1176. [CrossRef]

50. Pasco, J.A.; Kotowicz, M.A.; Henry, M.J.; Nicholson, G.C.; Spilsbury, H.J.; Box, J.D.; Schneider, H.G. High-sensitivity C-reactive protein and fracture risk in elderly women. *JAMA* **2006**, *296*, 1353–1355. [CrossRef]
51. Hardy, R.; Cooper, M.S. Bone loss in inflammatory disorders. *J. Endocrinol.* **2009**, *201*, 309. [CrossRef] [PubMed]
52. Wei, S.; Kitaura, H.; Zhou, P.; Ross, F.P.; Teitelbaum, S.L. IL-1 mediates TNF-induced osteoclastogenesis. *J. Clin. Investig.* **2005**, *115*, 282–290. [CrossRef] [PubMed]
53. Palmqvist, P.; Persson, E.; Conaway, H.H.; Lerner, U.H. IL-6, leukemia inhibitory factor, and oncostatin M stimulate bone resorption and regulate the expression of receptor activator of NF-kappa B ligand, osteoprotegerin, and receptor activator of NF-kappa B in mouse calvariae. *J. Immunol.* **2002**, *169*, 3353–3362. [CrossRef] [PubMed]
54. Yoshitake, F.; Itoh, S.; Narita, H.; Ishihara, K.; Ebisu, S. Interleukin-6 directly inhibits osteoclast differentiation by suppressing receptor activator of NF-kappaB signaling pathways. *J. Biol. Chem.* **2008**, *283*, 11535–11540. [CrossRef]
55. Kotake, S.; Udagawa, N.; Takahashi, N.; Matsuzaki, K.; Itoh, K.; Ishiyama, S.; Saito, S.; Inoue, K.; Kamatani, N.; Gillespie, M.T.; et al. IL-17 in synovial fluids from patients with rheumatoid arthritis is a potent stimulator of osteoclastogenesis. *J. Clin. Investig.* **1999**, *103*, 1345–1352. [CrossRef]
56. Ragab, A.A.; Nalepka, J.L.; Bi, Y.; Greenfield, E.M. Cytokines synergistically induce osteoclast differentiation: Support by immortalized or normal calvarial cells. *Am. J. Physiol. Cell Physiol.* **2002**, *283*, C679–C687. [CrossRef]
57. Kawai, T.; Matsuyama, T.; Hosokawa, Y.; Makihira, S.; Seki, M.; Karimbux, N.Y.; Goncalves, R.B.; Valverde, P.; Dibart, S.; Li, Y.P.; et al. B and T lymphocytes are the primary sources of RANKL in the bone resorptive lesion of periodontal disease. *Am. J. Pathol.* **2006**, *169*, 987–998. [CrossRef]
58. Sato, K.; Suematsu, A.; Okamoto, K.; Yamaguchi, A.; Morishita, Y.; Kadono, Y.; Tanaka, S.; Kodama, T.; Akira, S.; Iwakura, Y.; et al. Th17 functions as an osteoclastogenic helper T cell subset that links T cell activation and bone destruction. *J. Exp. Med.* **2006**, *203*, 2673–2682. [CrossRef]
59. Takayanagi, H.; Ogasawara, K.; Hida, S.; Chiba, T.; Murata, S.; Sato, K.; Takaoka, A.; Yokochi, T.; Oda, H.; Tanaka, K.; et al. T-cell-mediated regulation of osteoclastogenesis by signalling cross-talk between RANKL and IFN-gamma. *Nature* **2000**, *408*, 600–605. [CrossRef]
60. Rifas, L.; Weitzmann, M.N. A novel T cell cytokine, secreted osteoclastogenic factor of activated T cells, induces osteoclast formation in a RANKL-independent manner. *Arthritis Rheum.* **2009**, *60*, 3324–3335. [CrossRef]
61. Abbas, S.; Zhang, Y.H.; Clohisy, J.C.; Abu-Amer, Y. Tumor necrosis factor-alpha inhibits pre-osteoblast differentiation through its type-1 receptor. *Cytokine* **2003**, *22*, 33–41. [CrossRef]
62. Jilka, R.L.; Weinstein, R.S.; Bellido, T.; Parfitt, A.M.; Manolagas, S.C. Osteoblast Programmed Cell Death (Apoptosis): Modulation by Growth Factors and Cytokines. *J. Bone Miner. Res.* **1998**, *13*, 793–802. [CrossRef] [PubMed]
63. Kaneshiro, S.; Ebina, K.; Shi, K.; Higuchi, C.; Hirao, M.; Okamoto, M.; Koizumi, K.; Morimoto, T.; Yoshikawa, H.; Hashimoto, J. IL-6 negatively regulates osteoblast differentiation through the SHP2/MEK2 and SHP2/Akt2 pathways in vitro. *J. Bone Miner. Metab.* **2014**, *32*, 378–392. [CrossRef] [PubMed]
64. Redlich, K.; Görtz, B.; Hayer, S.; Zwerina, J.; Doerr, N.; Kostenuik, P.; Bergmeister, H.; Kollias, G.; Steiner, G.; Smolen, J.S.; et al. Repair of local bone erosions and reversal of systemic bone loss upon therapy with anti-tumor necrosis factor in combination with osteoprotegerin or parathyroid hormone in tumor necrosis factor-mediated arthritis. *Am. J. Pathol.* **2004**, *164*, 543–555. [CrossRef]
65. van Staa, T.P.; Leufkens, H.G.; Cooper, C. The epidemiology of corticosteroid-induced osteoporosis: A meta-analysis. *Osteoporos. Int.* **2002**, *13*, 777–787. [CrossRef]
66. Weinstein, R.S.; Jilka, R.L.; Parfitt, A.M.; Manolagas, S.C. Inhibition of osteoblastogenesis and promotion of apoptosis of osteoblasts and osteocytes by glucocorticoids. Potential mechanisms of their deleterious effects on bone. *J. Clin. Investig.* **1998**, *102*, 274–282. [CrossRef]

67. Zhou, H.; Mak, W.; Zheng, Y.; Dunstan, C.R.; Seibel, M.J. Osteoblasts directly control lineage commitment of mesenchymal progenitor cells through Wnt signaling. *J. Biol. Chem.* **2008**, *283*, 1936–1945. [CrossRef]
68. Mak, W.; Shao, X.; Dunstan, C.R.; Seibel, M.J.; Zhou, H. Biphasic glucocorticoid-dependent regulation of Wnt expression and its inhibitors in mature osteoblastic cells. *Calcif. Tissue Int.* **2009**, *85*, 538–545. [CrossRef]
69. O'Brien, C.A.; Jia, D.; Plotkin, L.I.; Bellido, T.; Powers, C.C.; Stewart, S.A.; Manolagas, S.C.; Weinstein, R.S. Glucocorticoids act directly on osteoblasts and osteocytes to induce their apoptosis and reduce bone formation and strength. *Endocrinology* **2004**, *145*, 1835–1841. [CrossRef]
70. Brunetti, G.; Faienza, M.F.; Piacente, L.; Ventura, A.; Oranger, A.; Carbone, C.; Benedetto, A.D.; Colaianni, G.; Gigante, M.; Mori, G.; et al. High dickkopf-1 levels in sera and leukocytes from children with 21-hydroxylase deficiency on chronic glucocorticoid treatment. *Am. J. Physiol. Endocrinol. Metab.* **2013**, *304*, E546–E554. [CrossRef]
71. Rauch, A.; Seitz, S.; Baschant, U.; Schilling, A.F.; Illing, A.; Stride, B.; Kirilov, M.; Takacz, A.; Schmidt-Ullrich, R.; Ostermay, S.; et al. Glucocorticoids suppress bone formation by attenuating osteoblast differentiation via the monomeric glucocorticoid receptor. *Cell Metab.* **2010**, *11*, 517–531. [CrossRef] [PubMed]
72. Jia, D.; O'Brien, C.A.; Stewart, S.A.; Manolagas, S.C.; Weinstein, R.S. Glucocorticoids act directly on osteoclasts to increase their life span and reduce bone density. *Endocrinology* **2006**, *147*, 5592–5599. [CrossRef] [PubMed]
73. Rubin, J.; Biskobing, D.M.; Jadhav, L.; Fan, D.; Nanes, M.S.; Perkins, S.; Fan, X. Dexamethasone promotes expression of membrane-bound macrophage colony-stimulating factor in murine osteoblast-like cells. *Endocrinology* **1998**, *139*, 1006–1012. [CrossRef] [PubMed]
74. Swanson, C.; Lorentzon, M.; Conaway, H.H.; Lerner, U.H. Glucocorticoid Regulation of Osteoclast Differentiation and Expression of Receptor Activator of Nuclear Factor-κB (NF-κB) Ligand, Osteoprotegerin, and Receptor Activator of NF-κB in Mouse Calvarial Bones. *Endocrinology* **2006**, *147*, 3613–3622. [CrossRef] [PubMed]
75. Hofbauer, L.C.; Gori, F.; Riggs, B.L.; Lacey, D.L.; Dunstan, C.R.; Spelsberg, T.C.; Khosla, S. Stimulation of osteoprotegerin ligand and inhibition of osteoprotegerin production by glucocorticoids in human osteoblastic lineage cells: Potential paracrine mechanisms of glucocorticoid-induced osteoporosis. *Endocrinology* **1999**, *140*, 4382–4389. [CrossRef] [PubMed]
76. Humphrey, E.L.; Williams, J.H.; Davie, M.W.; Marshall, M.J. Effects of dissociated glucocorticoids on OPG and RANKL in osteoblastic cells. *Bone* **2006**, *38*, 652–661. [CrossRef]
77. Faienza, M.F.; Brunetti, G.; Colucci, S.; Piacente, L.; Ciccarelli, M.; Giordani, L.; Del Vecchio, G.C.; D'Amore, M.; Albanese, L.; Cavallo, L.; et al. Osteoclastogenesis in children with 21-hydroxylase deficiency on long-term glucocorticoid therapy: The role of receptor activator of nuclear factor-kappaB ligand/osteoprotegerin imbalance. *J. Clin. Endocrinol. Metab.* **2009**, *94*, 2269–2276. [CrossRef]
78. Chen, J.; Yoon, S.H.; Grynpas, M.D.; Mitchell, J. Pre-treatment with Pamidronate Improves Bone Mechanical Properties in Mdx Mice Treated with Glucocorticoids. *Calcif. Tissue Int.* **2019**, *104*, 182–192. [CrossRef]
79. Kim, H.J.; Zhao, H.; Kitaura, H.; Bhattacharyya, S.; Brewer, J.A.; Muglia, L.J.; Ross, F.P.; Teitelbaum, S.L. Glucocorticoids suppress bone formation via the osteoclast. *J. Clin. Investig.* **2006**, *116*, 2152–2160. [CrossRef]
80. Fenton, C.G.; Webster, J.M.; Martin, C.S.; Fareed, S.; Wehmeyer, C.; Mackie, H.; Jones, R.; Seabright, A.P.; Lewis, J.W.; Lai, Y.C.; et al. Therapeutic glucocorticoids prevent bone loss but drive muscle wasting when administered in chronic polyarthritis. *Arthritis Res. Ther.* **2019**, *21*, 182. [CrossRef]
81. Güler-Yüksel, M.; Bijsterbosch, J.; Goekoop-Ruiterman, Y.P.M.; de Vries-Bouwstra, J.K.; Hulsmans, H.M.J.; de Beus, W.M.; Han, K.H.; Breedveld, F.C.; Dijkmans, B.A.C.; Allaart, C.F.; et al. Changes in bone mineral density in patients with recent onset, active rheumatoid arthritis. *Ann. Rheum. Dis.* **2008**, *67*, 823–828. [CrossRef] [PubMed]
82. Sambrook, P.N.; Cohen, M.L.; Eisman, J.A.; Pocock, N.A.; Champion, G.D.; Yeates, M.G. Effects of low dose corticosteroids on bone mass in rheumatoid arthritis: A longitudinal study. *Ann. Rheum. Dis.* **1989**, *48*, 535–538. [CrossRef] [PubMed]
83. Sambrook, P.N.; Eisman, J.A.; Yeates, M.G.; Pocock, N.A.; Eberl, S.; Champion, G.D. Osteoporosis in rheumatoid arthritis: Safety of low dose corticosteroids. *Ann. Rheum. Dis.* **1986**, *45*, 950–953. [CrossRef] [PubMed]

84. Wijbrandts, C.A.; Klaasen, R.; Dijkgraaf, M.G.W.; Gerlag, D.M.; van Eck-Smit, B.L.F.; Tak, P.P. Bone mineral density in rheumatoid arthritis patients 1 year after adalimumab therapy: Arrest of bone loss. *Ann. Rheum. Dis.* **2009**, *68*, 373–376. [CrossRef]
85. Haugeberg, G.; Uhlig, T.; Falch, J.A.; Halse, J.I.; Kvien, T.K. Bone mineral density and frequency of osteoporosis in female patients with rheumatoid arthritis: Results from 394 patients in the Oslo County rheumatoid arthritis register. *Arthritis Rheum.* **2000**, *43*, 522–530. [CrossRef]
86. Pereira, R.M.; Corrente, J.E.; Chahade, W.H.; Yoshinari, N.H. Evaluation by dual X-ray absorptiometry (DXA) of bone mineral density in children with juvenile chronic arthritis. *Clin. Exp. Rheumatol.* **1998**, *16*, 495–501.
87. Varonos, S.; Ansell, B.M.; Reeve, J. Vertebral collapse in juvenile chronic arthritis: Its relationship with glucocorticoid therapy. *Calcif. Tissue Int.* **1987**, *41*, 75–78. [CrossRef]
88. Bergström, J.; Hermansen, L.; Hultman, E.; Saltin, B. Diet, Muscle Glycogen and Physical Performance. *Acta Physiol. Scand.* **1967**, *71*, 140–150. [CrossRef]
89. Coleman, M.E.; DeMayo, F.; Yin, K.C.; Lee, H.M.; Geske, R.; Montgomery, C.; Schwartz, R.J. Myogenic vector expression of insulin-like growth factor I stimulates muscle cell differentiation and myofiber hypertrophy in transgenic mice. *J. Biol. Chem.* **1995**, *270*, 12109–12116. [CrossRef]
90. Lai, K.M.V.; Gonzalez, M.; Poueymirou, W.T.; Kline, W.O.; Na, E.; Zlotchenko, E.; Stitt, T.N.; Economides, A.N.; Yancopoulos, G.D.; Glass, D.J. Conditional activation of akt in adult skeletal muscle induces rapid hypertrophy. *Mol. Cell. Biol.* **2004**, *24*, 9295–9304. [CrossRef]
91. Harwood, A.J. Regulation of GSK-3: A Cellular Multiprocessor. *Cell* **2001**, *105*, 821–824. [CrossRef]
92. Schiaffino, S.; Mammucari, C. Regulation of skeletal muscle growth by the IGF1-Akt/PKB pathway: Insights from genetic models. *Skelet. Muscle* **2011**, *1*, 4. [CrossRef] [PubMed]
93. Booth, F.W.; Tseng, B.S.; FlÜCk, M.; Carson, J.A. Molecular and cellular adaptation of muscle in response to physical training. *Acta Physiol. Scand.* **1998**, *162*, 343–350. [CrossRef] [PubMed]
94. Pallafacchina, G.; Calabria, E.; Serrano, A.L.; Kalhovde, J.M.; Schiaffino, S. A protein kinase B-dependent and rapamycin-sensitive pathway controls skeletal muscle growth but not fiber type specification. *Proc. Nat. Acad. Sci. USA* **2002**, *99*, 9213–9218. [CrossRef]
95. Brunn, G.J.; Hudson, C.C.; Sekulić, A.; Williams, J.M.; Hosoi, H.; Houghton, P.J.; Lawrence, J.C.; Abraham, R.T. Phosphorylation of the Translational Repressor PHAS-I by the Mammalian Target of Rapamycin. *Science* **1997**, *277*, 99. [CrossRef]
96. Gingras, A.C.; Raught, B.; Sonenberg, N. eIF4 Initiation Factors: Effectors of mRNA Recruitment to Ribosomes and Regulators of Translation. *Annu. Rev. Biochem.* **1999**, *68*, 913–963. [CrossRef]
97. Ma, X.M.; Blenis, J. Molecular mechanisms of mTOR-mediated translational control. *Nat. Rev. Mol. Cell Biol.* **2009**, *10*, 307–318. [CrossRef]
98. Hardt Stefan, E.; Tomita, H.; Katus Hugo, A.; Sadoshima, J. Phosphorylation of Eukaryotic Translation Initiation Factor 2Bε by Glycogen Synthase Kinase-3β Regulates β-Adrenergic Cardiac Myocyte Hypertrophy. *Circ. Res.* **2004**, *94*, 926–935. [CrossRef]
99. Rommel, C.; Bodine, S.C.; Clarke, B.A.; Rossman, R.; Nunez, L.; Stitt, T.N.; Yancopoulos, G.D.; Glass, D.J. Mediation of IGF-1-induced skeletal myotube hypertrophy by PI(3)K/Akt/mTOR and PI(3)K/Akt/GSK3 pathways. *Nat. Cell Biol.* **2001**, *3*, 1009–1013. [CrossRef]
100. Cross, D.A.; Alessi, D.R.; Cohen, P.; Andjelkovich, M.; Hemmings, B.A. Inhibition of glycogen synthase kinase-3 by insulin mediated by protein kinase B. *Nature* **1995**, *378*,785–789. [CrossRef]
101. Latres, E.; Amini, A.R.; Amini, A.A.; Griffiths, J.; Martin, F.J.; Wei, Y.; Lin, H.C.; Yancopoulos, G.D.; Glass, D.J. Insulin-like Growth Factor-1 (IGF-1) Inversely Regulates Atrophy-induced Genes via the Phosphatidylinositol 3-Kinase/Akt/Mammalian Target of Rapamycin (PI3K/Akt/mTOR) Pathway. *J. Biol. Chem.* **2005**, *280*, 2737–2744. [CrossRef] [PubMed]
102. Sandri, M.; Sandri, C.; Gilbert, A.; Skurk, C.; Calabria, E.; Picard, A.; Walsh, K.; Schiaffino, S.; Lecker, S.H.; Goldberg, A.L. Foxo transcription factors induce the atrophy-related ubiquitin ligase atrogin-1 and cause skeletal muscle atrophy. *Cell* **2004**, *117*, 399–412. [CrossRef]
103. Calnan, D.R.; Brunet, A. The FoxO code. *Oncogene* **2008**, *27*, 2276–2288. [CrossRef] [PubMed]
104. Brunet, A.; Bonni, A.; Zigmond, M.J.; Lin, M.Z.; Juo, P.; Hu, L.S.; Anderson, M.J.; Arden, K.C.; Blenis, J.; Greenberg, M.E. Akt Promotes Cell Survival by Phosphorylating and Inhibiting a Forkhead Transcription Factor. *Cell* **1999**, *96*, 857–868. [CrossRef]

105. Mammucari, C.; Milan, G.; Romanello, V.; Masiero, E.; Rudolf, R.; Del Piccolo, P.; Burden, S.J.; Di Lisi, R.; Sandri, C.; Zhao, J.; et al. $FoxO_3$ Controls Autophagy in Skeletal Muscle In Vivo. *Cell Metab.* **2007**, *6*, 458–471. [CrossRef] [PubMed]
106. Sandri, M. Autophagy in skeletal muscle. *FEBS Lett.* **2010**, *584*, 1411–1416. [CrossRef] [PubMed]
107. Stitt, T.N.; Drujan, D.; Clarke, B.A.; Panaro, F.; Timofeyva, Y.; Kline, W.O.; Gonzalez, M.; Yancopoulos, G.D.; Glass, D.J. The IGF-1/PI3K/Akt pathway prevents expression of muscle atrophy-induced ubiquitin ligases by inhibiting FOXO transcription factors. *Mol. Cell* **2004**, *14*, 395–403. [CrossRef]
108. Evenson, A.R.; Fareed, M.U.; Menconi, M.J.; Mitchell, J.C.; Hasselgren, P.O. GSK-3beta inhibitors reduce protein degradation in muscles from septic rats and in dexamethasone-treated myotubes. *Int. J. Biochem. Cell Biol.* **2005**, *37*, 2226–2238. [CrossRef]
109. Glickman, M.H.; Ciechanover, A. The Ubiquitin-Proteasome Proteolytic Pathway: Destruction for the Sake of Construction. *Physiol. Rev.* **2002**, *82*, 373–428. [CrossRef]
110. Hershko, A.; Ciechanover, A. The ubiquitin system. *Annu. Rev. Biochem.* **1998**, *67*, 425–479. [CrossRef]
111. Gomes, M.D.; Lecker, S.H.; Jagoe, R.T.; Navon, A.; Goldberg, A.L. Atrogin-1, a muscle-specific F-box protein highly expressed during muscle atrophy. *Proc. Natl. Acad. Sci. USA* **2001**, *98*, 14440–14445. [CrossRef] [PubMed]
112. Bodine, S.C.; Latres, E.; Baumhueter, S.; Lai, V.K.M.; Nunez, L.; Clarke, B.A.; Poueymirou, W.T.; Panaro, F.J.; Na, E.; Dharmarajan, K.; et al. Identification of ubiquitin ligases required for skeletal muscle atrophy. *Science* **2001**, *294*, 1704–1708. [CrossRef] [PubMed]
113. Polge, C.; Heng, A.E.; Jarzaguet, M.; Ventadour, S.; Claustre, A.; Combaret, L.; Béchet, D.; Matondo, M.; Uttenweiler-Joseph, S.; Monsarrat, B.; et al. Muscle actin is polyubiquitinylated in vitro and in vivo and targeted for breakdown by the E3 ligase MuRF1. *FASEB J.* **2011**, *25*, 3790–3802. [CrossRef] [PubMed]
114. Lokireddy, S.; Wijesoma, I.W.; Sze, S.K.; McFarlane, C.; Kambadur, R.; Sharma, M. Identification of atrogin-1-targeted proteins during the myostatin-induced skeletal muscle wasting. *Am. J. Physiol. Cell Physiol.* **2012**, *303*, C512–C529. [CrossRef]
115. Csibi, A.; Cornille, K.; Leibovitch, M.P.; Poupon, A.; Tintignac, L.A.; Sanchez, A.M.; Leibovitch, S.A. The translation regulatory subunit eIF3f controls the kinase-dependent mTOR signaling required for muscle differentiation and hypertrophy in mouse. *PLoS ONE* **2010**, *5*, e8994. [CrossRef]
116. Lagirand-Cantaloube, J.; Cornille, K.; Csibi, A.; Batonnet-Pichon, S.; Leibovitch, M.P.; Leibovitch, S.A. Inhibition of atrogin-1/MAFbx mediated MyoD proteolysis prevents skeletal muscle atrophy in vivo. *PLoS ONE* **2009**, *4*, e4973. [CrossRef]
117. Centner, T.; Yano, J.; Kimura, E.; McElhinny, A.S.; Pelin, K.; Witt, C.C.; Bang, M.L.; Trombitas, K.; Granzier, H.; Gregorio, C.C.; et al. Identification of muscle specific ring finger proteins as potential regulators of the titin kinase domain. *J. Mol. Biol.* **2001**, *306*, 717–726. [CrossRef]
118. Kedar, V.; McDonough, H.; Arya, R.; Li, H.H.; Rockman, H.A.; Patterson, C. Muscle-specific RING finger 1 is a bona fide ubiquitin ligase that degrades cardiac troponin I. *Proc. Natl. Acad. Sci. USA* **2004**, *101*, 18135–18140. [CrossRef]
119. Cohen, S.; Brault, J.J.; Gygi, S.P.; Glass, D.J.; Valenzuela, D.M.; Gartner, C.; Latres, E.; Goldberg, A.L. During muscle atrophy, thick, but not thin, filament components are degraded by MuRF1-dependent ubiquitylation. *J. Cell Biol.* **2009**, *185*, 1083. [CrossRef]
120. Mizushima, N.; Yamamoto, A.; Matsui, M.; Yoshimori, T.; Ohsumi, Y. In Vivo Analysis of Autophagy in Response to Nutrient Starvation Using Transgenic Mice Expressing a Fluorescent Autophagosome Marker. *Mol. Biol. Cell* **2003**, *15*, 1101–1111. [CrossRef]
121. Hanna, R.A.; Quinsay, M.N.; Orogo, A.M.; Giang, K.; Rikka, S.; Gustafsson, A.B. Microtubule-associated protein 1 light chain 3 (LC3) interacts with Bnip3 protein to selectively remove endoplasmic reticulum and mitochondria via autophagy. *J. Biol. Chem.* **2012**, *287*, 19094–19104. [CrossRef] [PubMed]
122. Masiero, E.; Agatea, L.; Mammucari, C.; Blaauw, B.; Loro, E.; Komatsu, M.; Metzger, D.; Reggiani, C.; Schiaffino, S.; Sandri, M. Autophagy Is Required to Maintain Muscle Mass. *Cell Metab.* **2009**, *10*, 507–515. [CrossRef] [PubMed]
123. Yu, M.; Wang, H.; Xu, Y.; Yu, D.; Li, D.; Liu, X.; Du, W. Insulin-like growth factor-1 (IGF-1) promotes myoblast proliferation and skeletal muscle growth of embryonic chickens via the PI3K/Akt signalling pathway. *Cell Biol. Int.* **2015**, *39*, 910–922. [CrossRef] [PubMed]

124. Florini, J.R.; Ewton, D.Z.; Magri, K.A. Hormones, growth factors, and myogenic differentiation. *Annu. Rev. Physiol.* **1991**, *53*, 201–216. [CrossRef]
125. Thomas, M.; Langley, B.; Berry, C.; Sharma, M.; Kirk, S.; Bass, J.; Kambadur, R. Myostatin, a negative regulator of muscle growth, functions by inhibiting myoblast proliferation. *J. Biol. Chem.* **2000**, *275*, 40235–40243. [CrossRef]
126. Rios, R.; Carneiro, I.; Arce, V.M.; Devesa, J. Myostatin is an inhibitor of myogenic differentiation. *Am. J. Physiol. Cell Physiol.* **2002**, *282*, C993–C999. [CrossRef]
127. Windner, S.E.; Doris, R.A.; Ferguson, C.M.; Nelson, A.C.; Valentin, G.; Tan, H.; Oates, A.C.; Wardle, F.C.; Devoto, S.H. Tbx6, Mesp-b and Ripply1 regulate the onset of skeletal myogenesis in zebrafish. *Development* **2015**, *142*, 1159–1168. [CrossRef]
128. Biolo, G.; Maggi, S.P.; Williams, B.D.; Tipton, K.D.; Wolfe, R.R. Increased rates of muscle protein turnover and amino acid transport after resistance exercise in humans. *Am. J. Physiol.* **1995**, *268 Pt 1*, E514–E520. [CrossRef]
129. Phillips, S.M. The science of muscle hypertrophy: Making dietary protein count. *Proc. Nutr. Soc.* **2011**, *70*, 100–103. [CrossRef]
130. Rudnicki, M.A.; Schnegelsberg, P.N.J.; Stead, R.H.; Braun, T.; Arnold, H.-H.; Jaenisch, R. MyoD or Myf-5 is required for the formation of skeletal muscle. *Cell* **1993**, *75*, 1351–1359. [CrossRef]
131. Nabeshima, Y.; Hanaoka, K.; Hayasaka, M.; Esuml, E.; Li, S.; Nonaka, I.; Nabeshima, Y.I. Myogenin gene disruption results in perinatal lethality because of severe muscle defect. *Nature* **1993**, *364*, 532–535. [CrossRef] [PubMed]
132. Kassar-Duchossoy, L.; Gayraud-Morel, B.; Gomès, D.; Rocancourt, D.; Buckingham, M.; Shinin, V.; Tajbakhsh, S. Mrf4 determines skeletal muscle identity in Myf5:Myod double-mutant mice. *Nature* **2004**, *431*, 466–471. [CrossRef] [PubMed]
133. Tajbakhsh, S.; Rocancourt, D.; Cossu, G.; Buckingham, M. Redefining the Genetic Hierarchies Controlling Skeletal Myogenesis: Pax-3 and Myf-5 Act Upstream of MyoD. *Cell* **1997**, *89*, 127–138. [CrossRef]
134. Roubenoff, R.; Roubenoff, R.A.; Ward, L.M.; Holland, S.M.; Hellmann, D.B. Rheumatoid cachexia: Depletion of lean body mass in rheumatoid arthritis. Possible association with tumor necrosis factor. *J. Rheumatol.* **1992**, *19*, 1505–1510. [PubMed]
135. Londhe, P.; Guttridge, D.C. Inflammation induced loss of skeletal muscle. *Bone* **2015**, *80*, 131–142. [CrossRef] [PubMed]
136. Pedersen, M.; Bruunsgaard, H.; Weis, N.; Hendel, H.W.; Andreassen, B.U.; Eldrup, E.; Dela, F.; Pedersen, B.K. Circulating levels of TNF-alpha and IL-6-relation to truncal fat mass and muscle mass in healthy elderly individuals and in patients with type-2 diabetes. *Mech. Ageing Dev.* **2003**, *124*, 495–502. [CrossRef]
137. Jonsdottir, I.H.; Schjerling, P.; Ostrowski, K.; Asp, S.; Richter, E.A.; Pedersen, B.K. Muscle contractions induce interleukin-6 mRNA production in rat skeletal muscles. *J. Physiol.* **2000**, *528*, 157–163. [CrossRef]
138. Goodman, M.N. Interleukin-6 induces skeletal muscle protein breakdown in rats. *Proc. Soc. Exp. Biol. Med.* **1994**, *205*, 182–185. [CrossRef]
139. Cai, D.; Frantz, J.D.; Tawa, N.E., Jr.; Melendez, P.A.; Oh, B.C.; Lidov, H.G.; Hasselgren, P.O.; Frontera, W.R.; Lee, J.; Glass, D.J.; et al. IKKβ/NF-κB Activation Causes Severe Muscle Wasting in Mice. *Cell* **2004**, *119*, 285–298. [CrossRef]
140. Li, Y.P.; Chen, Y.; John, J.; Moylan, J.; Jin, B.; Mann, D.L.; Reid, M.B. TNF-alpha acts via p38 MAPK to stimulate expression of the ubiquitin ligase atrogin1/MAFbx in skeletal muscle. *FASEB J.* **2005**, *19*, 362–370. [CrossRef]
141. Guttridge, D.C.; Mayo, M.W.; Madrid, L.V.; Wang, C.Y.; Baldwin, A.S., Jr. NF-kappaB-induced loss of MyoD messenger RNA: Possible role in muscle decay and cachexia. *Science* **2000**, *289*, 2363–2366. [CrossRef] [PubMed]
142. Layne, M.D.; Farmer, S.R. Tumor necrosis factor-alpha and basic fibroblast growth factor differentially inhibit the insulin-like growth factor-I induced expression of myogenin in C2C12 myoblasts. *Exp. Cell Res.* **1999**, *249*, 177–187. [CrossRef] [PubMed]
143. Li, Y.P.; Reid, M.B. NF-kappaB mediates the protein loss induced by TNF-alpha in differentiated skeletal muscle myotubes. *Am. J. Physiol. Regul. Integr. Comp. Physiol.* **2000**, *279*, R1165–R1170. [CrossRef] [PubMed]

144. Fernandez-Celemin, L.; Pasko, N.; Blomart, V.; Thissen, J.P. Inhibition of muscle insulin-like growth factor I expression by tumor necrosis factor-alpha. *Am. J. Physiol. Endocrinol. Metab.* **2002**, *283*, E1279–E1290. [CrossRef]
145. Frost, R.A.; Lang, C.H.; Gelato, M.C. Transient exposure of human myoblasts to tumor necrosis factor-alpha inhibits serum and insulin-like growth factor-I stimulated protein synthesis. *Endocrinology* **1997**, *138*, 4153–4159. [CrossRef]
146. Zhang, L.; Rajan, V.; Lin, E.; Hu, Z.; Han, H.Q.; Zhou, X.; Song, Y.; Min, H.; Wang, X.; Du, J.; et al. Pharmacological inhibition of myostatin suppresses systemic inflammation and muscle atrophy in mice with chronic kidney disease. *FASEB J.* **2011**, *25*, 1653–1663. [CrossRef]
147. Brandt, C.; Nielsen, A.R.; Fischer, C.P.; Hansen, J.; Pedersen, B.K.; Plomgaard, P. Plasma and muscle myostatin in relation to type 2 diabetes. *PLoS ONE* **2012**, *7*, e37236. [CrossRef]
148. Lecker, S.H.; Solomon, V.; Mitch, W.E.; Goldberg, A.L. Muscle protein breakdown and the critical role of the ubiquitin-proteasome pathway in normal and disease states. *J. Nutr.* **1999**, *129* (Suppl. S1), 227S–237S. [CrossRef]
149. Hall-Angeras, M.; Angeras, U.; Zamir, O.; Hasselgren, P.O.; Fischer, J.E. Effect of the glucocorticoid receptor antagonist RU 38486 on muscle protein breakdown in sepsis. *Surgery* **1991**, *109*,468–473.
150. Schakman, O.; Dehoux, M.; Bouchuari, S.; Delaere, S.; Lause, P.; Decroly, N.; Shoelson, S.E.; Thissen, J.P. Role of IGF-I and the TNFalpha/NF-kappaB pathway in the induction of muscle atrogenes by acute inflammation. *Am. J. Physiol. Endocrinol. Metab.* **2012**, *303*, E729–E739. [CrossRef]
151. Lecker, S.H.; Jagoe, R.T.; Gilbert, A.; Gomes, M.; Baracos, V.; Bailey, J.; Price, S.R.; Mitch, W.E.; Goldberg, A.L. Multiple types of skeletal muscle atrophy involve a common program of changes in gene expression. *FASEB J.* **2004**, *18*, 39–51. [CrossRef] [PubMed]
152. de Theije, C.C.; Schols, A.M.; Lamers, W.H.; Ceelen, J.J.; van Gorp, R.H.; Hermans, J.R.; Köhler, S.E.; Langen, R.C. Glucocorticoid Receptor Signaling Impairs Protein Turnover Regulation in Hypoxia-Induced Muscle Atrophy in Male Mice. *Endocrinology* **2018**, *159*, 519–534. [CrossRef] [PubMed]
153. Smith, I.J.; Alamdari, N.; O'Neal, P.; Gonnella, P.; Aversa, Z.; Hasselgren, P.O. Sepsis increases the expression and activity of the transcription factor Forkhead Box O 1 (FOXO1) in skeletal muscle by a glucocorticoid-dependent mechanism. *Int. J. Biochem. Cell Biol.* **2010**, *42*, 701–711. [CrossRef] [PubMed]
154. Schakman, O.; Gilson, H.; de Coninck, V.; Lause, P.; Verniers, J.; Havaux, X.; Ketelslegers, J.M.; Thissen, J.P. Insulin-like growth factor-I gene transfer by electroporation prevents skeletal muscle atrophy in glucocorticoid-treated rats. *Endocrinology* **2005**, *146*, 1789–1797. [CrossRef]
155. Tomas, F.M.; Munro, H.N.; Young, V.R. Effect of glucocorticoid administration on the rate of muscle protein breakdown in vivo in rats, as measured by urinary excretion of N tau-methylhistidine. *Biochem. J.* **1979**, *178*, 139–146. [CrossRef]
156. Hilton-Jones, D. Diagnosis and treatment of inflammatory muscle diseases. *J.Neurol. Neurosurg. Psychiatry* **2003**, *74* (Suppl. 2), ii25–ii31. [CrossRef]
157. Gayan-Ramirez, G.; Vanderhoydonc, F.; Verhoeven, G.; Decramer, M. Acute treatment with corticosteroids decreases IGF-1 and IGF-2 expression in the rat diaphragm and gastrocnemius. *Am. J. Respir. Crit. Care Med.* **1999**, *159*, 283–289. [CrossRef]
158. Fournier, M.; Huang, Z.S.; Li, H.; Da, X.; Cercek, B.; Lewis, M.I. Insulin-like growth factor I prevents corticosteroid-induced diaphragm muscle atrophy in emphysematous hamsters. *Am. J. Physiol. Regul. Integr. Comp. Physiol.* **2003**, *285*, R34–R43. [CrossRef]
159. Wang, H.; Kubica, N.; Ellisen, L.W.; Jefferson, L.S.; Kimball, S.R. Dexamethasone represses signaling through the mammalian target of rapamycin in muscle cells by enhancing expression of REDD1. *J. Biol. Chem.* **2006**, *281*, 39128–39134. [CrossRef]
160. Imae, M.; Fu, Z.; Yoshida, A.; Noguchi, T.; Kato, H. Nutritional and hormonal factors control the gene expression of FoxOs, the mammalian homologues of DAF-16. *J. Mol. Endocrinol.* **2003**, *30*, 253–262. [CrossRef]
161. Artaza, J.N.; Bhasin, S.; Mallidis, C.; Taylor, W.; Ma, K.; Gonzalez-Cadavid, N.F. Endogenous expression and localization of myostatin and its relation to myosin heavy chain distribution in C2C12 skeletal muscle cells. *J. Cell. Physiol.* **2002**, *190*, 170–179. [CrossRef] [PubMed]

162. Ma, K.; Mallidis, C.; Artaza, J.; Taylor, W.; Gonzalez-Cadavid, N.; Bhasin, S. Characterization of 5'-regulatory region of human myostatin gene: Regulation by dexamethasone in vitro. *Am. J. Physiol. Endocrinol. Metab.* **2001**, *281*, E1128–E1136. [CrossRef] [PubMed]
163. Ma, K.; Mallidis, C.; Bhasin, S.; Mahabadi, V.; Artaza, J.; Gonzalez-Cadavid, N.; Arias, J.; Salehian, B. Glucocorticoid-induced skeletal muscle atrophy is associated with upregulation of myostatin gene expression. *Am. J. Physiol. Endocrinol. Metab.* **2003**, *285*, E363–E371. [CrossRef] [PubMed]
164. Ponyi, A.; Borgulya, G.; Constantin, T.; Vancsa, A.; Gergely, L.; Danko, K. Functional outcome and quality of life in adult patients with idiopathic inflammatory myositis. *Rheumatology* **2005**, *44*, 83–88. [CrossRef] [PubMed]
165. Angelini, C.; Pegoraro, E.; Turella, E.; Intino, M.T.; Pini, A.; Costa, C. Deflazacort in Duchenne dystrophy: Study of long-term effect. *Muscle Nerve* **1994**, *17*, 386–391. [CrossRef] [PubMed]
166. Brooke, M.H.; Fenichel, G.M.; Griggs, R.C.; Mendell, J.R.; Moxley, R.T., 3rd; Miller, J.P.; Kaiser, K.K.; Florence, J.M.; Pandya, S.; Signore, L.; et al. Clinical investigation of Duchenne muscular dystrophy. Interesting results in a trial of prednisone. *Arch. Neurol.* **1987**, *44*, 812–817. [CrossRef] [PubMed]
167. Fenichel, G.M.; Mendell, J.R.; Moxley, R.T., 3rd; Griggs, R.C.; Brooke, M.H.; Miller, J.P.; Pestronk, A.; Robison, J.; King, W.; Signore, L.; et al. A comparison of daily and alternate-day prednisone therapy in the treatment of Duchenne muscular dystrophy. *Arch. Neurol.* **1991**, *48*, 575–579. [CrossRef]
168. Fenichel, G.M.; Florence, J.M.; Pestronk, A.; Mendell, J.R.; Moxley, R.T., 3rd; Griggs, R.C.; Brooke, M.H.; Miller, J.P.; Robison, J.; King, W.; et al. Long-term benefit from prednisone therapy in Duchenne muscular dystrophy. *Neurology* **1991**, *41*, 1874–1877. [CrossRef]
169. Griggs, R.C.; Moxley, R.T., 3rd; Mendell, J.R.; Fenichel, G.M.; Brooke, M.H.; Pestronk, A.; Miller, J.P. Prednisone in Duchenne dystrophy. A randomized, controlled trial defining the time course and dose response. Clinical Investigation of Duchenne Dystrophy Group. *Arch. Neurol.* **1991**, *48*, 383–388. [CrossRef]
170. Lemmey, A.B.; Wilkinson, T.J.; Perkins, C.M.; Nixon, L.A.; Sheikh, F.; Jones, J.G.; Ahmad, Y.A.; O'Brien, T.D. Muscle loss following a single high-dose intramuscular injection of corticosteroids to treat disease flare in patients with rheumatoid arthritis. *Eur. J. Rheumatol.* **2018**, *5*, 160–164. [CrossRef]
171. Gibson, J.N.; Poyser, N.L.; Morrison, W.L.; Scrimgeour, C.M.; Rennie, M.J. Muscle protein synthesis in patients with rheumatoid arthritis: Effect of chronic corticosteroid therapy on prostaglandin F2 alpha availability. *Eur. J. Clin. Investig.* **1991**, *21*, 406–412. [CrossRef] [PubMed]
172. Tiao, G.; Fagan, J.; Roegner, V.; Lieberman, M.; Wang, J.J.; Fischer, J.E.; Hasselgren, P.O. Energy-ubiquitin-dependent muscle proteolysis during sepsis in rats is regulated by glucocorticoids. *J. Clin. Investig.* **1996**, *97*, 339–348. [CrossRef] [PubMed]
173. Gathercole, L.L.; Lavery, G.G.; Morgan, S.A.; Cooper, M.S.; Sinclair, A.J.; Tomlinson, J.W.; Stewart, P.M. 11beta-hydroxysteroid dehydrogenase 1: Translational and therapeutic aspects. *Endocr. Rev.* **2013**, *34*, 525–555. [CrossRef] [PubMed]
174. Hardy, R.S.; Doig, C.L.; Hussain, Z.; O'leary, M.; Morgan, S.A.; Pearson, M.J.; Naylor, A.; Jones, S.W.; Filer, A.; Stewart, P.M.; et al. 11beta-hydroxysteroid dehydrogenase type 1 within muscle protects against the adverse effects of local inflammation. *J. Pathol.* **2016**, *240*, 472–483. [CrossRef] [PubMed]
175. Bujalska, I.; Shimojo, M.; Howie, A.; Stewart, P.M. Human 11 beta-hydroxysteroid dehydrogenase: Studies on the stably transfected isoforms and localization of the type 2 isozyme within renal tissue. *Steroids* **1997**, *62*, 77–82. [CrossRef]
176. Fenton, C.G.; Doig, C.L.; Fareed, S.; Naylor, A.; Morrell, A.P.; Addison, O.; Wehmeyer, C.; Buckley, C.D.; Cooper, M.S.; Lavery, G.G.; et al. 11beta-HSD1 plays a critical role in trabecular bone loss associated with systemic glucocorticoid therapy. *Arthritis Res. Ther.* **2019**, *21*, 188. [CrossRef]
177. Morgan, S.A.; McCabe, E.L.; Gathercole, L.L.; Hassan-Smith, Z.K.; Larner, D.P.; Bujalska, I.J.; Stewart, P.M.; Tomlinson, J.W.; Lavery, G.G. 11beta-HSD1 is the major regulator of the tissue-specific effects of circulating glucocorticoid excess. *Proc. Nat. Acad. Sci. USA* **2014**, *111*, E2482–E2491. [CrossRef]
178. Feig, P.U.; Shah, S.; Hermanowski-Vosatka, A.; Plotkin, D.; Springer, M.S.; Donahue, S.; Thach, C.; Klein, E.J.; Lai, E.; Kaufman, K.D. Effects of an 11beta-hydroxysteroid dehydrogenase type 1 inhibitor, MK-0916, in patients with type 2 diabetes mellitus and metabolic syndrome. *Diabetes Obes. Metab.* **2011**, *13*, 498–504. [CrossRef]

179. Rosenstock, J.; Banarer, S.; Fonseca, V.A.; Inzucchi, S.E.; Sun, W.; Yao, W.; Hollis, G.; Flores, R.; Levy, R.; Williams, W.V.; et al. The 11-beta-hydroxysteroid dehydrogenase type 1 inhibitor INCB13739 improves hyperglycemia in patients with type 2 diabetes inadequately controlled by metformin monotherapy. *Diabetes Care* **2010**, *33*, 1516–1522. [CrossRef]
180. Ahasan, M.M.; Hardy, R.; Jones, C.; Kaur, K.; Nanus, D.; Juarez, M.; Morgan, S.A.; Hassan-Smith, Z.; Bénézech, C.; Caamano, J.H.; et al. Inflammatory regulation of glucocorticoid metabolism in mesenchymal stromal cells. *Arthritis Rheum.* **2012**, *64*, 2404–2413. [CrossRef]
181. Kaur, K.; Hardy, R.; Ahasan, M.M.; Eijken, M.; Van Leeuwen, J.P.; Filer, A.; Thomas, A.M.; Raza, K.; Buckley, C.D.; Stewart, P.M.; et al. Synergistic induction of local glucocorticoid generation by inflammatory cytokines and glucocorticoids: Implications for inflammation associated bone loss. *Ann. Rheum. Dis.* **2010**, *69*, 1185–1190. [CrossRef] [PubMed]
182. Coutinho, A.E.; Gray, M.; Brownstein, D.G.; Salter, D.M.; Sawatzky, D.A.; Clay, S.; Gilmour, J.S.; Seckl, J.R.; Savill, J.S.; Chapman, K.E. 11beta-Hydroxysteroid dehydrogenase type 1, but not type 2, deficiency worsens acute inflammation and experimental arthritis in mice. *Endocrinology* **2012**, *153*, 234–240. [CrossRef] [PubMed]
183. Hardy, R.S.; Fenton, C.; Croft, A.P.; Naylor, A.J.; Begum, R.; Desanti, G.; Buckley, C.D.; Lavery, G.; Cooper, M.S.; Raza, K. 11 Beta-hydroxysteroid dehydrogenase type 1 regulates synovitis, joint destruction, and systemic bone loss in chronic polyarthritis. *J. Autoimmun.* **2018**, *92*, 104–113. [CrossRef] [PubMed]